Electric Power Engineering Handbook
Second Edition

Electric Power Generation, Transmission, and Distribution

Edited by

LEONARD L. GRIGSBY

CRC Press
Taylor & Francis Group

Electric Power Engineering Handbook

Second Edition

Edited by

Leonard L. Grigsby

Electric Power Generation, Transmission, and Distribution

Edited by Leonard L. Grigsby

Electric Power Transformer Engineering, Second Edition

Edited by James H. Harlow

Electric Power Substations Engineering, Second Edition

Edited by John D. McDonald

Power Systems

Edited by Leonard L. Grigsby

Power System Stability and Control

Edited by Leonard L. Grigsby

The Electrical Engineering Handbook Series

Series Editor
Richard C. Dorf
University of California, Davis

Titles Included in the Series

The Handbook of Ad Hoc Wireless Networks, Mohammad Ilyas
The Biomedical Engineering Handbook, *Third Edition,* Joseph D. Bronzino
The Circuits and Filters Handbook, Second Edition, Wai-Kai Chen
The Communications Handbook, Second Edition, Jerry Gibson
The Computer Engineering Handbook, Second Edtion, Vojin G. Oklobdzija
The Control Handbook, William S. Levine
The CRC Handbook of Engineering Tables, Richard C. Dorf
The Digital Avionics Handbook, *Second Edition* Cary R. Spitzer
The Digital Signal Processing Handbook, Vijay K. Madisetti and Douglas Williams
The Electrical Engineering Handbook, *Third Edition,* Richard C. Dorf
The Electric Power Engineering Handbook, *Second Edition*, Leonard L. Grigsby
The Electronics Handbook, *Second Edition,* Jerry C. Whitaker
The Engineering Handbook, Third Edition, Richard C. Dorf
The Handbook of Formulas and Tables for Signal Processing, Alexander D. Poularikas
The Handbook of Nanoscience, Engineering, and Technology, Second Edition,
William A. Goddard, III, Donald W. Brenner, Sergey E. Lyshevski, and Gerald J. Iafrate
The Handbook of Optical Communication Networks, Mohammad Ilyas and
Hussein T. Mouftah
The Industrial Electronics Handbook, J. David Irwin
The Measurement, Instrumentation, and Sensors Handbook, John G. Webster
The Mechanical Systems Design Handbook, Osita D.I. Nwokah and Yidirim Hurmuzlu
The Mechatronics Handbook, *Second Edition,* Robert H. Bishop
The Mobile Communications Handbook, *Second Edition*, Jerry D. Gibson
The Ocean Engineering Handbook, Ferial El-Hawary
The RF and Microwave Handbook, *Second Edition,* Mike Golio
The Technology Management Handbook, Richard C. Dorf
The Transforms and Applications Handbook, *Second Edition,* Alexander D. Poularikas
The VLSI Handbook, *Second Edition*, Wai-Kai Chen

Electric Power Engineering Handbook
Second Edition

ELECTRIC POWER GENERATION, TRANSMISSION, and DISTRIBUTION

Edited by
Leonard L. Grigsby

CRC Press
Taylor & Francis Group
Boca Raton London New York

CRC Press is an imprint of the
Taylor & Francis Group, an informa business

CRC Press
Taylor & Francis Group
6000 Broken Sound Parkway NW, Suite 300
Boca Raton, FL 33487-2742

Printed in the United States of America on acid-free paper
10 9 8 7 6 5 4 3 2 1

International Standard Book Number-10: 0-8493-9292-6 (Hardcover)
International Standard Book Number-13: 978-0-8493-9292-4 (Hardcover)

Library of Congress Cataloging-in-Publication Data

Electric power generation, transmission, and distribution / editor, Leonard Lee Grigsby.
p. cm.
Includes bibliographical references and index.
ISBN-13: 978-0-8493-9292-4 (alk. paper)
ISBN-10: 0-8493-9292-6 (alk. paper)
1. Electric power production. 2. Electric power distribution. 3. Electric power transmission. I. Grigsby, Leonard L. II. Title.

TK1001.E25 2007
621.31--dc22 2007006454

Visit the Taylor & Francis Web site at
http://www.taylorandfrancis.com

and the CRC Press Web site at
http://www.crcpress.com

Table of Contents

IV Distribution Systems

V Electric Power Utilization

VI Power Quality

33 Power Quality Monitoring

Patrick Coleman

Preface

The generation, delivery, and utilization of electric power and energy remain one of the most challenging and exciting fields of electrical engineering. The astounding technological developments of our age are highly dependent upon a safe, reliable, and economic supply of electric power. The objective of *Electric Power Engineering Handbook*, 2nd Edition is to provide a contemporary overview of this far-reaching field as well as to be a useful guide and educational resource for its study. It is intended to define electric power engineering by bringing together the core of knowledge from all of the many topics encompassed by the field. The chapters are written primarily for the electric power engineering professional who is seeking factual information, and secondarily for the professional from other engineering disciplines who wants an overview of the entire field or specific information on one aspect of it.

The handbook is published in five volumes. Each is organized into topical sections and chapters in an attempt to provide comprehensive coverage of the generation, transformation, transmission, distribution, and utilization of electric power and energy as well as the modeling, analysis, planning, design, monitoring, and control of electric power systems. The individual chapters are different from most technical publications. They are not journal-type chapters nor are they textbook in nature. They are intended to be tutorials or overviews providing ready access to needed information while at the same time providing sufficient references to more in-depth coverage of the topic. This work is a member of the Electrical Engineering Handbook Series published by CRC Press. Since its inception in 1993, this series has been dedicated to the concept that when readers refer to a handbook on a particular topic they should be able to find what they need to know about the subject most of the time. This has indeed been the goal of this handbook.

This volume of the handbook is devoted to the subjects of electric power generation by both conventional and nonconventional methods, transmission systems, distribution systems, power utilization, and power quality. If your particular topic of interest is not included in this list, please refer to the list of companion volumes seen at the beginning of this book.

In reading the individual chapters of this handbook, I have been most favorably impressed by how well the authors have accomplished the goals that were set. Their contributions are, of course, most key to the success of the work. I gratefully acknowledge their outstanding efforts. Likewise, the expertise and dedication of the editorial board and section editors have been critical in making this handbook possible. To all of them I express my profound thanks. I also wish to thank the personnel at Taylor & Francis who have been involved in the production of this book, with a special word of thanks to Nora Konopka, Allison Shatkin, and Jessica Vakili. Their patience and perseverance have made this task most pleasant.

Leo Grigsby
Editor-in-Chief

Editor

Leonard L. ("Leo") Grigsby received his BS and MS in electrical engineering from Texas Tech University and his PhD from Oklahoma State University. He has taught electrical engineering at Texas Tech, Oklahoma State University, and Virginia Polytechnic Institute and University. He has been at Auburn University since 1984 first as the Georgia power distinguished professor, later as the Alabama power distinguished professor, and currently as professor emeritus of electrical engineering. He also spent nine months during 1990 at the University of Tokyo as the Tokyo Electric Power Company endowed chair of electrical engineering. His teaching interests are in network analysis, control systems, and power engineering.

During his teaching career, Professor Grigsby has received 13 awards for teaching excellence. These include his selection for the university-wide William E. Wine Award for Teaching Excellence at Virginia Polytechnic Institute and University in 1980, his selection for the ASEE AT&T Award for Teaching Excellence in 1986, the 1988 Edison Electric Institute Power Engineering Educator Award, the 1990–1991 Distinguished Graduate Lectureship at Auburn University, the 1995 IEEE Region 3 Joseph M. Beidenbach Outstanding Engineering Educator Award, the 1996 Birdsong Superior Teaching Award at Auburn University, and the IEEE Power Engineering Society Outstanding Power Engineering Educator Award in 2003.

Professor Grigsby is a fellow of the Institute of Electrical and Electronics Engineers (IEEE). During 1998–1999 he was a member of the board of directors of IEEE as director of Division VII for power and energy. He has served the Institute in 30 different offices at the chapter, section, regional, and international levels. For this service, he has received seven distinguished service awards, the IEEE Centennial Medal in 1984, the Power Engineering Society Meritorious Service Award in 1994, and the IEEE Millennium Medal in 2000.

During his academic career, Professor Grigsby has conducted research in a variety of projects related to the application of network and control theory to modeling, simulation, optimization, and control of electric power systems. He has been the major advisor for 35 MS and 21 PhD graduates. With his students and colleagues, he has published over 120 technical papers and a textbook on introductory network theory. He is currently the series editor for the Electrical Engineering Handbook Series published by CRC Press. In 1993 he was inducted into the Electrical Engineering Academy at Texas Tech University for distinguished contributions to electrical engineering.

Contributors

Math H.J. Bollen
STRI
Ludvika, Sweden

Simon W. Bowen
Alabama Power Company
Birmingham, Alabama

Robert P. Broadwater
Virginia Polytechnic Institute
and State University
Blacksburg, Virginia

Steven R. Brockschink
Stantec Consulting
Portland, Oregon

Kristine Buchholz
Pacific Gas & Electric Company
Danville, California

Jim Burke
InfraSource Technology
Cary, North Carolina

Wilford Caulkins
Sherman & Reilly
Chattanooga, Tennessee

William A. Chisholm
Kinectrics/UQAC
Toronto, Ontario, Canada

George L. Clark
Alabama Power Company
Birmingham, Alabama

Patrick Coleman
Alabama Power Company
Birmingham, Alabama

Murat Dilek
Electrical Distribution
Design, Inc.
Blacksburg, Virginia

D.A. Douglass
Power Delivery Consultants, Inc.
Niskayuna, New York

Michael L. Dyer
Salt River Project
Phoenix, Arizona

Richard G. Farmer
Arizona State University
Tempe, Arizona

Charles A. Gross
Auburn University
Auburn, Alabama

John V. Grubbs
Alabama Power Company
Birmingham, Alabama

James H. Gurney
BC Transmission Corporation
Vancouver, British Columbia, Canada

S.M. Halpin
Auburn University
Auburn, Alabama

Andrew Hanson
PowerComm Engineering
Raleigh, North Carolina

Gary L. Johnson
Kansas State University
Manhattan, Kansas

John G. Kappenman
Metatech Corporation
Duluth, Minnesota

George G. Karady
Arizona State University
Tempe, Arizona

John R. Kennedy
Georgia Power Company
Atlanta, Georgia

William H. Kersting
New Mexico State University
Las Cruces, New Mexico

Christopher J. Melhorn
EPRI
Knoxville, Tennessee

Roger A. Messenger
Florida Atlantic University
Boca Raton, Florida

Paul I. Nippes
Magnetic Products and Services, Inc.
Holmdel, New Jersey

Joe C. Pohlman
Consultant
Pittsburgh, Pennsylvania

Saifur Rahman
Virginia Polytechnic Institute
and State University
Alexandria, Virginia

Rama Ramakumar
Oklahoma State University
Stillwater, Oklahoma

Manuel Reta-Hernández
Universidad Autónoma
de Zacatecas
Zacatecas, Mexico

Kenneth H. Sebra
Baltimore Gas and
Electric Company
Dameron, Maryland

Douglas B. Seely
Stantec Consulting
Portland, Oregon

Raymond R. Shoults
University of Texas at Arlington
Arlington, Texas

Larry D. Swift
University of Texas at Arlington
Arlington, Texas

Rao S. Thallam
Salt River Project
Phoenix, Arizona

Ridley Thrash
Southwire Company
Carollton, Georgia

Giao N. Trinh
Retired from Hydro-Québec
Institute of Research
Boucherville, Quebec, Canada

I

Electric Power Generation: Nonconventional Methods

Saifur Rahman
Virginia Polytechnic Institute and State University

1

Wind Power

Gary L. Johnson
Kansas State University

The wind is a free, clean, and inexhaustible energy source. It has served humankind well for many centuries by propelling ships and driving wind turbines to grind grain and pump water. Denmark was the first country to use wind for generation of electricity. The Danes were using a 23-m diameter wind turbine in 1890 to generate electricity. By 1910, several hundred units with capacities of 5 to 25 kW were in operation in Denmark (Johnson, 1985). By about 1925, commercial wind-electric plants using two- and three-bladed propellers appeared on the American market. The most common brands were Wincharger (200 to 1200 W) and Jacobs (1.5 to 3 kW). These were used on farms to charge storage batteries which were then used to operate radios, lights, and small appliances with voltage ratings of 12, 32, or 110 volts. A good selection of 32-VDC appliances was developed by the industry to meet this demand.

In addition to home wind-electric generation, a number of utilities around the world have built larger wind turbines to supply power to their customers. The largest wind turbine built before the late 1970s was a 1250-kW machine built on Grandpa's Knob, near Rutland, Vermont, in 1941. This turbine, called the Smith-Putnam machine, had a tower that was 34 m high and a rotor 53 m in diameter. The rotor turned an ac synchronous generator that produced 1250 kW of electrical power at wind speeds above 13 m/s.

After World War II, we entered the era of cheap oil imported from the Middle East. Interest in wind energy died and companies making small turbines folded. The oil embargo of 1973 served as a wakeup call, and oil-importing nations around the world started looking at wind again. The two most important countries in wind power development since then have been the U.S. and Denmark (Brower et al., 1993).

The U.S. immediately started to develop utility-scale turbines. It was understood that large turbines had the potential for producing cheaper electricity than smaller turbines, so that was a reasonable decision. The strategy of getting large turbines in place was poorly chosen, however. The Department of Energy decided that only large aerospace companies had the manufacturing and engineering capability to build utility-scale turbines. This meant that small companies with good ideas would not have the revenue stream necessary for survival. The problem with the aerospace firms was that they had no desire to manufacture utility-scale wind turbines. They gladly took the government's money to build test turbines, but when the money ran out, they were looking for other research projects. The government funded a number of test turbines, from the 100 kW MOD-0 to the 2500 kW MOD-2. These ran for brief periods of time, a few years at most. Once it was obvious that a particular design would never be cost competitive, the turbine was quickly salvaged.

Denmark, on the other hand, established a plan whereby a landowner could buy a turbine and sell the electricity to the local utility at a price where there was at least some hope of making money. The early

TABLE 1.1 Wind Power Installed Capacity

Canada	83
China	224
Denmark	1450
India	968
Ireland	63
Italy	180
Germany	2874
Netherlands	363
Portugal	60
Spain	834
Sweden	150
U.K.	334
U.S.	1952
Other	304
Total	9839

turbines were larger than what a farmer would need for himself, but not what we would consider utility scale. This provided a revenue stream for small companies. They could try new ideas and learn from their mistakes. Many people jumped into this new market. In 1986, there were 25 wind turbine manufacturers in Denmark. The Danish market gave them a base from which they could also sell to other countries. It was said that Denmark led the world in exports of two products: wind turbines and butter cookies! There has been consolidation in the Danish industry since 1986, but some of the companies have grown large. Vestas, for example, has more installed wind turbine capacity worldwide than any other manufacturer.

Prices have dropped substantially since 1973, as performance has improved. It is now commonplace for wind power plants (collections of utility-scale turbines) to be able to sell electricity for under four cents per kilowatt hour.

Total installed worldwide capacity at the start of 1999 was almost 10,000 MW, according to the trade magazine *Wind Power Monthly* (1999). The countries with over 50 MW of installed capacity at that time are shown in Table 1.1.

1.1 Applications

There are perhaps four distinct categories of wind power which should be discussed. These are

1. small, non-grid connected
2. small, grid connected
3. large, non-grid connected
4. large, grid connected

By small, we mean a size appropriate for an individual to own, up to a few tens of kilowatts. Large refers to utility scale.

1.1.1 Small, Non-Grid Connected

If one wants electricity in a location not serviced by a utility, one of the options is a wind turbine, with batteries to level out supply and demand. This might be a vacation home, a remote antenna and transmitter site, or a Third-World village. The costs will be high, on the order of $0.50/kWh, but if the total energy usage is small, this might be acceptable. The alternatives, photovoltaics, microhydro, and diesel generators, are not cheap either, so a careful economic study needs to be done for each situation.

1.1.2 Small, Grid Connected

The small, grid connected turbine is usually not economically feasible. The cost of wind-generated electricity is less because the utility is used for storage rather than a battery bank, but is still not competitive.

In order for the small, grid connected turbine to have any hope of financial breakeven, the turbine owner needs to get something close to the retail price for the wind-generated electricity. One way this is done is for the owner to have an arrangement with the utility called net metering. With this system, the meter runs backward when the turbine is generating more than the owner is consuming at the moment. The owner pays a monthly charge for the wires to his home, but it is conceivable that the utility will sometimes write a check to the owner at the end of the month, rather than the other way around. The utilities do not like this arrangement. They want to buy at wholesale and sell at retail. They feel it is unfair to be used as a storage system without remuneration.

For most of the twentieth century, utilities simply refused to connect the grid to wind turbines. The utility had the right to generate electricity in a given service territory, and they would not tolerate competition. Then a law was passed that utilities had to hook up wind turbines and pay them the avoided cost for energy. Unless the state mandated net metering, the utility typically required the installation of a second meter, one measuring energy consumption by the home and the other energy production by the turbine. The owner would pay the regular retail rate, and the utility would pay their estimate of avoided cost, usually the fuel cost of some base load generator. The owner might pay \$0.08 to \$0.15 per kWh, and receive \$0.02 per kWh for the wind-generated electricity. This was far from enough to economically justify a wind turbine, and had the effect of killing the small wind turbine business.

1.1.3 Large, Non-Grid Connected

These machines would be installed on islands or in native villages in the far north where it is virtually impossible to connect to a large grid. Such places are typically supplied by diesel generators, and have a substantial cost just for the imported fuel. One or more wind turbines would be installed in parallel with the diesel generators, and act as fuel savers when the wind was blowing.

This concept has been studied carefully and appears to be quite feasible technically. One would expect the market to develop after a few turbines have been shown to work for an extended period in hostile environments. It would be helpful if the diesel maintenance companies would also carry a line of wind turbines so the people in remote locations would not need to teach another group of maintenance people about the realities of life at places far away from the nearest hardware store.

1.1.4 Large, Grid Connected

We might ask if the utilities should be forced to buy wind-generated electricity from these small machines at a premium price which reflects their environmental value. Many have argued this over the years. A better question might be whether the small or the large turbines will result in a lower net cost to society. Given that we want the environmental benefits of wind generation, should we get the electricity from the wind with many thousands of individually owned small turbines, or should we use a much smaller number of utility-scale machines?

If we could make the argument that a dollar spent on wind turbines is a dollar not spent on hospitals, schools, and the like, then it follows that wind turbines should be as efficient as possible. Economies of scale and costs of operation and maintenance are such that the small, grid connected turbine will always need to receive substantially more per kilowatt hour than the utility-scale turbines in order to break even. There is obviously a niche market for turbines that are not connected to the grid, but small, grid connected turbines will probably not develop a thriving market. Most of the action will be from the utility-scale machines.

Sizes of these turbines have been increasing rapidly. Turbines with ratings near 1 MW are now common, with prototypes of 2 MW and more being tested. This is still small compared to the needs of a utility, so clusters of turbines are placed together to form wind power plants with total ratings of 10 to 100 MW.

1.2 Wind Variability

One of the most critical features of wind generation is the variability of wind. Wind speeds vary with time of day, time of year, height above ground, and location on the earth's surface. This makes wind generators into what might be called energy producers rather than power producers. That is, it is easier to estimate the energy production for the next month or year than it is to estimate the power that will be produced at 4:00 PM next Tuesday. Wind power is not dispatchable in the same manner as a gas turbine. A gas turbine can be scheduled to come on at a given time and to be turned off at a later time, with full power production in between. A wind turbine produces only when the wind is available. At a good site, the power output will be zero (or very small) for perhaps 10% of the time, rated for perhaps another 10% of the time, and at some intermediate value the remaining 80% of the time.

This variability means that some sort of storage is necessary for a utility to meet the demands of its customers, when wind turbines are supplying part of the energy. This is not a problem for penetrations of wind turbines less than a few percent of the utility peak demand. In small concentrations, wind turbines act like negative load. That is, an increase in wind speed is no different in its effect than a customer turning off load. The control systems on the other utility generation sense that generation is greater than load, and decrease the fuel supply to bring generation into equilibrium with load. In this case, storage is in the form of coal in the pile or natural gas in the well.

An excellent form of storage is water in a hydroelectric lake. Most hydroelectric plants are sized large enough to not be able to operate full-time at peak power. They therefore must cut back part of the time because of the lack of water. A combination hydro and wind plant can conserve water when the wind is blowing, and use the water later, when the wind is not blowing.

When high-temperature superconductors become a little less expensive, energy storage in a magnetic field will be an exciting possibility. Each wind turbine can have its own superconducting coil storage unit. This immediately converts the wind generator from an energy producer to a peak power producer, fully dispatchable. Dispatchable peak power is always worth more than the fuel cost savings of an energy producer. Utilities with adequate base load generation (at low fuel costs) would become more interested in wind power if it were a dispatchable peak power generator.

The variation of wind speed with time of day is called the diurnal cycle. Near the earth's surface, winds are usually greater during the middle of the day and decrease at night. This is due to solar heating, which causes "bubbles" of warm air to rise. The rising air is replaced by cooler air from above. This thermal mixing causes wind speeds to have only a slight increase with height for the first hundred meters or so above the earth. At night, however, the mixing stops, the air near the earth slows to a stop, and the winds above some height (usually 30 to 100 m) actually increase over the daytime value. A turbine on a short tower will produce a greater proportion of its energy during daylight hours, while a turbine on a very tall tower will produce a greater proportion at night.

As tower height is increased, a given generator will produce substantially more energy. However, most of the extra energy will be produced at night, when it is not worth very much. Standard heights have been increasing in recent years, from 50 to 65 m or even more. A taller tower gets the blades into less turbulent air, a definite advantage. The disadvantages are extra cost and more danger from overturning in high winds. A very careful look should be given the economics before buying a tower that is significantly taller than whatever is sold as a standard height for a given turbine.

Wind speeds also vary strongly with time of year. In the southern Great Plains (Kansas, Oklahoma, and Texas), the winds are strongest in the spring (March and April) and weakest in the summer (July and August). Utilities here are summer peaking, and hence need the most power when winds are the lowest and the least power when winds are highest. The diurnal variation of wind power is thus a fairly good match to utility needs, while the yearly variation is not.

The variability of wind with month of year and height above ground is illustrated in Table 1.2. These are actual wind speed data for a good site in Kansas, and projected electrical generation of a Vestas turbine (V47-660) at that site. Anemometers were located at 10, 40, and 60 m above ground. Wind

TABLE 1.2 Monthly Average Wind Speed in MPH and Projected Energy Production at 65 m, at a Good Site in Southern Kansas

Month	10 m Speed	60 m Speed	Energy (MWh)	Month	10 m Speed	60 m Speed	Energy (MWh)
1/96	14.9	20.3	256	1/97	15.8	21.2	269
2/96	16.2	22.4	290	2/97	14.7	19.0	207
3/96	17.6	22.3	281	3/97	17.4	22.8	291
4/96	19.8	25.2	322	4/97	15.9	20.4	242
5/96	18.4	23.1	297	5/97	15.2	19.8	236
6/96	13.5	18.2	203	6/97	11.9	16.3	167
7/96	12.5	16.5	169	7/97	13.3	18.5	212
8/96	11.6	16.0	156	8/97	11.7	16.9	176
9/96	12.4	17.2	182	9/97	13.6	19.0	211
10/96	17.1	23.3	320	10/97	15.0	21.1	265
11/96	15.3	20.0	235	11/97	14.3	19.7	239
12/96	15.1	20.1	247	12/97	13.6	19.5	235

speeds at 40 and 60 m were used to estimate the wind speed at 65 m (the nominal tower height of the V47-660) and to calculate the expected energy production from this turbine at this height. Data have been normalized for a 30-day month.

There can be a factor of two between a poor month and an excellent month (156 MWh in 8/96 to 322 MWh in 4/96). There will not be as much variation from one year to the next, perhaps 10 to 20%. A wind power plant developer would like to have as long a data set as possible, with an absolute minimum of one year. If the one year of data happens to be for the best year in the decade, followed by several below average years, a developer could easily get into financial trouble. The risk gets smaller if the data set is at least two years long.

One would think that long-term airport data could be used to predict whether a given data set was collected in a high or low wind period for a given part of the country, but this is not always true. One study showed that the correlation between average annual wind speeds at Russell, Kansas, and Dodge City, Kansas, was 0.596 while the correlation between Russell and Wichita was 0.115. The terrain around Russell is very similar to that around Wichita, and there is no obvious reason why wind speeds should be high at one site and low at the other for one year, and then swap roles the next year.

There is also concern about long-term variation in wind speeds. There appears to be an increase in global temperatures over the past decade or so, which would probably have an impact on wind speeds. It also appears that wind speeds have been somewhat lower as temperatures have risen, at least in Kansas. It appears that wind speeds can vary significantly over relatively short distances. A good data set at one location may underpredict or overpredict the winds at a site a few miles away by as much as 10 to 20%. Airport data collected on a 7-m tower in a flat river valley may underestimate the true surrounding hilltop winds by a factor of two. If economics are critical, a wind power plant developer needs to acquire rights to a site and collect wind speed data for at least one or two years before committing to actually constructing turbines there.

1.2.1 Land Rights

Spacing of turbines can vary widely with the type of wind resource. In a tradewind or a mountain pass environment where there are only one or two prevailing wind directions, the turbines can be located "shoulder to shoulder" crossways to the wind direction. A downwind spacing of ten times the rotor diameter is usually assumed to be adequate to give the wind space to recover its speed. In open areas, a crosswind spacing of four rotor diameters is usually considered a minimum. In the Great Plains, the prevailing winds are from the south (Kansas, Oklahoma, and Texas) or north (the Dakotas). The energy in the winds from east and west may not be more than 10% of the total

energy. In this situation, a spacing of ten rotor diameters north–south and four rotor diameters east–west would be minimal. Adjustments would be made to avoid roads, pipelines, power lines, houses, ponds, and creeks.

The results of a detailed site layout will probably not predict much more than 20 MW of installed capacity per square mile (640 acres). This figure can be used for initial estimates without great error. That is, if a developer is considering installing a 100-MW wind plant, rights to at least five square miles should be acquired.

One issue that has not received much attention in the wind power community is that of a fair compensation to the land owner for the privilege of installing wind turbines. The developer could buy the land, hopefully with a small premium. The original deal could be an option to buy at some agreed upon price, if two years of wind data were satisfactory. The developer might lease the land back to the original landowner, since the agricultural production capability is only slightly affected by the presence of wind turbines. Outright purchase between a willing and knowledgeable buyer and seller would be as fair an arrangement as could be made.

But what about the case where the landowner does not want to sell? Rights have been acquired by a large variety of mechanisms, including a large one-time payment for lease signing, a fixed yearly fee, a royalty payment based on energy produced, and combinations of the above. The one-time payment has been standard utility practice for right-of-way acquisitions, and hence will be preferred by at least some utilities. A key difference is that wind turbines require more attention than a transmission line. Roads are not usually built to transmission line towers, while they are built to wind turbines. Roads and maintenance operations around wind turbines provide considerably more hassle to the landowner. The original owner got the lease payment, and 20 years later the new owner gets the nuisance. There is no incentive for the new landowner to be cooperative or to lobby county or state officials on behalf of the developer.

A one-time payment also increases the risk to the developer. If the project does not get developed, there has been a significant outlay of cash which will have no return on it. These disadvantages mean that the one-time payment with no yearly fees or royalties will probably not be the long-term norm in the industry.

To discuss what might be a fair price for a lease, it will be helpful to use an example. We will assume the following:

- 20 MW per square mile
- Land fair-market value \$500/acre
- Plant factor 0.4
- Developer desired internal rate of return 0.2
- Electricity value \$0.04/kWh
- Installed cost of wind turbine \$1000/kW

A developer that purchased the land at \$500/acre would therefore want a return of \$(500) (0.2) = \$100/acre. America's cheap food policy means that production agriculture typically gets a much smaller return on investment than the developer wants. Actual cash rent on grassland might be \$15/acre, or a return of 0.03 on investment. We see an immediate opportunity for disagreement, even hypocrisy. The developer might offer the landowner \$15/acre when the developer would want \$100/acre if he bought the land. This hardly seems equitable.

The gross income per acre is

$$I = \frac{(20{,}000 \text{ kW})\ (0.4)\ (8760 \text{ hours/year})\ (\$0.04)}{640 \text{ acres}} = \$4380/\text{acre/year} \tag{1.1}$$

The cost of wind turbines per acre is

$$CT_a = \frac{(20{,}000 \text{ kW})\ (\$1000/\text{kW})}{640 \text{ acres}} = \$31{,}250/\text{acre} \tag{1.2}$$

We see that the present fair-market value for the land is tiny compared with the installed cost of the wind turbines. A lease payment of $100/acre/year is slightly over 2% of the gross income. It is hard to imagine financial arrangements so tight that they would collapse if the landowner (either rancher or developer) were paid this yearly fee. That is, it seems entirely reasonable for a figure like 2% of gross income to be a starting point for negotiations.

There is another factor that might result in an even higher percentage. Landowners throughout the Great Plains are accustomed to royalty payments of 12.5% of wholesale price for oil and gas leases. This is determined independently of any agricultural value for the land. The most worthless mesquite in Texas gets the same terms as the best irrigated corn ground in Kansas. We might ask if this rate is too high. A royalty of 12.5% of wholesale amounts to perhaps 6% of retail. Cutting the royalty in half would have the potential of reducing the price of gasoline about 3%. In a market where gasoline prices swing by 20%, this reduction is lost in the noise. If a law were passed which cut royalty payments in half, it is hard to argue that it would have much impact on our gasoline buying habits, the size of vehicles we buy, or the general welfare of the nation.

One feature of the 12.5% royalty is that it is high enough to get most oil and gas producing land under lease. Would 6.25% have been enough to get the same amount of land leased? If we assumed that some people would sign a lease for 12.5% that would not sign if the offer were 6.25%, then we have the interesting possibility that the supply would be less. If we assume the law of supply and demand to apply, the price of gasoline and natural gas would increase. The possible increase is shear speculation, but could easily be more than the 6.25% that was "saved" by cutting the royalty payment in half.

The point is that the royalty needs to be high enough to get the very best sites under lease. If the best site produces 10% more energy than the next best, it makes no economic sense to pay a 2% royalty for the second best when a 6% royalty would get the best site. In this example, the developer would get 10% more energy for 4% more royalty. The developer could either pocket the difference or reduce the price of electricity a proportionate amount.

References

Brower, M.C., Tennis, M.W., Denzler, E.W., and Kaplan, M.M., *Powering the Midwest*, A Report by the Union of Concerned Scientists, 1993.

Johnson, G.L., *Wind Energy Systems*, Prentice-Hall, New York, 1985.

Wind Power Monthly, 15(6), June, 1999.

2

Advanced Energy Technologies

Saifur Rahman
Virginia Polytechnic Institute and State University

2.1 Storage Systems

Energy storage technologies are of great interest to electric utilities, energy service companies, and automobile manufacturers (for electric vehicle application). The ability to store large amounts of energy would allow electric utilities to have greater flexibility in their operation because with this option the supply and demand do not have to be matched instantaneously. The availability of the proper battery at the right price will make the electric vehicle a reality, a goal that has eluded the automotive industry thus far. Four types of storage technologies (listed below) are discussed in this section, but most emphasis is placed on storage batteries because it is now closest to being commercially viable. The other storage technology widely used by the electric power industry, pumped-storage power plants, is not discussed as this has been in commercial operation for more than 60 years in various countries around the world.

- Flywheel storage
- Compressed air energy storage
- Superconducting magnetic energy storage
- Battery storage

2.1.1 Flywheel Storage

Flywheels store their energy in their rotating mass, which rotates at very high speeds (approaching 75,000 rotations per minute), and are made of composite materials instead of steel because of the composite's ability to withstand the rotating forces exerted on the flywheel. In order to store energy the flywheel is placed in a sealed container which is then placed in a vacuum to reduce air resistance. Magnets embedded in the flywheel pass near pickup coils. The magnet induces a current in the coil changing the rotational energy into electrical energy. Flywheels are still in research and development, and commercial products are several years away.

2.1.2 Compressed Air Energy Storage

As the name implies, the compressed air energy storage (CAES) plant uses electricity to compress air which is stored in underground reservoirs. When electricity is needed, this compressed air is withdrawn, heated with gas or oil, and run through an expansion turbine to drive a generator. The compressed air can be stored in several types of underground structures, including caverns in salt or rock formations, aquifers, and depleted natural gas fields. Typically the compressed air in a CAES plant uses about one third of the premium fuel needed to produce the same amount of electricity as in a conventional plant. A 290-MW CAES plant has been in operation in Germany since the early 1980s with 90% availability and 99% starting reliability. In the U.S., the Alabama Electric Cooperative runs a CAES plant that stores compressed air in a 19-million cubic foot cavern mined from a salt dome. This 110-MW plant has a storage capacity of 26 h. The fixed-price turnkey cost for this first-of-a-kind plant is about $400/kW in constant 1988 dollars.

The turbomachinery of the CAES plant is like a combustion turbine, but the compressor and the expander operate independently. In a combustion turbine, the air that is used to drive the turbine is compressed just prior to combustion and expansion and, as a result, the compressor and the expander must operate at the same time and must have the same air mass flow rate. In the case of a CAES plant, the compressor and the expander can be sized independently to provide the utility-selected "optimal" MW charge and discharge rate which determines the ratio of hours of compression required for each hour of turbine-generator operation. The MW ratings and time ratio are influenced by the utility's load curve, and the price of off-peak power. For example, the CAES plant in Germany requires 4 h of compression per hour of generation. On the other hand, the Alabama plant requires 1.7 h of compression for each hour of generation. At 110-MW net output, the power ratio is 0.818 kW output for each kilowatt input. The heat rate (LHV) is 4122 BTU/kWh with natural gas fuel and 4089 BTU/kWh with fuel oil. Due to the storage option, a partial-load operation of the CAES plant is also very flexible. For example, the heat rate of the expander increases only by 5%, and the airflow decreases nearly linearly when the plant output is turned down to 45% of full load. However, CAES plants have not reached commercial viability beyond some prototypes.

2.1.3 Superconducting Magnetic Energy Storage

A third type of advanced energy storage technology is superconducting magnetic energy storage (SMES), which may someday allow electric utilities to store electricity with unparalled efficiency (90% or more). A simple description of SMES operation follows.

The electricity storage medium is a doughnut-shaped electromagnetic coil of superconducting wire. This coil could be about 1000 m in diameter, installed in a trench, and kept at superconducting temperature by a refrigeration system. Off-peak electricity, converted to direct current (DC), would be fed into this coil and stored for retrieval at any moment. The coil would be kept at a low-temperature superconducting state using liquid helium. The time between charging and discharging could be as little as 20 ms with a round-trip AC–AC efficiency of over 90%.

Developing a commercial-scale SMES plant presents both economic and technical challenges. Due to the high cost of liquiud helium, only plants with 1000-MW, 5-h capacity are economically attractive. Even then the plant capital cost can exceed several thousand dollars per kilowatt. As ceramic superconductors, which become superconducting at higher temperatures (maintained by less expensive liquid nitrogen), become more widely available, it may be possible to develop smaller scale SMES plants at a lower price.

2.1.4 Battery Storage

Even though battery storage is the oldest and most familiar energy storage device, significant advances have been made in this technology in recent years to deserve more attention. There has been renewed interest in this technology due to its potential application in non-polluting electric vehicles. Battery

systems are quiet and non-polluting, and can be installed near load centers and existing suburban substations. These have round-trip AC–AC efficiencies in the range of 85%, and can respond to load changes within 20 ms. Several U.S., European, and Japanese utilities have demonstrated the application of lead–acid batteries for load-following applications. Some of them have been as large as 10 MW with 4 h of storage.

The other player in battery development is the automotive industry for electric vehicle application. In 1991, General Motors, Ford, Chrysler, Electric Power Research Institute (EPRI), several utilities, and the U.S. Department of Energy (DOE) formed the U.S. Advanced Battery Consortium (USABC) to develop better batteries for electric vehicle (EV) applications. A brief introduction to some of the available battery technologies as well some that are under study is presented in the following (Source: http://www.eren.doe.gov/consumerinfo/refbriefs/fa1/html).

2.1.4.1 Battery Types

Chemical batteries are individual cells filled with a conducting medium-electrolyte that, when connected together, form a battery. Multiple batteries connected together form a battery bank. At present, there are two main types of batteries: primary batteries (non-rechargeable) and secondary batteries (rechargeable). Secondary batteries are further divided into two categories based on the operating temperature of the electrolyte. Ambient operating temperature batteries have either aqueous (flooded) or nonaqueous electrolytes. High operating temperature batteries (molten electrodes) have either solid or molten electrolytes. Batteries in EVs are the secondary-rechargeable-type and are in either of the two subcategories. A battery for an EV must meet certain performance goals. These goals include quick discharge and recharge capability, long cycle life (the number of discharges before becoming unserviceable), low cost, recyclability, high specific energy (amount of usable energy, measured in watt-hours per pound [lb] or kilogram [kg]), high energy density (amount of energy stored per unit volume), specific power (determines the potential for acceleration), and the ability to work in extreme heat or cold. No battery currently available meets all these criteria.

2.1.4.2 Lead–Acid Batteries

Lead–acid starting batteries (shallow-cycle lead–acid secondary batteries) are the most common battery used in vehicles today. This battery is an ambient temperature, aqueous electrolyte battery. A cousin to this battery is the deep-cycle lead–acid battery, now widely used in golf carts and forklifts. The first electric cars built also used this technology. Although the lead–acid battery is relatively inexpensive, it is very heavy, with a limited usable energy by weight (specific energy). The battery's low specific energy and poor energy density make for a very large and heavy battery pack, which cannot power a vehicle as far as an equivalent gas-powered vehicle. Lead–acid batteries should not be discharged by more than 80% of their rated capacity or depth of discharge (DOD). Exceeding the 80% DOD shortens the life of the battery. Lead–acid batteries are inexpensive, readily available, and are highly recyclable, using the elaborate recycling system already in place. Research continues to try to improve these batteries.

A lead–acid nonaqueous (gelled lead acid) battery uses an electrolyte paste instead of a liquid. These batteries do not have to be mounted in an upright position. There is no electrolyte to spill in an accident. Nonaqueous lead–acid batteries typically do not have as high a life cycle and are more expensive than flooded deep-cycle lead–acid batteries.

2.1.4.3 Nickel Iron and Nickel Cadmium Batteries

Nickel iron (Edison cells) and nickel cadmium (nicad) pocket and sintered plate batteries have been in use for many years. Both of these batteries have a specific energy of around 25 Wh/lb (55 Wh/kg), which is higher than advanced lead–acid batteries. These batteries also have a long cycle life. Both of these batteries are recyclable. Nickel iron batteries are non-toxic, while nicads are toxic. They can also be discharged to 100% DOD without damage. The biggest drawback to these batteries is their cost. Depending on the size of battery bank in the vehicle, it may cost between $20,000 and $60,000 for the batteries. The batteries should last at least 100,000 mi (160,900 km) in normal service.

2.1.4.4 Nickel Metal Hydride Batteries

Nickel metal hydride batteries are offered as the best of the next generation of batteries. They have a high specific energy: around 40.8 Wh/lb (90 Wh/kg). According to a U.S. DOE report, the batteries are benign to the environment and are recyclable. They also are reported to have a very long cycle life. Nickel metal hydride batteries have a high self-discharge rate: they lose their charge when stored for long periods of time. They are already commercially available as "AA" and "C" cell batteries, for small consumer appliances and toys. Manufacturing of larger batteries for EV applications is only available to EV manufacturers. Honda is using these batteries in the EV Plus, which is available for lease in California.

2.1.4.5 Sodium Sulfur Batteries

This battery is a high-temperature battery, with the electrolyte operating at temperatures of 572°F (300°C). The sodium component of this battery explodes on contact with water, which raises certain safety concerns. The materials of the battery must be capable of withstanding the high internal temperatures they create, as well as freezing and thawing cycles. This battery has a very high specific energy: 50 Wh/lb (110 Wh/kg). The Ford Motor Company uses sodium sulfur batteries in their Ecostar, a converted delivery minivan that is currently sold in Europe. Sodium sulfur batteries are only available to EV manufacturers.

2.1.4.6 Lithium Iron and Lithium Polymer Batteries

The USABC considers lithium iron batteries to be the long-term battery solution for EVs. The batteries have a very high specific energy: 68 Wh/lb (150 Wh/kg). They have a molten-salt electrolyte and share many features of a sealed bipolar battery. Lithium iron batteries are also reported to have a very long cycle life. These are widely used in laptop computers. These batteries will allow a vehicle to travel distances and accelerate at a rate comparable to conventional gasoline-powered vehicles. Lithium polymer batteries eliminate liquid electrolytes. They are thin and flexible, and can be molded into a variety of shapes and sizes. Neither type will be ready for EV commercial applications until early in the 21st century.

2.1.4.7 Zinc and Aluminum Air Batteries

Zinc air batteries are currently being tested in postal trucks in Germany. These batteries use either aluminum or zinc as a sacrificial anode. As the battery produces electricity, the anode dissolves into the electrolyte. When the anode is completely dissolved, a new anode is placed in the vehicle. The aluminum or zinc and the electrolyte are removed and sent to a recycling facility. These batteries have a specific energy of over 97 Wh/lb (200 Wh/kg). The German postal vans currently carry 80 kWh of energy in their battery, giving them about the same range as 13 gallons (49.2 liters) of gasoline. In their tests, the vans have achieved a range of 615 mi (990 km) at 25 miles per hour (40 km/h).

2.2 Fuel Cells

In 1839, a British Jurist and an amateur physicist named William Grove first discovered the principle of the fuel cell. Grove utilized four large cells, each containing hydrogen and oxygen, to produce electricity and water which was then used to split water in a different container to produce hydrogen and oxygen. However, it took another 120 years until NASA demonstrated its use to provide electricity and water for some early space flights. Today the fuel cell is the primary source of electricity on the space shuttle. As a result of these successes, industry slowly began to appreciate the commercial value of fuel cells. In addition to stationary power generation applications, there is now a strong push to develop fuel cells for automotive use. Even though fuel cells provide high performance characterisitics, reliability, durability, and environmental benefits, a very high investment cost is still the major barrier against large-scale deployments.

2.2.1 Basic Principles

The fuel cell works by processing a hydrogen-rich fuel—usually natural gas or methanol—into hydrogen, which, when combined with oxygen, produces electricity and water. This is the reverse electrolysis process. Rather than burning the fuel, however, the fuel cell converts the fuel to electricity using a highly efficient electrochemical process. A fuel cell has few moving parts, and produces very little waste heat or gas.

A fuel cell power plant is basically made up of three subsystems or sections. In the fuel-processing section, the natural gas or other hydrocarbon fuel is converted to a hydrogen-rich fuel. This is normally accomplished through what is called a steam catalytic reforming process. The fuel is then fed to the power section, where it reacts with oxygen from the air in a large number of individual fuel cells to produce direct current (DC) electricity, and by-product heat in the form of usable steam or hot water. For a power plant, the number of fuel cells can vary from several hundred (for a 40-kW plant) to several thousand (for a multi-megawatt plant). In the final, or third stage, the DC electricity is converted in the power conditioning subsystem to electric utility-grade alternating current (AC).

In the power section of the fuel cell, which contains the electrodes and the electrolyte, two separate electrochemical reactions take place: an oxidation half-reaction occurring at the anode and a reduction half-reaction occurring at the cathode. The anode and the cathode are separated from each other by the electrolyte. In the oxidation half-reaction at the anode, gaseous hydrogen produces hydrogen ions, which travel through the ionically conducting membrane to the cathode. At the same time, electrons travel through an external circuit to the cathode. In the reduction half-reaction at the cathode, oxygen supplied from air combines with the hydrogen ions and electrons to form water and excess heat. Thus, the final products of the overall reaction are electricity, water, and excess heat.

2.2.2 Types of Fuel Cells

The electrolyte defines the key properties, particularly the operating temperature, of the fuel cell. Consequently, fuel cells are classified based on the types of electrolyte used as described below.

1. Polymer Electrolyte Membrane (PEM)
2. Alkaline Fuel Cell (AFC)
3. Phosphoric Acid Fuel Cell (PAFC)
4. Molten Carbonate Fuel Cell (MCFC)
5. Solid Oxide Fuel Cell (SOFC)

These fuel cells operate at different temperatures and each is best suited to particular applications. The main features of the five types of fuel cells are summarized in Table 2.1.

2.2.3 Fuel Cell Operation

Basic operational characteristics of the four most common types of fuel cells are discussed in the following.

2.2.3.1 Polymer Electrolyte Membrane (PEM)

The PEM cell is one in a family of fuel cells that are in various stages of development. It is being considered as an alternative power source for automotive application for electric vehicles. The electrolyte in a PEM cell is a type of polymer and is usually referred to as a membrane, hence the name. Polymer electrolyte membranes are somewhat unusual electrolytes in that, in the presence of water, which the membrane readily absorbs, the negative ions are rigidly held within their structure. Only the positive (H) ions contained within the membrane are mobile and are free to carry positive charges through the membrane in one direction only, from anode to cathode. At the same time, the organic nature of the polymer electrolyte membrane structure makes it an electron insulator, forcing it to travel through the outside circuit providing electric power to the load. Each of the two electrodes consists of porous

TABLE 2.1 Comparison of Five Fuel Cell Technologies

Type	Electrolyte	Operating Temperature (°C)	Applications	Advantages
Polymer Electrolyte Membrane (PEM)	Solid organic polymer poly-perflouro-sulfonic acid	60–100	Electric utility, transportation, portable power	Solid electrolyte reduces corrosion, low temperature, quick start-up
Alkaline (AFC)	Aqueous solution of potassium hydroxide soaked in a matrix	90–100	Military, space	Cathode reaction faster in alkaline electrolyte; therefore high performance
Phosphoric Acid (PAFC)	Liquid phosphoric acid soaked in a matrix	175–200	Electric utility, transportation, and heat	Up to 85% efficiency in co-generation of electricity
Molten Carbonate (MCFC)	Liquid solution of lithium, sodium, and/or potassium carbonates soaked in a matrix	600–1000	Electric utility	Higher efficiency, fuel flexibility, inexpensive catalysts
Solid Oxide (SOFC)	Solid zirconium oxide to which a small amount of yttria is added	600–1000	Electric utility	Higher efficiency, fuel flexibility, inexpensive catalysts. Solid electrolyte advantages like PEM

carbon to which very small platinum (Pt) particles are bonded. The electrodes are somewhat porous so that the gases can diffuse through them to reach the catalyst. Moreover, as both platinum and carbon conduct electrons well, they are able to move freely through the electrodes. Chemical reactions that take place inside a PEM fuel cell are presented in the following.

Anode

$$2H_2 \rightarrow 4H^+ + 4e^-$$

Cathode

$$O_2 + 4H^+ + 4e^- \rightarrow 2H_2O$$

$$\text{Net reaction: } 2H_2 + O_2 = 2H_2O$$

Hydrogen gas diffuses through the polymer electrolyte until it encounters a Pt particle in the anode. The Pt catalyzes the dissociation of the hydrogen molecule into two hydrogen atoms (H) bonded to two neighboring Pt atoms. Only then can each H atom release an electron to form a hydrogen ion (H^+) which travels to the cathode through the electrolyte. At the same time, the free electron travels from the anode to the cathode through the outer circuit. At the cathode the oxygen molecule interacts with the hydrogen ion and the electron from the outside circuit to form water. The performance of the PEM fuel cell is limited primarily by the slow rate of the oxygen reduction half-reaction at the cathode, which is 100 times slower than the hydrogen oxidation half-reaction at the anode.

2.2.3.2 Phosphoric Acid Fuel Cell (PAFC)

Phosphoric acid technology has moved from the laboratory research and development to the first stages of commercial application. Turnkey 200-kW plants are now available and have been installed at more than 70 sites in the U.S., Japan, and Europe. Operating at about 200°C, the PAFC plant also produces heat for domestic hot water and space heating, and its electrical efficiency approaches 40%. The principal obstacle against widespread commercial acceptance is cost. Capital costs of about $2500 to

$4000/kW must be reduced to $1000 to $1500/kW if the technology is to be accepted in the electric power markets.

The chemical reactions occurring at two electrodes are written as follows:

$$\begin{aligned} &\text{At anode:} && 2H_2 \rightarrow 4H^+ + 4e^- \\ &\text{At cathode:} && O_2 + 4H^+ + 4e^- \rightarrow 2H_2O \end{aligned}$$

2.2.3.3 Molten Carbonate Fuel Cell (MCFC)

Molten carbonate technology is attractive because it offers several potential advantages over PAFC. Carbon monoxide, which poisons the PAFC, is indirectly used as a fuel in the MCFC. The higher operating temperature of approximately 650°C makes the MCFC a better candidate for combined cycle applications whereby the fuel cell exhaust can be used as input to the intake of a gas turbine or the boiler of a steam turbine. The total thermal efficiency can approach 85%. This technology is at the stage of prototype commercial demonstrations and is estimated to enter the commercial market by 2003 using natural gas, and by 2010 with gas made from coal. Capital costs are expected to be lower than PAFC. MCFCs are now being tested in full-scale demonstration plants. The following equations illustrate the chemical reactions that take place inside the cell.

$$\begin{aligned} &\text{At anode:} && 2H_2 + 2CO_3^{2-} \rightarrow 2H_2O + 2CO_2 + 4e^- \\ &\text{and} && 2CO + 2CO_3^{2-} \rightarrow 4CO_2 + 4e^- \\ &\text{At cathode:} && O_2 + 2CO_2 + 4e^- \rightarrow 2O_3^{2-} \end{aligned}$$

2.2.3.4 Solid Oxide Fuel Cell (SOFC)

A solid oxide fuel cell is currently being demonstrated at a 100-kW plant. Solid oxide technology requires very significant changes in the structure of the cell. As the name implies, the SOFC uses a solid electrolyte, a ceramic material, so the electrolyte does not need to be replenished during the operational life of the cell. This simplifies design, operation, and maintenance, as well as having the potential to reduce costs. This offers the stability and reliability of all solid-state construction and allows higher temperature operation. The ceramic make-up of the cell lends itself to cost-effective fabrication techniques. The tolerance to impure fuel streams make SOFC systems especially attractive for utilizing H_2 and CO from natural gas steam-reforming and coal gasification plants. The chemical reactions inside the cell may be written as follows:

$$\begin{aligned} &\text{At anode:} && 2H_2 + 2O^{2-} \rightarrow 2H_2O + 4e^- \\ &\text{and} && 2CO + 2O^{2-} \rightarrow 2CO_2 + 4e^- \\ &\text{At cathode:} && O_2 + 4e^- \rightarrow 2O^{2-} \end{aligned}$$

2.3 Summary

Fuel cells can convert a remarkably high proportion of the chemical energy in a fuel to electricity. With the efficiencies approaching 60%, even without co-generation, fuel cell power plants are nearly twice as efficient as conventional power plants. Unlike large steam plants, the efficiency is not a function of the plant size for fuel cell power plants. Small-scale fuel cell plants are just as efficient as the large ones, whether they operate at full load or not. Fuel cells contribute significantly to the cleaner environment; they produce dramtically fewer emissions, and their by-products are primarily hot water and carbon dioxide in small amounts. Because of their modular nature, fuel cells can be placed at or near load centers, resulting in savings of transmission network expansion.

3

Photovoltaics

Roger A. Messenger
Florida Atlantic University

3.1 Types of PV Cells

3.1.1 Silicon Cells

Silicon PV cells come in several varieties. The most common cell is the single-crystal silicon cell. Other variations include multicrystalline (polycrystalline), thin silicon (buried contact) cells, and amorphous silicon cells.

3.1.1.1 Single-Crystal Silicon Cells

While single crystal silicon cells are still the most common cells, the fabrication process of these cells is relatively energy intensive, resulting in limits to cost reduction for these cells. Since single-crystal silicon is an indirect bandgap semiconductor ($E_g = 1.1$ eV), its absorption constant is smaller than that of direct bandgap materials. This means that single-crystal silicon cells need to be thicker than other cells in order to absorb a sufficient percentage of incident radiation. This results in the need for more material and correspondingly more energy involved in cell processing, especially since the cells are still produced mostly by sawing of single-crystal silicon ingots into wafers that are about 200 μm thick. To achieve maximum fill of the module, round ingots are first sawed to achieve closer to a square cross-section prior to wafering.

After chemical etching to repair surface damage from sawing, the junction is diffused into the wafers. Improved cell efficiency can then be achieved by using a preferential etch on the cell surfaces to produce textured surfaces. The textured surfaces reflect photons back toward the junction at an angle, thus increasing the path length and increasing the probability of the photon being absorbed within a minority carrier diffusion length of the junction. Following the chemical etch, contacts, usually aluminum, are evaporated and annealed and the front surface is covered with an antireflective coating.

The cells are then assembled into modules, consisting of approximately 33 to 36 individual cells connected in series. Since the open-circuit output voltage of an individual silicon cell typically ranges from 0.5 to 0.6 V, depending upon irradiance level and cell temperature, this results in a module open-circuit voltage between 18 and 21.6 V. The cell current is directly proportional to the irradiance and the cell area. A 4-ft^2 (0.372-m^2) module (active cell area) under full sun will typically produce a maximum power close to 55 W at approximately 17 V and 3.2 A.

3.1.1.2 Multicrystalline Silicon Cells

By pouring molten silicon into a crucible and controlling the cooling rate, it is possible to grow multicrystalline silicon with a rectangular cross-section. This eliminates the "squaring-up" process and the associated loss of material. The ingot must still be sawed into wafers, but the resulting wafers completely fill the module. The remaining processing follows the steps of single-crystal silicon, and cell efficiencies in excess of 15% have been achieved for relatively large area cells. Multicrystalline material still maintains the basic properties of single-crystal silicon, including the indirect bandgap. Hence, relatively thick cells with textured surfaces have the highest conversion efficiencies. Multicrystalline silicon modules are commercially available and are recognized by their "speckled" surface appearance.

3.1.1.3 Thin Silicon (Buried Contact) Cells

The current flow direction in most PV cells is between the front surface and the back surface. In the thin silicon cell, a dielectric layer is deposited on an insulating substrate, followed by alternating layers of n-type and p-type silicon, forming multiple pn junctions. Channels are then cut with lasers and contacts are buried in the channels, so the current flow is parallel to the cell surfaces in multiple parallel conduction paths. These cells minimize resistance from junction to contact with the multiple parallel conduction paths and minimize blocking of incident radiation by the front contact. Although the material is not single crystal, grain boundaries cause minimal degradation of cell efficiency. The collection efficiency is very high, since essentially all photon-generated carriers are generated within a diffusion length of a pn junction. This technology is relatively new, but has already been licensed to a number of firms worldwide (Green and Wenham, 1994).

3.1.1.4 Amorphous Silicon Cells

Amorphous silicon has no predictable crystal structure. As a result, the uniform covalent bond structure of single-crystal silicon is replaced with a random bonding pattern with many open covalent bonds. These bonds significantly degrade the performance of amorphous silicon by reducing carrier mobilities and the corresponding diffusion lengths. However, if hydrogen is introduced into the material, its electron will pair up with the dangling bonds of the silicon, thus passivating the material. The result is a direct bandgap material with a relatively high absorption constant. A film with a thickness of a few micrometers will absorb nearly all incident photons with energies higher than the 1.75 eV bandgap energy.

Maximum collection efficiency for a-Si:H is achieved by fabricating the cell with a pin junction. Early work on the cells revealed, however, that if the intrinsic region is too thick, cell performance will degrade over time. This problem has now been overcome by the manufacture of multi-layer cells with thinner pin junctions. In fact, it is possible to further increase cell efficiency by stacking cells of a-SiC:H on top, a-Si:H in the center, and a-SiGe:H on the bottom. Each successive layer from the top has a smaller bandgap, so the high-energy photons can be captured soon after entering the material, followed by middle-energy photons and then lower energy photons.

While the theoretical maximum efficiency of a-Si:H is 27% (Zweibel, 1990), small-area lab cells have been fabricated with efficiencies of 14% and large-scale devices have efficiencies in the 10% range (Yang et al., 1997).

Amorphous silicon cells have been adapted to the building integrated PV (BIPV) market by fabricating the cells on stainless steel (Guha et al., 1997) and polymide substrates (Huang et al., 1997). The "solar shingle" is now commercially available, and amorphous silicon cells are commonly used in solar calculators and solar watches.

3.1.2 Gallium Arsenide Cells

Gallium arsenide (GaAs), with its 1.43 eV direct bandgap, is a nearly optimal PV cell material. The only problem is that it is very costly to fabricate cells. GaAs cells have been fabricated with conversion efficiencies above 30% and with their relative insensitivity to severe temperature cycling and radiation exposure, they are the preferred material for extraterrestrial applications, where performance and weight are the dominating factors.

Gallium and arsenic react exothermically when combined, so formation of the host material is more complicated than formation of pure, single-crystal silicon. Modern GaAs cells are generally fabricated by growth of a GaAs film on a suitable substrate, such as Ge. A typical GaAs cell has a Ge substrate with a layer of n-GaAs followed by a layer of p-GaAs and then a thin layer of p-GaAlAs between the p-GaAs and the top contacts. The p-GaAlAs has a wider bandgap (1.8 eV) than the GaAs, so the higher energy photons are not absorbed at the surface, but are transmitted through to the GaAs pn junction, where they are then absorbed.

Recent advances in III-V technology have produced tandem cells similar to the a-Si:H tandem cell. One cell consists of two tandem GaAs cells, separated by thin tunnel junctions of GaInP, followed by a third tandem GaInP cell, separated by AlInP tunnel junctions (Lammasniemi et al., 1997). The tunnel junctions mitigate voltage drop of the otherwise forward-biased pn junction that would appear between any two tandem pn junctions in opposition to the photon-induced cell voltage. Cells have also been fabricated of InP (Hoffman et al., 1997).

3.1.3 Copper Indium (Gallium) Diselenide Cells

Another promising thin film material is copper indium (gallium) diselenide (CIGS). While the basic copper indium diselenide cell has a bandgap of 1.0 eV, the addition of gallium increases the bandgap to closer to 1.4 eV, resulting in more efficient collection of photons near the peak of the solar spectrum. CIGS has a high absorption constant and essentially all incident photons are absorbed within a distance of 2 μm, as in a-Si:H. Indium is the most difficult component to obtain, but the quantity needed for a module is relatively minimal.

The CIGS cell is fabricated on a soda glass substrate by first applying a thin layer of molybdenum as the back contact, since the CIGS will form an ohmic contact with Mo. The next layer is p-type CIGS, followed by a layer of n-type CdS, rather than n-type CIGS, because the pn homojunction in CIGS is neither stable nor efficient. While the cells discussed thus far have required metals to obtain ohmic front contacts, it is possible to obtain an ohmic contact on CdS with a transparent conducting oxide (TCO) such as ZnO. The top surface is first passivated with a thin layer (50 nm) of intrinsic ZnO to prevent minority carrier surface recombination. Then a thicker layer (350 nm) of n^+ ZnO is added, followed by an MgF_2 antireflective coating.

Efficiencies of laboratory cells are now near 18% (Tuttle et al., 1996), with a module efficiency of 11.1% reported in 1998 (Tarrant and Gay, 1998). Although at the time of this writing, CIGS modules were not commercially available, the technology has been under field tests for nearly 10 years. It has been projected that the cells may be manufactured on a large scale for $1/W or less. At this cost level, area-related costs become significant, so that it becomes important to increase cell efficiency to maximize power output for a given cell area.

3.1.4 Cadmium Telluride Cells

Of the II-VI semiconductor materials, CdTe has a theoretical maximum efficiency of near 25%. The material has a favorable direct bandgap (1.44 eV) and a large absorption constant. As in the other thin film materials, a 2-μm thickness is adequate for the absorption of most of the incident photons. Small laboratory cells have been fabricated with efficiencies near 15% and module efficiencies close to 10% have been achieved (Ullal et al., 1997). Some concern has been expressed about the Cd content of the cells, particularly in the event of fire dispersing the Cd. It has been determined that anyone endangered by Cd in a fire would be far more endangered by the fire itself, due to the small quantity of Cd in the cells. Decommissioning of the module has also been analyzed and it has been concluded that the cost to recycle module components is pennies per watt (Fthenakis and Moskowitz, 1997).

The CdTe cell is fabricated on a glass superstrate covered with a thin TCO (1 μm). The next layer is n-type CdS with a thickness of approximately 100 nm, followed by a 2-μm thick CdTe layer and a back contact of an appropriate metal for ohmic contact, such as Au, Cu/Au, Ni, Ni/Al, ZnTe:Cu or (Cu, HgTe). The back contact is then covered with a layer of ethylene vinyl acetate (EVA) or other suitable encapsulant and another layer of glass. The front glass is coated with an antireflective coating.

Experimental CdTe arrays up to 25 kW have been under test for several years with no reports of degradation. It has been estimated that the cost for large-scale production can be reduced to below $1/W. Once again, as in the CIGS case, module efficiency needs to be increased to reduce the area-related costs.

3.1.5 Emerging Technologies

The PV field is moving so quickly that by the time information appears in print, it is generally outdated. Reliability of cells, modules, and system components continues to improve. Efficiencies of cells and modules continue to increase, and new materials and cell fabrication techniques continue to evolve.

One might think that Si cells will soon become historical artifacts. This may not be the case. Efforts are underway to produce Si cells that have good charge carrier transport properties while improving photon absorption and reducing the energy for cell production. Ceramic and graphite substrates have been used with thinner layers of Si. Processing steps have been doubled up. Metal insulator semiconductor inversion layer (MIS-IL) cells have been produced in which the diffused junction is replaced with a Schottky junction. By use of clever geometry of the back electrode to reduce the rear surface recombination velocity along with front surface passivation, an efficiency of 18.5% has been achieved for a laboratory MIS-IL cell. Research continues on ribbon growth in an effort to eliminate wafering, and combining crystalline and amorphous Si in a tandem cell to take advantage of the two different bandgaps for increasing photon collection efficiency has been investigated.

At least eight different CIS-based materials have been proposed for cells. The materials have direct bandgaps ranging from 1.05 to 2.56 eV. A number of III-V materials have also emerged that have favorable photon absorption properties. In addition, quantum well cells have been proposed that have theoretical efficiencies in excess of 40% under concentrating conditions.

The PV market seems to have taken a strong foothold, with the likelihood that annual PV module shipments will exceed 200 MW before the end of the century and continue to increase by approximately 15% annually as new markets open as cost continues to decline and reliability continues to improve.

3.2 PV Applications

PV cells were first used to power satellites. Through the middle of the 1990s the most common terrestrial PV applications were stand-alone systems located where connection to the utility grid was impractical. By the end of the 1990s, PV electrical generation was cost-competitive with the marginal cost of central station power when it replaced gas turbine peaking in areas with high afternoon irradiance levels. Encouraged by consumer approval, a number of utilities have introduced utility-interactive PV systems to supply a portion of their total customer demand. Some of these systems have been residential and commercial rooftop systems and other systems have been larger ground-mounted systems. PV systems are generally classified as utility interactive (grid connected) or stand-alone.

Orientation of the PV modules for optimal energy collection is an important design consideration, whether for a utility interactive system or for a stand-alone system. Best overall energy collection on an annual basis is generally obtained with a south-facing collector having a tilt at an angle with the horizontal approximately 90% of the latitude of the site. For optimal winter performance, a tilt of latitude $+15^\circ$ is best and for optimal summer performance a tilt of latitude -15° is best. In some cases, when it is desired to have the PV output track utility peaking requirements, a west-facing array may be preferred, since its maximum output will occur during summer afternoon utility peaking hours. Monthly peak sun tables for many geographical locations are available from the National Renewable Energy Laboratory (Sandia National Laboratories, 1996; Florida Solar Energy Center).

3.2.1 Utility-Interactive PV Systems

Utility-interactive PV systems are classified by IEEE Standard 929 as small, medium, or large (ANSI/IEEE, 1999). Small systems are less than 10 kW, medium systems range from 10 to 500 kW,

and large systems are larger than 500 kW. Each size range requires different consideration for the utility interconnect. In addition to being able to offset utility peak power, the distributed nature of PV systems also results in the reduction of load on transmission and distribution lines. Normally, utility-interactive systems do not incorporate any form of energy storage—they simply supply power to the grid when they are operating. In some instances, however, where grid power may not be as reliable as the user may desire, battery back-up is incorporated to ensure uninterrupted power.

Since the output of PV modules is DC, it is necessary to convert the module output to AC before connecting it to the grid. This is done with an inverter, also known as a power conditioning unit (PCU). Modern PCUs must meet the standards set by IEEE 929. If the PCU is connected on the customer side of the revenue meter, the PV system must meet the requirements of the *National Electrical Code*® (*NEC*®) (National Fire Protection Association, 1998). For a system to meet *NEC* requirements, it must consist of UL listed components. In particular, the PCU must be tested under UL 1741 (Underwriters Laboratories, 1997). But UL 1741 has been set up to test for compliance with IEEE 929, so any PCU that passes the UL 1741 test is automatically qualified under the requirements of the *NEC*.

Utility-interactive PCUs are generally pulse code modulated (PCM) units with nearly all *NEC*-required components, such as fusing of PV output circuits, DC and AC disconnects, and automatic utility disconnect in the event of loss of utility voltage. They also often contain surge protectors on input and output, ground fault protection circuitry, and maximum power tracking circuitry to ensure that the PV array is loaded at its maximum power point. The PCUs act as current sources, synchronized by the utility voltage. Since the PCUs are electronic, they can sample the line voltage at a high rate and readily shut down under conditions of utility voltage or frequency as specified by IEEE 929.

The typical small utility-interactive system of a few kilowatts consists of an array of modules selected by either a total cost criterion or, perhaps, by an available roof area criterion. The modules are connected to produce an output voltage ranging from 48 V to 300 V, depending upon the DC input requirements of the PCU. One or two PCUs are used to interface the PV output to the utility at 120 V or, perhaps, 120/240 V. The point of utility connection is typically the load side of a circuit breaker in the distribution panel of the occupancy if the PV system is connected on the customer side of the revenue meter. Connections on the utility side of the meter will normally be with double lugs on the line side of the meter. Section 690 of the *NEC* provides the connection and installation requirements for systems connected on the customer side of the revenue meter. Utility-side interconnects are regulated by the local utility.

Since the cost of PCUs is essentially proportional to their power handling capability, to date there has been no particular economy of scale for PV system size. As a result, systems are often modular. One form of modularity is the AC module. The AC module incorporates a small PCU ($\approx$300 W) mounted on the module itself so the output of the module is 120 V AC. This simplifies the hook-up of the PV system, since *NEC* requirements for PV output circuits are avoided and only the requirements for PCU output circuits need to be met.

Medium- and large-scale utility-interactive systems differ from small-scale systems only in the possibility that the utility may require different interfacing conditions relating to power quality and/or conditions for disconnect. Since medium-and large-scale systems require more area than is typically available on the rooftop of a residential occupancy, they are more typically found either on commercial industrial rooftops or, in the case of large systems, are typically ground-mounted. Rooftop mounts are attractive since they require no additional space other than what is already available on the rooftop. The disadvantage is when roof repair is needed, the PV system may need to be temporarily removed and then reinstalled. Canopies for parking lots present attractive possibilities for large utility-interactive PV systems.

3.2.2 Stand-Alone PV Systems

Stand-alone PV systems are used when it is impractical to connect to the utility grid. Common stand-alone systems include PV-powered fans, water pumping systems, portable highway signs, and power

systems for remote installations, such as cabins, communications repeater stations, and marker buoys. The design criteria for stand-alone systems is generally more complex than the design criteria for utility-interactive systems, where most of the critical system components are incorporated in the PCU. The PV modules must supply all the energy required unless another form of backup power, such as a gasoline generator, is also incorporated into the system. Stand-alone systems also often incorporate battery storage to run the system under low sun or no sun conditions.

3.2.2.1 PV-Powered Fans

Perhaps the simplest of all PV systems is the connection of the output of a PV module directly to a DC fan. When the module output is adequate, the fan operates. When the sun goes down, the fan stops. Such an installation is reasonable for use in remote bathrooms or other locations where it is desirable to have air circulation while the sun is shining, but not necessarily when the sun goes down. The advantage of such a system is its simplicity. The disadvantage is that it does not run when the sun is down, and under low sun conditions, the system operates very inefficiently due to a mismatch between the fan I-V characteristic and the module I-V characteristic that results in operation far from the module maximum power point.

If the fan is to run continuously, or beyond normal sunlight hours, then battery storage will be needed. The PV array must then be sized to provide the daily ampere-hour (Ah) load of the fan, plus any system losses. A battery system must be selected to store sufficient energy to last for several days of low sun, depending upon whether the need for the fan is critical, and an electronic controller is normally provided to prevent overcharge or overdischarge of the batteries.

3.2.2.2 PV-Powered Water Pumping System

If the water reservoir is adequate to provide a supply of water at the desired rate of pumping, then a water pumping system may not require battery storage. Instead, the water pumped can be stored in a storage tank for availability during low sun times. If this is the case, then the PV array needs to be sized to meet the power requirements of the water pump plus any system losses. If the reservoir provides water at a limited rate, the pumping rate may be limited by the reservoir replenishment rate, and battery storage may be required to extend the pumping time.

While it is possible to connect the PV array output directly to the pump, it is generally better to employ the use of an electronic maximum power tracker (MPT) to better match the pump to the PV array output. The MPT is a DC–DC converter that either increases or decreases pump voltage as needed to maximize pump power. This generally results in pumping approximately 20% more water in a day. Alternatively, it allows for the use of a smaller pump with a smaller array to pump the same amount of water, since the system is being used more efficiently.

3.2.2.3 PV-Powered Highway Information Sign

The PV-powered highway information sign is now a familiar sight to most motorists. The simpler signs simply employ bidirectional arrows to direct traffic to change lanes. The more complex signs display a message. The array size for a PV-powered highway information sign is limited by how it can be mounted without becoming a target for vandalism. Generally this means the modules must be mounted on the top of the sign itself to get them sufficiently above grade level to reduce temptation. This limits the array dimensions to the width of the trailer (about 8 ft) and the length of the modules (about 4 ft). At full sun, such a 32-ft^2 array, if 15% efficient, can produce approximately 450 W. Depending on location and time of year, about 5 h of full sun is typically available on an average day. This means the production of approximately 2250 Wh of energy on the typical day. Taking into account system losses in the batteries, the control circuitry, and degraded module performance due to dirty surfaces, about 70 to 75% of this energy can be delivered to the display, or about 1600 Wh/d. Hence, the average power available to the display over a 24-h period is 67 W. While this may not seem to be very much power, it is adequate for efficient display technology to deliver a respectable message.

If the system is a 12 V DC system, a set of deep discharge batteries will need to have a capacity of 185 Ah for each day of battery back-up (day of autonomy). For 3 d of autonomy, a total of 555 Ah of storage will be needed, which equates to eight batteries rated at 70 Ah each.

3.2.2.4 Hybrid PV-Powered Single Family Dwelling

In areas where winter sunlight is significantly less than summer sunlight, and/or where winter electrical loads are higher than summer electrical loads, if sufficient PV is deployed to meet winter needs, then the system produces excess power for many months of the year. If this power is not used, then the additional capacity of the system is wasted. Thus, for such cases, it often makes sense to size the PV system to

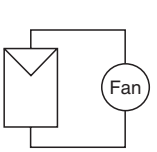

a. Simple PV-powered fan.

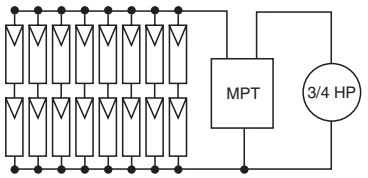

b. Water pump with maximum power tracking.

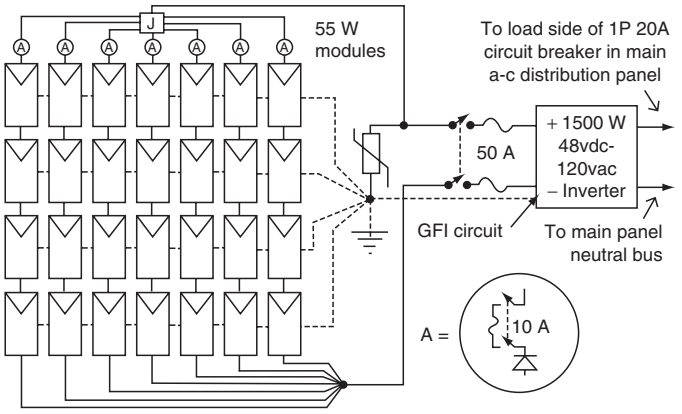

c. A 1.5 kW residential rooftop utility interactive system connected on customer side of revenue meter.

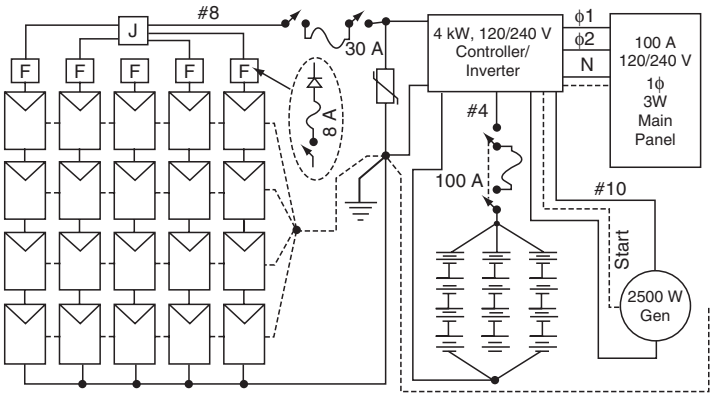

d. A hybrid residential installation.

FIGURE 3.1 Examples of PV systems.

completely meet the system needs during the month(s) with the most sunlight, and then provide backup generation of another type, such as a gasoline generator, to provide the difference in energy during the remaining months.

Such a system poses an interesting challenge for the system controller. It needs to be designed to make maximum use of PV power before starting the generator. Since generators operate most efficiently at about 90% of full load, the controller must provide for battery charging by the generator at the appropriate rate to maximize generator efficiency. Typically the generator will be sized to charge the batteries from 20 to 70% charge in about 5 h. When the batteries have reached 70% charge, the generator shuts down to allow available sunlight to complete the charging cycle. If the sunlight is not available, the batteries discharge to 20% and the cycle is repeated.

Figure 3.1 shows schematic diagrams of a few typical PV applications.

References

ANSI/IEEE P929, IEEE Recommended Practice for Utility Interface of Residential and Intermediate Photovoltaic (PV) Systems, IEEE Standards Coordinating Committee 21, Photovoltaics, Draft 10, February 1999.

Florida Solar Energy Center site with extensive links to other sites, including solar radiation tables. http://alpha.fsec.ucf.edu/~pv/inforesource/links/

Fthenakis, V.M. and Moskowitz, P.D., Emerging photovoltaic technologies: environmental and health issues update, *NREL/SNL Photovoltaics Program Review*, AIP Press, New York, 1997.

Green, M.A. and Wenham, S.R., Novel parallel multijunction solar cell, *Appl. Phys. Lett.*, 65, 2907, 1994.

Guha, S., Yang, J., et al., *Proc. 26th IEEE PV Spec. Conf.*, 607–610, 1997.

Hoffman, R., et al., *Proc. 26th IEEE PV Spec. Conf.*, 815–818, 1997.

Huang, J., Lee, Y., et al., *Proc. 26th IEEE PV Spec. Conf.*, 699–702, 1997.

Lammasniemi, J., et al., *Proc. 26th IEEE PV Spec. Conf.*, 823–826, 1997.

Messenger, R., and Ventre, J., *Photovoltaic Systems Engineering*, CRC Press, Boca Raton, FL, 1999.

NFPA 70 National Electrical Code, 1999 Edition, National Fire Protection Association, Quincy, MA, 1998.

Stand-Alone Photovoltaic Systems: A Handbook of Recommended Design Practices, Sandia National Laboratories, Albuquerque, NM, 1996.

Tarrant, D.E. and Gay, R.R., *CIS-Based Thin Film PV Technology, Phase 2 Technical Report, October 1996—October 1997*, NREL, Golden, CO, May 1998.

Tuttle, J.R., et al., *Proc. 14th NREL PV Program Review*, AIP Conf. Proceedings 394, Lakewood, CO, 1996, 83–105.

UL Subject 1741, Standard for Power Conditioning Units for Use in Residential Photovoltaic Power Systems, Underwriters Laboratories Inc., 1997.

Ullal, H.S., Zweibel, K., and von Roedern, B., *Proc. 26th IEEE PV Spec. Conf.*, 301–305, 1997.

Yang, J., Banerjee, A., et al., *Proc. 26th IEEE PV Spec Conf.*, 563–568, 1997.

Zweibel, K., *Harnessing Solar Power*, Plenum Press, New York, 1990.

II

Electric Power Generation: Conventional Methods

Rama Ramakumar
Oklahoma State University

4

Hydroelectric Power Generation

Steven R. Brockschink
Stantec Consulting

James H. Gurney
BC Transmission Corporation

Douglas B. Seely
Stantec Consulting

Hydroelectric power generation involves the storage of a hydraulic fluid, water, conversion of the hydraulic (potential) energy of the fluid into mechanical (kinetic) energy in a hydraulic turbine, and conversion of the mechanical energy to electrical energy in an electric generator.

The first hydroelectric power plants came into service in the 1880s and now comprise approximately 20% (700 GW) of the world's installed generation capacity (World Energy Council, 2001). Hydroelectricity is an important source of renewable energy and provides significant flexibility in base loading, peaking, and energy storage applications. While initial capital costs are high, the inherent simplicity of hydroelectric plants, coupled with their low operating and maintenance costs, long service life, and high reliability, make them a very cost-effective and flexible source of electricity generation. Especially valuable is their operating characteristic of fast response for start-up, loading, unloading, and following of system load variations. Other useful features include their ability to start without the availability of power system voltage (black start capability), ability to transfer rapidly from generation mode to synchronous-condenser mode, and pumped storage application.

Hydroelectric units have been installed in capacities ranging from a few kilowatts to nearly 1 GW. Multi-unit plant sizes range from a few kilowatts to a maximum of 18 GW.

4.1 Planning of Hydroelectric Facilities

4.1.1 Siting

Hydroelectric plants are located in geographic areas where they will make economic use of hydraulic energy sources. Hydraulic energy is available wherever there is a flow of liquid and accumulated head. Head represents potential energy and is the vertical distance through which the fluid falls in the energy conversion process. The majority of sites utilize the head developed by freshwater; however, other

liquids such as saltwater and treated sewage have been utilized. The siting of a prospective hydroelectric plant requires careful evaluation of technical, economic, environmental, and social factors. A significant portion of the project cost may be required for mitigation of environmental effects on fish and wildlife and relocation of infrastructure and population from flooded areas.

4.1.2 Hydroelectric Plant Schemes

There are three main types of hydroelectric plant arrangements, classified according to the method of controlling the hydraulic flow at the site:

1. Run-of-the-river plants, having small amounts of water storage and thus little control of the flow through the plant.
2. Storage plants, having the ability to store water and thus control the flow through the plant on a daily or seasonal basis.
3. Pumped storage plants, in which the direction of rotation of the turbines is reversed during off-peak hours, pumping water from a lower reservoir to an upper reservoir, thus "storing energy" for later production of electricity during peak hours.

4.1.3 Selection of Plant Capacity, Energy, and Other Design Features

The generating capacity of a hydroelectric plant is a function of the head and flow rate of water discharged through the hydraulic turbines, as shown in the following equation:

$$P = 9.8\ \eta\, Q\, H \tag{4.1}$$

where P = power (kilowatts)
η = plant efficiency
Q = discharge flow rate (m^3/s)
H = head (m)

Flow rate and head are influenced by reservoir inflow, storage characteristics, plant and equipment design features, and flow restrictions imposed by irrigation, minimum downstream releases, or flood control requirements. Historical daily, seasonal, maximum (flood), and minimum (drought) flow conditions are carefully studied in the planning stages of a new development. Plant capacity, energy, and physical features such as the dam and spillway structures are optimized through complex economic studies that consider the hydrological data, planned reservoir operation, performance characteristics of plant equipment, construction costs, the value of capacity and energy, and financial discount rates. The costs of substation, transmission, telecommunications, and off-site control facilities are also important considerations in the economic analysis. If the plant has storage capability, then societal benefits from flood control may be included in the economic analysis.

Another important planning consideration is the selection of the number and size of generating units installed to achieve the desired plant capacity and energy, taking into account installed unit costs, unit availability, and efficiencies at various unit power outputs (American Society of Mechanical Engineers–Hydropower Technical Committee, 1996).

4.2 Hydroelectric Plant Features

Figures 4.1 and 4.2 illustrate the main components of a hydroelectric generating unit. The generating unit may have its shaft oriented in a vertical, horizontal, or inclined direction depending on the physical conditions of the site and the type of turbine applied. Figure 4.1 shows a typical vertical shaft Francis turbine unit and Fig. 4.2 shows a horizontal shaft propeller turbine unit. The following sections will describe the main components such as the turbine, generator, switchgear, and generator transformer, as well as the governor, excitation system, and control systems.

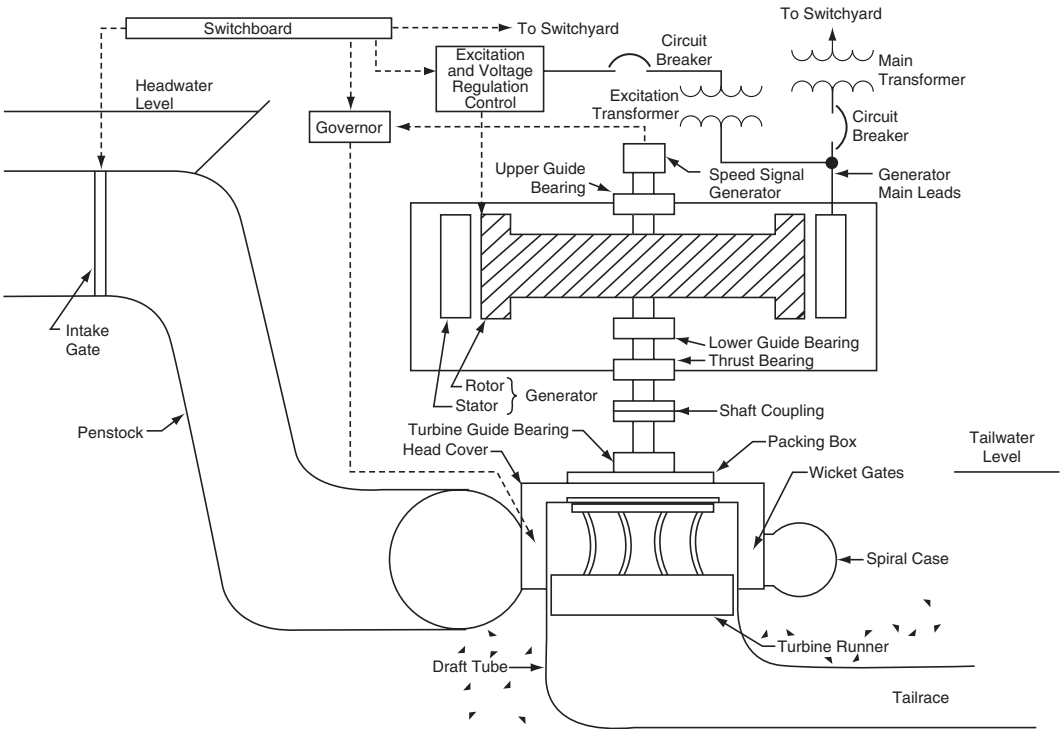

FIGURE 4.1 Vertical Francis unit arrangement. (From IEEE Standard 1020, IEEE Guide for Control of Small Hydroelectric Power Plants. Copyright IEEE. All rights reserved.)

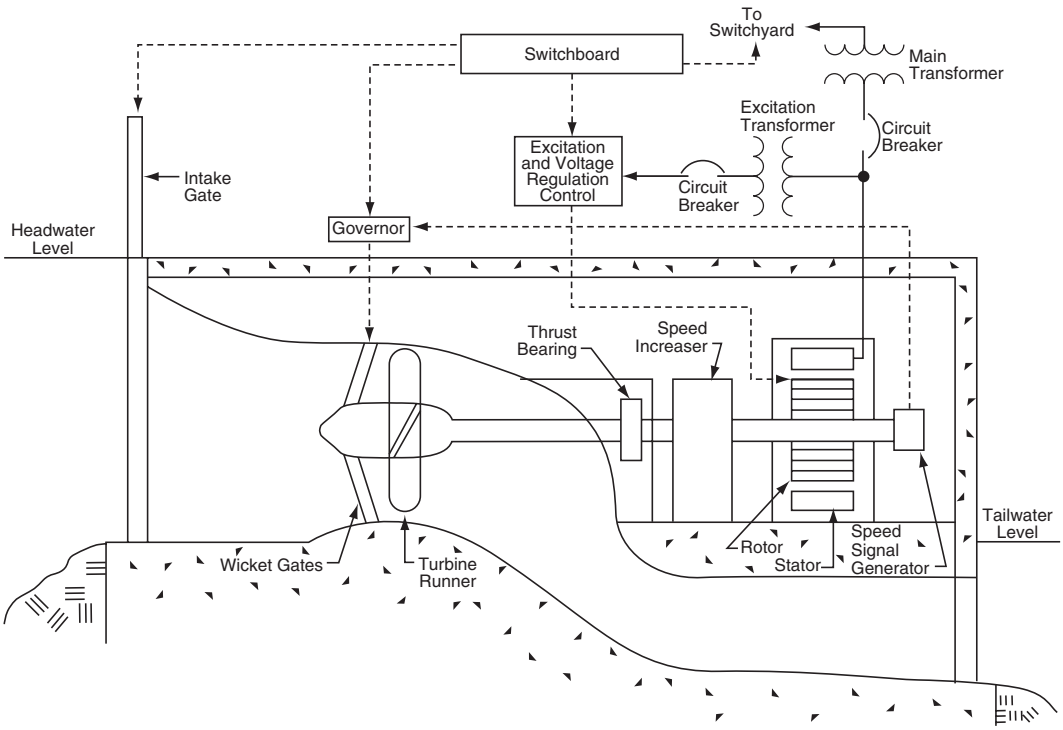

FIGURE 4.2 Horizontal axial-flow unit arrangement. (From IEEE Standard 1020, IEEE Guide for Control of Small Hydroelectric Power Plants. Copyright IEEE. All rights reserved.)

4.2.1 Turbine

The type of turbine selected for a particular application is influenced by the head and flow rate. There are two classifications of hydraulic turbines: impulse and reaction.

The impulse turbine is used for high heads—approximately 300 m or greater. High-velocity jets of water strike spoon-shaped buckets on the runner which is at atmospheric pressure. Impulse turbines may be mounted horizontally or vertically and include perpendicular jets (known as a Pelton type), diagonal jets (known as a Turgo type), or cross-flow types.

In a reaction turbine, the water passes from a spiral casing through stationary radial guide vanes, through control gates and onto the runner blades at pressures above atmospheric. There are two categories of reaction turbine—Francis and propeller. In the Francis turbine, installed at heads up to approximately 360 m, the water impacts the runner blades tangentially and exits axially. The propeller turbine uses a propeller-type runner and is used at low heads—below approximately 45 m. The propeller runner may use fixed blades or variable pitch blades—known as a Kaplan or double regulated type—that allows control of the blade angle to maximize turbine efficiency at various hydraulic heads and generation levels. Francis and propeller turbines may also be arranged in a slant, tubular, bulb, and rim generator configurations.

Water discharged from the turbine is directed into a draft tube where it exits to a tailrace channel, lower reservoir, or directly to the river.

4.2.2 Flow Control Equipment

The flow through the turbine is controlled by wicket gates on reaction turbines and by needle nozzles on impulse turbines. A turbine inlet valve or penstock intake gate is provided for isolation of the turbine during shutdown and maintenance.

Spillways and additional control valves and outlet tunnels are provided in the dam structure to pass flows that normally cannot be routed through the turbines.

4.2.3 Generator

Synchronous generators and induction generators are used to convert the mechanical energy output of the turbine to electrical energy. Induction generators are used in small hydroelectric applications (less than 5 MVA) due to their lower cost which results from elimination of the exciter, voltage regulator, and synchronizer associated with synchronous generators. The induction generator draws its excitation current from the electrical system and thus cannot be used in an isolated power system.

The majority of hydroelectric installations utilize salient pole synchronous generators. Salient pole machines are used because the hydraulic turbine operates at low speeds, requiring a relatively large number of field poles to produce the rated frequency. A rotor with salient poles is mechanically better suited for low-speed operation, compared to round rotor machines, which are applied in horizontal axis high-speed turbo-generators.

Generally, hydroelectric generators are rated on a continuous-duty basis to deliver net kVA output at a rated speed, frequency, voltage, and power factor and under specified service conditions including the temperature of the cooling medium (air or direct water). Industry standards specify the allowable temperature rise of generator components (above the coolant temperature) that are dependent on the voltage rating and class of insulation of the windings (ANSI, C50.12; IEC, 60034-1). The generator capability curve (Fig. 4.3) describes the maximum real and reactive power output limits at rated voltage within which the generator rating will not be exceeded with respect to stator and rotor heating and other limits. Standards also provide guidance on short-circuit capabilities and continuous and short-time current unbalance requirements (ANSI, C50.12; IEEE, 492).

Synchronous generators require direct current field excitation to the rotor, provided by the excitation system described in the section entitled "Excitation System". The generator saturation curve (Fig. 4.4) describes the relationship of terminal voltage, stator current, and field current.

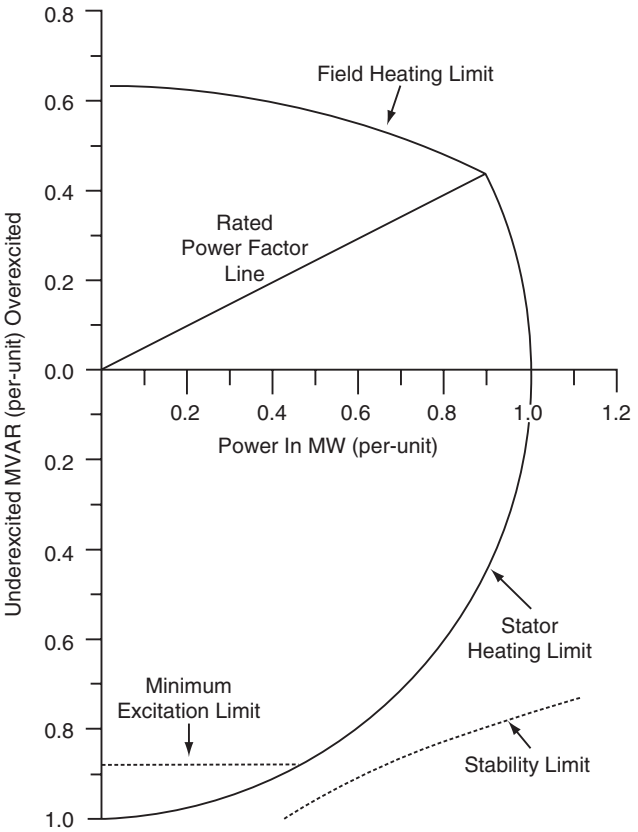

FIGURE 4.3 Typical hydro-generator capability curve (0.9 power factor, rated voltage). (From IEEE Standard 492, IEEE Guide for Operation and Maintenance of Hydro-Generators. Copyright 2006 IEEE. All rights reserved.)

While the generator may be vertical or horizontal, the majority of new installations are vertical. The basic components of a vertical generator are the stator (frame, magnetic core, and windings), rotor (shaft, thrust block, spider, rim, and field poles with windings), thrust bearing, one or two guide bearings, upper and lower brackets for the support of bearings and other components, and sole plates which are bolted to the foundation. Other components may include a direct connected exciter, speed signal generator, rotor brakes, rotor jacks, and ventilation systems with surface air coolers (IEEE, 1095).

The stator core is composed of stacked steel laminations attached to the stator frame. The stator winding may consist of single turn or multiturn coils or half-turn bars, connected in series to form a three phase circuit. Double layer windings, consisting of two coils per slot, are most common. One or more circuits are connected in parallel to form a complete phase winding. The stator winding is normally connected in wye configuration, with the neutral grounded through one of a number of alternative methods that depend on the amount of phase-to-ground fault current that is permitted to flow (IEEE, C62.92.2, C37.101). Generator output voltages range from approximately 480 VAC to 22 kVAC line-to-line, depending on the MVA rating of the unit. Temperature detectors are installed between coils in a number of stator slots.

The rotor is normally comprised of a spider frame attached to the shaft, a rim constructed of solid steel or laminated rings, and field poles attached to the rim. The rotor construction will vary significantly depending on the shaft and bearing system, unit speed, ventilation type, rotor dimensions, and characteristics of the driving hydraulic turbine. Damper windings or amortisseurs in the form of copper or brass rods are embedded in the pole faces for damping rotor speed oscillations.

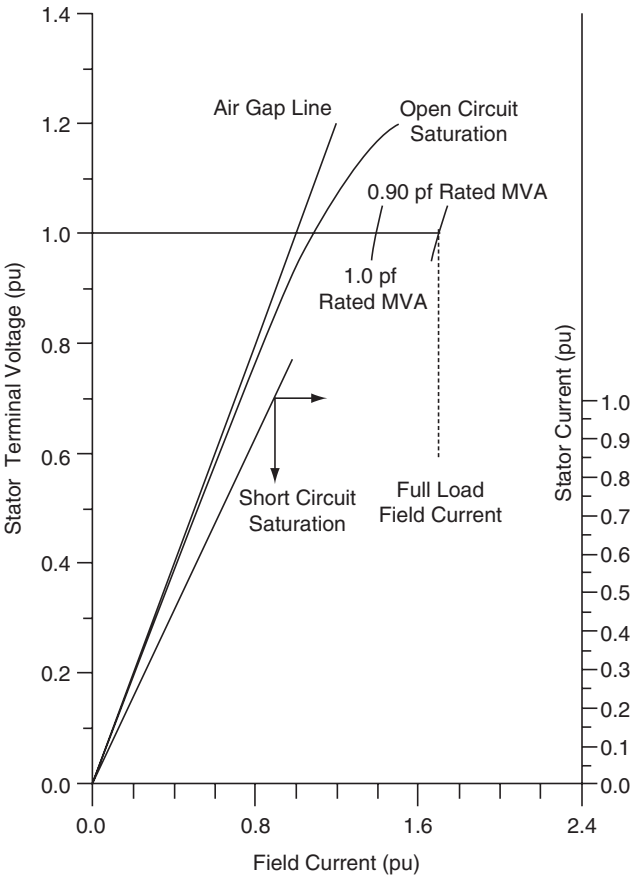

FIGURE 4.4 Typical hydro-generator saturation curves. (From IEEE Standard 492, IEEE Guide for Operation and Maintenance of Hydro-Generators. Copyright IEEE. All rights reserved.)

The thrust bearing supports the mass of both the generator and turbine plus the hydraulic thrust imposed on the turbine runner and is located either above the rotor (suspended unit) or below the rotor (umbrella unit). Thrust bearings are constructed of oil-lubricated, segmented, babbit-lined shoes. One or two oil-lubricated generator guide bearings are used to restrain the radial movement of the shaft.

Fire protection systems are normally installed to detect combustion products in the generator enclosure, initiate rapid de-energization of the generator, and release extinguishing material. Carbon dioxide and water are commonly used as the fire quenching medium.

Excessive unit vibrations may result from mechanical or magnetic unbalance. Vibration monitoring devices such as proximity probes to detect shaft run out are provided to initiate alarms and unit shutdown.

The choice of generator inertia is an important consideration in the design of a hydroelectric plant. The speed rise of the turbine-generator unit under load rejection conditions, caused by the instantaneous disconnection of electrical load, is inversely proportional to the combined inertia of the generator and turbine. Turbine inertia is normally about 5% of the generator inertia. During design of the plant, unit inertia, effective wicket gate or nozzle closing and opening times, and penstock dimensions are optimized to control the pressure fluctuations in the penstock and speed variations of the turbine-generator during load rejection and load acceptance. Speed variations may be reduced by increasing the generator inertia at added cost. Inertia can be added by increasing the mass of the generator, adjusting the rotor diameter, or by adding a flywheel. The unit inertia also has a significant effect on the transient

stability of the electrical system, as this factor influences the rate at which energy can be moved in or out of the generator to control the rotor angle acceleration during system fault conditions. [see *Power System Stability and Control,* Kundur (1994) and Section 2 of title *Power System Stability and Control* of this handbook.]

4.2.4 Generator Terminal Equipment

The generator output is connected to terminal equipment via cable, busbar, or isolated phase bus. The terminal equipment comprises current transformers (CTs), voltage transformers (VTs), and surge suppression devices. The CTs and VTs are used for unit protection, metering and synchronizing, and for governor and excitation system functions. The surge protection devices, consisting of surge arresters and capacitors, protect the generator and low-voltage windings of the step-up transformer from lightning and switching-induced surges.

4.2.5 Generator Switchgear

The generator circuit breaker and associated isolating disconnect switches are used to connect and disconnect the generator to and from the power system. The generator circuit breaker may be located on either the low-voltage or high-voltage side of the generator step-up transformer. In some cases, the generator is connected to the system by means of circuit breakers located in the switchyard of the generating plant. The generator circuit breaker may be of the oil filled, air magnetic, air blast, or compressed gas insulated type, depending on the specific application. The circuit breaker is closed as part of the generator synchronizing sequence and is opened (tripped) either by operator control, as part of the automatic unit stopping sequence, or by operation of protective relay devices in the event of unit fault conditions.

4.2.6 Generator Step-Up Transformer

The generator transformer steps up the generator terminal voltage to the voltage of the power system or plant switchyard. Generator transformers are generally specified and operated in accordance with international standards for power transformers, with the additional consideration that the transformer will be operated close to its maximum rating for the majority of its operating life. Various types of cooling systems are specified depending on the transformer rating and physical constraints of the specific application. In some applications, dual low-voltage windings are provided to connect two generating units to a single bank of step-up transformers. Also, transformer tertiary windings are sometimes provided to serve the AC station service requirements of the power plant.

4.2.7 Excitation System

The excitation system fulfills two main functions:

1. It produces DC voltage (and power) to force current to flow in the field windings of the generator. There is a direct relationship between the generator terminal voltage and the quantity of current flowing in the field windings as described in Fig. 4.4.
2. It provides a means for regulating the terminal voltage of the generator to match a desired setpoint and to provide damping for power system oscillations.

Prior to the 1960s, generators were generally provided with rotating exciters that fed the generator field through a slip ring arrangement, a rotating pilot exciter feeding the main exciter field, and a regulator controlling the pilot exciter output. Since the 1960s, the most common arrangement is thyristor bridge rectifiers fed from a transformer connected to the generator terminals, referred to as a "potential source controlled rectifier high initial response exciter" or "bus-fed static exciter" (IEEE, 421.1, 421.2, 421.4, 421.5). Another system used for smaller high-speed units is a brushless exciter with a rotating AC generator and rotating rectifiers.

Modern static exciters have the advantage of providing extremely fast response times and high field ceiling voltages for forcing rapid changes in the generator terminal voltage during system faults. This is necessary to overcome the inherent large time constant in the response between terminal voltage and field voltage (referred to as $T'_{do'}$, typically in the range of 5–10 s). Rapid terminal voltage forcing is necessary to maintain transient stability of the power system during and immediately after system faults. Power system stabilizers are also applied to static exciters to cause the generator terminal voltage to vary in phase with the speed deviations of the machine, for damping power system dynamic oscillations. [see *Power System Stability and Control,* Kundur (1994) and Section 2 of title *Power System Stability and Control* of this handbook.]

Various auxiliary devices are applied to the static exciter to allow remote setting of the generator voltage and to limit the field current within rotor thermal and under excited limits. Field flashing equipment is provided to build up generator terminal voltage during starting to the point at which the thyristor can begin gating. Power for field flashing is provided either from the station battery or alternating current station service.

4.2.8 Governor System

The governor system is the key element of the unit speed and power control system (IEEE, 125, 1207; IEC, 61362; ASME, 29). It consists of control and actuating equipment for regulating the flow of water through the turbine, for starting and stopping the unit, and for regulating the speed and power output of the turbine generator. The governor system includes setpoint and sensing equipment for speed, power and actuator position, compensation circuits, and hydraulic power actuators which convert governor control signals to mechanical movement of the wicket gates (Francis and Kaplan turbines), runner blades (Kaplan turbine), and nozzle jets (Pelton turbine). The hydraulic power actuator system includes high-pressure oil pumps, pressure tanks, oil sump, actuating valves, and servomotors.

Older governors are of the mechanical-hydraulic type, consisting of ballhead speed sensing, mechanical dashpot and compensation, gate limit, and speed droop adjustments. Modern governors are of the electro-hydraulic type where the majority of the sensing, compensation, and control functions are performed by electronic or microprocessor circuits. Compensation circuits utilize proportional plus integral (PI) or proportional plus integral plus derivative (PID) controllers to compensate for the phase lags in the penstock–turbine–generator–governor control loop. PID settings are normally adjusted to ensure that the hydroelectric unit remains stable when serving an isolated electrical load. These settings ensure that the unit contributes to the damping of system frequency disturbances when connected to an integrated power system. Various techniques are available for modeling and tuning the governor (IEEE Standard P1207).

A number of auxiliary devices are provided for remote setting of power, speed, and actuator limits and for electrical protection, control, alarming, and indication. Various solenoids are installed in the hydraulic actuators for controlling the manual and automatic start-up and shutdown of the turbine-generator unit.

4.2.9 Control Systems

Detailed information on the control of hydroelectric power plants is available in industry standards (IEEE, 1010, 1020, 1249). A general hierarchy of control is illustrated in Table 4.1. Manual controls, normally installed adjacent to the device being controlled, are used during testing and maintenance, and as a backup to the automatic control systems. Figure 4.5 illustrates the relationship of control locations and typical functions available at each location. Details of the control functions available at each location are described in IEEE 1249. Automatic sequences implemented for starting, synchronizing, and shutdown of hydroelectric units are detailed in IEEE 1010.

Modern hydroelectric plants and plants undergoing rehabilitation and life extension are incorporating higher levels of computer automation (IEEE, 1249, 1147). The relative simplicity of

TABLE 4.1 Summary of Control Hierarchy for Hydroelectric Plants

Control Category	Subcategory	Remarks
Location	Local	Control is local at the controlled equipment or within sight of the equipment.
	Centralized	Control is remote from the controlled equipment, but within the plant.
	Off-site	Control location is remote from the project.
Mode	Manual	Each operation needs a separate and discrete initiation; could be applicable to any of the three locations.
	Automatic	Several operations are precipitated by a single initiation; could be applicable to any of the three locations.
Operation (supervision)	Attended	Operator is available at all times to initiate control action.
	Unattended	Operation staff is not normally available at the project site.

Source: IEEE Standard 1249, IEEE Guide for Computer-Based Control for Hydroelectric Power Plant Automation. With permission.

hydroelectric plant control allows most plants to be operated in an unattended mode from off-site control centers.

The current trend is to apply automated condition monitoring systems for hydroelectric plant equipment. Condition monitoring systems, coupled with expert system computer programs, allow plant owners and operators to more fully utilize the capacity of plant equipment and water resources, make better maintenance and replacement decisions, and maximize the value of installed assets.

4.2.10 Protection Systems

The turbine-generator unit and related equipment are protected against mechanical, electrical, hydraulic, and thermal damage that may occur as a result of abnormal conditions within the plant or

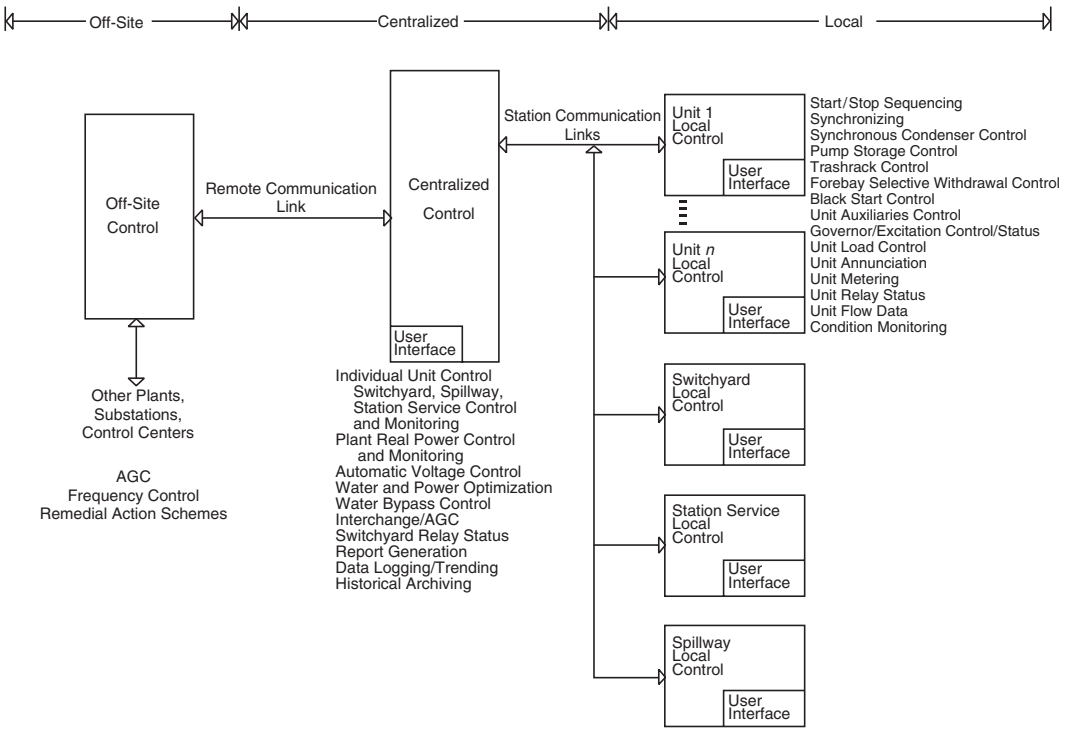

FIGURE 4.5 Relationship of local, centralized, and off-site control. (From IEEE Standard 1249, IEEE Guide for Computer-Based Control for Hydroelectric Power Plant Automation.)

on the power system to which the plant is connected. Abnormal conditions are detected automatically by means of protective relays and other devices and measures are taken to isolate the faulty equipment as quickly as possible while maintaining the maximum amount of equipment in service. Typical protective devices include electrical fault detecting relays, temperature, pressure, level, speed, and fire sensors, and vibration monitors associated with the turbine, generator, and related auxiliaries. The protective devices operate in various isolation and unit shutdown sequences, depending on the severity of the fault.

The type and extent of protection will vary depending on the size of the unit, manufacturer's recommendations, owner's practices, and industry standards.

Specific guidance on application of protection systems for hydroelectric plants is provided in IEEE 1010, 1020, C37.102, C37.91.

4.2.11 Plant Auxiliary Equipment

A number of auxiliary systems and related controls are provided throughout the hydroelectric plant to support the operation of the generating units (IEEE, 1010, 1020). These include:

1. Switchyard systems (see Chapter 5).
2. Alternating current (AC) station service. Depending on the size and criticality of the plant, multiple sources are often supplied, with emergency backup provided by a diesel generator.
3. Direct current (DC) station service. It is normally provided by one or more battery banks, for supply of protection, control, emergency lighting, and exciter field flashing.
4. Lubrication systems, particularly for supply to generator and turbine bearings and bushings.
5. Drainage pumps, for removing leakage water from the plant.
6. Air compressors, for supply to the governors, generator brakes, and other systems.
7. Cooling water systems, for supply to the generator air coolers, generator and turbine bearings, and step-up transformer.
8. Fire detection and extinguishing systems.
9. Intake gate or isolation valve systems.
10. Draft tube gate systems.
11. Reservoir and tailrace water level monitoring.
12. Synchronous condenser equipment, for dewatering the draft tube to allow the runner to spin in air during synchronous condenser operation. In this case, the generator acts as a synchronous motor, supplying or absorbing reactive power.
13. Service water systems.
14. Overhead crane.
15. Heating, ventilation, and air conditioning.
16. Environmental systems.

4.3 Special Considerations Affecting Pumped Storage Plants

A pumped storage unit is one in which the turbine and generator are operated in the reverse direction to pump water from the lower reservoir to the upper reservoir. The generator becomes a motor, drawing its energy from the power system, and supplies mechanical power to the turbine which acts as a pump. The motor is started with the wicket gates closed and the draft tube water depressed with compressed air. The motor is accelerated in the pump direction and when at full speed and connected to the power system, the depression air is expelled, the pump is primed, and the wicket gates are opened to commence pumping action.

4.3.1 Pump Motor Starting

Various methods are utilized to accelerate the generator/motor in the pump direction during starting (IEEE, 1010). These include:

1. Full voltage, across the line starting—Used primarily on smaller units, the unit breaker is closed and the unit is started as an induction generator. Excitation is applied near rated speed and machine reverts to synchronous motor operation.
2. Reduced voltage, across the line starting—A circuit breaker connects the unit to a starting bus tapped from the unit step-up transformer at one third to one half rated voltage. Excitation is applied near rated speed and the unit is connected to the system by means of the generator circuit breaker. Alternative methods include use of a series reactor during starting and energization of partial circuits on multiple circuit machines.
3. Pony motor starting—A variable speed wound-rotor motor attached to the AC station service and coupled to the motor/generator shaft is used to accelerate the machine to synchronous speed.
4. Synchronous starting—A smaller generator, isolated from the power system, is used to start the motor by connecting the two in parallel on a starting bus, applying excitation to both units, and opening the wicket gates on the smaller generator. When the units reach synchronous speed, the motor unit is disconnected from the starting bus and connected to the power system.
5. Semisynchronous (reduced frequency, reduced voltage) starting—An isolated generator is accelerated to about 80% rated speed and paralleled with the motor unit by means of a starting bus. Excitation is applied to the generating unit and the motor unit starts as an induction motor. When the speed of the two units is approximately equal, excitation is applied to the motor unit, bringing it into synchronism with the generating unit. The generating unit is then used to accelerate both units to rated speed and the motor unit is connected to the power system.
6. Static starting—A static converter/inverter connected to the AC station service is used to provide variable frequency power to accelerate the motor unit. Excitation is applied to the motor unit at the beginning of the start sequence and the unit is connected to the power system when it reaches synchronous speed. The static starting system can be used for dynamic braking of the motor unit after disconnection from the power system, thus extending the life of the unit's mechanical brakes.

4.3.2 Phase Reversing of the Generator/Motor

It is necessary to reverse the direction of rotation of the generator/motor by interchanging any two of the three phases. This is achieved with multipole motor operated switches or with circuit breakers.

4.3.3 Draft Tube Water Depression

Water depression systems using compressed air are provided to lower the level of the draft tube water below the runner to minimize the power required to accelerate the motor unit during the transition to pumping mode. Water depression systems are also used during motoring operation of a conventional hydroelectric unit while in synchronous condenser mode. Synchronous condenser operation is used to provide voltage support for the power system and to provide spinning reserve for rapid loading response when required by the power system.

4.4 Commissioning of Hydroelectric Plants

The commissioning of a new hydroelectric plant, rehabilitation of an existing plant, or replacement of existing equipment requires a rigorous plan for inspection and testing of equipment and systems and for organizing, developing, and documenting the commissioning program (IEEE, 1248).

References

American Society of Mechanical Engineers–Hydropower Technical Committee, *The Guide to Hydropower Mechanical Design*, HCI Publications, Kansas City, KS, 1996.

ANSI Standard C50.12, Synchronous Generators and Generator/Motors for Hydraulic Turbine Applications.

ASME PTC 29, Speed Governing Systems for Hydraulic Turbine Generator Units.
IEC Standard 60034-1, Rotating Electrical Machines—Part 1: Rating and Performance.
IEC Standard 61362, Guide to Specification of Hydraulic Turbine Control Systems.
IEEE Standard C37.91, IEEE Guide for Protective Relay Applications to Power Transformers.
IEEE Standard 421.1, IEEE Standard Definitions for Excitation Systems for Synchronous Machines.
IEEE Standard 1010, IEEE Guide for Control of Hydroelectric Power Plants.
IEEE Standard 125, IEEE Recommended Practice for Preparation of Equipment Specifications for Speed-Governing of Hydraulic Turbines Intended to Drive Electric Generators.
IEEE Standard 1207, IEEE Guide for the Application of Turbine Governing Systems for Hydroelectric Generating Units.
IEEE Standard 1020, IEEE Guide for Control of Small Hydroelectric Power Plants.
IEEE Standard C62.92.2, IEEE Guide for the Application of Neutral Grounding in Electrical Utility Systems, Part II—Grounding of Synchronous Generator Systems.
IEEE Standard 1095, IEEE Guide for Installation of Vertical Generators and Generator/Motors for Hydroelectric Applications.
IEEE Standard 421.2, IEEE Guide for Identification, Testing and Evaluation of the Dynamic Performance of Excitation Control Systems.
IEEE Standard 421.4, IEEE Guide for the Preparation of Excitation System Specifications.
IEEE Standard 1147, IEEE Guide for the Rehabilitation of Hydroelectric Power Plants.
IEEE Standard 421.5, IEEE Recommended Practice for Excitation Systems for Power Stability Studies.
IEEE Standard C37.101, IEEE Guide for Generator Ground Protection.
IEEE Standard C37.102, IEEE Guide for AC Generator Protection.
IEEE Standard 1249, IEEE Guide for Computer-Based Control for Hydroelectric Power Plant Automation.
IEEE Standard 1248, IEEE Guide for the Commissioning of Electrical Systems in Hydroelectric Power Plants.
IEEE Standard 492, IEEE Guide for Operation and Maintenance of Hydro-Generators.
Kundur, P., *Power System Stability and Control*, McGraw-Hill, New York, 1994.
Working Group on Prime Mover and Energy Supply Models for System Dynamic Performance Studies, Hydraulic turbine and turbine control models for system dynamic studies, *IEEE Transactions on Power Systems*, 7(1), February 1992.
World Energy Council, Survey of Energy Resources, 2001.

5

Synchronous Machinery

Paul I. Nippes
Magnetic Products and Services, Inc.

5.1 General

Synchronous motors convert electrical power to mechanical power; synchronous generators convert mechanical power to electrical power; and synchronous condensers supply only reactive power to stabilize system voltages.

Synchronous motors, generators, and condensers perform similarly, except for a heavy cage winding on the rotor of motors and condensers for self-starting.

A rotor has physical magnetic poles, arranged to have alternating north and south poles around the rotor diameter which are excited by electric current, or uses permanent magnets, having the same number of poles as the stator electromagnetic poles.

The rotor RPM = 120 × Electrical System Frequency/Poles.

The stator winding, fed from external AC multi-phase electrical power, creates rotating electromagnetic poles.

At speed, rotor poles turn in synchronism with the stator rotating electromagnetic poles, torque being transmitted magnetically across the "air gap" power angle, lagging in generators and leading in motors.

Synchronous machine sizes range from fractional watts, as in servomotors, to 1500 MW, as in large generators.

Voltages vary, up to 25,000 V AC stator and 1500 V DC rotor.

Installed horizontal or vertical at speed ranges up to 130,000 RPM, normally from 40 RPM (waterwheel generators) to 3600 RPM (turbine generators).

Frequency at 60 or 50 Hz mostly, 400 Hz military; however, synthesized variable frequency electrical supplies are increasingly common and provide variable motor speeds to improve process efficiency.

Typical synchronous machinery construction and performance are described; variations may exist on special smaller units.

This document is intentionally general in nature. Should the reader want specific application information, refer to standards: NEMA MG-1; IEEE 115, C50-10 and C50-13; IEC 600034: 1-11, 14-16, 18, 20, 44, 72, and 136, plus other applicable specifications.

5.2 Construction (See Fig. 5.1)

5.2.1 Stator

5.2.1.1 Frame

The exterior frame, made of steel, either cast or a weldment, supports the laminated stator core and has feet, or flanges, for mounting to the foundation. Frame vibration from core magnetic forcing or rotor unbalance is minimized by resilient mounting the core and/or by designing to avoid frame resonance with forcing frequencies. If bracket type bearings are employed, the frame must support the bearings, oil seals, and gas seals when cooled with hydrogen or gas other than air. The frame also provides protection from the elements and channels cooling air, or gas, into and out of the core, stator windings, and rotor. When the unit is cooled by gas contained within the frame, heat from losses is removed by coolers having water circulating through finned pipes of a heat exchanger mounted within the frame. Where cooling water is unavailable and outside air cannot circulate through the frame because of its dirty or toxic condition, large air-to-air heat exchangers are employed, the outside air being forced through the cooler by an externally shaft-mounted blower.

5.2.1.2 Stator Core Assembly

The stator core assembly of a synchronous machine is almost identical to that of an induction motor. A major component of the stator core assembly is the core itself, providing a high permeability path for magnetism. The stator core is comprised of thin silicon steel laminations and insulated by a surface coating minimizing eddy current and hysteresis losses generated by alternating magnetism. The laminations are stacked as full rings or segments, in accurate alignment, either in a fixture or in the stator frame, having ventilation spacers inserted periodically along the core length. The completed core is compressed and clamped axially to about 10 kg/cm^2 using end fingers and heavy clamping plates. Core end heating from stray magnetism is minimized, especially on larger machines, by using non-magnetic materials at the core end or by installing a flux shield of either tapered laminations or copper shielding.

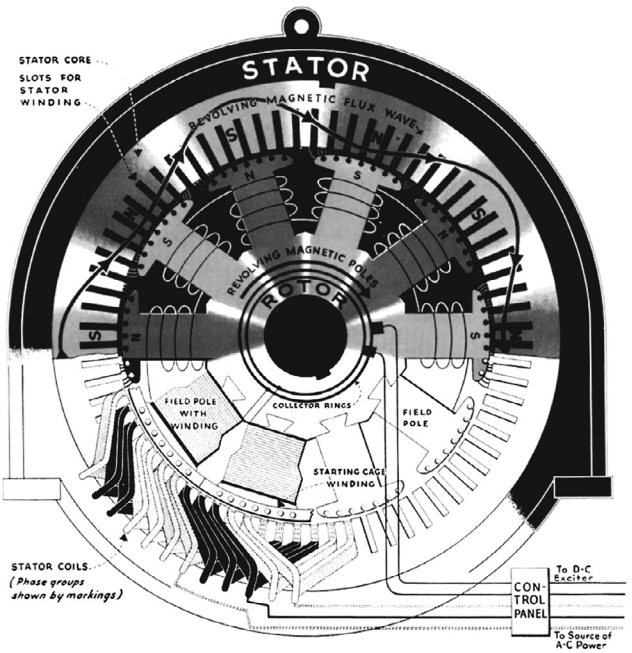

FIGURE 5.1 Magnetic "skeleton" (upper half) and structural parts (lower half) of a ten-pole (720 rpm at 60 cycles) synchronous motor. (From *The ABC's of Synchronous Motors*, 7(1), 5, 1944. The Electric Machinery Company, Inc. With permission.)

A second major component is the stator winding made up of insulated coils placed in axial slots of the stator core inside diameter. The coil make-up, pitch, and connections are designed to produce rotating stator electromagnetic poles in synchronism with the rotor magnetic poles. The stator coils are retained into the slots by slot wedges driven into grooves in the top of the stator slots. Coil end windings are bound together and to core-end support brackets. If the synchronous machine is a generator, the rotating rotor pole magnetism generates voltage in the stator winding which delivers power to an electric load. If the synchronous machine is a motor, its electrically powered stator winding generates rotating electromagnetic poles and the attraction of the rotor magnets, operating in synchronism, produces torque and delivery of mechanical power to the drive shaft.

5.2.2 Rotor

5.2.2.1 The Rotor Assembly

The rotor of a synchronous machine is a highly engineered unitized assembly capable of rotating satisfactorily at synchronous speed continuously according to standards or as necessary for the application. The central element is the shaft, having journals to support the rotor assembly in bearings. Located at the rotor assembly axial mid-section is the rotor core embodying magnetic poles. When the rotor is round it is called "non-salient pole", or turbine generator type construction and when the rotor has protruding pole assemblies, it is called "salient pole" construction.

The non-salient pole construction, used mainly on turbine generators (and also as wind tunnel fan drive motors), has two or four magnetic poles created by direct current in coils located in slots at the rotor outside diameter. Coils are restrained in the slots by slot wedges and at the ends by retaining rings on large high-speed rotors, and fiberglass tape on other units where stresses permit. This construction is not suited for use on a motor requiring self-starting as the rotor surface, wedges, and retaining rings overheat and melt from high currents of self-starting.

A single piece forging is sometimes used on salient pole machines, usually with four or six poles. Salient poles can also be integral with the rotor lamination and can be mounted directly to the shaft or fastened to an intermediate rotor spider. Each distinct pole has an exciting coil around it carrying excitation current or else it employs permanent magnets. In a generator, a moderate cage winding in the face of the rotor poles, usually with pole-to-pole connections, is employed to dampen shaft torsional oscillation and to suppress harmonic variation in the magnetic waveform. In a motor, heavy bars and end connections are required in the pole face to minimize and withstand the high heat of starting duty.

Direct current excites the rotor windings of salient, and non-salient pole motors and generators, except when permanent magnets are employed. The excitation current is supplied to the rotor from either an external DC supply through collector rings or a shaft-mounted brushless exciter. Positive and negative polarity bus bars or cables pass along and through the shaft as required to supply excitation current to the windings of the field poles.

When supplied through collector rings, the DC current could come from a shaft-driven DC or AC exciter rectified output, from an AC-DC motor-generator set, or from plant power. DC current supplied by a shaft-mounted AC generator is rectified by a shaft-mounted rectifier assembly.

As a generator, excitation current level is controlled by the voltage regulator. As a motor, excitation current is either set at a fixed value, or is controlled to regulate power factor, motor current, or system stability.

In addition, the rotor also has shaft-mounted fans or blowers for cooling and heat removal from the unit plus provision for making balance weight additions or corrections.

5.2.2.2 Bearings and Couplings

Bearings on synchronous machinery are anti-friction, grease, or oil-lubricated on smaller machines, journal type oil-lubricated on large machines, and tilt-pad type on more sophisticated machines, especially where rotor dynamics are critical. Successful performance of magnetic bearings, proving to be successful on turbo-machinery, may also come to be used on synchronous machinery as well.

As with bearings on all large electrical machinery, precautions are taken with synchronous machines to prevent bearing damage from stray electrical shaft currents. An elementary measure is the application of insulation on the outboard bearing, if a single-shaft end unit, and on both bearing and coupling at the same shaft end for double-shaft end drive units. Damage can occur to bearings even with properly applied insulation, when solid-state controllers of variable frequency drives, or excitation, cause currents at high frequencies to pass through the bearing insulation as if it were a capacitor. Shaft grounding and shaft voltage and grounding current monitoring can be employed to predict and prevent bearing and other problems.

5.3 Performance

5.3.1 Synchronous Machines, in General

This section covers performance common to synchronous motors, generators, and condensers.

Saturation curves (Fig. 5.2) are either calculated or obtained from test and are the basic indicators of machine design suitability. From these the full load field, or excitation, amperes for either motors

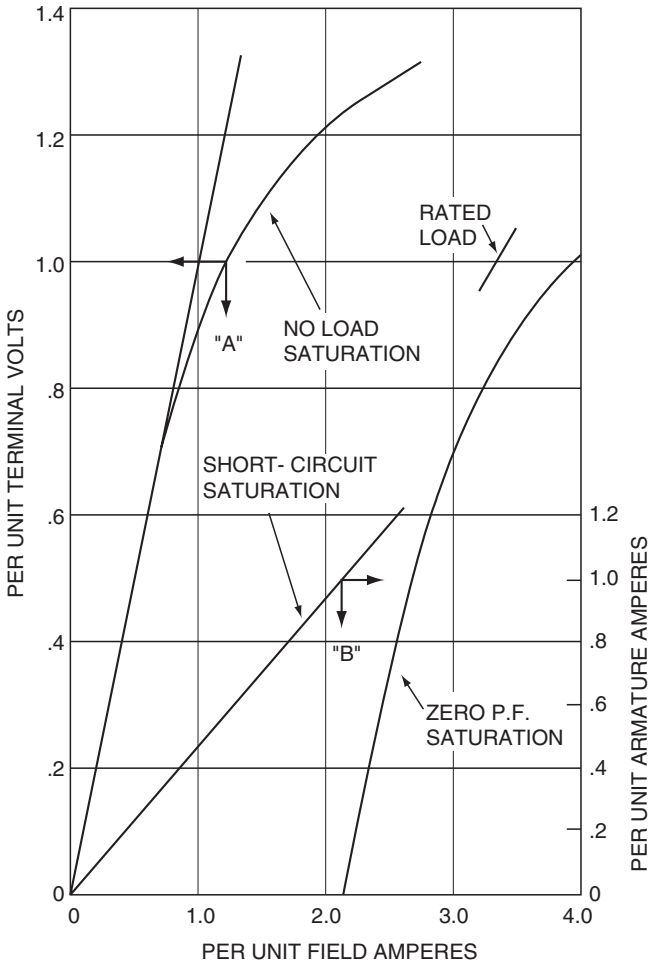

FIGURE 5.2 Saturation curves.

or generators are determined as shown, on the rated voltage line, as "*Rated Load*." For synchronous condensers, the field current is at the crossing of the zero P.F. saturation line at 1.0 V. As an approximate magnetic figure of merit, the no-load saturation curve should not exceed its extrapolated straight line by more than 25%, unless of a special design. From these criteria, and the knowledge of the stator current and cooling system effectiveness, the manufacturer can project the motor component heating, and thus insulation life, and the efficiency of the machine at different loads.

Vee curves (Fig. 5.3) show overall loading performance of a synchronous machine for different loads and power factors, but more importantly show how heating and stability limit loads. For increased hydrogen pressures in a generator frame, the load capability increases markedly.

The characteristics of all synchronous machines when their stator terminals are short-circuited are similar (see Fig. 5.4). There is an initial subtransient period of current increase of 8 to 10 times rated, with one phase offsetting an equal amount. These decay in a matter of milliseconds to a transient value of 3 to 5 times rated, decaying in tenths of a second to a relatively steady value. Coincident with this, the

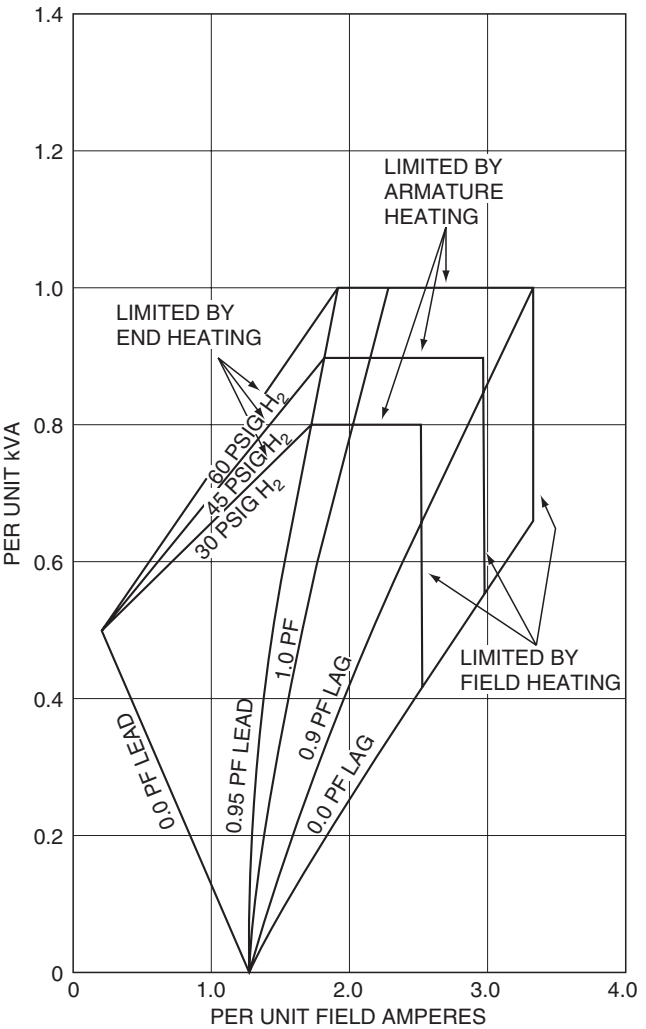

FIGURE 5.3 Vee curves.

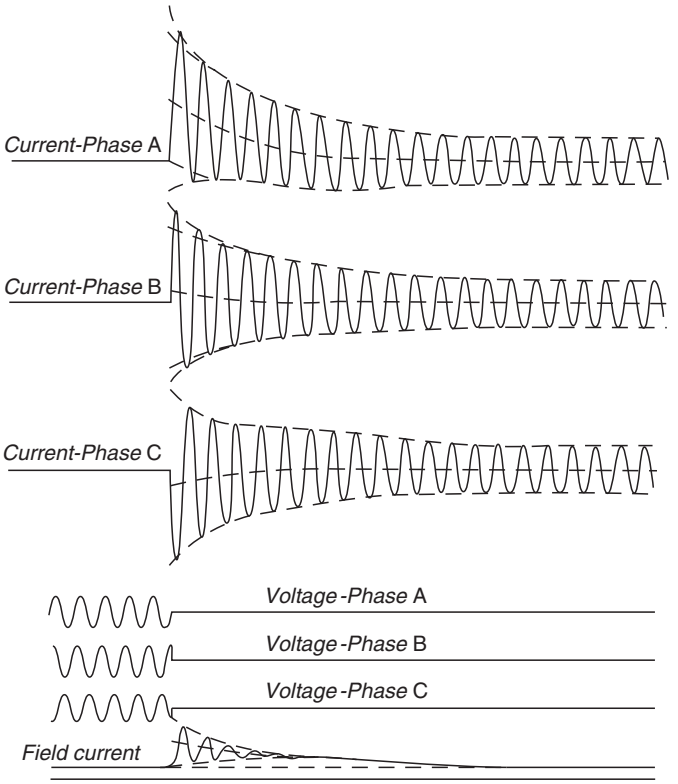

FIGURE 5.4 Typical oscillogram of a sudden three-phase short circuit.

field current increases suddenly by 3 to 5 times, decaying in tenths of a second. The stator voltage on the shorted phases drops to zero and remains so until the short circuit is cleared.

5.3.2 Synchronous Generator Capability

The synchronous generator normally has easy starting duty as it is brought up to speed by a prime mover. Then the rotor excitation winding is powered with DC current, adjusted to rated voltage, and transferred to voltage regulator control. It is then synchronized to the power system, closing the interconnecting circuit breaker as the prime mover speed is advancing, at a snail's pace, leading the electric system. Once on line, its speed is synchronized with the power system and KW is raised by increasing the prime mover KW input. The voltage regulator adjusts excitation current to hold voltage. Increasing the voltage regulator set point increases KVAR input to the system, reducing the power factor toward lagging and vice versa. Steady operating limits are provided by its Reactive Capability Curve (see Fig. 5.5). This curve shows the possible kVA reactive loading, lagging, or leading, for given KW loading. Limitations consist of field heating, armature heating, stator core end heating, and operating stability over different regions of the reactive capability curve.

5.3.3 Synchronous Motor and Condenser Starting

The duty on self-starting synchronous motors and condensors is severe, as there are large induction currents in the starting cage winding once the stator winding is energized (see Fig. 5.6).

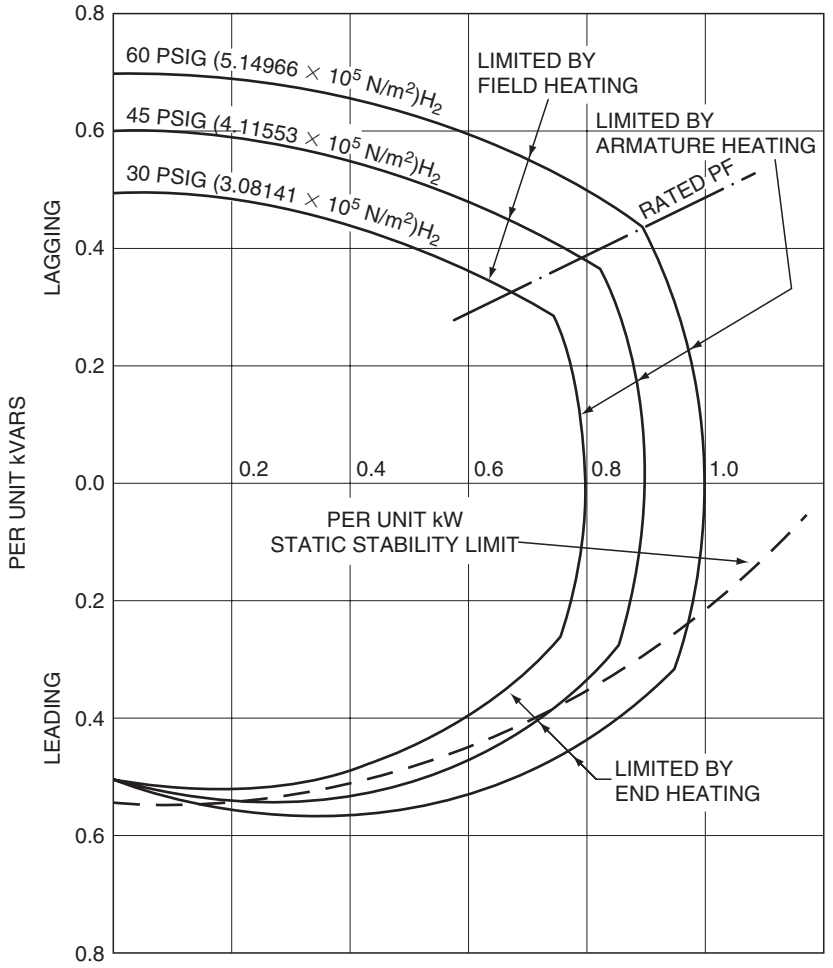

FIGURE 5.5 Typical reactive capability curve.

These persist as the motor comes up to speed, similar to but not identical to starting an induction motor. Similarities exist to the extent that extremely high torque impacts the rotor initially and decays rapidly to an average value, increasing with time. Different from the induction motor is the presence of a large oscillating torque. The oscillating torque decreases in frequency as the rotor speed increases. This oscillating frequency is caused by the saliency effect of the protruding poles on the rotor. Meanwhile, the stator current remains constant until 80% speed is reached. The oscillating torque at decaying frequency may excite train torsional natural frequencies during acceleration, a serious train design consideration. An anomaly occurs at half speed as a dip in torque and current due to the coincidence of line frequency torque with oscillating torque frequency. Once the rotor is close to rated speed, excitation is applied to the field coils and the rotor pulls into synchronism with the rotating electromagnetic poles. At this point, stable steady-state operation begins.

Increasingly, variable frequency power is supplied to synchronous machinery primarily to deliver the optimum motor speed to meet load requirements, improving the process efficiency. It can also be used

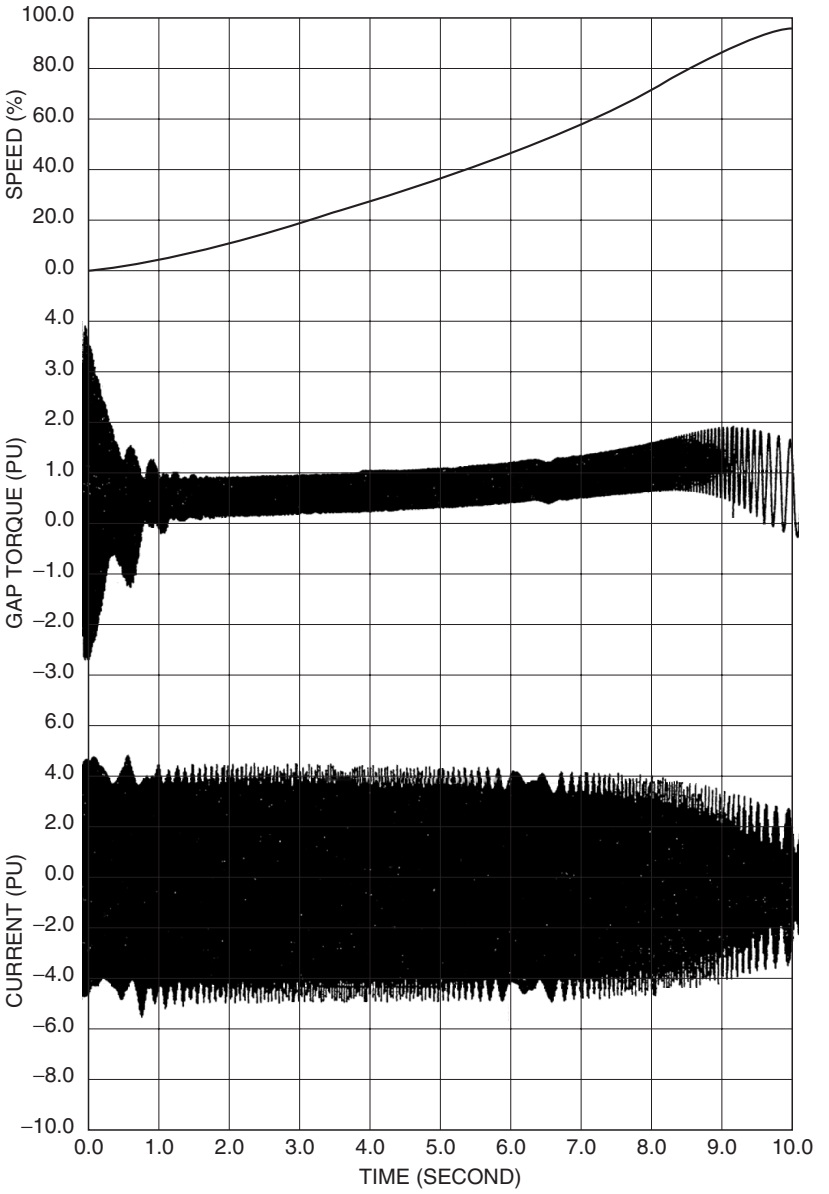

FIGURE 5.6 Synchronous motor and condensor starting.

for soft-starting the synchronous motor or condenser. Special design and control are employed to avert problems imposed, such as excitation of train torsional natural frequencies and extra heating from harmonics of the supply power.

6

Thermal Generating Plants

Kenneth H. Sebra
Baltimore Gas and Electric Company

Thermal generating plants are designed and constructed to convert energy from fuel (coal, oil, gas, or radiation) into electric power. The actual conversion is accomplished by a turbine-driven generator. Thermal generating plants differ from industrial plants in that the nature of the product never changes. The plant will always produce electric energy. The things that may change are the fuel used (coal, oil, or gas) and environmental requirements. Many plants that were originally designed for coal were later converted to oil, converted back to coal, and then converted to gas. Environmental requirements have changed, which has required the construction of air and water emissions control systems. Plant electrical systems should be designed to allow for further growth. Sizing of

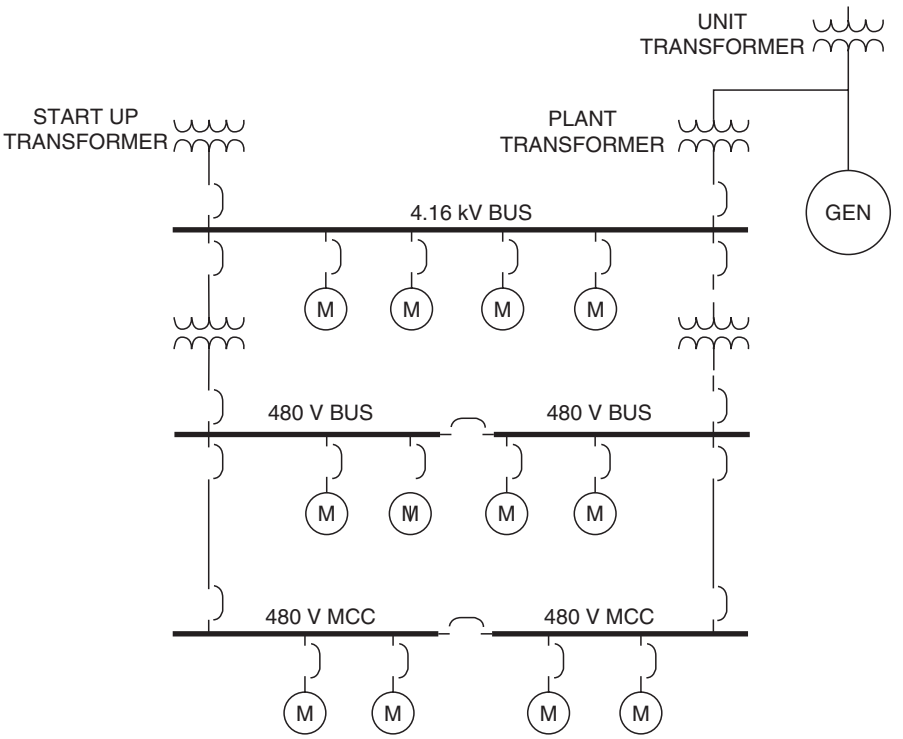

FIGURE 6.1 Typical plant layout.

transformers and buses is at best a matter of guesswork. The plant electrical system should be sized at 5 to 10% the size of the generating unit depending on the plant configuration and number of units at the plant site. The layout of a typical system is seen in Fig. 6.1.

6.1 Plant Auxiliary System

6.1.1 Selection of Auxiliary System Voltages

The most common plant auxiliary system voltages are 13,800 V, 6900 V, 4160 V, 2400 V, and 480 V. The highest voltage is determined by the largest motor. If motors of 4000 hp or larger are required, one should consider using 13,800 V. If the largest motor required is less than 4000 hp, then 4160 V should be satisfactory.

6.1.2 Auxiliary System Loads

Auxiliary load consists of motors and transformers. Transformers supply lower level buses which supply smaller motors and transformers which supply lower voltage buses. Generation plants built before 1950 may have an auxiliary generator that is connected to the main generator shaft. The auxiliary generator will supply plant loads when the plant is up and running.

6.1.3 Auxiliary System Power Sources

The power sources for a generating plant consist of one or more off-site sources and one or more on-site sources. The on-site sources are the generator and, in some cases, a black start diesel generator or a gas turbine generator which may be used as a peaker.

6.1.4 Auxiliary System Voltage Regulation Requirements

Most plants will not require voltage regulation. A load flow study will indicate if voltage regulation is required. Transformers with tap changers, static var compensators, or induction regulators may be used to keep plant bus voltages within acceptable limits. Switched capacitor banks and overexcited synchronous motors may also be used to regulate bus voltage.

6.2 Plant One-Line Diagram

The one-line diagram is the most important document you will use. Start with a conceptual one-line and add detail as it becomes available. The one-line diagram will help you think about your design and make it easier to discuss with others. Do not be afraid to get something on paper very early and modify as you get more information about the design. Consider how the plant will be operated. Will there be a start-up source and a running source? Are there on-site power sources?

6.3 Plant Equipment Voltage Ratings

Establish at least one bus for each voltage rating in the plant. Two or more buses may be required depending on how the plant will be operated.

6.4 Grounded vs. Ungrounded Systems

A method of grounding must be determined for each voltage level in the plant.

6.4.1 Ungrounded

Most systems will be grounded in some manner with the exception for special cases of 120-V control systems which may be operated ungrounded for reliability reasons. An ungrounded system may be allowed to continue to operate with a single ground on the system. Ungrounded systems are undesirable because ground faults are difficult to locate. Also, ground faults can result in system overvoltage, which can damage equipment that is connected to the ungrounded system.

6.4.2 Grounded

Most systems 480 V and lower will be solidly grounded.

6.4.3 Low-Resistance Grounding

Low-resistance grounding systems are used at 2400 V and above. This system provides enough ground fault current to allow relay coordination and limits ground fault current to a value low enough to prevent equipment damage.

6.4.4 High-Resistance Grounding

High-resistance grounding systems limit ground fault current to a very low value but make relay coordination for ground faults difficult.

6.5 Miscellaneous Circuits

6.5.1 Essential Services

Essential services such as critical control required for plant shutdown, fire protection, and emergency lighting should be supplied by a battery-backed inverter. This is equipment that must continue to

operate after a loss of off-site power. Some of these loads may be supplied by an on-site diesel generator or gas turbine if a delay after loss of off-site power is acceptable.

6.5.2 Lighting Supply

Lighting circuits should be designed with consideration to emergency lighting to the control room and other vital areas of the plant. Consideration should be given to egress lighting and lighting requirements for plant maintenance.

6.6 DC Systems

The plant will require at least one DC system for control and operation of essential systems when off-site power is lost. The required operating time for the emergency equipment that will be operated from the DC systems must be established in order to size the batteries. The installation of a diesel generator may reduce the size of the battery.

6.6.1 125-V DC

A 125-V DC system is supplied for circuit breaker and protective relaying. The system voltage may collapse to close to zero during fault conditions and would not be capable of supplying relay control and breaker trip current when it is needed to operate.

6.6.2 250-V DC

A 250-V DC system may be required to supply turbine generator emergency motors such as turning gear motors and emergency lube oil motors.

6.7 Power Plant Switchgear

6.7.1 High-Voltage Circuit Breakers

High-voltage circuit breakers of 34.5 kV and above may be used in the switchyard associated with the generating plant, but are rarely used in a generating plant.

6.7.2 Medium-Voltage Switchgear

Medium-voltage breakers are 2.4 to 13.8 kV. Breakers in this range are used for large motors in the plant. The most prevalent is 4.16 kV.

6.7.2.1 Medium-Voltage Air Circuit Breakers

Air circuit breakers were the most common type of breaker until about 1995. Due to large size and high maintenance requirements of air circuit breakers, they have been replaced by vacuum breakers.

6.7.2.2 Medium-Voltage Vacuum Circuit Breakers

Vacuum circuit breakers are the most common type of circuit breaker used in new installations. Vacuum circuit breakers are being used to replace air circuit breakers. Vacuum breakers are smaller and can provide additional space if the plant needs to be expanded to meet new requirements. Before using vacuum circuit breakers, a transient analysis study should be performed to determine if there is a need for surge protection. If required, surge protection can be supplied by the installation of capacitors and/or surge suppressors can be used to eliminate voltage surge problems.

6.7.2.3 Medium-Voltage SF6 Circuit Breakers

SF6 circuit breakers have the same advantages as vacuum circuit breakers but there is some environmental concern with the SF6 gas.

6.7.3 Low-Voltage Switchgear

Low voltage is 600 V and below. The most common voltage used is 480 V.

6.7.3.1 Low-Voltage Air Circuit Breakers

Air circuit breakers are used in load centers that may include a power transformer. Air circuit breakers are used for motors greater than 200 hp and less than about 600 hp. Low-voltage circuit breakers are self-contained in that fault protection is an integral part of the breaker. Low-voltage devices, which do not contain fault protection devices, are referred to as low-voltage switches. Low-voltage breakers may be obtained with various combinations of trip elements. Long time, short time, and ground trip elements may be obtained in various combinations.

Low-voltage breakers manufactured before 1970 will contain oil dashpot time delay trip elements. Breakers manufactured after the mid-1970s until about 1990 will contain solid-state analog trip elements. Breakers manufactured after 1990 will contain digital trip elements. The digital elements provide much more flexibility.

A circuit that may be large enough for a load center circuit breaker but is operated several times a day should not be put on a load center circuit breaker. The circuit breaker would be put through its useful life in a very short time. A motor starter would be a better choice.

6.7.4 Motor Control Centers

Motor control centers are self-contained and may include molded case breakers or combination starters. Molded case breakers are available as either magnetic or thermal-magnetic. The magnetic trip breakers are instantaneous trip only and the thermal-magnetic trip breakers are time delay with instantaneous trip. Magnetic breakers can be used with a contactor to make a combination starter. Time delay trip is provided by overload relays mounted on the contactor. Solid-state equipment is available to use in motor control centers and allows much greater flexibility.

6.7.5 Circuit Interruption

The purpose of a circuit breaker is to provide a method of interrupting the circuit either to turn the load on and off or to interrupt fault current. The first requirement is based on the full load current of the load. The second requirement is based on the maximum fault current as determined by the fault current study. There is no relationship between the load current and the fault current. If modifications are made to the electric power system, the fault interrupting current requirement may increase. Failure to recognize this could result in the catastrophic failure of a breaker.

6.8 Auxiliary Transformers

6.8.1 Selection of Percent Impedance

The transformer impedance is always compromised. High transformer impedance will limit fault current and reduce the required interrupting capability of switchgear and, therefore, reduce the cost. Low impedance will reduce the voltage drop through the transformer and therefore improve voltage regulation. A careful analysis using a load flow study will help in arriving at the best compromise.

6.8.2 Rating of Voltage Taps

Transformers should be supplied with taps to allow adjustment in bus voltage. Optimum tap settings can be determined using a load flow study.

6.9 Motors

6.9.1 Selection of Motors

Many motors are required in a thermal generating plant and range in size from fractional horsepower to several thousand horsepower. These motors may be supplied with the equipment they drive or they may be specified by the electrical engineer and purchased separately. The small motors are usually supplied by the equipment supplier and the large motors specified by the electrical engineer. How this will be handled must be resolved very early in the project. The horsepower cut-off point for each voltage level must be decided. The maximum plant voltage level must be established. A voltage of 13.8 kV may be required if very large horsepower motors are to be used. This must be established very early in the plant design so that a preliminary one-line diagram may be developed.

6.9.2 Types of Motors

6.9.2.1 Squirrel Cage Induction Motors

The squirrel cage induction motor is the most common type of large motor used in a thermal generating plant. Squirrel cage induction motors are very rugged and require very little maintenance.

6.9.2.2 Wound Rotor Induction Motors

The wound rotor induction motor has a rotor winding which is brought out of the motor through slip rings and brushes. While more flexible than a squire cage induction motor, the slip rings and brushes are an additional maintenance item. Wound rotor motors are only used in special applications in a power plant.

6.9.2.3 Synchronous Motors

Synchronous motors may be required in some applications. Large slow-speed, 1800 rpm or less may require a synchronous motor. A synchronous motor may used to supply VARs and improve voltage regulation. If the synchronous motor is going to be used as a VAR source, the field supply must be sized large enough to over-excite the field.

6.9.2.4 Direct Current Motors

Direct current motors are used primarily on emergency systems such as turbine lube oil and turbine turning gear. Direct current motors may also be used on some control valves.

6.9.2.5 Single-Phase Motors

Single-phase motors are fractional horsepower motors and are usually supplied with the equipment.

6.9.2.6 Motor Starting Limitations

The starting current for induction motors is about 6 times full load current. This must be taken into account when sizing transformers and should be part of the load flow analysis. If the terminal voltage is allowed to drop too low, below 80%, the motor will stall. Methods of reduced voltage starting are available, but should be avoided if possible. The most reliable designs are the simplest.

6.10 Main Generator

The turbine generator will be supplied as a unit. The size and characteristics are usually determined by the system planners as a result of system load requirements and system stability requirements.

6.10.1 Associated Equipment

6.10.1.1 Exciters and Excitation Equipment

The excitation system will normally be supplied with the generator.

6.10.2 Electronic Exciters

Modern excitation systems are solid state and, in recent years, most have digital control systems.

6.10.3 Generator Neutral Grounding

The generator neutral is never connected directly to ground. The method used to limit the phase to ground fault current to a value equal to or less than the three-phase fault current is determined by the way the generator is connected to the power system. If the generator is connected directly to the power system, a resistor or inductor connected between the neutral of the generator and ground will be used to limit the ground fault current. If the generator is connected to the power system through a transformer in a unit configuration, the neutral of the generator may be connected to ground through a distribution transformer with a resistor connected across the secondary of the transformer. The phase-to-ground fault current can be limited to 5 to 10 A using this method.

6.10.4 Isolated Phase Bus

The generator is usually connected to the step-up transformer through an isolated phase bus. This separated phase greatly limits the possibility of a phase-to-phase fault at the terminals of the generator.

6.11 Cable

Large amounts of cable are required in a thermal generating plant. Power, control, and instrumentation cable should be selected carefully with consideration given to long life. Great care should be given in the installation of all cable. Cable replacement can be very expensive.

6.12 Electrical Analysis

All electrical studies should be well-documented for use in plant modifications. These studies will be of great value in evaluating plant problems.

6.12.1 Load Flow

A load flow study should be performed as early in the design as possible even if the exact equipment is not known. The load flow study will help in getting an idea of transformer size and potential voltage drop problems.

A final load flow study should be performed to document the final design and will be very helpful if modifications are required in the future.

6.12.2 Short-Circuit Analysis

Short-circuit studies must be performed to determine the requirements for circuit breaker interrupting capability. Relay coordination should be studied as well.

6.12.3 Surge Protection

Surge protection may be required to limit transient overvoltage caused by lightning and circuit switching. A surge study should be performed to determine the needs of each plant configuration. Surge arrestors and/or capacitors may be required to limit transient voltages to acceptable levels.

6.12.4 Phasing

A phasing diagram should be made to determine correct transformer connections. An error here could prevent busses from being paralleled.

6.12.5 Relay Coordination Studies

Relay coordination studies should be performed to ensure proper coordination of the relay protection system. The protective relay system may include overcurrent relays, bus differential relays, transformer differential relays, voltage relays, and various special function relays.

6.13 Maintenance and Testing

A good plant design will take into account maintenance and testing requirements. Equipment must be accessible for maintenance and provisions should be made for test connections.

6.14 Start-Up

A start-up plan should be developed to ensure equipment will perform as expected. This plan should include insulation testing. Motor starting current magnitude and duration should be recorded and relay coordination studies verified. Voltage level and load current readings should be taken to verify load flow studies. This information will also be very helpful when evaluating plant operating conditions and problems.

References

General

Beeman, D., Ed., *Industrial Power Systems Handbook*, McGraw-Hill, New York.

Electrical Transmission and Distribution Reference Book, Westinghouse Electric Corporation.

IEEE Standard 666-1991, IEEE Design Guide for Electric Power Service Systems for Generating Stations.

Grounding

IEEE 665-1955, IEEE Guide for Generating Station Grounding.

IEEE 1050-1996, IEEE Guide for Instrumentation and control Grounding in Generating Stations.

DC Systems

IEEE 485-1997, IEEE Recommended Practice for Sizing Lead-Acid Batteries for Station Applications.

IEEE 946-1992, IEEE Recommended Practice for the Design of DC Auxiliary Power Systems for Generating Stations.

Switchgear

IEEE Standards Collection: Power and Energy-Switchgear, 1998 Edition.

Auxiliary Transformers

IEEE Distribution, Power and Regulating Transformers Standards Collection, 1998 Edition.

Motors

IEEE Electric Machinery Standards Collection, 1997 Edition.

Cable

IEEE 835-1994, IEEE Standard Power Cable Ampacity Tables.

Electrical Analysis

Clarke, E., *Circuit Analysis of AC Power Systems*, General Electric Company, 1961.

Stevenson, W.D., *Elements of Power Systems Analysis*, McGraw-Hill, New York, 1962.

Wager, C.F. and Evans, R.D., *Symmetrical Components*, McGraw-Hill, New York, 1933.

7

Distributed Utilities

John R. Kennedy
Georgia Power Company

Distributed utilities (sometimes referred to as DU) is the current term used in describing distributed generation and storage devices operating separately and in parallel with the utility grid. In most cases, these devices are small in comparison to traditional utility base or peaking generation, but can range up to several megawatts. For the purposes of this section, DU will be limited to devices 5 MW and below applied at either the secondary voltage level, 120 V single phase to 480 V three phase, and at the medium voltage level, 2.4 kV to 25 kV, although many of the issues discussed would apply to the larger units as well.

In this section, we will give an overview of the different issues associated with DU, including available technologies, interfacing, a short discussion on economics and possible regulatory treatment, applications, and some practical examples. Emerging technologies discussed will include fuel cells, microturbines, and small turbines. A brief discussion of storage technologies is also included. Interfacing issues include general protection, overcurrent protection, islanding issues, communication and control, voltage regulation, frequency control, fault detection, safety issues, and synchronization. In the applications section, deferred investment, demand reduction, peak shaving, ancillary services, reliability, and power quality will be discussed. Economics and possible regulatory treatment will be discussed briefly.

7.1 Available Technologies

Many of the "new" technologies have been around for several years, but the relative cost per kilowatt of small generators compared to conventional power plants has made their use limited. Utility rules and interconnect requirements have also limited the use of small generators and storage devices to mostly emergency, standby, and power quality applications. The prospect of deregulation has changed all that. Utilities are no longer assured that they can recover the costs of large base generation plants, and stranded investment of transmission and distribution facilities is a subject of debate. This, coupled with improvements in the cost and reliability of DU technologies, has opened an emerging market for small power plants. In the near future, these new technologies should be competitive with conventional plants, providing high reliability with less investment risk. Some of the technologies are listed below. All of the energy storage devices and many of the small emerging generation devices are inverter/converter

Technology	Size	Fuel Sources	AC Interface Type	Applications
Fuel Cells	.5Kw– Larger units With Stacking	Natural Gas Hydrogen Petroleum Products	Inverter type	Continuous
Microturbines	10Kw-100Kw Larger sizes	Natural Gas Petroleum Products	Inverter type	Continuous Standby
Batteries	.1Kw-2Mw+	Storage	Inverter type	PQ, Peaking
Flywheel	>.1Kw-.5Kw	Storage	Inverter type	PQ, Peaking
PV	>.1Kw-1Kw	Sunlight	Inverter type	Peaking
Gas Turbine	10Kw–5Mw+	Natural Gas Petroleum Products	Rotary type	Continuous, Peaking Standby

FIGURE 7.1 Distributed generation technology chart.

based. Figure 7.1 is a listing of different technologies, their size ranges, fuel sources, and AC interface type, and most likely applications.

7.2 Fuel Cells

Fuel cell technology has been around since its invention by William Grove in 1839. From the 1960s to the present, fuel cells have been the power source used for space flight missions. Unlike other generation technologies, fuel cells act like continuously fueled batteries, producing direct current (DC) by using an electrochemical process. The basic design of all fuel cells consists of an anode, electrolyte, and cathode. Hydrogen or a hydrogen-rich fuel gas is passed over the anode, and oxygen or air is passed over the cathode. A chemical combination then takes place producing a constant supply of electrons (DC current) with by-products of water, carbon dioxide, and heat. The DC power can be used directly or it can be fed to a power conditioner and converted to AC power (see Fig. 7.2).

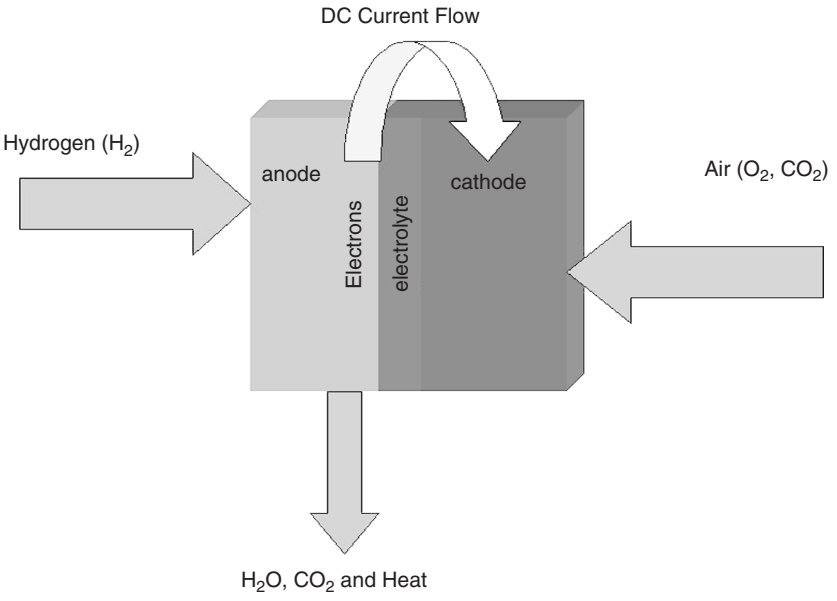

FIGURE 7.2 Basic fuel cell operation.

	PAFC	MCFC	SOFC	PEMFC
Electrolyte	Phosphoric acid	Molten carbonate salt	Ceramic	Polymer
Operating Temperature	375°F (190°C)	1200°F (650°C)	1830°F (1000°C)	175°F (80°C)
Fuels	Hydrogen (H_2)	H_2/CO	$H_2/CO_2/CH_4$	H_2
	Reformate	Reformate	Reformate	Reformate
Reforming	External	External	External	External
Oxidant	O_2/Air	CO_2/O_2/Air	O_2/Air	O_2/Air
Efficiency (HHV)	40–50%	50–60%	45–55%	40–50%

FIGURE 7.3 Comparison of fuel cell types. (From DoD Website, www.dodfuelcell.com/fcdescriptions.html.)

Most of the present technologies have a fuel reformer or processor that can take most hydrocarbon-based fuels, separate out the hydrogen, and produce high-quality power with negligible emissions. This would include gasoline, natural gas, coal, methanol, light oil, or even landfill gas. In addition, fuel cells can be more efficient than conventional generators. Theoretically they can obtain efficiencies as high as 85% when the excess heat produced in the reaction is used in a combined cycle mode. These features, along with relative size and weight, have also made the fuel cell attractive to the automotive industry as an alternative to battery power for electric vehicles. The major differences in fuel cell technology concern the electrolyte composition. The major types are the Proton Exchange Membrane Fuel Cell (PEFC) also called the PEM, the Phosphoric Acid Fuel Cell (PAFC), the Molten Carbonate Fuel Cell (MCFC), and the Solid Oxide Fuel Cell (SOFC) (Fig. 7.3).

Fuel cell power plants can come in sizes ranging from a few watts to several megawatts with stacking. The main disadvantage to the fuel cell is the initial high cost of installation. With the interest in efficient and environmentally friendly generation, coupled with the automotive interest in an EV alternative power source, improvements in the technology and lower costs are expected. As with all new technologies, volume of sales should also lower the unit price.

7.3 Microturbines

Experiments with microturbine technology have been around for many decades, with the earliest attempts of wide-scale applications being targeted at the automotive and transportation markets. These experiments later expanded into markets associated with military and commercial aircraft and mobile systems. Microturbines are typically defined as systems with an output power rating of between 10 kW up to a few hundred kilowatts. As shown in Fig. 7.4, these systems are usually a single-shaft design with compressor, turbine, and generator all on the common shaft, although some companies are engineering dual-shaft systems. Like the large combustion turbines, the microturbines are Brayton Cycle systems, and will usually have a recuperator in the system.

The recuperator is incorporated as a means of increasing efficiency by taking the hot turbine exhaust through a heavy (and relatively expensive) metallic heat exchanger and transferring the heat to the input air, which is also passed through parallel ducts of the recuperator. This increase in inlet air temperature helps reduce the amount of fuel needed to raise the temperature of the gaseous mixture during combustion to levels required for total expansion in the turbine. A recuperated Brayton Cycle microturbine can operate at efficiencies of approximately 30%, while these aeroderivative systems operating without a recuperator would have efficiencies in the mid-teens.

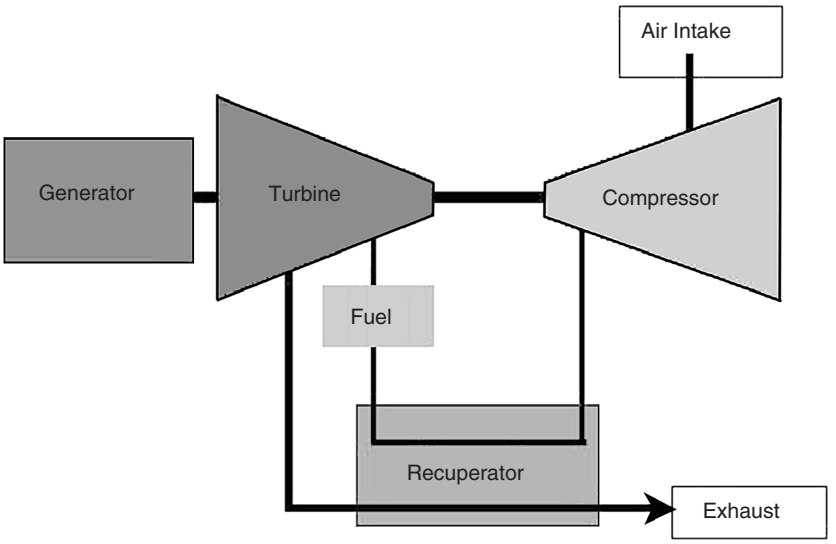

FIGURE 7.4 Turbine block diagram configuration with recuperator.

Another requirement of microturbine systems is that the shaft must spin at very high speeds, in excess of 50,000 RPM and in some cases doubling that rate, due to the low inertia of the shaft and connected components. This high speed is used to keep the weight of the system low and increase the power density over other generating technologies. Although many of the microturbines are touted as having only a single moving part, there are numerous ancillary devices required that do incorporate moving parts such as cooling fans, fuel compressors, and pumps.

Since the turbine requires extremely high speeds for optimal performance, the generator cannot operate as a synchronous generator. Typical microturbines have a permanent magnet motor/generator incorporated onto the shaft of the system. The high rotational speed gives an AC output in excess of 1000 Hz, depending on the number of poles and actual rotational speed of the microturbine. This high-frequency AC source is rectified, forming a common DC bus voltage that is then converted to a 60-Hz AC output by an onboard inverter.

The onboard electronics are also used to start the microturbine, either in a stand-alone mode or in grid parallel applications. Typically, the utility voltage will be rectified and the electronics are used to convert this DC voltage into a variable frequency AC source. This variable frequency drive will power the permanent magnet motor/generator (which is operating as a motor), and will ramp the turbine speed up to a preset RPM, a point where stabile combustion and control can be maintained. Once this preset speed is obtained and stabile combustion is taking place, the drive shuts down and the turbine speed increases until the operating point is maintained and the system operates as a generator. The time from a "Shaft Stop" to full load condition is anywhere from 30 sec to 3 min, depending on manufacturer recommendations and experiences.

Although things are in the early stages of commercialization of the microturbine products, there are cost targets that have been announced from all of the major manufacturers of these products. The early market entry price of these systems is in excess of $600 per kW, more than comparably sized units of alternative generation technologies, but all of the major suppliers have indicated that costs will fall as the number of units being put into the field increases.

The microturbine family has a very good environmental rating, due to natural gas being a primary choice for fuel and the inherent operating characteristics, which puts these units at an advantage over diesel generation systems.

7.4 Combustion Turbines

There are two basic types of combustion turbines (CTs) other than the microturbines: the heavy frame industrial turbines and the aeroderivative turbines. The heavy frame systems are derived from similar models that were steam turbine designs. As can be identified from the name, they are of very heavy construction. The aeroderivative systems have a design history from the air flight industry, and are of a much lighter and higher speed design. These types of turbines, although similar in operation, do have some significant design differences in areas other than physical size. These include areas such as turbine design, combustion areas, rotational speed, and air flows.

Although these units were not originally designed as a "distributed generation" technology, but more so for central station and large co-generation applications, the technology is beginning to economically produce units with ratings in the hundreds of kilowatts and single-digit megawatts. These turbines operate as Brayton Cycle systems and are capable of operating with various fuel sources. Most applications of the turbines as distributed generation will operate on either natural gas or fuel oil. The operating characteristics between the two systems can best be described in tabular form as shown in Fig. 7.5.

The combustion turbine unit consists of three major mechanical components: a compressor, a combustor, and a turbine. The compressor takes the input air and compresses it, which will increase the temperature and decrease the volume per the Brayton Cycle. The fuel is then added and the combustion takes place in the combustor, which increases both the temperature and volume of the gaseous mixture, but leaves the pressure as a constant. This gas is then expanded through the turbine where the power is extracted through the decrease in pressure and temperature and the increase in volume.

If efficiency is the driving concern, and the capital required for the increased efficiency is available, the Brayton Cycle systems can have either co-generation systems, heat recovery steam generators, or simple recuperators added to the combustion turbine unit. Other equipment modifications and improvements can be incorporated into these types of combustion turbines such as multistage turbines with fuel re-injection, inter-cooler between multistage compressors, and steam/water injection.

Typical heat rates for simple cycle combustion turbines vary across manufacturers, but are in a range from 11,000 to 20,000 BTU/kWh. However, these numbers decrease as recuperation and co-generation are added. CTs typically have a starting reliability in the 99% range and operating reliability approaching 98%. The operating environment has a major effect on the performance of combustion turbines. The elevation at which the CT is operating has a degradation factor of around 3.5% per 1000 ft of increased elevation and the ambient temperature has a similar degradation per 10° increase.

Figure 7.6 shows a block diagram of a simple cycle combustion turbine with a recuperator (left) and a combustion turbine with multistage turbine and fuel re-injection (right).

	Heavy Frame	Aeroderivative
Size (Same General Rating)	Large	Compact
Shaft Speed	Synchronous	Higher Speed (coupled through a gear box)
Air Flow	High (lower compression)	Lower (high compression)
Start-up Time	15 Minutes	2-3 minutes

FIGURE 7.5 Basic combustion turbine operating characteristics.

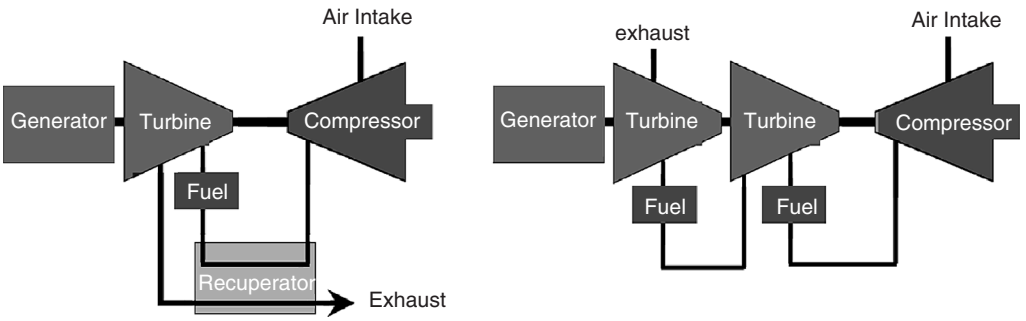

FIGURE 7.6 Basic combustion turbine designs.

7.5 Storage Technologies

Storage technologies include batteries, flywheels, ultra-capacitors, and to some extent photovoltaics. Most of these technologies are best suited for power quality and reliability enhancement applications, due to their relative energy storage capabilities and power density characteristics, although some large battery installations could be used for peak shaving. All of the storage technologies have a power electronic converter interface and can be used in conjunction with other DU technologies to provide "seamless" transitions when power quality is a requirement.

7.6 Interface Issues

A whole chapter could be written just about interface issues, but this discussion will touch on the highlights. Most of the issues revolve around safety and quality of service. We will discuss some general guidelines and the general utility requirements and include examples of different considerations. In addition to the interface issues, the DU installation must also provide self-protection to prevent short circuit or other damage to the unit. Self-protection will not be discussed here. The most important issues are listed in Table 7.1.

In addition to the interface issues identified in Table 7.1, there are also operating limits that must be considered. These are listed in Table 7.2.

TABLE 7.1 Interface Issues

Issue	Definition	Concern
Automatic reclosing	Utility circuit breakers can test the line after a fault.	If a generator is still connected to the system, it may not be in synchronization, thus damaging the generator or causing another trip.
Faults	Short circuit condition on the utility system.	Generator may contribute additional current to the fault, causing a miss operation of relay equipment.
Islanding	A condition where a portion of the system continues to operate isolated from the utility system.	Power quality, safety, and protection may be compromised in addition to possible synchronization problems.
Protection	Relays, instrument transformers, circuit breakers.	Devices must be utility grade rather than industrial grade for better accuracy. Devices must also be maintained on a regular schedule by trained technicians.
Communication	Devices necessary for utility control during emergency conditions.	Without control of the devices, islanding and other undesirable operation of devices.

TABLE 7.2 Operating Limits

1.	Voltage—The operating range for voltage must maintain a level of ±15% of nominal for service voltage (ANSI C84.1), and have a means of automatic separation if the level gets out of the acceptable range within a specified time.
2.	Flicker—Flicker must be within the limits as specified by the connecting utility. Methods of controlling flicker are discussed in IEEE Std. 519-1992, 10.5.
3.	Frequency—Frequency must be maintained within ±0.5 Hz of 60 Hz and have an automatic means of disconnecting if this is not maintained. If the system is small and isolated, there might be a larger frequency window. Larger units may require an adjustable frequency range to allow for clock synchronizaton.
4.	Power factor—The power factor should be within 0.85 lagging or leading for normal operation. Some systems that are designed for compensation may operate outside these limits.
5.	Harmonics—Both voltage and current harmonics must comply with the values for generators as specified in IEEE Std. 519-1992 for both total and individual harmonics.

Utility requirements vary but generally depend on the application of a distributed source. If the unit is being used strictly for emergency operation, open transition peak shaving, or any other stand-alone type operation, the interface requirements are usually fairly simple, since the units will not be operating in parallel with the utility system. When parallel operation is anticipated or required, the interface requirements become more complex. Protection, safety, power quality, and system coordination become issues that must be addressed. In the case of parallel operation, there are generally three major factors that determine the degree of protection required. These would include the size and type of the generation, the location on the system, and how the installation will operate (one-way vs. two-way). Generator sizes are generally classified as:

Large: Greater than 3 MVA or possibility of "islanding" a portion of the system
Small: Between large and extremely small
Extremely small: Generation less than 100 kVA

Location on the system and individual system characteristics determine impedance of a distribution line, which in turn determines the available fault current and other load characteristics that influence "islanding" and make circuit protection an issue. This will be discussed in more detail later.

The type of operation is the other main issue and is one of the main determinants in the amount of protection required. One-way power flow where power will not flow back into the utility has a fairly simple interface, but is dependent on the other two factors, while two-way interfaces can be quite complex. An example is shown in Fig. 7.7. Smaller generators and "line-commutated" units would have less stringent requirements. Commutation methods will be discussed later. Reciprocating engines such as diesel and turbines with mass, and "self-commutating" units which could include microturbines and fuel cells, would require more stringent control packages due to their islanding and reverse power capabilities.

Most of the new developing technologies are inverter based and there are efforts now in IEEE to revise the old Standard P929 *Recommended Practice for Utility Interface of Photovoltaic (PV) Systems* to include other inverter-based devices. The standards committee is looking at the issues with inverter-based devices in an effort to develop a standard interface design that will simplify and reduce the cost, while not sacrificing the safety and operational concerns. Inverter interfaces generally fall into two classes: line-commutated inverters and self-commutated inverters.

7.6.1 Line-Commutated Inverters

These inverters require a switching signal from the line voltage in order to operate. Therefore, they will cease operation if the line signal, i.e., utility voltage, is abnormal or interrupted. These are not as popular today for single-phase devices due to the filtering elements required to meet the harmonic distortion requirements, but are appearing in some of the three-phase devices where phase cancellation minimizes the use of the additional components.

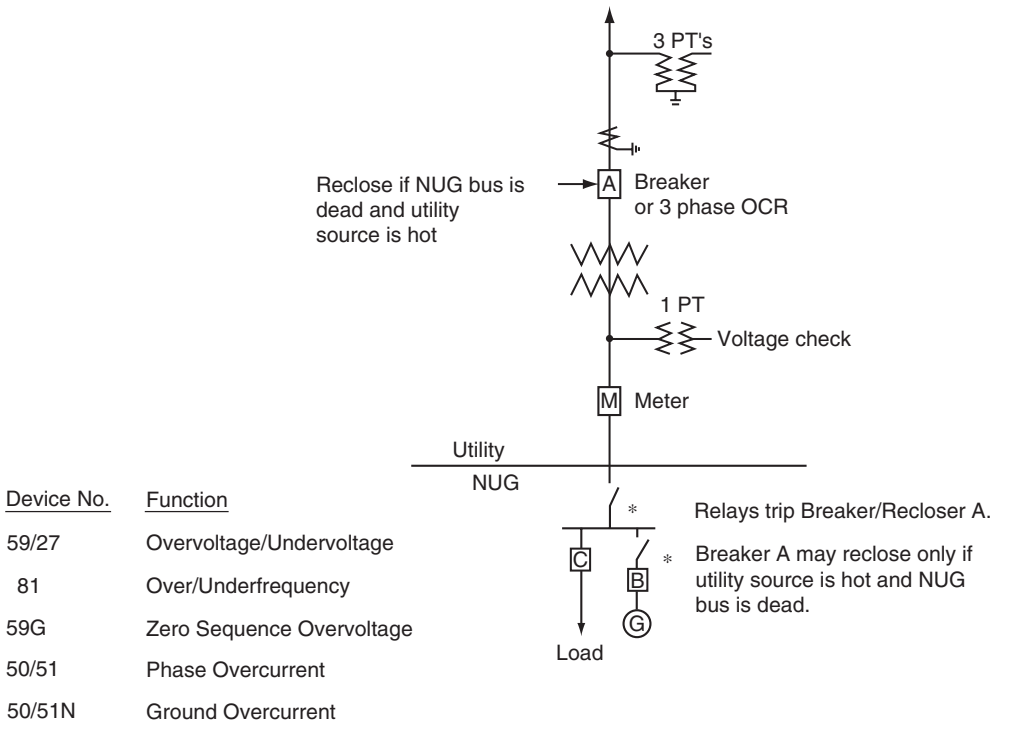

FIGURE 7.7 Example of large generator interface requirements for distribution. (From *Georgia Power Bulletin*, 18–8, generator interface requirements.)

7.6.2 Self-Commutated Inverters

These inverters, as implied by the name, are self-commutating. All stand-alone units are self-commutated, but not all self-commutated inverters are stand-alone. They can be designed as either voltage or current sources and most that are now being designed to be connected to the utility system are designed to be current sources. These units still use the utility voltage signal as a comparison and produce current at that voltage and frequency. A great deal of effort has gone into the development of non-islanding inverters that are of this type.

7.7 Applications

Applications vary and will become more diverse as utilities unbundle. Listed below are some examples of the most likely.

7.7.1 Ancillary Services

Ancillary services support the basic electrical services and are essential for the reliability and operation of the electric power system. The electrical services that are supported include generating capacity, energy supply, and the power delivery system. FERC requires six ancillary services, including system control, regulation (frequency), contingency reserves (both spinning and supplemental), voltage control, and energy imbalance. In addition, load following, backup supply, network stability, system "black-start", loss replacement, and dynamic scheduling are necessary for the operation of the system. Utilities have been performing these functions for decades, but as vertically integrated regulated monopoly

organizations. As these begin to disappear, and a new structure with multiple competing parties emerges, distributed utilities might be able to supply several of these.

The distributed utilities providing these services could be owned by the former traditional utility, customers, or third-party brokers, depending on the application. The main obstacles to this approach are aggregation and communication when dealing with many small resources rather than large central station sources.

7.7.2 "Traditional Utility" Applications

Traditional utilities may find the use of DU a practical way to solve loading and reliability problems if each case is evaluated on a stand-alone individual basis. Deferring investment is one likely way that DU can be applied. In many areas, substations and lines have seasonal peaks that are substantially higher than the rest of the year. In these cases, the traditional approach has been to increase the capacity to meet the demand. Based on the individual situation, delaying the upgrade for 2 to 5 years with a DU system could be a more economical solution. This would be especially true if different areas had different seasonal peaks and the DU system was portable, thus deferring two upgrades. DU could also be used instead of conventional facilities when backup feeds are required or to improve reliability or power quality.

In addition, peak shaving and generation reserve could be provided with strategically placed DU systems that take advantage of reducing system losses as well as offsetting base generation. Again, these have to be evaluated on an individual case basis and not a system average basis as is done in many economic studies. The type of technology used will depend on the particular requirements. In general, storage devices such as flywheels and batteries are better for power quality applications due to their fast response time, in many cases half a cycle. Generation devices are better suited for applications that require more than 30 min of supply, such as backup systems, alternate feeds, peak shaving, and demand deferrals. Generation sources can also be used instead of conventional facilities in certain cases.

7.7.3 Customer Applications

Individual customers with special requirements may find DU technologies that meet their needs. Customers who require "enhanced" power quality and reliability of service already utilize UPS systems with battery backup to condition the power to sensitive equipment, and many hospitals, waste treatment plants, and other emergency services providers have emergency backup systems supplied by standby generator systems. As barriers go down and technologies improve, customer-sited DU facilities could provide many of the ancillary services as well as sell excess power into the grid. Fuel cell and even diesel generators could be especially attractive for customers with requirements of heat and steam. Many of the fuel cell technologies are now looking at the residential market with small units that would be connected to the grid but supply the additional requirements for customers with special power quality needs.

7.7.4 Third-Party Service Providers

Third-party service providers could provide all the services listed above for the utilities and customers, in addition to selling power across the grid. In many cases, an end user does not have the expertise to operate and maintain generation systems and would prefer to purchase the services.

7.8 Conclusions

Disbursed generation will be a part of the distribution utility system of the future. Economics, regulatory requirements, and technology improvements will determine the speed at which they are integrated.

References

ANSI/IEEE Std. 1001–1998, *IEEE Guide for Interfacing Dispersed Storage and Generation Facilities with Electric Utility Systems*, IEEE Standards Coordinating Committee 23, Feb. 9, 1989.

Davis, M.W. *Microturbines—An Economic and Reliability Evaluation for Commercial, Residential, and Remote Load Applications*, IEEE Transactions PE-480-PWRS-0-10-1998.

Delmerico, R.W., Miller, N.W., and Owen, E.L. *Power System Integration Strategies for Distributed Generation*, Power Systems Energy Consulting GE International, Inc., Distributed Electricity Generation Conference, Denver, CO, Jan. 25, 1999.

Department of Defense Website, www.dodfuelcell.com/fcdescriptions.html.

Goldstein, H.L. *Small Turbines in Distributed Utility Application Natural Gas Pressure Supply Requirements*, NREL/SP-461-21073, May, 1996.

Hirschenhofer, J.H. DOE Forum on Fuel Cell Technologies, IEEE Winter Power Meeting, Parsons Corporation Presentation, Feb. 4, 1999.

Kirby, B. *Distributed Generation: A Natural for Ancillary Services*, Distributed Electric Generation Conference, Denver CO, Jan. 25, 1999.

Oplinger, J.L. *Methodology to Assess the Market Potential of Distributed Generation*, Power Systems Energy Consulting GE International, Inc., Distributed Electric Generation Conference, Denver, CO, Jan. 25, 1999.

Recommended Practice for Utility Interface of Photovoltaic (PV) Systems, IEEE Standard P929, Draft 10, Feb. 1999.

Southern Company Parallel Operation Requirements, Protection and Control Committee, Aug. 4, 1998.

Technology Overviews, DOE Forum on Fuel Cell Technology, IEEE Winter Power Meeting, Feb. 4, 1999.

III

Transmission System

George G. Karady
Arizona State University

8

Concept of Energy Transmission and Distribution

George G. Karady
Arizona State University

The purpose of the electric transmission system is the interconnection of the electric energy producing power plants or generating stations with the loads. A three-phase AC system is used for most transmission lines. The operating frequency is 60 Hz in the U.S. and 50 Hz in Europe, Australia, and part of Asia. The three-phase system has three phase conductors. The system voltage is defined as the rms voltage between the conductors, also called line-to-line voltage. The voltage between the phase conductor and ground, called line-to-ground voltage, is equal to the line-to-line voltage divided by the square root of three. Figure 8.1 shows a typical system.

The figure shows the Phoenix area 230-kV system, which interconnects the local power plants and the substations supplying different areas of the city. The circles are the substations and the squares are the generating stations. The system contains loops that assure that each load substation is supplied by at least two lines. This assures that the outage of a single line does not cause loss of power to any customer. For example, the Aqua Fria generating station (marked: Power plant) has three outgoing lines. Three high-voltage cables supply the Country Club Substation (marked: Substation with cables). The Pinnacle Peak Substation (marked: Substation with transmission lines) is a terminal for six transmission lines. This example shows that the substations are the node points of the electric system. The system is interconnected with the neighboring systems. As an example, one line goes to Glen Canyon and the other to Cholla from the Pinnacle Peak substation.

In the middle of the system, which is in a congested urban area, high-voltage cables are used. In open areas, overhead transmission lines are used. The cost per mile of overhead transmission lines is 6 to 10% less than underground cables.

The major components of the electric system, the transmission lines, and cables are described briefly below [1].

8.1 Generation Stations

The generating station converts the stored energy of gas, oil, coal, nuclear fuel, or water position to electric energy. The most frequently used power plants are:

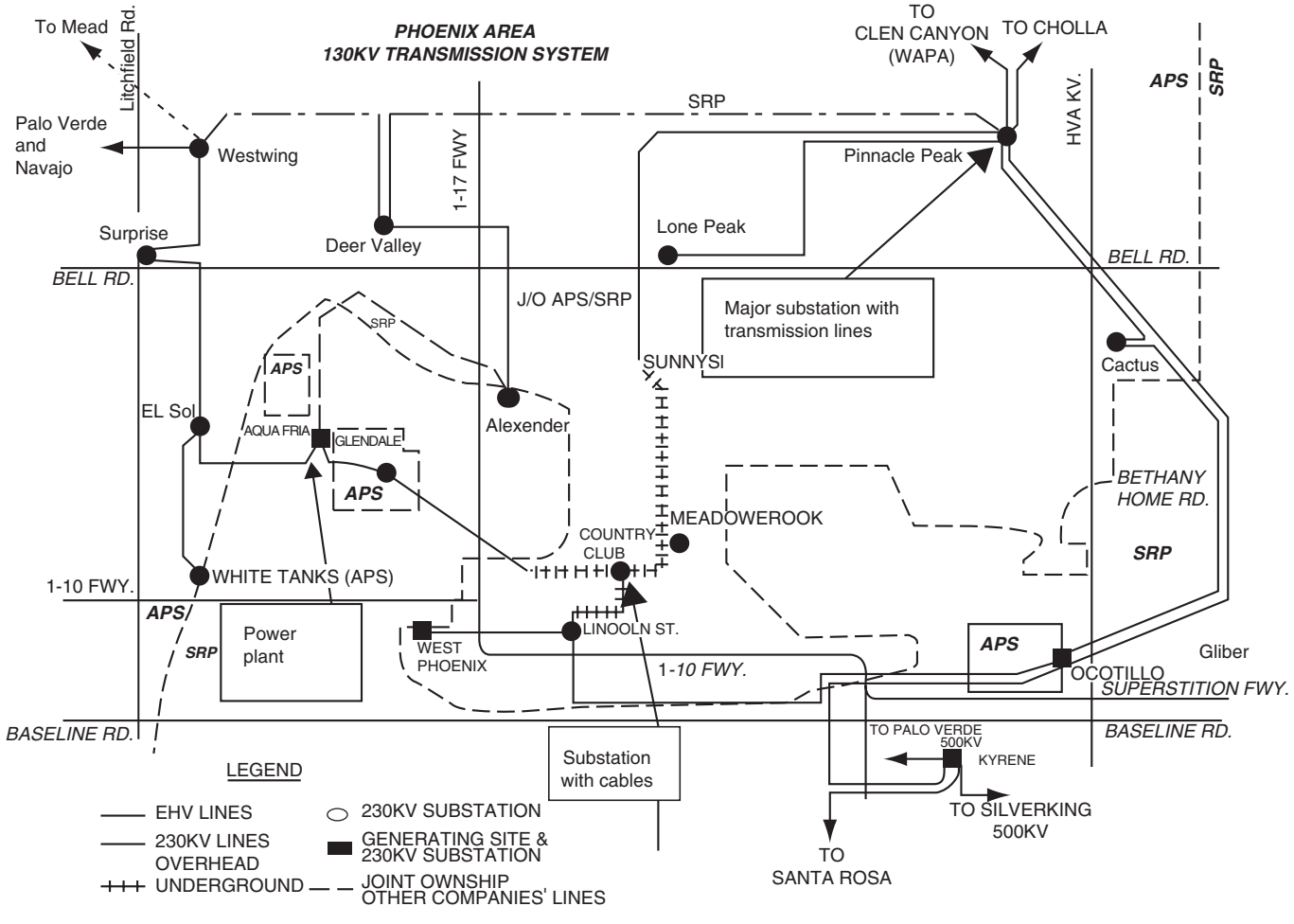

FIGURE 8.1 One line diagram of a high voltage electric transmission system.

Thermal Power Plant. The fuel is pulverized coal or natural gas. Older plants may use oil. The fuel is mixed with air and burned in a boiler that generates steam. The high-pressure and high-temperature steam drives the turbine, which turns the generator that converts the mechanical energy to electric energy.

Nuclear Power Plant. Enriched uranium produces atomic fission that heats water and produces steam. The steam drives the turbine and generator.

Hydro Power Plants. A dam increases the water level on a river, which produces fast water flow to drive a hydro-turbine. The hydro-turbine drives a generator that produces electric energy.

Gas Turbine. Natural gas is mixed with air and burned. This generates a high-speed gas flow that drives the turbine, which turns the generator.

Combined Cycle Power Plant. This plant contains a gas turbine that generates electricity. The exhaust from the gas turbine is high-temperature gas. The gas supplies a heat exchanger to preheat the combustion air to the boiler of a thermal power plant. This process increases the efficiency of the combined cycle power plant. The steam drives a second turbine, which drives the second generator. This two-stage operation increases the efficiency of the plant.

8.2 Switchgear

The safe operation of the system requires switches to open lines automatically in case of a fault, or manually when the operation requires it. Figure 8.2 shows the simplified connection diagram of a generating station.

The generator is connected directly to the low-voltage winding of the main transformer. The transformer high-voltage winding is connected to the bus through a circuit breaker, disconnect switch, and current transformer. The generating station auxiliary power is supplied through an auxiliary transformer through a circuit breaker, disconnect switch, and current transformer. Generator circuit breakers, connected between the generator and transformer, are frequently used in Europe. These breakers have to interrupt the very large short-circuit current of the generators, which results in high cost.

The high-voltage bus supplies two outgoing lines. The station is protected from lightning and switching surges by a surge arrester.

Circuit breaker (CB) is a large switch that interrupts the load and fault current. Fault detection systems automatically open the CB, but it can be operated manually.

Disconnect switch provides visible circuit separation and permits CB maintenance. It can be operated only when the CB is open, in no-load condition.

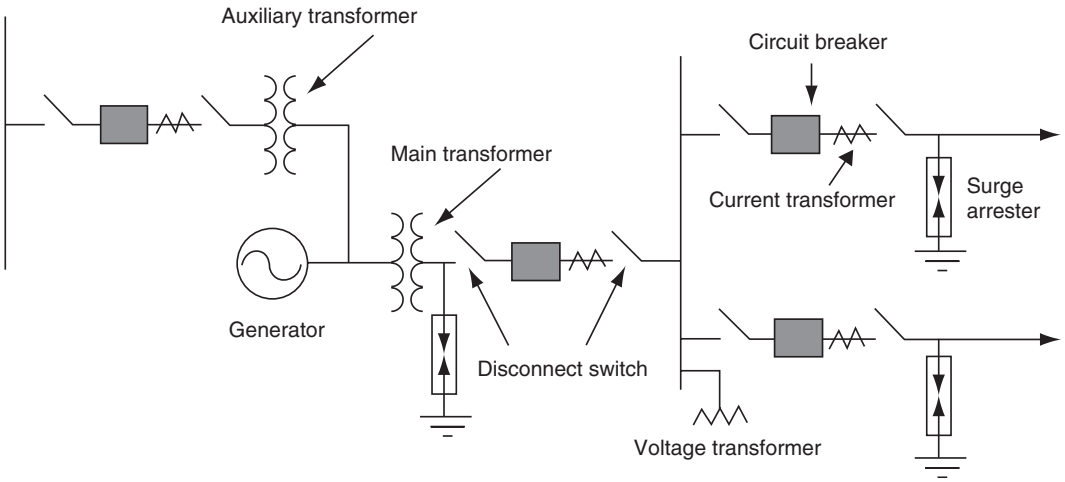

FIGURE 8.2 Simplified connection diagram of a generating station.

Potential transformers (PT) and current transformers (CT) reduce the voltage to 120 V, the current to 5 A, and insulates the low-voltage circuit from the high-voltage. These quantities are used for metering and protective relays. The relays operate the appropriate CB in case of a fault.

Surge arresters are used for protection against lightning and switching overvoltages. They are voltage dependent, nonlinear resistors.

8.3 Control Devices

In an electric system the voltage and current can be controlled. The voltage control uses parallel connected devices, while the flow or current control requires devices connected in series with the lines.

Tap-changing transformers are frequently used to control the voltage. In this system, the turns-ratio of the transformer is regulated, which controls the voltage on the secondary side. The ordinary tap changer uses a mechanical switch. A thyristor-controlled tap changer has recently been introduced.

A shunt capacitor connected in parallel with the system through a switch is the most frequently used voltage control method. The capacitor reduces lagging-power-factor reactive power and improves the power factor. This increases voltage and reduces current and losses. Mechanical and thyristor switches are used to insert or remove the capacitor banks.

The frequently used Static Var Compensator (SVC) consists of a switched capacitor bank and a thyristor-controlled inductance. This permits continuous regulation of reactive power.

The current of a line can be controlled by a capacitor connected in series with the line. The capacitor reduces the inductance between the sending and receiving points of the line. The lower inductance increases the line current if a parallel path is available.

In recent years, electronically controlled series compensators have been installed in a few transmission lines. This compensator is connected in series with the line, and consists of several thyristor-controlled capacitors in series or parallel, and may include thyristor-controlled inductors.

Medium- and low-voltage systems use several other electronic control devices. The last part in this section gives an outline of the electronic control of the system.

8.4 Concept of Energy Transmission and Distribution

Figure 8.3 shows the concept of typical energy transmission and distribution systems. The generating station produces the electric energy. The generator voltage is around 15 to 25 kV. This relatively low voltage is not appropriate for the transmission of energy over long distances. At the generating station a transformer is used to increase the voltage and reduce the current. In Fig. 8.3 the voltage is increased to 500 kV and an extra-high-voltage (EHV) line transmits the generator-produced energy to a distant substation. Such substations are located on the outskirts of large cities or in the center of several large loads. As an example, in Arizona, a 500-kV transmission line connects the Palo Verde Nuclear Station to the Kyrene and Westwing substations, which supply a large part of the city of Phoenix.

The voltage is reduced at the 500 kV/220 kV EHV substation to the high-voltage level and high-voltage lines transmit the energy to high-voltage substations located within cities.

At the high-voltage substation the voltage is reduced to 69 kV. Sub-transmission lines connect the high-voltage substation to many local distribution stations located within cities. Sub-transmission lines are frequently located along major streets [2,3].

The voltage is reduced to 12 kV at the distribution substation. Several distribution lines emanate from each distribution substation as overhead or underground lines. Distribution lines distribute the energy along streets and alleys. Each line supplies several step-down transformers distributed along the line. The distribution transformer reduces the voltage to 230/115 V, which supplies houses, shopping centers, and other local loads. The large industrial plants and factories are supplied directly by a subtransmission line or a dedicated distribution line as shown in Fig. 8.3.

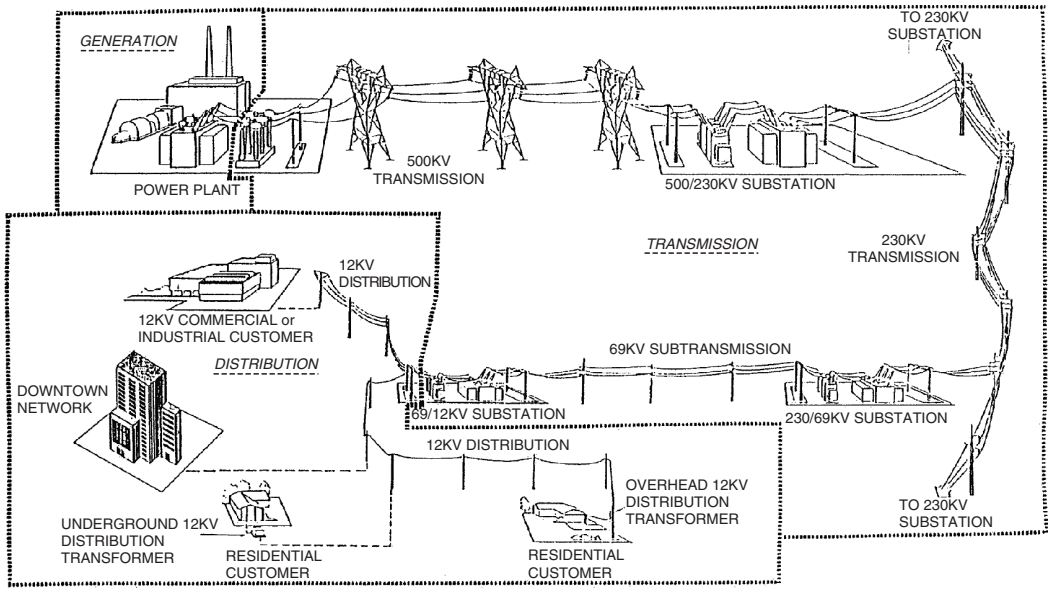

FIGURE 8.3 Concept of electric energy transmission.

The overhead transmission lines are used in open areas such as interconnections between cities or along wide roads within the city. In congested areas within cities, underground cables are used for electric energy transmission. The underground transmission system is environmentally preferable but has a significantly higher cost. In Fig. 8.3 the 12-kV line is connected to a 12-kV cable which supplies commercial or industrial customers [4]. The figure also shows 12-kV cable networks supplying downtown areas in a large city. Most newly developed residential areas are supplied by 12-kV cables through pad-mounted step-down transformers as shown in Fig. 8.3.

8.4.1 High-Voltage Transmission Lines

Highvoltage and extra-high-voltage (EHV) transmission lines interconnect power plants and loads, and form an electric network. Figure 8.4 shows a typical high-voltage and EHV system.

This system contains 500-kV, 345-kV, 230-kV, and 115-kV lines. The figure also shows that the Arizona (AZ) system is interconnected with transmission systems in California, Utah, and New Mexico. These interconnections provide instantaneous help in case of lost generation in the AZ system. This also permits the export or import of energy, depending on the needs of the areas.

Presently, synchronous ties (AC lines) interconnect all networks in the eastern U.S. and Canada. Synchronous ties also (AC lines) interconnect all networks in the western U.S. and Canada. Several non-synchronous ties (DC lines) connect the East and the West. These interconnections increase the reliability of the electric supply systems.

In the U.S., the nominal voltage of the high-voltage lines is between 100 kV and 230 kV. The voltage of the extra-high-voltage lines is above 230 kV and below 800 kV. The voltage of an ultra-high-voltage line is above 800 kV. The maximum length of high-voltage lines is around 200 miles. Extra-high-voltage transmission lines generally supply energy up to 400–500 miles without intermediate switching and var support. Transmission lines are terminated at the bus of a substation.

The physical arrangement of most extra-high-voltage (EHV) lines is similar. Figure 8.5 shows the major components of an EHV, which are:

1. Tower: The figure shows a lattice, steel tower.
2. Insulator: V strings hold four bundled conductors in each phase.
3. Conductor: Each conductor is stranded, steel reinforced aluminum cable.

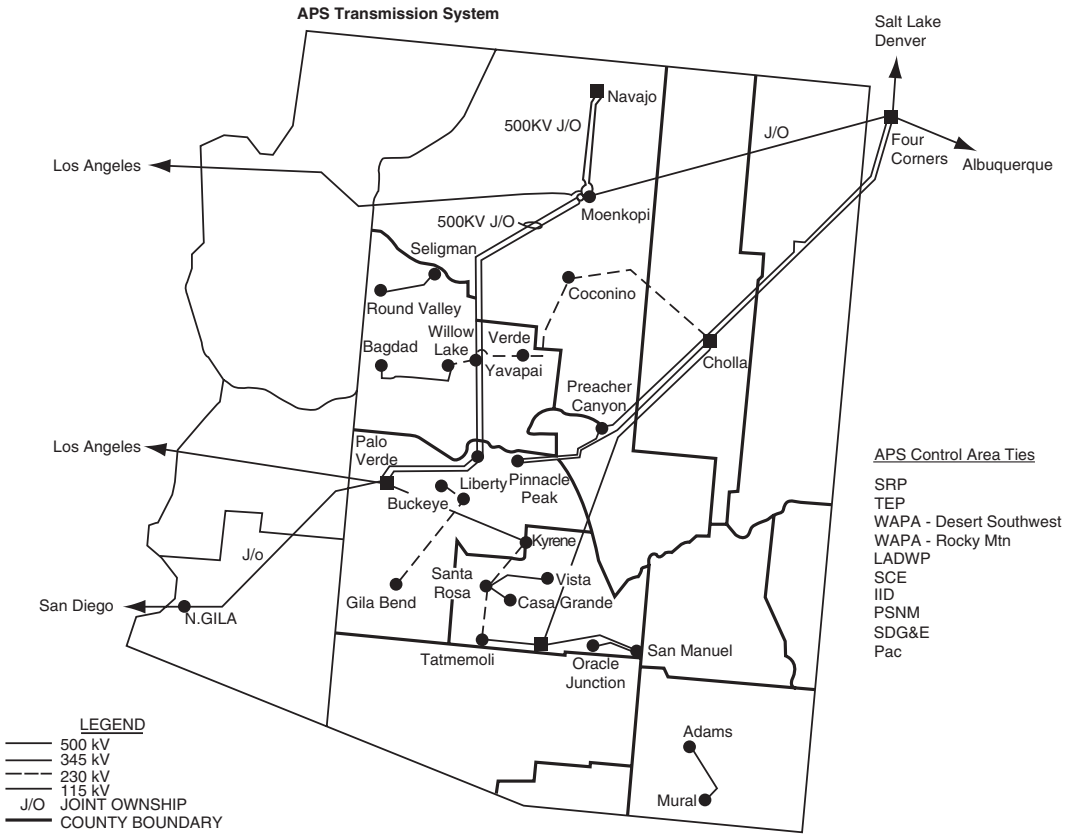

FIGURE 8.4 Typical high-voltage and EHV transmission system (Arizona Public Service, Phoenix area system).

4. Foundation and grounding: Steel-reinforced concrete foundation and grounding electrodes placed in the ground.
5. Shield conductors: Two grounded shield conductors protect the phase conductors from lightning.

At lower voltages the appearance of lines can be improved by using more aesthetically pleasing steel tubular towers. Steel tubular towers are made out of a tapered steel tube equipped with banded arms. The arms hold the insulators and the conductors. Figure 8.6 shows typical 230-kV steel tubular and lattice double-circuit towers. Both lines carry two three-phase circuits and are built with two conductor bundles to reduce corona and radio and TV noise. Grounded shield conductors protect the phase conductors from lightning [1].

8.4.2 High-Voltage DC Lines

High-voltage DC lines are used to transmit large amounts of energy over long distances or through waterways. One of the best known is the Pacific HVDC Intertie, which interconnects southern California with Oregon. Another DC system is the $\pm$400 kV Coal Creek-Dickenson lines. Another famous HVDC system is the interconnection between England and France, which uses underwater cables. In Canada, Vancouver Island is supplied through a DC cable.

In an HVDC system the AC voltage is rectified and a DC line transmits the energy. At the end of the line an inverter converts the DC voltage to AC. A typical example is the Pacific HVDC Intertie that operates with $\pm$500 kV voltage and interconnects Southern California with the hydro stations in Oregon.

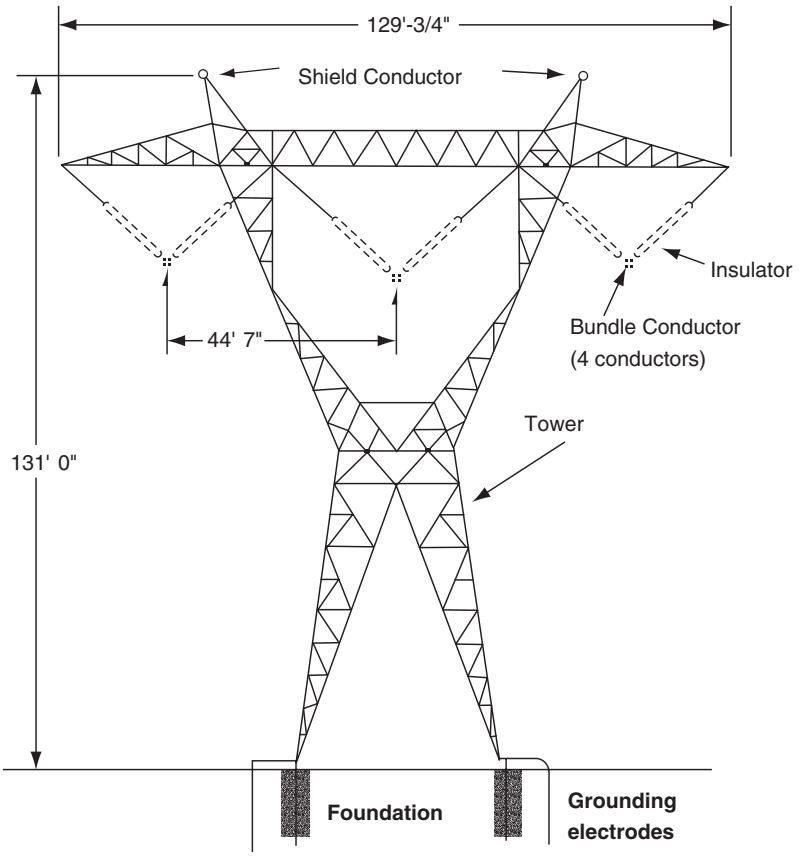

FIGURE 8.5 Typical high-voltage transmission line. (From Fink, D.G. and Beaty, H.W., *Standard Handbook for Electrical Engineering*, 11th ed., McGraw-Hill, New York, 1978.)

Figure 8.7 shows a guyed tower arrangement used on the Pacific HVDC Intertie. Four guy wires balance the lattice tower. The tower carries a pair of two-conductor bundles supported by suspension insulators.

8.4.3 Sub-Transmission Lines

Typical sub-transmission lines interconnect the high-voltage substations with distribution stations within a city. The voltage of the subtransmission system is between 46 kV, 69 kV, and 115 kV. The maximum length of sub-transmission lines is in the range of 50–60 miles. Most subtransmission lines are located along streets and alleys. Figure 8.8 shows a typical sub-transmission system.

This system operates in a looped mode to enhance continuity of service. This arrangement assures that the failure of a line will not interrupt the customer's power.

Figure 8.9 shows a typical double-circuit sub-transmission line, with a wooden pole and post-type insulators. Steel tube or concrete towers are also used. The line has a single conductor in each phase. Post insulators hold the conductors without metal cross arms. One grounded shield conductor on the top of the tower shields the phase conductors from lightning. The shield conductor is grounded at each tower. Plate or vertical tube electrodes (ground rod) are used for grounding.

8.4.4 Distribution Lines

The distribution system is a radial system. Figure 8.10 shows the concept of a typical urban distribution system. In this system a main three-phase feeder goes through the main street. Single-phase subfeeders

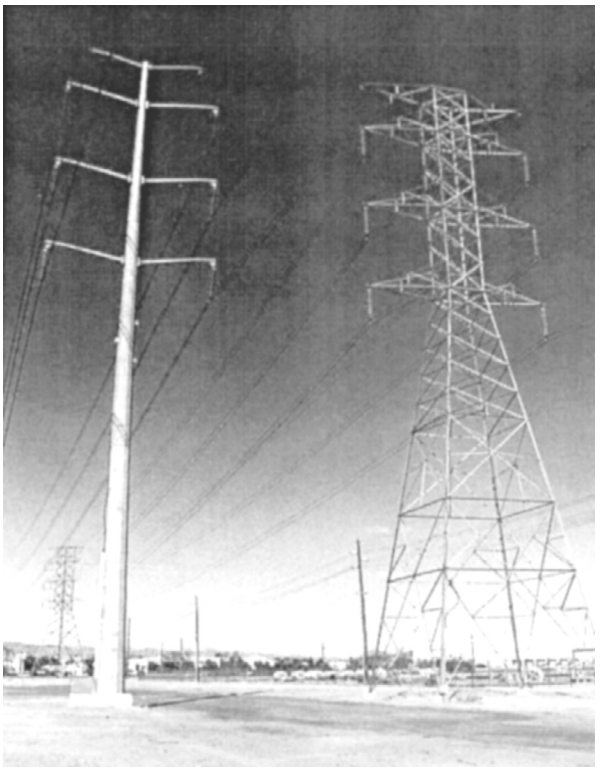

FIGURE 8.6 Typical 230-kV constructions.

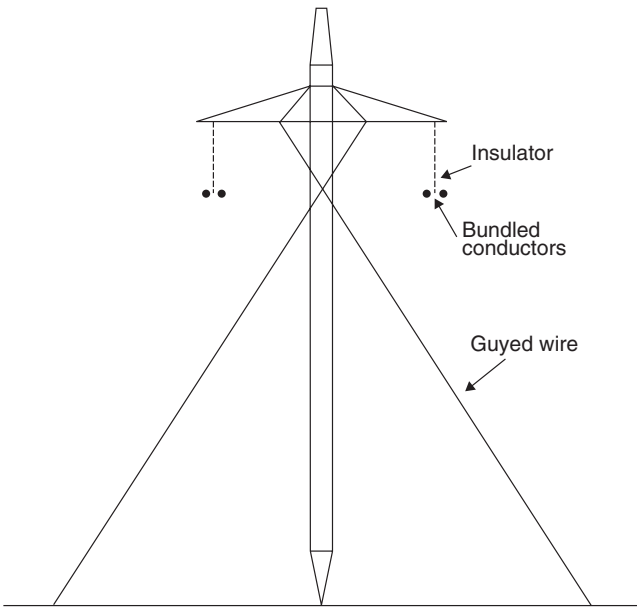

FIGURE 8.7 HVDC tower arrangement. (From Fink, D.G. and Beaty, H.W., *Standard Handbook for Electrical Engineering*, 11th ed., McGraw-Hill, New York, 1978.)

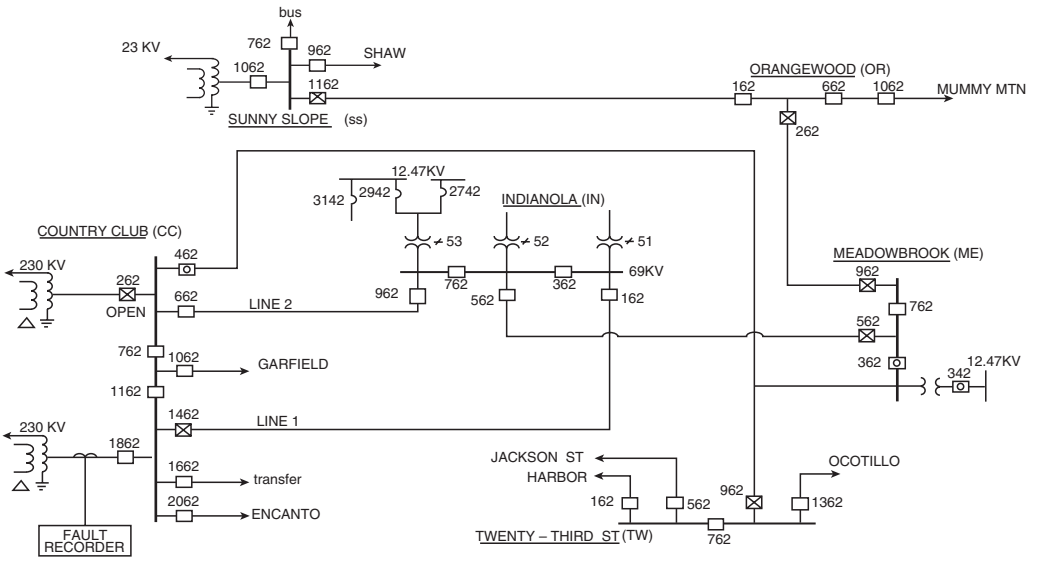

FIGURE 8.8 Subtransmission system.

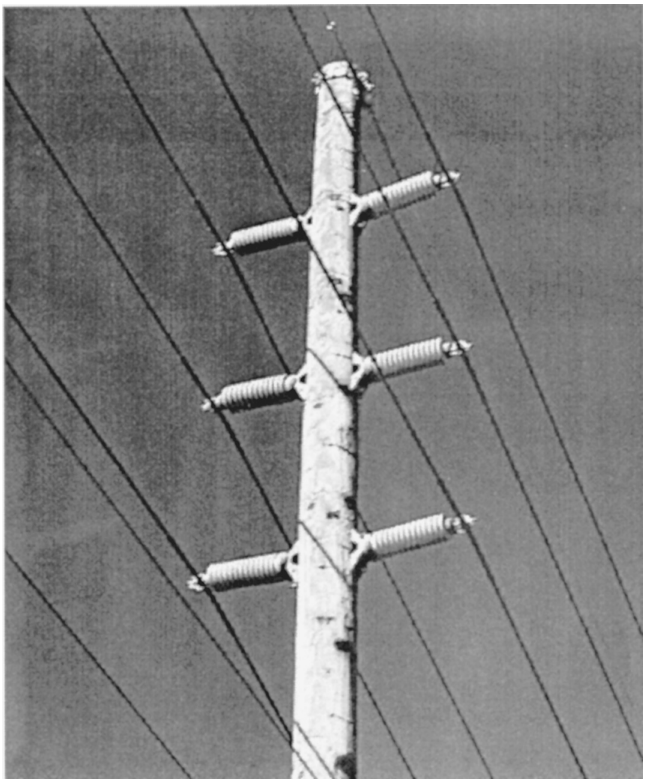

FIGURE 8.9 Typical subtransmission line.

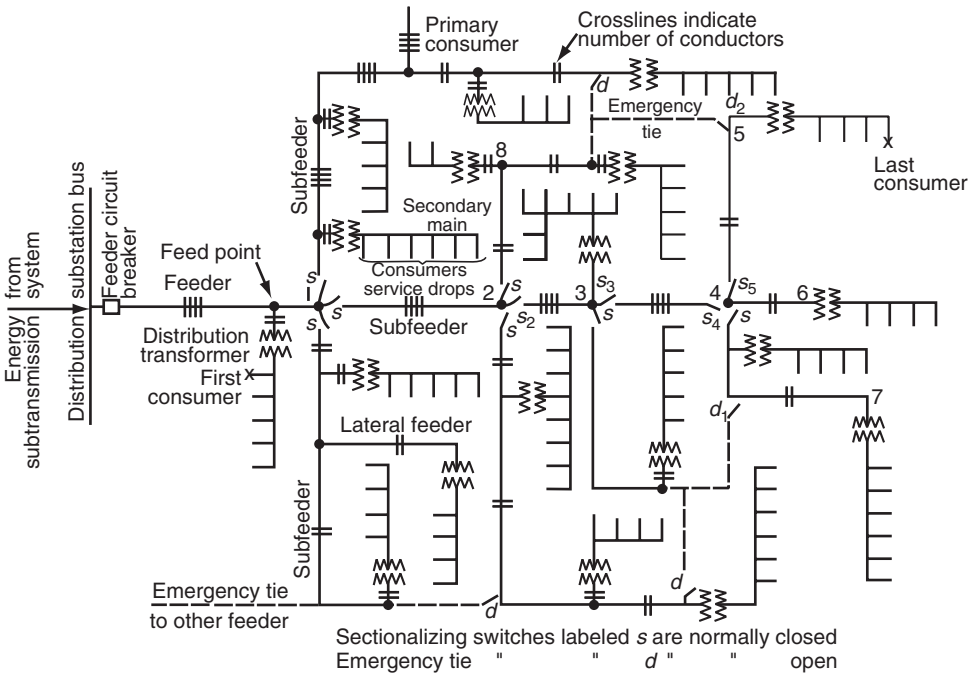

FIGURE 8.10 Concept of radial distribution system.

supply the crossroads. Secondary mains are supplied through transformers. The consumer's service drops supply the individual loads. The voltage of the distribution system is between 4.6 and 25 kV. Distribution feeders can supply loads up to 20–30 miles.

Many distribution lines in the U.S. have been built with a wood pole and cross arm. The wood is treated with an injection of creosote or other wood preservative that protects the wood from rotting and termites. Most poles are buried in a hole without foundation. Lines built recently may use a simple concrete block foundation. Small porcelain or non-ceramic, pin-type insulators support the conductors. The insulator pin is grounded to eliminate leakage current, which can cause burning of the wood tower. A simple vertical copper rod is used for grounding. Shield conductors are seldom used. Figure 8.11 shows typical distribution line arrangements.

Because of the lack of space in urban areas, distribution lines are often installed on the subtransmission line towers. This is referred to as underbuild. A typical arrangement is shown in Fig. 8.12.

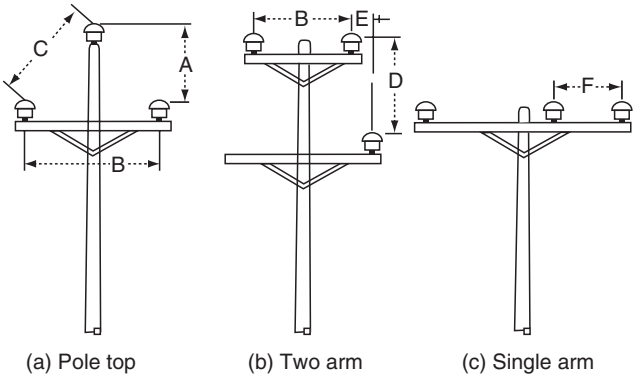

FIGURE 8.11 Distribution line arrangements.

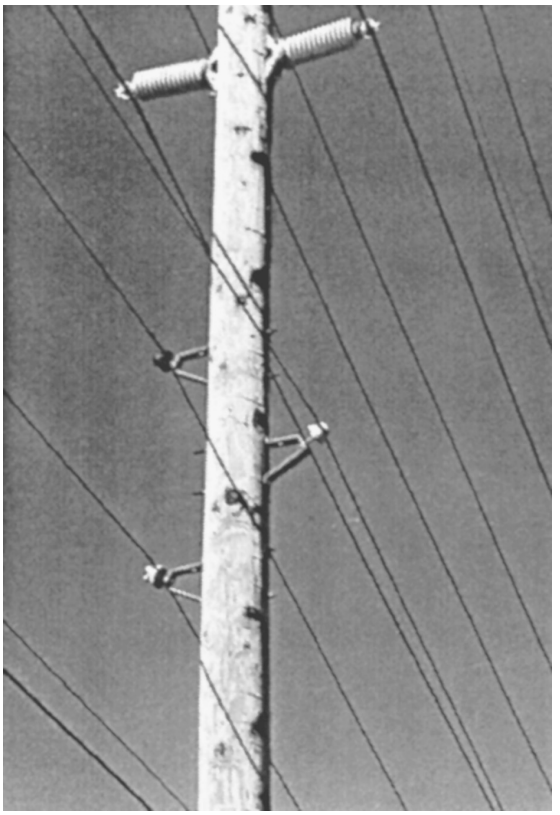

FIGURE 8.12 Distribution line installed under the subtransmission line.

The figure shows that small porcelain insulators support the conductors. The insulators are installed on metal brackets that are bolted onto the wood tower. This arrangement reduces the right-of-way requirement and saves space.

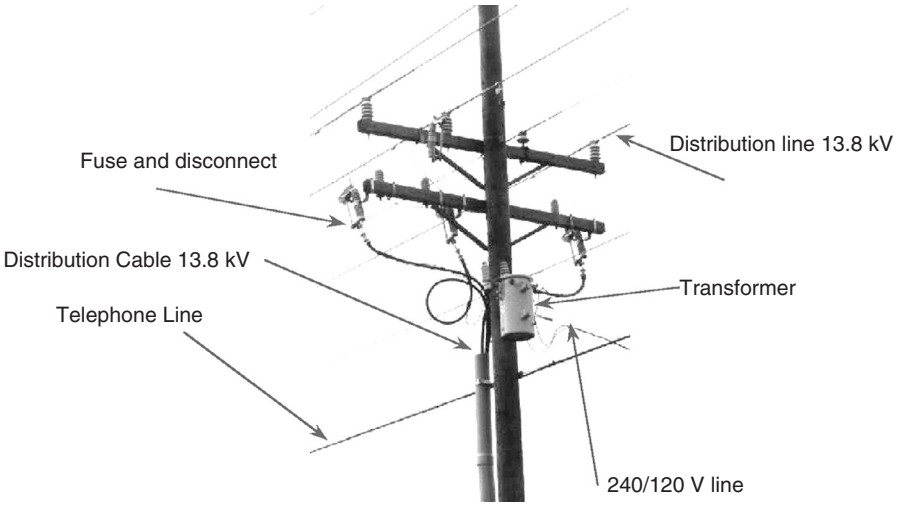

FIGURE 8.13 Service drop.

Transformers mounted on distribution poles frequently supply individual houses or groups of houses. Figure 8.13 shows a typical transformer pole, consisting of a transformer that supplies a 240/120-V service drop, and a 13.8-kV distribution cable. The latter supplies a nearby shopping center, located on the other side of the road. The 13.8-kV cable is protected by a cut-off switch that contains a fuse mounted on a pivoted insulator. The lineman can disconnect the cable by pulling the cut-off open with a long insulated rod (hot stick).

References

1. Electric Power Research Institute, *Transmission Line Reference Book, 345 kV and Above*, Electric Power Research Institute, Palo Alto, CA, 1987.
2. Fink, D.G. and Beaty, H.W., *Standard Handbook for Electrical Engineering*, 11th ed., McGraw-Hill, New York, Sec. 18, 1978.
3. Gonen, T., *Electric Power Distribution System Engineering*, Wiley, New York, 1986.
4. Gonen, T., *Electric Power Transmission System Engineering*, Wiley, New York, 1986.

9

Transmission Line Structures

Joe C. Pohlman
Consultant

An overhead transmission line (OHTL) is a very complex, continuous, electrical/mechanical system. Its function is to transport power safely from the circuit breaker on one end to the circuit breaker on the other. It is physically composed of many individual components made up of different materials having a wide variety of mechanical properties, such as:

- flexible vs. rigid
- ductile vs. brittle
- variant dispersions of strength
- wear and deterioration occurring at different rates when applied in different applications within one micro-environment or in the same application within different micro-environments

This discussion will address the nature of the structures which are required to provide the clearances between the current-carrying conductors, as well as their safe support above the earth. During this discussion, reference will be made to the following definitions:

Capability:	Capacity (×) availability
Reliability level:	Ability of a line (or component) to perform its expected capability
Security level:	Ability of a line to restrict progressive damage after the failure of the first component
Safety level:	Ability of a line to perform its function safely

9.1 Traditional Line Design Practice

Present line design practice views the support structure as an isolated element supporting half span of conductors and overhead ground wires (OHGWs) on either side of the structure. Based on the voltage level of the line, the conductors and OHGWs are configured to provide, at least, the minimum clearances mandated by the National Electrical Safety Code (NESC) (IEEE, 1990), as well as other applicable codes. This configuration is designed to control the separation of:

- energized parts from other energized parts
- energized parts from the support structure of other objects located along the r-o-w
- energized parts above ground

The NESC divides the U.S. into three large global loading zones: heavy, medium, and light and specifies radial ice thickness/wind pressure/temperature relationships to define the minimum load levels that must be used within each loading zone. In addition, the Code introduces the concept of an Overload Capacity Factor (OCF) to cover uncertainties stemming from the:

- likelihood of occurrence of the specified load
- dispersion of structure strength
- grade of construction
- deterioration of strength during service life
- structure function (suspension, dead-end, angle)
- other line support components (guys, foundations, etc.)

Present line design practice normally consists of the following steps:

1. The owning utility prepares an agenda of loading events consisting of:
   - mandatory regulations from the NESC and other codes
   - climatic events believed to be representative of the line's specific location
   - contingency loading events of interest; i.e., broken conductor
   - special requirements and expectations

Each of these loading events is multiplied by its own OCF to cover uncertainties associated with it to produce an agenda of final ultimate design loads (see Fig. 9.1).

2. A ruling span is identified based on the sag/tension requirements for the preselected conductor.
3. A structure type is selected based on past experience or on recommendations of potential structure suppliers.
4. Ultimate design loads resulting from the ruling span are applied statically as components in the longitudinal, transverse, and vertical directions, and the structure deterministically designed.
5. Using the loads and structure configuration, ground line reactions are calculated and used to accomplish the foundation design.
6. The ruling span line configuration is adjusted to fit the actual r-o-w profile.
7. Structure/foundation designs are modified to account for variation in actual span lengths, changes in elevation, and running angles.
8. Since most utilities expect the tangent structure to be the weakest link in the line system, hardware, insulators, and other accessory components are selected to be stronger than the structure.

Inasmuch as structure types are available in a wide variety of concepts, materials, and costs, several iterations would normally be attempted in search of the most cost effective line design based on total installed costs (see Fig. 9.2).

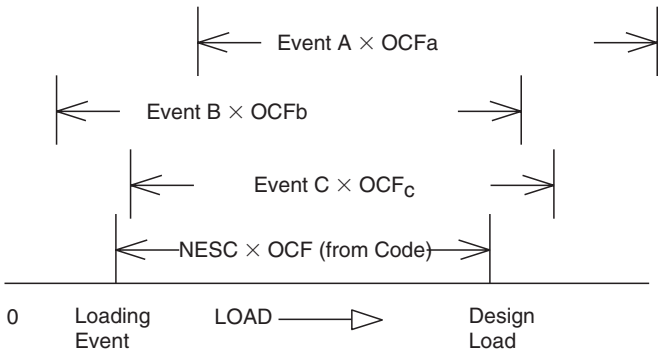

FIGURE 9.1 Development of a loading agenda.

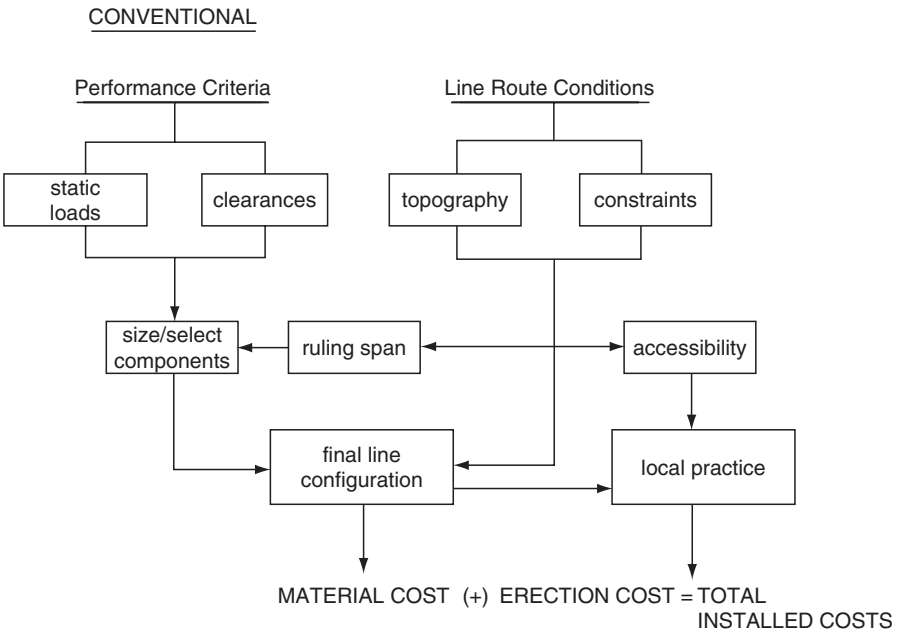

FIGURE 9.2 Search for cost effectiveness.

While deterministic design using static loads applied in quadrature is a convenient mathematical approach, it is obviously not representative of the real-world exposure of the structural support system. OHTLs are tens of yards wide and miles long and usually extend over many widely variant microtopographical and microclimatic zones, each capable of delivering unique events consisting of magnitude of load at a probability-of-occurrence. That component along the r-o-w that has the highest probability of occurrence of failure from a loading event becomes the weak link in the structure design and establishes the reliability level for the total line section. Since different components are made from different materials that have different response characteristics and that wear, age, and deteriorate at different rates, it is to be expected that the weak link:

- will likely be different in different line designs
- will likely be different in different site locations within the same line
- can change from one component to another over time

9.1.1 Structure Types in Use

Structures come in a wide variety of styles:

- lattice towers
- cantilevered or guyed poles and masts
- framed structures
- combinations of the above

They are available in a wide variety of materials:

- Metal
  galvanized steel and aluminum rods, bars and rolled shapes
  fabricated plate
  tubes

- Concrete
  spun with pretensioned or post-tensioned reinforcing cable
  statically cast nontensioned reinforcing steel
  single or multiple piece
- Wood
  as grown
  glued laminar
- Plastics
- Composites
- Crossarms and braces
- Variations of all of the above

Depending on their style and material contents, structures vary considerably in how they respond to load. Some are rigid. Some are flexible. Those structures that can safely deflect under load and absorb energy while doing so, provide an ameliorating influence on progressive damage after the failure of the first element (Pohlman and Lummis, 1969).

9.1.2 Factors Affecting Structure Type Selection

There are usually many factors that impact on the selection of the structure type for use in an OHTL. Some of the more significant are briefly identified below.

Erection Technique: It is obvious that different structure types require different erection techniques. As an example, steel lattice towers consist of hundreds of individual members that must be bolted together, assembled, and erected onto the four previously installed foundations. A tapered steel pole, on the other hand, is likely to be produced in a single piece and erected directly on its previously installed foundation in one hoist. The lattice tower requires a large amount of labor to accomplish the considerable number of bolted joints, whereas the pole requires the installation of a few nuts applied to the foundation anchor bolts plus a few to install the crossarms. The steel pole requires a large-capacity crane with a high reach which would probably not be needed for the tower. Therefore, labor needs to be balanced against the need for large, special equipment and the site's accessibility for such equipment.

Public Concerns: Probably the most difficult factors to deal with arise as a result of the concerns of the general public living, working, or coming in proximity to the line. It is common practice to hold public hearings as part of the approval process for a new line. Such public hearings offer a platform for neighbors to express individual concerns that generally must be satisfactorily addressed before the required permit will be issued. A few comments demonstrate this problem.

The general public usually perceives transmission structures as "eyesores" and distractions in the local landscape. To combat this, an industry study was made in the late 1960s (Dreyfuss, 1968) sponsored by the Edison Electric Institute and accomplished by Henry Dreyfuss, the internationally recognized industrial designer. While the guidelines did not overcome all the objections, they did provide a means of satisfying certain very highly controversial installations (Pohlman and Harris, 1971).

Parents of small children and safety engineers often raise the issue of lattice masts, towers, and guys, constituting an "attractive challenge" to determined climbers, particularly youngsters.

Inspection, Assessment, and Maintenance: Depending on the owning utility, it is likely their in-house practices will influence the selection of the structure type for use in a specific line location. Inspections and assessment are usually made by human inspectors who use diagnostic technologies to augment their personal senses of sight and touch. The nature and location of the symptoms of critical interest are such that they can be most effectively examined from specific perspectives. Inspectors must work from the most advantageous location when making inspections. Methods can include observations from ground or fly-by patrol, climbing, bucket trucks, or helicopters. Likewise, there are certain maintenance activities that are known or believed to be required for particular structure types. The equipment necessary to maintain the structure should be taken into consideration during the structure type selection process to assure there will be no unexpected conflict between maintenance needs and r-o-w restrictions.

Future Upgrading or Uprating: Because of the difficulty of procuring r-o-w's and obtaining the necessary permits to build new lines, many utilities improve their future options by selecting structure types for current line projects that will permit future upgrading and/or uprating initiatives.

9.2 Current Deterministic Design Practice

Figure 9.3 shows a loading agenda for a double-circuit, 345-kV line built in the upper Midwest region of the U.S. on steel lattice towers. Over and above the requirements of the NESC, the utility had specified these loading events:

- a heavy wind condition (Pohlman and Harris, 1971)
- a wind on bare tower (Carton and Peyrot, 1992)
- two maximum vertical loads on the OHGW and conductor supports (Osterdorp, 1998; CIGRE, 1995)
- two broken wire contingencies (Pohlman and Lummis, 1969; Dreyfuss, 1968)

It was expected that this combination of loading events would result in a structural support design with the capability of sustaining 50-year recurrence loads likely to occur in the general area where the line was

TANGENT AND LIGHT ANGLE SUSPENSION TOWER – 345 DOUBLE CIRCUIT

OHGW: Two 7/16" diameter galvanized steel strand
Conductors: Six twin conductor bundles of 1431 KCM 45/7 ACSR
Weight span: 1,650 feet
Wind span: 1,100 feet
Line angle: 0° to 2°

Load Case	Load Event	Radial Ice (")	Wind Pressure Wire (psf)	Wind Pressure Structure (psf)	Load Direction	OCF
1	NESC Heavy	1/2	4	5.1	T L V	2.54 1.65 1.27
2	One broken OHGW combined with wind and ice	1/2	8	13.0	T L V	1.0 1.0 1.0
3	One broken conductor bundle combined with wind and ice	1/2	8	13.0	T L V	1.0 1.0 1.0
4	Heavy wind	0	16	42.0	T L V	1.0 1.0 1.0
5	Wind on bare tower (no conductors or OHGW)	0	0	46.2	T L V	1.0 1.0 1.0
6	Vertical load at any OHGW support of 3780 lbs. (not simultaneously)	0	0	0	V	1.0
7	Vertical load at any conductor support of 17,790 lbs. (not simultaneously)	0	0	0	V	1.0

FIGURE 9.3 Example of loading agenda.

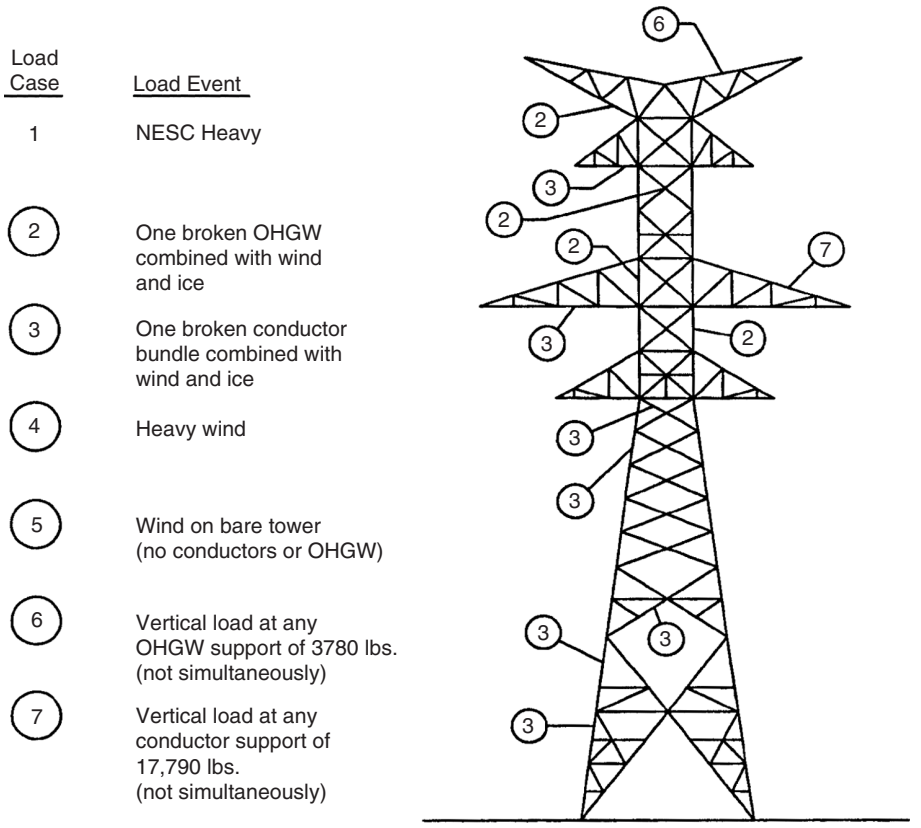

FIGURE 9.4 Results of deterministic design.

built. Figure 9.4 shows that different members of the structure, as designed, were under the control of different loading cases from this loading agenda. While interesting, this does not:

- provide a way to identify weak links in the support structure
- provide a means for predicting performance of the line system
- provide a framework for decision-making

9.2.1 Reliability Level

The shortcomings of deterministic design can be demonstrated by using 3D modeling/simulation technology which is in current use (Carton and Peyrot, 1992) in forensic investigation of line failures. The approach is outlined in Fig. 9.5. After the structure (as designed) is properly modeled, loading events of increasing magnitude are analytically applied from different directions until the actual critical capacity for each key member of interest is reached. The probability of occurrence for those specific loading events can then be predicted for the specific location of that structure within that line section by professionals skilled in the art of micrometerology.

Figure 9.6 shows a few of the key members in the example for Fig. 9.4:

- The legs had a probability of failure in that location of once in 115 years.
- Tension chords in the conductor arm and OHGW arm had probabilities of failure of 110 and 35 years, respectively.
- A certain wind condition at an angle was found to be critical for the foundation design with a probability of occurrence at that location of once in 25 years.

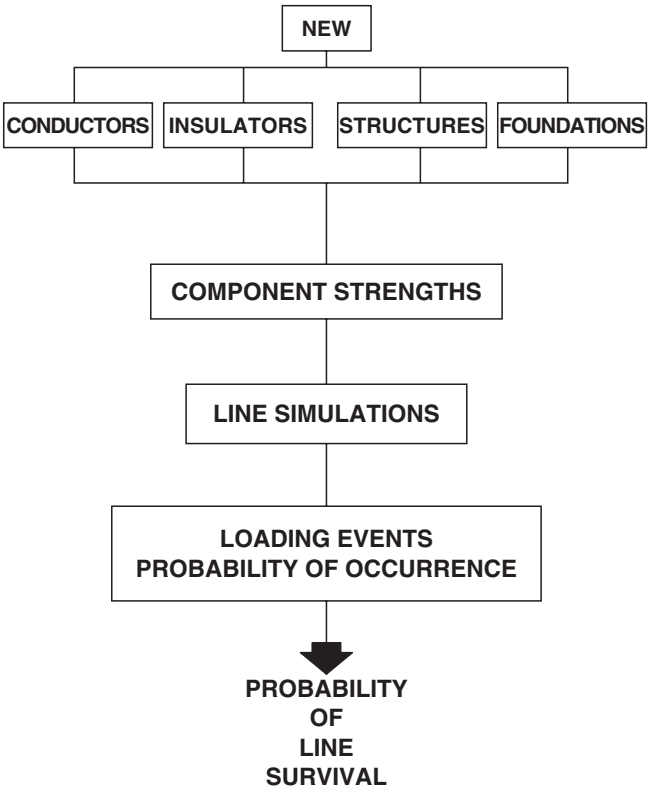

FIGURE 9.5 Line simulation study.

Member	Controlling Climatic Load Condition	Controlling Load Return Period (years)
Legs	Wind, no ice	115
Tension chord of conductor arm	Ice, no wind	110
Tension chord of OHGW arm	Ice, no wind	35
Foundation	Wind, no ice	25

Controlling Climatic Loads

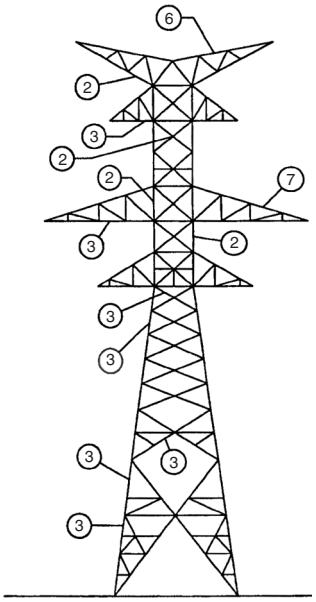

FIGURE 9.6 Simulation study output.

Some interesting observations can be drawn:

- The legs were conservatively designed.
- The loss of an OHGW is a more likely event than the loss of a conductor.
- The foundation was found to be the weak link.

In addition to the interesting observations on relative reliability levels of different components within the structural support system, the output of the simulation study also provides the basis for a decision-making process which can be used to determine the cost effectiveness of management initiatives. Under the simple laws of statistics, when there are two independent outcomes to an event, the probability of the first outcome is equal to one minus the probability of the second. When these outcomes are survival and failure:

$$\begin{gathered}\text{Annual probability of survival} = 1 - \text{Annual probability of failure} \\ \text{Ps} = 1 - \text{Pf}\end{gathered} \tag{9.1}$$

If it is desired to know what the probability of survival is over an extended length of time, i.e., n years of service life:

$$[\text{Ps1} \times \text{Ps2} \times \text{Ps3} \times \ldots \text{Psn}] = (\text{ps})\text{n} \tag{9.2}$$

Applying this principle to the components in the deterministic structure design and considering a 50-year service life as expected by the designers:

- the legs had a Ps of 65%
- the tension chord in the conductor arm had a Ps of 63%
- the tension chord of the OHGW arm had a Ps of 23%
- the foundation had a Ps of 13%

9.2.2 Security Level

It should be remembered, however, that the failure of every component does not necessarily progress into extensive damage. A comparison of the total risk that would result from the initial failure of components of interest can be accomplished by making a security-level check of the line design (Osterdorp, 1998).

Since the OHTL is a contiguous mechanical system, the forces from the conductors and OHGWs on one side of each tangent structure are balanced and restrained by those on the other side. When a critical component in the conductor/OHGW system fails, energy stored within the conductor system is released suddenly and sets up unbalanced transients that can cause failure of critical components at the next structure. This can set off a cascading effect that will continue to travel downline until it encounters a point in the line strong enough to withstand the unbalance. Unfortunately, a security check of the total line cannot be accomplished from the information describing the one structure in Fig. 9.4; but perhaps some generalized observations can be drawn for demonstration purposes.

Since the structure was designed for broken conductor bundle and broken OHGW contingencies, it appears the line would not be subjected to a cascade from a broken bare conductor, but what if the conductor was coated with ice at the time? Since ice increases the energy trapped within the conductor prior to release, it might be of interest to determine how much ice would be "enough." Three-dimensional modeling would be employed to simulate ice coating of increasing thicknesses until the critical amount is defined. A proper micrometerological study could then identify the probability of occurrence of a storm system capable of delivering that amount of ice at that specific location.

In the example, a wind condition with no ice was identified that would be capable of causing foundation failure once every 25 years. A security-level check would predict the amount

of resulting losses and damages that would be expected from this initiating event compared to the broken-conductor-under-ice-load contingencies.

9.3 Improved Design Approaches

The above discussion indicates that technologies are available today for assessing the true capability of an OHTL that was created using the conventional practice of specifying ultimate static loads and designing a structure that would properly support them. Because there are many different structure types made from different materials, this was not always straightforward. Accordingly, many technical societies prepared guidelines on how to design the specific structure needed. These are listed in the accompanying references. The interested reader should realize that these documents are subject to periodic review and revision and should, therefore, seek the most current version.

While the technical fraternity recognizes that the mentioned technologies are useful for analyzing existing lines and determining management initiatives, something more direct for designing new lines is needed. There are many efforts under way. The most promising of these is *Improved Design Criteria of OHTLs Based on Reliability Concepts* (Ostendorp, 1998), currently under development by CIGRE Study Committee 22: Recommendations for Overhead Lines. Appendix A outlines the methodology involved in words and in a diagram. The technique is based on the premise that loads and strengths are stochastic variables and the combined reliability is computable if the statistical functions of loads and strength are known. The referenced report has been circulated internationally for trial use and comment. It is expected that the returned comments will be carefully considered, integrated into the report, and the final version submitted to the International Electrotechnical Commission (IEC) for consideration as an International Standard.

References

1. Carton, T. and Peyrot, A., Computer Aided Structural and Geometric Design of Power Lines, *IEEE Trans. on Power Line Syst.*, 7(1), 1992.
2. Dreyfuss, H., *Electric Transmission Structures*, Edison Electric Institute Publication No. 67–61, 1968.
3. Guide for the Design and Use of Concrete Poles, ASCE 596–6, 1987.
4. Guide for the Design of Prestressed Concrete Poles, ASCE/PCI Joint Commission on Concrete Poles, February, 1992. Draft.
5. Guide for the Design of Transmission Towers, *ASCE Manual on Engineering Practice*, 52, 1988.
6. Guide for the Design Steel Transmission Poles, *ASCE Manual on Engineering Practice*, 72, 1990.
7. IEEE Trial-Use Design Guide for Wood Transmission Structures, IEEE Std. 751, February, 1991.
8. *Improved Design Criteria of Overhead Transmission Lines Based on Reliability Concepts, CIGRE SC-22 Report*, October 1995.
9. *National Electrical Safety Code ANSI C-2*, IEEE, 1990.
10. Ostendorp, M., Longitudinal Loading and Cascading Failure Assessment for Transmission Line Upgrades, *ESMO Conference '98*, Orlando, Florida, April 26–30, 1998.
11. Pohlman, J. and Harris, W., Tapered Steel H-Frames Gain Acceptance Through Scenic Valley, *Electric Light and Power Magazine*, 48(vii), 55–58, 1971.
12. Pohlman, J. and Lummis, J., Flexible Structures Offer Broken Wire Integrity at Low Cost, *Electric Light and Power*, 46(V, 144–148.4), 1969.

Appendix A General Design Criteria—Methodology

The recommended methodology for designing transmission line components is summarized in Fig. 9.7 and can be described as follows:

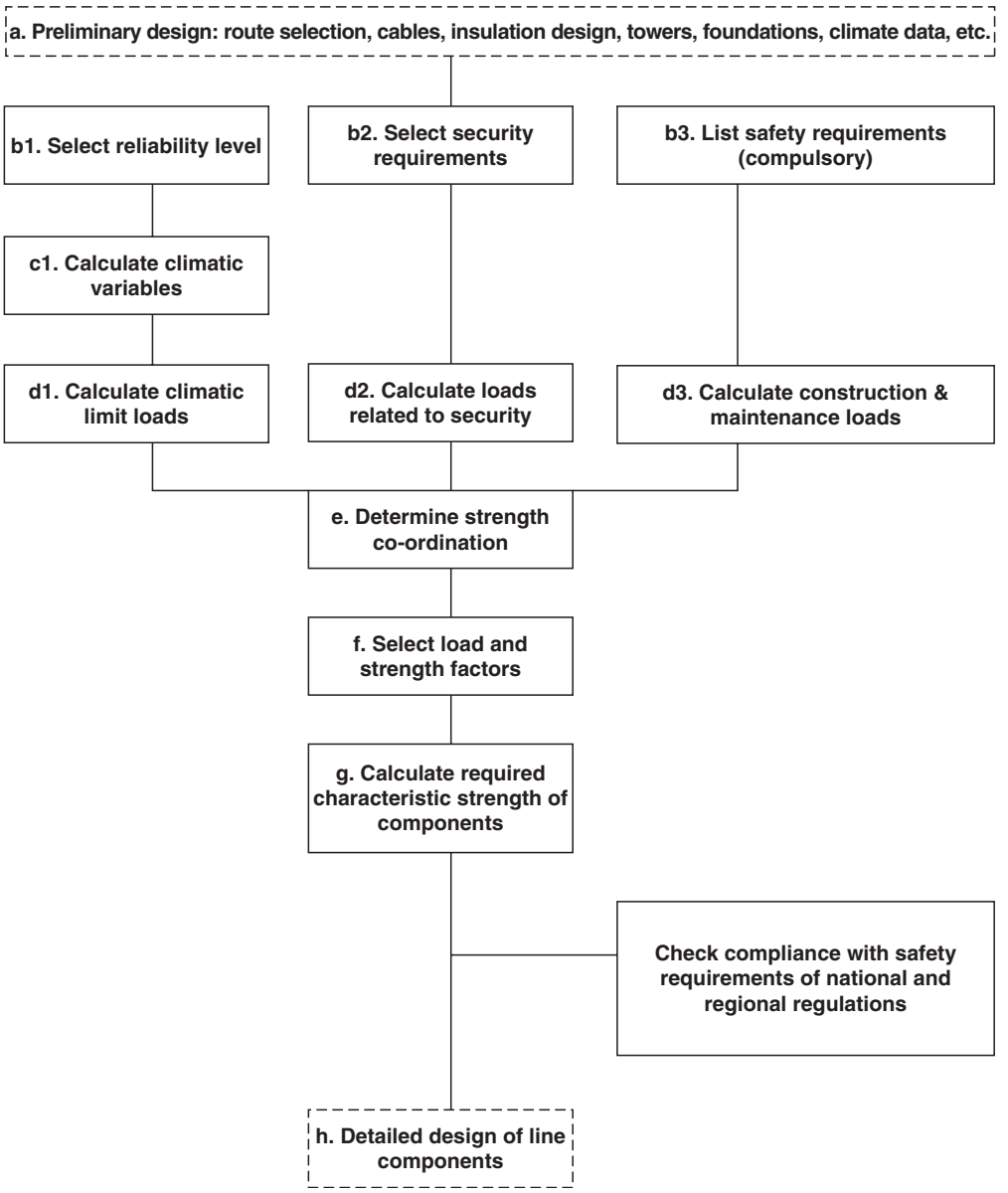

FIGURE 9.7 Methodology.

a) Gather preliminary line design data and available climatic data.[1]
b1) Select the reliability level in terms of return period of design loads. (Note: Some national regulations and/or codes of practice sometimes impose design requirements, directly or indirectly, that may restrict the choice offered to designers).
b2) Select the security requirements (failure containment).
b3) List safety requirements imposed by mandatory regulations and construction and maintenance loads.

[1]In some countries, design wind speed, such as the 50-year return period, is given in National Standards.

c) Calculate climatic variables corresponding to selected return period of design loads.
d1) Calculate climatic limit loadings on components.
d2) Calculate loads corresponding to security requirements.
d3) Calculate loads related to safety requirements during construction and maintenance.
e) Determine the suitable strength coordination between line components.
f) Select appropriate load and strength factors applicable to load and strength equations.
g) Calculate the characteristic strengths required for components.
h) Design line components for the above strength requirements.

This document deals with items b) to g). Items a) and h) are not part of the scope of this document. They are identified by a dotted frame in Fig. 9.7.

Source: Improved design criteria of overhead transmission lines based on reliability concepts, *CIGRE SC22 Report*, October, 1995.

10

Insulators and Accessories

George G. Karady
Arizona State University

Richard G. Farmer
Arizona State University

Electric insulation is a vital part of an electrical power system. Although the cost of insulation is only a small fraction of the apparatus or line cost, line performance is highly dependent on insulation integrity. Insulation failure may cause permanent equipment damage and long-term outages. As an example, a short circuit in a 500-kV system may result in a loss of power to a large area for several hours. The potential financial losses emphasize the importance of a reliable design of the insulation.

The insulation of an electric system is divided into two broad categories:

1. Internal insulation
2. External insulation

Apparatus or equipment has mostly internal insulation. The insulation is enclosed in a grounded housing which protects it from the environment. External insulation is exposed to the environment. A typical example of internal insulation is the insulation for a large transformer where insulation between turns and between coils consists of solid (paper) and liquid (oil) insulation protected by a steel tank. An overvoltage can produce internal insulation breakdown and a permanent fault.

External insulation is exposed to the environment. Typical external insulation is the porcelain insulators supporting transmission line conductors. An overvoltage caused by flashover produces only a temporary fault. The insulation is self-restoring.

This section discusses external insulation used for transmission lines and substations.

10.1 Electrical Stresses on External Insulation

The external insulation (transmission line or substation) is exposed to electrical, mechanical, and environmental stresses. The applied voltage of an operating power system produces electrical stresses. The weather and the surroundings (industry, rural dust, oceans, etc.) produce additional environmental

stresses. The conductor weight, wind, and ice can generate mechanical stresses. The insulators must withstand these stresses for long periods of time. It is anticipated that a line or substation will operate for more than 20–30 years without changing the insulators. However, regular maintenance is needed to minimize the number of faults per year. A typical number of insulation failure-caused faults is 0.5–10 per year, per 100 mi of line.

10.1.1 Transmission Lines and Substations

Transmission line and substation insulation integrity is one of the most dominant factors in power system reliability. We will describe typical transmission lines and substations to demonstrate the basic concept of external insulation application.

Figure 10.1 shows a high-voltage transmission line. The major components of the line are:

1. Conductors
2. Insulators
3. Support structure tower

The insulators are attached to the tower and support the conductors. In a suspension tower, the insulators are in a vertical position or in a V-arrangement. In a dead-end tower, the insulators are in a horizontal position. The typical transmission line is divided into sections and two dead-end towers terminate each section. Between 6 and 15 suspension towers are installed between the two dead-end towers. This sectionalizing prevents the propagation of a catastrophic mechanical fault beyond each section. As an example, a tornado caused collapse of one or two towers could create a domino effect, resulting in the collapse of many miles of towers, if there are no dead ends.

FIGURE 10.1 A 500-kV suspension tower with V string insulators.

Figure 10.2 shows a lower voltage line with post-type insulators. The rigid, slanted insulator supports the conductor. A high-voltage substation may use both suspension and post-type insulators. References [1,2] give a comprehensive description of transmission lines and discuss design problems.

10.1.2 Electrical Stresses

The electrical stresses on insulation are created by:

1. Continuous power frequency voltages
2. Temporary overvoltages
3. Switching overvoltages
4. Lightning overvoltages

10.1.2.1 Continuous Power Frequency Voltages

The insulation has to withstand normal operating voltages. The operating voltage fluctuates from changing load. The normal range of fluctuation is around $\pm 10\%$. The line-to-ground voltage causes the voltage stress on the insulators. As an example, the insulation requirement of a 220-kV line is at least:

$$1.1 \times \frac{220\,\text{kV}}{\sqrt{3}} \cong 140\ \text{kV} \tag{10.1}$$

This voltage is used for the selection of the number of insulators when the line is designed. The insulation can be laboratory tested by measuring the dry flashover voltage of the insulators. Because the line insulators are self-restoring, flashover tests do not

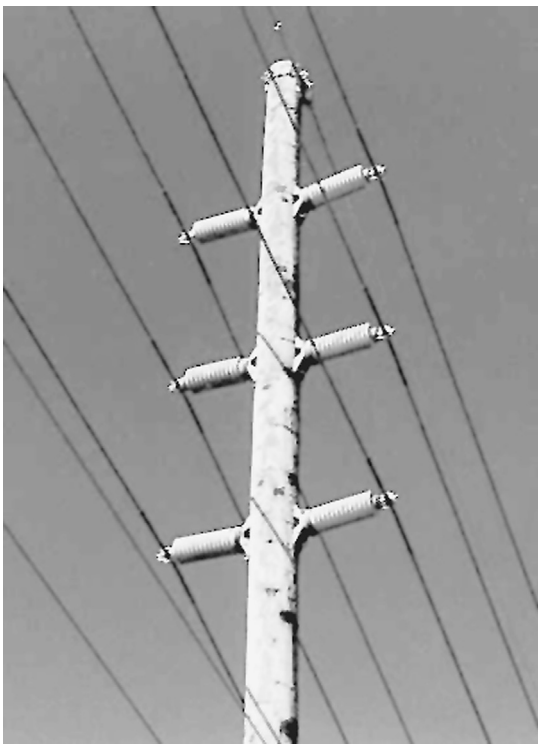

FIGURE 10.2 69-kV transmission line with post insulators.

cause any damage. The flashover voltage must be larger than the operating voltage to avoid outages. For a porcelain insulator, the required dry flashover voltage is about 2.5–3 times the rated voltage. A significant number of the apparatus standards recommend dry withstand testing of every kind of insulation to be two (2) times the rated voltage plus 1 kV for 1 min of time. This severe test eliminates most of the deficient units.

10.1.2.2 Temporary Overvoltages

These include ground faults, switching, load rejection, line energization and resonance, cause power frequency, or close-to-power frequency, and relatively long duration overvoltages. The duration is from 5 sec to several minutes. The expected peak amplitudes and duration are listed in Table 10.1.

The base is the crest value of the rated voltage. The dry withstand test, with two times the maximum operating voltage plus 1 kV for 1 minute, is well-suited to test the performance of insulation under temporary overvoltages.

10.1.2.3 Switching Overvoltages

The opening and closing of circuit breakers causes switching overvoltages. The most frequent causes of switching overvoltages are fault or ground fault clearing, line energization, load interruption, interruption of inductive current, and switching of capacitors.

Switching produces unidirectional or oscillatory impulses with durations of 5000–20,000 μsec. The amplitude of the overvoltage varies between 1.8 and 2.5 per unit. Some modern circuit breakers use preinsertion resistance, which reduces the overvoltage amplitude to 1.5–1.8 per unit. The base is the crest value of the rated voltage.

Switching overvoltages are calculated from computer simulations that can provide the distribution and standard deviation of the switching overvoltages. Figure 10.3 shows typical switching impulse voltages. Switching surge performance of the insulators is determined by flashover tests. The test is performed by applying a standard impulse with a time to crest of 250 μsec and time to half value of

TABLE 10.1 Expected Amplitude of Temporary Overvoltages

Type of Overvoltage	Expected Amplitude	Duration
Fault overvoltages		
Effectively grounded	1.3 per unit	1 sec
Resonant grounded	1.73 per unit or greater	10 sec
Load rejection		
System substation	1.2 per unit	1–5 sec
Generator station	1.5 per unit	3 sec
Resonance	3 per unit	2–5 min
Transformer energization	1.5–2.0 per unit	1–20 sec

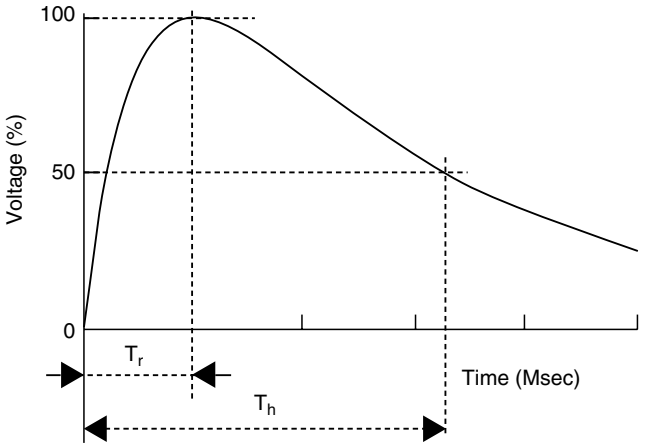

FIGURE 10.3 Switching overvoltages. $T_r = 20-5000$ μsec, $T_h < 20{,}000$ μsec, where T_r is the time-to-crest value and T_h is the time-to-half value.

5000 μsec. The test is repeated 20 times at different voltage levels and the number of flashovers is counted at each voltage level. These represent the statistical distribution of the switching surge impulse flashover probability. The correlation of the flashover probability with the calculated switching impulse voltage distribution gives the probability, or risk, of failure. The measure of the risk of failure is the number of flashovers expected by switching surges per year.

10.1.2.4 Lightning Overvoltages

Lightning overvoltages are caused by lightning strikes:

1. to the phase conductors
2. to the shield conductor (the large current-caused voltage drop in the grounding resistance may cause flashover to the conductors [back flash]).
3. to the ground close to the line (the large ground current induces voltages in the phase conductors).

Lighting strikes cause a fast-rising, short-duration, unidirectional voltage pulse. The time-to-crest is between 0.1–20 μsec. The time-to-half value is 20–200 μsec.

The peak amplitude of the overvoltage generated by a direct strike to the conductor is very high and is practically limited by the subsequent flashover of the insulation. Shielding failures and induced voltages cause somewhat less overvoltage. Shielding failure caused overvoltage is around 500 kV–2000 kV. The lightning-induced voltage is generally less than 400 kV. The actual stress on the insulators is equal to the impulse voltage.

The insulator BIL is determined by using standard lightning impulses with a time-to-crest value of 1.2 μsec and time-to-half value of 50 μsec. This is a measure of the insulation strength for lightning. Figure 10.4 shows a typical lightning pulse.

When an insulator is tested, peak voltage of the pulse is increased until the first flashover occurs. Starting from this voltage, the test is repeated 20 times at different voltage levels and the number of flashovers are counted at each voltage level. This provides the statistical distribution of the lightning impulse flashover probability of the tested insulator.

10.1.3 Environmental Stresses

Most environmental stress is caused by weather and by the surrounding environment, such as industry, sea, or dust in rural areas. The environmental stresses affect both mechanical and electrical performance of the line.

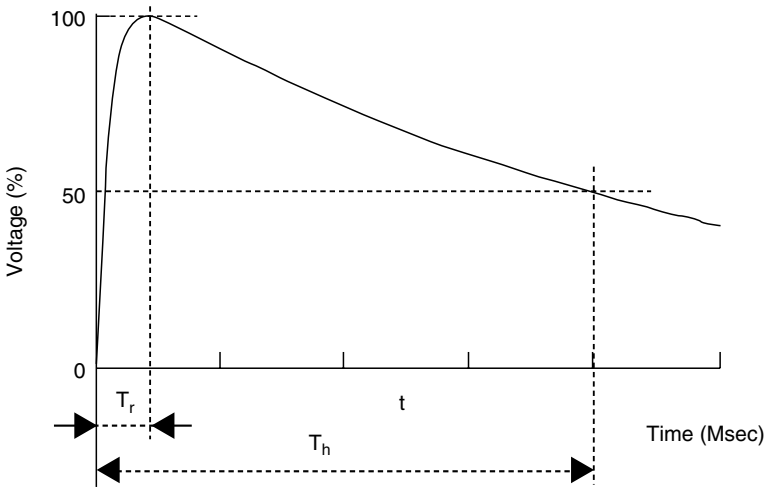

FIGURE 10.4 Lightning overvoltages. $T_r = 0.1-20$ μsec, T_h 20−200 μsec, where T_r is the time-to-crest value and T_h is the time-to-half value.

10.1.3.1 Temperature

The temperature in an outdoor station or line may fluctuate between −50°C and +50°C, depending upon the climate. The temperature change has no effect on the electrical performance of outdoor insulation. It is believed that high temperatures may accelerate aging. Temperature fluctuation causes an increase of mechanical stresses, however it is negligible when well-designed insulators are used.

10.1.3.2 UV Radiation

UV radiation accelerates the aging of nonceramic composite insulators, but has no effect on porcelain and glass insulators. Manufacturers use fillers and modified chemical structures of the insulating material to minimize the UV sensitivity.

10.1.3.3 Rain

Rain wets porcelain insulator surfaces and produces a thin conducting layer most of the time. This reduces the flashover voltage of the insulators. As an example, a 230-kV line may use an insulator string with 12 standard ball-and-socket-type insulators. Dry flashover voltage of this string is 665 kV and the wet flashover voltage is 502 kV. The percentage reduction is about 25%.

Nonceramic polymer insulators have a water-repellent hydrophobic surface that reduces the effects of rain. As an example, with a 230-kV composite insulator, dry flashover voltage is 735 kV and wet flashover voltage is 630 kV. The percentage reduction is about 15%. The insulator's wet flashover voltage must be higher than the maximum temporary overvoltage.

10.1.3.4 Icing

In industrialized areas, conducting water may form ice due to water-dissolved industrial pollution. An example is the ice formed from acid rain water. Ice deposits form bridges across the gaps in an insulator string that result in a solid surface. When the sun melts the ice, a conducting water layer will bridge the insulator and cause flashover at low voltages. Melting ice-caused flashover has been reported in the Quebec and Montreal areas.

10.1.3.5 Pollution

Wind drives contaminant particles into insulators. Insulators produce turbulence in airflow, which results in the deposition of particles on their surfaces. The continuous depositing of the particles increases the thickness of these deposits. However, the natural cleaning effect of wind, which blows

TABLE 10.2 Site Severity (IEEE Definitions)

Description	ESDD (mg/cm^2)
Very light	0–0.03
Light	0.03–0.06
Moderate	0.06–0.1
Heavy	<0.1

loose particles away, limits the growth of deposits. Occasionally, rain washes part of the pollution away. The continuous depositing and cleaning produces a seasonal variation of the pollution on the insulator surfaces. However, after a long time (months, years), the deposits are stabilized and a thin layer of solid deposit will cover the insulator. Because of the cleaning effects of rain, deposits are lighter on the top of the insulators and heavier on the bottom. The development of a continuous pollution layer is compounded by chemical changes. As an example, in the vicinity of a cement factory, the interaction between the cement and water produces a tough, very sticky layer. Around highways, the wear of car tires produces a slick, tar-like carbon deposit on the insulator's surface.

Moisture, fog, and dew wet the pollution layer, dissolve the salt, and produce a conducting layer, which in turn reduces the flashover voltage. The pollution can reduce the flashover voltage of a standard insulator string by about 20–25%.

Near the ocean, wind drives salt water onto insulator surfaces, forming a conducting salt-water layer which reduces the flashover voltage. The sun dries the pollution during the day and forms a white salt layer. This layer is washed off even by light rain and produces a wide fluctuation in pollution levels.

The Equivalent Salt Deposit Density (ESDD) describes the level of contamination in an area. Equivalent Salt Deposit Density is measured by periodically washing down the pollution from selected insulators using distilled water. The resistivity of the water is measured and the amount of salt that produces the same resistivity is calculated. The obtained mg value of salt is divided by the surface area of the insulator. This number is the ESDD. The pollution severity of a site is described by the average ESDD value, which is determined by several measurements.

Table 10.2 shows the criteria for defining site severity.

The contamination level is light or very light in most parts of the U.S. and Canada. Only the seashores and heavily industrialized regions experience heavy pollution. Typically, the pollution level is very high in Florida and on the southern coast of California. Heavy industrial pollution occurs in the industrialized areas and near large highways. Table 10.3 gives a summary of the different sources of pollution.

The flashover voltage of polluted insulators has been measured in laboratories. The correlation between the laboratory results and field experience is weak. The test results provide guidance, but insulators are selected using practical experience.

TABLE 10.3 Typical Sources of Pollution

Pollution Type	Source of Pollutant	Deposit Characteristics	Area
Rural areas	Soil dust	High resitivity layer, effective rain washing	Large areas
Desert	Sand	Low resistivity	Large areas
Coastal area	Sea salt	Very low resistivity, easily washed by rain	10–20 km from the sea
Industrial	Steel mill, coke plants, chemical plants, generating stations, quarries	High conductivity, extremely difficult to remove, insoluble	Localized to the plant area
Mixed	Industry, highway, desert	Very adhesive, medium resistivity	Localized to the plant area

10.1.3.6 Altitude

The insulator's flashover voltage is reduced as altitude increases. Above 1500 feet, an increase in the number of insulators should be considered. A practical rule is a 3% increase of clearance or insulator strings' length per 1000 ft as the elevation increases.

10.1.4 Mechanical Stresses

Suspension insulators need to carry the weight of the conductors and the weight of occasional ice and wind loading.

In northern areas and in higher elevations, insulators and lines are frequently covered by ice in the winter. The ice produces significant mechanical loads on the conductor and on the insulators. The transmission line insulators need to support the conductor's weight and the weight of the ice in the adjacent spans. This may increase the mechanical load by 20–50%.

The wind produces a horizontal force on the line conductors. This horizontal force increases the mechanical load on the line. The wind-force-produced load has to be added vectorially to the weight-produced forces. The design load will be the larger of the combined wind and weight, or ice and wind load.

The dead-end insulators must withstand the longitudinal load, which is higher than the simple weight of the conductor in the half span.

A sudden drop in the ice load from the conductor produces large-amplitude mechanical oscillations, which cause periodic oscillatory insulator loading (stress changes from tension to compression and back).

The insulator's one-minute tension strength is measured and used for insulator selection. In addition, each cap-and-pin or ball-and-socket insulator is loaded mechanically for one minute and simultaneously energized. This mechanical and electrical (M&E) value indicates the quality of insulators. The maximum load should be around 50% of the M&E load.

The Bonneville Power Administration uses the following practical relation to determine the required M&E rating of the insulators.

1. M&E $>$ 5* Bare conductor weight/span
2. M&E $>$ Bare conductor weight + Weight of 3.81 cm (1.5 in) of ice on the conductor (3 lb/sq ft)
3. M&E $>$ 2* (Bare conductor weight + Weight of 0.63 cm (1/4 in) of ice on the conductor and loading from a wind of 1.8 kg/sq ft (4 lb/sq ft)

The required M&E value is calculated from all equations above and the largest value is used.

10.2 Ceramic (Porcelain and Glass) Insulators

10.2.1 Materials

Porcelain is the most frequently used material for insulators. Insulators are made of wet, processed porcelain. The fundamental materials used are a mixture of feldspar (35%), china clay (28%), flint (25%), ball clay (10%), and talc (2%). The ingredients are mixed with water. The resulting mixture has the consistency of putty or paste and is pressed into a mold to form a shell of the desired shape. The alternative method is formation by extrusion bars that are machined into the desired shape. The shells are dried and dipped into a glaze material. After glazing, the shells are fired in a kiln at about 1200°C. The glaze improves the mechanical strength and provides a smooth, shiny surface. After a cooling-down period, metal fittings are attached to the porcelain with Portland cement. Reference [3] presents the history of porcelain insulators and discusses the manufacturing procedure.

Toughened glass is also frequently used for insulators [4]. The melted glass is poured into a mold to form the shell. Dipping into hot and cold baths cools the shells. This thermal treatment shrinks the surface of the glass and produces pressure on the body, which increases the mechanical strength of the glass. Sudden mechanical stresses, such as a blow by a hammer or bullets, will break the glass into small pieces. The metal end-fitting is attached by alumina cement.

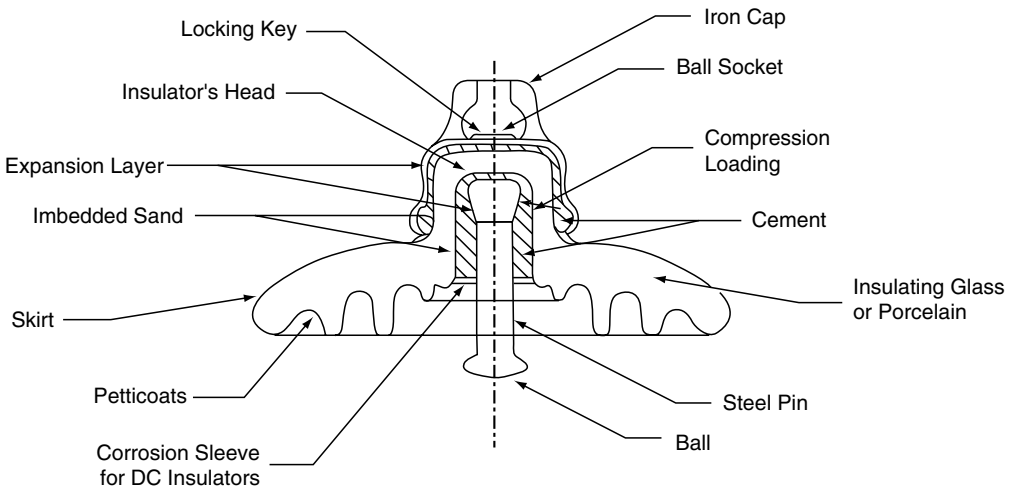

FIGURE 10.5 Cross-section of a standard ball-and-socket insulator.

10.2.2 Insulator Strings

Most high-voltage lines use ball-and-socket-type porcelain or toughened glass insulators. These are also referred to as "cap and pin." The cross section of a ball-and-socket-type insulator is shown in Fig. 10.5.

Table 10.4 shows the basic technical data of these insulators.

The porcelain skirt provides insulation between the iron cap and steel pin. The upper part of the porcelain is smooth to promote rain washing and cleaning of the surface. The lower part is corrugated, which prevents wetting and provides a longer protected leakage path. Portland cement attaches the cup and pin. Before the application of the cement, the porcelain is sandblasted to generate a rough surface. A thin expansion layer (e.g., bitumen) covers the metal surfaces. The loading compresses the cement and provides high mechanical strength.

The metal parts of the standard ball-and-socket insulator are designed to fail before the porcelain fails as the mechanical load increases. This acts as a mechanical fuse protecting the tower structure.

The ball-and-socket insulators are attached to each other by inserting the ball in the socket and securing the connection with a locking key. Several insulators are connected together to form an insulator string. Figure 10.6 shows a ball-and-socket insulator string and the clevis-type string, which is used less frequently for transmission lines.

Fog-type, long leakage distance insulators are used in polluted areas, close to the ocean, or in industrial environments. Figure 10.7 shows representative fog-type insulators, the mechanical strength of which is higher than standard insulator strength. As an example, a 6 1/2 × 12 1/2 fog-type insulator is rated to 180 kN (40 klb) and has a leakage distance of 50.1 cm (20 in.).

Insulator strings are used for high-voltage transmission lines and substations. They are arranged vertically on support towers and horizontally on dead-end towers. Table 10.5 shows the typical number of insulators used by utilities in the U.S. and Canada in lightly polluted areas.

TABLE 10.4 Technical Data of a Standard Insulator

Diameter	25.4 cm	(10 in.)
Spacing	14.6 cm	(5-3/4 in.)
Leakage distance	305 cm	(12 ft)
Typical operating voltage	10 kV	
Mechanical strength	75 kN	(15 klb)

10.2.3 Post-Type Insulators

Post-type insulators are used for medium- and low-voltage transmission lines, where insulators replace the cross-arm (Fig. 10.3). However, the majority of post insulators are used in substations where insulators support conductors, bus bars, and

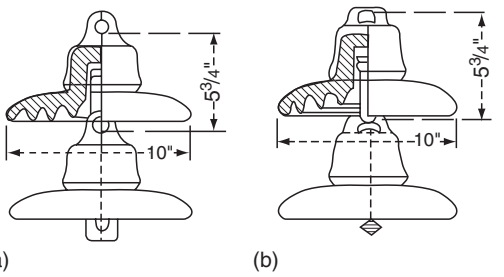

FIGURE 10.6 Insulator string: (a) clevis type, (b) ball-and-socket type.

equipment. A typical example is the interruption chamber of a live tank circuit breaker. Typical post-type insulators are shown in Fig. 10.8.

Older post insulators are built somewhat similar to cap-and-pin insulators, but with hardware that permits stacking of the insulators to form a high-voltage unit. These units can be found in older stations. Modern post insulators consist of a porcelain column, with weather skirts or corrugation on the outside surface to increase leakage distance. For indoor use, the outer surface is corrugated. For outdoor use, a deeper weather shed is used. The end-fitting seals the inner part of the tube to prevent water penetration. Figure 10.8 shows a representative unit used at a substation. Equipment manufacturers use the large post-type insulators to house capacitors, fiber-optic cables and electronics, current transformers, and operating mechanisms. In some cases, the insulator itself rotates and operates disconnect switches.

Post insulators are designed to carry large compression loads, smaller bending loads, and small tension stresses.

10.2.4 Long Rod Insulators

The long rod insulator is a porcelain rod with an outside weather shed and metal end fittings. The long rod is designed for tension load and is applied on transmission lines in Europe. Figure 10.9 shows a typical long rod insulator. These insulators are not used in the U.S. because vandals may shoot the insulators, which will break and cause outages. The main advantage of the long rod design is the elimination of metal parts between the units, which reduces the insulator's length.

10.3 Nonceramic (Composite) Insulators

Nonceramic insulators use polymers instead of porcelain. High-voltage composite insulators are built with mechanical load-bearing fiberglass rods, which are covered by polymer weather sheds to assure high electrical strength.

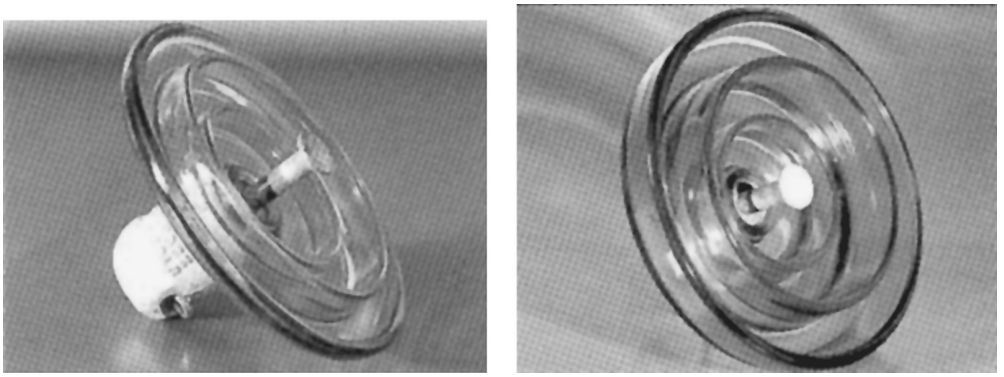

FIGURE 10.7 Standard and fog-type insulators. (Courtesy of Sediver, Inc., Nanterre Cedex, France.)

TABLE 10.5 Typical Number of Standard (5-1/4 ft × 10 in.) Insulators at Different Voltage Levels

Line Voltage (kV)	Number of Standard Insulators
69	4–6
115	7–9
138	8–10
230	12
287	15
345	18
500	24
765	30–35

FIGURE 10.8 Post insulators.

The first insulators were built with bisphenol epoxy resin in the mid-1940s and are still used in indoor applications. Cycloaliphatic epoxy resin insulators were introduced in 1957. Rods with weather sheds were molded and cured to form solid insulators. These insulators were tested and used in England for several years. Most of them were exposed to harsh environmental stresses and failed. However, they have been successfully used indoors. The first composite insulators, with fiberglass rods and rubber weather sheds, appeared in the mid-1960s. The advantages of these insulators are [5–7]:

- Lightweight, which lowers construction and transportation costs.
- More vandalism resistant.
- Higher strength-to-weight ratio, allowing longer design spans.
- Better contamination performance.
- Improved transmission line aesthetics, resulting in better public acceptance of a new line.

However, early experiences were discouraging because several failures were observed during operation. Typical failures experienced were:

- Tracking and erosion of the shed material, which led to pollution and caused flashover.
- Chalking and crazing of the insulator's surface, which resulted in increased contaminant collection, arcing, and flashover.
- Reduction of contamination flashover strength and subsequent increased contamination-induced flashover.
- Deterioration of mechanical strength, which resulted in confusion in the selection of mechanical line loading.
- Loosening of end fittings.
- Bonding failures and breakdowns along the rod-shed interface.
- Water penetration followed by electrical failure.

As a consequence of reported failures, an extensive research effort led to second- and third-generation nonceramic transmission line insulators. These improved units have tracking free sheds, better corona resistance, and slip-free end fittings. A better understanding of failure mechanisms and of mechanical strength-time dependency has resulted in newly designed insulators that are expected to last 20–30 years [8,9]. Increased production quality control and automated manufacturing technology has further improved the quality of these third-generation nonceramic transmission line insulators.

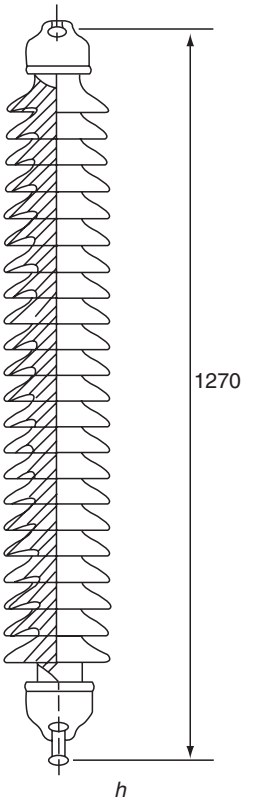

FIGURE 10.9 Long rod insulator.

10.3.1 Composite Suspension Insulators

A cross-section of a third-generation composite insulators is shown in Fig. 10.10. The major components of a composite insulator are:

- End fittings
- Corona ring(s)
- Fiberglass-reinforced plastic rod
- Interface between shed and sleeve
- Weather shed

10.3.1.1 End Fittings

End fittings connect the insulator to a tower or conductor. It is a heavy metal tube with an oval eye, socket, ball, tongue, and a clevis ending. The tube is attached to a fiberglass rod. The duty of the end fitting is to provide a reliable, non-slip attachment without localized stress in the fiberglass rod. Different manufacturers use different technologies. Some methods are:

1. The ductile galvanized iron-end fitting is wedged and glued with epoxy to the rod.
2. The galvanized forged steel-end fitting is swaged and compressed to the rod.
3. The malleable cast iron, galvanized forged steel, or aluminous bronze-end fitting is attached to the rod by controlled swaging. The material is selected according to the corrosion resistance requirement. The end fitting coupling zone serves as a mechanical fuse and determines the strength of the insulator.
4. High-grade forged steel or ductile iron is crimped to the rod with circumferential compression.

The interface between the end fitting and the shed material must be sealed to avoid water penetration. Another technique, used mostly in distribution insulators, involves the weather shed overlapping the end fitting.

10.3.1.2 Corona Ring(s)

Electrical field distribution along a nonceramic insulator is nonlinear and produces very high electric fields near the end of the insulator. High fields generate corona and surface discharges, which are the source of insulator aging. Above 230 kV, each manufacturer recommends aluminum corona rings be installed at the line end of the insulator. Corona rings are used at both ends at higher voltages (>500 kV).

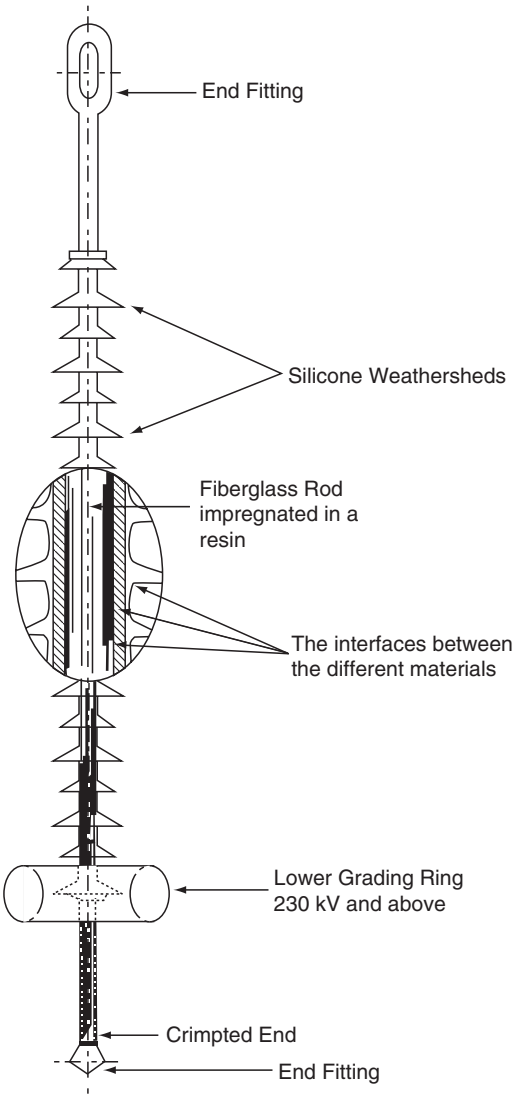

FIGURE 10.10 Cross-section of a typical composite insulator. (From *Toughened Glass Insulators.* Sediver, Inc., Nanterre Cedex, France. With permission.)

10.3.1.3 Fiberglass-Reinforced Plastic Rod

The fiberglass is bound with epoxy or polyester resin. Epoxy produces better-quality rods but polyester is less expensive. The rods are manufactured in a continuous process or in a batch mode, producing the required length. The even distribution of the glass fibers assures equal loading, and the uniform impregnation assures good bonding between the fibers and the resin. To improve quality, some manufacturers use E-glass to avoid brittle fractures. Brittle fracture can cause sudden shattering of the rod.

10.3.1.4 Interfaces Between Shed and Fiberglass Rod

Interfaces between the fiberglass rod and weather shed should have no voids. This requires an appropriate interface material that assures bonding of the fiberglass rod and weather shed. The most frequently used techniques are:

1. The fiberglass rod is primed by an appropriate material to assure the bonding of the sheds.
2. Silicon rubber or ethylene propylene diene monomer (EPDM) sheets are extruded onto the fiberglass rod, forming a tube-like protective covering.
3. The gap between the rod and the weather shed is filled with silicon grease, which eliminates voids.

10.3.1.5 Weather Shed

All high-voltage insulators use rubber weather sheds installed on fiberglass rods. The interface between the weather shed, fiberglass rod, and the end fittings are carefully sealed to prevent water penetration. The most serious insulator failure is caused by water penetration to the interface.

The most frequently used weather shed technologies are:

1. Ethylene propylene copolymer (EPM) and silicon rubber alloys, where hydrated-alumina fillers are injected into a mold and cured to form the weather sheds. The sheds are threaded to the fiberglass rod under vacuum. The inner surface of the weather shed is equipped with O-ring type grooves filled with silicon grease that seals the rod-shed interface. The gap between the end-fittings and the sheds is sealed by axial pressure. The continuous slow leaking of the silicon at the weather shed junctions prevents water penetration.
2. High-temperature vulcanized silicon rubber (HTV) sleeves are extruded on the fiberglass surface to form an interface. The silicon rubber weather sheds are injection-molded under pressure and placed onto the sleeved rod at a predetermined distance. The complete subassembly is vulcanized at high temperatures in an oven. This technology permits the variation of the distance between the sheds.
3. The sheds are directly injection-molded under high pressure and high temperature onto the primed rod assembly. This assures simultaneous bonding to both the rod and the end-fittings. Both EPDM and silicon rubber are used. This one-piece molding assures reliable sealing against moisture penetration.
4. One piece of silicon or EPDM rubber shed is molded directly to the fiberglass rod. The rubber contains fillers and additive agents to prevent tracking and erosion.

10.3.2 Composite Post Insulators

The construction and manufacturing method of post insulators is similar to that of suspension insulators. The major difference is in the end fittings and the use of a larger diameter fiberglass rod. The latter is necessary because bending is the major load on these insulators. The insulators are flexible, which permits bending in case of sudden overload. A typical post-type insulator used for 69-kV lines is shown in Fig. 10.11.

Post-type insulators are frequently used on transmission lines. Development of station-type post insulators has just begun. The major problem is the fabrication of high strength, large diameter fiberglass tubes and sealing of the weather shed.

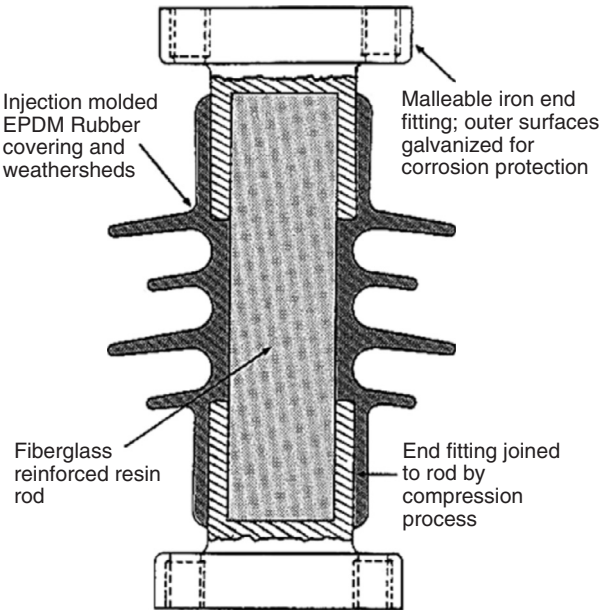

FIGURE 10.11 Post-type composite insulator. (From *Toughened Glass Insulators*. Sediver, Inc., Nanterre Cedex, France. With permission.)

10.4 Insulator Failure Mechanism

10.4.1 Porcelain Insulators

Cap-and-pin porcelain insulators are occasionally destroyed by direct lightning strikes, which generate a very steep wave front. Steep-front waves break down the porcelain in the cap, cracking the porcelain. The penetration of moisture results in leakage currents and short circuits of the unit.

Mechanical failures also crack the insulator and produce short circuits. The most common cause is water absorption by the Portland cement used to attach the cap to the porcelain. Water absorption expands the cement, which in turn cracks the porcelain. This reduces the mechanical strength, which may cause separation and line dropping.

Short circuits of the units in an insulator string reduce the electrical strength of the string, which may cause flashover in polluted conditions.

Glass insulators use alumina cement, which reduces water penetration and the head-cracking problem. A great impact, such as a bullet, can shatter the shell, but will not reduce the mechanical strength of the unit.

The major problem with the porcelain insulators is pollution, which may reduce the flashover voltage under the rated voltages. Fortunately, most areas of the U.S. are lightly polluted. However, some areas with heavy pollution experience flashover regularly.

10.4.2 Insulator Pollution

Insulation pollution is a major cause of flashovers and of long-term service interruptions. Lightning-caused flashovers produce short circuits. The short circuit current is interrupted by the circuit breaker and the line is reclosed successfully. The line cannot be successfully reclosed after pollution-caused flashover because the contamination reduces the insulation's strength for a long time. Actually, the insulator must dry before the line can be reclosed.

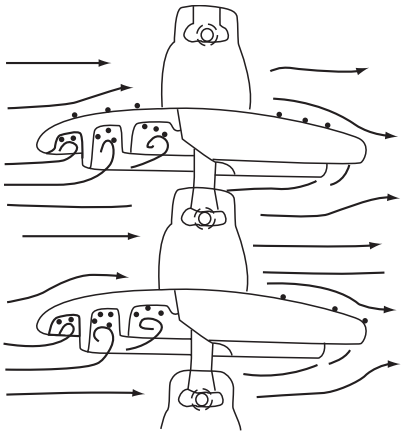

FIGURE 10.12 Deposit accumulation. (From *Application Guide for Composite Suspension Insulators*. Sediver, Inc., York, SC, 1993. With permission.)

10.4.2.1 Ceramic Insulators

Pollution-caused flashover is an involved process that begins with the pollution source. Some sources of pollution are: salt spray from an ocean, salt deposits in the winter, dust and rubber particles during the summer from highways and desert sand, industrial emissions, engine exhaust, fertilizer deposits, and generating station emissions. Contaminated particles are carried in the wind and deposited on the insulator's surface. The speed of accumulation is dependent upon wind speed, line orientation, particle size, material, and insulator shape. Most of the deposits lodge between the insulator's ribs and behind the cap because of turbulence in the airflow in these areas (Fig. 10.12).

The deposition is continuous, but is interrupted by occasional rain. Rain washes the pollution away and high winds clean the insulators. The top surface is cleaned more than the ribbed bottom. The horizontal and V strings are cleaned better by the rain than the I strings. The deposit on the insulator forms a well-dispersed layer and stabilizes around an average value after longer exposure times. However, this average value varies with the changing of the seasons.

Fog, dew, mist, or light rain wets the pollution deposits and forms a conductive layer. Wetting is dependent upon the amount of dissolvable salt in the contaminant, the nature of the insoluble material, duration of wetting, surface conditions, and the temperature difference between the insulator and its surroundings. At night, the insulators cool down with the low night temperatures. In the early morning, the air temperature begins increasing, but the insulator's temperature remains constant. The temperature difference accelerates water condensation on the insulator's surface. Wetting of the contamination layer starts leakage currents.

Leakage current density depends upon the shape of the insulator's surface. Generally, the highest current density is around the pin. The current heats the conductive layer and evaporates the water at the areas with high current density. This leads to the development of dry bands around the pin. The dry bands modify the voltage distribution along the surface. Because of the high resistance of the dry bands, it is across them that most of the voltages will appear. The high voltage produces local arcing. Short arcs (Fig. 10.13) will bridge the dry bands.

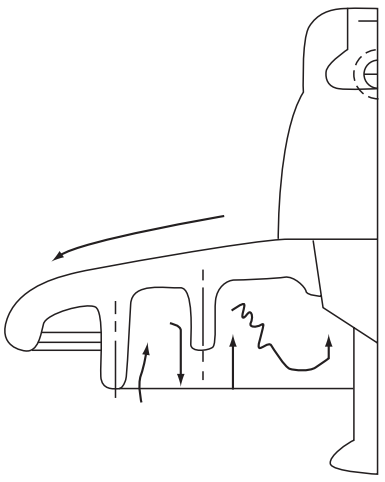

FIGURE 10.13 Dry-band arcing. (From *Application Guide for Composite Suspension Insulators*. Sediver, Inc., York, SC, 1993. With permission.)

Leakage current flow will be determined by the voltage drop of the arcs and by the resistance of the wet layer in series with the dry bands. The arc length may increase or decrease, depending on the layer resistance. Because of the large layer resistance, the arc first extinguishes, but further wetting reduces the resistance, which leads to increases in arc length. In adverse conditions, the level of contamination is high and the layer resistance becomes low because of intensive wetting. After several arcing periods, the length of the dry band will increase and the arc will extend across the insulator. This contamination causes flashover.

In favorable conditions when the level of contamination is low, layer resistance is high and arcing continues until the

sun or wind dries the layer and stops the arcing. Continuous arcing is harmless for ceramic insulators, but it ages nonceramic and composite insulators.

The mechanism described above shows that heavy contamination and wetting may cause insulator flashover and service interruptions. Contamination in dry conditions is harmless. Light contamination and wetting causes surface arcing and aging of nonceramic insulators.

10.4.2.2 Nonceramic Insulators

Nonceramic insulators have a dirt and water repellent (hydrophobic) surface that reduces pollution accumulation and wetting. The different surface properties slightly modify the flashover mechanism.

Contamination buildup is similar to that in porcelain insulators. However, nonceramic insulators tend to collect less pollution than ceramic insulators. The difference is that in a composite insulator, the diffusion of low-molecular-weight silicone oil covers the pollution layer after a few hours. Therefore, the pollution layer will be a mixture of the deposit (dust, salt) and silicone oil. A thin layer of silicone oil, which provides a hydrophobic surface, will also cover this surface.

Wetting produces droplets on the insulator's hydrophobic surface. Water slowly migrates to the pollution and partially dissolves the salt in the contamination. This process generates high resistivity in the wet region. The connection of these regions starts leakage current. The leakage current dries the surface and increases surface resistance. The increase of surface resistance is particularly strong on the shaft of the insulator where the current density is higher.

Electrical fields between the wet regions increase. These high electrical fields produce spot discharges on the insulator's surface. The strongest discharge can be observed at the shaft of the insulator. This discharge reduces hydrophobicity, which results in an increase of wet regions and an intensification of the discharge. At this stage, dry bands are formed at the shed region. In adverse conditions, this phenomenon leads to flashover. However, most cases of continuous arcing develop as the wet and dry regions move on the surface.

The presented flashover mechanism indicates that surface wetting is less intensive in nonceramic insulators. Partial wetting results in higher surface resistivity, which in turn leads to significantly higher flashover voltage. However, continuous arcing generates local hot spots, which cause aging of the insulators.

10.4.3 Effects of Pollution

The flashover mechanism indicates that pollution reduces flashover voltage. The severity of flashover voltage reduction is shown in Fig. 10.14. This figure shows the surface electrical stress (field), which causes flashover as a function of contamination, assuming that the insulators are wet. This means that the salt in the deposit is completely dissolved. The Equivalent Salt Deposit Density (ESDD) describes the level of contamination.

These results show that the electrical stress, which causes flashover, decreases by increasing the level of pollution on all of the insulators. This figure also shows that nonceramic insulator performance is better than ceramic insulator performance. The comparison between EPDM and silicone shows that flashover performance is better for the latter.

Table 10.6 shows the number of standard insulators required in contaminated areas. This table can be used to select the number of insulators, if the level of contamination is known.

Pollution and wetting cause surface discharge arcing, which is harmless on ceramic insulators, but produces aging on composite insulators. Aging is a major problem and will be discussed in the next section.

10.4.4 Composite Insulators

The Electric Power Research Institute (EPRI) conducted a survey analyzing the cause of composite insulator failures and operating conditions. The survey was based on the statistical evaluation of failures reported by utilities.

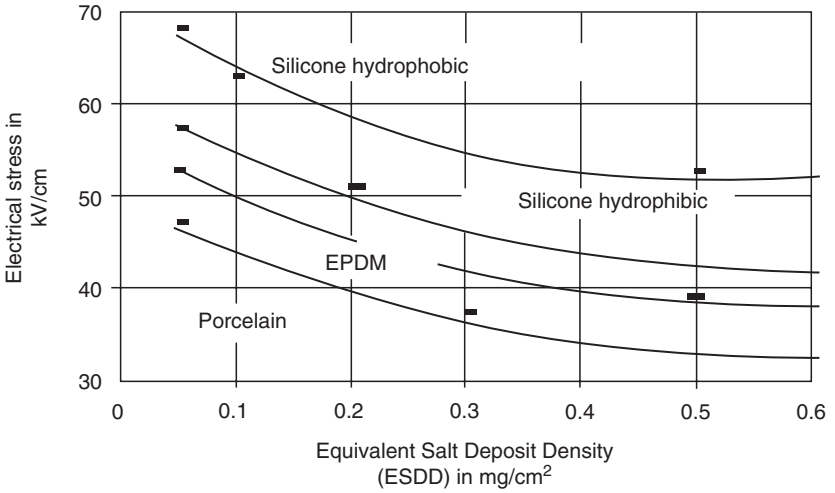

FIGURE 10.14 Surface electrical stress vs. ESDD of fully wetted insulators (laboratory test results). (From *Application Guide for Composite Suspension Insulators*. Sediver, Inc., York, SC, 1993. With permission.)

Results show that a majority of insulators (48%) are subjected to very light pollution and only 7% operate in heavily polluted environments. Figure 10.15 shows the typical cause of composite insulator failures. The majority of failures are caused by deterioration and aging. Most electrical failures are caused by water penetration at the interface, which produces slow tracking in the fiberglass rod surface. This tracking produces a conduction path along the fiberglass surface and leads to internal breakdown of the insulator. Water penetration starts with corona or erosion-produced cuts, holes on the weather shed, or mechanical load-caused separation of the end-fitting and weather shed interface.

Most of the mechanical failures are caused by breakage of the fiberglass rods in the end fitting. This occurs because of local stresses caused by inappropriate crimping. Another cause of mechanical failures is brittle fracture. Brittle fracture is initiated by the penetration of water containing slight acid from pollution. The acid may be produced by electrical discharge and acts as a cathalizator, attacking the bonds and the glass fibers to produce a smooth fracture. The brittle fractures start at high mechanical stress points, many times in the end fitting.

10.4.5 Aging of Composite Insulators

Most technical work concentrates on the aging of nonceramic insulators and the development of test methods that simulate the aging process. Transmission lines operate in a polluted atmosphere.

TABLE 10.6 Number of Standard Insulators for Contaminated Areas

System Voltage KV	Level of Contamination			
	Very light	Light	Moderate	Heavy
138	6/6	8/7	9/7	11/8
230	11/10	14/12	16/13	19/15
345	16/15	21/17	24/19	29/22
500	25/22	32/27	37/29	44/33
765	36/32	47/39	53/42	64/48

Note: First number is for I-string; second number is for V-string.

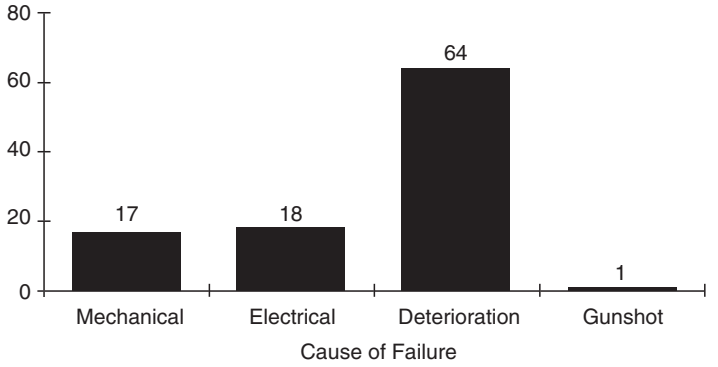

FIGURE 10.15 Cause of composite insulator failure. (From Schneider et al., Nonceramic insulators for transmission lines, *IEEE Transaction on Power Delivery*, 4(4), 2214–2221, April, 1989.)

Inevitably, insulators will become polluted after several months in operation. Fog and dew cause wetting and produce uneven voltage distribution, which results in surface discharge. Observations of transmission lines at night by a light magnifier show that surface discharge occurs in nearly every line in wet conditions. UV radiation and surface discharge cause some level of deterioration after long-term operation. These are the major causes of aging in composite insulators which also lead to the uncertainty of an insulator's life span. If the deterioration process is slow, the insulator can perform well for a long period of time. This is true of most locations in the U.S. and Canada. However, in areas closer to the ocean or areas polluted by industry, deterioration may be accelerated and insulator failure may occur after a few years of exposure [10,11]. Surveys indicate that some insulators operate well for 18–20 years and others fail after a few months. An analysis of laboratory data and literature surveys permit the formulation of the following aging hypothesis:

1. Wind drives dust and other pollutants into the composite insulator's water-repellent surface. The combined effects of mechanical forces and UV radiation produces slight erosion of the surface, increasing surface roughness and permitting the slow buildup of contamination.
2. Diffusion drives polymers out of the bulk skirt material and embeds the contamination. A thin layer of polymer will cover the contamination, assuring that the surface maintains hydrophobicity.
3. High humidity, fog, dew, or light rain produce droplets on the hydrophobic insulator surface. Droplets may roll down from steeper areas. In other areas, contaminants diffuse through the thin polymer layer and droplets become conductive.
4. Contamination between the droplets is wetted slowly by the migration of water into the dry contaminant. This generates a high resistance layer and changes the leakage current from capacitive to resistive.
5. The uneven distribution and wetting of the contaminant produces an uneven voltage stress distribution along the surface. Corona discharge starts around the droplets at the high stress areas. Additional discharge may occur between the droplets.
6. The discharge consumes the thin polymer layer around the droplets and destroys hydrophobicity.
7. The deterioration of surface hydrophobicity results in dispersion of droplets and the formation of a continuous conductive layer in the high stress areas. This increases leakage current.
8. Leakage current produces heating, which initiates local dry band formation.
9. At this stage, the surface consists of dry regions, highly resistant conducting surfaces, and hydrophobic surfaces with conducting droplets. The voltage stress distribution will be uneven on this surface.

10. Uneven voltage distribution produces arcing and discharges between the different dry bands. These cause further surface deterioration, loss of hydrophobicity, and the extension of the dry areas.
11. Discharge and local arcing produces surface erosion, which ages the insulator's surface.
12. A change in the weather, such as the sun rising, reduces the wetting. As the insulator dries, the discharge diminishes.
13. The insulator will regain hydrophobicity if the discharge-free dry period is long enough. Typically, silicon rubber insulators require 6–8 h; EPDM insulators require 12–15 h to regain hydrophobicity.
14. Repetition of the described procedure produces erosion on the surface. Surface roughness increases and contamination accumulation accelerates aging.
15. Erosion is due to discharge-initiated chemical reactions and a rise in local temperature. Surface temperature measurements, by temperature indicating point, show local hot-spot temperatures between 260°C and 400°C during heavy discharge.

The presented hypothesis is supported by the observation that the insulator life spans in dry areas are longer than in areas with a wetter climate. Increasing contamination levels reduce an insulator's life span. The hypothesis is also supported by observed beneficial effects of corona rings on insulator life.

DeTourreil et al. (1990) reported that aging reduces the insulator's contamination flashover voltage. Different types of insulators were exposed to light natural contamination for 36–42 months at two different sites. The flashover voltage of these insulators was measured using the "quick flashover salt fog" technique, before and after the natural aging. The quick flashover salt fog procedure subjects the insulators to salt fog (80 kg/m^3 salinity). The insulators are energized and flashed over 5–10 times. Flashover was obtained by increasing the voltage in 3% steps every 5 min from 90% of the estimated flashover value until flashover. The insulators were washed, without scrubbing, before the salt fog test. The results show that flashover voltage on the new insulators was around 210 kV and the aged insulators flashed over around 184–188 kV. The few years of exposure to light contamination caused a 10–15% reduction of salt fog flashover voltage.

Natural aging and a follow-up laboratory investigation indicated significant differences between the performance of insulators made by different manufacturers. Natural aging caused severe damage on some insulators and no damage at all on others.

10.5 Methods for Improving Insulator Performance

Contamination caused flashovers produce frequent outages in severely contaminated areas. Lines closer to the ocean are in more danger of becoming contaminated. Several countermeasures have been proposed to improve insulator performance. The most frequently used methods are:

1. **Increasing leakage distance by increasing the number of units or by using fog-type insulators**. The disadvantages of the larger number of insulators are that both the polluted and the impulse flashover voltages increase. The latter jeopardizes the effectiveness of insulation coordination because of the increased strike distance, which increases the overvoltages at substations.
2. **Application insulators are covered with a semiconducting glaze**. A constant leakage current flows through the semiconducting glaze. This current heats the insulator's surface and reduces the moisture of the pollution. In addition, the resistive glaze provides an alternative path when dry bands are formed. The glaze shunts the dry bands and reduces or eliminates surface arcing. The resistive glaze is exceptionally effective near the ocean.
3. **Periodic washing of the insulators with high-pressure water**. The transmission lines are washed by a large truck carrying water and pumping equipment. Trained personnel wash the insulators by aiming the water spray toward the strings. Substations are equipped with permanent washing systems. High-pressure nozzles are attached to the towers and water is supplied from a central pumping station. Safe washing requires spraying large amounts of water at the insulators in a

short period of time. Fast washing prevents the formation of dry bands and pollution-caused flashover. However, major drawbacks of this method include high installation and operational costs.

4. **Periodic cleaning of the insulators by high pressure driven abrasive material, such as ground corn cobs or walnut shells**. This method provides effective cleaning, but cleaning of the residual from the ground is expensive and environmentally undesirable.
5. **Replacement of porcelain insulators with nonceramic insulators**. Nonceramic insulators have better pollution performance, which eliminates short-term pollution problems at most sites. However, insulator aging may affect the long-term performance.
6. **Covering the insulators with a thin layer of room-temperature vulcanized (RTV) silicon rubber coating**. This coating has a hydrophobic and dirt-repellent surface, with pollution performance similar to nonceramic insulators. Aging causes erosion damage to the thin layer after 5–10 years of operation. When damage occurs, it requires surface cleaning and a reapplication of the coating. Cleaning by hand is very labor intensive. The most advanced method is cleaning with high pressure driven abrasive materials like ground corn cobs or walnut shells. The coating is sprayed on the surface using standard painting techniques.
7. **Covering the insulators with a thin layer of petroleum or silicon grease**. Grease provides a hydrophobic surface and absorbs the pollution particles. After one or two years of operation, the grease saturates the particles and it must be replaced. This requires cleaning of the insulator and application of the grease, both by hand. Because of the high cost and short life span of the grease, it is not used anymore.

References

1. *Transmission Line Reference Book (345 kV and Above)*, 2nd ed., EL 2500 Electric Power Research Institute (EPRI), Palo Alto, CA, 1987.
2. Fink, D.G. and Beaty, H.W., *Standard Handbook for Electrical Engineers*, 11th ed., McGraw-Hill, New York, 1978.
3. Looms, J.S.T., *Insulators for High Voltages*, Peter Peregrinus Ltd., London, 1988.
4. *Toughened Glass Insulators*. Sediver Inc., Nanterre Cedex, France.
5. *Application Guide for Composite Suspension Insulators*, Sediver Inc., York, SC, 1993.
6. Hall, J.F., History and bibliography of polymeric insulators for outdoor application, *IEEE Transaction on Power Delivery*, 8(1), 376–385, January, 1993.
7. Schneider, H., Hall, J.F., Karady, G., and Rendowden, J., Nonceramic insulators for transmission lines, *IEEE Transaction on Power Delivery*, 4(4), 2214–2221, April, 1989.
8. Karady, G.G., Outdoor insulation, *Proceedings of the Sixth International Symposium on High Voltage Engineering*, New Orleans, LA, September, 1989, 30.01–30.08.
9. DeTourreil, C.H. and Lambeth, P.J., Aging of composite insulators: Simulation by electrical tests, *IEEE Trans. on Power Delivery*, 5(3), 1558–1567, July, 1990.
10. Karady, G.G., Rizk, F.A.M., and Schneider, H.H., Review of CIGRE and IEEE Research into Pollution Performance of Nonceramic Insulators: Field Aging Effect and Laboratory Test Techniques, in *International Conference on Large Electric High Tension Systems (CIGRE), Group 33*, (33–103), Paris, 1–8, August, 1994.
11. Gorur, R.S., Karady, G.G., Jagote, A., Shah, M., and Yates, A., Aging in silicon rubber used for outdoor insulation, *IEEE Transaction on Power Delivery*, 7(2), 525–532, March, 1992.

11

Transmission Line Construction and Maintenance

Wilford Caulkins
Sherman & Reilly

Kristine Buchholz
Pacific Gas & Electric Company

The information herein was derived from personal observation and participation in the construction of overhead transmission lines for over 40 years. Detailed information, specific tools and equipment have been provided previously and are available in IEEE Standard 524-2003 and IEEE Standard 524A-1993.

The purpose of this chapter is to give a general overview of the steps that are necessary in the planning and construction of a typical overhead transmission line, to give newcomers to the trade a general format to follow, and assist transmission design engineers in understanding how such lines are built.

Stringing overhead conductors in transmission is a very specialized type of construction requiring years of experience, as well as equipment and tools that have been designed, tried, and proven to do the work. Because transmission of electrical current is normally at higher voltages (69 kV and above), conductors must be larger in diameter and span lengths must be longer than in normal distribution. Although proximity to other energized lines may be limited on the right-of-way, extra care must be exercised to protect the conductor so that when energized, power loss and corona are not a problem.

There are four methods that can be used to install overhead transmission conductors:

1. Slack stringing
2. Semi-tension stringing
3. Full-tension stringing
4. Helicopter stringing

Slack stringing can only be utilized if it is not necessary to keep the conductor off of the ground, and if no energized lines lie beneath the line being strung. In this method the pulling lines are pulled out on the ground, threaded through the stringing blocks, and the conductor is pulled in with less tension than is required to keep it off the ground. This is not considered to be an acceptable method when demands involve maximum utilization of transmission requirements.

Semi-tension methods are merely an upgrading of slack stringing, but do not necessarily keep the conductor completely clear of the ground, or the lines used to pull.

Full-tension stringing is a method of installing the conductors and overhead groundwire in which sufficient pulling capabilities on one end and tension capabilities on the other, keep the wires clear of any obstacles during the movement of the conductor from the reel to its final sag position. This ensures that

these current-carrying cables are "clipped" into the support clamps in the best possible condition, which is the ultimate goal of the work itself.

Stringing with helicopters, which is much more expensive per hour of work, can be much less expensive when extremely arduous terrain exists along the right-of-way and when proper pre-planning is utilized. Although pulling conductors themselves with a helicopter can be done, it is limited and normally not practical. Maximum efficiency can be achieved when structures are set and pilot lines are pulled with the helicopter, and then the conductor stringing is done in a conventional manner. Special tools (such as stringing blocks) are needed if helicopters are used.

So that maximum protection of the conductor is realized and maximum safety of personnel is attained, properly designed and constructed tools and equipment are tantamount to a successful job. Because the initial cost of these tools and equipment represent such a small percentage of the overall cost of the project, the highest quality should be used, thus minimizing "down time" and possible failure during the course of construction.

11.1 Tools

Basic tools needed to construct overhead transmission lines are as follows:

1. Conductor blocks
2. Overhead groundwire blocks
3. Catch-off blocks
4. Sagging blocks
5. Pulling lines
6. Pulling grips
7. Catch-off grips
8. Swivels
9. Running boards
10. Conductor lifting hooks
11. Hold-down blocks

Conductor blocks are made in the following configurations:

1. Single conductor
2. Multiple conductor
3. Multiversal type (can be converted from bundle to single, and vice versa)
4. Helicopter

Conductor blocks should be large enough to properly accommodate the conductor and be lined with a resilient liner such as neoprene or polyurethane and constructed of lightweight, high-strength materials. Some sheaves are made of synthetic material such as nylatron. Sheaves should be mounted on anti-friction ball bearings to reduce the tension required in stringing and facilitate proper sagging. Conductor blocks are available for stringing single conductors or multiple conductors. Some are convertible, thus enhancing their versatility. When stringing multiple conductors, it is desirable to pull all conductors with a single pulling line so that all conductors in the bundle have identical tension history. The running board makes this possible. Pulling lines are divided into two categories:

1. Steel cable
2. Synthetic rope

Because of the extra high tension required in transmission line construction, steel pulling lines and pilot lines are most practical to use. Torque-resistant, stranded, and swagged cable are used so that ball bearing swivels can be utilized to prevent torque buildup from being transferred to the conductor. Some

braided or woven steel cables are also used. If synthetic ropes are utilized, the most important features should include:

1. No torque
2. Very minimum elongation
3. No "kinking"
4. Easily spliced
5. High strength/small diameter
6. Excellent dielectric properties

Stringing overhead groundwires does not normally require the care of current-carrying conductors. Most overhead groundwires are stranded steel construction and the use of steel wire with a fiber-optic core for communications has become a common practice. Special care should be taken to ensure that excessive bending does not occur when erecting overhead groundwires with fiber-optic centers, such as OPT-GW (Optical Power Telecommunications—Ground Wire) and ADSS (All Dielectric Self-Supporting Cable). New types of conductor such as ACCR, Aluminum Conductor Composite Reinforced, need special care. Use of array (multi-sheave in tandem) blocks may be necessary. Special instructions are available from the manufacturer, which specify minimum sheave and bullwheel diameter for construction. OPT-GW should be strung using an antirotational device to prevent the cable from twisting.

11.2 Equipment

Pullers are used to bring in the main pulling line. Multi-drum pullers, called pilot line winders, are used to tension string the heavy pulling cable.

Primary pullers are used to tension string the conductors. These pullers are either drum type or bullwheel type. The drum type is used more extensively in many areas of North America because the puller and pulling cable are stored on one piece of equipment, but it is not practical in other areas because it is too heavy. Thus, the bullwheel type is used allowing the puller and pulling cable to be separated onto two pieces of equipment. Also, the pulling cable can be separated into shorter lengths to allow easier handling, especially if manual labor is preferred.

Tensioners should be bullwheel type using multigroove wheels for more control. Although V groove machines are used on some lighter, smaller conductors, they are not recommended in transmission work because of the crushing effect on the conductor. Tensioners are either mounted on a truck or trailer.

Reel stands are used to carry the heavy reels of conductor and are equipped with brakes to hold "tailing tension" on the conductor as it is fed into the bullwheel tensioner. These stands are usually mounted on a trailer separated from the tensioner.

Helicopters are normally used to fly in a light line which can be used to pull in the heavier cable.

11.3 Procedures

Once the right-of-way has been cleared, the following are normal steps taken in construction:

1. Framing
2. Pulling
3. Pulling overhead groundwire up to sag and installation
4. Pulling in main line with pilot line
5. Stringing conductors
6. Sagging conductors
7. Clipping in conductors
8. Installing spacer or spacer dampers where applicable

Framing normally consists of erecting poles, towers, or other structures, including foundations and anchors on guyed structures. It is desirable for the stringing blocks to be installed, with finger lines, on

the ground before structures are set, to eliminate an extra climb later. Helicopters are used to set structures, especially where rough terrain exists or right-of-way clearances are restricted.

Once structures are secure, overhead groundwire and pilot lines are pulled in together with a piece of equipment such as a caterpillar or other track vehicle. A helicopter is also used to fly in these lines. Once the overhead groundwires are in place, they are sagged and secured, thus giving the structures more stability for the stringing of the conductors. This is especially important for guyed structures.

Normally the three pilot lines (typically 3/8 in. diameter swagged steel cable) pull in the heavier pulling line (typically 3/4 in. diameter or 7/8 in. diameter swagged steel) under tension. The main pulling line is then attached to the conductor which is strung under full tension. Once the conductor is "caught off," the main pulling line is returned for pulling of the next phase.

Once the conductors are in place, they are then brought up to final sag and clipped into the conductor clamps provided. If the conductor is a part of a bundle per phase, the spacers or spacer dampers are installed, using a spacer cart which is either pulled along from the ground or self-propelled.

Coordination between design engineers and construction personnel is very important in the planning and design of transmission lines. Although it is sometimes impossible to accommodate the most efficient capabilities of the construction department (or line contractor), much time and money can be conserved if predesign meetings are held to discuss items such as the clearances needed for installing overhead groundwire blocks, hardware equipped with "work" holes to secure lifting hooks or blocks, conductor reel sizes compatible with existing reel stands, length of pull most desirable, or towers equipped to facilitate climbing.

For maximum safety of personnel constructing transmission lines, proper and effective grounding procedures should be utilized. Grounding can be accomplished by:

1. adequate grounding of conductors being strung and pulling cables being used, or
2. fully insulating equipment and operator,
3. isolating equipment and personnel.

All equipment, conductors, anchors, and structures within a defined work area must be bonded together and connected to the ground source. The recommended procedures of personnel protection are the following:

1. Establish equipotential work zones.
2. Select grounding equipment for the worst-case fault.
3. Discontinue all work when the possibility of lightning exists which may affect the work site.

In addition to the grounding system, the best safety precaution is to treat all equipment as if it could become energized.

11.4 Helicopters

As already mentioned, the use of helicopters is another option that is being chosen more frequently for transmission system construction and maintenance. There are a wide variety of projects where helicopters become involved, making the projects easier, safer, or more economical. When choosing any construction or maintenance method, identify the work to be accomplished, analyze the potential safety aspects, list the possible alternatives, and calculate the economics. Helicopters add a new dimension to this analytical process by adding to the alternatives, frequently reducing the risks of accident or injury, and potentially reducing costs. The most critical consideration in the use of a helicopter is the ability to safely position the helicopter and line worker at the work location.

11.4.1 Conductor Stringing

Helicopters are used for conductor stringing on towers through the use of pilot lines. Special stringing blocks are installed at each tower and a helicopter is brought in and attached to a pilot line. The

helicopter flies along the tower line and slips the pilot line in through each stringing block until it reaches the end of the set of towers for conductor pulling, where it disconnects and the pilot line is transferred to a ground crew. The ground crew then proceeds to pull the conductor in the conventional manner (Caulkins, 1987). The helicopter may also be used to monitor the conductor pulling and is readily available to assist if the conductor stalls at any tower location.

11.4.2 Structure and Material Setting

The most obvious use of helicopters is in the setting of new towers and structures. Helicopters are frequently used in rough terrain to fly in the actual tower to a location where a ground crew is waiting to spot the structure into a preconstructed foundation. In addition, heavy material can be transported to remote locations, as well as the construction crew.

The use of helicopters can be especially critical if the tower line is being replaced following a catastrophe or failure. Frequently, roads and even construction paths are impassable or destroyed following natural disasters. Helicopters can carry crews and materials with temporary structures that can be erected within hours to restore tower lines. Again, depending on the terrain and current conditions, whether the existing structure is repaired or temporary tower structures are utilized, the helicopter is invaluable to carry in the needed supplies and personnel.

11.4.3 Insulator Replacement

A frequent maintenance requirement on a transmission system is replacing insulators. This need is generated for various reasons, including line upgrading, gunshots, environmental damage, or defects in the original insulator manufacturing. With close coordinated crews, helicopters can maximize the efficiency of the replacement project.

Crews are located at several towers to perform the actual insulator removal and installation. The crews will do the required setup for a replacement, but the helicopter can be used to bring in the necessary tools and equipment. The crew removes the old insulator string and sets it to one side of the work location. When the crews are ready, the helicopter flies in the new insulator string to each tower. The crew on the tower detaches the new insulator string from the helicopter, positions it, and then attaches the old string to the helicopter, which removes the string to the staging area. With a well-coordinated team of helicopters and experienced line workers, it is not unusual to achieve a production rate of replacing all insulators on four three-phase structures per crew per day. Under ideal conditions, crews are able to replace the insulators on a structure in one hour (Buchholz, 1987).

11.4.4 Replacing Spacers

One of the first uses of helicopters in live-line work was the replacement of spacers in the early 1980s. This method was a historic step in live-line work since it circumvented the need for hot sticks or insulated aerial lift devices.

The first projects involved a particular spacer wearing into the conductor strands, causing the separation of the conductor. Traditionally, the transmission line would have been de-energized, grounded, and either a line worker would have utilized a spacer cart to move out on the line to replace the spacer, or the line would have been lowered and the spacer replaced and the conductor strengthened. The obvious safety dilemma was whether the conductor could support a line worker on a spacer cart or whether it was physically able to withstand the tensions of lowering it to the ground. By utilizing a helicopter and bare-hand work methods, the spacers were able to be replaced and the conductor strengthened where necessary with full-tension compression splices while providing total safety to the line workers and a continuous supply of energy over the transmission lines. One of the early projects achieved a replacement and installation of 25,000 spacers without a single accident or injury. A typical spacer replacement required about 45 sec, including the travel time between work locations (Buchholz, 1987).

11.4.5 Insulator Washing

Another common practice is to utilize helicopters for insulator washing. Again, this is a method that allows for the line to remain energized during the process. The helicopter carries a water tank that is refilled at a staging area near the work location. A hose and nozzle are attached to a structure on the helicopter and are operated by a qualified line worker who directs the water spray and adequately cleans the insulator string. Again, with the ease of access afforded by the helicopter, the speed of this operation can result in a typical three-phase tower being cleaned in a few minutes.

11.4.6 Inspections

Helicopters are invaluable for tower line and structure inspections. Due to the ease of the practice and the large number of inspections that can be accomplished, utilities have increased the amount of maintenance inspections being done, thus promoting system reliability.

Helicopters typically carry qualified line workers who utilize stabilizing binoculars to visually inspect the transmission tower for signs of rusting or weakness and the transmission hardware and conductor for damage and potential failure. Infrared inspections and photographic imaging can also be accomplished from the helicopter, either by mounting the cameras on the helicopter or through direct use by the crew. During these inspections, the helicopter provides a comfortable situation for accomplishing the necessary recording of specific information, tower locations, etc. In addition, inspections from helicopters are required following a catastrophic event or system failure. It is the only logical method of quickly inspecting a transmission system for the exact location and extent of damage.

11.4.7 Helicopter Method Considerations

The ability to safely position a helicopter and worker at the actual work site is the most critical consideration when deciding if a helicopter method can be utilized for construction or maintenance. The terrain and weather conditions are obvious factors, as well as the physical spacing needed to position the helicopter and worker in the proximity required for the work method. If live-line work methods are to be utilized, the minimum approach distance required for energized line work must be calculated very carefully for every situation. The geometry of each work structure, the geometry of the individual helicopter, and the positioning of the helicopter and worker for the specific work method must be analyzed. There are calculations that are available to analyze the approach distances (IEEE Task Force 15.07.05.05, 1999).

When choosing between construction and maintenance work methods, the safety of the line workers is the first consideration. Depending on circumstances, a helicopter method may be the safest work method. Terrain has always been a primary reason for choosing helicopters to assist with projects since the ability to drive to each work site may not be possible. However, helicopters may still be the easiest and most economic alternative when the terrain is open and flat, especially when there are many individual tower locations that will be contacted. Although helicopters may seem to be expensive on a per person basis, the ability to quickly position workers and easily move material can drastically reduce costs. When live-line methods can be utilized, the positioning of workers, material, and equipment becomes comparatively easier.

Finally, if the safe use of the helicopter allows the transmission systems to remain energized throughout the project, the helicopter may be the only possible alternative. Since the transmission system is a major link in the competitive energy markets, transmission operation will have reliability performance measures which must be achieved. Purchasing replacement energy through alternate transmission paths, as was done in the regulated world, is no longer an option. Transmission system managers are required to keep systems operational and will be fined if high levels of performance are not attained. The option of de-energizing systems for maintenance practices may be too costly in the deregulated world.

References

Buchholz, F., Helicopter application in transmission system maintenance and repair, in *IEEE/CSEE Joint Conference on High-Voltage Transmission Systems in China*, October 1987.

Caulkins, III., W., Practical applications and experiences in the installation of overhead transmission line conductors, in *IEEE/CSEE Joint Conference on High-Voltage Transmission Systems in China*, October, 1987.

Guide to Grounding During the Installation of Overhead Transmission Line Conductors: Supplement to IEEE Guide to the Installation of Overhead Transmission Line Conductors, IEEE 524A–1993, 1998.

Guide to the Installation of Overhead Transmission Line Conductors, IEEE 524–1992, 1998.

IEEE Task Force 15.07.05.05, PE 046 PRD (04–99), Recommended Practices for Helicopter Bonding Procedures for Live Line Work.

12

Insulated Power Cables Used in Underground Applications

Michael L. Dyer
Salt River Project

Aesthetics is primarily the major reason for installing power cables underground, providing open views of the landscape free of poles and wires. One could also argue that underground lines are more reliable than overhead lines as they are not susceptible to weather and tree caused outages, common to overhead power lines. This is particularly true of temporary outages caused by wind, which represents approximately 80% of all outages occurring on overhead systems. However, underground lines are susceptible to being damaged by excavations (reason behind "call before digging" locating programs implemented by many states in the U.S.). The time required to repair a damaged underground line may be considerably longer than an overhead line. Underground lines are typically ten times more expensive to install than overhead lines. The ampacity, current carrying capacity, of an underground line is less than an equivalent sized overhead line. Underground lines require a higher degree of planning than overhead, because it is costly to add or change facilities in an existing system. Underground cables do not have an infinite life, because the dielectric insulation is subjected to aging; therefore, systems should be designed with future replacement or repair as a consideration.

12.1 Underground System Designs

There are two types of underground systems (Fig. 12.1).

A. Radial—where the transformers are served from a single source.
B. Looped—where the transformers are capable of being served from one of two sources. During normal operation an open is located at one of the transformers, usually the midpoint.

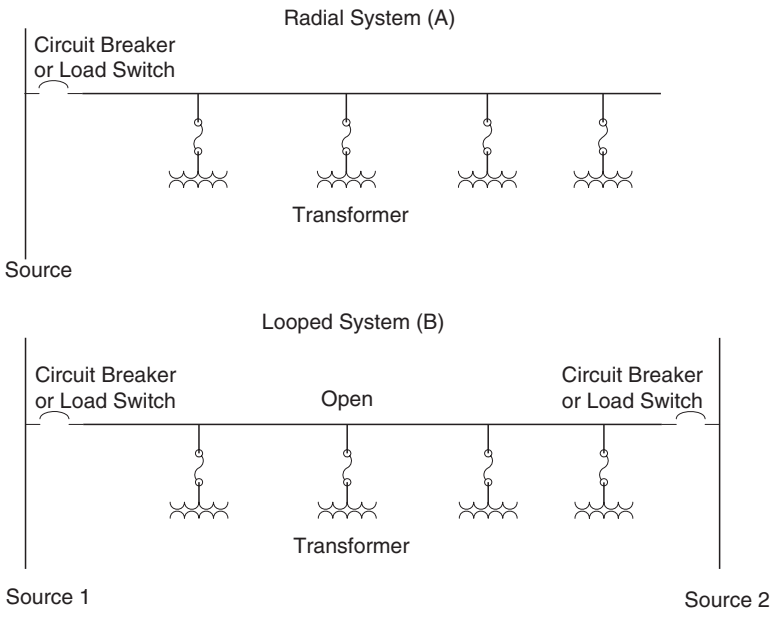

FIGURE 12.1 (A) Radial system and (B) looped system.

A radial system has the lowest initial cost, because a looped system requires the additional facilities to the second source. Outage restoration on a radial system requires either a cable repair or replacement, whereas on a looped system, switching to the alternate source is all that is required.

Underground cable can be directly buried in earth, which is the lowest initial cost, allows splicing at the point of failure as a repair option and allows for maximum ampacity. Cables may also be installed in conduit, which is an additional cost, requires replacement of a complete section as the repair option, reduces the ampacity, because the conduit wall and surrounding air are additional thermal resistances, but provides protection to the cable.

Underground power cables have three classifications.

1. Low voltage—limited to 2 kV. Primarily used as service cables
2. Medium voltage—2–46 kV. Primarily used to supply distribution transformers
3. High voltage—above 46 kV. Primarily used to supply substation transformers

American Standards Testing Material (ASTM), Insulated Cable Engineering Association (ICEA), National Electrical Manufacturing Association (NEMA), and Association of Edison Illuminating Companies (AEIC) have published standards for the various types of power cables.

12.2 Conductor

Common among all classes in function is the central conductor, the purpose of which is to conduct power (current and voltage) to serve a load. The metals of choice are either copper or aluminum. This central conductor may be composed of a single element (solid) or composed of multiple elements (stranded), on the basis of a geometric progression of 6, 12, 18, etc. of individual strands for each layer. Each layer is helically applied in the opposite direction of the underlying layer.

There are three common types of stranding available.

1. Concentric round
2. Compressed round (97% of the diameter of concentric)
3. Compact round (90–91% of the diameter of concentric)

Note: Some types of connectors may be suitable for stranded types 1 and 2 but not type 3 for the same size.

To improve manufacturing, 19 wire combination unilay stranding (helically applied in one direction one operation) has become popular in low-voltage applications, where some of the outer strands are of a smaller diameter, but the same outside diameter as compressed round is retained. Another stranding method which retains the same overall diameter is single input wire (SIW) compressed, which can be used to produce a wide range of conductors using a smaller range of the individual strands.

Conductors used at transmission voltages may have exotic stranding to reduce the voltage stress.

Cables requiring greater flexibility such as portable power cable utilize very fine strands with a rope type stranding.

Typical sizes for power conductors are #6 American Wire Gage (AWG) through 1000 kcmils. One cmil is defined as the area of a circle having a diameter of one mil (0.0001 in.). Solid conductors are usually limited to a maximum of #1/0 because of flexibility.

The metal type and size determines the ampacity and losses (I^2R). Copper having a higher intrinsic conductivity will have a greater ampacity and lower resistance than an equivalent size aluminum conductor. Aluminum 1350 alloy medium hardness is typical for power cable use.

12.3 Insulation

In order to install power cables underground, the conductor must be insulated. For low-voltage applications, a layer of insulation is extruded onto the conductor. Many types of insulation compounds have been used from natural or synthetic rubber, polyvinyl chloride (PVC), high molecular weight polyethylene (HMWPE), and cross-linked polyethylene (XLPE) to name a few. Although each insulation type has various characteristics, operating temperature and durability are probably the most important. XLPE is probably the most widely used insulation for low-voltage cables. XLPE is a thermoset plastic with its hydrocarbon molecular chains cross-linked. Cross-linking is a curing process, which occurs under heat and pressure, or as used for low-voltage cables, moisture and allows an operating temperature of 90°C.

Multiple layer cable insulation composed of a softer compound under a harder compound, a single layer harder insulation, or a self-healing insulation are used to address protection of the conductor, typically for direct buried low-voltage power cables.

12.4 Medium- and High-Voltage Power Cables

Medium- and high-voltage power cables, in addition to being insulated, are shielded to contain and evenly distribute the electric field within the insulation.

The components and function of a medium- and high-voltage cable are as follows (Figs. 12.2A and 12.2B):

1. The center conductor—metallic path to carry power.
2. The conductor shield—a semiconducting layer placed over the conductor to provide a smooth conducting cylinder around the conductor. Typical of today's cables, this layer is a semiconducting plastic, polymer with a carbon filler, extruded directly over the conductor. This layer represents a very smooth surface, which, because of direct contact with the conductor, is elevated to the applied voltage on the conductor.
3. The insulation—a high dielectric material to isolate the conductor. The two basic types used today are XLPE or ethylene propylene rubber (EPR). Because of an aging effect known as treeing (Fig. 12.3), on the basis of its visual appearance, caused by moisture in the presence of an electric field, a modified version of XLPE designated tree retardant (TRXLPE) has replaced the use of XLPE for medium-voltage applications. High-voltage transmission cables still utilize XLPE, but they usually have a moisture barrier. TRXLPE is a very low loss dielectric that is reasonably

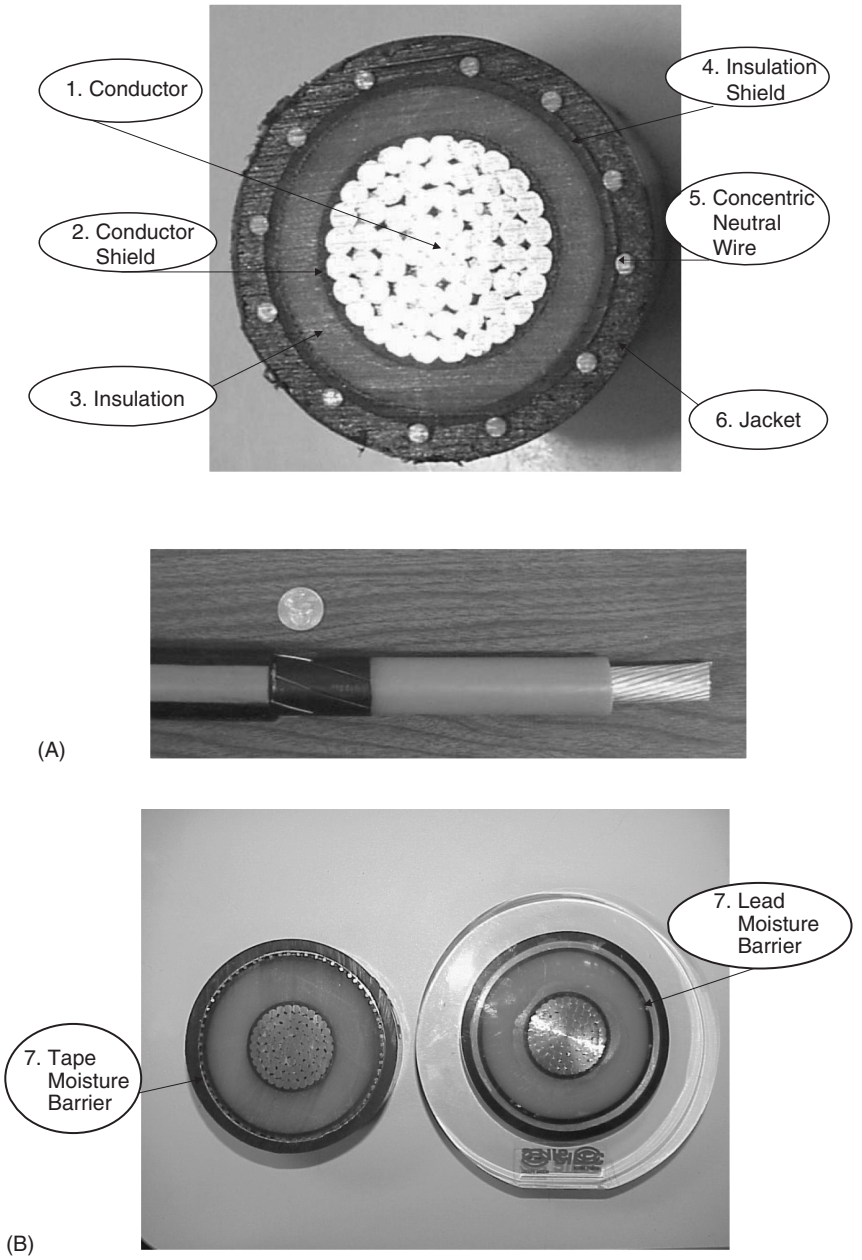

FIGURE 12.2 (A) Medium-voltage cable components, (B) high-voltage cable components.

flexible and has an operating temperature limit of 90°C or 105°C depending on type. TRXLPE because it is cross-linked, does not melt at high operating temperatures but softens. EPR is a rubber-based insulation having higher losses than TRXLPE and is very flexible and has an operating temperature limit of 105°C. EPR does not melt or soften as much as TRXLPE at high operating temperatures, because of its high filler content.

4. The insulation shield—a semiconducting layer to provide a smooth cylinder around the outside surface of the insulation. Typical shield compound is a polymer with a carbon filler that is extruded directly over the insulation. This layer, for medium-voltage applications, is not fully

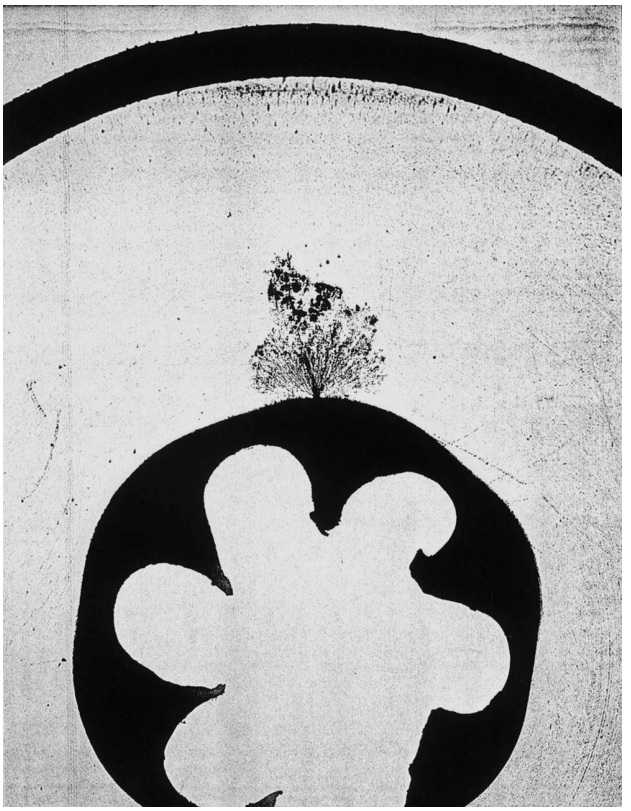

FIGURE 12.3 Tree in XLPE.

bonded to the insulation (strippable) to allow relatively easy removal for the installation of cable accessories. Transmission cables have this layer bonded to the insulation, which requires shaving tools to remove.

5. The metallic shield—a metallic layer, which may be composed of wires, tapes, or corrugated tube. This shield is connected to the ground, which keeps the insulation shield at ground potential and provides a return path for fault current. Medium-voltage cables can utilize the metallic shield as the neutral return conductor if sized accordingly. Typical metallic shield sizing criteria:

   A. Equal in ampacity to the central conductor for one phase applications.
   B. One-third the ampacity for three-phase applications.
   C. Fault duty for three-phase feeders and transmission applications.

6. Overall jacket—a plastic layer applied over the metallic shield for physical protection. This polymer layer may be extruded as a loose tube or directly over the metallic shield (encapsulated). Although both provide physical protection, the encapsulated jacket removes the space present in a loose tube design, which may allow longitudinal water migration. The typical compound used for jackets is linear low density polyethylene (LLDPE), because of its ruggedness and relatively low water vapor transmission rate. Jackets can be specified insulating (most common) or semiconducting (when jointly buried and randomly laid with communication cables).
7. Moisture barrier—a sealed metallic barrier applied either over or under the overall jacket. Typically used for transmission cables, this barrier may be a sealed tape, corrugated tube, or lead sheath.

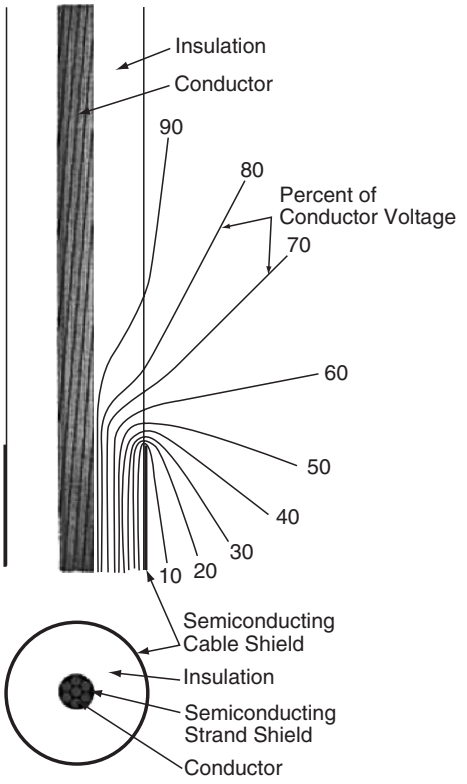

FIGURE 12.4 Voltage distribution in the insulation with the cable shield removed.

Cable components 1–4 comprise the cable core, which in cross-section, is a capacitor with the conductor shield and insulation shield making up the plates on each side of a dielectric. These plates evenly distribute the electric field radially in all directions within the insulation; however, until the metallic shield is added and effectively grounded, the insulation shield is subject to capacitive charging and presents a shock hazard. To be considered effectively grounded, the National Electrical Safety Code (NESC) requires a minimum of four ground connections per mile of line or eight grounds per mile when jointly buried with communication cables for insulating jackets. Semiconducting jackets are considered grounded when in contact with earth.

Because medium- and high-voltage cables are shielded, special methods are required to connect them to devices or other cables. Since the insulation shield is conductive and effectively grounded, it must be carefully removed a specific distance from the conductor end, on the basis of the operating voltage. Once the insulation shield has been removed, the electric field will no longer be contained within the insulation and the highest electrical stress will be concentrated at the end of the insulation shield (Fig. 12.4). Premolded, cold or heat shrink, or special tapes are applied at this location to control this stress, allowing the cable to be connected to various devices (Fig. 12.5).

12.5 Shield Bonding Practice

Generally, the metallic shields on distribution circuits are grounded at every device. Transmission circuits, however, may use one of the following configurations.

Multiple ground connections (multigrounded) (Fig. 12.6A): The metallic shield will carry an induced current because they surround the alternating current in the central conductor. This circulating current results in an I^2R heating loss, which adversely affects the ampacity of the cable.

Single point grounded (Fig. 12.6B): The metallic shield is grounded at a single point and no current can flow in the metallic shield because there is no closed circuit. This configuration allows the maximum ampacity rating for the cable; however, a voltage will be present on the open end, which may be a hazard. This voltage is dependent on the cable spacing, current, and cable length.

Cross-bonding (Fig. 12.6C): The three-phase circuit is divided into three equal segments. The metallic shield between each segment is connected to an adjacent phase using insulated conductor. Splices at these segments must interrupt the insulation shield to be effective.

12.6 Installation Practice

When cables are directly buried in earth, the trench bottom may require bedding sand or select backfill free from rocks that could damage the cable over time. When the cable is installed in conduit, the pulling tension must be limited so as not to damage the conductor, insulation, or shields. Typical value when using a wire basket grip is 3000 lbs. When the cable is pulled around a bend, the pulling tension results in

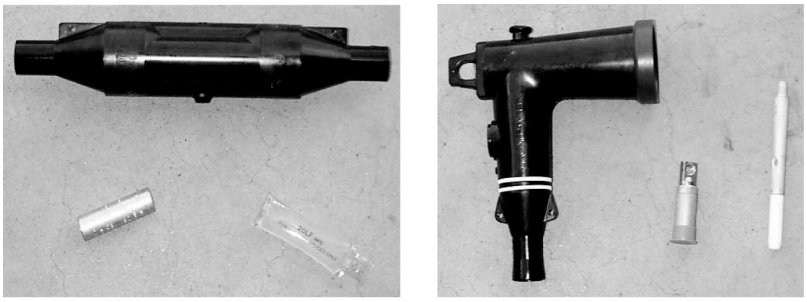

Cable Splice

Cable Elbow Termination

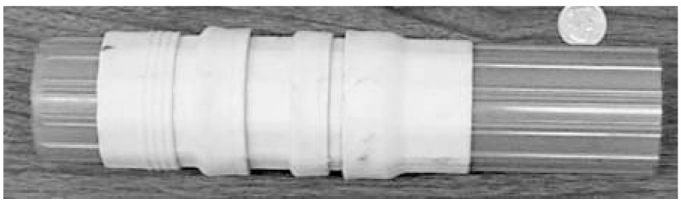

Cable Outdoor Termination

FIGURE 12.5 Cable accessories.

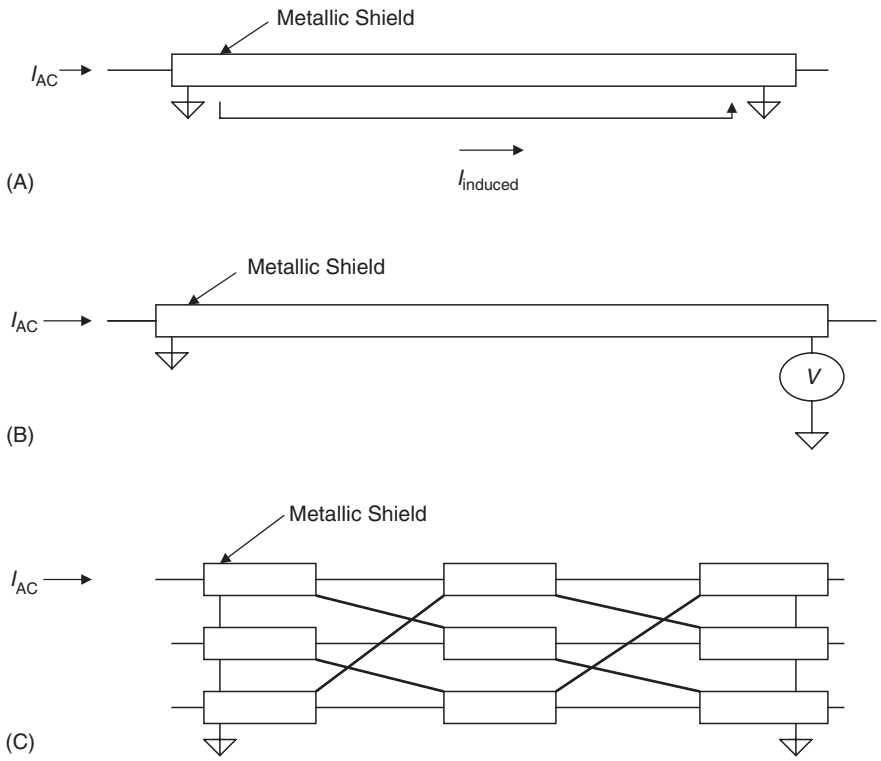

FIGURE 12.6 (A) Multigrounded shield, (B) single point grounded shield, (C) cross-bonding shields.

a side-wall bearing force against the inside surface of the elbow. This force must be limited to avoid crushing the cable components. Cables also have a minimum bending radius limit that prevents distortion of the cable components.

12.7 System Protection Devices

Two types of protecting devices are used on cable systems.

A. Overcurrent—fuses or circuit breakers. These devices isolate the cable from its source, preventing the flow of damaging levels of current during an overload, or remove a faulted cable from the system allowing restoration of the unfaulted parts.
B. Overvoltage—surge arrester. This device prevents damaging overvoltages caused by lightning or switching surges from entering the cable by clamping the voltage to a level tolerated by the cable insulation.

12.8 Common Calculations used with Cable

Inductance

$$L_{\text{cable}} = \frac{\mu_o}{2\pi}\left(\ln\left(\frac{2s_{\text{cable}}}{d}\right) + \frac{1}{4}\right) \quad \mu_o = 4\pi 10^{-7}\,\frac{\text{H}}{\text{m}},$$

where s_{cable} = center-to-center conductor spacing
for three single cables s_{cable} = cube root of each conductor spacing
d = conductor diameter
μ_o = permeability of free space

Inductive reactance

$$X_{\text{cable}} = \omega L_{\text{cable}} L \qquad \omega = 2\pi f,$$

where f = frequency
L_{cable} = inductance
L = length

Capacitance

$$C_{\text{cable}} = \frac{2\pi\varepsilon_o\varepsilon}{\ln\left(\frac{D}{d}\right)} \quad \varepsilon_o = \frac{10^{-9}}{36\pi}\,\frac{\text{F}}{\text{m}},$$

where ε = relative dielectric constant of the insulation (2.4 – XLPE, 2.9 – EPR)
ε_o = free space permittivity
D = diameter of insulation under insulation shield when present
d = diameter of the conductor in inches over the conductor shield when present

Charging current

$$I_{\text{cap}} = V_n(\omega C_{\text{cable}} L),$$

where C_{cable} = capacitance
V_n = voltage line to neutral
L = length

Ampacity

$$I_{\text{amp}} = \sqrt{\frac{T_c - T_a}{R_{ac} R_{th}}},$$

where T_c = conductor temperature
T_a = ambient temperature
R_{ac} = AC resistance at the operating temperature
R_{th} = thermal resistance of surrounding environment

Voltage drop

$$\text{Voltage drop} = I_{\text{cable}}(R_{\text{cable}} \cos(\phi) + X_{\text{cable}} \sin(\phi)),$$

where I_{cable} = current in conductor
R_{cable} = total ac resistance of the cable
X_{cable} = total ac reactance of the cable
ϕ = phase angle between supply voltage and current

For single-phase calculations the values of the main and the return conductors must be used.
Pulling tension single cable in straight conduit

$$T = \mu W L,$$

where μ = coefficient of dynamic friction (0.2–0.7 dependent on cable exterior and type of conduit)
W = cable weight per unit length
L = length

Pulling tension single cable through conduit bend

$$T_{\text{out}} = T_{\text{in}}\ e^{\mu\phi}\ (\text{pounds}),$$

where T_{in} = the tension entering the bend
μ = coefficient of dynamic friction (0.2–0.7 dependent on cable exterior and type of conduit)
ϕ = bend angle in radians

The pulling tensions of each segment of the conduit path are added together to determine the total pulling tension.

When multiple single cables are installed in a conduit, a multiplier must be applied to the cable weight, accounting for configuration as follows:

For three cables with a triangular configuration the weight multiplier is

$$W_{\text{multiplier triangular}} = \frac{2}{\sqrt{1 - \left(\frac{d}{D-d}\right)^2}}.$$

For three cables with a cradled configuration

$$W_{\text{multiplier cradled}} = 1 + \frac{4}{3}\left(\frac{d}{D-d}\right)^2,$$

where d = single cable outside diameter
D = conduit inside diameter.

General References

Aluminum Electrical Conductor Handbook, edited by Mark Walker, The Aluminum Association, 1982.

ANSI/IEEE 575-1988, IEEE Guide for the Application of Sheath-Bonding Methods for Single-Conductor Cables and the Calculation of Induced Voltages and Currents in Cable Sheaths.

Association of Edison Illuminating Companies, AEIC.

CS8-05, Specification for Extruded Dielectric, Shielded Power Cables Rated 5 through 46 kV.

IEEE 404-1993, IEEE Standard for Cable Joints for use with Extruded Dielectric Cable Rated 5000–138,000 V and Cable Joints for use with Laminated Dielectric Cable Rated 2500–500,000 V.

IEEE 48-1996, IEEE Standard Test Procedures and Requirements for Alternating Current Cable Terminations 2.5 kV through 765 kV.

IEEE 1215-2001, IEEE Guide for the Application of Separable Insulated Connectors.

IEEE 386-2005, IEEE Standard for Separable Insulated Connector Systems for Power Distribution Systems above 600 V.

Insulated Cable Engineering Association, ICEA standards.

P-53-426, Ampacities, 15–69 kV 1/c Power Cable Including Effect of Shield Losses (Solid Dielectric).

S-81-570-2005, 600 Volt Rated Cables of Ruggedized Design for Direct Burial Installations as Single Conductors or Assemblies of Single Conductors.

S-94-694-2004, Concentric Neutral Cables Rated 5 through 46 kV.

S-97-682-2000, Utility Shielded Power Cables Rated 5 through 46 kV.

S-105-692-2004, 600 Volt Single layer Thermoset Insulated Utility Underground Distribution Cables.

S-108-720-2004, Extruded Insulation Power Cables Rated above 46 through 345 kV.

Southwire Company Power Cable Manual, Second edition, edited by Thomas P. Arnold, Southwire Company, 1997.

13

Transmission Line Parameters

Manuel Reta-Hernández
Universidad Autónoma de Zacatecas

The power transmission line is one of the major components of an electric power system. Its major function is to transport electric energy, with minimal losses, from the power sources to the load centers, usually separated by long distances. The design of a transmission line depends on four electrical parameters:

1. Series resistance
2. Series inductance
3. Shunt capacitance
4. Shunt conductance

The series resistance relies basically on the physical composition of the conductor at a given temperature. The series inductance and shunt capacitance are produced by the presence of magnetic and electric fields around the conductors, and depend on their geometrical arrangement. The shunt conductance is due to leakage currents flowing across insulators and air. As leakage current is considerably small compared to nominal current, it is usually neglected, and therefore, shunt conductance is normally not considered for the transmission line modeling.

13.1 Equivalent Circuit

Once evaluated, the line parameters are used to model the transmission line and to perform design calculations. The arrangement of the parameters (equivalent circuit model) representing the line depends upon the length of the line.

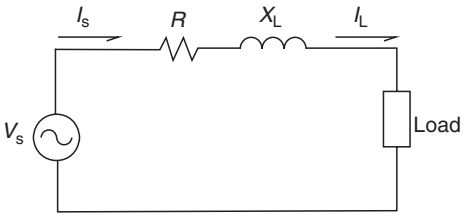

FIGURE 13.1 Equivalent circuit of a short-length transmission line.

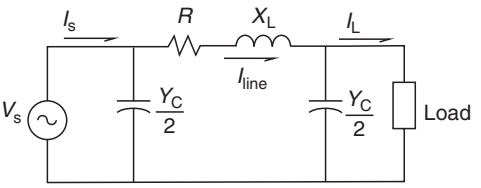

FIGURE 13.2 Equivalent circuit of a medium-length transmission line.

A transmission line is defined as a short-length line if its length is less than 80 km (50 miles). In this case, the shut capacitance effect is negligible and only the resistance and inductive reactance are considered. Assuming balanced conditions, the line can be represented by the equivalent circuit of a single phase with resistance R, and inductive reactance X_L in series (series impedance), as shown in Fig. 13.1. If the transmission line has a length between 80 km (50 miles) and 240 km (150 miles), the line is considered a medium-length line and its single-phase equivalent circuit can be represented in a nominal π circuit configuration [1]. The shunt capacitance of the line is divided into two equal parts, each placed at the sending and receiving ends of the line. Figure 13.2 shows the equivalent circuit for a medium-length line.

Both short- and medium-length transmission lines use approximated lumped-parameter models. However, if the line is larger than 240 km, the model must consider parameters uniformly distributed along the line. The appropriate series impedance and shunt capacitance are found by solving the corresponding differential equations, where voltages and currents are described as a function of distance and time. Figure 13.3 shows the equivalent circuit for a long line.

The calculation of the three basic transmission line parameters is presented in the following sections [1–7].

13.2 Resistance

The AC resistance of a conductor in a transmission line is based on the calculation of its DC resistance. If DC current is flowing along a round cylindrical conductor, the current is uniformly distributed over its cross-section area and its DC resistance is evaluated by

$$R_{DC} = \frac{\rho l}{A} \ (\Omega) \tag{13.1}$$

where ρ = conductor resistivity at a given temperature (Ω-m)
l = conductor length (m)
A = conductor cross-section area (m^2)

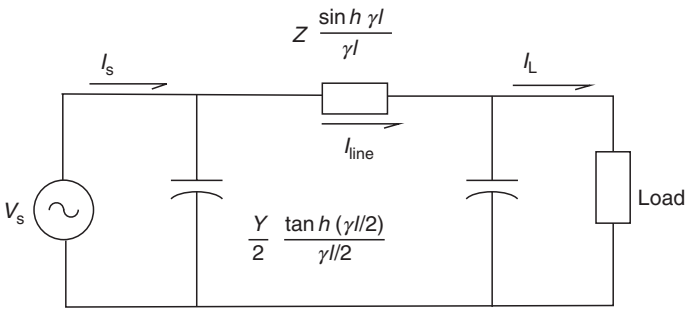

FIGURE 13.3 Equivalent circuit of a long-length transmission line. $Z = zl$ = equivalent total series impedance (Ω), $Y = yl$ = equivalent total shunt admittance (S), z = series impedance per unit length (Ω/m), y = shunt admittance per unit length (S/m), $\gamma = \sqrt{Z\,Y}$ = propagation constant.

If AC current is flowing, rather than DC current, the conductor effective resistance is higher due to frequency or skin effect.

13.2.1 Frequency Effect

The frequency of the AC voltage produces a second effect on the conductor resistance due to the nonuniform distribution of the current. This phenomenon is known as skin effect. As frequency increases, the current tends to go toward the surface of the conductor and the current density decreases at the center. Skin effect reduces the effective cross-section area used by the current, and thus, the effective resistance increases. Also, although in small amount, a further resistance increase occurs when other current-carrying conductors are present in the immediate vicinity. A skin correction factor k, obtained by differential equations and Bessel functions, is considered to reevaluate the AC resistance. For 60 Hz, k is estimated around 1.02

$$R_{AC} = R_{AC}k \tag{13.2}$$

Other variations in resistance are caused by

- Temperature
- Spiraling of stranded conductors
- Bundle conductors arrangement

13.2.2 Temperature Effect

The resistivity of any conductive material varies linearly over an operating temperature, and therefore, the resistance of any conductor suffers the same variations. As temperature rises, the conductor resistance increases linearly, over normal operating temperatures, according to the following equation:

$$R_2 = R_1\left(\frac{T + t_2}{T + t_1}\right) \tag{13.3}$$

where R_2 = resistance at second temperature t_2
R_1 = resistance at initial temperature t_1
T = temperature coefficient for the particular material (°C)

Resistivity (ρ) and temperature coefficient (T) constants depend upon the particular conductor material. Table 13.1 lists resistivity and temperature coefficients of some typical conductor materials [3].

13.2.3 Spiraling and Bundle Conductor Effect

There are two types of transmission line conductors: overhead and underground. Overhead conductors, made of naked metal and suspended on insulators, are preferred over underground conductors because of the lower cost and easy maintenance. Also, overhead transmission lines use aluminum conductors, because of the lower cost and lighter weight compared to copper conductors, although more cross-section area is needed to conduct the same amount of current. There are different types of commercially available aluminum conductors: aluminum-conductor-steel-reinforced (ACSR), aluminum-conductor-alloy-reinforced (ACAR), all-aluminum-conductor (AAC), and all-aluminum-alloy-conductor (AAAC).

TABLE 13.1 Resistivity and Temperature Coefficient of Some Conductors

Material	Resistivity at 20°C (Ω-m)	Temperature Coefficient (°C)
Silver	1.59×10^{-8}	243.0
Annealed copper	1.72×10^{-8}	234.5
Hard-drawn copper	1.77×10^{-8}	241.5
Aluminum	2.83×10^{-8}	228.1

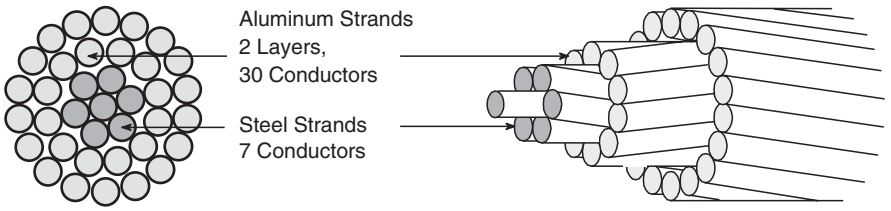

FIGURE 13.4 Stranded aluminum conductor with stranded steel core (ACSR).

ACSR is one of the most used conductors in transmission lines. It consists of alternate layers of stranded conductors, spiraled in opposite directions to hold the strands together, surrounding a core of steel strands. Figure 13.4 shows an example of aluminum and steel strands combination.

The purpose of introducing a steel core inside the stranded aluminum conductors is to obtain a high strength-to-weight ratio. A stranded conductor offers more flexibility and easier to manufacture than a solid large conductor. However, the total resistance is increased because the outside strands are larger than the inside strands on account of the spiraling [8]. The resistance of each wound conductor at any layer, per unit length, is based on its total length as follows:

$$R_{\text{cond}} = \frac{\rho}{A}\sqrt{1+\left(\pi\frac{1}{p}\right)^2}\ (\Omega/\text{m}) \tag{13.4}$$

where R_{cond} = resistance of wound conductor (Ω)

$\sqrt{1+\left(\pi\frac{1}{p}\right)^2}$ = length of wound conductor (m)

$p_{\text{cond}} = \frac{l_{\text{turn}}}{2r_{\text{layer}}}$ = relative pitch of wound conductor

l_{turn} = length of one turn of the spiral (m)

$2r_{\text{layer}}$ = diameter of the layer (m)

The parallel combination of n conductors, with same diameter per layer, gives the resistance per layer as follows:

$$R_{\text{layer}} = \frac{1}{\sum_{i=1}^{n}\frac{1}{R_i}}\ (\Omega/\text{m}) \tag{13.5}$$

Similarly, the total resistance of the stranded conductor is evaluated by the parallel combination of resistances per layer.

In high-voltage transmission lines, there may be more than one conductor per phase (bundle configuration) to increase the current capability and to reduce corona effect discharge. Corona effect occurs when the surface potential gradient of a conductor exceeds the dielectric strength of the surrounding air (30 kV/cm during fair weather), producing ionization in the area close to the conductor, with consequent corona losses, audible noise, and radio interference. As corona effect is a function of conductor diameter, line configuration, and conductor surface condition, then meteorological conditions play a key role in its evaluation. Corona losses under rain or snow, for instance, are much higher than in dry weather.

Corona, however, can be reduced by increasing the total conductor surface. Although corona losses rely on meteorological conditions, their evaluation takes into account the conductance between conductors and between conductors and ground. By increasing the number of conductors per phase, the total cross-section area increases, the current capacity increases, and the total AC resistance decreases proportionally to the number of conductors per bundle. Conductor bundles may be applied to any

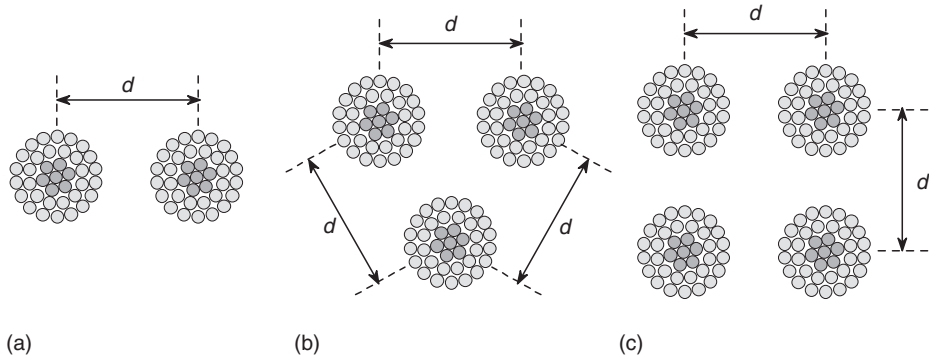

FIGURE 13.5 Stranded conductors arranged in bundles per phase of (a) two, (b) three, and (c) four.

voltage but are always used at 345 kV and above to limit corona. To maintain the distance between bundle conductors along the line, spacers made of steel or aluminum bars are used. Figure 13.5 shows some typical arrangement of stranded bundle configurations.

13.3 Current-Carrying Capacity (Ampacity)

In overhead transmission lines, the current-carrying capacity is determined mostly by the conductor resistance and the heat dissipated from its surface [8]. The heat generated in a conductor (Joule's effect) is dissipated from its surface area by convection and radiation given by

$$I^2R = S(w_c + w_r)\ (\text{W}) \tag{13.6}$$

where R = conductor resistance (Ω)
I = conductor current-carrying (A)
S = conductor surface area (sq. in.)
w_c = convection heat loss (W/sq. in.)
w_r = radiation heat loss (W/sq. in.)
Heat dissipation by convection is defined as

$$w_c = \frac{0.0128\sqrt{pv}}{T_{air}^{0.123}\sqrt{d_{cond}}}\ \Delta t\ (\text{W}) \tag{13.7}$$

where p = atmospheric pressure (atm)
v = wind velocity (ft/s)
d_{cond} = conductor diameter (in.)
T_{air} = air temperature (kelvin)
$\Delta t = T_c - T_{air}$ = temperature rise of the conductor (°C)
Heat dissipation by radiation is obtained from Stefan–Boltzmann law and is defined as

$$w_r = 36.8\,E\left[\left(\frac{T_c}{1000}\right)^4 - \left(\frac{T_{air}}{1000}\right)^4\right] \quad (\text{W/sq. in.}) \tag{13.8}$$

where w_r = radiation heat loss (W/sq. in.)
E = emissivity constant (1 for the absolute black body and 0.5 for oxidized copper)
T_c = conductor temperature (°C)
T_{air} = ambient temperature (°C)

Substituting Eqs. (13.7) and (13.8) in Eq. (13.6) we can obtain the conductor ampacity at given temperatures

$$I = \sqrt{\frac{S(w_c + w_r)}{R}} \quad \text{(A)} \tag{13.9}$$

$$I = \sqrt{\frac{S}{R}\left(\frac{\Delta t\left(0.0128\sqrt{pv}\right)}{T_{air}^{0.123}\sqrt{d_{cond}}} + 36.8E\left(\frac{T_c^4 - T_{air}^4}{1000^4}\right)\right)} \text{ (A)} \tag{13.10}$$

Some approximated current-carrying capacity for overhead ACSR and AACs are presented in the section "Characteristics of Overhead Conductors" [3,9].

13.4 Inductance and Inductive Reactance

A current-carrying conductor produces concentric magnetic flux lines around the conductor. If the current varies with the time, the magnetic flux changes and a voltage is induced. Therefore, an inductance is present, defined as the ratio of the magnetic flux linkage and the current. The magnetic flux produced by the current in transmission line conductors produces a total inductance whose magnitude depends on the line configuration. To determine the inductance of the line, it is necessary to calculate, as in any magnetic circuit with permeability μ, the following factors:

1. Magnetic field intensity H
2. Magnetic field density B
3. Flux linkage λ

13.4.1 Inductance of a Solid, Round, Infinitely Long Conductor

Consider an infinitely long, solid cylindrical conductor with radius r, carrying current I as shown in Fig. 13.6. If the conductor is made of a nonmagnetic material, and the current is assumed uniformly distributed (no skin effect), then the generated internal and external magnetic field lines are concentric circles around the conductor with direction defined by the right-hand rule.

13.4.2 Internal Inductance Due to Internal Magnetic Flux

To obtain the internal inductance, a magnetic field with radius x inside the conductor of length l is chosen, as shown in Fig. 13.7.

The fraction of the current I_x enclosed in the area of the circle chosen is determined by

$$I_x = I\frac{\pi x^2}{\pi r^2} \quad \text{(A)} \tag{13.11}$$

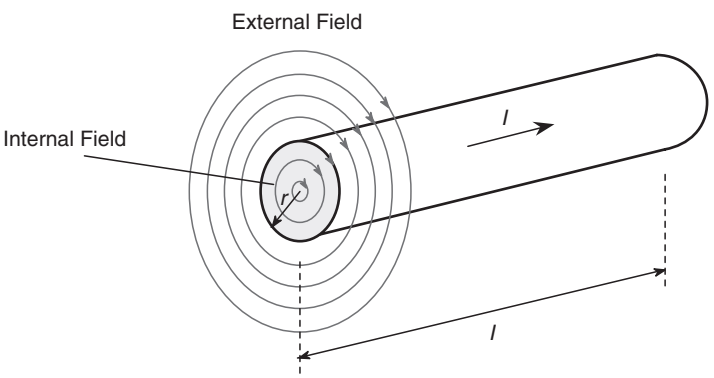

FIGURE 13.6 External and internal concentric magnetic flux lines around the conductor.

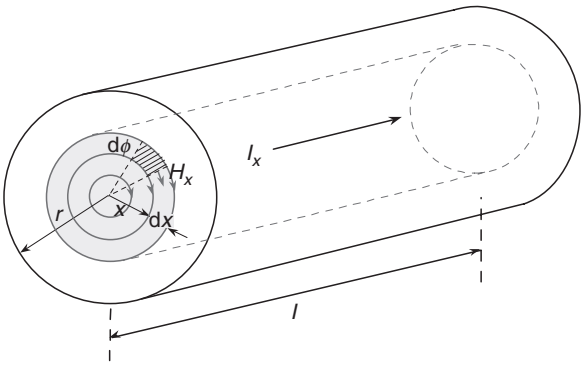

FIGURE 13.7 Internal magnetic flux.

Ampere's law determines the magnetic field intensity H_x, constant at any point along the circle contour as

$$H_x = \frac{I_x}{2\pi x} = \frac{I}{2\pi r^2} x \text{ (A/m)} \tag{13.12}$$

The magnetic flux density B_x is obtained by

$$B_x = \mu H_x = \frac{\mu_0}{2\pi}\left(\frac{Ix}{r^2}\right) \text{ (T)} \tag{13.13}$$

where $\mu = \mu_0 = 4\pi \times 10^{-7}$ H/m for a nonmagnetic material.

The differential flux $d\phi$ enclosed in a ring of thickness dx for a 1-m length of conductor and the differential flux linkage $d\lambda$ in the respective area are

$$d\phi = B_x\, dx = \frac{\mu_0}{2\pi}\left(\frac{Ix}{r^2}\right) dx \text{ (Wb/m)} \tag{13.14}$$

$$d\lambda = \frac{\pi x^2}{\pi r^2} d\phi = \frac{\mu_0}{2\pi}\left(\frac{Ix^3}{r^4}\right) dx \text{ (Wb/m)} \tag{13.15}$$

The internal flux linkage is obtained by integrating the differential flux linkage from $x = 0$ to $x = r$

$$\lambda_{\text{int}} = \int_0^r d\lambda = \frac{\mu_0}{8\pi} I \text{ (Wb/m)} \tag{13.16}$$

Therefore, the conductor inductance due to internal flux linkage, per unit length, becomes

$$L_{\text{int}} = \frac{\lambda_{\text{int}}}{I} = \frac{\mu_0}{8\pi} \text{ (H/m)} \tag{13.17}$$

13.4.3 External Inductance

The external inductance is evaluated assuming that the total current I is concentrated at the conductor surface (maximum skin effect). At any point on an external magnetic field circle of radius y (Fig. 13.8), the magnetic field intensity H_y and the magnetic field density B_y, per unit length, are

$$H_y = \frac{I}{2\pi y} \text{ (A/m)} \tag{13.18}$$

$$B_y = \mu H_y = \frac{\mu_0}{2\pi}\frac{I}{y} \text{ (T)} \tag{13.19}$$

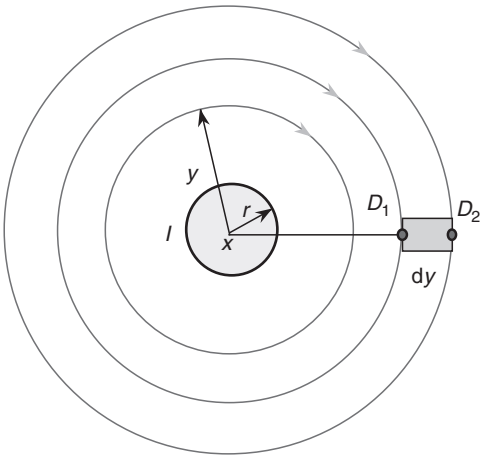

The differential flux $d\phi$ enclosed in a ring of thickness dy, from point D_1 to point D_2, for a 1-m length of conductor is

$$d\phi = B_y\, dy = \frac{\mu_0}{2\pi}\frac{I}{y}\, dy \ (\text{Wb/m}) \tag{13.20}$$

As the total current I flows in the surface conductor, then the differential flux linkage $d\lambda$ has the same magnitude as the differential flux $d\phi$.

$$d\lambda = d\phi = \frac{\mu_0}{2\pi}\frac{I}{y}\, dy \ (\text{Wb/m}) \tag{13.21}$$

The total external flux linkage enclosed by the ring is obtained by integrating from D_1 to D_2

FIGURE 13.8 External magnetic field.

$$\lambda_{1-2} = \int_{D_1}^{D_2} d\lambda = \frac{\mu_0}{2\pi} I \int_{D_1}^{D_2} \frac{dy}{y} = \frac{\mu_0}{2\pi} I \ln\left(\frac{D_1}{D_2}\right) \ (\text{Wb/m}) \tag{13.22}$$

In general, the total external flux linkage from the surface of the conductor to any point D, per unit length, is

$$\lambda_{\text{ext}} = \int_r^D d\lambda = \frac{\mu_0}{2\pi}\, I \ln\left(\frac{D}{r}\right) \ (\text{Wb/m}) \tag{13.23}$$

The summation of the internal and external flux linkage at any point D permits evaluation of the total inductance of the conductor L_{tot}, per unit length, as follows:

$$\lambda_{\text{intl}} + \lambda_{\text{ext}} = \frac{\mu_0}{2\pi}\, I \left[\frac{1}{4} + \ln\left(\frac{D}{r}\right)\right] = \frac{\mu_0}{2\pi} I \ln\left(\frac{D}{e^{-1/4} r}\right) \ (\text{Wb/m}) \tag{13.24}$$

$$L_{\text{tot}} = \frac{\lambda_{\text{int}} + \lambda_{\text{ext}}}{I} = \frac{\mu_0}{2\pi} \ln\left(\frac{D}{\text{GMR}}\right) \ (\text{H/m}) \tag{13.25}$$

where GMR (geometric mean radius) $= e^{-1/4} r = 0.7788r$

GMR can be considered as the radius of a fictitious conductor assumed to have no internal flux but with the same inductance as the actual conductor with radius r.

13.4.4 Inductance of a Two-Wire Single-Phase Line

Now, consider a two-wire single-phase line with solid cylindrical conductors A and B with the same radius r, same length l, and separated by a distance D, where $D > r$, and conducting the same current I, as shown in Fig. 13.9. The current flows from the source to the load in conductor A and returns in conductor B ($I_A = -I_B$).

The magnetic flux generated by one conductor links the other conductor. The total flux linking conductor A, for instance, has two components: (a) the flux generated by conductor A and (b) the flux generated by conductor B which links conductor A.

As shown in Fig. 13.10, the total flux linkage from conductors A and B at point P is

$$\lambda_{AP} = \lambda_{AAP} + \lambda_{ABP} \tag{13.26}$$

$$\lambda_{BP} = \lambda_{BBP} + \lambda_{BAP} \tag{13.27}$$

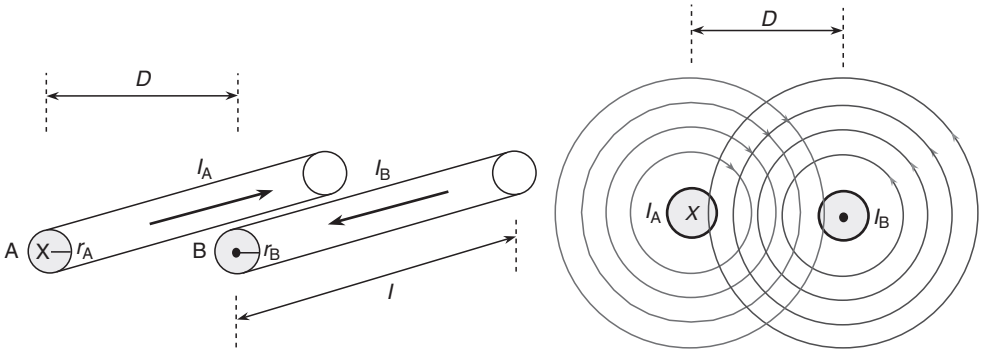

FIGURE 13.9 External magnetic flux around conductors in a two-wire single-phase line.

where λ_{AAP} = flux linkage from magnetic field of conductor A on conductor A at point P
λ_{ABP} = flux linkage from magnetic field of conductor B on conductor A at point P
λ_{BBP} = flux linkage from magnetic field of conductor B on conductor B at point P
λ_{BAP} = flux linkage from magnetic field of conductor A on conductor B at point P

The expressions of the flux linkages above, per unit length, are

$$\lambda_{AAP} = \frac{\mu_0}{2\pi} I \ln\left(\frac{D_{AP}}{\text{GMR}_A}\right) \text{ (Wb/m)} \tag{13.28}$$

$$\lambda_{ABP} = \int_D^{D_{BP}} B_{BP}\, dP = -\frac{\mu_0}{2\pi} I \ln\left(\frac{D_{BP}}{D}\right) \text{ (Wb/m)} \tag{13.29}$$

$$\lambda_{BAP} = \int_D^{D_{AP}} B_{AP}\, dP = -\frac{\mu_0}{2\pi} I \ln\left(\frac{D_{AP}}{D}\right) \text{ (Wb/m)} \tag{13.30}$$

$$\lambda_{BBP} = \frac{\mu_0}{2\pi} I \ln\left(\frac{D_{BP}}{\text{GMR}_B}\right) \text{ (Wb/m)} \tag{13.31}$$

The total flux linkage of the system at point P is the algebraic summation of λ_{AP} and λ_{BP}

$$\lambda_P = \lambda_{AP} + \lambda_{BP} = (\lambda_{AAP} + \lambda_{ABP}) + (\lambda_{BAP} + \lambda_{BBP}) \tag{13.32}$$

$$\lambda_P = \frac{\mu_0}{2\pi} I \ln\left[\left(\frac{D_{AP}}{\text{GMR}_A}\right)\left(\frac{D}{D_{AP}}\right)\left(\frac{D_{BP}}{\text{GMR}_B}\right)\left(\frac{D}{D_{BP}}\right)\right] = \frac{\mu_0}{2\pi} I \ln\left(\frac{D^2}{\text{GMR}_A \text{GMR}_B}\right) \text{ (Wb/m)} \tag{13.33}$$

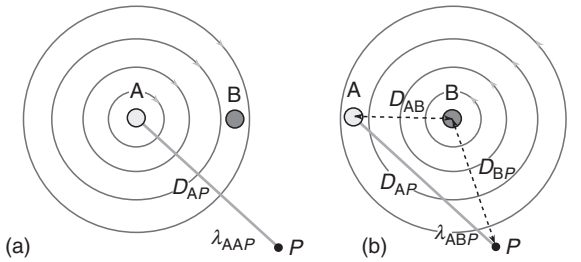

FIGURE 13.10 Flux linkage of (a) conductor A at point P and (b) conductor B on conductor A at point P. Single-phase system.

If the conductors have the same radius, $r_A = r_B = r$, and the point P is shifted to infinity, then the total flux linkage of the system becomes

$$\lambda = \frac{\mu_0}{\pi} I \ln\left(\frac{D}{\text{GMR}}\right) \text{ (Wb/m)} \tag{13.34}$$

and the total inductance per unit length becomes

$$L_{1\text{-phase system}} = \frac{\lambda}{I} = \frac{\mu_0}{\pi} \ln\left(\frac{D}{\text{GMR}}\right) \text{ (H/m)} \tag{13.35}$$

Comparing Eqs. (13.25) and (13.35), it can be seen that the inductance of the single-phase system is twice the inductance of a single conductor.

For a line with stranded conductors, the inductance is determined using a new GMR value named $\text{GMR}_{\text{stranded}}$, evaluated according to the number of conductors. If conductors A and B in the single-phase system, are formed by n and m solid cylindrical identical subconductors in parallel, respectively, then

$$\text{GMR}_{\text{A\_stranded}} = \sqrt[n^2]{\prod_{i=1}^{n}\prod_{j=1}^{n} D_{ij}} \tag{13.36}$$

$$\text{GMR}_{\text{B\_stranded}} = \sqrt[m^2]{\prod_{i=1}^{m}\prod_{j=1}^{m} D_{ij}} \tag{13.37}$$

Generally, the $\text{GMR}_{\text{stranded}}$ for a particular cable can be found in conductor tables given by the manufacturer.

If the line conductor is composed of bundle conductors, the inductance is reevaluated taking into account the number of bundle conductors and the separation among them. The $\text{GMR}_{\text{bundle}}$ is introduced to determine the final inductance value. Assuming the same separation among bundle conductors, the equation for $\text{GMR}_{\text{bundle}}$, up to three conductors per bundle, is defined as

$$\text{GMR}_{n \text{ bundle conductors}} = \sqrt[n]{d^{n-1}\text{GMR}_{\text{stranded}}} \tag{13.38}$$

where n = number of conductors per bundle
$\text{GMR}_{\text{stranded}}$ = GMR of the stranded conductor
d = distance between bundle conductors

For four conductors per bundle with the same separation between consecutive conductors, the $\text{GMR}_{\text{bundle}}$ is evaluated as

$$\text{GMR}_{4 \text{ bundle conductors}} = 1.09\sqrt[4]{d^3\text{GMR}_{\text{stranded}}} \tag{13.39}$$

13.4.5 Inductance of a Three-Phase Line

The derivations for the inductance in a single-phase system can be extended to obtain the inductance per phase in a three-phase system. Consider a three-phase, three-conductor system with solid cylindrical conductors with identical radius r_A, r_B, and r_C, placed horizontally with separation D_{AB}, D_{BC}, and D_{CA} (where $D > r$) among them. Corresponding currents I_A, I_B, and I_C flow along each conductor as shown in Fig. 13.11.

The total magnetic flux enclosing conductor A at a point P away from the conductors is the sum of the flux produced by conductors A, B, and C as follows:

$$\phi_{AP} = \phi_{AAP} + \phi_{ABP} + \phi_{ACP} \tag{13.40}$$

where ϕ_{AAP} = flux produced by current I_A on conductor A at point P
ϕ_{ABP} = flux produced by current I_B on conductor A at point P
ϕ_{ACP} = flux produced by current I_C on conductor A at point P

Considering 1-m length for each conductor, the expressions for the fluxes above are

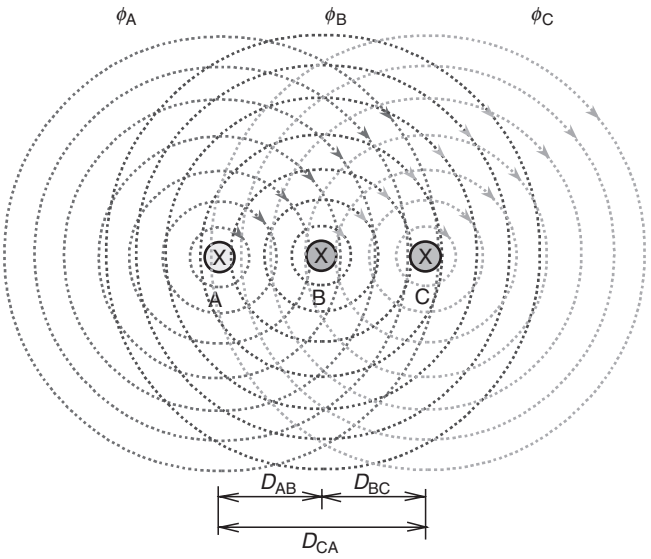

FIGURE 13.11 Magnetic flux produced by each conductor in a three-phase system.

$$\phi_{AAP} = \frac{\mu_0}{2\pi} I_A \ln\left(\frac{D_{AP}}{\text{GMR}_A}\right) \text{ (Wb/m)} \tag{13.41}$$

$$\phi_{ABP} = \frac{\mu_0}{2\pi} I_B \ln\left(\frac{D_{BP}}{D_{AB}}\right) \text{ (Wb/m)} \tag{13.42}$$

$$\phi_{ACP} = \frac{\mu_0}{2\pi} I_C \ln\left(\frac{D_{CP}}{D_{AC}}\right) \text{ (Wb/m)} \tag{13.43}$$

The corresponding flux linkage of conductor A at point P (Fig. 13.12) is evaluated as

$$\lambda_{AP} = \lambda_{AAP} + \lambda_{ABP} + \lambda_{ACP} \tag{13.44}$$

having

$$\lambda_{AAP} = \frac{\mu_0}{2\pi} I_A \ln\left(\frac{D_{AP}}{\text{GMR}_A}\right) \text{ (Wb/m)} \tag{13.45}$$

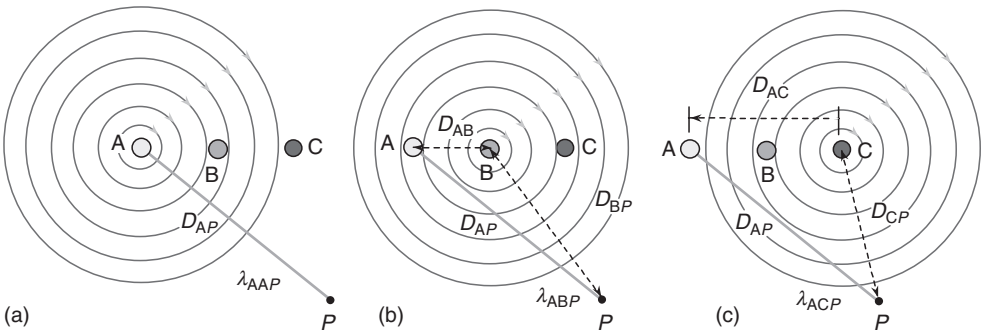

FIGURE 13.12 Flux linkage of (a) conductor A at point *P*, (b) conductor B on conductor A at point *P*, and (c) conductor C on conductor A at point *P*. Three-phase system.

$$\lambda_{ABP} = \int_{D_{AB}}^{D_{BP}} B_{BP}\, dP = \frac{\mu_0}{2\pi} I_B \ln\left(\frac{D_{BP}}{D_{AB}}\right) \text{ (Wb/m)} \tag{13.46}$$

$$\lambda_{ACP} = \int_{D_{AC}}^{D_{CP}} B_{CP}\, dP = \frac{\mu_0}{2\pi} I_C \ln\left(\frac{D_{CP}}{D_{AC}}\right) \text{ (Wb/m)} \tag{13.47}$$

where λ_{AP} = total flux linkage of conductor A at point P
λ_{AAP} = flux linkage from magnetic field of conductor A on conductor A at point P
λ_{ABP} = flux linkage from magnetic field of conductor B on conductor A at point P
λ_{ACP} = flux linkage from magnetic field of conductor C on conductor A at point P

Substituting Eqs. (13.45) through (13.47) in Eq. (13.44) and rearranging, according to natural logarithms law, we have

$$\lambda_{AP} = \frac{\mu_0}{2\pi}\left[I_A \ln\left(\frac{D_{AP}}{GMR_A}\right) + I_B \ln\left(\frac{D_{BP}}{D_{AB}}\right) + I_C \ln\left(\frac{D_{CP}}{D_{AC}}\right)\right] \text{ (Wb/m)} \tag{13.48}$$

$$\lambda_{AP} = \frac{\mu_0}{2\pi}\left[I_A \ln\left(\frac{1}{GMR_A}\right) + I_B \ln\left(\frac{1}{D_{AB}}\right) + I_C \ln\left(\frac{1}{D_{AC}}\right)\right] + \frac{\mu_0}{2\pi}\left[I_A \ln(D_{AP}) + I_B \ln(D_{BP}) + I_C \ln(D_{CP})\right] \text{ (Wb/m)} \tag{13.49}$$

The arrangement of Eq. (13.48) into Eq. (13.49) is algebraically correct according to natural logarithms law. However, as the calculation of any natural logarithm must be dimensionless, the numerator in the expressions $\ln(1/GMR_A)$, $\ln(1/D_{AB})$, and $\ln(1/D_{AC})$ must have the same dimension as the denominator. The same applies for the denominator in the expressions $\ln(D_{AP})$, $\ln(D_{BP})$, and $\ln(D_{CP})$.

Assuming a balanced three-phase system, where $I_A + I_B + I_C = 0$, and shifting the point P to infinity in such a way that $D_{AP} = D_{BP} = D_{CP}$, then the second part of Eq. (13.49) is zero, and the flux linkage of conductor A becomes

$$\lambda_A = \frac{\mu_0}{2\pi}\left[I_A \ln\left(\frac{1}{GMR_A}\right) + I_B \ln\left(\frac{1}{D_{AB}}\right) + I_C \ln\left(\frac{1}{D_{AC}}\right)\right] \text{ (Wb/m)} \tag{13.50}$$

Similarly, the flux linkage expressions for conductors B and C are

$$\lambda_B = \frac{\mu_0}{2\pi}\left[I_A \ln\left(\frac{1}{D_{BA}}\right) + I_B \ln\left(\frac{1}{GMR_B}\right) + I_C \ln\left(\frac{1}{D_{BC}}\right)\right] \text{ (Wb/m)} \tag{13.51}$$

$$\lambda_C = \frac{\mu_0}{2\pi}\left[I_A \ln\left(\frac{1}{D_{CA}}\right) + I_B \ln\left(\frac{1}{D_{CB}}\right) + I_C \ln\left(\frac{1}{GMR_C}\right)\right] \text{ (Wb/m)} \tag{13.52}$$

The flux linkage of each phase conductor depends on the three currents, and therefore, the inductance per phase is not only one as in the single-phase system. Instead, three different inductances (self and mutual conductor inductances) exist. Calculating the inductance values from the equations above and arranging the equations in a matrix form we can obtain the set of inductances in the system

$$\begin{bmatrix}\lambda_A \\ \lambda_B \\ \lambda_C\end{bmatrix} = \begin{bmatrix}L_{AA} & L_{AB} & L_{AC} \\ L_{BA} & L_{BB} & L_{BC} \\ L_{CA} & L_{CB} & L_{CC}\end{bmatrix}\begin{bmatrix}I_A \\ I_B \\ I_C\end{bmatrix} \tag{13.53}$$

where λ_A, λ_B, λ_C = total flux linkages of conductors A, B, and C
L_{AA}, L_{BB}, L_{CC} = self-inductances of conductors A, B, and C field of conductor A at point P
L_{AB}, L_{BC}, L_{CA}, L_{BA}, L_{CB}, L_{AC} = mutual inductances among conductors

With nine different inductances in a simple three-phase system the analysis could be a little more complicated. However, a single inductance per phase can be obtained if the three conductors are arranged with the same separation among them (symmetrical arrangement), where $D = D_{AB} = D_{BC} = D_{CA}$. For a balanced three-phase system ($I_A + I_B + I_C = 0$, or $I_A = -I_B - I_C$), the flux linkage of each conductor, per unit length, will be the same. From Eq. (13.50) we have

$$\lambda_A = \frac{\mu_0}{2\pi}\left[(-I_B - I_C)\ln\left(\frac{1}{GMR_A}\right) + I_B \ln\left(\frac{1}{D}\right) + I_C \ln\left(\frac{1}{D}\right)\right]$$

$$\lambda_A = \frac{\mu_0}{2\pi}\left[-I_B \ln\left(\frac{D}{GMR_A}\right) - I_C \ln\left(\frac{D}{GMR_A}\right)\right]$$

$$\lambda_A = \frac{\mu_0}{2\pi}\left[I_A \ln\left(\frac{D}{GMR_A}\right)\right] \text{ (Wb/m)} \tag{13.54}$$

If GMR value is the same for all conductors (either single or bundle GMR), the total flux linkage expression is the same for all phases. Therefore, the equivalent inductance per phase is

$$L_{phase} = \frac{\mu_0}{2\pi}\ln\left(\frac{D}{GMR_{phase}}\right) \text{ (H/m)} \tag{13.55}$$

13.4.6 Inductance of Transposed Three-Phase Transmission Lines

In actual transmission lines, the phase conductors cannot maintain symmetrical arrangement along the whole length because of construction considerations, even when bundle conductor spacers are used. With asymmetrical spacing, the inductance will be different for each phase, with a corresponding unbalanced voltage drop on each conductor. Therefore, the single-phase equivalent circuit to represent the power system cannot be used.

However, it is possible to assume symmetrical arrangement in the transmission line by transposing the phase conductors. In a transposed system, each phase conductor occupies the location of the other two phases for one-third of the total line length as shown in Fig. 13.13. In this case, the average distance geometrical mean distance (GMD) substitutes distance D, and the calculation of phase inductance derived for symmetrical arrangement is still valid.

The inductance per phase per unit length in a transmission line becomes

$$L_{phase} = \frac{\mu_0}{2\pi}\ln\left(\frac{GMD}{GMR_{phase}}\right) \text{ (H/m)} \tag{13.56}$$

Once the inductance per phase is obtained, the inductive reactance per unit length is

$$X_{L_{phase}} = 2\pi f L_{phase} = \mu_0 f \ln\left(\frac{GMD}{GMR_{phase}}\right) (\Omega/\text{m}) \tag{13.57}$$

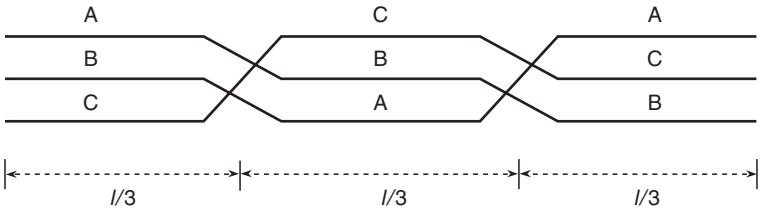

FIGURE 13.13 Arrangement of conductors in a transposed line.

For bundle conductors, the GMR_{bundle} value is determined, as in the single-phase transmission line case, by the number of conductors, and by the number of conductors per bundle and the separation among them. The expression for the total inductive reactance per phase yields

$$X_{L_{phase}} = \mu_0 f \ln\left(\frac{GMD}{GMR_{bundle}}\right) \ (\Omega/m) \tag{13.58}$$

where $GMR_{bundle} = (d^{n-1}\ GMR_{stranded})^{1/n}$ up to three conductors per bundle (m)
$GMR_{bundle} = 1.09(d^4\ GMR_{stranded})^{1/4}$ for four conductors per bundle (m)
GMR_{phase} = geometric mean radius of phase conductor, either solid or stranded (m)
$GMD = \sqrt[3]{D_{AB}D_{BC}D_{CA}}$ = geometrical mean distance for a three-phase line (m)
d = distance between bundle conductors (m)
n = number of conductor per bundle
f = frequency (Hz)

13.5 Capacitance and Capacitive Reactance

Capacitance exists among transmission line conductors due to their potential difference. To evaluate the capacitance between conductors in a surrounding medium with permittivity ε, it is necessary to determine the voltage between the conductors, and the electric field strength of the surrounding.

13.5.1 Capacitance of a Single-Solid Conductor

Consider a solid, cylindrical, long conductor with radius r, in a free space with permittivity ε_0, and with a charge of q^+ coulombs per meter, uniformly distributed on the surface. There is a constant electric field strength on the surface of cylinder (Fig. 13.14). The resistivity of the conductor is assumed to be zero (perfect conductor), which results in zero internal electric field due to the charge on the conductor.

The charge q^+ produces an electric field radial to the conductor with equipotential surfaces concentric to the conductor. According to Gauss's law, the total electric flux leaving a closed surface is equal to the total charge inside the volume enclosed by the surface. Therefore, at an outside point P separated x meters from the center of the conductor, the electric field flux density and the electric field intensity are

$$\text{Density}_P = \frac{q}{A} = \frac{q}{2\pi x} \ (C) \tag{13.59}$$

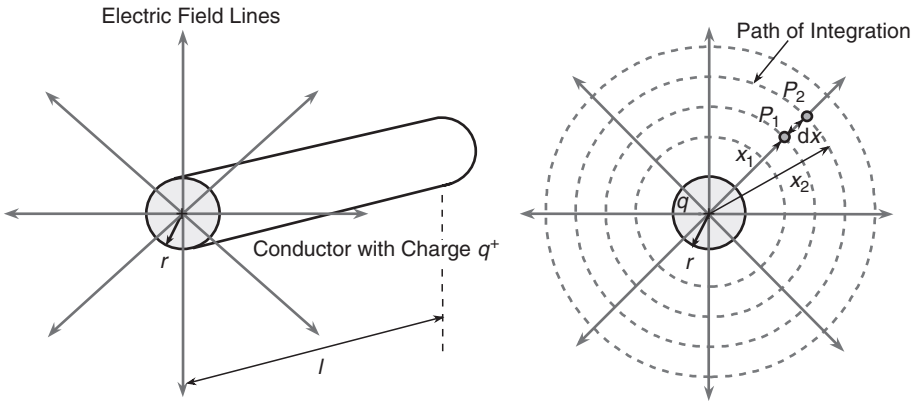

FIGURE 13.14 Electric field produced from a single conductor.

$$E_P = \frac{\text{Density}_P}{\varepsilon} = \frac{q}{2\pi\varepsilon_0 x} \text{ (V/m)} \tag{13.60}$$

where Density_P = electric flux density at point P

E_P = electric field intensity at point P

A = surface of a concentric cylinder with 1-m length and radius x (m^2)

$\varepsilon = \varepsilon_0 = \dfrac{10^{-9}}{36\pi}$ = permittivity of free space assumed for the conductor (F/m)

The potential difference or voltage difference between two outside points P_1 and P_2 with corresponding distances x_1 and x_2 from the conductor center is defined by integrating the electric field intensity from x_1 to x_2

$$V_{1-2} = \int_{x_1}^{x_2} E_P \frac{dx}{x} = \int_{x_1}^{x_2} \frac{q}{2\pi\varepsilon_0}\frac{dx}{x} = \frac{q}{2\pi\varepsilon_0} \ln\left[\frac{x_2}{x_1}\right] \text{ (V)} \tag{13.61}$$

Then, the capacitance between points P_1 and P_2 is evaluated as

$$C_{1-2} = \frac{q}{V_{1-2}} = \frac{2\pi\varepsilon_0}{\ln\left[\dfrac{x_2}{x_1}\right]} \text{ (F/m)} \tag{13.62}$$

If point P_1 is located at the conductor surface ($x_1 = r$), and point P_2 is located at ground surface below the conductor ($x_2 = h$), then the voltage of the conductor and the capacitance between the conductor and ground are

$$V_{\text{cond}} = \frac{q}{2\pi\varepsilon_0} \ln\left[\frac{h}{r}\right] \text{ (V)} \tag{13.63}$$

$$C_{\text{cond-ground}} = \frac{q}{V_{\text{cond}}} = \frac{2\pi\varepsilon_0}{\ln\left[\dfrac{h}{r}\right]} \text{ (F/m)} \tag{13.64}$$

13.5.2 Capacitance of a Single-Phase Line with Two Wires

Consider a two-wire single-phase line with conductors A and B with the same radius r, separated by a distance $D > r_A$ and r_B. The conductors are energized by a voltage source such that conductor A has a charge q^+ and conductor B a charge q^- as shown in Fig. 13.15.

The charge on each conductor generates independent electric fields. Charge q^+ on conductor A generates a voltage V_{AB-A} between both conductors. Similarly, charge q^- on conductor B generates a voltage V_{AB-B} between conductors.

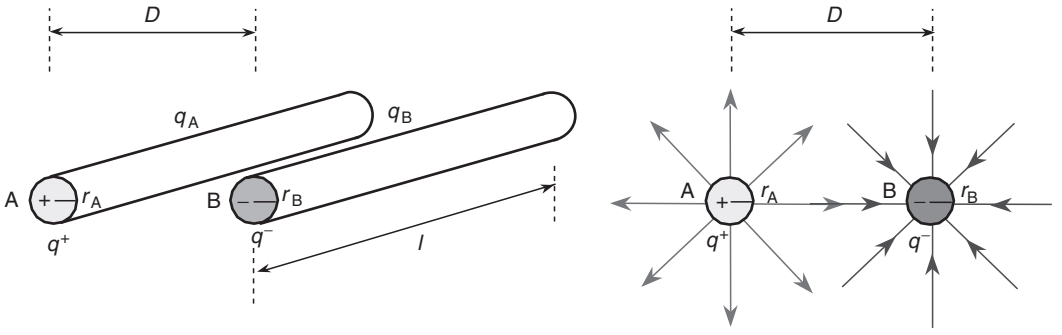

FIGURE 13.15 Electric field produced from a two-wire single-phase system.

V_{AB-A} is calculated by integrating the electric field intensity, due to the charge on conductor A, on conductor B from r_A to D

$$V_{AB-A} = \int_{r_A}^{D} E_A \, dx = \frac{q}{2\pi\varepsilon_0} \ln\left[\frac{D}{r_A}\right] \tag{13.65}$$

V_{AB-B} is calculated by integrating the electric field intensity due to the charge on conductor B from D to r_B

$$V_{AB-B} = \int_{D}^{r_B} E_B \, dx = \frac{-q}{2\pi\varepsilon_0} \ln\left[\frac{r_B}{D}\right] \tag{13.66}$$

The total voltage is the sum of the generated voltages V_{AB-A} and V_{AB-B}

$$V_{AB} = V_{AB-A} + V_{AB-B} = \frac{q}{2\pi\varepsilon_0} \ln\left[\frac{D}{r_A}\right] - \frac{q}{2\pi\varepsilon_0} \ln\left[\frac{r_B}{D}\right] = \frac{q}{2\pi\varepsilon_0} \ln\left[\frac{D^2}{r_A r_B}\right] \tag{13.67}$$

If the conductors have the same radius, $r_A = r_B = r$, then the voltage between conductors V_{AB}, and the capacitance between conductors C_{AB}, for a 1-m line length are

$$V_{AB} = \frac{q}{\pi\varepsilon_0} \ln\left[\frac{D}{r}\right] \text{ (V)} \tag{13.68}$$

$$C_{AB} = \frac{\pi\varepsilon_0}{\ln\left[\frac{D}{r}\right]} \text{ (F/m)} \tag{13.69}$$

The voltage between each conductor and ground (G) (Fig. 13.16) is one-half of the voltage between the two conductors. Therefore, the capacitance from either line to ground is twice the capacitance between lines

$$V_{AG} = V_{BG} = \frac{V_{AB}}{2} \text{ (V)} \tag{13.70}$$

$$C_{AG} = \frac{q}{V_{AG}} = \frac{2\pi\varepsilon_0}{\ln\left[\frac{D}{r}\right]} \text{ (F/m)} \tag{13.71}$$

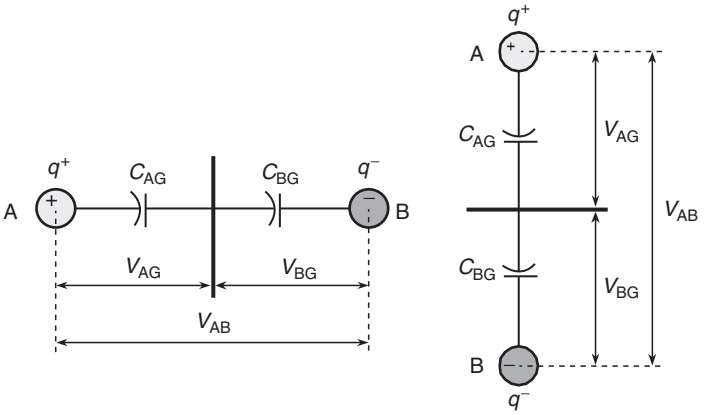

FIGURE 13.16 Capacitance between line to ground in a two-wire single-phase line.

13.5.3 Capacitance of a Three-Phase Line

Consider a three-phase line with the same voltage magnitude between phases, and assuming a balanced system with abc (positive) sequence such that $q_A + q_B + q_C = 0$. The conductors have radii r_A, r_B, and r_C, and the space between conductors are D_{AB}, D_{BC}, and D_{AC} (where D_{AB}, D_{BC}, and $D_{AC} > r_A$, r_B, and r_C). Also, the effect of earth and neutral conductors is neglected.

The expression for voltages between two conductors in a single-phase system can be extended to obtain the voltages between conductors in a three-phase system. The expressions for V_{AB} and V_{AC} are

$$V_{AB} = \frac{1}{2\pi\varepsilon_0}\left[q_A \ln\left[\frac{D_{AB}}{r_A}\right] + q_B \ln\left[\frac{r_B}{D_{AB}}\right] + q_C \ln\left[\frac{D_{BC}}{D_{AC}}\right]\right] \text{ (V)} \tag{13.72}$$

$$V_{AC} = \frac{1}{2\pi\varepsilon_0}\left[q_A \ln\left[\frac{D_{CA}}{r_A}\right] + q_B \ln\left[\frac{D_{BC}}{D_{AB}}\right] + q_C \ln\left[\frac{r_C}{D_{AC}}\right]\right] \text{ (V)} \tag{13.73}$$

If the three-phase system has triangular arrangement with equidistant conductors such that $D_{AB} = D_{BC} = D_{AC} = D$, with the same radii for the conductors such that $r_A = r_B = r_C = r$ (where $D > r$), the expressions for V_{AB} and V_{AC} are

$$\begin{aligned} V_{AB} &= \frac{1}{2\pi\varepsilon_0}\left[q_A \ln\left[\frac{D}{r}\right] + q_B \ln\left[\frac{r}{D}\right] + q_C \ln\left[\frac{D}{D}\right]\right] \\ &= \frac{1}{2\pi\varepsilon_0}\left[q_A \ln\left[\frac{D}{r}\right] + q_B \ln\left[\frac{r}{D}\right]\right] \text{ (V)} \end{aligned} \tag{13.74}$$

$$\begin{aligned} V_{AC} &= \frac{1}{2\pi\varepsilon_0}\left[q_A \ln\left[\frac{D}{r}\right] + q_B \ln\left[\frac{D}{D}\right] + q_C \ln\left[\frac{r}{D}\right]\right] \\ &= \frac{1}{2\pi\varepsilon_0}\left[q_A \ln\left[\frac{D}{r}\right] + q_C \ln\left[\frac{r}{D}\right]\right] \text{ (V)} \end{aligned} \tag{13.75}$$

Balanced line-to-line voltages with sequence abc, expressed in terms of the line-to-neutral voltage are

$$V_{AB} = \sqrt{3}\, V_{AN} \angle 30^\circ \text{ and } V_{AC} = -V_{CA} = \sqrt{3}\, V_{AN} \angle -30^\circ;$$

where V_{AN} is the line-to-neutral voltage. Therefore, V_{AN} can be expressed in terms of V_{AB} and V_{AC} as

$$V_{AN} = \frac{V_{AB} + V_{AC}}{3} \tag{13.76}$$

and thus, substituting V_{AB} and V_{AC} from Eqs. (13.67) and (13.68) we have

$$\begin{aligned} V_{AN} &= \frac{1}{6\pi\varepsilon_0}\left[\left[q_A \ln\left[\frac{D}{r}\right] + q_B \ln\left[\frac{r}{D}\right]\right] + \left[q_A \ln\left[\frac{D}{r}\right] + q_C \ln\left[\frac{r}{D}\right]\right]\right] \\ &= \frac{1}{6\pi\varepsilon_0}\left[2q_A \ln\left[\frac{D}{r}\right] + \left(q_B + q_C\right) \ln\left[\frac{r}{D}\right]\right] \text{ (V)} \end{aligned} \tag{13.77}$$

Under balanced conditions $q_A + q_B + q_C = 0$, or $-q_A = (q_B + q_C)$ then, the final expression for the line-to-neutral voltage is

$$V_{AN} = \frac{1}{2\pi\varepsilon_0} q_A \ln\left[\frac{D}{r}\right] \text{ (V)} \tag{13.78}$$

The positive sequence capacitance per unit length between phase A and neutral can now be obtained. The same result is obtained for capacitance between phases B and C to neutral

$$C_{AN} = \frac{q_A}{V_{AN}} = \frac{2\pi\varepsilon_0}{\ln\left[\frac{D}{r}\right]} \text{ (F/m)} \tag{13.79}$$

13.5.4 Capacitance of Stranded Bundle Conductors

The calculation of the capacitance in the equation above is based on

1. Solid conductors with zero resistivity (zero internal electric field)
2. Charge uniformly distributed
3. Equilateral spacing of phase conductors

In actual transmission lines, the resistivity of the conductors produces a small internal electric field and therefore, the electric field at the conductor surface is smaller than the estimated. However, the difference is negligible for practical purposes.

Because of the presence of other charged conductors, the charge distribution is nonuniform, and therefore the estimated capacitance is different. However, this effect is negligible for most practical calculations. In a line with stranded conductors, the capacitance is evaluated assuming a solid conductor with the same radius as the outside radius of the stranded conductor. This produces a negligible difference.

Most transmission lines do not have equilateral spacing of phase conductors. This causes differences between the line-to-neutral capacitances of the three phases. However, transposing the phase conductors balances the system resulting in equal line-to-neutral capacitance for each phase and is developed in the following manner.

Consider a transposed three-phase line with conductors having the same radius r, and with space between conductors D_{AB}, D_{BC}, and D_{AC} , where D_{AB}, D_{BC}, and $D_{AC} > r$.

Assuming abc positive sequence, the expressions for V_{AB} on the first, second, and third section of the transposed line are

$$V_{AB\ first} = \frac{1}{2\pi\varepsilon_0}\left[q_A \ln\left[\frac{D_{AB}}{r}\right] + q_B \ln\left[\frac{r}{D_{AB}}\right] + q_C \ln\left[\frac{D_{AB}}{D_{AC}}\right]\right] \text{ (V)} \tag{13.80}$$

$$V_{AB\ second} = \frac{1}{2\pi\varepsilon_0}\left[q_A \ln\left[\frac{D_{BC}}{r}\right] + q_B \ln\left[\frac{r}{D_{BC}}\right] + q_C \ln\left[\frac{D_{AC}}{D_{AB}}\right]\right] \text{ (V)} \tag{13.81}$$

$$V_{AB\ third} = \frac{1}{2\pi\varepsilon_0}\left[q_A \ln\left[\frac{D_{AC}}{r}\right] + q_B \ln\left[\frac{r}{D_{AC}}\right] + q_C \ln\left[\frac{D_{AB}}{D_{BC}}\right]\right] \text{ (V)} \tag{13.82}$$

Similarly, the expressions for V_{AC} on the first, second, and third section of the transposed line are

$$V_{AC\ first} = \frac{1}{2\pi\varepsilon_0}\left[q_A \ln\left[\frac{D_{AC}}{r}\right] + q_B \ln\left[\frac{D_{BC}}{D_{AB}}\right] + q_C \ln\left[\frac{r}{D_{AC}}\right]\right] \tag{13.83}$$

$$V_{AC\ second} = \frac{1}{2\pi\varepsilon_0}\left[q_A \ln\left[\frac{D_{AB}}{r}\right] + q_B \ln\left[\frac{D_{AC}}{D_{BC}}\right] + q_C \ln\left[\frac{r}{D_{AB}}\right]\right] \tag{13.84}$$

$$V_{AC\ third} = \frac{1}{2\pi\varepsilon_0}\left[q_A \ln\left[\frac{D_{BC}}{r}\right] + q_B \ln\left[\frac{D_{AB}}{D_{AC}}\right] + q_C \ln\left[\frac{r}{D_{BC}}\right]\right] \tag{13.85}$$

Taking the average value of the three sections, we have the final expressions of V_{AB} and V_{AC} in the transposed line

$$V_{\text{AB transp}} = \frac{V_{\text{AB first}} + V_{\text{AB second}} + V_{\text{AB third}}}{3}$$
$$= \frac{1}{6\pi\varepsilon_0}\left[q_A \ln\left[\frac{D_{AB}D_{AC}D_{BC}}{r^3}\right] + q_B \ln\left[\frac{r^3}{D_{AB}D_{AC}D_{BC}}\right] + q_C \ln\left[\frac{D_{AC}D_{AC}D_{BC}}{D_{AC}D_{AC}D_{BC}}\right]\right] (\text{V}) \quad (13.86)$$

$$V_{\text{AC transp}} = \frac{V_{\text{AC first}} + V_{\text{AC second}} + V_{\text{AC third}}}{3}$$
$$= \frac{1}{6\pi\varepsilon_0}\left[q_A \ln\left[\frac{D_{AB}D_{AC}D_{BC}}{r^3}\right] + q_B \ln\left[\frac{D_{AC}D_{AC}D_{BC}}{D_{AB}D_{AC}D_{BC}}\right] + q_C \ln\left[\frac{r^3}{D_{AC}D_{AC}D_{BC}}\right]\right] (\text{V}) \quad (13.87)$$

For a balanced system where $-q_A = (q_B + q_C)$, the phase-to-neutral voltage V_{AN} (phase voltage) is

$$V_{\text{AN transp}} = \frac{V_{\text{AB transp}} + V_{\text{AC transp}}}{3}$$
$$= \frac{1}{18\pi\varepsilon_0}\left[2\, q_A \ln\left[\frac{D_{AB}D_{AC}D_{BC}}{r^3}\right] + (q_B + q_C)\ln\left[\frac{r^3}{D_{AB}D_{AC}D_{BC}}\right]\right]$$
$$= \frac{1}{6\pi\varepsilon_0} q_A \ln\left[\frac{D_{AB}D_{AC}D_{BC}}{r^3}\right] = \frac{1}{2\pi\varepsilon_0} q_A \ln\left[\frac{\text{GMD}}{r}\right] (\text{V}) \quad (13.88)$$

where GMD $= \sqrt[3]{D_{AB}D_{BC}D_{CA}}$ = geometrical mean distance for a three-phase line.

For bundle conductors, an equivalent radius r_e replaces the radius r of a single conductor and is determined by the number of conductors per bundle and the spacing of conductors. The expression of r_e is similar to $\text{GMR}_{\text{bundle}}$ used in the calculation of the inductance per phase, except that the actual outside radius of the conductor is used instead of the $\text{GMR}_{\text{phase}}$. Therefore, the expression for V_{AN} is

$$V_{\text{AN transp}} = \frac{1}{2\pi\varepsilon_0} q_A \ln\left[\frac{\text{GMD}}{r_e}\right] (\text{V}) \quad (13.89)$$

where $r_e = (d^{n-1}r)^{1/n}$ = equivalent radius for up to three conductors per bundle (m)
$r_e = 1.09\ (d^3 r)^{1/4}$ = equivalent radius for four conductors per bundle (m)
d = distance between bundle conductors (m)
n = number of conductors per bundle

Finally, the capacitance and capacitive reactance, per unit length, from phase to neutral can be evaluated as

$$C_{\text{AN transp}} = \frac{q_A}{V_{\text{AN transp}}} = \frac{2\pi\varepsilon_0}{\ln\left[\frac{\text{GMD}}{r_e}\right]} (\text{F/m}) \quad (13.90)$$

$$X_{\text{AN transp}} = \frac{1}{2\pi f C_{\text{AN transp}}} = \frac{1}{4\pi f \varepsilon_0} \ln\left[\frac{\text{GMD}}{r_e}\right] (\Omega/\text{m}) \quad (13.91)$$

13.5.5 Capacitance Due to Earth's Surface

Considering a single-overhead conductor with a return path through the earth, separated a distance H from earth's surface, the charge of the earth would be equal in magnitude to that on the conductor but of opposite sign. If the earth is assumed as a perfectly conductive horizontal plane with infinite length, then the electric field lines will go from the conductor to the earth, perpendicular to the earth's surface (Fig. 13.17).

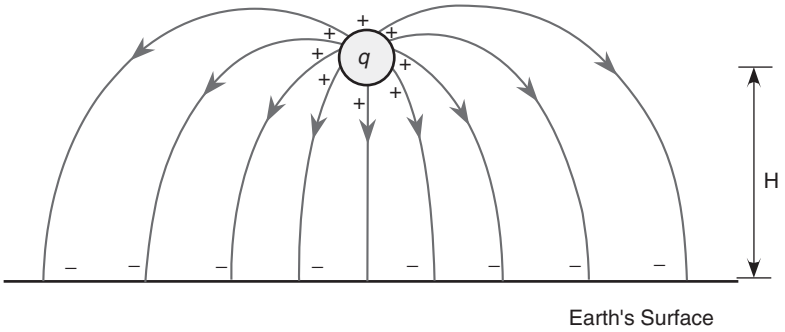

FIGURE 13.17 Distribution of electric field lines from an overhead conductor to earth's surface.

To calculate the capacitance, the negative charge of the earth can be replaced by an equivalent charge of an image conductor with the same radius as the overhead conductor, lying just below the overhead conductor (Fig. 13.18).

The same principle can be extended to calculate the capacitance per phase of a three-phase system. Figure 13.19 shows an equilateral arrangement of identical single conductors for phases A, B, and C carrying the charges q_A, q_B, and q_C and their respective image conductors A′, B′, and C′.

D_A, D_B, and D_C are perpendicular distances from phases A, B, and C to earth's surface. $D_{AA'}$, $D_{BB'}$, and $D_{CC'}$ are the perpendicular distances from phases A, B, and C to the image conductors A′, B′, and C′. Voltage V_{AB} can be obtained as

$$V_{AB} = \frac{1}{2\pi\varepsilon_0}\left[\begin{array}{l} q_A \ln\left[\dfrac{D_{AB}}{r_A}\right] + q_B \ln\left[\dfrac{r_B}{D_{AB}}\right] + q_C \ln\left[\dfrac{D_{BC}}{D_{AC}}\right] - \\ -q_A \ln\left[\dfrac{D_{AB'}}{D_{AA'}}\right] - q_B \ln\left[\dfrac{D_{BB'}}{D_{AB'}}\right] - q_C \ln\left[\dfrac{D_{BC'}}{D_{AC'}}\right] \end{array}\right] \text{ (V)} \qquad (13.92)$$

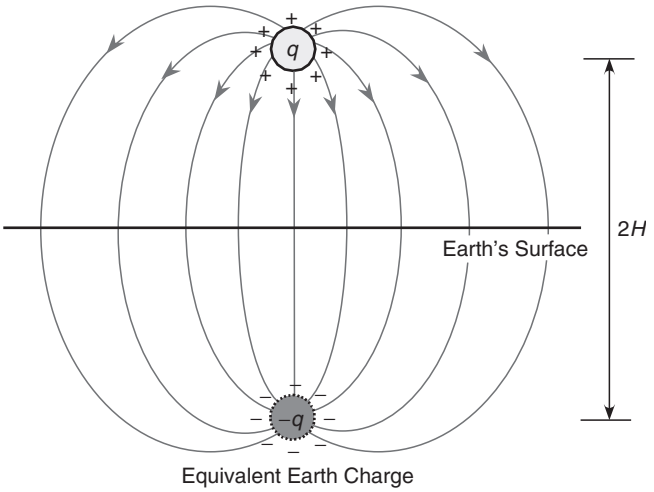

FIGURE 13.18 Equivalent image conductor representing the charge of the earth.

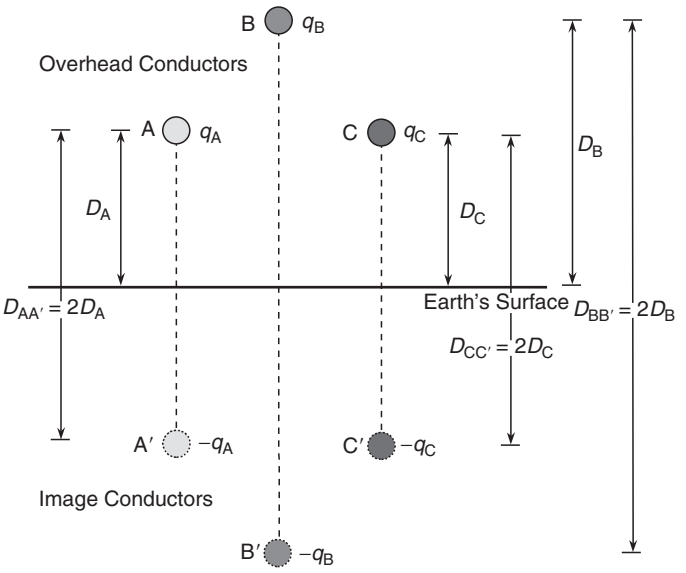

FIGURE 13.19 Arrangement of image conductors in a three-phase transmission line.

As overhead conductors are identical, then $r = r_A = r_B = r_C$. Also, as the conductors have equilateral arrangement, $D = D_{AB} = D_{BC} = D_{CA}$

$$V_{AB} = \frac{1}{2\pi\varepsilon_0}\left[q_A\left(\ln\left[\frac{D}{r}\right] - \ln\left[\frac{D_{AB'}}{D_{AA'}}\right]\right) + q_B\left(\ln\left[\frac{r}{D}\right] - \ln\left[\frac{D_{BB'}}{D_{AB'}}\right]\right) - q_C \ln\left[\frac{D_{BC'}}{D_{AC'}}\right]\right] \text{ (V)} \quad (13.93)$$

Similarly, expressions for V_{BC} and V_{AC} are

$$V_{BC} = \frac{1}{2\pi\varepsilon_0}\left[-q_A \ln\left[\frac{D_{CA'}}{D_{BA'}}\right] + q_B\left(\ln\left[\frac{D}{r}\right] - \ln\left[\frac{D_{CB'}}{D_{BB'}}\right]\right) + q_C\left(\ln\left[\frac{r}{D}\right] - \ln\left[\frac{D_{CC'}}{D_{BC'}}\right]\right)\right] \text{ (V)} \quad (13.94)$$

$$V_{AC} = \frac{1}{2\pi\varepsilon_0}\left[q_A\left(\ln\left[\frac{D}{r}\right] - \ln\left[\frac{D_{CA'}}{D_{AA'}}\right]\right) - q_B \ln\left[\frac{D_{CB'}}{D_{AB'}}\right] + q_C\left(\ln\left[\frac{r}{D}\right] - \ln\left[\frac{D_{CC'}}{D_{AC'}}\right]\right)\right] \text{ (V)} \quad (13.95)$$

The phase voltage V_{AN} becomes, through algebraic reduction,

$$\begin{aligned} V_{AN} &= \frac{V_{AB} + V_{AC}}{3} \\ &= \frac{1}{2\pi\varepsilon_0} q_A\left(\ln\left[\frac{D}{r}\right] - \ln\left[\frac{\sqrt[3]{D_{AB'} D_{BC'} D_{CA'}}}{\sqrt[3]{D_{AA'} D_{BB'} D_{CC'}}}\right]\right) \text{ (V)} \end{aligned} \quad (13.96)$$

Therefore, the phase capacitance C_{AN}, per unit length, is

$$C_{AN} = \frac{q_A}{V_{AN}} = \frac{2\pi\varepsilon_0}{\ln\left[\frac{D}{r}\right] - \ln\left[\frac{\sqrt[3]{D_{AB'} D_{BC'} D_{CA'}}}{\sqrt[3]{D_{AA'} D_{BB'} D_{CC'}}}\right]} \text{ (F/m)} \quad (13.97)$$

Equations (13.79) and (13.97) have similar expressions, except for the term $\ln\left((D_{AB'}\, D_{BC'}\, D_{CA'})^{1/3}/(D_{AA'}\, D_{BB'}\, D_{CC'})^{1/3}\right)$ included in Eq. (13.97). That term represents the effect of the earth on phase capacitance, increasing its total value. However, the capacitance increment is really small, and is usually

TABLE 13.2a Characteristics of Aluminum Cable Steel Reinforced Conductors (ACSR)

Code	Cross-Section Area			Stranding	Diameter		Layers	Approx. Current-Carrying Capacity	Resistance (mΩ/km)				GMR	60 Hz Reactances (Dm = 1 m)	
	Total	Aluminum			Conductor	Core			DC	AC (60 Hz)					
	(mm^2)	(kcmil)	(mm^2)	Al/Steel	(mm)	(mm)		(Amperes)	25°C	25°C	50°C	75°C	(mm)	X_1 (Ω/km)	X_0 (MΩ/km)
–	1521	2 776	1407	84/19	50.80	13.87	4		21.0	24.5	26.2	28.1	20.33	0.294	0.175
Joree	1344	2 515	1274	76/19	47.75	10.80	4		22.7	26.0	28.0	30.0	18.93	0.299	0.178
Thrasher	1235	2 312	1171	76/19	45.77	10.34	4		24.7	27.7	30.0	32.2	18.14	0.302	0.180
Kiwi	1146	2 167	1098	72/7	44.07	8.81	4		26.4	29.4	31.9	34.2	17.37	0.306	0.182
Bluebird	1181	2 156	1092	84/19	44.75	12.19	4		26.5	29.0	31.4	33.8	17.92	0.303	0.181
Chukar	976	1 781	902	84/19	40.69	11.10	4		32.1	34.1	37.2	40.1	16.28	0.311	0.186
Falcon	908	1 590	806	54/19	39.24	13.08	3	1 380	35.9	37.4	40.8	44.3	15.91	0.312	0.187
Lapwing	862	1 590	806	45/7	38.20	9.95	3	1 370	36.7	38.7	42.1	45.6	15.15	0.316	0.189
Parrot	862	1 510	765	54/19	38.23	12.75	3	1 340	37.8	39.2	42.8	46.5	15.48	0.314	0.189
Nuthatch	818	1 510	765	45/7	37.21	9.30	3	1 340	38.7	40.5	44.2	47.9	14.78	0.318	0.190
Plover	817	1 431	725	54/19	37.21	12.42	3	1 300	39.9	41.2	45.1	48.9	15.06	0.316	0.190
Bobolink	775	1 431	725	45/7	36.25	9.07	3	1 300	35.1	42.6	46.4	50.3	14.39	0.320	0.191
Martin	772	1 351	685	54/19	36.17	12.07	3	1 250	42.3	43.5	47.5	51.6	14.63	0.319	0.191
Dipper	732	1 351	685	45/7	35.20	8.81	3	1 250	43.2	44.9	49.0	53.1	13.99	0.322	0.193
Pheasant	726	1 272	645	54/19	35.10	11.71	3	1 200	44.9	46.1	50.4	54.8	14.20	0.321	0.193
Bittern	689	1 272	644	45/7	34.16	8.53	3	1 200	45.9	47.5	51.9	56.3	13.56	0.324	0.194
Grackle	681	1 192	604	54/19	34.00	11.33	3	1 160	47.9	49.0	53.6	58.3	13.75	0.323	0.194
Bunting	646	1 193	604	45/7	33.07	8.28	3	1 160	48.9	50.4	55.1	59.9	13.14	0.327	0.196
Finch	636	1 114	564	54/19	32.84	10.95	3	1 110	51.3	52.3	57.3	62.3	13.29	0.326	0.196
Bluejay	603	1 113	564	45/7	31.95	8.00	3	1 110	52.4	53.8	58.9	64.0	12.68	0.329	0.197
Curlew	591	1 033	523	54/7	31.62	10.54	3	1 060	56.5	57.4	63.0	68.4	12.80	0.329	0.198

Ortolan	560	1 033	525	45/7	30.78	7.70	3	1 060	56.5	57.8	63.3	68.7	12.22	0.332	0.199
Merganser	596	954	483	30/7	31.70	13.60	2	1 010	61.3	61.8	67.9	73.9	13.11	0.327	0.198
Cardinal	546	954	483	54/7	30.38	10.13	3	1 010	61.2	62.0	68.0	74.0	12.31	0.332	0.200
Rail	517	954	483	45/7	29.59	7.39	3	1 010	61.2	62.4	68.3	74.3	11.73	0.335	0.201
Baldpate	562	900	456	30/7	30.78	13.21	2	960	65.0	65.5	71.8	78.2	12.71	0.329	0.199
Canary	515	900	456	54/7	29.51	9.83	3	970	64.8	65.5	72.0	78.3	11.95	0.334	0.201
Ruddy	478	900	456	45/7	28.73	7.19	3	970	64.8	66.0	72.3	78.6	11.40	0.337	0.202
Crane	501	875	443	54/7	29.11	9.70	3	950	66.7	67.5	74.0	80.5	11.80	0.335	0.202
Willet	474	874	443	45/7	28.32	7.09	3	950	66.7	67.9	74.3	80.9	11.25	0.338	0.203
Skimmer	479	795	403	30/7	29.00	12.40	2	940	73.5	74.0	81.2	88.4	11.95	0.334	0.202
Mallard	495	795	403	30/19	28.96	12.42	2	910	73.5	74.0	81.2	88.4	11.95	0.334	0.202
Drake	469	795	403	26/7	28.14	10.36	2	900	73.3	74.0	81.2	88.4	11.43	0.337	0.203
Condor	455	795	403	54/7	27.74	9.25	3	900	73.4	74.1	81.4	88.6	11.22	0.339	0.204
Cuckoo	455	795	403	24/7	27.74	9.25	2	900	73.4	74.1	81.4	88.5	11.16	0.339	0.204
Tern	431	795	403	45/7	27.00	6.76	3	900	73.4	74.4	81.6	88.8	10.73	0.342	0.205
Coot	414	795	403	36/1	26.42	3.78	3	910	73.0	74.4	81.5	88.6	10.27	0.345	0.206
Buteo	447	715	362	30/7	27.46	11.76	2	840	81.8	82.2	90.2	98.3	11.34	0.338	0.204
Redwing	445	715	362	30/19	27.46	11.76	2	840	81.8	82.2	90.2	98.3	11.34	0.338	0.204
Starling	422	716	363	26/7	26.7	9.82	2	840	81.5	82.1	90.1	98.1	10.82	0.341	0.206
Crow	409	715	362	54/7	26.31	8.76	3	840	81.5	82.2	90.2	98.2	10.67	0.342	0.206

Current capacity evaluated at 75°C conductor temperature, 25°C air temperature, wind speed of 1.4 mi/h, and frequency of 60 Hz.

Sources: *Transmission Line Reference Book 345 kV and Above*, 2nd ed., Electric Power Research Institute, Palo Alto, California, 1987. With permission.
Glover, J.D. and Sarma, M.S., *Power System Analysis and Design*, 3rd ed., Brooks/Cole, 2002. With permission.

TABLE 13.2b Characteristics of Aluminum Cable Steel Reinforced Conductors (ACSR)

	Cross-Section Area				Diameter			Approx. Current-Carrying Capacity	Resistance (mΩ/km)					60 Hz Reactances (Dm = 1 m)	
		Aluminum								AC (60 Hz)					
Code	Total (mm^2)	(kcmil)	(mm^2)	Stranding Al/Steel	Conductor (mm)	Core (mm)	Layers	(Amperes)	DC 25°C	25°C	50°C	75°C	GMR (mm)	X_1 (Ω/km)	X_0 (MΩ/km)
Stilt	410	716	363	24/7	26.31	8.76	2	840	81.5	82.2	90.2	98.1	10.58	0.343	0.206
Grebe	388	716	363	45/7	25.63	6.4	3	840	81.5	82.5	90.4	98.4	10.18	0.346	0.208
Gannet	393	666	338	26/7	25.76	9.5	2	800	87.6	88.1	96.6	105.3	10.45	0.344	0.208
Gull	382	667	338	54/7	25.4	8.46	3	800	87.5	88.1	96.8	105.3	10.27	0.345	0.208
Flamingo	382	667	338	24/7	25.4	8.46	2	800	87.4	88.1	96.7	105.3	10.21	0.346	0.208
Scoter	397	636	322	30/7	25.88	11.1	2	800	91.9	92.3	101.4	110.4	10.70	0.342	0.207
Egret	396	636	322	30/19	25.88	11.1	2	780	91.9	92.3	101.4	110.4	10.70	0.342	0.207
Grosbeak	375	636	322	26/7	25.15	9.27	2	780	91.7	92.2	101.2	110.3	10.21	0.346	0.209
Goose	364	636	322	54/7	24.82	8.28	3	770	91.8	92.4	101.4	110.4	10.06	0.347	0.208
Rook	363	636	322	24/7	24.82	8.28	2	770	91.7	92.3	101.3	110.3	10.06	0.347	0.209
Kingbird	340	636	322	18/1	23.88	4.78	2	780	91.2	92.2	101.1	110.0	9.27	0.353	0.211
Swirl	331	636	322	36/1	23.62	3.38	3	780	91.3	92.4	101.3	110.3	9.20	0.353	0.212
Wood Duck	378	605	307	30/7	25.25	10.82	2	760	96.7	97.0	106.5	116.1	10.42	0.344	0.208
Teal	376	605	307	30/19	25.25	10.82	2	770	96.7	97.0	106.5	116.1	10.42	0.344	0.208
Squab	356	605	356	26/7	25.54	9.04	2	760	96.5	97.0	106.5	116.0	9.97	0.347	0.208
Peacock	346	605	307	24/7	24.21	8.08	2	760	96.4	97.0	106.4	115.9	9.72	0.349	0.210
Duck	347	606	307	54/7	24.21	8.08	3	750	96.3	97.0	106.3	115.8	9.81	0.349	0.210
Eagle	348	557	282	30/7	24.21	10.39	2	730	105.1	105.4	115.8	126.1	10.00	0.347	0.210
Dove	328	556	282	26/7	23.55	8.66	2	730	104.9	105.3	115.6	125.9	9.54	0.351	0.212
Parakeet	319	557	282	24/7	23.22	7.75	2	730	104.8	105.3	115.6	125.9	9.33	0.352	0.212

Osprey	298	556	282	18/1	22.33	4.47	2	740	104.4	105.2	115.4	125.7	8.66	0.358	0.214
Hen	298	477	242	30/7	22.43	9.6	2	670	122.6	122.9	134.9	147.0	9.27	0.353	0.214
Hawk	281	477	242	26/7	21.79	8.03	2	670	122.4	122.7	134.8	146.9	8.84	0.357	0.215
Flicker	273	477	273	24/7	21.49	7.16	2	670	122.2	122.7	134.7	146.8	8.63	0.358	0.216
Pelican	255	477	242	18/1	20.68	4.14	2	680	121.7	122.4	134.4	146.4	8.02	0.364	0.218
Lark	248	397	201	30/7	20.47	8.76	2	600	147.2	147.4	161.9	176.4	8.44	0.360	0.218
Ibis	234	397	201	26/7	19.89	7.32	2	590	146.9	147.2	161.7	176.1	8.08	0.363	0.220
Brant	228	398	201	24/7	19.61	6.53	2	590	146.7	147.1	161.6	176.1	7.89	0.365	0.221
Chickadee	213	397	201	18/1	18.87	3.78	2	590	146.1	146.7	161.0	175.4	7.32	0.371	0.222
Oriole	210	336	170	30/7	18.82	8.08	2	530	173.8	174.0	191.2	208.3	7.77	0.366	0.222
Linnet	198	336	170	26/7	18.29	6.73	2	530	173.6	173.8	190.9	208.1	7.41	0.370	0.224
Widgeon	193	336	170	24/7	18.03	6.02	2	530	173.4	173.7	190.8	207.9	7.25	0.371	0.225
Merlin	180	336	170	18/1	16.46	3.48	2	530	173.0	173.1	190.1	207.1	6.74	0.377	0.220
Piper	187	300	152	30/7	17.78	7.62	2	500	195.0	195.1	214.4	233.6	7.35	0.370	0.225
Ostrich	177	300	152	26/7	17.27	6.38	2	490	194.5	194.8	214.0	233.1	7.01	0.374	0.227
Gadwall	172	300	152	24/7	17.04	5.69	2	490	194.5	194.8	213.9	233.1	6.86	0.376	0.227
Phoebe	160	300	152	18/1	16.41	3.28	2	490	193.5	194.0	213.1	232.1	6.37	0.381	0.229
Junco	167	267	135	30/7	16.76	7.19	2	570	219.2	219.4	241.1	262.6	6.92	0.375	0.228
Partridge	157	267	135	26/7	16.31	5.99	2	460	218.6	218.9	240.5	262.0	6.61	0.378	0.229
Waxwing	143	267	135	18/1	15.47	3.1	2	460	217.8	218.1	239.7	261.1	6.00	0.386	0.232

Current capacity evaluated at 75°C conductor temperature, 25°C air temperature, wind speed of 1.4 mi/h, and frequency of 60 Hz.

Sources: *Transmission Line Reference Book 345 kV and Above,* 2nd ed., Electric Power Research Institute, Palo Alto, California, 1987. With permission.
Glover, J.D. and Sarma, M.S., *Power System Analysis and Design,* 3rd ed., Brooks/Cole, 2002. With permission.

TABLE 13.3a Characteristics of All-Aluminum-Conductors (AAC)

	Cross-Section Area			Diameter		Approx. Current-Carrying Capacity	Resistance (mΩ/km)					60 Hz Reactances (Dm = 1 m)	
								AC (60 Hz)					
Code	(mm^2)	kcmil or AWG	Stranding	(mm)	Layers	(Amperes)	DC 25°C	25°C	50°C	75°C	GMR (mm)	X_L (Ω/km)	X_C (MΩ/km)
Coreopsis	806.2	1591	61	36.93	4	1380	36.5	39.5	42.9	46.3	14.26	0.320	0.190
Gladiolus	765.8	1511	61	35.99	4	1340	38.4	41.3	44.9	48.5	13.90	0.322	0.192
Carnation	725.4	1432	61	35.03	4	1300	40.5	43.3	47.1	50.9	13.53	0.324	0.193
Columbine	865.3	1352	61	34.04	4	1250	42.9	45.6	49.6	53.6	13.14	0.327	0.196
Narcissus	644.5	1272	61	33.02	4	1200	45.5	48.1	52.5	56.7	12.74	0.329	0.194
Hawthorn	604.1	1192	61	31.95	4	1160	48.7	51.0	55.6	60.3	12.34	0.331	0.197
Marigold	564.2	1113	61	30.89	4	1110	52.1	54.3	59.3	64.3	11.92	0.334	0.199
Larkspur	524	1034	61	29.77	4	1060	56.1	58.2	63.6	69.0	11.49	0.337	0.201
Bluebell	524.1	1034	37	29.71	3	1060	56.1	58.2	63.5	68.9	11.40	0.337	0.201
Goldenrod	483.7	955	61	28.6	4	1010	60.8	62.7	68.6	74.4	11.03	0.340	0.203
Magnolia	483.6	954	37	28.55	3	1010	60.8	62.7	68.6	74.5	10.97	0.340	0.203
Crocus	443.6	875	61	27.38	4	950	66.3	68.1	74.5	80.9	10.58	0.343	0.205
Anemone	443.5	875	37	27.36	3	950	66.3	68.1	74.5	80.9	10.49	0.344	0.205
Lilac	403.1	796	61	26.11	4	900	73.0	74.6	81.7	88.6	10.09	0.347	0.207
Arbutus	402.9	795	37	26.06	3	900	73.0	74.6	81.7	88.6	10.00	0.347	0.207
Nasturtium	362.5	715	61	24.76	4	840	81.2	82.6	90.5	98.4	9.57	0.351	0.209
Violet	362.8	716	37	24.74	3	840	81.1	82.5	90.4	98.3	9.48	0.351	0.209
Orchid	322.2	636	37	23.32	3	780	91.3	92.6	101.5	110.4	8.96	0.356	0.212
Mistletoe	281.8	556	37	21.79	3	730	104.4	105.5	115.8	126.0	8.38	0.361	0.215
Dahlia	281.8	556	19	21.72	2	730	104.4	105.5	115.8	125.9	8.23	0.362	0.216
Syringa	241.5	477	37	20.19	3	670	121.8	122.7	134.7	146.7	7.74	0.367	0.219
Cosmos	241.9	477	19	20.14	2	670	121.6	122.6	134.5	146.5	7.62	0.368	0.219
Canna	201.6	398	19	18.36	2	600	145.9	146.7	161.1	175.5	6.95	0.375	0.224
Tulip	170.6	337	19	16.92	2	530	172.5	173.2	190.1	207.1	6.40	0.381	0.228
Laurel	135.2	267	19	15.06	2	460	217.6	218.1	239.6	261.0	5.70	0.390	0.233
Daisy	135.3	267	7	14.88	1	460	217.5	218	239.4	260.8	5.39	0.394	0.233
Oxlip	107.3	212 or (4/0)	7	13.26	1	340	274.3	274.7	301.7	328.8	4.82	0.402	0.239
Phlox	85	168 or (3/0)	7	11.79	1	300	346.4	346.4	380.6	414.7	4.27	0.411	0.245
Aster	67.5	133 or (2/0)	7	10.52	1	270	436.1	439.5	479.4	522.5	3.81	0.40	0.25
Poppy	53.5	106 or (1/0)	7	9.35	1	230	550	550.2	604.5	658.8	3.38	0.429	0.256
Pansy	42.4	#1 AWG	7	8.33	1	200	694.2	694.2	763.2	831.6	3.02	0.438	0.261
Iris	33.6	#2 AWG	7	7.42	1	180	874.5	874.5	960.8	1047.9	2.68	0.446	0.267
Rose	21.1	#3 AWG	7	5.89	1	160	1391.5	1391.5	1528.9	1666.3	2.13	0.464	0.278
Peachbell	13.3	#4 AWG	7	4.67	1	140	2214.4	2214.4	2443.2	2652	1.71	0.481	0.289

Current capacity evaluated at 75°C conductor temperature, 25°C air temperature, wind speed of 1.4 mi/h, and frequency of 60 Hz.

Sources: *Transmission Line Reference Book 345 kV and Above*, 2nd ed., Electric Power Research Institute, Palo Alto, California, 1987. With permission.
Glover, J.D. and Sarma, M.S., *Power System Analysis and Design*, 3rd ed., Brooks/Cole, 2002. With permission.

TABLE 13.3b Characteristics of All-Aluminum-Conductors (AAC)

	Cross-Section Area			Diameter		Approx. Current-Carrying Capacity	Resistance (mΩ/km)					60 Hz Reactances (Dm = 1 m)	
							DC	AC (60 Hz)			GMR	X_L	X_C
Code	(mm^2)	kcmil or AWG	Stranding	(mm)	Layers	(Amperes)	25°C	25°C	50°C	75°C	(mm)	(Ω/km)	(MΩ/km)
EVEN SIZES													
Bluebonnet	1773.3	3500	7	54.81	6		16.9	22.2	23.6	25.0	21.24	0.290	0.172
Trillium	1520.2	3000	127	50.75	6		19.7	24.6	26.2	27.9	19.69	0.296	0.175
Lupine	1266.0	2499	91	46.30	5		23.5	27.8	29.8	31.9	17.92	0.303	0.180
Cowslip	1012.7	1999	91	41.40	5		29.0	32.7	35.3	38.0	16.03	0.312	0.185
Jessamine	887.0	1750	61	38.74	4		33.2	36.5	39.5	42.5	14.94	0.317	0.188
Hawkweed	506.7	1000	37	29.24	3	1030	58.0	60.0	65.5	71.2	11.22	0.339	0.201
Camelia	506.4	999	61	29.26	4	1030	58.1	60.1	65.5	71.2	11.31	0.338	0.201
Snapdragon	456.3	900	61	27.79	4	970	64.4	66.3	72.5	78.7	10.73	0.342	0.204
Cockscomb	456.3	900	37	27.74	3	970	64.4	66.3	72.5	78.7	10.64	0.343	0.204
Cattail	380.1	750	61	25.35	4	870	77.4	78.9	86.4	93.9	9.78	0.349	0.208
Petunia	380.2	750	37	23.85	3	870	77.4	78.9	86.4	93.9	9.72	0.349	0.208
Flag	354.5	700	61	24.49	4	810	83.0	84.4	92.5	100.6	9.45	0.352	0.210
Verbena	354.5	700	37	24.43	3	810	83.0	84.4	92.5	100.6	9.39	0.352	0.210
Meadowsweet	303.8	600	37	2.63	3	740	96.8	98.0	107.5	117.0	8.69	0.358	0.214
Hyacinth	253.1	500	37	20.65	3	690	116.2	117.2	128.5	140.0	7.92	0.365	0.218
Zinnia	253.3	500	19	20.60	2	690	116.2	117.2	128.5	139.9	7.80	0.366	0.218
Goldentuft	228.0	450	19	19.53	2	640	129.0	129.9	142.6	155.3	7.41	0.370	0.221
Daffodil	177.3	350	19	17.25	2	580	165.9	166.6	183.0	199.3	6.52	0.379	0.227
Peony	152.1	300	19	15.98	2	490	193.4	194.0	213.1	232.1	6.04	0.385	0.230
Valerian	126.7	250	19	14.55	2	420	232.3	232.8	255.6	278.6	5.52	0.392	0.235
Sneezewort	126.7	250	7	14.40	1	420	232.2	232.7	255.6	278.4	5.21	0.396	0.235

Current capacity evaluated at 75°C conductor temperature, 25°C air temperature, wind speed of 1.4 mi/h, and frequency of 60 Hz.

Sources: *Transmission Line Reference Book 345 kV and Above*, 2nd ed., Electric Power Research Institute, Palo Alto, California, 1987. With permission.
Glover, J.D. and Sarma, M.S., *Power System Analysis and Design*, 3rd ed., Brooks/Cole, 2002. With permission.

neglected, because distances from overhead conductors to ground are always greater than distances among conductors.

13.6 Characteristics of Overhead Conductors

Tables 13.2a and 13.2b present typical values of resistance, inductive reactance and capacitance reactance, per unit length, of ACSR conductors. The size of the conductors (cross-section area) is specified in square millimeters and kcmil, where a cmil is the cross-section area of a circular conductor with a diameter of 1/1000 in. The tables include also the approximate current-carrying capacity of the conductors assuming 60 Hz, wind speed of 1.4 mi/h, and conductor and air temperatures of 75°C and 25°C, respectively. Tables 13.3a and 13.3b present the corresponding characteristics of AACs.

References

1. Yamayee, Z.A. and Bala, J.L. Jr., *Electromechanical Energy Devices and Power Systems*, John Wiley and Sons, Inc., New York, 1994.
2. Glover, J.D. and Sarma, M.S., *Power System Analysis and Design*, 3rd ed., Brooks/Cole, 2002.
3. Stevenson, W.D. Jr., *Elements of Power System Analysis*, 4th ed. McGraw-Hill, New York, 1982.
4. Saadat, H., *Power System Analysis*, McGraw-Hill, Boston, MA, 1999.
5. Gross, Ch.A., *Power System Analysis*, John Wiley and Sons, New York, 1979.
6. Gungor, B.R., *Power Systems*, Harcourt Brace Jovanovich, Orlando, FL, 1988.
7. Zaborszky, J. and Rittenhouse, J.W., *Electric Power Transmission. The Power System in the Steady State*, The Ronald Press Company, New York, 1954.
8. Barnes, C.C., *Power Cables. Their Design and Installation*, 2nd ed., Chapman and Hall, London, 1966.
9. Electric Power Research Institute, *Transmission Line Reference Book 345 kV and Above*, 2nd ed., Palo Alto, CA, 1987.

14

Sag and Tension of Conductor

D.A. Douglass
Power Delivery Consultants, Inc.

Ridley Thrash
Southwire Company

The energized conductors of transmission and distribution lines must be placed to totally eliminate the possibility of injury to people. Overhead conductors, however, elongate with time, temperature, and tension, thereby changing their original positions after installation. Despite the effects of weather and loading on a line, the conductors must remain at safe distances from buildings, objects, and people or vehicles passing beneath the line at all times. To ensure this safety, the shape of the terrain along the right-of-way, the height and lateral position of the conductor support points, and the position of the conductor between support points under all wind, ice, and temperature conditions must be known.

Bare overhead transmission or distribution conductors are typically quite flexible and uniform in weight along their length. Because of these characteristics, they take the form of a catenary (Ehrenberg, 1935; Winkelmann, 1959) between support points. The shape of the catenary changes with conductor temperature, ice and wind loading, and time. To ensure adequate vertical and horizontal clearance under all weather and electrical loadings, and to ensure that the breaking strength of the conductor is not exceeded, the behavior of the conductor catenary under all conditions must be known before the line is designed. The future behavior of the conductor is determined through calculations commonly referred to as sag-tension calculations.

Sag-tension calculations predict the behavior of conductors based on recommended tension limits under varying loading conditions. These tension limits specify certain percentages of the conductor's

rated breaking strength that are not to be exceeded upon installation or during the life of the line. These conditions, along with the elastic and permanent elongation properties of the conductor, provide the basis for determinating the amount of resulting sag during installation and long-term operation of the line.

Accurately determined initial sag limits are essential in the line design process. Final sags and tensions depend on initial installed sags and tensions and on proper handling during installation. The final sag shape of conductors is used to select support point heights and span lengths so that the minimum clearances will be maintained over the life of the line. If the conductor is damaged or the initial sags are incorrect, the line clearances may be violated or the conductor may break during heavy ice or wind loadings.

14.1 Catenary Cables

A bare-stranded overhead conductor is normally held clear of objects, people, and other conductors by periodic attachment to insulators. The elevation differences between the supporting structures affect the shape of the conductor catenary. The catenary's shape has a distinct effect on the sag and tension of the conductor, and therefore, must be determined using well-defined mathematical equations.

14.1.1 Level Spans

The shape of a catenary is a function of the conductor weight per unit length, w, the horizontal component of tension, H, span length, S, and the maximum sag of the conductor, D. Conductor sag and span length are illustrated in Fig. 14.1 for a level span.

The exact catenary equation uses hyperbolic functions. Relative to the low point of the catenary curve shown in Fig. 14.1, the height of the conductor, $y(x)$, above this low point is given by the following equation:

$$y(x) = \frac{H}{w}\cosh\left(\left(\frac{w}{H}x\right) - 1\right) = \frac{w(x^2)}{2H} \tag{14.1}$$

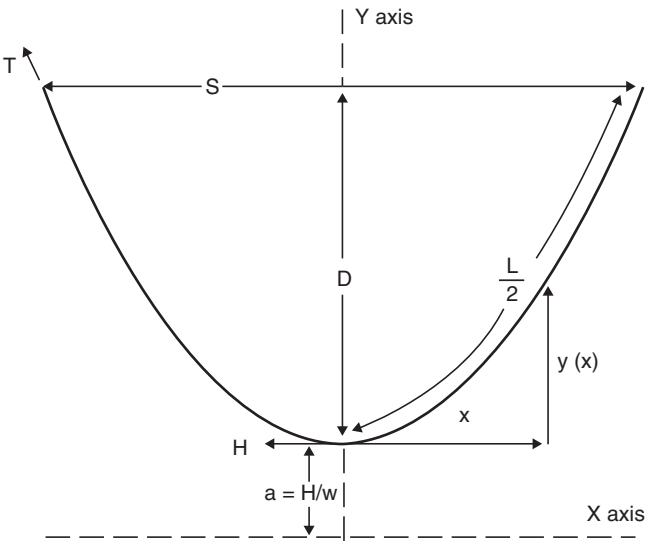

FIGURE 14.1 The catenary curve for level spans.

Note that x is positive in either direction from the low point of the catenary. The expression to the right is an approximate parabolic equation based upon a MacLaurin expansion of the hyperbolic cosine.

For a level span, the low point is in the center, and the sag, D, is found by substituting $x = S/2$ in the preceding equations. The exact and approximate parabolic equations for sag become the following:

$$D = \frac{H}{w}\left(\cosh\left(\frac{wS}{2H}\right) - 1\right) = \frac{w(S^2)}{8H} \tag{14.2}$$

The ratio, H/w, which appears in all of the preceding equations, is commonly referred to as the catenary constant. An increase in the catenary constant, having the units of length, causes the catenary curve to become shallower and the sag to decrease. Although it varies with conductor temperature, ice and wind loading, and time, the catenary constant typically has a value in the range of several thousand feet for most transmission-line catenaries.

The approximate or parabolic expression is sufficiently accurate as long as the sag is less than 5% of the span length. As an example, consider a 1000-ft span of Drake conductor ($w = 1.096$ lb/ft) installed at a tension of 4500 lb. The catenary constant equals 4106 ft. The calculated sag is 30.48 ft and 30.44 ft using the hyperbolic and approximate equations, respectively. Both estimates indicate a sag-to-span ratio of 3.4% and a sag difference of only 0.5 in.

The horizontal component of tension, H, is equal to the conductor tension at the point in the catenary where the conductor slope is horizontal. For a level span, this is the midpoint of the span length. At the ends of the level span, the conductor tension, T, is equal to the horizontal component plus the conductor weight per unit length, w, multiplied by the sag, D, as shown in the following:

$$T = H + wD \tag{14.3}$$

Given the conditions in the preceding example calculation for a 1000-ft level span of Drake ACSR, the tension at the attachment points exceeds the horizontal component of tension by 33 lb. It is common to perform sag-tension calculations using the horizontal tension component, but the average of the horizontal and support point tension is usually listed in the output.

14.1.2 Conductor Length

Application of calculus to the catenary equation allows the calculation of the conductor length, $L(x)$, measured along the conductor from the low point of the catenary in either direction.

The resulting equation becomes:

$$L(x) = \frac{H}{w}\mathrm{SINH}\left(\frac{wx}{H}\right) = x\left(1 + \frac{x^2(w^2)}{6H^2}\right) \tag{14.4}$$

For a level span, the conductor length corresponding to $x = S/2$ is half of the total conductor length and the total length, L, is:

$$L = \left(\frac{2H}{w}\right)\mathrm{SINH}\left(\frac{Sw}{2H}\right) = S\left(1 + \frac{S^2(w^2)}{24H^2}\right) \tag{14.5}$$

The parabolic equation for conductor length can also be expressed as a function of sag, D, by substitution of the sag parabolic equation, giving:

$$L = S + \frac{8D^2}{3S} \tag{14.6}$$

14.1.3 Conductor Slack

The difference between the conductor length, L, and the span length, S, is called slack. The parabolic equations for slack may be found by combining the preceding parabolic equations for conductor length, L, and sag, D:

$$L - S = S^3\left(\frac{w^2}{24H^2}\right) = D^2\left(\frac{8}{3S}\right) \tag{14.7}$$

While slack has units of length, it is often expressed as the percentage of slack relative to the span length. Note that slack is related to the cube of span length for a given H/w ratio and to the square of sag for a given span. For a series of spans having the same H/w ratio, the total slack is largely determined by the longest spans. It is for this reason that the ruling span is nearly equal to the longest span rather than the average span in a series of suspension spans.

Equation (14.7) can be inverted to obtain a more interesting relationship showing the dependence of sag, D, upon slack, L-S:

$$D = \sqrt{\frac{3S(L-S)}{8}} \tag{14.8}$$

As can be seen from the preceding equation, small changes in slack typically yield large changes in conductor sag.

14.1.4 Inclined Spans

Inclined spans may be analyzed using essentially the same equations that were used for level spans. The catenary equation for the conductor height above the low point in the span is the same. However, the span is considered to consist of two separate sections, one to the right of the low point and the other to the left as shown in Fig. 14.2 (Winkelmann, 1959). The shape of the catenary relative to the low point is unaffected by the difference in suspension point elevation (span inclination).

In each direction from the low point, the conductor elevation, y(x), relative to the low point is given by:

$$y(x) = \frac{H}{w}\cosh\left(\left(\frac{w}{H}x\right) - 1\right) = \frac{w(x^2)}{2H} \tag{14.9}$$

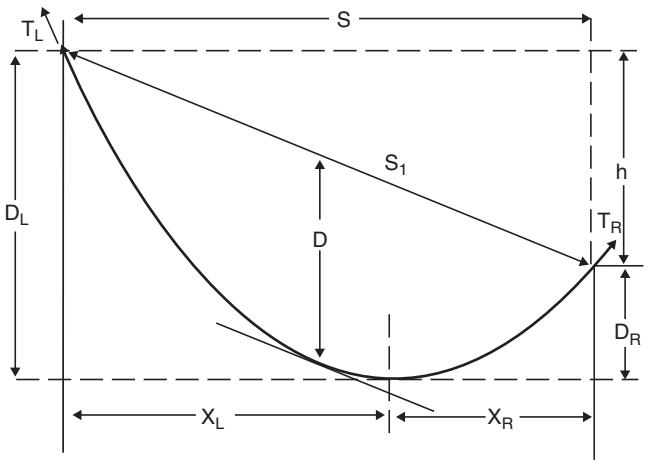

FIGURE 14.2 Inclined catenary span.

Note that x is considered positive in either direction from the low point.

The horizontal distance, x_L, from the left support point to the low point in the catenary is:

$$x_L = \frac{S}{2}\left(1 + \frac{h}{4D}\right) \tag{14.10}$$

The horizontal distance, x_R, from the right support point to the low point of the catenary is:

$$x_R = \frac{S}{2}\left(1 - \frac{h}{4D}\right) \tag{14.11}$$

where S = horizontal distance between support points.
h = vertical distance between support points.
S_l = straight-line distance between support points.
D = sag measured vertically from a line through the points of conductor support to a line tangent to the conductor.

The midpoint sag, D, is approximately equal to the sag in a horizontal span equal in length to the inclined span, S_l.

Knowing the horizonal distance from the low point to the support point in each direction, the preceding equations for $y(x)$, L, D, and T can be applied to each side of the inclined span.

The total conductor length, L, in the inclined span is equal to the sum of the lengths in the x_R and x_L sub-span sections:

$$L = S + \left(x_R^3 + x_L^3\right)\left(\frac{w^2}{6H^2}\right) \tag{14.12}$$

In each sub-span, the sag is relative to the corresponding support point elevation:

$$D_R = \frac{wx_R^2}{2H} \quad D_L = \frac{wx_L^2}{2H} \tag{14.13}$$

or in terms of sag, D, and the vertical distance between support points:

$$D_R = D\left(1 - \frac{h}{4D}\right)^2 \quad D_L = D\left(1 + \frac{h}{4D}\right)^2 \tag{14.14}$$

and the maximum tension is:

$$T_R = H + wD_R \quad T_L = H + wD_L \tag{14.15}$$

or in terms of upper and lower support points:

$$T_u = T_l + wh \tag{14.16}$$

where D_R = sag in right sub-span section
D_L = sag in left sub-span section
T_R = tension in right sub-span section
T_L = tension in left sub-span section
T_u = tension in conductor at upper support
T_l = tension in conductor at lower support

The horizontal conductor tension is equal at both supports. The vertical component of conductor tension is greater at the upper support and the resultant tension, T_u, is also greater.

14.1.5 Ice and Wind Conductor Loads

When a conductor is covered with ice and/or is exposed to wind, the effective conductor weight per unit length increases. During occasions of heavy ice and/or wind load, the conductor catenary tension increases dramatically along with the loads on angle and deadend structures. Both the conductor and its supports can fail unless these high-tension conditions are considered in the line design.

The National Electric Safety Code (NESC) suggests certain combinations of ice and wind corresponding to heavy, medium, and light loading regions of the United States. Figure 14.3 is a map of the U.S. indicating those areas (NESC, 1993). The combinations of ice and wind corresponding to loading region are listed in Table 14.1.

The NESC also suggests that increased conductor loads due to high wind loads without ice be considered. Figure 14.4 shows the suggested wind pressure as a function of geographical area for the United States (ASCE Std 7–88).

Certain utilities in very heavy ice areas use glaze ice thicknesses of as much as two inches to calculate iced conductor weight. Similarly, utilities in regions where hurricane winds occur may use wind loads as high as 34 lb/ft^2.

As the NESC indicates, the degree of ice and wind loads varies with the region. Some areas may have heavy icing, whereas some areas may have extremely high winds. The loads must be accounted for in the line design process so they do not have a detrimental effect on the line. Some of the effects of both the individual and combined components of ice and wind loads are discussed in the following.

14.1.5.1 Ice Loading

The formation of ice on overhead conductors may take several physical forms (glaze ice, rime ice, or wet snow). The impact of lower density ice formation is usually considered in the design of line sections at high altitudes.

The formation of ice on overhead conductors has the following influence on line design:

- Ice loads determine the maximum vertical conductor loads that structures and foundations must withstand.
- In combination with simultaneous wind loads, ice loads also determine the maximum transverse loads on structures.

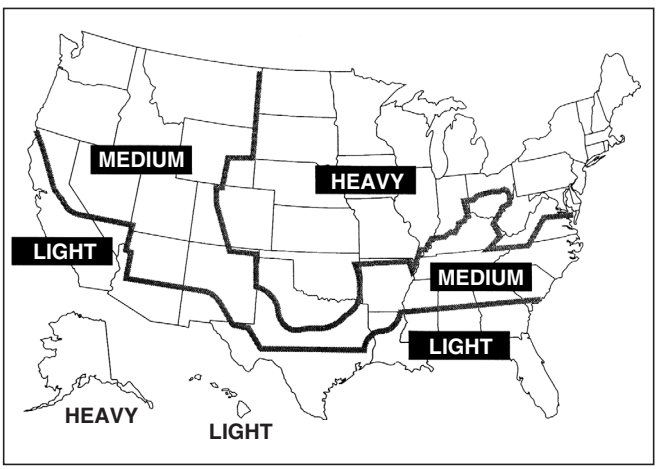

FIGURE 14.3 Ice and wind load areas of the U.S.

TABLE 14.1 Definitions of Ice and Wind Load for NESC Loading Areas

	Loading Districts			
	Heavy	Medium	Light	Extreme Wind Loading
Radial thickness of ice				
(in.)	0.50	0.25	0	0
(mm)	12.5	6.5	0	0
Horizontal wind pressure				
(lb/ft^2)	4	4	9	See Fig. 14.4
(Pa)	190	190	430	
Temperature				
(°F)	0	+15	+30	+60
(°C)	−20	−10	−1	+15
Constant to be added to the resultant for all conductors				
(lb/ft)	0.30	0.20	0.05	0.0
(N/m)	4.40	2.50	0.70	0.0

- In regions of heavy ice loads, the maximum sags and the permanent increase in sag with time (difference between initial and final sags) may be due to ice loadings.

Ice loads for use in designing lines are normally derived on the basis of past experience, code requirements, state regulations, and analysis of historical weather data. Mean recurrence intervals for heavy ice loadings are a function of local conditions along various routings. The impact of varying assumptions concerning ice loading can be investigated with line design software.

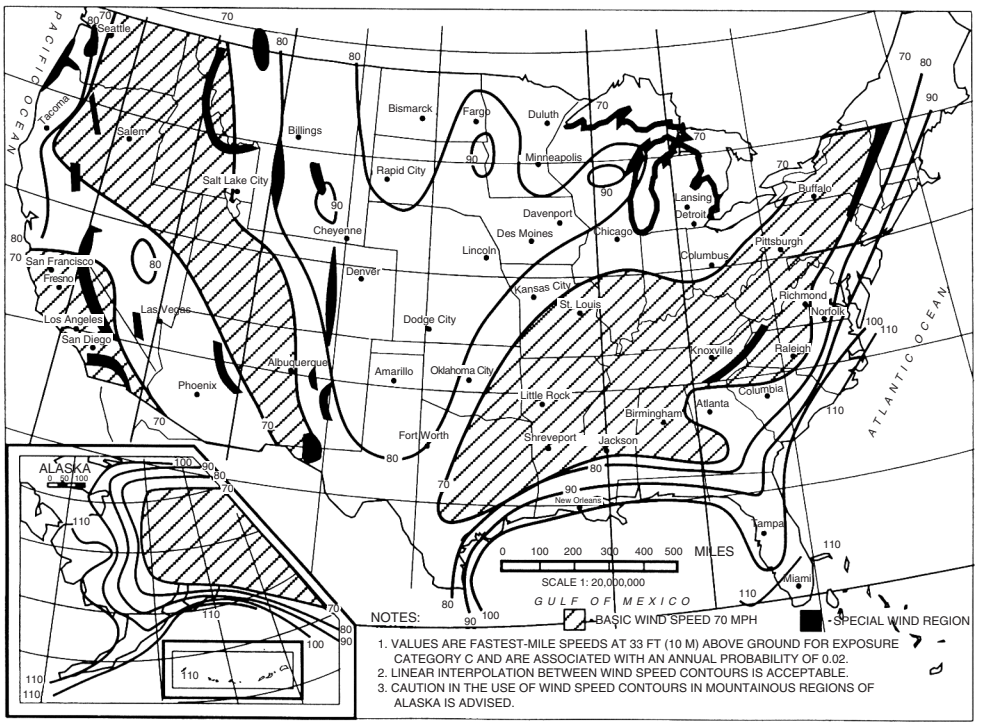

FIGURE 14.4 Wind pressure design values in the United States. Maximum recorded wind speed in miles/hour. (From Overend, P.R. and Smith, S., *Impulse Time Method of Sag Measurement*, American Society of Civil Engineers. With permission.)

TABLE 14.2 Ratio of Iced to Bare Conductor Weight

ACSR Conductor	D_c, in.	W_{bare}, lb/ft	W_{ice}, lb/ft	$\frac{W_{bare} + W_{ice}}{W_{bare}}$
#1/0 AWG -6/1 "Raven"	0.398	0.1451	0.559	4.8
477 kcmil-26/7 "Hawk"	0.858	0.6553	0.845	2.3
1590 kcmil-54/19 "Falcon"	1.545	2.042	1.272	1.6

The calculation of ice loads on conductors is normally done with an assumed glaze ice density of 57 lb/ft^3. The weight of ice per unit length is calculated with the following equation:

$$w_{ice} = 1.244t(D_c + t) \tag{14.17}$$

where t = thickness of ice, in.
D_c = conductor outside diameter, in.
w_{ice} = resultant weight of ice, lb/ft

The ratio of iced weight to bare weight depends strongly upon conductor diameter. As shown in Table 14.2 for three different conductors covered with 0.5-in radial glaze ice, this ratio ranges from 4.8 for #1/0 AWG to 1.6 for 1590-kcmil conductors. As a result, small diameter conductors may need to have a higher elastic modulus and higher tensile strength than large conductors in heavy ice and wind loading areas to limit sag.

14.1.5.2 Wind Loading

Wind loadings on overhead conductors influence line design in a number of ways:

- The maximum span between structures may be determined by the need for horizontal clearance to edge of right-of-way during moderate winds.
- The maximum transverse loads for tangent and small angle suspension structures are often determined by infrequent high wind-speed loadings.
- Permanent increases in conductor sag may be determined by wind loading in areas of light ice load.

Wind pressure load on conductors, P_w, is commonly specified in lb/ft^2. The relationship between P_w and wind velocity is given by the following equation:

$$P_w = 0.0025(V_w)^2 \tag{14.18}$$

where V_w = the wind speed in miles per hour.

The wind load per unit length of conductor is equal to the wind pressure load, P_w, multiplied by the conductor diameter (including radial ice of thickness t, if any), is given by the following equation:

$$W_w = P_w \frac{(D_c + 2t)}{12} \tag{14.19}$$

14.1.5.3 Combined Ice and Wind Loading

If the conductor weight is to include both ice and wind loading, the resultant magnitude of the loads must be determined vectorially. The weight of a conductor under both ice and wind loading is given by the following equation:

$$w_{w+i} = \sqrt{(w_b + w_i)^2 + (W_w)^2} \tag{14.20}$$

where w_b = bare conductor weight per unit length, lb/ft
w_i = weight of ice per unit length, lb/ft
w_w = wind load per unit length, lb/ft
$w_{w \pm i}$ = resultant of ice and wind loads, lb/ft

The NESC prescribes a safety factor, K, in pounds per foot, dependent upon loading district, to be added to the resultant ice and wind loading when performing sag and tension calculations. Therefore, the total resultant conductor weight, w, is:

$$w = w_{w+i} + K \tag{14.21}$$

14.1.6 Conductor Tension Limits

The NESC recommends limits on the tension of bare overhead conductors as a percentage of the conductor's rated breaking strength. The tension limits are: 60% under maximum ice and wind load, 33.3% initial unloaded (when installed) at 60°F, and 25% final unloaded (after maximum loading has occurred) at 60°F. It is common, however, for lower unloaded tension limits to be used. Except in areas experiencing severe ice loading, it is not unusual to find tension limits of 60% maximum, 25% unloaded initial, and 15% unloaded final. This set of specifications could easily result in an actual maximum tension on the order of only 35 to 40%, an initial tension of 20% and a final unloaded tension level of 15%. In this case, the 15% tension limit is said to govern.

Transmission-line conductors are normally not covered with ice, and winds on the conductor are usually much lower than those used in maximum load calculations. Under such everyday conditions, tension limits are specified to limit aeolian vibration to safe levels. Even with everyday lower tension levels of 15 to 20%, it is assumed that vibration control devices will be used in those sections of the line that are subject to severe vibration. Aeolian vibration levels, and thus appropriate unloaded tension limits, vary with the type of conductor, the terrain, span length, and the use of dampers. Special conductors, such as ACSS, SDC, and VR, exhibit high self-damping properties and may be installed to the full code limits, if desired.

14.2 Approximate Sag-Tension Calculations

Sag-tension calculations, using exacting equations, are usually performed with the aid of a computer; however, with certain simplifications, these calculations can be made with a handheld calculator. The latter approach allows greater insight into the calculation of sags and tensions than is possible with complex computer programs. Equations suitable for such calculations, as presented in the preceding section, can be applied to the following example:

It is desired to calculate the sag and slack for a 600-ft level span of 795 kcmil-26/7 ACSR "Drake" conductor. The bare conductor weight per unit length, w_b, is 1.094 lb/ft. The conductor is installed with a horizontal tension component, H, of 6300 lb, equal to 20% of its rated breaking strength of 31,500 lb.

By use of Eq. (14.2), the sag for this level span is:

$$D = \frac{1.094(600^2)}{(8)6300} = 7.81 \text{ ft } (2.38 \text{ m})$$

The length of the conductor between the support points is determined using Eq. (14.6):

$$L = 600 + \frac{8(7.81)^2}{3(600)} = 600.27 \text{ ft } (182.96 \text{ m})$$

Note that the conductor length depends solely on span and sag. It is not directly dependent on conductor tension, weight, or temperature. The conductor slack is the conductor length minus the span length; in this example, it is 0.27 ft (0.0826 m).

14.2.1 Sag Change with Thermal Elongation

ACSR and AAC conductors elongate with increasing conductor temperature. The rate of linear thermal expansion for the composite ACSR conductor is less than that of the AAC conductor because the steel strands in the ACSR elongate at approximately half the rate of aluminum. The effective linear thermal expansion coefficient of a non-homogenous conductor, such as Drake ACSR, may be found from the following equations (Fink and Beatty):

$$E_{AS} = E_{AL}\left(\frac{A_{AL}}{A_{TOTAL}}\right) + E_{ST}\left(\frac{A_{ST}}{A_{TOTAL}}\right) \tag{14.22}$$

$$\alpha_{AS} = \alpha_{AL}\left(\frac{E_{AL}}{E_{AS}}\right)\left(\frac{A_{AL}}{A_{TOTAL}}\right) + \alpha_{ST}\left(\frac{E_{ST}}{E_{AS}}\right)\left(\frac{A_{ST}}{A_{TOTAL}}\right) \tag{14.23}$$

where E_{AL} = Elastic modulus of aluminum, psi
E_{ST} = Elastic modulus of steel, psi
E_{AS} = Elastic modulus of aluminum-steel composite, psi
A_{AL} = Area of aluminum strands, square units
A_{ST} = Area of steel strands, square units
A_{TOTAL} = Total cross-sectional area, square units
α_{AL} = Aluminum coefficient of linear thermal expansion, per °F
α_{ST} = Steel coefficient of thermal elongation, per °F
α_{AS} = Composite aluminum-steel coefficient of thermal elongation, per °F

The elastic moduli for solid aluminum wire is 10 million psi and for steel wire is 30 million psi. The elastic moduli for stranded wire is reduced. The modulus for stranded aluminum is assumed to be 8.6 million psi for all strandings. The moduli for the steel core of ACSR conductors varies with stranding as follows:

- 27.5×10^6 for single-strand core
- 27.0×10^6 for 7-strand core
- 26.5×10^6 for 19-strand core

Using elastic moduli of 8.6 and 27.0 million psi for aluminum and steel, respectively, the elastic modulus for Drake ACSR is:

$$E_{AS} = (8.6 \times 10^6)\left(\frac{0.6247}{0.7264}\right) + (27.0 \times 10^6)\left(\frac{0.1017}{0.7264}\right) = 11.2 \times 10^6 \text{ psi}$$

and the coefficient of linear thermal expansion is:

$$\begin{aligned}\alpha_{AS} &= 12.8 \times 10^{-6}\left(\frac{8.6 \times 10^6}{11.2 \times 10^6}\right)\left(\frac{0.6247}{0.7264}\right) + 6.4 \times 10^{-6}\left(\frac{27.0 \times 10^6}{11.2 \times 10^6}\right)\left(\frac{0.1017}{0.7264}\right) \\ &= 10.6 \times 10^{-6}/^\circ\text{F}\end{aligned}$$

If the conductor temperature changes from a reference temperature, T_{REF}, to another temperature, T, the conductor length, L, changes in proportion to the product of the conductor's effective thermal elongation coefficient, α_{AS}, and the change in temperature, $T - T_{REF}$, as shown below:

$$L_T = L_{T_{REF}}(1 + \alpha_{AS}(T - T_{REF})) \tag{14.24}$$

For example, if the temperature of the Drake conductor in the preceding example increases from 60°F (15°C) to 167°F (75°C), then the length at 60°F increases by 0.68 ft (0.21 m) from 600.27 ft (182.96 m) to 600.95 ft (183.17 m):

$$L_{(167^\circ F)} = 600.27(1 + (10.6 \times 10^{-6})(167 - 60)) = 600.95 \text{ ft}$$

Ignoring for the moment any change in length due to change in tension, the sag at 167°F (75°C) may be calculated for the conductor length of 600.95 ft (183.17 m) using Eq. (14.8):

$$D = \sqrt{\frac{3(600)(0.95)}{8}} = 14.62 \text{ ft}$$

Using a rearrangement of Eq. (14.2), this increased sag is found to correspond to a decreased tension of:

$$H = \frac{w(S^2)}{8D} = \frac{1.094(600^2)}{8(14.62)} = 3367 \text{ lb}$$

If the conductor were inextensible, that is, if it had an infinite modulus of elasticity, then these values of sag and tension for a conductor temperature of 167°F would be correct. For any real conductor, however, the elastic modulus of the conductor is finite and changes in tension do change the conductor length. Use of the preceding calculation, therefore, will overstate the increase in sag.

14.2.2 Sag Change Due to Combined Thermal and Elastic Effects

With moduli of elasticity around the 8.6 million psi level, typical bare aluminum and ACSR conductors elongate about 0.01% for every 1000 psi change in tension. In the preceding example, the increase in temperature caused an increase in length and sag and a decrease in tension, but the effect of tension change on length was ignored.

As discussed later, concentric-lay stranded conductors, particularly non-homogenous conductors such as ACSR, are not inextensible. Rather, they exhibit quite complex elastic and plastic behavior. Initial loading of conductors results in elongation behavior substantially different from that caused by loading many years later. Also, high tension levels caused by heavy ice and wind loads cause a permanent increase in conductor length, affecting subsequent elongation under various conditions.

Accounting for such complex stress-strain behavior usually requires a sophisticated, computer-aided approach. For illustration purposes, however, the effect of permanent elongation of the conductor on sag and tension calculations will be ignored and a simplified elastic conductor assumed. This idealized conductor is assumed to elongate linearly with load and to undergo no permanent increase in length regardless of loading or temperature. For such a conductor, the relationship between tension and length is as follows:

$$L_H = L_{H_{REF}}\left(1 + \frac{H - H_{REF}}{E_C A}\right) \tag{14.25}$$

where L_H = Length of conductor under horizontal tension H
$L_{H_{REF}}$ = Length of conductor under horizontal reference tension H_{REF}
E_C = Elastic modulus of elasticity of the conductor, psi
A = Cross-sectional area, in.^{2}

In calculating sag and tension for extensible conductors, it is useful to add a step to the preceding calculation of sag and tension for elevated temperature. This added step allows a separation of thermal elongation and elastic elongation effects, and involves the calculation of a zero tension length, ZTL, at the conductor temperature of interest, T_{cdr}.

This ZTL(T_{cdr}) is the conductor length attained if the conductor is taken down from its supports and laid on the ground with no tension. By reducing the initial tension in the conductor to zero, the elastic elongation is also reduced to zero, shortening the conductor. It is possible, then, for the zero tension length to be less than the span length.

Consider the preceding example for Drake ACSR in a 600-ft level span. The initial conductor temperature is 60°F, the conductor length is 600.27 ft, and E_{AS} is calculated to be 11.2 million psi. Using Eq. (14.25), the reduction of the initial tension from 6300 lb to zero yields a ZTL (60°F) of:

$$ZTL_{(60^\circ F)} = 600.27\left(1 + \frac{0 - 6300}{(11.2 \times 10^6)0.7264}\right) = 599.81 \text{ ft}$$

Keeping the tension at zero and increasing the conductor temperature to 167°F yields a purely thermal elongation. The zero tension length at 167°F can be calculated using Eq. (14.24):

$$ZTL_{(167^\circ F)} = 599.81\left(1 + \left(10.6 \times 10^{-6}\right)\left(167 - 60\right)\right) = 600.49 \text{ ft}$$

According to Eqs. (14.2) and (14.8), this length corresponds to a sag of 10.5 ft and a horizontal tension of 4689 lb. However, this length was calculated for zero tension and will elongate elastically under tension. The actual conductor sag-tension determination requires a process of iteration as follows:

1. As described above, the conductor's zero tension length, calculated at 167°F (75°C), is 600.49 ft, sag is 10.5 ft, and the horizontal tension is 4689 lb.
2. Because the conductor is elastic, application of Eq. (14.25) shows the tension of 4689 lb will increase the conductor length from 600.49 ft to:

$$L_{l_{(167^\circ F)}} = 600.49\left(1 + \frac{4689 - 0}{0.7264(11.2 \times 10^6)}\right) = 600.84 \text{ ft}$$

3. The sag, $D_{1_{(167^\circ F)}}$, corresponding to this length is calculated using Eq. (14.8):

$$D_{l_{(167^\circ F)}} = \sqrt{\frac{3(600)(0.84)}{8}} = 13.72 \text{ ft}$$

4. Using Eq. (14.2), this sag yields a new horizontal tension, $H_{1_{(167^\circ F)}}$, of:

$$H_1 = \frac{1.094(600^2)}{8(13.7)} = 3588 \text{ lb}$$

A new trial tension is taken as the average of H and H_1, and the process is repeated. The results are described in Table 14.3.

TABLE 14.3 Interative Solution for Increased Conductor Temperature

Iteration #	Length, L_n, ft	Sag, D_n, ft	Tension, H_n, lb	New Trial Tension, lb
ZTL	600.550	11.1	4435	—
1	600.836	13.7	3593	$\frac{4435 + 3593}{2} = 4014$
2	600.809	13.5	3647	$\frac{3647 + 4014}{2} = 3831$
3	600.797	13.4	3674	$\frac{3674 + 3831}{2} = 3753$
4	600.792	13.3	3702	$\frac{3702 + 3753}{2} = 3727$

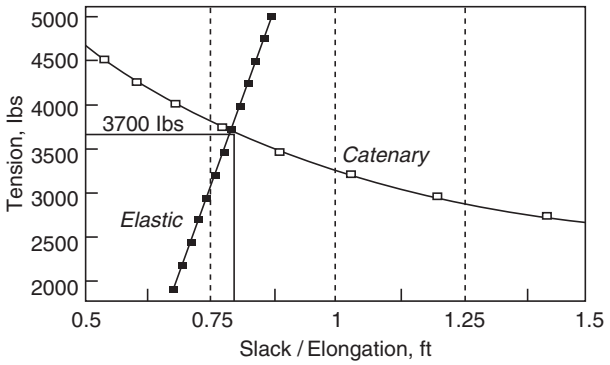

FIGURE 14.5 Sag-tension solution for 600-ft span of Drake at 167°F.

Note that the balance of thermal and elastic elongation of the conductor yields an equilibrium tension of approximately 3700 lbs and a sag of 13.3 ft. The calculations of the previous section, which ignored elastic effects, results in lower tension, 3440 lb, and a greater sag, 14.7 ft.

Slack is equal to the excess of conductor length over span length. The preceding table can be replaced by a plot of the catenary and elastic curves on a graph of slack vs tension. The solution occurs at the intersection of the two curves. Figure 14.5 shows the tension versus slack curves intersecting at a tension of 3700 lb, which agrees with the preceding calculations.

14.2.3 Sag Change Due to Ice Loading

As a final example of sag-tension calculation, calculate the sag and tension for the 600-ft Drake span with the addition of 0.5 inches of radial ice and a drop in conductor temperature to 0°F. Employing Eq. (14.17), the weight of the conductor increases by:

$$w_{ice} = 1.244t(D + t)$$

$$w_{ice} = 1.244(0.5)(1.108 + 0.5) = 1.000 \text{ lb/ft}$$

As in the previous example, the calculation uses the conductor's zero tension length at 60°F, which is the same as that found in the previous section, 599.81 ft. The ice loading is specified for a conductor temperature of 0°F, so the ZTL(0°F), using Eq. (14.24), is:

$$ZTL_{(0°F)} = 599.81[1 + (10.6 \times 10^{-6})(0 - 60)] = 599.43\text{ft}$$

As in the case of sag-tension at elevated temperatures, the conductor tension is a function of slack and elastic elongation. The conductor tension and the conductor length are found at the point of intersection of the catenary and elastic curves (Fig. 14.6). The intersection of the curves occurs at a horizontal tension component of 12,275 lb, not very far from the crude initial estimate of 12,050 lb that ignored elastic effects. The sag corresponding to this tension and the iced conductor weight per unit length is 9.2 ft.

In spite of doubling the conductor weight per unit length by adding 0.5 in. of ice, the sag of the conductor is much less than the sag at 167°F. This condition is generally true for transmission conductors where minimum ground clearance is determined by the high temperature rather than the heavy loading condition. Small distribution conductors, such as the 1/0 AWG ACSR in Table 14.1, experience a much larger ice-to-conductor weight ratio (4.8), and the conductor sag under maximum wind and ice load may exceed the sag at moderately higher temperatures.

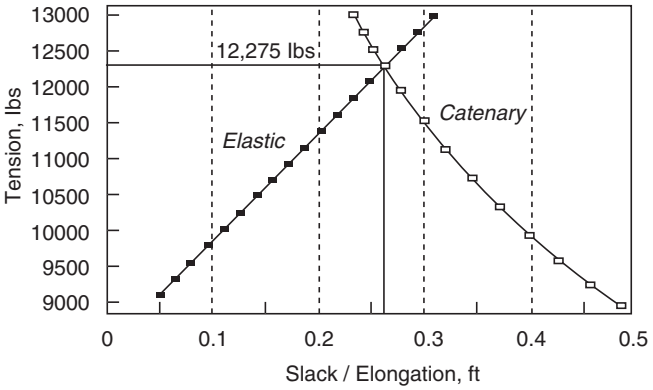

FIGURE 14.6 Sag-tension solution for 600-ft span of Drake at 0°F and 0.5 in. ice.

The preceding approximate tension calculations could have been more accurate with the use of actual stress-strain curves and graphic sag-tension solutions, as described in detail in *Graphic Method for Sag Tension Calculations for ACSR and Other Conductors* (Aluminum Company of America, 1961). This method, although accurate, is very slow and has been replaced completely by computational methods.

14.3 Numerical Sag-Tension Calculations

Sag-tension calculations are normally done numerically and allow the user to enter many different loading and conductor temperature conditions. Both initial and final conditions are calculated and multiple tension constraints can be specified. The complex stress-strain behavior of ACSR-type conductors can be modeled numerically, including both temperature, and elastic and plastic effects.

14.3.1 Stress-Strain Curves

Stress-strain curves for bare overhead conductor include a minimum of an initial curve and a final curve over a range of elongations from 0 to 0.45%. For conductors consisting of two materials, an initial and final curve for each is included. Creep curves for various lengths of time are typically included as well.

Overhead conductors are not purely elastic. They stretch with tension, but when the tension is reduced to zero, they do not return to their initial length. That is, conductors are plastic; the change in conductor length cannot be expressed with a simple linear equation, as for the preceding hand calculations. The permanent length increase that occurs in overhead conductors yields the difference in initial and final sag-tension data found in most computer programs.

Figure 14.7 shows a typical stress-strain curve for a 26/7 ACSR conductor (Aluminum Association, 1974); the curve is valid for conductor sizes ranging from 266.8 to 795 kcmil. A 795 kcmil-26/7 ACSR "Drake" conductor has a breaking strength of 31,500 lb (14,000 kg) and an area of 0.7264 in.^{2} (46.9 mm^2) so that it fails at an average stress of 43,000 psi (30 kg/mm^2). The stress-strain curve illustrates that when the percent of elongation at a stress is equal to 50% of the conductor's breaking strength (21,500 psi), the elongation is less than 0.3% or 1.8 ft (0.55 m) in a 600-ft (180 m) span.

Note that the component curves for the steel core and the aluminum stranded outer layers are separated. This separation allows for changes in the relative curve locations as the temperature of the conductor changes.

For the preceding example, with the Drake conductor at a tension of 6300 lb (2860 kg), the length of the conductor in the 600-ft (180 m) span was found to be 0.27 ft longer than the span. This tension corresponds to a stress of 8600 psi (6.05 kg/mm^2). From the stress-strain curve in Fig. 14.7, this corresponds to an initial elongation of 0.105% (0.63 ft). As in the preceding hand calculation, if the conductor is reduced to zero tension, its unstressed length would be less than the span length.

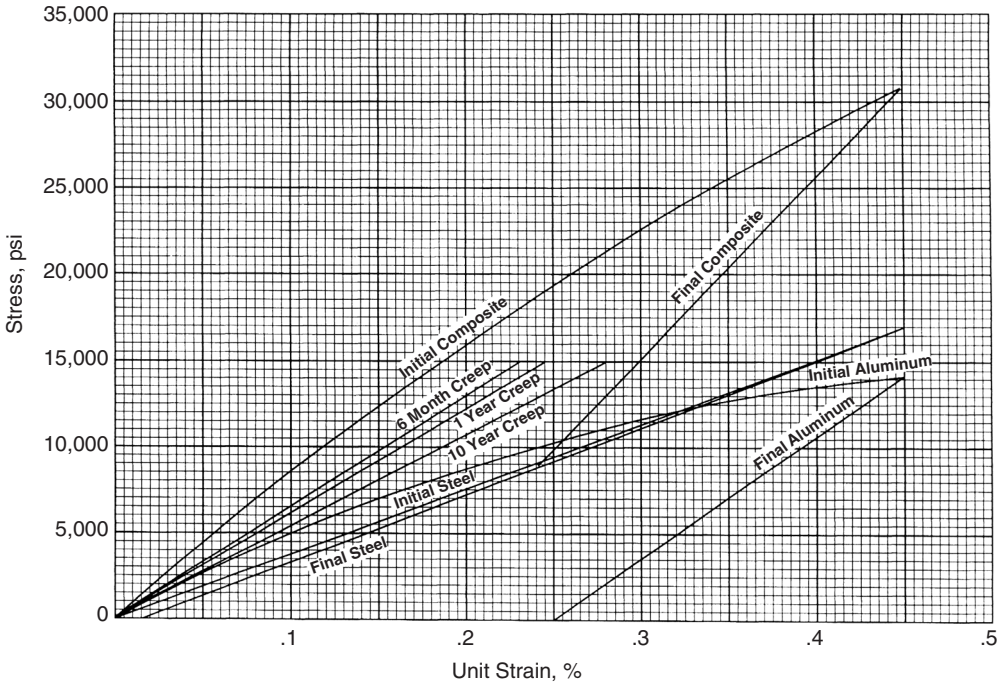

Equations for Curves (X = unit strain in %; Y = stress in psi) :

Initial composite: $X = 4.07 \times 10^{-3} + (1.28 \times 10^{-5})\ Y - (1.18 \times 10^{-10})\ Y^2 + (5.64 \times 10^{-15})\ Y^3$
$Y = -512 + (8.617 \times 10^{4})\ X - (1.18 \times 10^{4})\ X^2 - (5.76 \times 10^{-4})\ X^3$

Initial Steel: $Y = (37.15 \times 10^{3})\ X$

Initial Aluminum: $Y = -512 = (4.902 \times 10^{4})\ X - (1.18 \times 10^{4})\ X^2 - (5.76 \times 10^{4})\ X^3$

Final Composite: $Y = (107.55\ X - 17.65) \times 10^{3}$

Final Steel: $Y = (38.60\ X - 0.65) \times 10^{3}$

Final Aluminum: $Y = (68.95\ X - 17.00) \times 10^{3}$

6 Month Creep: $Y = (68.75 \times 10^{3})\ X$

1 Year Creep: $Y = (60.60 \times 10^{3})\ X$

10 Year Creep: $Y = (53.45 \times 10^{3})\ X$

Test Temperature 70°F to 75°F

FIGURE 14.7 Stress-strain curves for 26/7 ACSR.

Figure 14.8 is a stress-strain curve (Aluminum Association, 1974) for an all-aluminum 37-strand conductor ranging in size from 250 kcmil to 1033.5 kcmil. Because the conductor is made entirely of aluminum, there is only one initial and final curve.

14.3.1.1 Permanent Elongation

Once a conductor has been installed at an initial tension, it can elongate further. Such elongation results from two phenomena: permanent elongation due to high tension levels resulting from ice and wind loads, and creep elongation under everyday tension levels. These types of conductor elongation are discussed in the following sections.

14.3.1.2 Permanent Elongation Due to Heavy Loading

Both Figs. 14.7 and 14.8 indicate that when the conductor is initially installed, it elongates following the initial curve that is not a straight line. If the conductor tension increases to a relatively high level under ice and wind loading, the conductor will elongate. When the wind and ice loads abate, the conductor

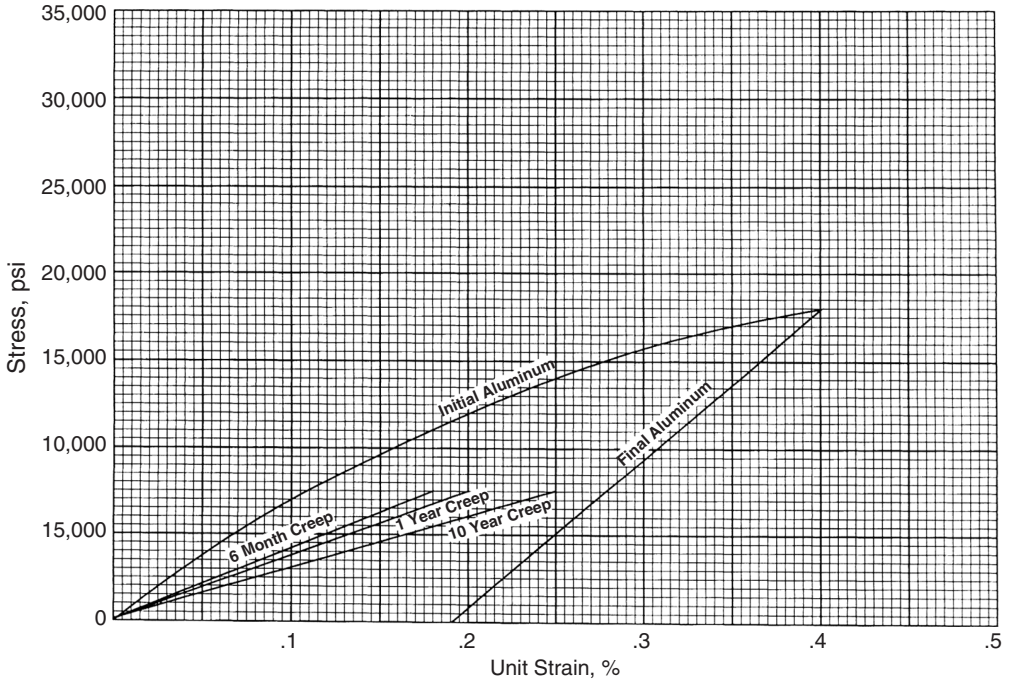

Equations for Curves (X = unit strain in %; Y = stress in psi):

Initial Aluminum: $X = -5.31 \times 10^{-3} + (1.74 \times 10^{-5})\,Y - (6.17 \times 10^{-10})\,Y^2 + (5.05 \times 10^{-14})\,Y^3$

$Y = 136 + (7.46 \times 10^4)\,X - (8.51 \times 10^4)\,X^2 + (2.33 \times 10^4)\,X^3$

Final Aluminum: $Y = (85.20\,X - 16.14) \times 10^3$

6 Month Creep: $Y = (42.30 \times 10^3)\,X$

1 Year Creep: $Y = (38.20 \times 10^3)\,X$

10 Year Creep: $Y = (30.60 \times 10^3)\,X$

Test Temperature 70°F to 75°F

FIGURE 14.8 Stress-strain curves for 37-strand AAC.

elongation will reduce along a curve parallel to the final curve, but the conductor will never return to its original length.

For example, refer to Fig. 14.8 and assume that a newly strung 795 kcmil-37 strand AAC "Arbutus" conductor has an everyday tension of 2780 lb. The conductor area is 0.6245 in.^{2}, so the everyday stress is 4450 psi and the elongation is 0.062%. Following an extremely heavy ice and wind load event, assume that the conductor stress reaches 18,000 psi. When the conductor tension decreases back to everyday levels, the conductor elongation will be permanently increased by more than 0.2%. Also the sag under everyday conditions will be correspondingly higher, and the tension will be less. In most numerical sag-tension methods, final sag-tensions are calculated for such permanent elongation due to heavy loading conditions.

14.3.1.3 Permanent Elongation at Everyday Tensions (Creep Elongation)

Conductors permanently elongate under tension even if the tension level never exceeds everyday levels. This permanent elongation caused by everyday tension levels is called creep (Aluminum Company of America, 1961). Creep can be determined by long-term laboratory creep tests, the results of which are used to generate creep curves. On stress-strain graphs, creep curves are usually shown for 6-mo, 1-yr, and 10-yr periods. Figure 14.8 shows these typical creep curves for a 37 strand 250.0 through 1033.5 kcmil AAC. In Fig. 14.8 assume that the conductor tension remains constant at the initial stress of 4450 psi. At the intersection of this stress level and the initial elongation curve, 6-month, 1-year, and 10-year creep

curves, the conductor elongation from the initial elongation of 0.062% increases to 0.11%, 0.12%, and 0.15%, respectively. Because of creep elongation, the resulting final sags are greater and the conductor tension is less than the initial values.

Creep elongation in aluminum conductors is quite predictable as a function of time and obeys a simple exponential relationship. Thus, the permanent elongation due to creep at everyday tension can be found for any period of time after initial installation. Creep elongation of copper and steel conductors is much less and is normally ignored.

Permanent increase in conductor length due to heavy load occurrences cannot be predicted at the time that a line is built. The reason for this unpredictability is that the occurrence of heavy ice and wind is random. A heavy ice storm may occur the day after the line is built or may never occur over the life of the line.

14.3.2 Sag-Tension Tables

To illustrate the result of typical sag-tension calculations, refer to Tables 14.4 through 14.9 showing initial and final sag-tension data for 795 kcmil-26/7 ACSR "Drake", 795 kcmil-37 strand AAC "Arbutus", and 795-kcmil Type 16 "Drake/SDC" conductors in NESC light and heavy loading areas for spans of

TABLE 14.4 Sag and Tension Data for 795 kcmil-26/7 ACSR "Drake" Conductor

Creep is ***not*** a factor				**Span = 600 ft** *NESC Heavy Loading District*				
					Final		Initial	
Temp, °F	Ice, in.	Wind, lb/ft^2	K, lb/ft	Resultant Weight, lb/ft	Sag, ft	Tension, lb	Sag, ft	Tension, lb
0	0.50	4.00	0.30	2.509	11.14	10153	11.14	10153
						5415 Al		5415 Al
						4738 St		4738 St
32	0.50	0.00	0.00	2.094	44.54	8185	11.09	8512
						3819 Al		4343 Al
						4366 St		4169 St
−20	0.00	0.00	0.00	1.094	6.68	7372	6.27	7855
						3871 Al		4465 Al
						3501 St		3390 St
0	0.00	0.00	0.00	1.094	7.56	6517	6.89	7147
						3111 Al		3942 Al
						3406 St		3205 St
30	0.00	0.00	0.00	1.094	8.98	5490	7.95	6197
						2133 Al		3201 Al
						3357 St		2996 St
60	0.00	0.00	0.00	1.094	10.44	4725[a]	9.12	5402
						1321 Al		2526 Al
						3404 St		2875 St
90	0.00	0.00	0.00	1.094	11.87	4157	10.36	4759
						634 Al		1922 Al
						3522 St		2837 St
120	0.00	0.00	0.00	1.094	13.24	3727	11.61	4248
						35 Al		1379 Al
						3692 St		2869 St
167	0.00	0.00	0.00	1.094	14.29	3456	13.53	3649
						0 Al		626 Al
						3456 St		3022 St
212	0.00	0.00	0.00	1.094	15.24	3241	15.24	3241
						0 Al		0 Al
						3241 St		3239 St

[a]Design condition.

TABLE 14.5 Tension Differences in Adjacent Dead-End Spans

Conductor: Drake
795 kcmil-26/7 ACSR
Area = 0.7264 in.^{2}
Creep ***is*** a factor

Span = 700 ft

NESC Heavy Loading District

					Final		Initial	
Temp, °F	Ice, in.	Wind, lb/ft^2	K, lb/ft	Resultant Weight, lb/ft	Sag, ft	Tension, lb	Sag, ft	Tension, lb
0	0.50	4.00	0.30	2.509	13.61	11318	13.55	11361
32	0.50	0.00	0.00	2.094	13.93	9224	13.33	9643
−20	0.00	0.00	0.00	1.094	8.22	8161	7.60	8824
0	0.00	0.00	0.00	1.094	9.19	7301	8.26	8115
30	0.00	0.00	0.00	1.094	10.75	6242	9.39	7142
60	0.00	0.00	0.00	1.094	12.36	5429	10.65	6300[a]
90	0.00	0.00	0.00	1.094	13.96	4809	11.99	5596
120	0.00	0.00	0.00	1.094	15.52	4330	13.37	5020
167	0.00	0.00	0.00	1.094	16.97	3960	15.53	4326
212	0.00	0.00	0.00	1.094	18.04	3728	17.52	3837

[a]Design condition.

Conductor: Drake
795 kcmil-26/7 ACSR
Area = 0.7264 in.^{2}
Creep is ***not*** a factor

Span = 1000 ft

NESC Heavy Loading District

					Final		Initial	
Temp, °F	Ice, in.	Wind, lb/ft^2	K, lb/ft	Resultant Weight, lb/ft	Sag, ft	Tension, lb	Sag, ft	Tension, lb
0	0.50	4.00	0.30	2.509	25.98	12116	25.98	12116
32	0.50	0.00	0.00	2.094	26.30	9990	25.53	10290
−20	0.00	0.00	0.00	1.094	18.72	7318	17.25	7940
0	0.00	0.00	0.00	1.094	20.09	6821	18.34	7469
30	0.00	0.00	0.00	1.094	22.13	6197	20.04	6840
60	0.00	0.00	0.00	1.094	24.11	5689	21.76	6300[a]
90	0.00	0.00	0.00	1.094	26.04	5271	23.49	5839
120	0.00	0.00	0.00	1.094	27.89	4923	25.20	5444
167	0.00	0.00	0.00	1.094	30.14	4559	27.82	4935
212	0.00	0.00	0.00	1.094	31.47	4369	30.24	4544

[a]Design condition.

1000 and 300 ft. Typical tension constraints of 15% final unloaded at 60°F, 25% initial unloaded at 60°F, and 60% initial at maximum loading are used.

With most sag-tension calculation methods, final sags are calculated for both heavy ice/wind load and for creep elongation. The final sag-tension values reported to the user are those with the greatest increase in sag.

14.3.2.1 Initial vs. Final Sags and Tensions

Rather than calculate the line sag as a function of time, most sag-tension calculations are determined based on initial and final loading conditions. Initial sags and tensions are simply the sags and tensions at the time the line is built. Final sags and tensions are calculated if (1) the specified ice and wind loading has occurred, and (2) the conductor has experienced 10 years of creep elongation at a conductor temperature of 60°F at the user-specified initial tension.

TABLE 14.6 Sag and Tension Data for 795 kcmil-26/7 ACSR "Drake" 600-ft Ruling Span

Conductor: Drake
795 kcmil-26/7 ACSR
Area = 0.7264 in.^{2}
Creep is ***not*** a factor

Span = 600 ft

NESC Heavy Loading District

					Final		Initial	
Temp, °F	Ice, in.	Wind, lb/ft^2	K, lb/ft	Resultant Weight, lb/ft	Sag, ft	Tension, lb	Sag, ft	Tension, lb
0	0.50	4.00	0.30	2.509	11.14	10153	11.14	10153
32	0.50	0.00	0.00	2.094	11.54	8185	11.09	8512
−20	0.00	0.00	0.00	1.094	6.68	7372	6.27	7855
0	0.00	0.00	0.00	1.094	7.56	6517	6.89	7147
30	0.00	0.00	0.00	1.094	8.98	5490	7.95	6197
60	0.00	0.00	0.00	1.094	10.44	4725[a]	9.12	5402
90	0.00	0.00	0.00	1.094	11.87	4157	10.36	4759
120	0.00	0.00	0.00	1.094	13.24	3727	11.61	4248
167	0.00	0.00	0.00	1.094	14.29	3456	13.53	3649
212	0.00	0.00	0.00	1.094	15.24	3241	15.24	3241

[a] Design condition.

TABLE 14.7 Stringing Sag Table for 795 kcmil-26/7 ACSR "Drake" 600-ft Ruling Span

600-ft Ruling Span

Controlling Design Condition:
15% RBS at 60°F, No Ice or Wind, Final

NESC Heavy Load District

Horizontal	6493	6193	5910	5645	5397	5166	4952	4753	4569
Tension, lb	20	30	40	50	60	70	80	90	100
Temp, °F Spans	Sag, ft-in.	Sag, ft-in.	Sag, ft-in.	Sag, ft-in.	Sag, ft-in.	Sag, ft-in.	Sag, ft-in.	Sag, ft-in.	Sag, ft-in.
400	3 - 4	3 - 6	3 - 8	3 - 11	4 - 1	4 - 3	4 - 5	4 - 7	4 - 9
410	3 - 6	3 - 9	3 - 11	4 - 1	4 - 3	4 - 5	4 - 8	4 - 10	5 - 0
420	3 - 9	3 - 11	4 - 1	4 - 3	4 - 6	4 - 8	4 - 10	5 - 1	5 - 3
430	3 - 11	4 - 1	4 - 3	4 - 6	4 - 8	4 - 11	5 - 1	5 - 4	5 - 6
440	4 - 1	4 - 3	4 - 6	4 - 8	4 - 11	5 - 2	5 - 4	5 - 7	5 - 10
450	4 - 3	4 - 6	4 - 8	4 - 11	5 - 2	5 - 4	5 - 7	5 - 10	6 - 1
460	4 - 5	4 - 8	4 - 11	5 - 2	5 - 4	5 - 7	5 - 10	6 - 1	6 - 4
470	4 - 8	4 - 11	5 - 1	5 - 4	5 - 7	5 - 10	6 - 1	6 - 4	6 - 7
480	4 - 10	5 - 1	5 - 4	5 - 7	5 - 10	6 - 1	6 - 4	6 - 8	6 - 11
490	5 - 1	5 - 4	5 - 7	5 - 10	6 - 1	6 - 4	6 - 8	6 - 11	7 - 2
500	5 - 3	5 - 6	5 - 9	6 - 1	6 - 4	6 - 7	6 - 11	7 - 2	7 - 6
510	5 - 6	5 - 9	6 - 0	6 - 4	6 - 7	6 - 11	7 - 2	7 - 6	7 - 9
520	5 - 8	6 - 0	6 - 3	6 - 7	6 - 10	7 - 2	7 - 6	7 - 9	8 - 1
530	5 - 11	6 - 2	6 - 6	6 - 10	7 - 1	7 - 5	7 - 9	8 - 1	8 - 5
540	6 - 2	6 - 5	6 - 9	7 - 1	7 - 5	7 - 9	8 - 1	8 - 5	8 - 9
550	6 - 4	6 - 8	7 - 0	7 - 4	7 - 8	8 - 0	8 - 4	8 - 8	9 - 1
560	6 - 7	6 - 11	7 - 3	7 - 7	7 - 11	8 - 4	8 - 8	9 - 0	9 - 5
570	6 - 10	7 - 2	7 - 6	7 - 10	8 - 3	8 - 7	9 - 0	9 - 4	9 - 9
580	7 - 1	7 - 5	7 - 9	8 - 2	8 - 6	8 - 11	9 - 4	9 - 8	10 - 1
590	7 - 4	7 - 8	8 - 1	8 - 5	8 - 10	9 - 3	9 - 7	10 - 0	10 - 5
600	7 - 7	7 - 11	8 - 4	8 - 9	9 - 1	9 - 6	9 - 11	10 - 4	10 - 9
610	7 - 1	8 - 3	8 - 7	9 - 0	9 - 5	9 - 10	10 - 3	10 - 9	11 - 2
620	8 - 1	8 - 6	8 - 11	9 - 4	9 - 9	10 - 2	10 - 7	11 - 1	11 - 6
630	8 -	8 - 9	9 - 2	9 - 7	10 - 1	10 - 6	11 - 0	11 - 5	11 - 11
640	8 - 8	9 - 1	9 - 6	9 - 11	10 - 5	10 - 10	11 - 4	11 - 9	12 - 3
650	8 - 11	9 - 4	9 - 9	10 - 3	10 - 9	11 - 2	11 - 8	12 - 2	12 - 8
660	9 - 2	9 - 7	10 - 1	10 - 7	11 - 1	11 - 6	12 - 0	12 - 6	13 - 1
670	9 - 5	9 - 11	10 - 5	10 - 11	11 - 5	11 - 11	12 - 5	12 - 11	13 - 5
680	9 - 9	10 - 3	10 - 8	11 - 2	11 - 9	12 - 3	12 - 9	13 - 4	13 - 10
690	10 - 0	10 - 6	11 - 0	11 - 6	12 - 1	12 - 7	13 - 2	13 - 8	14 - 3
700	10 - 4	10 - 10	11 - 4	11 - 11	12 - 5	13 - 0	13 - 6	14 - 1	14 - 8

TABLE 14.8 Time-Sag Table for Stopwatch Method

Return of Wave											
Sag, in.	3rd Time, sec	5th Time, sec	Sag, in.	3rd Time, sec	5th Time, sec	Sag, in.	3rd Time, sec	5th Time, sec	Sag, in.	3rd Time, sec	5th Time, sec
5	1.9	3.2	55	6.4	10.7	105	8.8	14.7	155	10.7	17.9
6	2.1	3.5	56	6.5	10.8	106	8.9	14.8	156	10.8	18.0
7	2.3	3.8	57	6.5	10.9	107	8.9	14.9	157	10.8	18.0
8	2.4	4.1	58	6.6	11.1	109	9.0	15.0	158	10.9	18.1
9	2.6	4.3	59	6.6	11.1	109	9.0	15.0	159	10.9	18.1
10	2.7	4.6	60	6.7	11.1	110	9.1	15.1	160	10.9	18.2
11	2.9	4.8	61	6.7	11.2	111	9.1	15.2	161	11.0	18.2
12	3.0	5.0	62	6.8	11.3	112	9.1	15.2	162	11.0	18.2
13	3.1	5.2	63	6.9	11.4	113	9.2	15.3	163	11.0	18.4
14	3.2	5.4	64	6.9	11.5	114	9.2	15.4	164	11.1	18.4
15	3.3	5.6	65	7.0	11.6	115	9.3	15.4	165	11.1	18.5
16	3.5	5.8	66	7.0	11.7	116	9.3	15.5	166	11.1	18.5
17	3.6	5.9	67	7.1	11.8	117	9.3	15.6	167	11.2	18.6
18	3.7	6.1	68	7.1	11.9	118	9.4	15.6	168	11.2	18.7
19	3.8	6.3	69	7.2	12.0	119	9.4	15.7	169	11.2	18.7
20	3.9	6.4	70	7.2	12.0	120	9.5	15.8	170	11.3	18.8
21	4.0	6.6	71	7.3	12.1	121	9.5	15.8	171	11.3	18.8
22	4.0	6.7	72	7.3	12.2	122	9.5	15.9	172	11.3	18.9
23	4.1	6.9	73	7.4	12.3	123	9.6	16.0	173	11.4	18.9
24	4.2	7.0	74	7.4	12.4	124	9.6	16.0	174	11.4	19.0
25	4.3	7.2	75	7.5	12.5	125	9.7	16.1	175	11.4	19.0
26	4.4	7.3	76	7.5	12.5	126	9.7	16.2	176	11.4	19.1
27	4.5	7.5	77	7.6	12.6	127	9.7	16.2	177	11.5	19.1
28	4.6	7.6	78	7.6	12.7	128	9.8	16.3	178	11.5	19.2
29	4.6	7.7	79	7.7	12.8	129	9.8	16.3	179	11.5	19.3
30	4.7	7.9	80	7.7	12.9	130	9.8	16.4	180	11.6	19.3
31	4.8	8.0	81	7.8	13.0	131	9.9	16.5	181	11.6	19.4
32	4.9	8.1	82	7.8	13.0	132	9.9	16.5	182	11.6	19.4
33	5.0	8.3	83	7.9	13.1	133	10.0	16.6	183	11.7	19.5
34	5.0	8.4	84	7.9	13.2	134	10.0	16.7	184	11.7	19.5
35	5.1	8.5	85	8.0	13.3	135	10.0	16.7	185	11.7	19.6
36	5.2	8.6	86	8.0	13.3	136	10.1	16.8	186	11.8	19.6
37	5.3	8.8	87	8.1	13.4	137	10.1	16.8	187	11.8	19.7
38	5.3	8.9	88	8.1	13.5	138	10.1	16.9	188	11.8	19.7
39	5.4	9.0	89	8.1	13.6	139	10.2	17.0	189	11.9	19.8
40	5.5	9.1	90	8.2	13.7	140	10.2	17.0	190	11.9	19.8
41	5.5	9.2	91	8.2	13.7	141	10.3	17.1	191	11.9	19.9
42	5.6	9.3	92	8.3	13.8	142	10.3	17.1	192	12.0	19.9
43	5.7	9.4	93	8.3	13.9	143	10.3	17.2	193	12.0	20.0
44	5.7	9.5	94	8.4	14.0	144	10.4	17.3	194	12.0	20.0
45	5.8	9.7	95	8.4	14.0	145	10.4	17.3	195	12.1	20.1
46	5.9	9.8	96	8.5	14.1	146	10.4	17.4	196	12.1	20.1
47	5.9	9.9	97	8.5	14.2	147	10.5	17.4	197	12.1	20.2
48	6.0	10.0	98	8.5	14.2	148	10.5	17.5	198	12.1	20.0
49	6.0	10.1	99	8.6	14.3	149	10.5	17.6	199	12.2	20.3
50	6.1	10.2	100	8.6	14.4	150	10.6	17.6	200	12.2	20.3
51	6.2	10.3	101	8.7	14.5	151	10.6	17.7	201	12.2	20.4
52	6.2	10.4	102	8.7	14.5	152	10.6	17.7	202	12.3	20.5
53	6.3	10.5	103	8.8	14.6	153	10.7	17.8	203	12.3	20.5
54	6.3	10.6	104	8.8	14.7	154	10.7	17.9	204	12.3	20.6

Note: To calculate the time of return of other waves, multiply the time in seconds for one wave return by the number of wave returns or, more simply, select the combination of values from the table that represents the number of wave returns desired. For example, the time of return of the 8th wave is the sum of the 3rd and 5th, while for the 10th wave it is twice the time of the 5^{th}.

The approximate formula giving the relationship between sag and time is given as:

$$D = 12.075\left(\frac{T}{N}\right)^2 \ (inches)$$

where $D =$ sag, in.
$T =$ time, sec
$N =$ number of return waves counted

TABLE 14.9 Typical Sag and Tension Data 795 kcmil-26/7 ACSR "Drake," 300- and 1000-ft Spans

Conductor: Drake
795 kcmil-26/7 ACSR
Area = 0.7264 in.^{2}
Creep ***is*** a factor

Span = 300 ft

NESC Heavy Loading District

Temp, °F	Ice, in.	Wind, lb/ft^2	K, lb/ft	Weight, lb/ft	Final Sag, ft	Final Tension, lb	Initial Sag, ft	Initial Tension, lb
30	0.00	9.00	0.05	1.424	2.37	6769	2.09	7664
30	0.00	0.00	0.00	1.094	1.93	6364	1.66	7404
60	0.00	0.00	0.00	1.094	2.61	4725[a]	2.04	6033
90	0.00	0.00	0.00	1.094	3.46	3556	2.57	4792
120	0.00	0.00	0.00	1.094	1.00	3077	3.25	3785
167	0.00	0.00	0.00	1.094	4.60	2678	4.49	2746
212	0.00	0.00	0.00	1.094	5.20	2371	5.20	2371

[a] Design condition.

Conductor: Drake
795 kcmil-26/7 ACSR
Area = 0.7264 in.^{2}
Creep ***is*** a factor

Span = 1000 ft

NESC Heavy Loading District

Temp, °F	Ice, in.	Wind, lb/ft^2	K, lb/ft	Weight, lb/ft	Final Sag, ft	Final Tension, lb	Initial Sag, ft	Initial Tension, lb
30	0.00	9.00	0.05	1.424	28.42	6290	27.25	6558
30	0.00	0.00	0.00	1.094	27.26	5036	25.70	5339
60	0.00	0.00	0.00	1.094	29.07	4725[a]	27.36	5018
90	0.00	0.00	0.00	1.094	30.82	4460	28.98	4740
120	0.00	0.00	0.00	1.094	32.50	4232	30.56	4498
167	0.00	0.00	0.00	1.094	34.49	3990	32.56	4175
212	0.00	0.00	0.00	1.094	35.75	3851	35.14	3917

[a] Design condition.

Note: **Calculations based on:** (1) NESC Light Loading District. (2) Tension Limits: a. Initial Loaded – 60% RBS @ 30°F; b. Initial Unloaded – 25% RBS @ 60°F; c. Final Unloaded – 15% RBS @ 60°F.

14.3.2.2 Special Aspects of ACSR Sag-Tension Calculations

Sag-tension calculations with ACSR conductors are more complex than such calculations with AAC, AAAC, or ACAR conductors. The complexity results from the different behavior of steel and aluminum strands in response to tension and temperature. Steel wires do not exhibit creep elongation or plastic elongation in response to high tensions. Aluminum wires do creep and respond plastically to high stress levels. Also, they elongate twice as much as steel wires do in response to changes in temperature.

Table 14.10 presents various initial and final sag-tension values for a 600-ft span of a Drake ACSR conductor under heavy loading conditions. Note that the tension in the aluminum and steel components is shown separately. In particular, some other useful observations are:

1. At 60°F, without ice or wind, the tension level in the aluminum strands decreases with time as the strands permanently elongate due to creep or heavy loading.
2. Both initially and finally, the tension level in the aluminum strands decreases with increasing temperature reaching zero tension at 212°F and 167°F for initial and final conditions, respectively.
3. At the highest temperature (212°F), where all the tension is in the steel core, the initial and final sag-tensions are nearly the same, illustrating that the steel core does not permanently elongate in response to time or high tension.

TABLE 14.10 Typical Sag and Tension Data 795 kcmil-26/7 ACSR "Drake," 300- and 1000-ft Spans

Conductor: Drake
795 kcmil-26/7 ACSR/SD
Area = 0.7264 in.^{2}
Creep ***is*** a factor

Span = 300 ft

NESC Heavy Loading District

					Final		Initial	
Temp, °F	Ice, in.	Wind, lb/ft^2	K, lb/ft	Weight, lb/ft	Sag, ft	Tension, lb	Sag, ft	Tension, lb
0	0.50	4.00	0.30	2.509	2.91	9695	2.88	9802
32	0.50	0.00	0.00	2.094	3.13	7528	2.88	8188
−20	0.00	0.00	0.00	1.094	1.26	9733	1.26	9756
0	0.00	0.00	0.00	1.094	1.48	8327	1.40	8818
30	0.00	0.00	0.00	1.094	1.93	6364	1.66	7404
60	0.00	0.00	0.00	1.094	2.61	4725[a]	2.04	6033
90	0.00	0.00	0.00	1.094	3.46	3556	2.57	4792
120	0.00	0.00	0.00	1.094	4.00	3077	3.25	3785
167	0.00	0.00	0.00	1.094	4.60	2678	4.49	2746
212	0.00	0.00	0.00	1.094	5.20	2371	5.20	2371

[a]Design condition.

Conductor: Drake
795 kcmil-26/7 ACSR
Area = 0.7264 in.^{2}
Creep is ***not*** a factor

Span = 1000 ft

NESC Heavy Loading District

					Final		Initial	
Temp, °F	Ice, in.	Wind, lb/ft^2	K, lb/ft	Weight, lb/ft	Sag, ft	Tension, lb	Sag, ft	Tension, lb
0	0.50	4.00	0.30	2.509	30.07	10479	30.07	10479
32	0.50	0.00	0.00	2.094	30.56	8607	29.94	8785
−20	0.00	0.00	0.00	1.094	24.09	5694	22.77	6023
0	0.00	0.00	0.00	1.094	25.38	5406	23.90	5738
30	0.00	0.00	0.00	1.094	27.26	5036	25.59	5362
60	0.00	0.00	0.00	1.094	29.07	4725[a]	27.25	5038
90	0.00	0.00	0.00	1.094	30.82	4460	28.87	4758
120	0.00	0.00	0.00	1.094	32.50	4232	30.45	4513
167	0.00	0.00	0.00	1.094	34.36	4005	32.85	4187
212	0.00	0.00	0.00	1.094	35.62	3865	35.05	3928

[a]Design condition.

Note: **Calculations based on:** (1) NESC Heavy Loading District. (2) Tension Limits: a. Initial Loaded – 60% RBS @ 0°F; b. Initial Unloaded – 25% RBS @ 60°F; c. Final Unloaded – 15% RBS @ 60°F.

14.4 Ruling Span Concept

Transmission lines are normally designed in line sections with each end of the line section terminated by a strain structure that allows no longitudinal (along the line) movement of the conductor (Winkelman, 1959). Structures within each line section are typically suspension structures that support the conductor vertically, but allow free movement of the conductor attachment point either longitudinally or transversely.

14.4.1 Tension Differences for Adjacent Dead-End Spans

Table 14.11 contains initial and final sag-tension data for a 700-ft and a 1000-ft dead-end span when a Drake ACSR conductor is initially installed to the same 6300-lb tension limits at 60°F. Note that the

TABLE 14.11 Typical Sag and Tension Data 795 kcmil-Type 16 ACSR/SD, 300- and 1000-ft Spans

Conductor: Drake
795 kcmil-Type 16 ACSR/SD
Area = 0.7261 in.^{2}
Creep ***is*** a factor

Span = 300 ft

NESC Heavy Loading District

					Final		Initial	
Temp, °F	Ice, in.	Wind, lb/ft^2	K, lb/ft	Weight, lb/ft	Sag, ft	Tension, lb	Sag, ft	Tension, lb
30	0.00	9.00	0.05	1.409	1.59	9980	1.31	12373
30	0.00	0.00	0.00	1.093	1.26	9776	1.03	11976
60	0.00	0.00	0.00	1.093	1.60	7688	1.16	10589[a]
90	0.00	0.00	0.00	1.093	2.12	5806	1.34	9159
120	0.00	0.00	0.00	1.093	2.69	4572	1.59	7713
167	0.00	0.00	0.00	1.093	3.11	3957	2.22	5545
212	0.00	0.00	0.00	1.093	3.58	3435	3.17	3877

[a] Design condition.

Conductor: Drake
795 kcmil-Type 16 ACSR/SD
Area = 0.7261 in.^{2}
Creep ***is*** a factor

Span = 1000 ft

NESC Heavy Loading District

					Final		Initial	
Temp, °F	Ice, in.	Wind, lb/ft^2	K, lb/ft	Weight, lb/ft	Sag, ft	Tension, lb	Sag, ft	Tension, lb
30	0.00	9.00	0.05	1.409	17.21	10250	15.10	11676
30	0.00	0.00	0.00	1.093	15.22	8988	12.69	10779
60	0.00	0.00	0.00	1.093	17.21	7950[a]	13.98	9780
90	0.00	0.00	0.00	1.093	19.26	7108	15.44	8861
120	0.00	0.00	0.00	1.093	21.31	6428	17.03	8037
167	0.00	0.00	0.00	1.093	24.27	5647	19.69	6954
212	0.00	0.00	0.00	1.093	25.62	5352	22.32	6136

[a] Design condition.

Note: **Calculations based on:** (1) NESC Light Loading District. (2) Tension Limits: a. Initial Loaded – 60% RBS @ 30°F; b. Initial Unloaded – 25% RBS @ 60°F; c. Final Unloaded – 15% RBS @ 60°F.

difference between the initial and final limits at 60°F is approximately 460 lb. Even the initial tension (equal at 60°F) differs by almost 900 lb at −20°F and 600 lb at 167°F.

14.4.2 Tension Equalization by Suspension Insulators

At a typical suspension structure, the conductor is supported vertically by a suspension insulator assembly, but allowed to move freely in the direction of the conductor axis. This conductor movement is possible due to insulator swing along the conductor axis. Changes in conductor tension between spans, caused by changes in temperature, load, and time, are normally equalized by insulator swing, eliminating horizontal tension differences across suspension structures.

14.4.3 Ruling Span Calculation

Sag-tension can be found for a series of suspension spans in a line section by use of the ruling span concept (Ehrenberg, 1935; Winkelman, 1959). The ruling span (RS) for the line section is defined by the following equation:

$$RS = \sqrt{\frac{S_1{}^3 + S_2{}^3 + \cdots + S_n{}^3}{S_1 + S_2 + \cdots + S_n}} \tag{14.26}$$

where RS = Ruling span for the line section containing n suspension spans
S_1 = Span length of first suspension span
S_2 = Span length of second suspension span
S_n = Span length of nth suspension span

Alternatively, a generally satisfactory method for estimating the ruling span is to take the sum of the average suspension span length plus two-thirds of the difference between the maximum span and the average span. However, some judgment must be exercised in using this method because a large difference between the average and maximum span may cause a substantial error in the ruling span value.

As discussed, suspension spans are supported by suspension insulators that are free to move in the direction of the conductor axis. This freedom of movement allows the tension in each suspension span to be assumed to be the same and equal to that calculated for the ruling span. This assumption is valid for the suspension spans and ruling span under the same conditions of temperature and load, for both initial and final sags. For level spans, sag in each suspension span is given by the parabolic sag equation:

$$D_i = \frac{w(S_i^2)}{8H_{RS}} \tag{14.27}$$

where D_i = sag in the ith span
S_i = span length of the ith span
H_{RS} = tension from ruling span sag-tension calculations

The sag in level suspension spans may also be calculated using the ratio:
where D_{RS} = sag in ruling span

Suspension spans vary in length, though typically not over a large range. Conductor temperature during sagging varies over a range considerably smaller than that used for line design purposes.

If the sag in any suspension span exceeds approximately 5% of the span length, a correction factor should be added to the sags obtained from the above equation or the sag should be calculated using catenary Eq. (14.29). This correction factor may be calculated as follows:

$$Correction = D^2 \frac{w}{6H} \tag{14.28}$$

where D = sag obtained from parabolic equation
w = weight of conductor, lb/ft
H = horizontal tension, lb

The catenary equation for calculating the sag in a suspension or stringing span is:

$$Sag = \frac{H}{w}\left(\cosh\frac{Sw}{2H} - 1\right) \tag{14.29}$$

where S = span length, ft
H = horizontal tension, lb
w = resultant weight, lb/ft

14.4.4 Stringing Sag Tables

Conductors are typically installed in line section lengths consisting of multiple spans. The conductor is pulled from the conductor reel at a point near one strain structure progressing through travelers attached to each suspension structure to a point near the next strain structure. After stringing, the

TABLE 14.12 Typical Sag and Tension Data 795 kcmil-Type 16 ACSR/SD, 300- and 1000-ft Span

Conductor: Drake
795 kcmil-Type 16 ACSR/SD
Area = 0.7261 in.^{2}
Creep ***is*** a factor

Span = 300 ft

NESC Heavy Loading District

Temp, °F	Ice, in.	Wind, lb/ft^2	K, lb/ft	Weight, lb/ft	Final Sag, ft	Final Tension, lb	Initial Sag, ft	Initial Tension, lb
0	0.50	4.00	0.30	2.486	2.19	12774	2.03	13757
32	0.50	0.00	0.00	2.074	2.25	10377	1.90	12256
−20	0.00	0.00	0.00	1.093	.91	13477	.87	14156
0	0.00	0.00	0.00	1.093	1.03	11962	.92	13305
30	0.00	0.00	0.00	1.093	1.26	9776	1.03	11976
60	0.00	0.00	0.00	1.093	1.60	7688	1.16	10589[a]
90	0.00	0.00	0.00	1.093	2.12	5806	1.34	9159
120	0.00	0.00	0.00	1.093	2.69	4572	1.59	7713
167	0.00	0.00	0.00	1.093	3.11	3957	2.22	5545
212	0.00	0.00	0.00	1.093	3.58	3435	3.17	3877

[a]Design Condition

Conductor: Drake
795 kcmil-Type 16 ACSR/SD
Area = 0.7261 in.^{2}
Creep ***is*** a factor

Span = 1000 ft

NESC Heavy Loading District

Temp, °F	Ice, in.	Wind, lb/ft^2	K, lb/ft	Weight, lb/ft	Final Sag, ft	Final Tension, lb	Initial Sag, ft	Initial Tension, lb
0	0.50	4.00	0.30	2.486	20.65	15089	20.36	15299
32	0.50	0.00	0.00	2.074	20.61	12607	19.32	13445
−20	0.00	0.00	0.00	1.093	12.20	11205	10.89	12552
0	0.00	0.00	0.00	1.093	13.35	10244	11.56	11832
30	0.00	0.00	0.00	1.093	15.22	8988	12.69	10779
60	0.00	0.00	0.00	1.093	17.21	7950[a]	13.98	9780
90	0.00	0.00	0.00	1.093	19.26	7108	15.44	8861
120	0.00	0.00	0.00	1.093	21.31	6428	17.03	8037
167	0.00	0.00	0.00	1.093	24.27	5647	19.69	6954
212	0.00	0.00	0.00	1.093	25.62	5352	22.32	6136

[a]Design condition.

Note: **Calculations based on:** (1) NESC Heavy Loading District. (2) Tension Limits: a. Initial Loaded – 60% RBS @ 0°F; b. Initial Unloaded – 25% RBS @ 60°F; Final Unloaded – 15% RBS @ 60°F.

conductor tension is increased until the sag in one or more suspension spans reaches the appropriate stringing sags based on the ruling span for the line section. The calculation of stringing sags is based on the preceding sag equation.

Table 14.13 shows a typical stringing sag table for a 600-ft ruling span of Drake ACSR with suspension spans ranging from 400 to 700 ft and conductor temperatures of 20–100°F. All values in this stringing table are calculated from ruling span initial tensions, shown in Table 14.12 using the parabolic sag equation.

14.5 Line Design Sag-Tension Parameters

In laying out a transmission line, the first step is to survey the route and draw up a plan-profile of the selected right-of-way. The plan-profile drawings serve an important function in linking together

TABLE 14.13 Typical Sag and Tension Data 795 kcmil-37 Strand AAC "Arbutus," 300- and 1000-ft Spans

Conductor: Arbutus
795 kcmil-37 Strands AAC
Area = 0.6245 in.^{2}
Creep ***is*** a factor

Span = 300 ft

NESC Heavy Loading District

					Final		Initial	
Temp, °F	Ice, in.	Wind, lb/ft^2	K, lb/ft	Weight, lb/ft	Sag, ft	Tension, lb	Sag, ft	Tension, lb
30	0.00	9.00	0.05	1.122	3.56	3546	2.82	4479
30	0.00	0.00	0.00	0.746	2.91	2889	2.06	4075
60	0.00	0.00	0.00	0.746	4.03	2085[a]	2.80	2999
90	0.00	0.00	0.00	0.746	5.13	1638	3.79	2215
120	0.00	0.00	0.00	0.746	6.13	1372	4.86	1732
167	0.00	0.00	0.00	0.746	7.51	1122	6.38	1319
212	0.00	0.00	0.00	0.746	8.65	975	7.65	1101

[a] Design condition.

Conductor: Arbutus
795 kcmil-37 Strands AAC
Area = 0.6245 in.^{2}
Creep ***is*** a factor

Span = 1000 ft

NESC Heavy Loading District

					Final		Initial	
Temp, °F	Ice, in.	Wind, lb/ft^2	K, lb/ft	Weight, lb/ft	Sag, ft	Tension, lb	Sag, ft	Tension, lb
30	0.00	9.00	0.05	1.122	44.50	3185	42.85	3305
30	0.00	0.00	0.00	0.746	43.66	2158	41.71	2258
60	0.00	0.00	0.00	0.746	45.24	2085[a]	43.32	2175
90	0.00	0.00	0.00	0.746	46.76	2018	44.89	2101
120	0.00	0.00	0.00	0.746	48.24	1958	46.42	2033
167	0.00	0.00	0.00	0.746	50.49	1873	48.72	1939
212	0.00	0.00	0.00	0.746	52.55	1801	50.84	1860

[a] Design condition.

Note: **Calculations based on:** (1) NESC Light Loading District. (2) Tension Limits: a. Initial Loaded – 60% RBS @ 30°F; b. Initial Unloaded – 25% RBS @ 60°F; c. Final Unloaded – 15% RBS @ 60°F.

the various stages involved in the design and construction of the line. These drawings, prepared based on the route survey, show the location and elevation of all natural and man-made obstacles to be traversed by, or adjacent to, the proposed line. These plan-profiles are drawn to scale and provide the basis for tower spotting and line design work.

Once the plan-profile is completed, one or more estimated ruling spans for the line may be selected. Based on these estimated ruling spans and the maximum design tensions, sag-tension data may be calculated providing initial and final sag values. From this data, sag templates may be constructed to the same scale as the plan-profile for each ruling span, and used to graphically spot structures.

14.5.1 Catenary Constants

The sag in a ruling span is equal to the weight per unit length, w, times the span length, S, squared, divided by 8 times the horizontal component of the conductor tension, H. The ratio of conductor horizontal tension, H, to weight per unit length, w, is the catenary constant, H/w. For a ruling span sag-tension calculation using eight loading conditions, a total of 16 catenary constant values could be defined, one for initial and final tension under each loading condition.

Catenary constants can be defined for each loading condition of interest and are used in any attempt to locate structures. Some typical uses of catenary constants for locating structures are to avoid

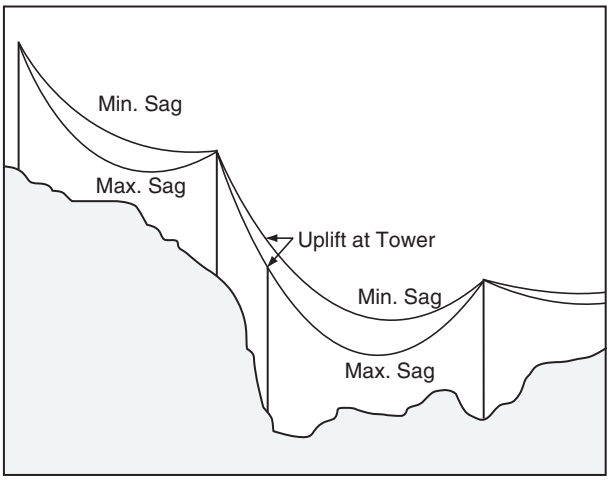

FIGURE 14.9 Conductor uplift.

overloading, assure ground clearance is sufficient at all points along the right-of-way, and minimize blowout or uplift under cold weather conditions. To do this, catenary constants are typically found for: (1) the maximum line temperature; (2) heavy ice and wind loading; (3) wind blowout; and (4) minimum conductor temperature. Under any of these loading conditions, the catenary constant allows sag calculation at any point within the span.

14.5.2 Wind Span

The maximum wind span of any structure is equal to the distance measured from center to center of the two adjacent spans supported by a structure. The wind span is used to determine the maximum horizontal force a structure must be designed to withstand under high wind conditions. Wind span is not dependent on conductor sag or tension, only on horizontal span length.

14.5.3 Weight Span

The weight span of a structure is a measure of the maximum vertical force a structure must be designed to withstand. The weight span is equal to the horizontal distance between the low points and the vertex of two adjacent spans. The maximum weight span for a structure is dependent on the loading condition being a minimum for heavy ice and wind load. When the elevations of adjacent structures are the same, the wind and weight spans are equal.

14.5.4 Uplift at Suspension Structures

Uplift occurs when the weight span of a structure is negative. On steeply inclined spans, the low point of sag may fall beyond the lower support. This indicates that the conductor in the uphill span is exerting a negative or upward force on the lower tower. The amount of this upward force is equal to the weight of the conductor from the lower tower to the low point in the sag. If the upward pull of the uphill span is greater than the downward load of the next adjacent span, actual uplift will be caused and the conductor will swing free of the tower. This usually occurs under minimum temperature conditions and must be dealt with by adding weights to the insulator suspension string or using a strain structure (Fig. 14.9).

14.5.5 Tower Spotting

Given sufficiently detailed plan-profile drawings, structure heights, wind/weight spans, catenary constants, and minimum ground clearances, structure locations can be chosen such that ground clearance is

maintained and structure loads are acceptable. This process can be done by hand using a sag template, plan-profile drawing, and structure heights, or numerically by one of several commercial programs.

14.6 Conductor Installation

Installation of a bare overhead conductor can present complex problems. Careful planning and a thorough understanding of stringing procedures are needed to prevent damage to the conductor during the stringing operations. The selection of stringing sheaves, tensioning method, and measurement techniques are critical factors in obtaining the desired conductors sagging results. Conductor stringing and sagging equipment and techniques are discussed in detail in the *IEEE Guide to the Installation of Overhead Transmission Line Conductors,* IEEE Std. 524–1992. Some basic factors concerning installation are covered in this section. Because the terminology used for equipment and installation procedures for overhead conductors varies throughout the utility industry, a limited glossary of terms and equipment definitions excerpted from IEEE Std. 524–1992 is provided in the chapter appendix. A complete glossary is presented in the *IEEE Guide to the Installation of Overhead Transmission Line Conductors.*

14.6.1 Conductor Stringing Methods

There are two basic methods of stringing conductors, categorized as either slack or tension stringing. There are as many variations of these methods as there are organizations installing conductors. The selected method, however, depends primarily on the terrain and conductor surface damage requirements.

14.6.1.1 Slack or Layout Stringing Method

Slack stringing of conductor is normally limited to lower voltage lines and smaller conductors. The conductor reel(s) is placed on reel stands or "jack stands" at the beginning of the stringing location. The conductor is unreeled from the shipping reel and dragged along the ground by means of a vehicle or pulling device. When the conductor is dragged past a supporting structure, pulling is stopped and the conductor placed in stringing sheaves attached to the structure. The conductor is then reattached to the pulling equipment and the pull continued to the next structure.

This stringing method is typically used during construction of new lines in areas where the right-of-way is readily accessible to vehicles used to pull the conductor. However, slack stringing may be used for repair or maintenance of transmission lines where rugged terrain limits use of pulling and tensioning equipment. It is seldom used in urban areas or where there is any danger of contact with high-voltage conductors.

14.6.1.2 Tension Stringing

A tension stringing method is normally employed when installing transmission conductors. Using this method, the conductor is unreeled under tension and is not allowed to contact the ground. In a typical tension stringing operation, travelers are attached to each structure. A pilot line is pulled through the travelers and is used, in turn, to pull in heavier pulling line. This pulling line is then used to pull the conductor from the reels and through the travelers. Tension is controlled on the conductor by the tension puller at the pulling end and the bullwheel tension retarder at the conductor payout end of the installation. Tension stringing is preferred for all transmission installations. This installation method keeps the conductor off the ground, minimizing the possibility of surface damage and limiting problems at roadway crossings. It also limits damage to the right-of-way by minimizing heavy vehicular traffic.

14.6.2 Tension Stringing Equipment and Setup

Stringing equipment typically includes bullwheel or drum pullers for back-tensioning the conductor during stringing and sagging; travelers (stringing blocks) attached to every phase conductor and shield wire attachment point on every structure; a bullwheel or crawler tractor for pulling the conductor through travelers; and various other special items of equipment. Figure 14.10 illustrates a typical stringing and sagging setup for a stringing section and the range of stringing equipment required.

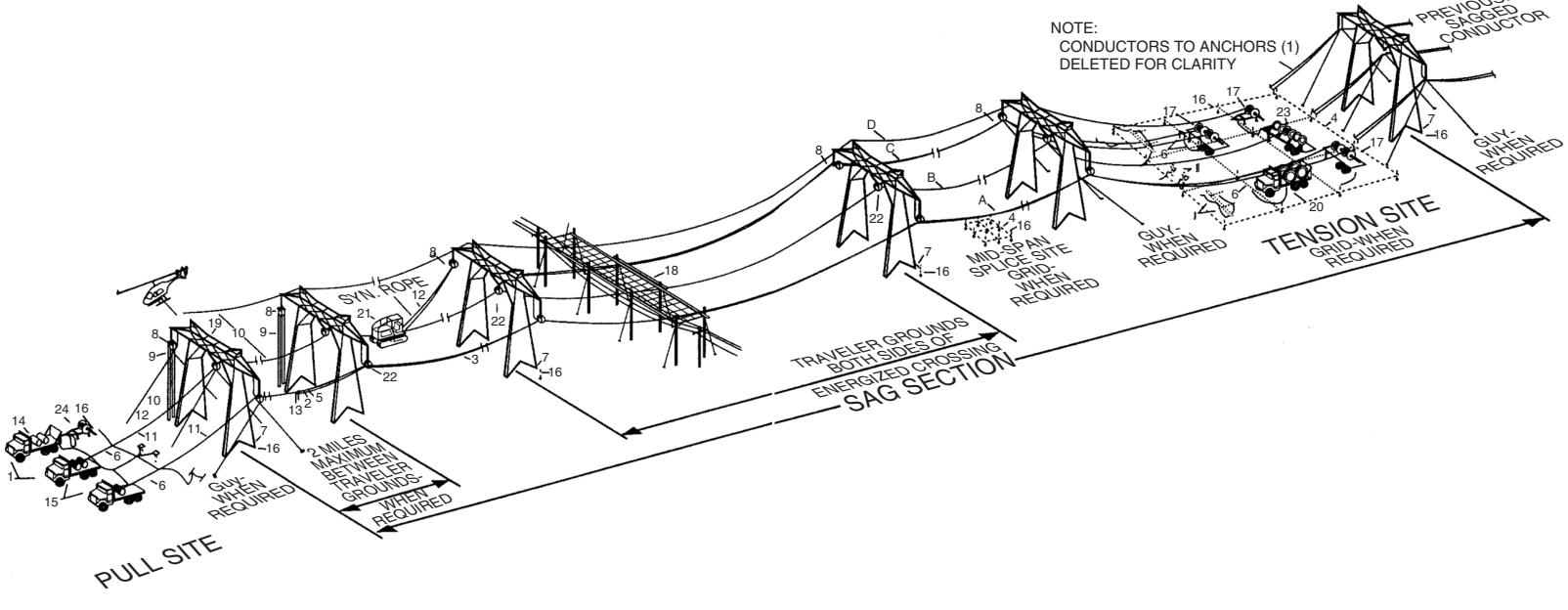

FIGURE 14.10 Tension stringing equipment setup.

FIGURE 14.11 Basket grip pulling device.

Provision for conductor splicing during stringing must be made at tension site or midspan sites to avoid pulling splices through the travelers.

During the stringing operation, it is necessary to use proper tools to grip the strands of the conductor evenly to avoid damaging the outer layer of wires. Two basic types or categories of grips are normally used in transmission construction. The first is a type of grip referred to as a pocketbook, suitcase, bolted, etc., that hinges to completely surround the conductor and incorporates a bail for attaching to the pulling line. The second type is similar to a Chinese finger grip and is often referred to as a basket or "Kellem" grip. Such a grip, shown in Fig. 14.11, is often used because of its flexibility and small size, making it easily pulled through sheaves during the stringing operation. Whatever type of gripping device is used, a swivel should be installed between the pulling grip and pulling line or running board to allow free rotation of both the conductor and the pulling line.

A traveler consists of a sheave or pulley wheel enclosed in a frame to allow it to be suspended from structures or insulator strings. The frame must have some type of latching mechanism to allow insertion and removal of the conductor during the stringing operation. Travelers are designed for a maximum safe working load. Always ensure that this safe working load will not be exceeded during the stringing operation. Sheaves are often lined with neoprene or urethane materials to prevent scratching of conductors in high-voltage applications; however, unlined sheaves are also available for special applications.

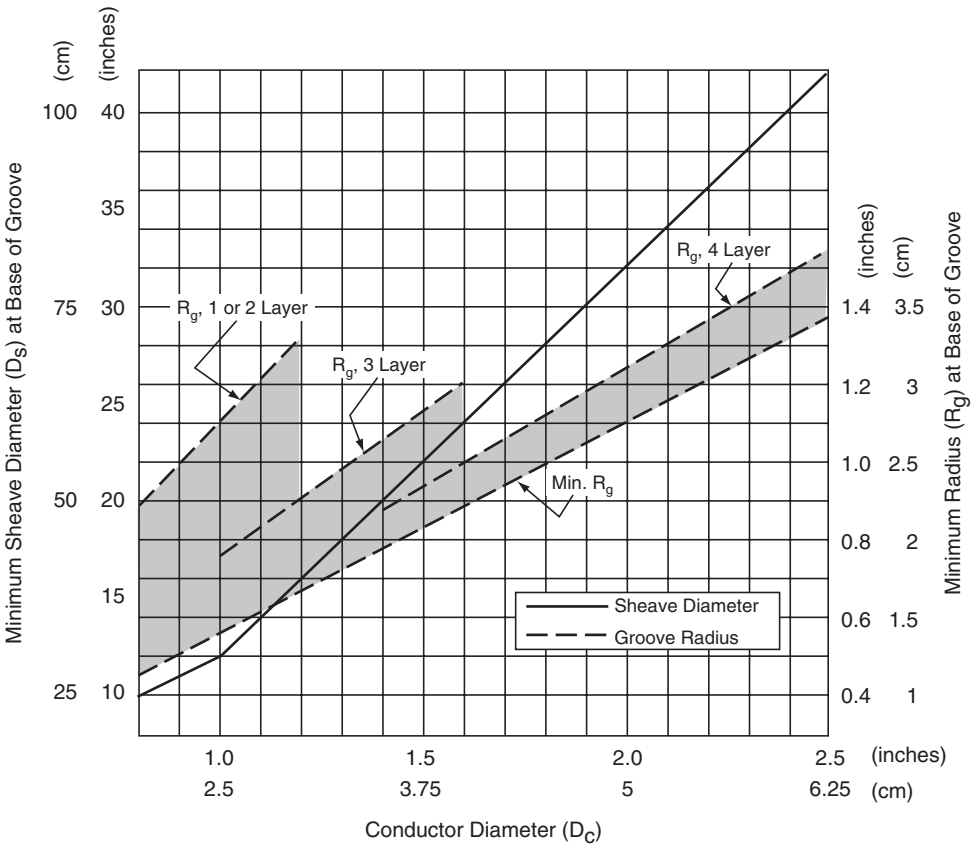

FIGURE 14.12 Recommended minimum sheave dimensions.

Travelers used in tension stringing must be free rolling and capable of withstanding high running or static loads without damage. Proper maintenance is essential. Very high longitudinal tension loads can develop on transmission structures if a traveler should "freeze" during tension stringing, possibly causing conductor and/or structure damage. Significant levels of rotation resistance will also yield tension differences between spans, resulting in incorrect sag.

Proper selection of travelers is important to assure that travelers operate correctly during tension stringing and sagging. The sheave diameter and the groove radius must be matched to the conductor.

Figure 14.12 illustrates the minimum sheave diameter for typical stringing and sagging operations. Larger diameter sheaves may be required where particularly severe installation conditions exist.

14.6.3 Sagging Procedure

It is important that the conductors be properly sagged at the correct stringing tension for the design ruling span. A series of several spans, a line section, is usually sagged in one operation. To obtain the correct sags and to insure the suspension insulators hang vertically, the horizontal tension in all spans must be equal. Figures 14.13 through 14.18 depict typical parabolic methods and computations required

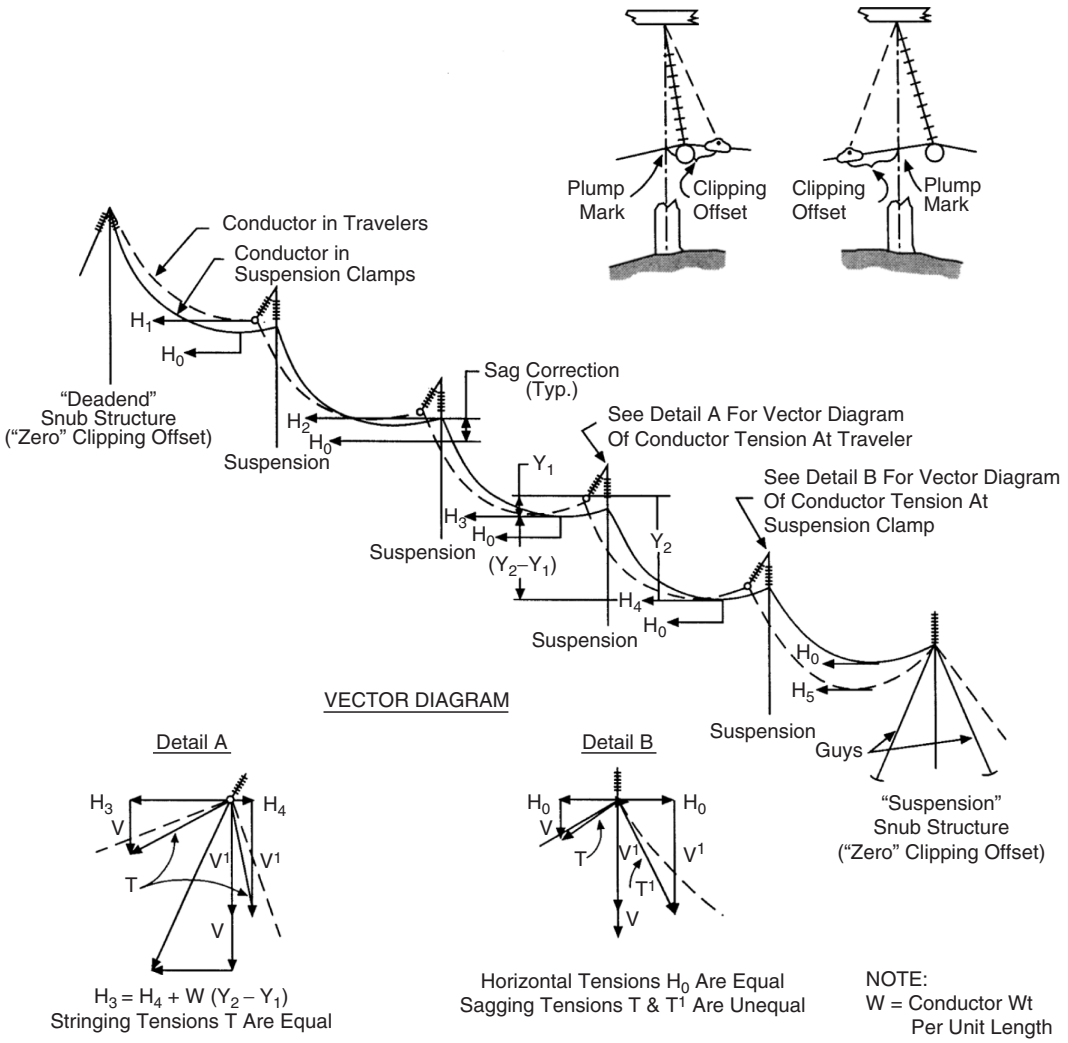

FIGURE 14.13 Clipping offset illustration.

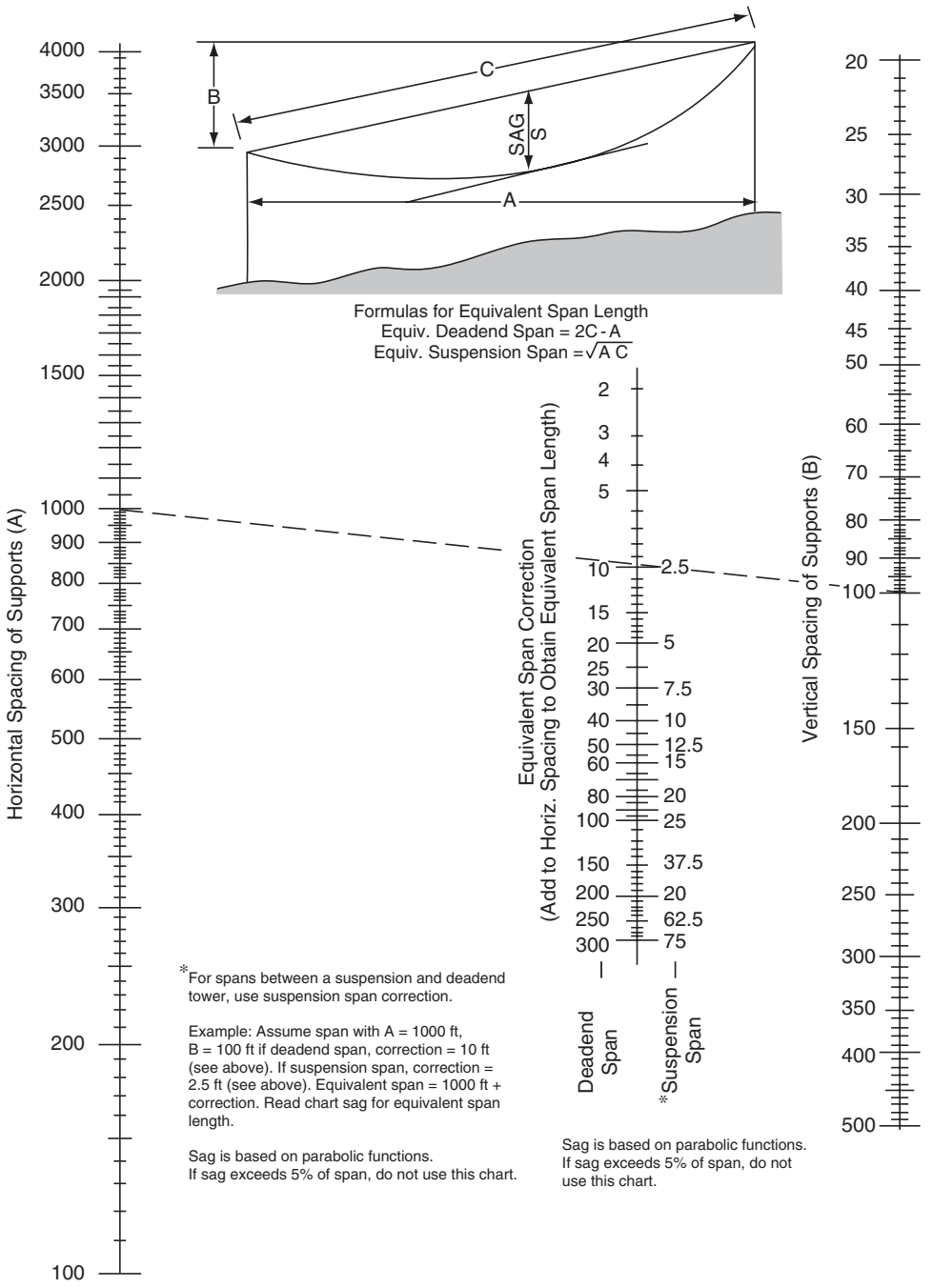

FIGURE 14.14 Nomograph for determining level span equivalents of non-level spans.

for sagging conductors. Factors that must be considered when sagging conductors are creep elongation during stringing and prestressing of the conductor.

Creep elongation during stringing: Upon completion of conductor stringing, a time of up to several days may elapse before the conductor is tensioned to design sag. Since the conductor tension during the stringing process is normally well below the initial sagging tension, and because the conductor remains in the stringing sheaves for only a few days or less, any elongation due to creep is neglected. The

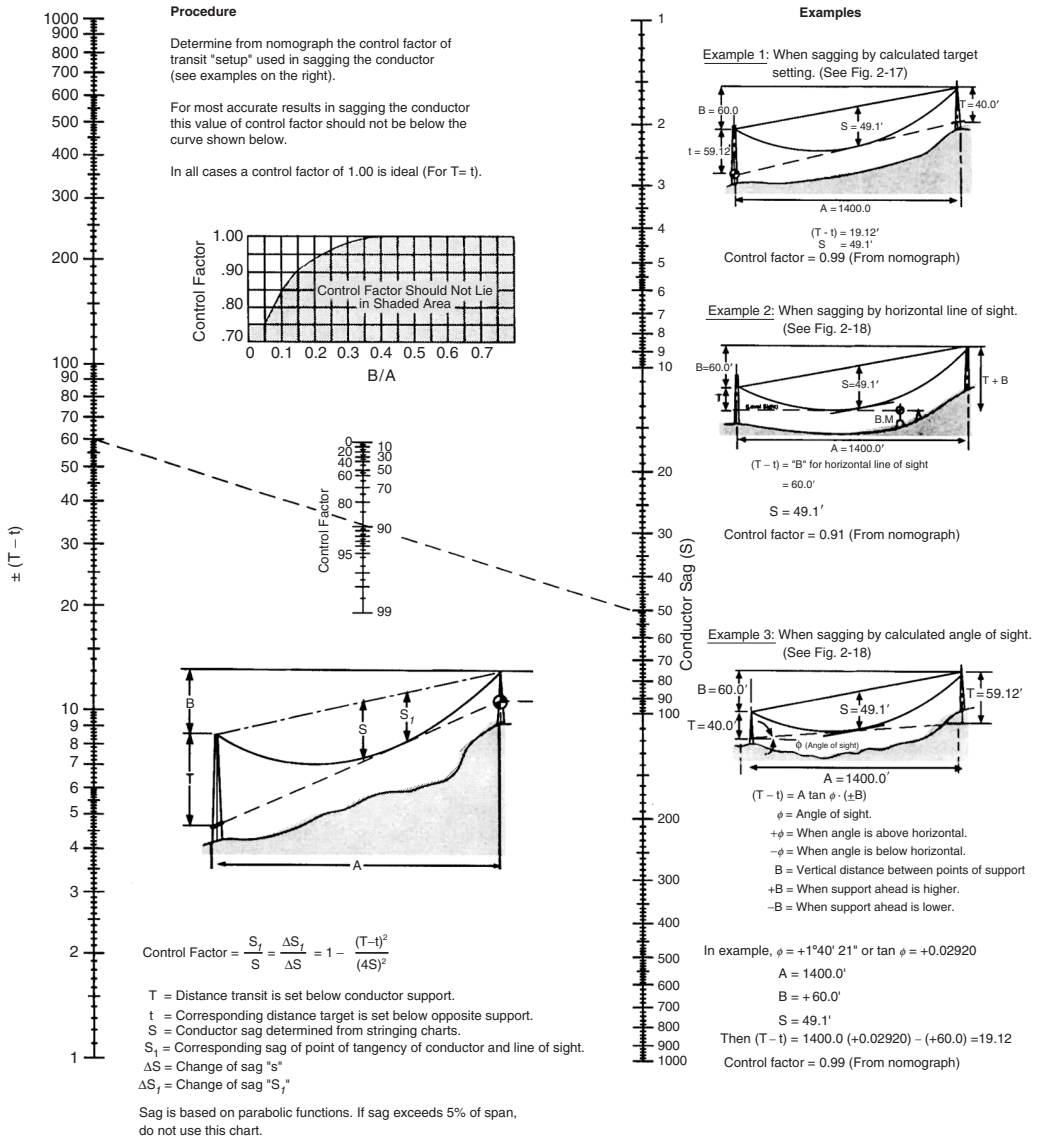

FIGURE 14.15 Nomograph for determining control factor for conductor sagging.

conductor should be sagged to the initial stringing sags listed in the sag tables. However, if the conductor tension is excessively high during stringing, or the conductor is allowed to remain in the blocks for an extended period of time, then the creep elongation may become significant and the sagging tables should be corrected prior to sagging.

Creep is assumed exponential with time. Thus, conductor elongation during the first day under tension is equal to elongation over the next week. Using creep estimation formulas, the creep strain can be estimated and adjustments made to the stringing sag tables in terms of an equivalent temperature. Also, should this become a concern, Southwire's Wire and Cable Technology Group will be happy to work with you to solve the problem.

Prestressing conductor: Prestressing is sometimes used to stabilize the elongation of a conductor for some defined period of time. The prestressing tension is normally much higher than the unloaded design tension for a conductor. The degree of stabilization is dependent upon the time maintained at the

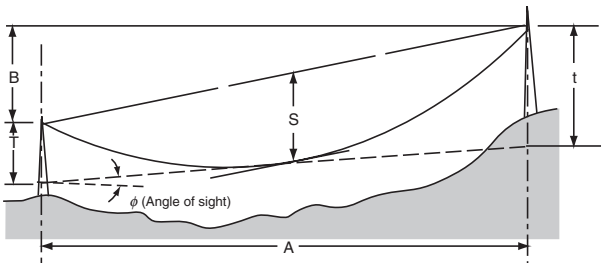

METHOD 1: $\text{Tan } \phi = \dfrac{T \pm B - t}{A}$

METHOD 2: $\text{Tan } \phi = \dfrac{B + 2T - S(2+M)}{A}$

ϕ = Angle of sight
+ ϕ When angle is above horizontal
– ϕ When angle is below horizontal
t = Vertical distance below support to line of sight. (See Fig. 2-17).
T = Vertical distance below support for transit.
S = Sag
A = Horizontal distance between points of support - obtained from structure list or plan & profile
B = Vertical distance between points of support - obtained from plan & profile, tower site data sheets or field measurement.
+ B when support ahead is higher.
– B when support ahead is lower.
M = Determined from cure on Fig. 2-17.

EXAMPLES:

Given:

A = 1400.0'
B = +60.0'
T = 40.0'

S = 49.1' @ 60°F
S = 51.2' @ 90°F
T = 59.12' @ 60°F
T = 63.76' @ 90°F

METHOD 1

$\text{Tan } \phi = \dfrac{T \pm B - t}{A}$

$\text{Tan } \phi_{60°F} = \dfrac{40.0 - 60.0 - 59.12}{1400.0} = 0.02920$

$\phi_{60°F} = +1° 40'21"$

$\text{Tan } \phi_{90°F} = \dfrac{40.0 - 60.0 - 63.76}{1400.0} = 0.02589$

$\phi_{90°F} = +1° 28' 59"$

Change in angle ϕ for 5°F = $(1° 40' 21" - 1° 28' 59") \left(\dfrac{5}{30}\right) = 0° 1' 54"$

METHOD 2

$\text{Tan } \phi = \dfrac{B + 2T - S(2 + M)}{A}$

$\text{Tan } \phi_{60°F} = \dfrac{60.0 + (40.0)(2) - (49.1)(2+0.019)}{1400.0} = 0.02919$

$\phi_{60°F} = +1° 40' 19"$

$\text{Tan } \phi_{90°F} = \dfrac{60.0 + (40.0)(2) - (51.2)(2+0.027)}{1400.0} = 0.02587$

$\phi_{90°F} = +1° 28' 55"$

Change in angle ϕ for 5° F = $(1° 40' 19" - 1° 28' 55") \left(\dfrac{5}{30}\right) = 0° 1' 54"$

Sag is based on parabolic functions. If sag exceeds 5% of span, do not use this chart.

FIGURE 14.16 Conductor sagging by calculated angle of sight.

prestress tension. After prestressing, the tension on the conductor is reduced to stringing or design tension limits. At this reduced tension, the creep or plastic elongation of the conductor has been slowed, reducing the permanent elongation due to strain and creep for a defined period of time. By tensioning a conductor to levels approaching 50% of its breaking strength for times on the order of a day, creep elongation will be temporarily halted (Cahill, 1973). This simplifies concerns about creep during subsequent installation but presents both equipment and safety problems.

14.6.3.1 Sagging by Stopwatch Method

A mechanical pulse imparted to a tensioned conductor moves at a speed proportional to the square root of tension divided by weight per unit length. By initiating a pulse on a tensioned conductor and measuring the time required for the pulse to move to the nearest termination, the tension, and thus

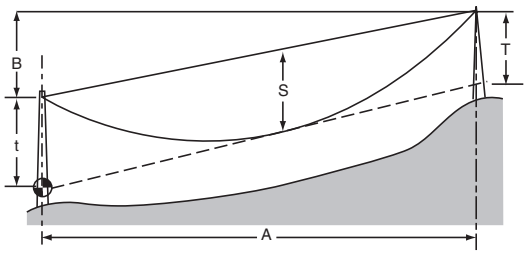

METHOD 1: $t = (2\sqrt{S} - \sqrt{T})^2$

METHOD 2: $t = 2S - T + SM$

t = Vertical distance below support for target.
T = Vertical distance below support for transit.
S = Sag.
A = Horizontal distance between structures - obtained from structure list or plan & profile.
B = Vertical distance between points of support - obtained from plan & profile, tower site data sheets or field measurement.
M = Determined from curve below.

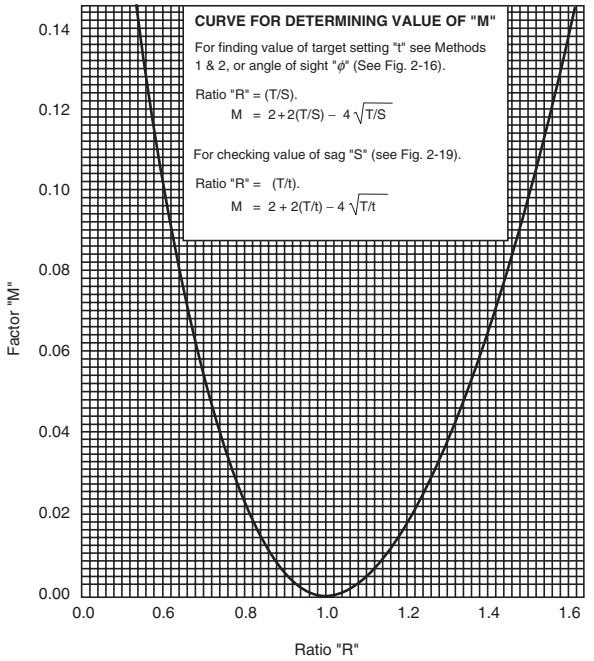

EXAMPLES

Given:

A = 1400.0'
B = 60.0'
T = 40.0'
S = 49.1' @ 60°F
S = 51.2' @ 90°F

METHOD 1

$t = (2\sqrt{S} - \sqrt{T})^2$

$\sqrt{T} = 6.325$

$\sqrt{S_{60°F}} = 7.007$

$2\sqrt{S_{60°F}} = 14.014$

$t_{60°F} = 59.12'$

$\sqrt{S_{90°F}} = 7.155$

$2\sqrt{S_{90°F}} = 14310$

$t_{90°F} = 63.76'$

Change in "t" for 5°F = $(63.76 - 59.12)\left(\frac{5}{30}\right) = 0.77'$

METHOD 2

$t = 2S - T + SM$

$T/S_{60°F} = 0.815$

$M_{60°F} = 0.019$

$2S_{60°F} = 98.2'$

$t_{60°F} = 59.13'$

$T/S_{90°F} = 0.781$

$M_{90°F} = 0.027$

$2S_{90°F} = 102.4'$

$t_{90°F} = 63.78'$

Change in "t" for 5°F = $(63.76 - 59.13)\left(\frac{5}{30}\right) = 0.78'$

Sag is based on parabolic functions.
If sag exceeds 5% of span, do not use this chart.

FIGURE 14.17 Conductor sagging by calculated target method.

the sag of the conductor, can be determined. This stopwatch method (Overend and Smith) has come into wide use even for long spans and large conductors.

The conductor is struck a sharp blow near one support and the stopwatch is started simultaneously. A mechanical wave moves from the point where the conductor was struck to the next support point at which it will be partially reflected. If the initiating blow is sharp, the wave will travel up and down the span many times before dying out. Time-sag tables such as the one shown in Table 14.14 are available from many sources. Specially designed sagging stopwatches are also available.

The reflected wave can be detected by lightly touching the conductor but the procedure is more likely to be accurate if the wave is both initiated and detected with a light rope over the conductor. Normally, the time for the return of the 3rd or 5th wave is monitored.

Traditionally, a transit sagging method has been considered to be more accurate for sagging than the stopwatch method. However, many transmission-line constructors use the stopwatch method exclusively, even with large conductors.

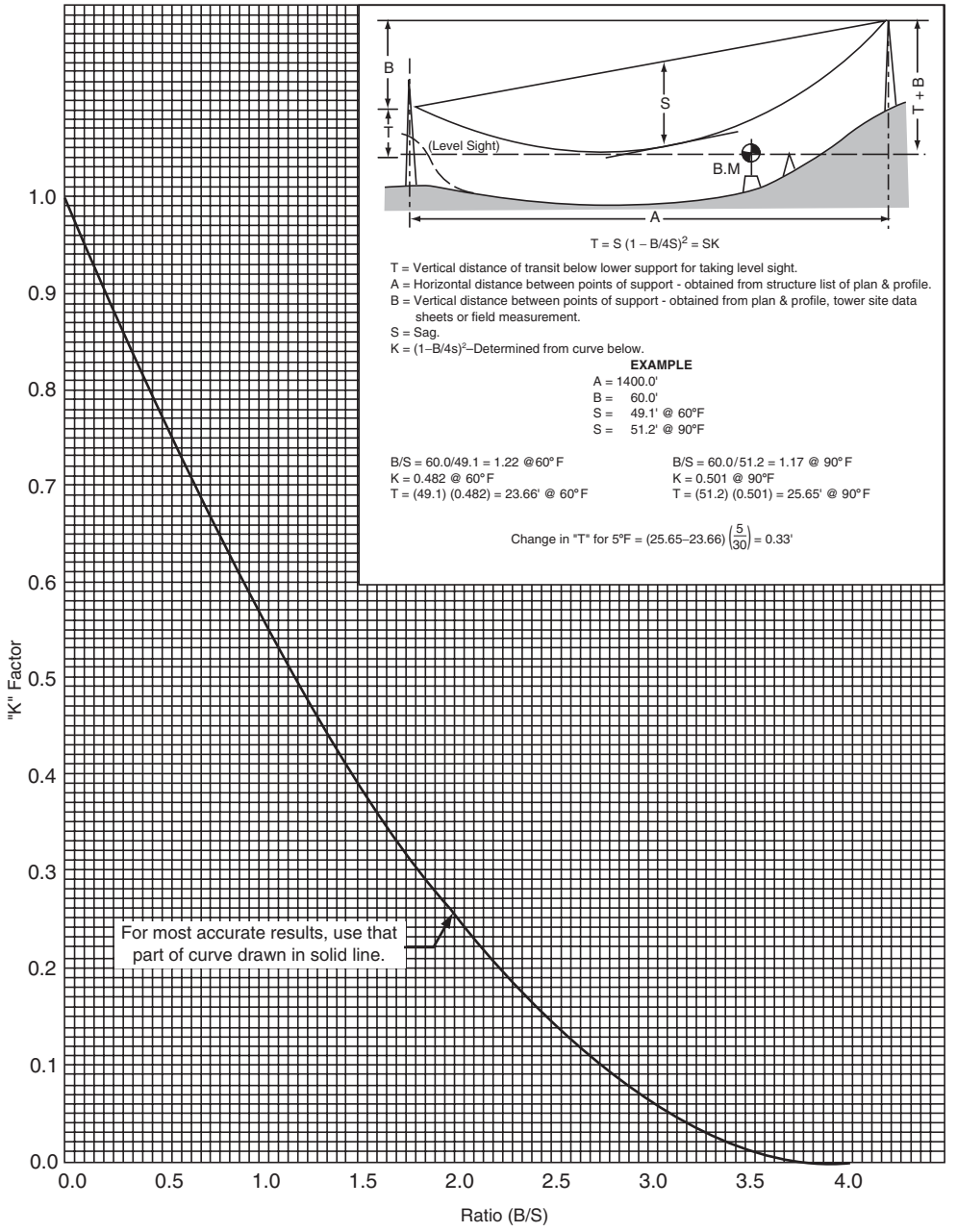

FIGURE 14.18 Conductor sagging by horizontal line of sight.

14.6.3.2 Sagging by Transit Methods

IEEE Guide Std. 524–1993 lists three methods of sagging conductor with a transit: "Calculated Angle of Sight," "Calculated Target Method," and "Horizontal Line of Sight." The method best suited to a particular line sagging situation may vary with terrain and line design.

TABLE 14.14 Typical Sag and Tension Data 795 kcmil-37 Strand AAC "Arbutus," 300- and 1000-ft Spans

Conductor: Arbutus
795 kcmil-37 Strands AAC
Area = 0.6245 in.^{2}
Creep ***is*** a factor

Span = 300 ft

					Final		Initial	
Temp, °F	Ice, in.	Wind, lb/ft^2	K, lb/ft	Weight, lb/ft	Sag, ft	Tension, lb	Sag, ft	Tension, lb
0	0.50	4.00	0.30	2.125	3.97	6033	3.75	6383
32	0.50	0.00	0.00	1.696	4.35	4386	3.78	5053
−20	0.00	0.00	0.00	0.746	1.58	5319	1.39	6055
0	0.00	0.00	0.00	0.746	2.00	4208	1.59	5268
30	0.00	0.00	0.00	0.746	2.91	2889	2.06	4075
60	0.00	0.00	0.00	0.746	4.03	2085[a]	2.80	2999
90	0.00	0.00	0.00	0.746	5.13	1638	3.79	2215
120	0.00	0.00	0.00	0.746	6.13	1372	4.86	1732
167	0.00	0.00	0.00	0.746	7.51	1122	6.38	1319
212	0.00	0.00	0.00	0.746	8.65	975	7.65	1101

[a]Design condition.

Conductor: Arbutus
795 kcmil-37 Strands AAC
Area = 0.6245 in.^{2}
Creep ***is*** a factor

Span = 1000 ft

NESC Heavy Loading District

					Final		Initial	
Temp, °F	Ice, in.	Wind, lb/ft^2	K, lb/ft	Weight, lb/ft	Sag, ft	Tension, lb	Sag, ft	Tension, lb
0	0.50	4.00	0.30	2.125	45.11	59.53	44.50	6033
32	0.50	0.00	0.00	1.696	45.80	4679	44.68	4794
−20	0.00	0.00	0.00	0.746	40.93	2300	38.89	2418
0	0.00	0.00	0.00	0.746	42.04	2240	40.03	2350
30	0.00	0.00	0.00	0.746	43.66	2158	41.71	2258
60	0.00	0.00	0.00	0.746	45.24	2085[a]	43.32	2175
90	0.00	0.00	0.00	0.746	46.76	2018	44.89	2101
120	0.00	0.00	0.00	0.746	48.24	1958	46.42	2033
167	0.00	0.00	0.00	0.746	50.49	1873	48.72	1939
212	0.00	0.00	0.00	0.746	52.55	1801	50.84	1860

[a]Design condition.

Note: **Calculations based on:** (1) NESC Light Loading District. (2) Tension Limits: a. Initial Loaded – 60% RBS @ 0°F; b. Initial Unloaded – 25% RBS @ 60°F; c. Final Unloaded – 15% RBS @ 60°F.

14.6.3.3 Sagging Accuracy

Sagging a conductor during construction of a new line or in the reconductoring of a old line involves many variables that can lead to a small degree of error. IEEE Std. 524–1993 suggests that all sags be within 6 in. of the stringing sag values. However, aside from measurement errors during sagging, errors in terrain measurement and variations in conductor properties, loading conditions, and hardware installation have led some utilities to allow up to 3 ft of margin in addition to the required minimum ground clearance.

14.6.3.4 Clipping Offsets

If the conductor is to be sagged in a series of suspension spans where the span lengths are reasonably close and where the terrain is reasonably level, then the conductor is sagged using conventional stringing sag tables and the conductor is simply clipped into suspension clamps that replace the travelers. If the

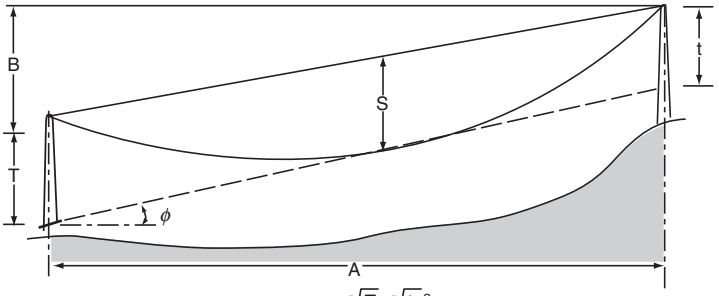

METHOD 1: $S = \left(\frac{\sqrt{T}+\sqrt{t}}{2}\right)^2$

METHOD 2: $S = \frac{B}{2} + \frac{t}{2} - \frac{tM}{8}$

S = Sag
t = Vertical distance below support to line of sight.
= T ± B – A tan ϕ when angle ϕ is above horizontal.
= T± B + A tan ϕ when angle ϕ is below horizontal.
T = Vertical distance below support for transit.
B = Vertical distance between points of support - obtanied from plan & profile, tower site data sheets or field measurement.
+ B when support ahead is higher.
– B when support ahead is lower.
A = Horizontal distance between points of support - obtained from structure list or plan & profile
ϕ = Angle of sight
M = Determined from cure on Fig. 2.17.

EXAMPLES

Given:

A = 1400.0' T = 40.0'
B = 60.0' ϕ = +1°40' 21″ @ 60°F (Field Measured)

METHOD 1

$S = \left(\frac{\sqrt{T}+\sqrt{t}^2}{2}\right)$

t = 40.0 + 60.0 – 1400.0 tan 1° 40' 21"

= 59.12'

$\sqrt{t}$ = 7.689

$\sqrt{T}$ = 6.325

$S_{60°F}$ = 49.1'

METHOD 2

Note: When using Method 2, value, "T" should lie between 3/4 "S" & 4/3 "S"

$S = \frac{B}{2} + \frac{t}{2} - \frac{tM}{8}$

t = 59.12'

t/2 = 29.56'

T/2 = 20.0″

M = 0.061

$S_{60°F} = 20.0 + 29.56 - \frac{(59.12)(0.061)}{8}$

$S_{60°F}$ = 49.1'

Sag is based on parabolic functions. if sag exceeds 5% of span, do not use this chart.

FIGURE 14.19 Conductor sagging for checking sag S.

conductor is to be sagged in a series of suspension spans where span lengths vary widely or more commonly, where the terrain is steep, then clipping offsets may need to be employed in order to yield vertical suspension strings after installation.

Clipping offsets are illustrated in Fig. 14.19, showing a series of steeply inclined spans terminated in a "snub" structure at the bottom and a "deadend" structure at the top. The vector diagram illustrates a balance of total conductor tension in the travelers but an imbalance in the horizontal component of tension.

14.7 Defining Terms

Block—A device designed with one or more single sheaves, a wood or metal shell, and an attachment hook or shackle. When rope is reeved through two of these devices, the assembly is commonly referred to as a *block and tackle.* A *set of 4s* refers to a block and tackle arrangement utilizing two 4-inch double-sheave blocks to obtain four load-bearing lines. Similarly, a *set of 5s* or a *set of 6s* refers to the same number of load bearing lines obtained using two 5-inch or two 6-inch double-sheave blocks, respectively.

Synonyms: set of 4s, set of 5s, set of 6s.

Bullwheel—A wheel incorporated as an integral part of a bullwheel puller or tensioner to generate pulling or braking tension on conductors or pulling lines, or both, through friction. A puller or tensioner normally has one or more pairs arranged in tandem incorporated in its design. The physical size of the wheels will vary for different designs, but 17-in. (43 cm) face widths and diameters of 5 ft (150 cm) are common. The wheels are power driven or retarded and lined with single- or multiple-groove neoprene or urethane linings. Friction is accomplished by reeving the pulling line or conductor around the groove of each pair.

Clipping-in—The transferring of sagged conductors from the traveler to their permanent suspension positions and the installing of the permanent suspension clamps.

Synonyms: clamping, clipping.

Clipping offset—A calculated distance, measured along the conductor from the plum mark to a point on the conductor at which the center of the suspension clamp is to be placed. When stringing in rough terrain, clipping offset may be required to balance the horizontal forces on each suspension structure.

Grip, conductor—A device designed to permit the pulling of conductor without splicing on fittings, eyes, etc. It permits the pulling of a *continuous* conductor where threading is not possible. The designs of these grips vary considerably. Grips such as the Klein (Chicago) and Crescent utilize an open-sided rigid body with opposing jaws and swing latch. In addition to pulling conductors, this type is commonly used to tension guys and, in some cases, pull wire rope. The design of the come-along (pocketbook, suitcase, four bolt, etc.) incorporates a bail attached to the body of a clamp which folds to completely surround and envelope the conductor. Bolts are then used to close the clamp and obtain a grip.

Synonyms: buffalo, Chicago grip, come-along, Crescent, four bolt, grip, Klein, pocketbook, seven bolt, six bolt, slip-grip, suitcase.

Line, pilot—A lightweight line, normally synthetic fiber rope, used to pull heavier pulling lines which in turn are used to pull the conductor. Pilot lines may be installed with the aid of finger lines or by helicopter when the insulators and travelers are hung.

Synonyms: lead line, leader, P-line, straw line.

Line, pulling—A high-strength line, normally synthetic fiber rope or wire rope, used to pull the conductor. However, on reconstruction jobs where a conductor is being replaced, the old conductor often serves as the pulling line for the new conductor. In such cases, the old conductor must be closely examined for any damage prior to the pulling operations.

Synonyms: bull line, hard line, light line, sock line.

Puller, bullwheel—A device designed to pull pulling lines and conductors during stringing operations. It normally incorporates one or more pairs of urethane- or neoprene-lined, power-driven, single- or multiple-groove bullwheels where each pair is arranged in tandem. Pulling is accomplished by friction generated against the pulling line which is reeved around the grooves of a pair of the bullwheels. The puller is usually equipped with its own engine which drives the bullwheels mechanically, hydraulically, or through a combination of both. Some of these devices function as either a puller or tensioner.

Synonym: puller.

Puller, drum—A device designed to pull a conductor during stringing operations. It is normally equipped with its own engine which drives the drum mechanically, hydraulically, or through a combination of both. It may be equipped with synthetic fiber rope or wire rope to be used as the

pulling line. The pulling line is payed out from the unit, pulled through the travelers in the sag section and attached to the conductor. The conductor is then pulled in by winding the pulling line back onto the drum. This unit is sometimes used with synthetic fiber rope acting as a pilot line to pull heavier pulling lines across canyons, rivers, etc.

Synonyms: hoist, single drum hoist, single drum winch, tugger.

Puller, reel—A device designed to pull a conductor during stringing operations. It is normally equipped with its own engine which drives the supporting shaft for the reel mechanically, hydraulically, or through a combination of both. The shaft, in turn, drives the reel. The application of this unit is essentially the same as that for the drum puller previously described. Some of these devices function as either a puller or tensioner.

Reel stand—A device designed to support one or more reels and having the possibility of being skid, trailer, or truck mounted. These devices may accommodate rope or conductor reels of varying sizes and are usually equipped with reel brakes to prevent the reels from turning when pulling is stopped. They are used for either slack or tension stringing. The designation of reel trailer or reel truck implies that the trailer or truck has been equipped with a reel stand (jacks) and may serve as a reel transport or *payout* unit, or both, for stringing operations. Depending upon the sizes of the reels to be carried, the transporting vehicles may range from single-axle trailers to semi-trucks with trailers having multiple axles.

Synonyms: reel trailer, reel transporter, reel truck.

Running board—A pulling device designed to permit stringing more than one conductor simultaneously with a single pulling line. For distribution stringing, it is usually made of lightweight tubing with the forward end curved gently upward to provide smooth transition over pole cross-arm rollers. For transmission stringing, the device is either made of sections hinged transversely to the direction of pull or of a hard-nose rigid design, both having a flexible pendulum tail suspended from the rear. This configuration stops the conductors from twisting together and permits smooth transition over the sheaves of bundle travelers.

Synonyms: alligator, bird, birdie, monkey tail, sled.

Sag section—The section of line between snub structures. More than one sag section may be required in order to properly sag the actual length of conductor which has been strung.

Synonyms: pull, setting, stringing section.

Site, pull—The location on the line where the puller, reel winder, and anchors (snubs) are located. This site may also serve as the pull or tension site for the next sag section.

Synonyms: reel setup, tugger setup.

Site, tension—The location on the line where the tensioner, reel stands and anchors (snubs) are located. This site may also serve as the pull or tension site for the next sag section.

Synonyms: conductor payout station, payout site, reel setup.

Snub structure—A structure located at one end of a sag section and considered as a *zero* point for sagging and clipping offset calculations. The section of line between two such structures is the sag section, but more than one sag section may be required in order to sag properly the actual length of conductor which has been strung.

Synonyms: *0* structure, zero structure.

Tensioner, bullwheel—A device designed to hold tension against a pulling line or conductor during the stringing phase. Normally, it consists of one or more pairs of urethane- or neoprene-lined, power braked, single- or multiple-groove bullwheels where each pair is arranged in tandem. Tension is accomplished by friction generated against the conductor which is reeved around the grooves of a pair of the bullwheels. Some tensioners are equipped with their own engines which retard the bullwheels mechanically, hydraulically, or through a combination of both. Some of these devices function as either a puller or tensioner. Other tensioners are only equipped with friction-type retardation.

Synonyms: retarder, tensioner.

Tensioner, reel—A device designed to generate tension against a pulling line or conductor during the stringing phase. Some are equipped with their own engines which retard the supporting shaft for

the reel mechanically, hydraulically, or through a combination of both. The shaft, in turn, retards the reel. Some of these devices function as either a puller or tensioner. Other tensioners are only equipped with friction type retardation.

Synonyms: retarder, tensioner.

Traveler—A sheave complete with suspension arm or frame used separately or in groups and suspended from structures to permit the stringing of conductors. These devices are sometimes bundled with a center drum or sheave, and another traveler, and used to string more than one conductor simultaneously. For protection of conductors that should not be nicked or scratched, the sheaves are often lined with nonconductive or semiconductive neoprene or with nonconductive urethane. Any one of these materials acts as a padding or cushion for the conductor as it passes over the sheave. Traveler grounds must be used with lined travelers in order to establish an electrical ground.

Synonyms: block, dolly, sheave, stringing block, stringing sheave, stringing traveler.

Winder reel—A device designed to serve as a recovery unit for a pulling line. It is normally equipped with its own engine which drives a supporting shaft for a reel mechanically, hydraulically, or through a combination of both. The shaft, in turn, drives the reel. It is normally used to rewind a pulling line as it leaves the bullwheel puller during stringing operations. This unit is not intended to serve as a puller, but sometimes serves this function where only low tensions are involved.

Synonyms: take-up reel.

References

Cahill, T., Development of Low-Creep ACSR Conductor, *Wire Journal*, July 1973.

Ehrenburg, D.O., Transmission Line Catenary Calculations, AIEE Paper, Committee on Power Transmission & Distribution, July 1935.

Fink, D.G. and Beaty, H.W., *Standard Handbook for Electrical Engineers*, 13th ed., McGraw-Hill.

IEEE Guide to the Installation of Overhead Transmission Line Conductors, IEEE Standard 524-1993, IEEE, New York, 1993.

Graphic Method for Sag Tension Calculations for ACSR and Other Conductors, Aluminum Company of America, 1961.

Minimum Design Loads for Buildings and Other Structures, American Society of Civil Engineers Standard, ASCE 7–88.

National Electrical Safety Code, 1993 edition.

Overend, P.R. and Smith, S., Impulse Time Method of Sag Measurement.

Stress-Strain-Creep Curves for Aluminum Overhead Electrical Conductors, Aluminum Association, 1974.

Winkelman, P.F., Sag-Tension Computations and Field Measurements of Bonneville Power Administration, AIEE Paper 59-900, June 1959.

15

Corona and Noise

Giao N. Trinh
Retired from Hydro-Québec Institute of Research

Modern electric power systems are often characterized by generating stations located far away from the consumption centers, with long overhead transmission lines to transmit the energy from the generating sites to the load centers. From the few tens of kilovolts in the early years of the 20th century, the line voltage has reached the extra-high voltage (EHV) levels of 800-kV AC (Lacroix and Charbonneau, 1968) and 500-kV DC (Bateman et al., 1969) in the 1970s, and touched the ultrahigh voltage (UHV) levels of 1200-kV AC (Bortnik et al., 1988) and 600-kV DC (Krishnayya et al., 1988). Although overhead lines operating at high voltages are the most economical means of transmitting large amounts of energy over long distances, their exposure to atmospheric conditions constantly alters the surface conditions of the conductors and causes large variations in the corona activities on the line conductors.

Corona discharges follow an electron avalanche process whereby neutral molecules are ionized by electron impacts under the effect of the applied field (Raether, 1964). Since air is a particular mixture of nitrogen (79%), oxygen (20%), and various impurities, the discharge development is significantly conditioned by the electronegative nature of oxygen molecules, which can readily capture free electrons to form negative ions and thus hamper the electron avalanche process (Loeb, 1965). Several modes of corona discharge can be distinguished; and while all corona modes produce energy losses, the streamer discharges also generate electromagnetic interference, and audible noise in the immediate vicinity of high-voltage (HV) lines (Trinh and Jordan, 1968; Trinh, 1995a,b). These parameters are currently used to evaluate the corona performance of conductor bundles and to predict the energy losses and environmental impact of HV lines before their installation.

Adequate control of line corona is obtained by controlling the surface gradient at the line conductors. The introduction of bundled conductors by Whitehead in 1910 has greatly influenced the development of HV lines to today's EHVs (Whitehead, 1910). In effect, HV lines as we know them today would not exist without the bundled conductors. This chapter reviews the physical processes leading to the development of corona discharges on the line conductors and presents the current practices in selecting the line conductors.

15.1 Corona Modes (Trinh and Jordan, 1968; Trinh, 1995a)

In a nonuniform field gap in atmospheric air, corona discharges can develop over a whole range of voltages in a small region near the highly stressed electrode before the gap breaks down. Several criteria

have been developed for the onset of corona discharge, the most familiar being the streamer criterion. They are all related to the development of an electron avalanche in the gas gap and can be expressed as

$$1 - \gamma \exp\left[\int (\alpha - \eta)\, dx\right] = 0 \tag{15.1}$$

where $\alpha' = \alpha - \eta$ is the net coefficient of ionization by electron impact of the gas, α and η are respectively the ionization and attachment coefficients in air, and γ is a coefficient representing the efficiency of secondary processes in maintaining the ionization activities in the gap. The net coefficient of ionization varies with the distance x from the highly stressed electrode and the integral is evaluated for values of x where α' is positive.

A physical meaning may be given to the above corona onset criteria. The onset conditions can be rewritten as

$$\exp\left[\int (\alpha - \eta) dx\right] = \frac{1}{\gamma} \tag{15.2}$$

The left-hand side represents the avalanche development from a single electron and $1/\gamma$ the critical size of the avalanche to assure the stable development of the discharge.

The nonuniform field necessary for the development of corona discharges and the electronegative nature of air favor the formation of negative ions during the discharge development. Due to their relatively slow mobility, ions of both polarities from several consecutive electron avalanches accumulate in the low-field region of the gap and form ion space charges. To properly interpret the development of corona discharges, account must be taken of the active role of these ion space charges, which continuously modify the local field intensity and, hence, the development of corona discharges according to their relative build-up and removal from the region around the highly stressed electrode.

15.1.1 Negative Corona Modes

When the highly stressed electrode is at a negative potential, electron avalanches are initiated at the cathode and develop toward the anode in a continuously decreasing field. Referring to Fig. 15.1, the nonuniformity of the field distribution causes the electron avalanche to stop at the boundary surface S_0, where the net ionization coefficient is zero, that is, $\alpha = \eta$. Since free electrons can move much faster than ions under the influence of the applied field, they concentrate at the avalanche head during its progression. A concentration of positive ions thus forms in the region of the gap between the cathode and the boundary surface, while free electrons continue to migrate across the gap. In air, free electrons rapidly attach themselves to oxygen molecules to form negative ions, which, because of the slow drift velocity, start to accumulate in the region of the gap beyond S_0. Thus, as soon as the first electron avalanche has developed, there are two ion space charges in the gap.

The presence of these space charges increases the field near the cathode, but it reduces the field intensity at the anode end of the gap. The boundary surface of zero ionization activity is therefore displaced toward the cathode. The subsequent electron avalanche develops in a region of slightly higher field intensity but covers a shorter distance than its predecessor. The influence of the ion space charge is such that it actually conditions the development of the discharge at the highly stressed electrode, producing three modes of corona discharge with distinct electrical, physical, and visual characteristics (Fig. 15.2). These are, respectively, with increasing field intensity: Trichel streamer, negative pulseless glow, and negative streamer. An interpretation of the physical mechanism of different corona modes is given below.

15.1.1.1 Trichel Streamer

Figure 15.2a shows the visual aspect of the discharge; its current and light characteristics are shown in Fig. 15.3. The discharge develops along a narrow channel from the cathode and follows a regular

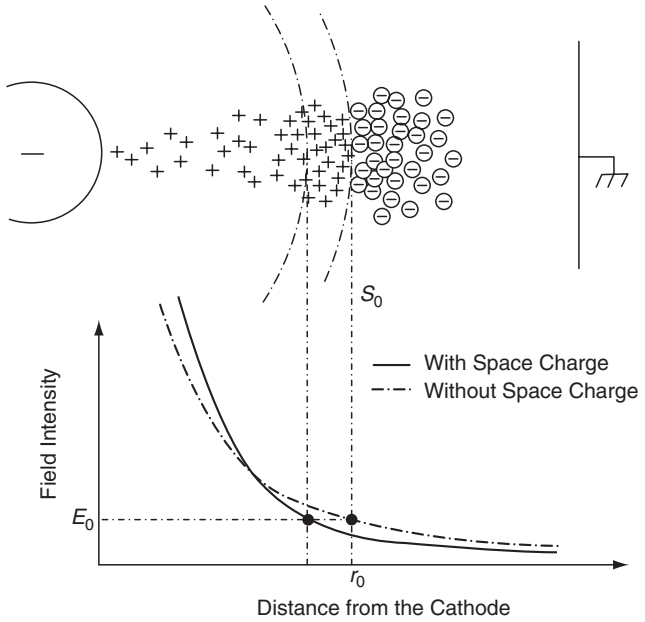

FIGURE 15.1 Development of an electron avalanche from the cathode. (From Trinh, N.G., *IEEE Electr. Insul. Mag.*, 11, 23, 1995a.)

pattern in which the streamer is initiated, is developed, and is suppressed; a short dead time follows before the cycle is repeated. The duration of an individual streamer is very short, a few tens of nanoseconds, while the dead time varies from a few microseconds to a few milliseconds, or even longer. The resulting discharge current consists of regular negative pulses of small amplitude and short duration, succeeding one another at the rate of a few thousand pulses per second. A typical Trichel current pulse is shown in Fig. 15.3 (above left) where, it should be noted, the wave shape is somewhat influenced by the time constant of the measuring circuit. The discharge duration may be significantly shorter, as depicted by the light pulse shown in Fig. 15.3 (below left).

The development of Trichel streamers cannot be explained without taking account of the active roles of the ion space charges and the applied field. The streamer is initiated from the cathode by a free electron. If the corona onset conditions are met, the secondary emissions are sufficient to trigger new electron avalanches from the cathode and maintain the discharge activity. During the streamer development, several generations of electron avalanches are initiated from the cathode and propagate along the streamer channel. The avalanche process also produces two ion space charges in the gap, which gradually moves the boundary surface S_0 closer to the cathode. The positive ion cloud thus finds itself compressed at the cathode and, in addition, is partially neutralized at the cathode and by the negative ions produced in subsequent avalanches. This results in a net negative ion space charge, which eventually reduces the local field intensity at the cathode below the onset field and suppresses the discharge. The dead time is a period during which the remaining ion space charges are dispersed by the applied field. A new streamer will develop when the space charges in the immediate surrounding of the cathode have been cleared to a sufficient extent.

This mechanism depends on a very active electron attachment process to suppress the ionization activity within a few tens of nanoseconds following the beginning of the discharge. The streamer repetition rate is essentially a function of the removal rate of ion space charges by the applied field, and generally shows a linear dependence on the applied voltage. However, at high fields a reduction in the pulse repetition rate may be observed, which corresponds to the transition to a new corona mode.

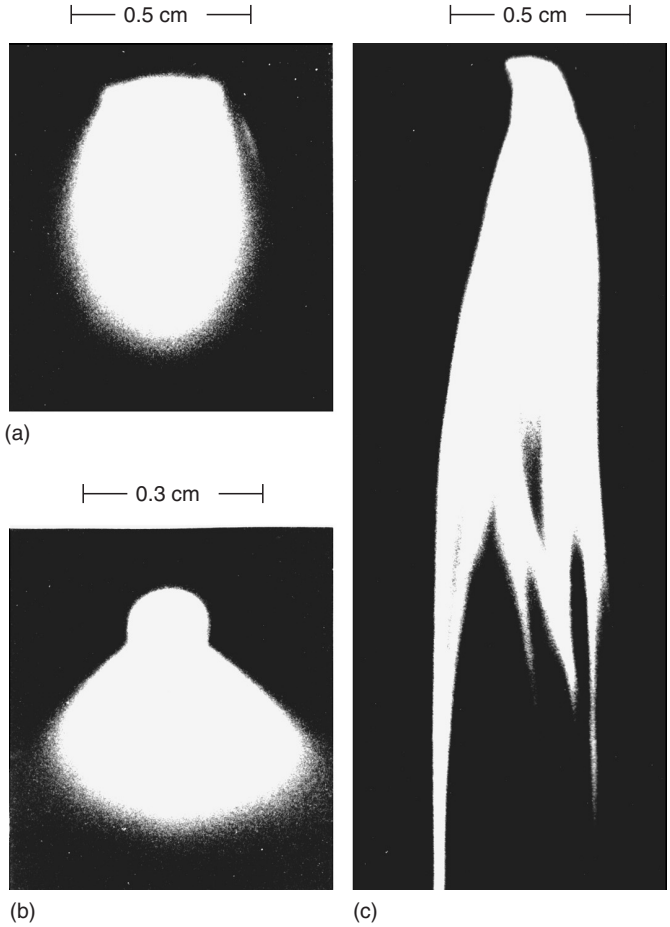

FIGURE 15.2 Corona modes at cathode: (a) Trichel streamers; (b) negative pulseless glow; (c) negative streamers. Cathode: spherical protrusion ($d = 0.8$ cm) on a sphere ($D = 7$ cm); gap 19 cm; time exposure 1/4 s. (From Trinh, N.G. and Jordan, I.B., *IEEE Trans.*, PAS-87, 1207, 1968; Trinh, N.G., *IEEE Electr. Insul. Mag.*, 11, 23, 1995a. With permission.)

15.1.1.2 Negative Pulseless Glow

The negative pulseless glow mode is characterized by a pulseless discharge current. As indicated by the well-defined visual aspect of the discharge (Fig. 15.2b), the discharge itself is particularly stable, which shows the basic characteristics of a miniature glow discharge. Starting from the cathode, a cathode dark space can be distinguished, followed by a negative glow region, a Faraday dark space and, finally, a positive column of conical shape. As with low-pressure glow discharges, these features of the pulseless glow discharge result from very stable conditions of electron emission from the cathode by ionic bombardment. The electrons, emitted with very low kinetic energy, are first propelled through the cathode dark space, where they acquire sufficient energy to ionize the gas, and intensive ionization occurs at the negative glow region. At the end of the negative glow region, the electrons lose most of their kinetic energy and are again accelerated across the Faraday dark space before they can ionize the gas atoms in the positive column. The conical shape of the positive column is attributed to the diffusion of the free electrons in the low-field region.

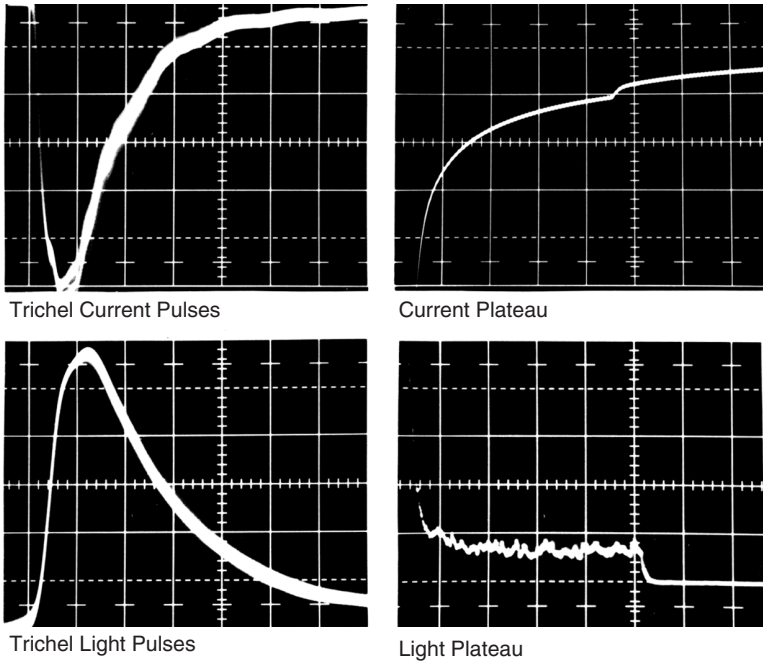

FIGURE 15.3 Current and light characteristics of Trichel streamer. Cathode: spherical protrusion ($d = 0.8$ cm) on a sphere ($D = 7$ cm); gap 19 cm. Scales: current 350 μA/div., 50 ns/div. (left), 50 μA/div., 2 μs/div. (right). Light: 0.5 V/div., 20 ns/div. (left), 0.2 V/div., 2 μs/div. (right). (From Trinh, N.G. and Jordan, I.B., *IEEE Trans.*, PAS-87, 1207, 1968; Trinh, N.G., *IEEE Electr. Insul. Mag.*, 11, 23, 1995a.)

These stable discharge conditions may be explained by the greater efficiency of the applied field in removing the ion space charges at higher field intensities. Negative ion space charges cannot build up sufficiently close to the cathode to effectively reduce the cathode field and suppress the ionization activities there. This interpretation of the discharge mechanism is further supported by the existence of a plateau in the Trichel streamer current and light pulses (Fig. 15.3), which indicates that an equilibrium state exists for a short time between the removal and the creation of the negative ion space charge. It has been shown (Trinh and Jordan, 1970) that the transition from the Trichel streamer mode to the negative pulseless glow corresponds to an indefinite prolongation in time of one such current plateau.

15.1.1.3 Negative Streamer

If the applied voltage is increased still further, negative streamers may be observed, as illustrated in Fig. 15.2c. The discharge possesses essentially the same characteristics observed in the negative pulseless glow discharge but here the positive column of the glow discharge is constricted to form the streamer channel, which extends farther into the gap. The glow discharge characteristics observed at the cathode imply that this corona mode also depends largely on electron emissions from the cathode by ionic bombardment, while the formation of a streamer channel characterized by intensive ionization denotes an even more effective space charge removal action by the applied field. The streamer channel is fairly stable. It projects from the cathode into the gap and back again, giving rise to a pulsating fluctuation of relatively low frequency in the discharge current.

15.1.2 Positive Corona Modes

When the highly stressed electrode is of positive polarity, the electron avalanche is initiated at a point on the boundary surface S_0 of zero net ionization and develops toward the anode in a continuously increasing field (Fig. 15.4). As a result, the highest ionization activity is observed at the anode. Here again, due to the lower mobility of the ions, a positive ion space charge is left behind along the development path of the avalanche. However, because of the high field-intensity at the anode, few electron attachments occur and the majority of free electrons created are neutralized at the anode. Negative ions are formed mainly in the low-field region farther in the gap. The following discharge behavior may be observed (Trinh and Jordan, 1968; Trinh, 1995a):

- The incoming free electrons are highly energetic and cannot be immediately absorbed by the anode. As a result, they tend to spread over the anode surface where they lose their energy through ionization of the gas particles, until they are neutralized at the anode, thus contributing to the development of the discharge over the anode surface.
- Since the positive ions are concentrated immediately next to the anode surface, they may produce a field enhancement in the gap that attracts secondary electron avalanches and promotes the radial propagation of the discharge into the gap along a streamer channel.
- During streamer discharge, the ionization activity is observed to extend considerably into the low-field region of the gap via the formation of corona globules, which propagate owing to the action of the electric field generated by their own positive ion space charge. Dawson (1965) has shown that if a corona globule is produced containing 10^8 positive ions within a spherical volume of 3×10^{-3} cm in radius, the ion space charge field is such that it attracts sufficient new electron avalanches to create a new corona globule a short distance away. In the meantime, the initial corona globule is neutralized, causing the corona globule to effectively move ahead toward the cathode.

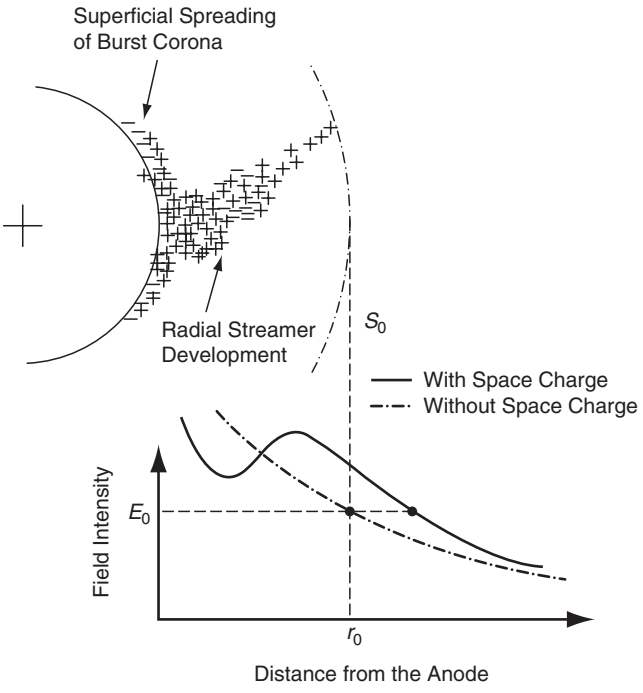

FIGURE 15.4 Development of an electron avalanche toward the anode. (From Trinh, N.G., *IEEE Electr. Insul. Mag.*, 11, 23, 1995a. With permission.)

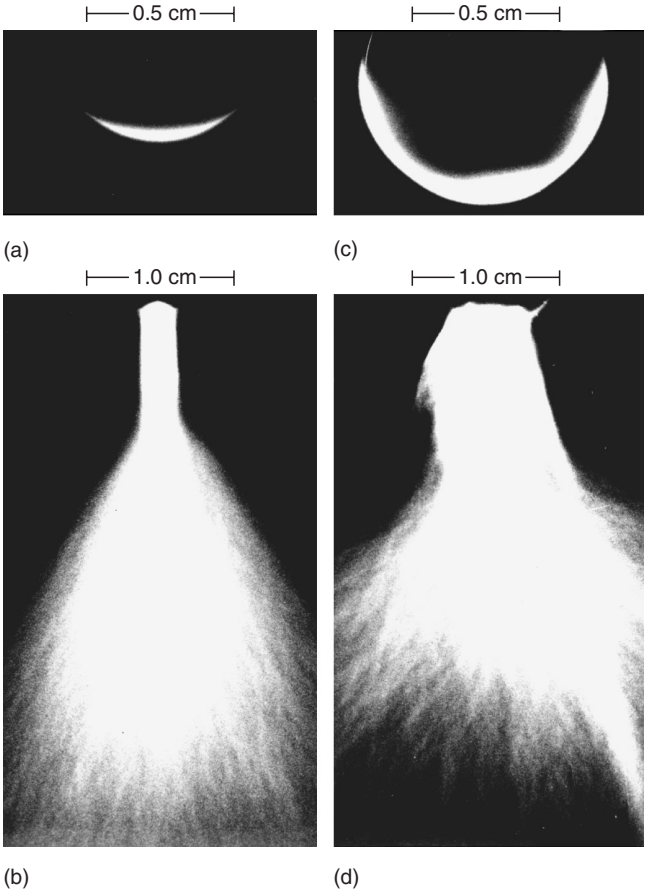

FIGURE 15.5 Corona modes at anode: (a) burst corona; (b) onset streamers; (c) positive glow corona; (d) breakdown streamers. Anode spherical protrusion ($d = 0.8$ cm) on a sphere ($D = 7$ cm); gap 35 cm; time exposure 1/4 s. (From Trinh, N.G. and Jordan, I.B., *IEEE Trans.*, PAS-87, 1207, 1968; Trinh, N.G., *IEEE Electr. Insul. Mag.*, 11, 23, 1995a.)

The presence of ion space charges of both polarities in the anode region greatly affects the local distribution of the field, and, consequently, the development of corona discharge at the anode. Four different corona discharge modes having distinct electrical, physical, and visual characteristics can be observed at a highly stressed anode, prior to flashover of the gap. These are, respectively, with increasing field intensity (Fig. 15.5): burst corona, onset streamers, positive glow, and breakdown streamers. An interpretation of the physical mechanisms leading to the development of these corona modes is given below.

15.1.2.1 Burst Corona

The burst corona appears as a thin luminous sheath adhering closely to the anode surface (Fig. 15.5a). The discharge results from the spread of ionization activities at the anode surface, which allows the high-energy incoming electrons to lose their energy before neutralization at the anode. During this process, a number of positive ions are created in a small area over the anode, which builds up a local positive space charge and suppresses the discharge. The spread of free electrons then moves to another part of the anode. The resulting discharge current consists of very small positive pulses (Fig. 15.6a),

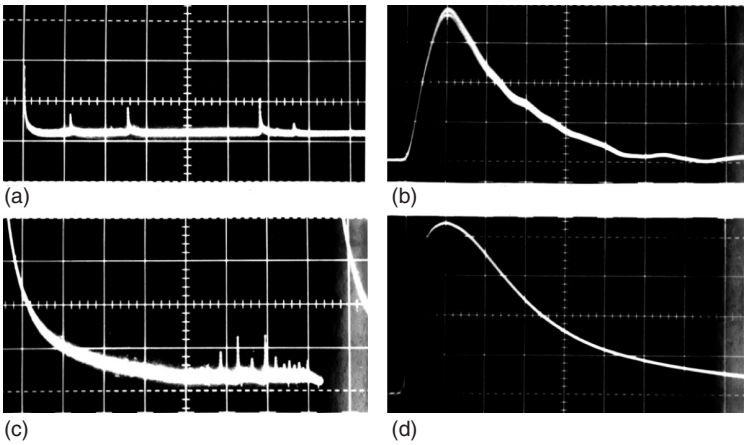

FIGURE 15.6 (a) Burst corona current pulse. Scales: 5 mA/div., 0.2 ms/div. (b) Development of burst corona following a streamer discharge. Scales: 5 mA/div., 0.2 ms/div. (c) Current characteristics of onset streamers. Scales: 7 mA/div., 50 ns/div. (d) Light characteristics of onset streamers. Scales: 1 V/div., 20 ns/div. (From Juette, G.W., *IEEE Trans.*, PAS-91, 865, 1972; Trinh, N.G. and Jordan, I.B., *IEEE Trans.*, PAS-87, 1207, 1968; Trinh, N.G., *IEEE Electr. Insul. Mag.*, 11, 23, 1995a. With permission.)

each corresponding to the ionization spreading over a small area at the anode and then being suppressed by the positive ion space charge produced.

15.1.2.2 Onset Streamer

The positive ion space charge formed adjacent to the anode surface causes a field enhancement in its immediate vicinity, which attracts subsequent electron avalanches and favors the radial development of onset streamers. This discharge mode is highly effective and the streamers are observed to extend farther into the low-field region of the gap along numerous filamentary channels, all originating from a common stem projecting from the anode (Fig. 15.5b). During this development of the streamers, a considerable number of positive ions are formed in the low-field region. As a result of the cumulative effect of the successive electron avalanches and the absorption at the anode of the free electrons created in the discharge, a net residual positive ion space charge forms in front of the anode. The local gradient at the anode then drops below the critical value for ionization and suppresses the streamer discharge. A dead time is consequently required for the applied field to remove the ion space charge and restore the proper conditions for the development of a new streamer. The discharge develops in a pulsating mode, producing a positive current pulse of short duration, high amplitude, and relatively low repetition rate due to the large number of ions created in a single streamer (Figs. 15.6c and 15.6d).

It has been observed that these first two discharge modes develop in parallel over a small range of voltages following corona onset. As the voltage is increased, the applied field rapidly becomes more effective in removing the ion space charge in the immediate vicinity of the electrode surface, thus promoting the lateral spread of burst corona at the anode. In fact, burst corona can be triggered just a few microseconds after suppression of the streamer (Fig. 15.6b). This behavior can be explained by the rapid clearing of the positive ion space charge at the anode region, while the incoming negative ions encounter a high enough gradient to shed their electrons, thus providing the seeding free electrons to initiate new avalanches and sustain the ionization activity over the anode surface in the form of burst corona. The latter will continue to develop until it is again suppressed by its own positive space charge.

As the voltage is raised even higher, the burst corona is further enhanced by a more effective space charge removal action of the field at the anode. During the development of the burst corona, positive ions are created and rapidly pushed away from the anode. The accumulation of positive ions in front of the anode results in the formation of a stable positive ion space charge that prevents the radial development of the discharge into the gap. Consequently, the burst corona develops more readily, at

the expense of the onset streamer, until the latter is completely suppressed. A new mode, the positive glow discharge, is then established at the anode.

15.1.2.3 Positive Glow

A photograph of a positive glow discharge developing at a spherical protrusion is presented in Fig. 15.5. This discharge is due to the development of the ionization activity over the anode surface, which forms a thin luminous layer immediately adjacent to the anode surface, where intense ionization activity takes place. The discharge current consists of a direct current superimposed by a small pulsating component with a high repetition rate, in the hundreds of kilohertz range. By analyzing the light signals obtained with photomultipliers pointing to different regions of the anode, it may be found that the luminous sheath is composed of a stable central region, from there, bursts of ionization activity may develop and project the ionizing sheath outward and back again, continuously, giving rise to the pulsating current component.

The development of the positive glow discharge may be interpreted as resulting from a particular combination of removal and creation of positive ions in the gap. The field is high enough for the positive ion space charge to be rapidly removed from the anode, thus promoting surface ionization activity. Meanwhile, the field intensity is not sufficient to allow radial development of the discharge and the formation of streamers. The main contribution of the negative ions is to supply the necessary triggering electrons to sustain ionization activity at the anode.

15.1.2.4 Breakdown Streamer

If the applied voltage is further increased, streamers are again observed and they eventually lead to breakdown of the gap. The development of breakdown streamers is preceded by local streamer spots of intense ionization activity, which may be seen moving slowly over the anode surface. The development of streamer spots is not accompanied by any marked change in the current or the light signal. Only when the applied field becomes sufficiently high to rapidly clear the positive ion space charges from the anode region does radial development of the discharge become possible, resulting in breakdown streamers.

Positive breakdown streamers develop more and more intensively with higher applied voltage and eventually cause the gap to break down. The discharge is essentially the same as the onset streamer type but can extend much farther into the gap. The streamer current is more intense and may occur at a higher repetition rate. A streamer crossing the gap does not necessarily result in gap breakdown, which proves that the filamentary region of the streamer is not fully conducting.

15.1.3 AC Corona

When alternating voltage is used, the gradient at the highly stressed electrode varies continuously, both in intensity and in polarity. Different corona modes can be observed in the same cycle of the applied voltage. Figure 15.7 illustrates the development of different corona modes at a spherical protrusion as a function of the applied voltage. The corona modes can be readily identified by the discharge current. The following observations can be made:

- For short gaps, the ion space charges created in one half-cycle are absorbed by the electrodes in the same half-cycle. The same corona modes that develop near onset voltages can be observed, namely: negative Trichel streamers, positive onset streamers, and burst corona.
- For long gaps, the ion space charges created in one half-cycle are not completely absorbed by the electrodes, leaving residual space charges in the gap. These residual space charges are drawn back to the region of high field intensity in the following half-cycle and can influence discharge development. Onset streamers are suppressed in favor of the positive glow discharge. The following corona modes can be distinguished: negative Trichel streamers, negative glow discharge, positive glow discharge, and positive breakdown streamers.
- Negative streamers are not observed under AC voltage, owing to the fact that their onset gradient is higher than the breakdown voltage that occurs during the positive half-cycle.

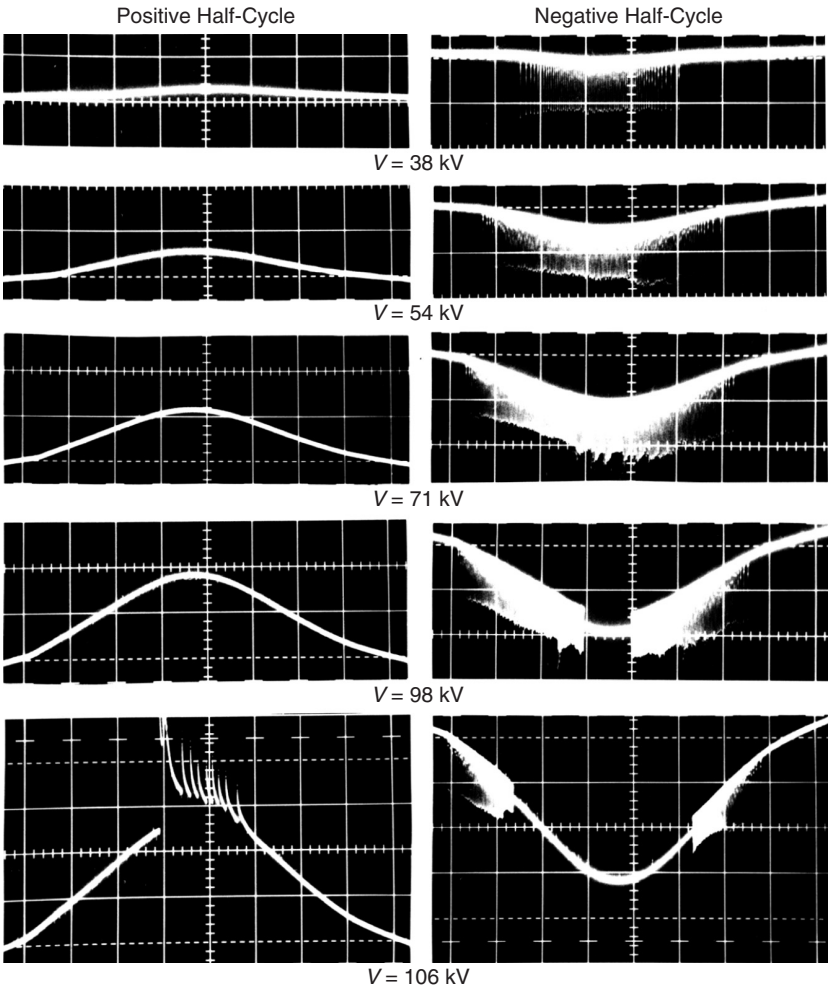

FIGURE 15.7 Corona modes under AC voltage. Electrode: conical protrusion ($\theta = 30°$) on a sphere ($D = 7$ cm); gap 25 cm; $R = 10$ kΩ. Scales: 50 μA/div., 1.0 ms/div. (From Trinh, N.G. and Jordan, I.B., *IEEE Trans.*, PAS-87, 1207, 1968; Trinh, N.G., *IEEE Electr. Insul. Mag.*, 11, 23, 1995a.)

15.2 Main Effects of Corona Discharges on Overhead Lines (Trinh, 1995b)

Impact of corona discharges on the design of high-voltage lines has been recognized since the early days of electric power transmission when the corona losses were the limiting factor. Even today, corona losses remain critical for HV lines below 300 kV. With the development of EHV lines operating at voltages between 300 and 800 kV, electromagnetic interferences become the designing parameters. For UHV lines operating at voltages above 800 kV, the audible noise appears to gain in importance over the other two parameters. The physical mechanisms of these effects—corona losses, electromagnetic interference, and audible noise—and their current evaluation methods are discussed below.

15.2.1 Corona Losses

The movement of ions of both polarities generated by corona discharges, and subjected to the applied field around the line conductors, is the main source of energy loss. For AC lines, the movement of the ion space charges is limited to the immediate vicinity of the line conductors, corresponding to their maximum displacement during one half-cycle, typically a few tens of centimeters, before the voltage changes polarity and reverses the ionic movement. For direct current (DC) lines, the ion displacement covers the whole distance separating the line conductors, and between the conductors and the ground.

Corona losses are generally described in terms of the energy losses per kilometer of the line. They are generally negligible under fair-weather conditions but can reach values of several hundreds of kilowatts per kilometer of line during foul weather. Direct measurement of corona losses is relatively complex, but foul-weather losses can be readily evaluated in test cages under artificial rain conditions, which yield the highest energy loss. The results are expressed in terms of the generated loss W, a characteristic of the conductor to produce corona losses under given operating conditions.

15.2.2 Electromagnetic Interference

Electromagnetic interference is associated with streamer discharges that inject current pulses into the conductor. These pulses of steep front and short duration have a high harmonic content, reaching the tens of megahertz range, as illustrated in Fig. 15.8, which shows the typical frequency spectra associated with various streamer modes (Juette, 1972). A tremendous research effort was devoted to the subject during the years 1950–1980 in an effort to evaluate the electromagnetic interference from HV lines. The most comprehensive contributions were made by Moreau and Gary (1972a,b) of Électricité de France, who introduced the concept of the excitation function, $\Gamma(\omega)$, which characterizes the ability of a line conductor to generate electromagnetic interference under the given operating conditions.

Consider first the case of a single-phase line, where the contribution to the electromagnetic interference at the measuring frequency, ω, from corona discharges developing at a section dx of the conductor is

$$j0(\omega) = \frac{C}{2\pi\varepsilon 0}\Gamma(\omega)\mathrm{d}x \tag{15.3}$$

where C is the capacitance per unit length of the line conductor to ground.

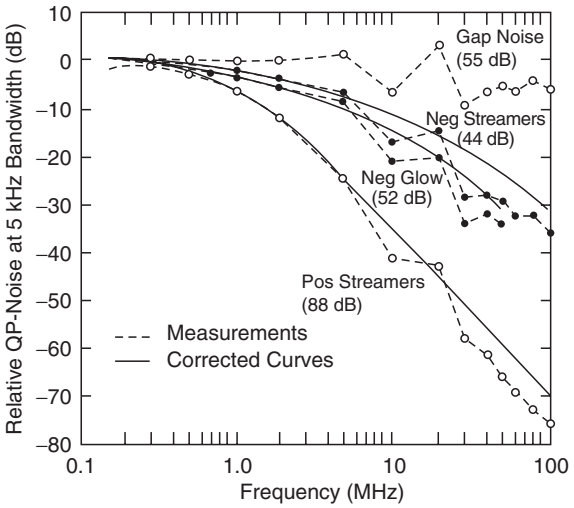

FIGURE 15.8 Relative frequency spectra for different noise types. (From Trinh, N.G., *IEEE Electr. Insul. Mag.*, 11, 5, 1995b; Juette, G.W., *IEEE Trans.*, PAS-91, 865, 1972.)

Upon injection, the discharge current pulse splits itself into two identical current pulses of half amplitude propagating in opposite directions away from the discharge site. At a point of observation located at a distance x along the line from the discharge site, the noise current is distorted according to

$$i(\omega, x)\ \mathrm{d}x = i0(\omega)\exp(-\gamma\ x)\ \mathrm{d}x = i0(\omega)\exp(-\alpha x)\,\mathrm{d}x \tag{15.4}$$

where γ represents the propagation constant, which can be approximated by its real component α.

The total noise current circulating in the line conductor is the sum of all contributions from the corona discharges along the conductor and is given by

$$I(\omega) = \sqrt{\int_{-\infty}^{\infty} [i(\omega, x)]^2\ \mathrm{d}x} = \frac{i0(\omega)}{\sqrt{\alpha}} \tag{15.5}$$

For a multiphase line, because of the high-frequency nature of the noise current, the calculation of the interference field must take account of the mutual coupling among the conductors, which further complicates the process (Gary, 1972; Moreau and Gary, 1972a,b). Modal analysis provides a convenient means of evaluating the noise currents on the line conductors. In this approach, the noise currents are first transposed into their modal components, which propagate without distortion along the line conductors at their own velocity according to the relation

$$[i0(\omega)\ \mathrm{d}x] = [M]\ [j0(\omega)\ \mathrm{d}x] \tag{15.6}$$

Consequently,

$$[j0(\omega)\ \mathrm{d}x] = [M]^{-1}[i0(\omega)\ \mathrm{d}x] \tag{15.7}$$

where $[M]$ is the modal transposition matrix and $j0(\omega)$ are the modal components of the injected noise current. The modal current at the measuring point located at a distance x from the injection point is

$$j(\omega, x)\ \mathrm{d}x = j0(\omega)\ \ \exp(-\alpha\ x)\ \mathrm{d}x \tag{15.8}$$

and the modal current component at the measuring point is

$$J(\omega) = \sqrt{\int_{-\infty}^{\infty} [\,j(\omega, x)]^2\ \mathrm{d}x} = \frac{j0(\omega)}{\sqrt{\alpha}} \tag{15.9}$$

or, in a general way

$$[\,J(\omega)] = \frac{1}{[\sqrt{\alpha}]}\,[\,j0(\omega)] = \frac{1}{[\sqrt{\alpha}]}\,[M]^{-1}[i0(\omega)] \tag{15.10}$$

Finally, the line current can be obtained from

$$[I(\omega)] = [M]\ [J(\omega)] \tag{15.11}$$

The magnetic and electric fields produced by the noise currents in the line conductors can then be evaluated for assessment of the electromagnetic interferences. Moreau and Gary (1972a,b) obtained good agreement between calculated and experimental results with the symmetrical modes of Clarke for the modal transposition:

$$[M] = \begin{bmatrix} 1/\sqrt{6} & 1/2 & 1/\sqrt{3} \\ -2/\sqrt{6} & 0 & 1/\sqrt{3} \\ 1/\sqrt{6} & -1/2 & 1/\sqrt{3} \end{bmatrix} \tag{15.12}$$

The attenuation coefficients at 0.5 MHz are 11.1, 54, and 342 Np/m for the modal currents, and the magnetic ground was assumed to be located at a depth equal to the penetration depth of the magnetic field, dp, as defined by

$$\mathrm{d}p = 2\sqrt{\frac{\rho}{\mu\omega}} \tag{15.13}$$

For a typical soil resistivity of 100 Ωm and a measuring frequency of 0.5 MHz, the depth of the magnetic ground is equal to 7.11 m. It is equal to 5.03 m at a measuring frequency of 1.0 MHz.

Circulation of the noise current in the line conductor effectively generates an electromagnetic interference field around the conductors, which is readily picked up by any radio or television receiver located in the vicinity of the HV line. The current practices characterize the interference field in terms of its electric component, $E(\omega)$, expressed in decibels (dB) above a reference level of 1 μV/m. Evaluation of the electromagnetic interference is usually made by first calculating the magnetic interference field $H(\omega)$ at the measuring point

$$H(\omega) = \sum_j \frac{1}{2\pi\ r_j} I_j(\omega)\ ar \tag{15.14}$$

The summation was made with respect to the number of phase conductors of the lines and their images with respect to the magnetic ground. The electric interference field can next be related to the magnetic interference field according to

$$E(\omega) = \sqrt{\frac{\mu 0}{\varepsilon 0}}\, H(\omega) \tag{15.15}$$

15.2.2.1 Television Interference

The frequency spectrum of corona discharges has cut-off frequencies around a few tens of megahertz. As a result, the interference levels at the television frequencies are very much attenuated. In fact, gap discharges, which generate sharp current pulse with nanosecond rise times, are the principal discharges that effectively interfere with the television reception. These discharges are produced by loose connections, a problem common on low-voltage distribution lines but rarely observed on high-voltage transmission lines. Another source of interference is related to reflections of television signals at high-voltage line towers, producing ghost images. However, the problem is not related in any way to corona activities on the line conductors (Juette, 1972).

15.2.3 Audible Noise

The high temperature in the discharge channel produced by the streamer creates a corresponding increase in the local air pressure. Consequently, a pulsating sound wave is generated from the discharge site, propagates through the surrounding ambient air, and is perfectly audible in the immediate vicinity of the HV lines. The typical octave-band frequency spectra of line corona in Fig. 15.9 contain discrete components corresponding to the second and higher harmonics of the line voltage superimposed on a relatively broadband noise, extending well into the ultrasonic range (Ianna et al., 1974). The octave-band measurements in this figure show a sharp drop at frequencies over 20 kHz, due principally to the limited frequency response of the microphone and associated sound-level meter.

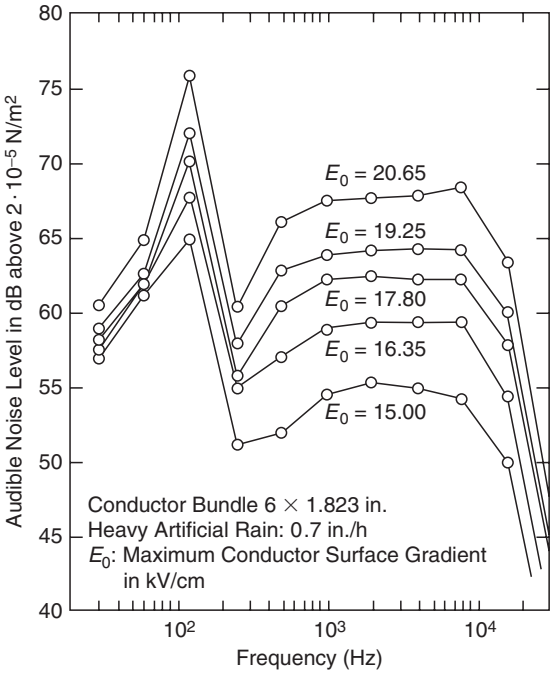

FIGURE 15.9 Octave-band frequency spectra of line corona audible noise at 10 m from the conductor. (From Trinh, N.G., *IEEE Electr. Insul. Mag.*, 11, 5, 1995b; Trinh, N.G. and Maruvada, P.S., *IEEE Trans.*, PAS-96, 312, 1977. With permission.)

Similar to the case of electromagnetic interference, the ability of the line conductors to produce audible noise is characterized by the generated acoustic power density A, defined as the acoustic power produced per unit length of the line conductor under specific operating conditions. The acoustic power generated by corona discharges developing in a portion dx of the conductor is then

$$\mathrm{d}A = A\ \mathrm{d}x \tag{15.16}$$

Its contribution to the acoustic intensity at a measuring point located at a distance r from the discharge site is

$$\mathrm{d}I = \frac{A}{4\pi r^2}\mathrm{d}x \tag{15.17}$$

The acoustic intensity at the measuring point is the sum of all contributions from corona discharge distributed along the conductor:

$$I(R) = 2A\int_{-\infty}^{\infty}\frac{1}{4\pi(R^2+x^2)}\mathrm{d}x = \frac{A}{2R} \tag{15.18}$$

where R is the distance from the measuring point to the conductor, and the integral is evaluated in terms of the longitudinal distance x along the conductor. Finally, the acoustic intensity at the measuring point is the sum of the contributions from the different phase conductors of the line

$$I(R) = \sum_j I_j\left(R_j\right) \tag{15.19}$$

The sound pressure, usually expressed in terms of decibel (dBA) above a reference level of 2×10^{-5} N/m^2 is

$$p(r) = \sqrt{\rho 0 \; C \; I} \tag{15.20}$$

15.2.4 Example of Calculation

It is obvious from the preceding sections that the effects of corona discharges on HV lines—the corona losses, the electromagnetic interferences, and audible noise—can be readily evaluated from the generated loss W, the excitation function $\Gamma(\omega)$, and the generated acoustic power density A of the conductor. The latter parameters are characteristics of the bundle conductor and are usually derived from tests in a test cage or on experimental line. An example calculation of the corona performance of an HV line is given below for the case of the Hydro-Québec's 735-kV lines under conditions of heavy rain. The line parameters are given in Table 15.1, together with the various corona-generated parameters taken from Trinh and Maruvada (1977). The calculation of the radio interference and audible noise levels will be made for a lateral distance of 15 m from the outer phase, i.e., at the limit of the right of way of the line.

Corona losses: The corona losses are the sum of the losses generated at the three phases of the line, which amount to 127.63 kW/km.

Radio interference: The calculation of the radio interference requires that the noise current be first transformed into its modal components. Consider a noise current of unit excitation function $\Gamma a(\omega) = 1.0$ μA/$\sqrt{\text{m}}$ circulating in phase A of the line. Because of the capacitive coupling, it induces currents to the other two phases of the line as well. For Hydro-Québec's 735-kV line, the capacitance matrix is

$$C = \begin{bmatrix} 11.204 & -2.241 & -0.73 \\ -2.241 & 11.605 & -2.241 \\ -0.73 & -2.241 & 11.204 \end{bmatrix}$$

and the noise current in phase A and its induced currents to phases B and C are

$$ia(\omega) = \begin{bmatrix} 11.204 \\ -2.241 \\ -0.73 \end{bmatrix}$$

The modal transformation using Eqs. (15.9)–(15.12) gives the following modal noise currents at the measuring point, taking into account the different attenuations of the modal currents:

$$Ja(\omega) = \begin{bmatrix} 16.472 & 10.321 & 2.31 \\ -30.497 & 0 & 1.998 \\ 16.472 & -10.321 & 2.31 \end{bmatrix}$$

TABLE 15.1 Hydro-Québec 735-kV Line

Distance between phase (m)	13.7	
Height of conductors (m)	19.8	
Number of subconductors	4	
Diameter of subconductor (cm)	3.05	
	Center phase	Outer phase
Electric field at the conductor surface (kVrms/cm)	19.79	18.46
Capacitance per unit length (pF/m)	10.57	
Generated loss W (W/m)	59.77	33.92
RI excitation function Γ (dB above 1 μA/$\sqrt{\text{m}}$)	43.52	39.59
Subconductor generated acoustic power density A (dBA above 1 μW/m)	3.28	−0.24

These modal currents, once transformed back to the current mode, Eq. (15.13), give the modal components of the noise currents flowing in the line conductors at the measuring point as related to the noise current injected to phase A:

$$Ia(\omega) = \begin{bmatrix} 6.725 & 7.298 & 1.333 \\ -13.449 & 0 & 1.333 \\ 6.725 & -7.298 & 1.333 \end{bmatrix}$$

These currents can then be used to calculate the magnetic and electric interference field using Eqs. (15.14) and (15.15):

$$Ha(\omega) = [0.0124 \quad 0.0449 \quad 0.0239]$$
$$Ea(\omega) = [4.674 \quad 16.938 \quad 9.017]$$

The corresponding electric interference level is 25.911 dB above 1 μV/m.

The above electric interference field and interference level are obtained assuming a noise excitation function of 1.0 $\mu A/\sqrt{m}$. For the case of interest, the excitation function at phase A is 39.59 dB and the corresponding interference level is 64.98 dB. By repeating the same process for the noise currents injected in phases B and C, one obtains effectively three sets of magnetic and electric field components generated by the circulation of the noise currents on the line conductors:

$$Eb(\omega) = [-8.653 \quad 0 \quad 7.80]$$
$$Ec(\omega) = [4.674 \quad -16.938 \quad 9.017]$$

Their contributions to the noise level are, respectively, 64.26 and 64.98 dB, resulting in a total noise level of 69.53 dB at the measuring point. The measuring frequency is 0.5 MHz.

Audible noise: Calculation of the audible noise is straightforward, since each phase of the line can be considered as an independent noise source. Consider the audible noise generated from phase A. The subconductor generated acoustic power density is -0.24 dBA or 1.58×10^{-5} μW/m for the bundle conductor. The acoustic intensity at 15 m from the outer phase of the line as given by Eq. (15.18) is 3.19×10^{-7} W/m^2 and the noise level is 55.14 dBA above 2×10^{-5} N/m^2.

By repeating the process for the other two phases of the line, the contributions to the acoustic intensity at the measuring point from the phases B and C of the line are 2.64×10^{-7} and 1.69×10^{-7} W/m^2, respectively, and the corresponding noise levels are 54.33 and 52.38 dBA. The total noise level is 58.87 dBA.

15.3 Impact on the Selection of Line Conductors

15.3.1 Corona Performance of HV Lines

Corona performance is a general term used to characterize the three main effects of corona discharges developing on the line conductors and their related hardware, namely corona losses (CL), electromagnetic interference (RI), and audible noise (AN). All are sensitive to weather conditions, which dictate the corona activities. Corona losses can be described by a lump figure, which is equal to the total energy losses per kilometer of the line. Both the RI and the AN levels vary with the distance from the line and are best described by lateral profiles, which show the variations in the RI and AN level with the lateral distance from the line. Typical lateral profiles are presented in Figs. 15.10 and 15.11 for a number of HV lines under foul-weather conditions. For convenience, the interference and noise levels at the edge

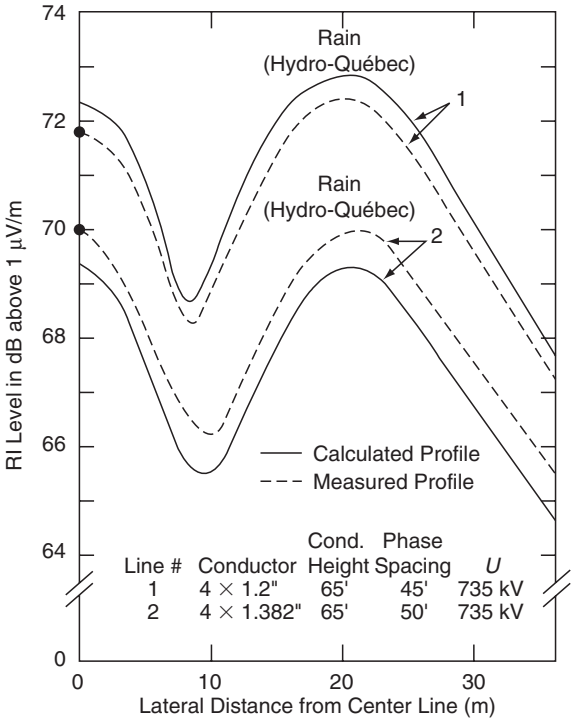

FIGURE 15.10 Comparison of calculated and measured RI performances of Hydro-Québec 735-kV lines at 1 MHz and using natural modes. (From Trinh, N.G., *IEEE Electr. Insul. Mag.*, 11, 5, 1995b; Trinh, N.G. and Maruvada, P.S., *IEEE Trans.*, PAS-96, 312, 1977. With permission.)

of the right-of-way, typically 15 m from the outside phases of the line, are generally used to quantify the interference and noise level.

The time variations in the corona performance of HV lines is best described in terms of a statistical distribution, which shows the proportion of time that the energy losses, the electromagnetic interference, and audible noise exceed their specified levels. Figure 15.12 illustrates typical corona performances of Hydro-Québec's 735-kV lines as measured at the edge of the right-of-way. It can be seen that the RI and AN levels vary over wide ranges. In addition, the cumulative distribution curves show a typical inverted-S shape, indicating that the recorded data actually result from the combination of more than one population, usually associated with fair- and foul-weather conditions.

DC coronas are less noisy than AC coronas. In effect, although DC lines can become very lossy during foul weather, the radio interference and audible noises are significantly reduced. This behavior is related to the fact that water drops become elongated, remain stable, and produce glow corona modes rather than streamers in a DC field (Ianna et al., 1974).

15.3.2 Approach to Control the Corona Performance

The occurrence of corona discharges on line conductors is dictated essentially by the local field intensity, which, in turn, is greatly affected by the surface conditions, e.g., rugosity, water drops, snow and ice particles, etc. For a smooth cylindrical conductor, the corona onset field is well described by Peek's experimental law

$$Ec = 30\ m\ \delta\left(1 + \frac{0.301}{\sqrt{\delta a}}\right) \tag{15.21}$$

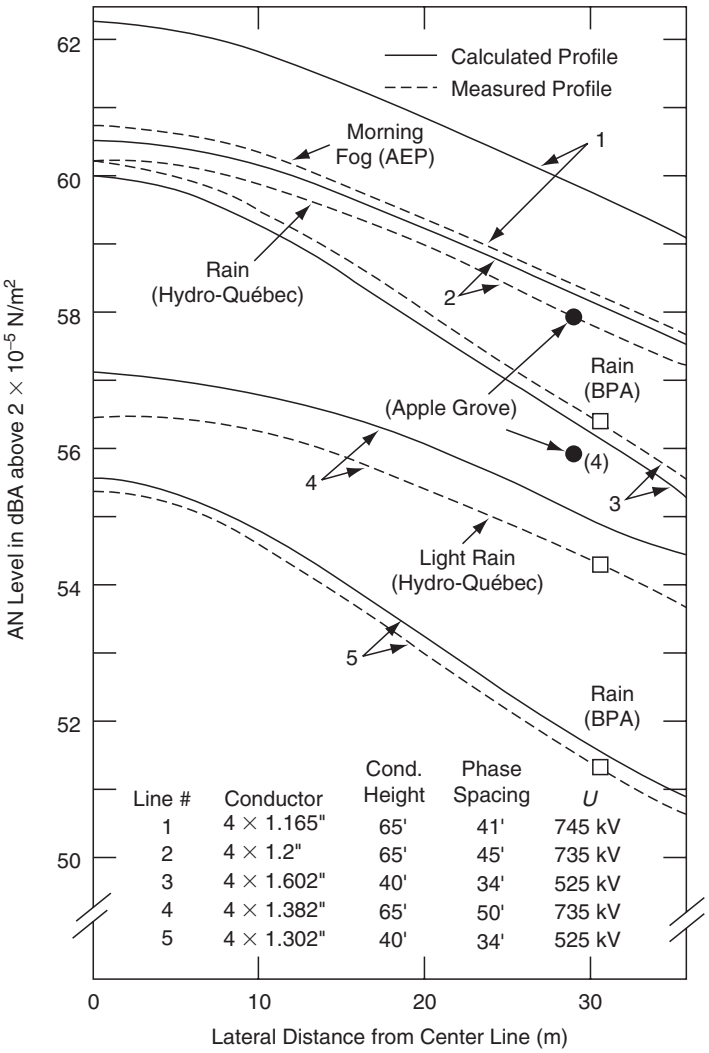

FIGURE 15.11 Comparison of calculated and measured AN performances of HV lines. (From Trinh, N.G., *IEEE Electr. Insul. Mag.*, 11, 5, 1995b; Trinh, N.G. and Maruvada, P.S., *IEEE Trans.*, PAS-96, 312, 1977.)

where *Ec* is the corona onset field, *a* is the radius of the conductor, and *m* is an experimental factor to take account of the surface conditions. Typical values of *m* are 0.8–0.9 for a dry-aged conductor, 0.5–0.7 for a conductor under foul-weather conditions, and δ is the relative air density factor.

The above corona-onset condition emphasizes the great sensitivity of corona activities to the conductor surface condition and, hence, to changes in weather conditions. In effect, although the line voltage and the nominal conductor surface gradient remain constant, the surface condition factor varies continuously due to the exposure of line conductors to atmospheric conditions. The changes are particularly pronounced during foul weather as a result of the numerous discharge sites associated with water drops, snow, and ice particles deposited on the conductor surface.

Adequate corona performance of HV lines is generally achieved by a proper control of the field intensity at the surface of the conductor. It can be well illustrated by the simple case of a single-phase, single-conductor line for which the field intensity at the conductor surface is

$$E_0 = \frac{1}{\ln\left(\frac{2h}{a}\right)} \frac{U}{a} \leq Ec \qquad (15.22)$$

It can be seen that the field intensity at the conductor surface is inversely proportional to its radius and, to a lesser extent, to the height of the conductor above ground. By properly dimensioning the conductor, the field intensity at its surface can be kept below the fair-weather corona-onset field for an adequate control of the corona activities and their undesirable effects.

With the single-conductor configuration, the size required for the conductor to be corona-free under fair-weather conditions is roughly proportional to the line voltage, and consequently will reach unrealistic values when the latter exceeds some 400 kV. Introduced in 1910 by Whitehead to increase the transmission capability of overhead lines (Whitehead, 1910), the concept of bundled conductors quickly revealed itself as an effective means of controlling the field intensity at the conductor surface, and hence, the line corona activities. This is well illustrated by the results in Table 15.2, which compare the single conductor design required to match the bundle performances in terms of power transmission capabilities, and the maximum conductor surface gradient for different line voltages. Bundled conductors are now used extensively in EHV lines rated 315 kV and higher; as a matter of fact, HV lines as we know them today would not exist without the introduction of conductor bundles.

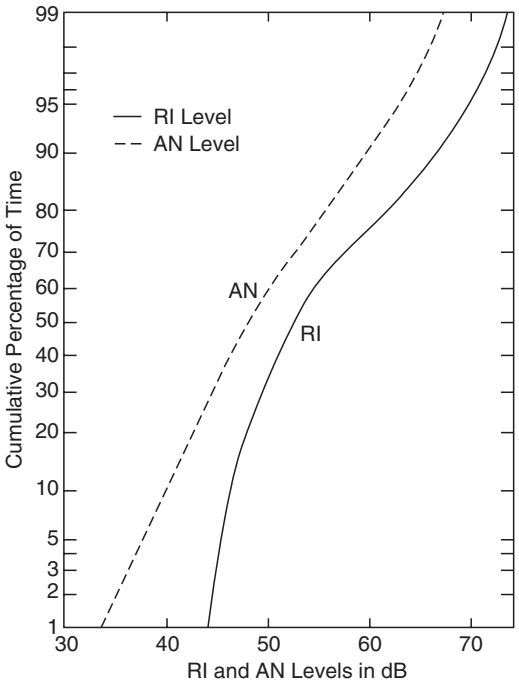

FIGURE 15.12 Cumulative distribution of RI and AN levels measured at 15 m from the outer phases of Hydro-Québec 735-kV lines. (From Trinh, N.G., *IEEE Electr. Insul. Mag.*, 11, 5, 1995b.)

15.3.3 Selection of Line Conductors

Even with the use of bundled conductors, it is not economically justifiable to design line conductors that would be corona-free under all weather conditions. The selection of line conductors is therefore made in terms of them being relatively corona-free under fair weather. While corona activities are tolerated under

TABLE 15.2 Comparison of Single and Bundled Conductors' Performances

Line voltage (kV)	400	735	1100
Distance between phases (m)	12	13.7	17
Number of subconductors	2	4	8
Bundle diameter (cm)	45	65	84
Conductor diameter (cm)	3.2	3.05	3.2
Corona onset gradient, $m = 0.85$, (kVrms/cm)	22.32	22.04	22.32
Maximum surface gradient (kVrms/cm)	16.3	19.79	17.3
Single conductor diameter of the same gradient (cm)	4.7	8.5	13.8
Transmission capability (GW)	0.5	2.0	4.9
Single conductor diameter of the same transmission capability (cm)	8.5	22	64

foul weather, their effects are controlled to acceptable levels at the edge of the rights-of-way of the line. For AC lines, the design levels of 70 dB for the radio interference and 60 dBA for the audible noise at the edge of the right-of-way are often used (Trinh et al., 1974). These levels may be reached during periods of foul weather, and for a specified annual proportion of time, typically 15–20%, depending on the local distribution of the weather pattern. The design process involves extensive field calculations and experimental testing to determine the number and size of the line conductors required to minimize the undesirable effects of corona discharges. Current practices in dimensioning HV-line conductors usually involve two stages of selection according to their worst-case and long-term corona performances.

15.3.3.1 Worst-Case Performance

Several conductor configurations (number, spacing, and diameter of the subconductors) are selected with respect to their worst-case performances which, for AC lines, correspond to foul-weather conditions, in particular heavy-rain. Evaluation of the conductor worst-case performance is best done in test cages under artificial heavy-rain conditions (Trinh and Maruvada, 1977). Test cages of square section, typically 3 m $\times$ 3 m, and a few tens of meters long, are adequate for evaluating full-size conductor bundles located along its central axis, for lines up to the 1500-kV class. The advantages of this experimental setup are the relatively modest test voltage required to reproduce the same field distribution on real-size bundled conductors, and the possibility of artificially producing the heavy-rain conditions. The worst-case performance of various bundled conductors can then be determined over a wide range of surface gradients.

Under DC voltage, the worst-case corona performance is not directly related to foul-weather conditions. Although heavy rain was found to produce the highest losses, both the electromagnetic interference and the audible noise levels decrease under rain conditions. This behavior is related to the fact that under DC field conditions, the water droplets have an optimum shape, favorable to the development of stable glow-corona modes (Ianna et al., 1974). For this reason, test cage is less effective in evaluating the worst-case DC performance of bundled conductors.

A significant amount of data was gathered in cage tests at IREQ during the 1970s and provided the database for the development of a method to predict the worst-case performance of bundled conductors for AC voltage (Trinh and Maravuda, 1977). The results presented in Figs. 15.10 and 15.11, which compare the calculated and measured lateral RI and AN profiles of a number of HV lines, illustrate the good concordance of this approach. Commercial software exist that evaluate the worst-case performance of HV-line conductors using available experimental data obtained in cage tests under conditions of artificial heavy rain, making it possible to avoid undergoing tedious and expensive tests to help select the best configurations for line conductors for a given rating of the line.

15.3.3.2 Long-Term Corona Performance

Because of their wide range of variation in different weather conditions, representative corona performances of HV line are best evaluated in their natural environment. Test lines are generally used in this study that involves energizing the conductors for a sufficiently long period, usually 1 year to cover most of the weather conditions, and recording their corona performances together with the weather conditions. The higher cost of the long-term corona performance study usually limits its application to a small number of conductor configurations selected from their worst-case performance.

It should be noted that best results for the long-term corona performance evaluated on test lines are obtained when the weather pattern at the test site is similar to that existing along the actual HV line. A direct transposition of the results is then possible. If this condition is not met, some interpretation of the experimental data is needed. This is done by first decomposing the recorded long-term data into two groups, corresponding to the fair- and foul-weather conditions, then recombining these data according to the local weather pattern to predict the long-term corona performance along the line.

15.4 Conclusions

This chapter on transmission systems has reviewed the physics of corona discharges and discussed their impact on the design of high-voltage lines, specifically in the selection of the line conductors. The following conclusions can be drawn.

Corona discharges can develop in different modes, depending on the equilibrium state existing under a given test condition, between the buildup and removal of ion space charges from the immediate vicinity of the highly stressed electrode. Three different corona modes—Trichel streamer, negative glow, and negative streamer—can be observed at the cathode with increasing applied field intensities. With positive polarity, four different corona modes are observed, namely burst corona, onset streamers, positive glow, and breakdown streamers.

While all corona modes produce energy losses, the streamer discharges also generate electromagnetic interference and audible noise in the immediate vicinity of HV lines. These parameters are currently used to evaluate the corona performance of conductor bundles and to predict the energy losses and environmental impact of HV lines before their installation.

Adequate control of line corona is obtained by controlling the surface gradient at the line conductors. The introduction of bundled conductors in 1910 has greatly influenced the development of HV lines to today's EHVs.

Commercial software is available to select the bundle configuration: number and size of the subconductors, with respect to corona performances, which can be verified in test cages and lines in the early stage of new HV-line projects.

References

Bateman, L.A., Haywood, R.W., and Brooks, R.F., Nelson River DC Transmission Project, *IEEE Trans.*, PAS-88, 688, 1969.

Bortnik, I.M., Belyakov, N.N., Djakov, A.F., Horoshev, M.I., Ilynichin, V.V., Kartashev, I.I., Nikitin, O.A., Rashkes, V.S., Tikhodeyev, N.N., and Volkova, O.V., 1200 kV Transmission Line in the USSR: The First Results of Operation, in CIGRE Report No. 38-09, Paris, August 1988.

Dawson, G.A., A model for streamer propagation, *Zeitchrift fur Physic*, 183, 159, 1965.

Gary, C.H., The theory of the excitation function: A demonstration of its physical meaning, *IEEE Trans.*, PAS-91, 305, 1972.

Ianna, F., Wilson, G.L., and Bosak, D.J., Spectral characteristics of acoustic noise from metallic protrusion and water droplets in high electric fields, *IEEE Trans.*, PAS-93, 1787, 1974.

Juette, G.W., Evaluation of television interference from high-voltage transmission lines, *IEEE Trans.*, PAS-91, 865, 1972.

Krishnayya, P.C.S., Lambeth, P.J., Maruvada, P.S., Trinh, N.G., and Desilets, G., An Evaluation of the R&D Requirements for Developing HVDC Converter Stations for Voltages above ± 600 kV, in CIGRE Report No. 14–07, Paris, August 1988.

Lacroix, R. and Charbonneau, H., Radio interference from the first 735-kV line of Hydro-Quebec, *IEEE Trans.*, PAS-87, 932, 1968.

Loeb, L.B., *Electrical Corona*, University of California Press, Berkeley, LA, 1965.

Moreau, M.R. and Gary, C.H., Predetermination of the radio-interference level of high voltage transmission lines—I: Predetermination of the excitation function, *IEEE Trans.*, PAS-91, 284, 1972a.

Moreau, M.R. and Gary, C.H., Predetermination of the radio-interference level of high voltage transmission lines—II: Field calculating method, *IEEE Trans.*, PAS-91, 292, 1972b.

Raether, H., *Electron Avalanches and Breakdown in Gases*, Butterworth Co., London, 1964.

Trinh, N.G., Partial discharge XIX: Discharge in air—Part I: Physical mechanisms, *IEEE Electr. Insul. Mag.*, 11, 23, 1995a.

Trinh, N.G., Partial discharge XX: Partial discharges in air—Part II: Selection of line conductors, *IEEE Electr. Insul. Mag.*, 11, 5, 1995b.

Trinh, N.G. and Jordan, I.B., Modes of corona discharges in air, *IEEE Trans.*, PAS-87, 1207, 1968.
Trinh, N.G. and Jordan, I.B., Trichel streamers and their transition into the pulseless glow discharge, *J. Appl. Physics*, 41, 3991, 1970.
Trinh, N.G. and Maruvada, P.S., A method of predicting the corona performance of conductor bundles based on cage test results, *IEEE Trans.*, PAS-96, 312, 1977.
Trinh, N.G., Maruvada, P.S., and Poirier, B., A comparative study of the corona performance of conductor bundles for 1200-kV transmission lines, *IEEE Trans.*, PAS-93, 940, 1974.
Whitehead, J.B., Systems of Electrical Transmission, U.S. Patent No. 1,078,711, 1910.

16

Geomagnetic Disturbances and Impacts upon Power System Operation

John G. Kappenman
Metatech Corporation

16.1 Introduction

Reliance of society on electricity for meeting essential needs has steadily increased for many years. This unique energy service requires coordination of electrical supply, demand, and delivery—all occurring at the same instant. Geomagnetic disturbances which arises from phenomena driven by solar activity commonly called space weather can cause correlated and geographically widespread disruption to these complex power grids. The disturbances to the Earth's magnetic field causes geomagnetically induced currents (GICs, a near-DC current typically with $f < 0.01$ Hz) to flow through the power system, entering and exiting the many grounding points on a transmission network. GICs are produced when shocks resulting from sudden and severe magnetic storms subject portions of the Earth's surface to fluctuations in the planet's normally quiescent magnetic field. These fluctuations induce electric fields across the Earth's surface—which causes GICs to flow through transformers, power system lines, and grounding points. Only a few amperes (A) are needed to disrupt transformer operation, but over 300 A have been measured in the grounding connections of transformers in affected areas. Unlike threats due to ordinary weather, space weather can readily create large-scale problems because the footprint of a storm can extend across a continent. As a result, simultaneous widespread stress occurs across a power grid to the point where correlated widespread failures and even regional blackouts may occur.

Large impulsive geomagnetic field disturbances pose the greatest concern for power grids in close proximity to these disturbance regions. Large GICs are most closely associated with geomagnetic field disturbances that have high rate-of-change; hence a high-cadence and region-specific analysis of dB/dt of the geomagnetic field provides a generally scalable means of quantifying the relative level of GIC threat. These threats have traditionally been understood as associated with auroral electrojet intensifications at an altitude of ~100 km which tend to locate at mid- and high-latitude locations during geomagnetic storms. However, both research and observational evidence have determined that the geomagnetic storm and associated GIC risks are broader and more complex than this traditional view (Kappenman, 2005). Large GIC and associated power system impacts have been observed for differing geomagnetic disturbance source regions and propagation processes and in power grids at low geomagnetic latitudes (Erinmez et al., 2002). This includes the traditionally perceived impulsive disturbances originating from ionospheric electrojet intensifications. However, large GICs have also been associated with impulsive geomagnetic field disturbances such as those during an arrival shock of a large solar wind structure called coronal mass ejection (CME) that will cause brief impulsive disturbances even at very low latitudes. As a result, large GICs can be observed even at low- and midlatitude locations for brief periods of time during these events (Kappenman, 2004). Recent observations also confirm that geomagnetic field disturbances usually associated with equatorial current system intensifications can be a source of large magnitude and long duration GIC in power grids at low and equatorial regions (Erinmez et al., 2002). High solar wind speed can also be the source of sustained pulsation of the geomagnetic field (Kelvin–Helmholtz shearing), which has caused large GICs. The wide geographic extent of these disturbances implies GIC risks to power grids that have never considered the risk of GIC previously, largely because they were not at high-latitude locations.

Geomagnetic disturbances will cause the simultaneous flow of GICs over large portions of the interconnected high-voltage transmission network, which now span most developed regions of the world. As the GIC enters and exits the thousands of ground points on the high-voltage network, the flow path takes this current through the windings of large high-voltage transformers. GIC, when present in transformers on the system will produce half-cycle saturation of these transformers, the root cause of all related power system problems. Since this GIC flow is driven by large geographic-scale magnetic field disturbances, the impacts to power system operation of these transformers will be occurring simultaneously throughout large portions of the interconnected network. Half-cycle saturation produces voltage regulation and harmonic distortion effects in each transformer in quantities that build cumulatively over the network. The result can be sufficient to overwhelm the voltage regulation capability and the protection margins of equipment over large regions of the network. The widespread but correlated impacts can rapidly lead to systemic failures of the network. Power system designers and operators expect networks to be challenged by the terrestrial weather, and where those challenges were fully understood in the past, the system design has worked extraordinarily well. Most of these terrestrial weather challenges have largely been confined to much smaller regions than those encountered due to space weather. The primary design approach undertaken by the industry for decades has been to weave together a tight network, which pools resources and provides redundancy to reduce failures. In essence, an unaffected neighbor helps out the temporarily weakened neighbor. Ironically, the reliability approaches that have worked to make the electric power industry strong for ordinary weather, introduce key vulnerabilities to the electromagnetic coupling phenomena of space weather. As will be explained, the large continental grids have become in effect a large antenna to these storms. Further, space weather has a planetary footprint, such that the concept of unaffected neighboring system and sharing the burden is not always realizable. To add to the degree of difficulty, the evolution of threatening space weather conditions are amazingly fast. Unlike ordinary weather patterns, the electromagnetic interactions of space weather are inherently instantaneous. Therefore, large geomagnetic field disturbances can erupt on a planetary-scale within the span of a few minutes.

16.2 Power Grid Damage and Restoration Concerns

The onset of important power system problems can be assessed in part by experience from contemporary geomagnetic storms. At geomagnetic field disturbance levels as low as 60–100 nT/min (a measure of the rate of change in the magnetic field flux density over the Earth's surface), power system operators have noted system upset events such as relay misoperation, the offline tripping of key assets, and even high levels of transformer internal heating due to stray flux in the transformer from GIC-caused half-cycle saturation of the transformer magnetic core. Reports of equipment damage have also included large electric generators and capacitor banks.

Power networks are operated using what is termed as "$N-1$" operation criterion. That is, the system must always be operated to withstand the next credible disturbance contingency without causing a cascading collapse of the system as a whole. This criterion normally works very well for the well-understood terrestrial environment challenges, which usually propagate more slowly and are more geographically confined. When a routine weather-related single-point failure occurs, the system needs to be rapidly adjusted (requirements typically allow a 10–30 min response time after the first incident) and positioned to survive the next possible contingency. Geomagnetic field disturbances during a severe storm can have a sudden onset and cover large geographic regions. Geomagnetic field disturbances can therefore cause near-simultaneous, correlated, multipoint failures in power system infrastructures, allowing little or no time for meaningful human interventions that are intended within the framework of the $N-1$ criterion. This is the situation that triggered the collapse of the Hydro Quebec power grid on March 13, 1989, when their system went from normal conditions to a situation where they sustained seven contingencies (i.e., $N-7$) in an elapsed time of 57 s; the province-wide blackout rapidly followed with a total elapsed time of 92 s from normal conditions to a complete collapse of the grid. For perspective, this occurred at a disturbance intensity of approximately 480 nT/min over the region (Fig. 16.1). A recent examination by Metatech of historically large disturbance intensities indicated that disturbance levels greater than 2000 nT/min have been observed even in contemporary storms on at least three occasions over the last 30 years at geomagnetic latitudes of concern for the North American power grid infrastructure and most other similar world locations: August 1972, July 1982, and March 1989. Anecdotal information from older storms suggests that disturbance levels may have reached nearly 5000 nT/min, a level $\sim$10 times greater than the environment which triggered the Hydro Quebec collapse (Kappenman, 2005). Both observations and simulations indicate that as the intensity of the disturbance increases, the relative levels of GICs and related power system impacts will also proportionately increase. Under these scenarios, the scale and speed of problems that could occur on exposed power grids has the potential to cause widespread and severe disruption of bulk power system operations. Therefore, as storm environments reach higher intensity levels, it becomes more likely that these events will precipitate widespread blackouts to exposed power grid infrastructures.

16.3 Weak Link in the Grid: Transformers

The primary concern with GIC is the effect that they have on the operation of a large power transformer. Under normal conditions the large power transformer is a very efficient device for converting one voltage level into another. Decades of design engineering and refinement have increased efficiencies and capabilities of these complex apparatus to the extent that only a few amperes of AC exciting current are necessary to provide the magnetic flux for the voltage transformation in even the largest modern power transformer.

However, in the presence of GIC, the near-direct current essentially biases the magnetic circuit of the transformer with resulting disruptions in performance. The three major effects produced by GIC in transformers are (1) the increased reactive power consumption of the affected transformer, (2) the

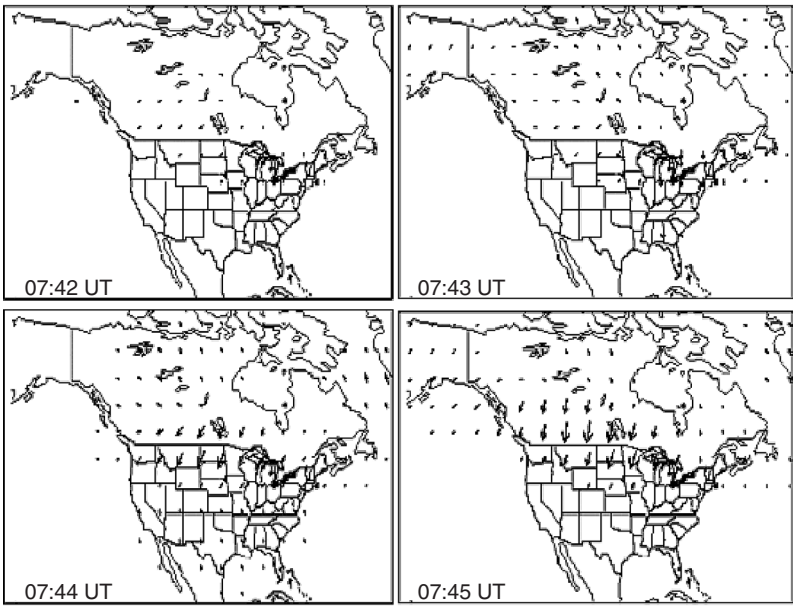

FIGURE 16.1 Four minutes of a superstorm. Space weather conditions capable of threatening power system reliability can rapidly evolve. The system operators at Hydro Quebec and other power system operators across North America faced such conditions during the March 13, 1989 Superstorm. The above slides show the rapid development and movement of a large geomagnetic field disturbance between the times 7:42 to 7:45 UT (2:42 to 2:45 EST) on March 13, 1989. The disturbance of the magnetic field began intensifying over the eastern US–Canada border and then rapidly intensified while moving to the west across North America over the span of a few minutes. With this rapid geomagnetic field disturbance onset, the Hydro Quebec system went from normal operating conditions to complete collapse in a span of just 90 s due to resulting GIC impacts on the grid. The magnetic field disturbances observed at the ground are caused by large electrojet current variations that interact with the geomagnetic field. The dB/dt intensities ranged from 400 nT/min at Ottawa at 7:44 UT to over 892 nT/min at Glen Lea. Large-scale rapid movement of this disturbance was evident.

increased even and odd harmonics generated by the half-cycle saturation, and (3) the possibilities of equipment damaging stray flux heating. These distortions can cascade problems by disrupting the performance of other network apparatus, causing them to trip off-line just when they are most needed to protect network integrity. For large storms, the spatial coverage of the disturbance is large and hundreds of transformers can be simultaneously saturated, a situation that can rapidly escalate into a network-wide voltage collapse. In addition, individual transformers may be damaged from overheating due to this unusual mode of operation, which can result in long-term outages to key transformers in the network. Damage of these assets can slow the full restoration of power grid operations.

Transformers use steel in their cores to enhance their transformation capability and efficiency, but this core steel introduces nonlinearities into their performance. Common design practice minimizes the effect of the nonlinearity while also minimizing the amount of core steel. Therefore, the transformers are usually designed to operate over a predominantly linear range of the core steel characteristics (as shown in Fig. 16.2) with only slightly nonlinear conditions occurring at the voltage peaks. This produces a relatively small exciting current (Fig. 16.3). With GIC present, the normal operating point on the core steel saturation curve is offset and the system voltage variation that is still impressed on the transformer causes operation in an extremely nonlinear portion of the core steel characteristic for half of the AC cycle (Fig. 16.2), hence, the term half-cycle saturation.

Because of the extreme saturation that occurs on half of the AC cycle, the transformer now draws an extremely large asymmetrical exciting current. The waveform in Fig. 16.3 depicts a typical example from field tests of the exciting current from a three-phase 600 MVA power transformer that has 75 A of

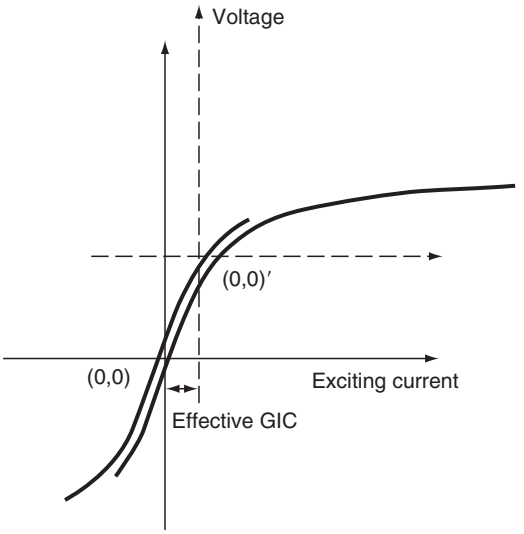

FIGURE 16.2 The presence of GIC causes the transformer magnetization characteristics to be biased or offset due to the DC. Therefore on one-half of the AC cycle, the transformer is driven into saturation by the combination of applied voltage and DC bias. Normal excitation operation is shown in the left curve, the biased operation in the right.

GIC in the neutral (25 A per phase). Spectrum analysis reveals this distorted exciting current to be rich in even, as well as odd harmonics. As is well documented, the presence of even a small amount of GIC (3 to 4 A per phase or less) will cause half-cycle saturation in a large transformer.

Since the exciting current lags the system voltage by 90°, it creates reactive power loss in the transformer and the impacted power system. Under normal conditions, transformer reactive power loss is very small. However, the several orders of magnitude increase in exciting current under half-cycle saturation also results in extreme reactive power losses in the transformer. For example, the three-phase reactive power loss associated with the abnormal exciting current of Fig. 16.3 produces a reactive power loss of over 40 MVars for this transformer alone. The same transformer would draw less than 1 MVar under normal conditions. Figure 16.4 provides a comparison of reactive power loss for two core types of transformers as a function of the amount of GIC flow.

Under a geomagnetic storm condition in which a large number of transformers are experiencing a simultaneous flow of GIC and undergoing half-cycle saturation, the cumulative increase in reactive power demand can be significant enough to impact voltage regulation across the network, and in extreme situations, lead to network voltage collapse.

The large and distorted exciting current drawn by the transformer under half-cycle saturation also poses a hazard to operation of the network because of the rich source of even and odd harmonic currents this injects into the network and the undesired interactions that these harmonics may cause with relay and protective systems or other power system apparatus. Figure 16.5 summarizes the spectrum analysis of the asymmetrical exciting current from Fig. 16.3. Even and odd harmonics are present typically in the first 10 orders and the variation of harmonic current production varies somewhat with the level of GIC, the degree of half-cycle saturation, and the type of transformer core.

With the magnetic circuit of the core steel saturated, the magnetic core will no longer contain the flow of flux within the transformer. This stray flux will impinge upon or flow through adjacent paths such as the transformer tank or core-clamping structures. The flux in these alternate paths can concentrate to the densities found in the heating elements of a kitchen stove. This abnormal operating regime can persist for extended periods as GIC flows from storm events can last for hours. The hot spots that may then form can severely damage the paper-winding insulation, produce gassing and combustion of the

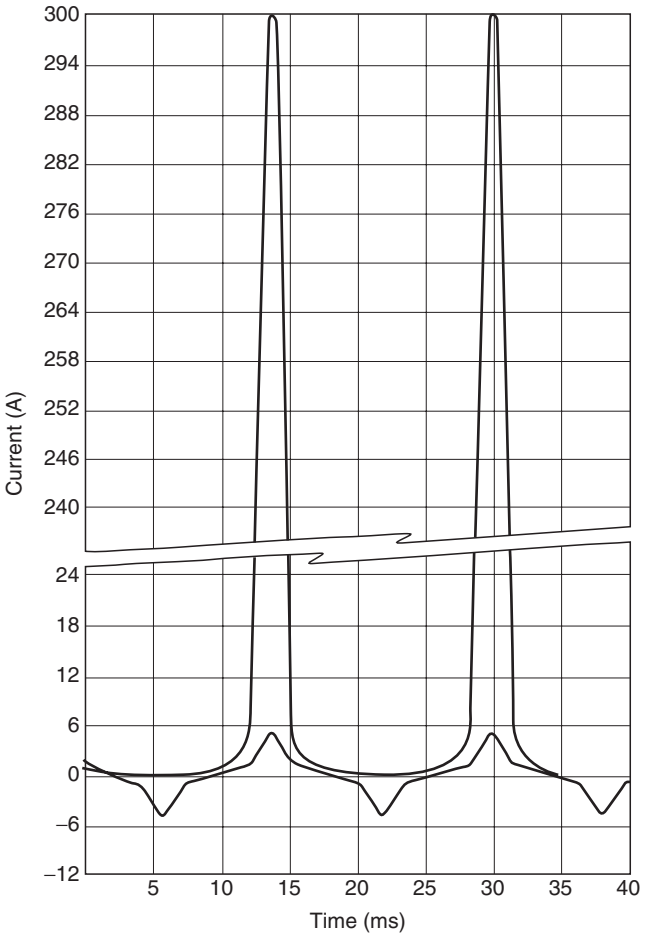

FIGURE 16.3 Under normal conditions, the excitation current of this 600 MVA 500/230 kV transformer is less than 1% of transformer rated current. However, with 25 A/phase of GIC present, the excitation current drawn by the transformer (top curve) is highly distorted by the half-cycle saturation conditions and has a large peak magnitude rich in harmonics.

transformer oil, or lead to other serious internal and or catastrophic failures of the transformer. Such saturation and the unusual flux patterns which result, are not typically considered in the design process and, therefore, a risk of damage or loss of life is introduced.

One of the more thoroughly investigated incidents of transformer stray flux heating occurred in the Allegheny Power System on a 350 MVA 500/138 kV autotransformer at their Meadow Brook Substation near Winchester, Virginia. The transformer was first removed from service on March 14, 1989, because of high gas levels in the transformer oil which were a by-product of internal heating. The gas-in-oil analysis showed large increases in the amounts of hydrogen, methane, and acetylene, indicating core and tank heating. External inspection of the transformer indicated four areas of blistering or discolored paint due to tank surface heating. In the case of the Meadow Brook transformer, calculations estimate the flux densities were high enough in proximity to the tank to create hot spots approaching 400°C. Reviews made by Allegheny Power indicated that similar heating events (though less severe) occurred in several other large power transformers in their system due to the March 13 disturbance. Figure 16.6 is a recording that Allegheny Power made on their Meadow Brook transformer during a storm in 1992. This measurement shows an immediate transformer tank hot spot developing in response to a surge in GIC

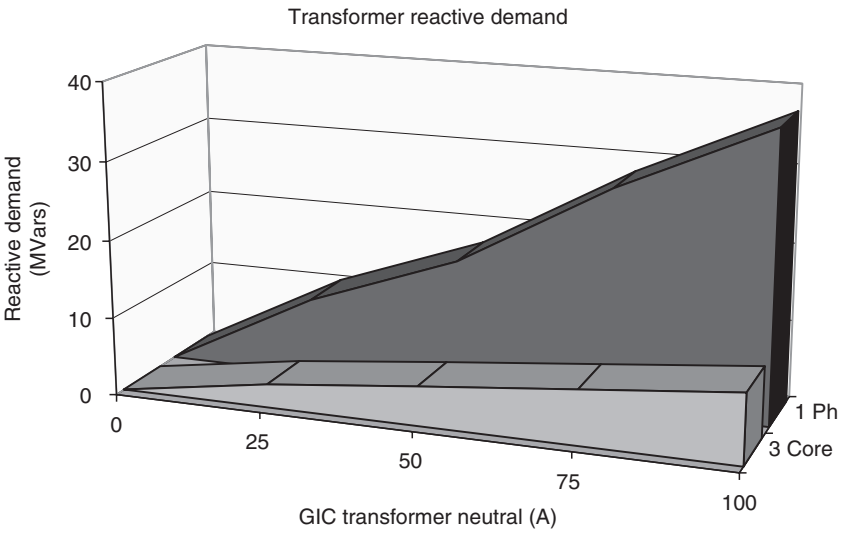

FIGURE 16.4 The exciting current drawn by half-cycle saturation conditions shown in Fig. 16.3 produces a reactive power loss in the transformer as shown in the top plot. This reactive loss varies with GIC flow as shown. This was measured from field tests of a three-phase bank of single-phase 500/230 kV transformers. Also shown in the bottom curve is measured reactive demand vs. GIC from a 230/115 kV three-phase three-legged core-form transformer. Transformer core design is a significant factor in estimating GIC reactive power impact.

entering the neutral of the transformer, while virtually no change is evident in the top oil readings. Because the hot spot is confined to a relatively small area, standard bulk top oil or other over temperature sensors would not be effective deterrents to use to alarm or limit exposures for the transformer to these conditions.

Designing a large transformer that would be immune to GIC would be technically difficult and prohibitively costly. The ampere turns of excitation (the product of the normal exciting current and the

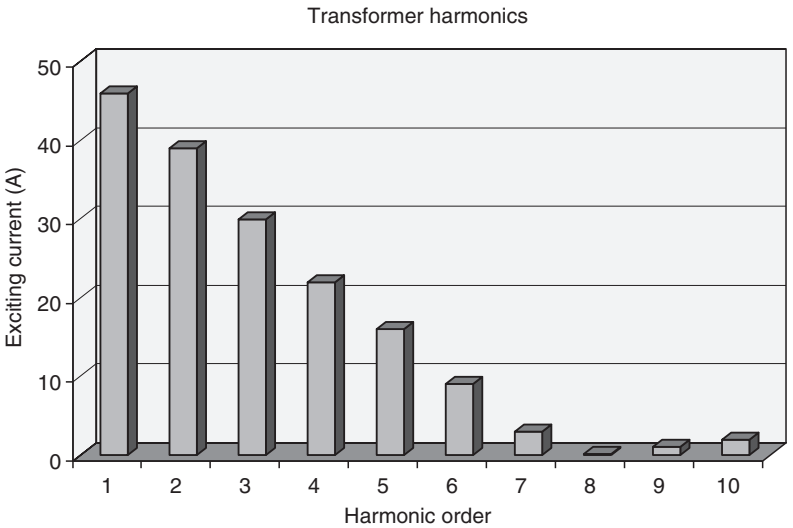

FIGURE 16.5 The distorted transformer exciting current shown in Fig. 16.3 has even and odd harmonic current distortion. This spectrum analysis was half-cycle saturation conditions resulting from a GIC flow of 25 A per phase.

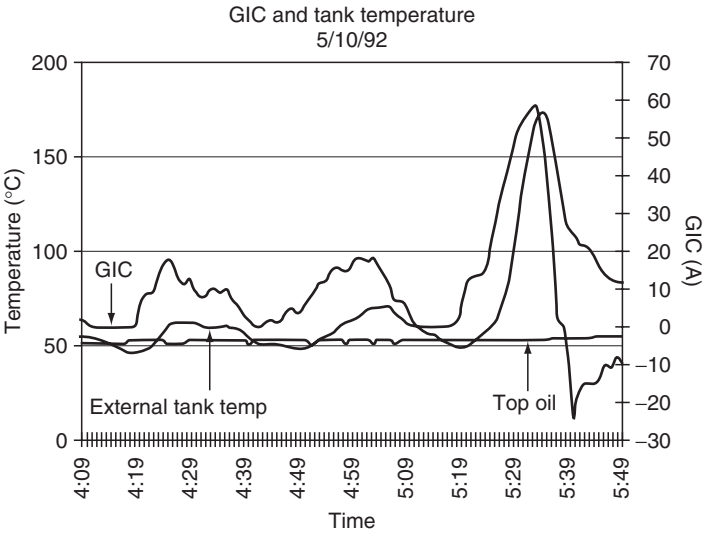

FIGURE 16.6 Transformer hot spot heating due to stray flux can be a concern in operation of a transformer with GIC present. This transformer experienced stray flux heating that could be monitored with a thermocouple mounted on the tank exterior surface. This storm demonstrated that the GIC and resulting half-cycle saturation produced a rapid heating in the tank hot spot. Notice also that transformer top-oil temperature did not show any significant change, indicating that the hot spot was relatively localized. (Courtesy Phil Gattens.)

number of winding turns) generally determine the core steel volume requirements of a transformer. Therefore, designing for unsaturated operation with the high level of GIC present would require a core of excessive size. The ability to even assess existing transformer vulnerability is a difficult undertaking and can only be confidently achieved in extensive case-by-case investigations. Each transformer design (even from the same manufacturer) can contain numerous subtle design variations. These variations complicate the calculation of how and at what density the stray flux can impinge on internal structures in the transformer. However, the experience from contemporary space weather events is revealing and potentially paints an ominous outcome for historically large storms that are yet to occur on today's infrastructure. As a case in point, during a September 2004 Electric Power Research Industry workshop on transformer damage due to GIC, Eskom, the power utility that operates the power grid in South Africa (geomagnetic latitudes $-27°$ to $-34°$), reported damage and loss of 15 large, high-voltage transformers (400 kV operating voltage) due to the geomagnetic storms of late October 2003. This damage occurred at peak disturbance levels of less than 100 nT/min in the region (Kappenman, 2005).

16.4 An Overview of Power System Reliability and Related Space Weather Climatology

The maintenance of the functional integrity of the bulk electric systems (i.e., power systems reliability) at all times is a very high priority for the planning and operation of power systems worldwide. Power systems are too large and critical in their operation to easily perform physical tests of their reliability performance for various contingencies. The ability of power systems to meet these requirements is commonly measured by deterministic study methods to test the system's ability to withstand probable disturbances through computer simulations. Traditionally, the design criterion consists of multiple outage and disturbance contingencies typical of what may be created from relatively localized terrestrial weather impacts. These stress tests are then applied against the network model under critical load or system transfer conditions to define important system design and operating constraints in the network.

System impact studies for geomagnetic storm scenarios can now be readily performed on large complex power systems. For cases in which utilities have performed such analysis, the impact results indicate that a severe geomagnetic storm event may pose an equal or greater stress on the network than most of the classic deterministic design criteria now in use. Further, by the very nature that these storms impact simultaneously over large regions of the network, they arguably pose a greater degree of threat for precipitating a system-wide collapse than more traditional threat scenarios.

The evaluation of power system vulnerability to geomagnetic storms is, of necessity, a two-stage process. The first stage is one of assessing the exposure to the network posed by the climatology. In other words, how large and how frequent can the storm driver be in a particular region? The second stage is one of assessment of the stress that probable and extreme climatology events may pose to reliable operation of the impacted network. This is measured through estimates of levels of GIC flow across the network and the manifestation of impacts such as sudden and dramatic increases in reactive power demands and implications on voltage regulation in the network. The essential aspects of risk management become the weighing of probabilities of storm events against the potential consequential impacts produced by a storm. From this analysis effort meaningful operational procedures can be further identified and refined to better manage the risks resulting from storms of various intensities (Kappenman et al., 2000).

Successive advances have been made in the ability to undertake detailed modeling of geomagnetic storm impacts upon terrestrial infrastructures. The scale of the problem is enormous, the physical processes entail vast volumes of the magnetosphere, ionosphere, and the interplanetary magnetic field conditions that trigger and sustain storm conditions. In addition, it is recognized that important aspects and uncertainties of the solid-earth geophysics need to be fully addressed in solving these modeling problems. Further, the effects to ground-based systems are essentially contiguous to the dynamics of the space environment. Therefore, the electromagnetic coupling and resulting impacts of the environment on ground-based systems require models of the complex network topologies overlaid on a complex geological base that can exhibit variation of conductivities that can span five orders of magnitude.

These subtle variations in the ground conductivity play an important role in determining the efficiency of coupling between disturbances of the local geomagnetic field caused by space environment influences and the resulting impact to ground-based systems that can be vulnerable to GIC. Lacking full understanding of this important coupling parameter hinders the ability to better classify the climatology of space weather on ground-based infrastructures.

16.5 Geological Risk Factors and Geoelectric Field Response

Considerable prior work has been done to model the geomagnetic induction effects in ground-based systems. As an extension to this fundamental work, numerical modeling of ground conductivity conditions have been demonstrated to provide accurate replication of observed geoelectric field conditions over a very broad frequency spectrum (Kappenman et al., 1997). Past experience has indicated that 1D Earth conductivity models are sufficient to compute the local electric fields. Lateral heterogeneity of ground conductivity conditions can be significant over mesoscale distances (Kappenman, 2001). In these cases, multiple 1D models can be used in cases where the conductivity variations are sufficiently large.

Ground conductivity models need to accurately reproduce geoelectric field variations that are caused by the considerable frequency ranges of geomagnetic disturbance events from the large magnitude/low-frequency electrojet-driven disturbances to the low amplitude but relatively high-frequency impulsive disturbances commonly associated with magnetospheric shock events. This variation of electromagnetic disturbances, therefore, require models accurate over a frequency range from 0.3 Hz to as low as 0.00001 Hz. At these low frequencies of the disturbance environments, diffusion aspects of ground conductivities must be considered to appropriate depths. Therefore skin depth theory can be used in the

frequency domain to determine the range of depths that are of importance. For constant Earth conductivities, the depths required are more than several hundred kilometers, although the exact depth is a function of the layers of conductivities present at a specific location of interest.

It is generally understood that the Earth's mantle conductivity increases with depth. In most locations, ground conductivity laterally varies substantially at the surface over mesoscale distances; these conductivity variations with depth can range from three to five orders of magnitude. Whereas surface conductivity can exhibit considerable lateral heterogeneity, conductivity at depth is more uniform, with conductivities ranging from 0.1 to 10 S/m at depths from 600 to 1000 km. If sufficient low-frequency measurements are available to characterize ground conductivity profiles, models of ground conductivity can be successfully applied over mesoscale distances and can be accurately represented by the use of layered conductivity profiles or models.

For illustration of the importance of ground models on the response of geoelectric fields, a set of four example ground models have been developed that illustrate the probable lower to upper quartile response characteristics of most known ground conditions, considering there is a high degree of uncertainty in the plausible diversity of upper layer conductivities. Figure 16.7 provides a plot of the layered ground conductivity conditions for these four ground models to depths of 700 km. As shown, there can be as much as four orders of magnitude variation in ground resistivity at various depths in the upper layers. Models A and B have very thin surface layers of relatively low resistivity. Models A and C are characterized by levels of relatively high resistivity until reaching depths exceeding 400 km, whereas models B and D have high variability of resistivity in only the upper 50 to 200 km of depth.

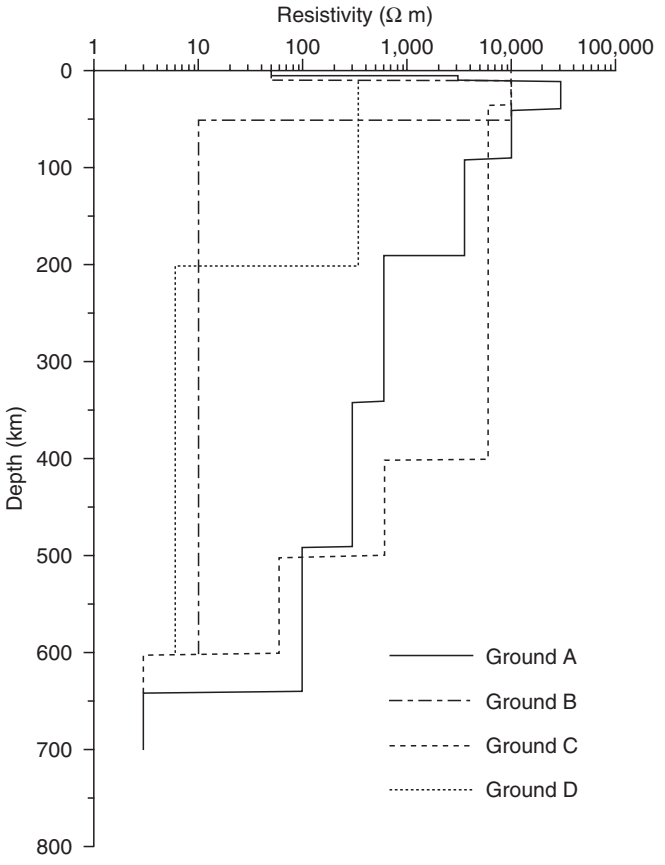

FIGURE 16.7 Resistivity profiles vs. depth for four example layered earth ground models.

Figure 16.8 provides the frequency response characteristics for these same four-layered earth ground models of Fig. 16.7. Each line plot represents the geoelectric field response for a corresponding incident magnetic field disturbance at each frequency. Whereas each ground model has unique response characteristics at each frequency, in general all ground models produce higher geoelectric field responses as the frequency of the incident disturbance increases. Also shown on this plot are the relative differences in geoelectric field response for the lowest and highest responding ground model at each decade of frequency. This illustrates that the response between the lowest and highest responding ground model can vary at discrete frequencies by more than a factor of 10. Also because the frequency content of an impulsive disturbance event can have higher frequency content (for instance due to a shock), the disturbance is acting upon the more responsive portion of the frequency range of the ground models (Kappenman, 2004). Therefore, the same disturbance energy input at these higher frequencies produces a proportionately larger response in geoelectric field. For example, in most of the ground models, the geoelectric field response is a factor of 50 higher at 0.1 Hz compared to the response at 0.0001 Hz.

From the frequency response plots of the ground models as provided in Fig. 16.8, some of the expected geoelectric field response due to geomagnetic field characteristics can be inferred. For example, Ground C provides the highest geoelectric field response across the entire spectral range, therefore, it would be expected that the time-domain response of the geoelectric field would be the highest for nearly all B field disturbances. At low frequencies, Ground B has the lowest geoelectric field response whereas at frequencies above 0.02 Hz, Ground A produces the lowest geoelectric field response. Because each of these ground models has both frequency-dependent and nonlinear variations in response, the resulting form of the geoelectric field waveforms would be expected to differ in form for the same B field input disturbance. In all cases, each of the ground models produces higher relative increasing geoelectric field response as the frequency of the incident B field disturbance increases. Therefore it should be expected that a higher peak geoelectric field should result for a higher spectral content disturbance condition.

A large electrojet-driven disturbance is capable of producing an impulsive disturbance as shown in Fig. 16.9, which reaches a peak delta B magnitude of ~2000 nT with a rate of change (dB/dt) of 2400 nT/min. This disturbance scenario can be used to simulate the estimated geoelectric field response of the four example ground models. Figure 16.10 provides the geoelectric field responses for each of the

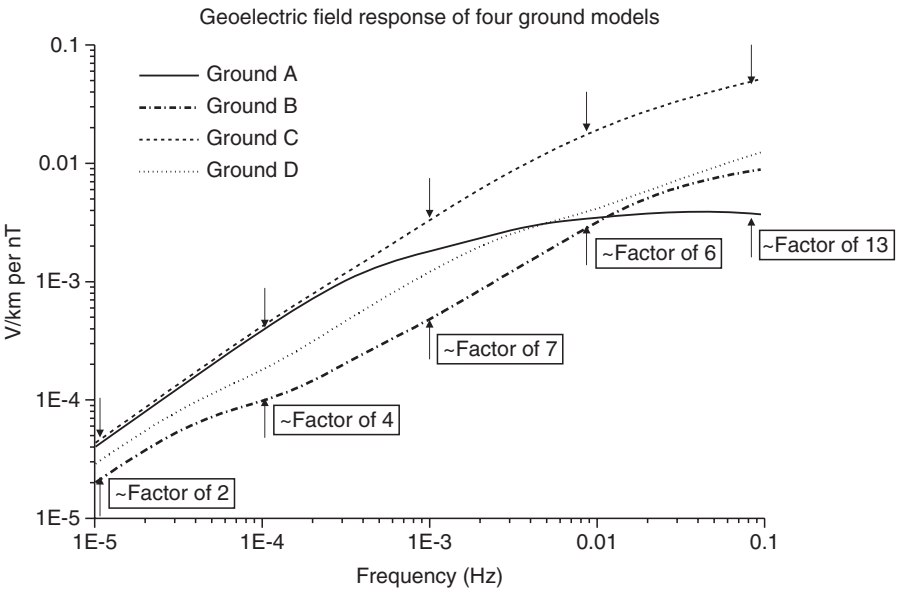

FIGURE 16.8 Frequency response of four example ground models of Fig. 16.1, max/min geoelectric field response characteristics shown at various discrete frequencies.

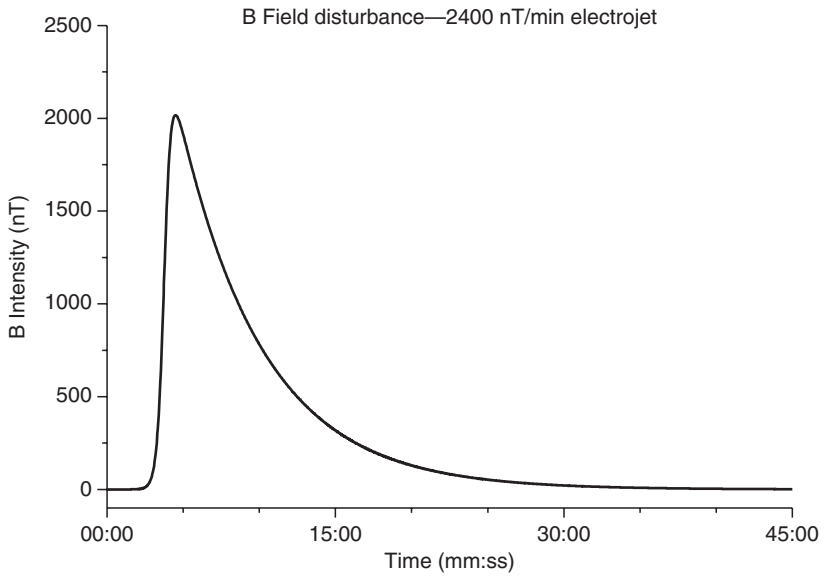

FIGURE 16.9 Waveform of example electrojet-driven geomagnetic field disturbance with 2400 nT/min rate of change intensity.

four ground models for this 2400 nT/min B field disturbance. As expected, the Ground C model produces the largest geoelectric field reaching a peak of ∼15 V/km, whereas Ground A is next largest and the Ground B model produces the smallest geoelectric field response. The Ground C geoelectric field peak is more than six times larger than the peak geoelectric field for the Ground B model. It is also

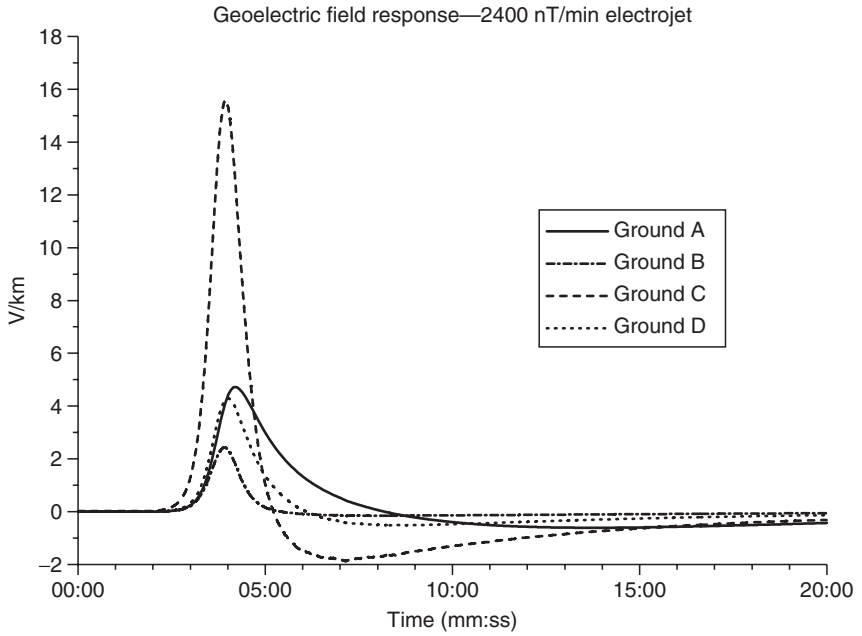

FIGURE 16.10 Geoelectric field response of the four example ground models to the 2400 nT/min disturbance conditions of Fig. 16.3.

evident that significant differences result in the overall shape and form of the geoelectric field response. For example, the peak geoelectric field for the Ground A model occurs 17 s later than the time of the peak geoelectric field for the Ground B model. In addition to the differences in the time of peak, the waveforms also exhibit differences in decay rates. As is implied from this example, both the magnitudes of the geoelectric field responses and the relative differences in responses between models will change dependent on the source disturbance characteristics.

16.6 Power Grid Design and Network Topology Risk Factors

While the previous discussion on ground conductivity conditions are important in determining the geoelectric field response, and in determining levels of GICs and their resulting impacts. Power grid design is also an important factor in the vulnerability of these critical infrastructures, a factor in particular that over time has greatly escalated the effective levels of GIC and operational impacts due to these increased GIC flows. Unfortunately, most research into space weather impacts on technology systems has focused upon the dynamics of the space environment. The role of the design and operation of the technology system in introducing or enhancing vulnerabilities to space weather is often overlooked. In the case of electric power grids, both the manner in which systems are operated and the accumulated design decisions engineered into present-day networks around the world have tended to significantly enhance geomagnetic storm impacts. The result is to increase the vulnerability of this critical infrastructure to space weather disturbances.

Both growth of the power grid infrastructure and design of its key elements have acted to introduce space weather vulnerabilities. The US high-voltage transmission grid and electric energy usage have grown dramatically over the last 50 years in unison with increasing electricity demands of society. The high-voltage transmission grid, which is the part of the power network that spans long distances, couples almost like an antenna through multiple ground points to the geoelectric field produced by disturbances in the geomagnetic field. From Solar Cycle 19 in the late 1950s through Solar Cycle 22 in the early 1980s, the high-voltage transmission grid and annual energy usage have grown nearly tenfold (Fig. 16.11). In short, the antenna that is sensitive to space weather disturbances is now very large. Similar development rates of transmission infrastructure have occurred simultaneously in other developed regions of the world.

As this network has grown in size, it has also grown in complexity and sets in place a compounding of risks that are posed to the power grid infrastructures for GIC events. Some of the more important changes in technology base that can increase impacts from GIC events include higher design voltages, changes in transformer design, and other related apparatus. The operating levels of high-voltage networks have increased from the 100–200 kV thresholds of the 1950s to 400 to 765 kV levels of present-day networks. With this increase in operating voltages, the average per unit length circuit resistance has decreased, whereas the average length of the grid circuit increases. In addition, power grids are designed to be tightly interconnected networks, which present a complex circuit that is continental in size. These interrelated design factors have acted to substantially increase the levels of GIC that are possible in modern power networks.

In addition to circuit topology, GIC levels are determined by the size and the resistive impedance of the power grid circuit itself when coupled with the level of geoelectric field, which result from the geomagnetic disturbance event. Given a geoelectric field imposed over the extent of a power grid, a current will be produced entering the neutral ground point at one location and exiting through other ground points elsewhere in the network. This can be best illustrated by examining the typical range of resistance per unit length for each kilovolt class of transmission lines and transformers.

As shown in Fig. 16.12, the average resistance per transmission line across the range of major kilovolt-rating classes used in the current US power grid decreases by a factor of more than 10. Therefore 115 and 765 kV transmission lines of equal length can have a factor of $\sim$10 difference in total circuit resistance. Ohm's law indicates that the higher voltage circuits when coupled to the same geoelectric field

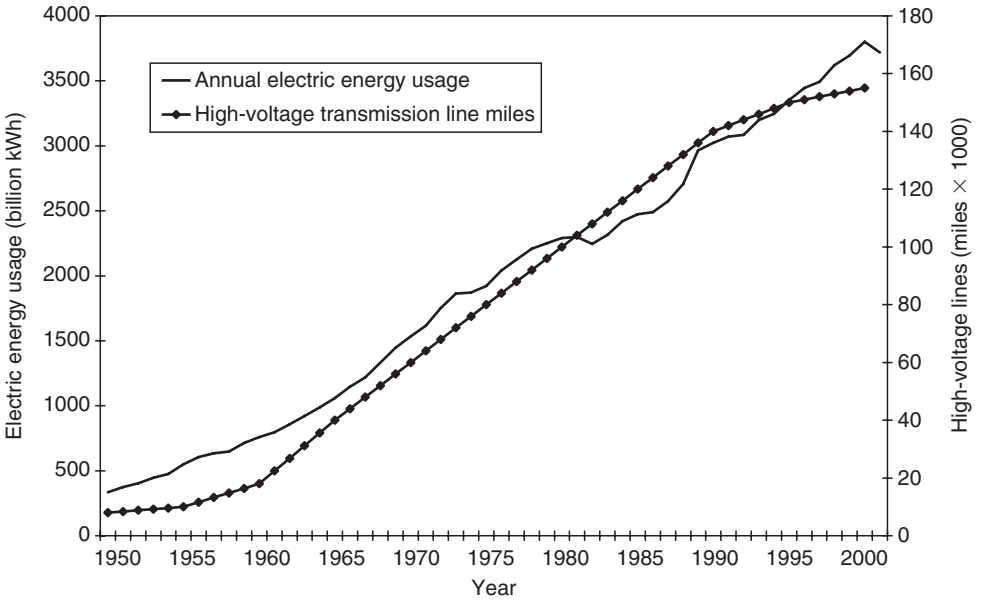

FIGURE 16.11 Growth of the US High Voltage Transmission Network and annual electric energy usage over the past 50 years. In addition to increasing total network size, the network has grown in complexity with introduction of higher kilovolt-rated lines that subsequently also tend to carry larger GIC flows. (Grid size derived from data in EHV Transmission Line Reference Book and NERC Electricity Supply and Demand Database; energy usage statistics from US Department of Energy—Energy Information Agency.)

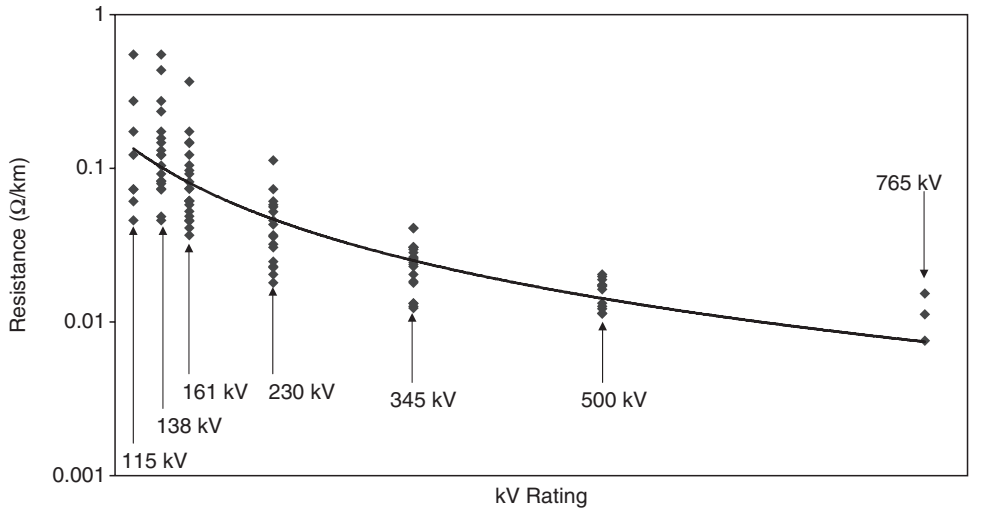

FIGURE 16.12 Range of transmission line resistance for the major kilovolt-rating classes for transmission lines in the US electric power grid infrastructure population. Also shown is a trend line of resistance weighted to average. The lower *R* for the higher voltage lines will also cause proportionately larger GIC flows in this portion of the power grid. (Derived from data in EHV Transmission Line Reference Book and from US Department of Energy, Energy Information Agency and FERC Form 1 Database.)

would result in as much as ~10 times larger GIC flows in the higher voltage portions of the power grid. The resistive impedance of large power system transformers follows a very similar pattern: the larger the power capacity and kilovolt-rating, the lower the resistance of the transformer. In combination, these design attributes will tend to collect and concentrate GIC flows in the higher kilovolt-rated equipment. More important, the higher kilovolt-rated lines and transformers are key network elements, as they are the long-distance heavy haulers of the power grid. The upset or loss of these key assets due to large GIC flows can rapidly cascade into geographically widespread disturbances to the power grid.

Most power grids are highly complex networks with numerous circuits or paths and transformers for GIC to flow through. This requires the application of highly sophisticated network and electromagnetic coupling models to determine the magnitude and path of GIC throughout the complex power grid. However for the purposes of illustrating the impact of power system design, a review will be provided using a single-transmission line terminated at each end with a single transformer to ground connection. To illustrate the differences that can occur in levels of GIC flow at higher voltage levels, the simple demonstration circuit has also been developed at 138, 230, 345, 500, and 765 kV, which are common grid voltages used in the United States and Canada. In Europe, voltages of 130, 275, and 400 kV are commonly used for the bulk power grid infrastructures. For these calculations, a uniform 1.0 V/km geoelectric field disturbance conditions are used, which means that the change in GIC levels will result from changes in the power grid resistances alone. Also for uniform comparison purposes, a 100 km long line is used in all kilovolt-rating cases.

Figure 16.13 illustrates the comparison of GIC flows that would result for various US infrastructure power grid kilovolt ratings using the simple circuit and a uniform 1.0 V/km geoelectric field disturbance. In complex networks, such as those in the United States, some scatter from this trend line is possible due to normal variations in circuit parameters such as line resistances, etc., which can occur in the overall population of infrastructure assets. Further, this was an analysis of simple "one-line" topology network, whereas real power grid networks have highly complex topologies, span large geographic regions, and present numerous paths for GIC flow, all of which tend to increase total GIC flows. Even this limited demonstration tends to illustrate that the power grid infrastructures of large grids in the United States and other locations of the world are increasingly exposed to higher GIC flows due to design changes that have resulted in reduced circuit resistance. Compounding this risk further, the higher kilovolt portions of the network handle the largest bulk power flows and form the backbone of the grid. Therefore the increased GIC risk is being placed at the most vital portions of this critical

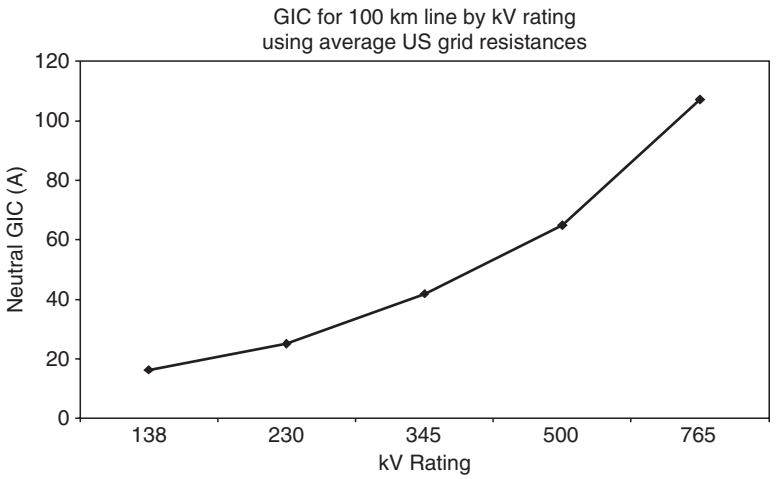

FIGURE 16.13 Average neutral GIC flows vs. kilovolt rating for a 100 km demonstration transmission circuit.

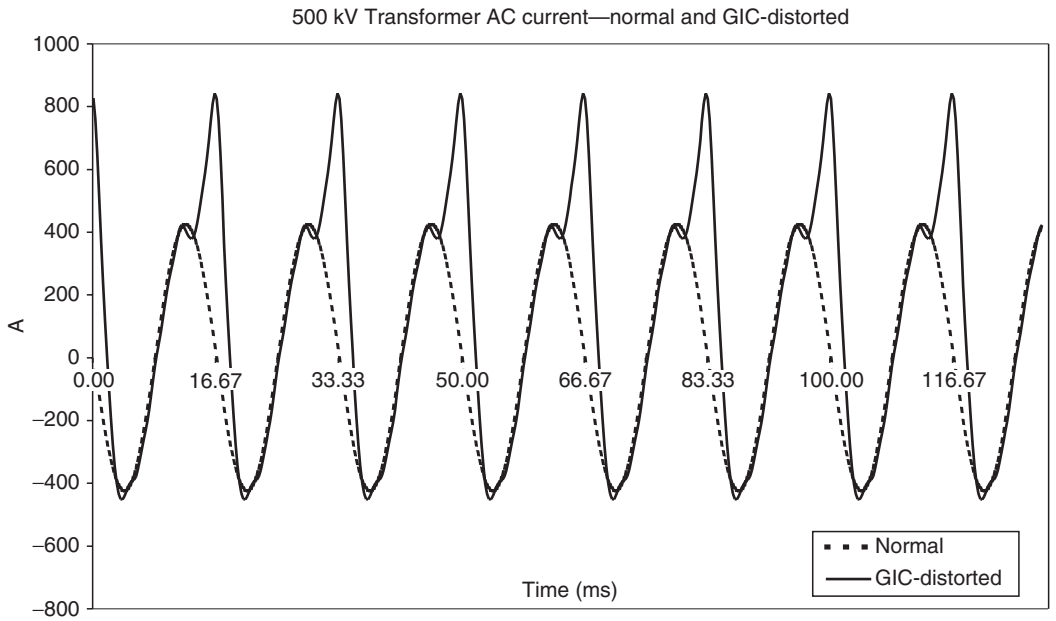

FIGURE 16.14 500 kV Simple demonstration circuit simulation results: transformer AC currents and distortion due to GIC.

infrastructure. In the United States, 345, 500, and 765 kV transmission systems are widely spread throughout and especially concentrated in areas of the United States with high population densities.

One of the best ways to illustrate the operational impacts of large GIC flows is to review the way in which the GIC can distort the AC output of a large power transformer due to half-cycle saturation. Under severe geomagnetic storm conditions, the levels of geoelectric field can be many times larger than the uniform 1.0 V/km used in the prior calculations. Under these conditions even larger GIC flows are possible. For example (see Fig. 16.14), the normal AC current waveform in the high-voltage winding of a 500 kV transformer under normal load conditions is shown (~300 A rms, ~400 A peak). With a large GIC flow in the transformer, the transformer experiences extreme saturation of the magnetic core for one-half of the AC cycle (half-cycle saturation). During this half-cycle of saturation, the magnetic core of the transformer draws an extremely large and distorted AC current from the power grid. This combines with the normal AC load current producing the highly distorted asymmetrically peaky waveform that now flows in the transformer. As shown, AC current peaks that are present are nearly twice as large compared to normal current for the transformer under this mode of operation. This highly distorted waveform is rich in both even and odd harmonics, which are injected into the system and can cause misoperations of sensors and protective relays throughout the network (Kappenman et al., 1981, 1989).

The design of transformers also acts to further compound the impacts of GIC flows in the high-voltage portion of the power grid. While proportionately larger GIC flows occur in these large high-voltage transformers, the larger high-voltage transformers are driven into saturation at the same few amperes of GIC exposure as those of lower voltage transformers. More ominously, another compounding of risk occurs as these higher kilovolt-rated transformers produce proportionately higher power system impacts than comparable lower voltage transformers. As shown in Fig. 16.15, because reactive power loss in a transformer is a function of the operating voltage, the higher kilovolt-rated transformers will also exhibit proportionately higher reactive power losses due to GIC. For example, a 765 kV transformer will have approximately six times larger reactive power losses for the same magnitude of GIC flow as that of a 115 kV transformer.

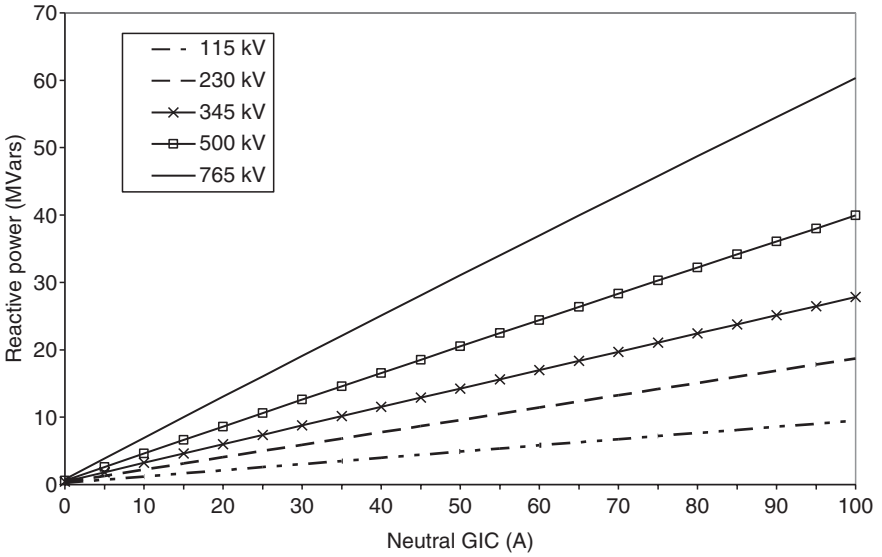

FIGURE 16.15 The impacts of GIC flows are further compounded by the behavior of transformers on the AC transmission network. Larger GIC flows will tend to occur in the higher kilovolt-rated transformers. As shown above these transformers also produce a proportionately larger reactive power consumption on the grid compared to the same level of GIC flow in lower kilovolt-rated transformers. (From "Space Weather and the Vulnerability of Electric Power Grids" J.G. Kappenman—NATO-ASI ESPRIT Conference, in press).

All transformers on the network can be exposed to similar conditions simultaneously due to the wide geographic extent of most disturbances. This means that the network needs to supply an extremely large amount of reactive power to each of these transformers or voltage collapse of the network could occur. The combination of voltage regulation stress, which occurs simultaneously with the loss of key elements due to relay misoperations can rapidly escalate to widespread progressive collapse of the exposed interconnected network. An example of these threat conditions can be provided for the US power grid for extreme but plausible geomagnetic storm conditions.

16.7 Extreme Geomagnetic Disturbance Events—Observational Evidence

Both the space weather community and the power industry have not fully understood these design implications. The application of detailed simulation models has provided tools for forensic analysis of recent storm activity and when adequately validated can be readily applied to examine impacts due to historically large storms. Some of the first reports of operational impacts to power systems date back to the early 1940s and the level of impacts has progressively become more frequent and significant as growth and development of technology has occurred in this infrastructure. In more contemporary times, major power system impacts in the United States have occurred in storms in 1957, 1958, 1968, 1970, 1972, 1974, 1979, 1982, 1983, and 1989 and several times in 1991. Both empirical and model extrapolations provide some perspective on the possible consequences of storms on present-day infrastructures.

Historic records of geomagnetic disturbance conditions and, more important, geoelectric field measurements provide a perspective on the ultimate driving force that can produce large GIC flows in power grids. Because geoelectric fields and resulting GIC are caused by the rate of change of the geomagnetic field, one of the most meaningful methods to measure the severity of impulsive geomagnetic field

disturbances is by the magnitude of the geomagnetic field change per minute, measured in nanoteslas per minute. For example, the regional disturbance intensity that triggered the Hydro Quebec collapse during the March 13, 1989 storm only reached an intensity of 479 nT/min. Large numbers of power system impacts in the United States were also observed for intensities that ranged from 300 to 600 nT/min during this storm. However, the most severe rate of change in the geomagnetic field observed during this storm reached a level of ∼2000 nT/min over the lower Baltic. The last such disturbance with an intensity of ∼2000 nT/min over North America was observed during a storm on August 4, 1972 when the power grid infrastructure was less than 40% of its current size.

Data assimilation models provide further perspectives on the intensity and geographic extent of the intense dB/dt of the March 1989 Superstorm. Figure 16.16 provides a synoptic map of the ground level geomagnetic field disturbance regions observed at time 22:00 UT. The previously mentioned lower Baltic region observations are embedded in an enormous westward electrojet complex during this period of time. Simultaneously with this intensification of the westward electrojet, an intensification of the eastward electrojet occupies a region across midlatitude portions of the western US. The features of the westward electrojet extend longitudinally ∼120° and have a north–south cross-section ranging as much as 5° to 10° in latitude.

Older storms provide even further guidance on the possible extremes of these specific electrojet-driven disturbance processes. A remarkable set of observations was conducted on rail communication circuits in Sweden that extend back nearly 80 years. These observations provide key evidence that allow for estimation of the geomagnetic disturbance intensity of historically important storms in an era where geomagnetic observatory data is unavailable. During a similarly intense westward electrojet disturbance on July 13–14, 1982, a ∼100 km length communication circuit from Stockholm to Torreboda measured a peak geopotential of 9.1 V/km (Lindahl). Simultaneous measurements at nearby Lovo observatory in central Sweden measured a dB/dt intensity of ∼2600 nT/min at 24:00 UT on July 13.

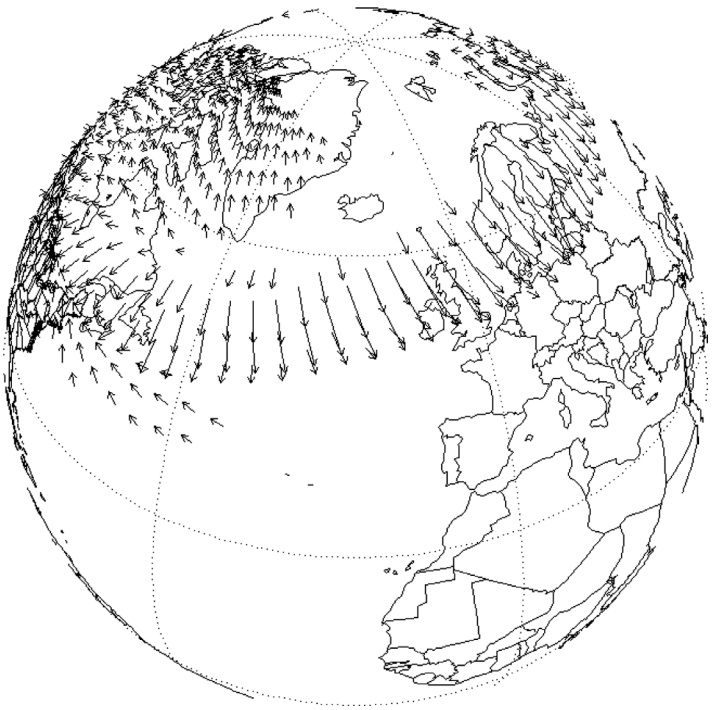

FIGURE 16.16 Extensive westward electrojet-driven geomagnetic field disturbances at time 22:00 UT on March 13, 1989.

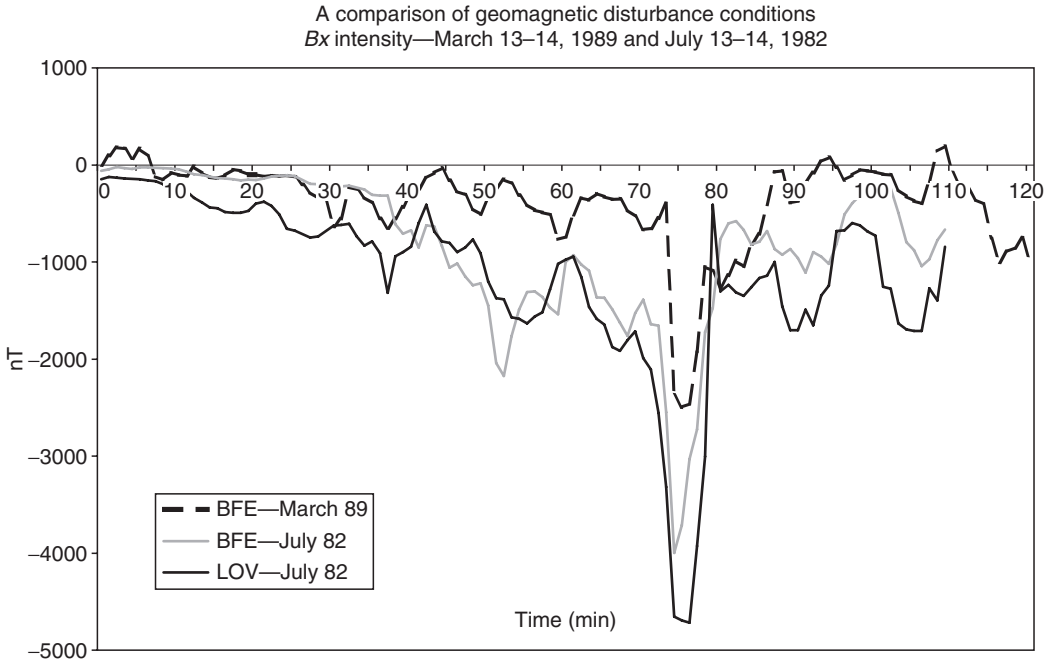

FIGURE 16.17 Comparison of observed delta *Bx* at Lovo and BFE during the July 13–14, 1982 and March 13, 1989 electrojet intensification events.

Figure 16.17 shows the delta *Bx* observed at BFE and Lovo during the peak disturbance times on July 13 and for comparison purposes the delta *Bx* observed at BFE during the large substorm on March 13, 1989. This illustrates that the comparative level of delta *Bx* is twice as large for the July 13, 1982 event than that observed on March 13, 1989. The large delta *Bx* of >4000 nT for the July 1982 disturbance suggests that these large field deviations are capable of producing even larger dB/dt impulses should faster onset or collapse of the *Bx* field occur over the region (Kappenman, 2006).

As previously discussed, unprecedented power system impacts were observed in North America on March 13–14, 1989 for storm intensities that reached levels of approximately 300–600 nT/min. However, the investigation of very large storms indicates that storm intensities over many of these same US regions could be as much as 4 to 10 times larger. These megastorms appear from historic data to be probable on a 1-in-50 to 1-in-100 year time frame. Modern critical infrastructures have not as yet been exposed to storms of this size. This increase in storm intensity causes a nearly proportional increase in resulting stress to power grid operations. These storms also have a footprint that can simultaneously threaten large geographic regions and can therefore plausibly trigger large regions of grid collapse.

16.8 Power Grid Simulations for Extreme Disturbance Events

Based upon these extreme disturbance events, a series of simulations were conducted for the entire US power grid using electrojet-driven disturbance scenarios with the disturbance at 50° geomagnetic latitude and at disturbance strengths of 2400, 3600, and 4800 nT/min. The electrojet disturbance footprint was also positioned over North America with the previously discussed longitudinal dimensions of a large westward electrojet disturbance. This extensive longitudinal structure will simultaneously expose a large portion of the US power grid.

In this analysis of disturbance impacts, the level of cumulative increased reactive demands (MVars) across the US power grid provides one of the more useful measures of overall stress on the network.

This cumulative MVar stress was also determined for the March 13, 1989 storm for the US power grid, which was estimated using the current system model as reaching levels of ~7000 to 8000 MVars at times 21:44 to 21:57 UT. At these times, corresponding dB/dt levels in midlatitude portions of the United States reached 350 to 545 nT/min as measured at various US observatories. This provides a comparison benchmark that can be used to either compare absolute MVar levels or, the relative MVar level increases for the more severe disturbance scenarios. The higher intensity disturbances of 2400 to 4800 nT/min will have a proportionate effect on levels of GIC in the exposed network. GIC levels more than five times larger than those observed during the above-mentioned periods in the March 1989 storm would be probable. With the increase in GIC, a linear and proportionate increase in other power system impacts is likely. For example, transformer MVar demands increase with increases in transformer GIC. As larger GICs cause greater degrees of transformer saturation, the harmonic order and magnitude of distortion currents increase in a more complex manner with higher GIC exposures. In addition, greater numbers of transformers would experience sufficient GIC exposure to be driven into saturation, as generally higher and more widely experienced GIC levels would occur throughout the extensive exposed power grid infrastructure.

Figure 16.18 provides a comparison summary of the peak cumulative MVar demands that are estimated for the US power grid for the March 1989 storm, and for the 2400, 3600, and 4800 nT/min disturbances at the different geomagnetic latitudes. As shown, all of these disturbance scenarios are far larger in magnitude than the levels experienced on the US power grid during the March 1989 Superstorm. All reactive demands for the 2400 to 4800 nT/min disturbance scenarios would produce unprecedented in size reactive demand increases for the US grid. The comparison with the MVar demand from the March 1989 Superstorm further indicates that even the 2400 nT/min disturbance scenarios would produce reactive demand levels at all of the latitudes that would be approximately six times larger than those estimated in March 1989. At the 4800 nT/min disturbance levels, the reactive demand is estimated, in total, to exceed 100,000 MVars. While these large reactive demand increases are calculated for illustration purposes, impacts on voltage regulation and probable large-scale voltage collapse across the network could conceivably occur at much lower levels.

This disturbance environment was further adapted to produce a footprint and onset progression that would be more geospatially typical of an electrojet-driven disturbance, using both the March 13, 1989 and July 13, 1982 storms as a template for the electrojet pattern. For this scenario, the intensity of the

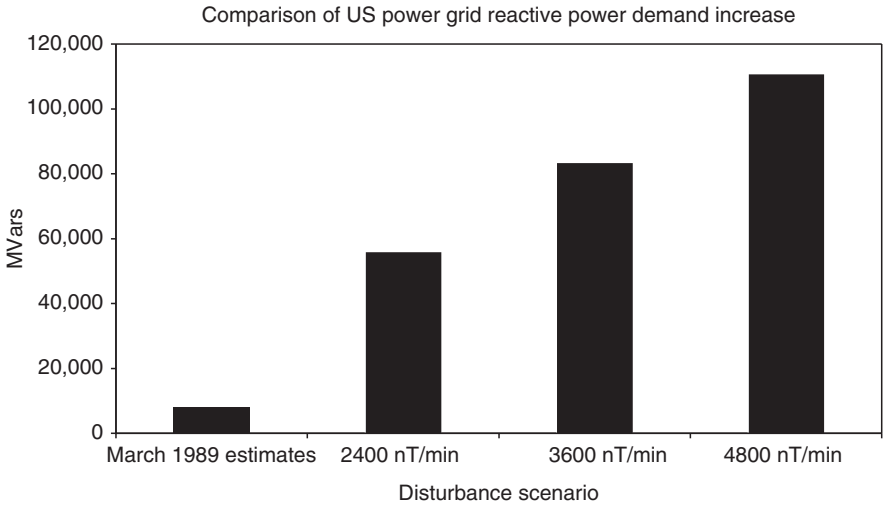

FIGURE 16.18 Comparison of estimated US power grid reactive demands during March 13, 1989 Superstorm and 2400, 3600, and 4800 nT/min disturbance scenarios at 50° geomagnetic latitude position over the United States.

disturbance is decreased as it progresses from the eastern to western US. The eastern portions of the United States are exposed to a 4800 nT/min disturbance intensity, while, west of the Mississippi, the disturbance intensity decreases to only 2400 nT/min. The extensive reactive power increase and extensive geographic boundaries of impact would be expected to trigger large-scale progressive collapse conditions, similar to the mode in which the Hydro Quebec collapse occurred. The most probable regions of expected power system collapse can be estimated based upon the GIC levels and reactive demand increases in combination with the disturbance criteria as it applies to the US power pools. Figure 16.19 provides a map of the peak GIC flows in the US power grid (size of circle at each node indicates relative GIC intensity) and estimated boundaries of regions that likely could experience system collapse due to this disturbance scenario. This example shows one of many possible scenarios for how a large storm could unfold.

While these complex models have been rigorously tested and validated, this is an exceedingly complex task with uncertainties that can easily be as much as a factor of two. However, just empirical evidence alone suggests that power grids in North America that were challenged to collapse for storms of 400 to 600 nT/min over a decade ago, are not likely to survive the plausible but rare disturbances of 2000 to 5000 nT/min that long-term observational evidence indicates have occurred before and therefore may be likely to occur again. Because large power system catastrophes due to space weather are not a zero probability event and because of the large-scale consequences of a major power grid blackout, it is important to discuss the potential societal and economic impacts of such an event should it ever reoccur. The August 14, 2003 US Blackout event provides a good case study, the utilities and various municipal organizations should be commended for the rapid and orderly restoration efforts that occurred. However, it should also acknowledge that in many respects this blackout occurred during highly optimal conditions, that were somewhat taken for granted and should not be counted upon in future blackouts. For example, an outage on January 14 rather than August 14 could have meant coincident cold weather conditions. Under these conditions, breakers and equipment at substations and power plants can be more difficult to reenergize when they become cold. Geomagnetic storms as previously discussed can also permanently damage key transformers on the grid which further burdens the restoration process, and delays could rapidly cause serious public health and safety concerns.

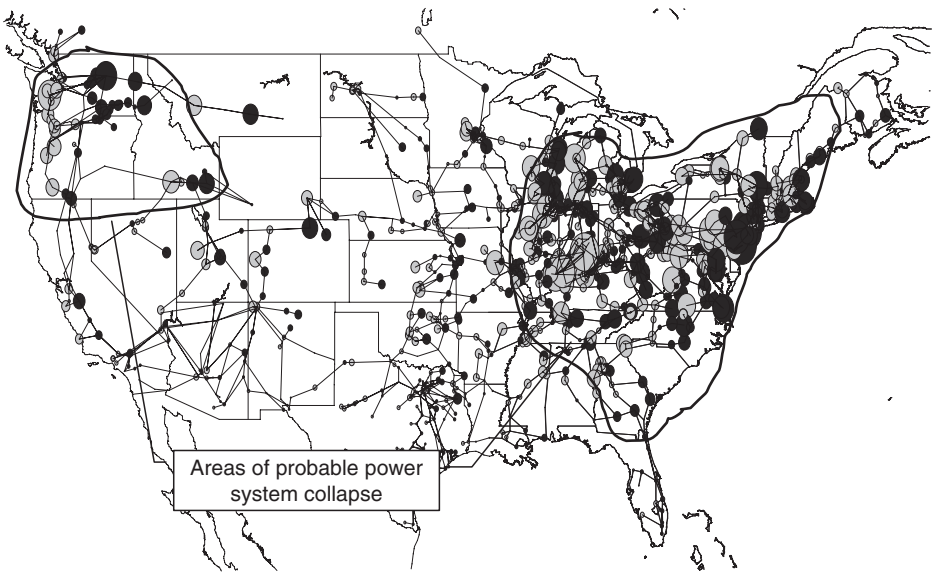

FIGURE 16.19 Regions of large GIC flows and possible power system collapse due to a 4800 nT/min disturbance scenario.

Because of the possible large geographic lay down of a severe storm event and resulting power grid collapse, the ability to provide meaningful emergency aid and response to an impacted population that may be in excess of 100 million people will be a difficult challenge. Even basic necessities such as potable water and replenishment of foods may need to come from boundary regions that are unaffected and these unaffected regions could be very remote to portions of the impacted US population centers. As previously suggested adverse terrestrial weather conditions could cause further complications in restoration and resupply logistics.

16.9 Conclusions

Contemporary models of large power grids and the electromagnetic coupling to these infrastructures by the geomagnetic disturbance environment have matured to a level in which it is possible to achieve very accurate benchmarking of storm geomagnetic observations and the resulting GIC. As abilities advance to model the complex interactions of the space environment with the electric power grid infrastructures, the ability to more rigorously quantify the impacts of storms on these critical systems also advances. This quantification of impacts due to extreme space weather events is leading to the recognition that geomagnetic storms are an important threat that has not been well recognized in the past.

References

Erinmez, I.A., Majithia, S., Rogers, C., Yasuhiro, T., Ogawa, S., Swahn, H., and Kappenman, J.G., Application of modelling techniques to assess geomagnetically induced current risks on the NGC transmission system, CIGRE Paper 39-304, Session 2002.

Kappenman, J.G., Chapter 13: An introduction to power grid impacts and vulnerabilities from space weather, in *NATO-ASI Book on Space Storms and Space Weather Hazards*, Vol. 38, edited by I.A. Daglis, Kluwer Academic Publishers, NATO Science Series, 2001, pp. 335–361.

Kappenman, J.G., Chapter 14: Space weather and the vulnerability of electric power grids, in *Effects of Space Weather on Technology Infrastructure*, Vol. 176, edited by I.A. Daglis, Kluwer Academic Publishers, Norwell, 2004, pp. 257–286.

Kappenman, J.G., An overview of the impulsive geomagnetic field disturbances and power grid impacts associated with the violent Sun–Earth connection events of 29–31 October 2003 and a comparative evaluation with other contemporary storms, *Space Weather*, 3, S08C01, 2005, doi:10.1029/2004SW000128.

Kappenman, J.G., Great geomagnetic storms and extreme impulsive geomagnetic field disturbance events—an analysis of observational evidence including the great storm of May 1921, *Advances in Space Research*, 38(2), 188–199, 2006.

Kappenman, J.G., Albertson, V.D., and Mohan, N., Current transformer and relay performance in the presence of geomagnetically-induced currents, *IEEE PAS Transactions*, PAS-100, 1078–1088, March 1981.

Kappenman, J.G., Carlson, D.L., and Sweezy, G.A., GIC effects on relay and CT performance, *Paper Presented at the EPRI Conference on Geomagnetically-Induced Currents*, November 8–10, San Francisco, CA, 1989.

Kappenman, J.G., Zanetti, L.J., and Radasky, W.A., Space weather from a user's perspective: Geomagnetic storm forecasts and the power industry, *EOS Transactions of the American Geophysical Union*, 78(4), 37–45, January 1997.

Kappenman, J.G., Radasky, W.A., Gilbert, J.L., and Erinmez, I.A., Advanced geomagnetic storm forecasting: A risk management tool for electric power operations, *IEEE Plasma Society Special Issue on Space Plasmas*, 28(6), 2114–2121, December 2000.

17

Lightning Protection

William A. Chisholm
Kinectrics/UQAC

The study of lightning predates electric power systems by many centuries. Observations of thunder were maintained in some areas for more than a millennium. Franklin and others established the electrical nature of lightning, and introduced the concepts of shielding and grounding to protect structures. Early power transmission lines used as many as six overhead shield wires, strung above the phase conductors and grounded at the towers for effective lightning protection. Later in the twentieth century, repeated strikes to tall towers, buildings, and power lines, contradicting the adage that "it never strikes twice," allowed systematic study of stroke current parameters. Improvements in electronics, computers, telecommunications, rocketry, and satellite technologies have all extended our knowledge about lightning, while at the same time exposing us to ever-increasing risks of economic damage from its consequences.

17.1 Ground Flash Density

The first, negative, downward, cloud-to-ground lightning stroke is the dominant risk element to power system components. Positive first strokes, negative subsequent strokes, and continuing currents can also cause specific problems. A traditional indicator of cloud-to-ground lightning activity is given by thunder observations, collected to World Meteorological Organization standards and converted to ground flash density (GFD) [1,2]:

$$\mathrm{GFD} = 0.04\mathrm{TD}^{1.25} \tag{17.1}$$

$$\mathrm{GFD} = 0.054\mathrm{TH}^{1.1} \tag{17.2}$$

where TD is the number of days with thunder per year, TH is the number of hours with thunder per year, and GFD is the number of first cloud-to-ground strokes per square kilometer per year.

Long-term thunder data suggest that GFD has a relative standard deviation of 30%. Observations of optical transient density have been performed using satellites starting from 1995. These data have some of the same defects as thunder observations: cloud-flash and ground-flash activity is equally weighted and the observations are sporadic. However, statistical considerations now favor the use of optical transient density, for example, as reported by Christian et al. [5] over thunder observations.

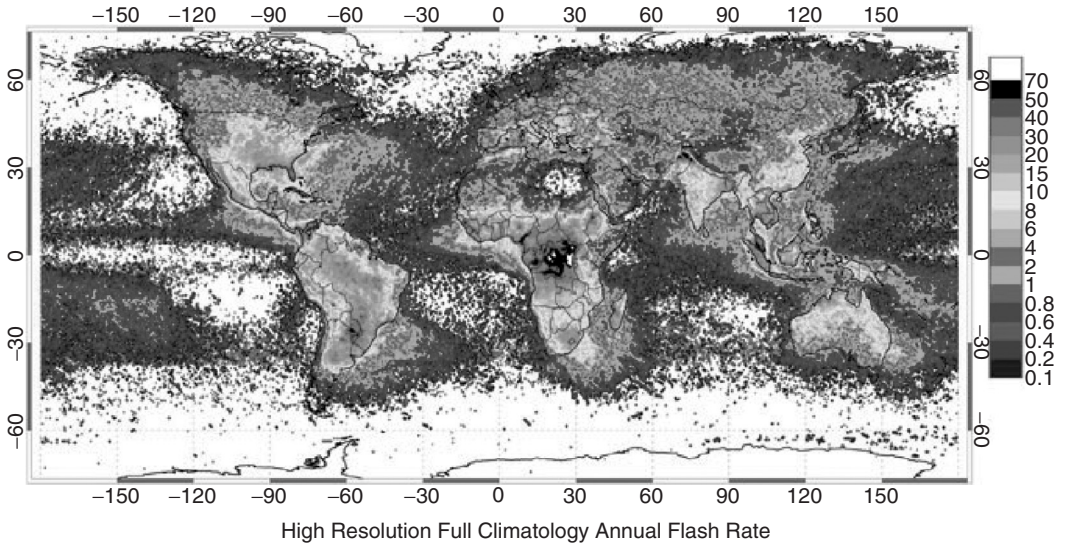

FIGURE 17.1 Observed optical transient density per km^2 per year from Ref. [5]. The optical transient density can be used to estimate lightning ground flash density (per km^2/year) by dividing the observed values by 3.0.

At present, a global estimate of GFD can be obtained by dividing the optical transient density in Fig. 17.1 by a factor of 3.0. This factor may vary across regions, possibly related to similar observed variations in the fraction of positive to negative flashes.

Electromagnetic signals from lightning are unique and have a high signal-to-noise ratio at large distances. Many single-station lightning flash counters have been developed and calibrated, each with good discrimination between cloud-flash and ground-flash activity using simple electronic circuits [3]. It has also been feasible for more than 30 years [4] to observe these signals with two or more stations, and to triangulate lightning stroke locations on a continent-wide basis. Lightning location networks [6] have improved continuously to the point where multiple ground strikes from a single flash can be resolved with high spatial and temporal accuracy and high probability of detection. A GFD value from these data should be based on approximately 400 counts in each cell to reduce relative standard deviation of the observation process below 5%. In areas with moderate flash density, a minimum cell size of 20×20 km is appropriate.

17.2 Stroke Incidence to Power Lines

The lightning leader, a thin column of electrically charged plasma, develops from cloud down to the ground in a series of step breakdowns [7]. Near the ground, electric fields are high enough to satisfy the conditions for continuous positive leader inception upward from tall objects or conductors. Analysis of a single overhead conductor with this approach [8] leads to

$$N_s = 3.8\text{GFD}h^{0.45} \tag{17.3}$$

where N_s is the number of strikes to the conductor per 100 km of line length per year and h is the average height of the conductor above ground in meters.

In areas of moderate- to high-GFD, one or more overhead shield wires are usually installed above the phase conductors. This shielding usually has a success rate of greater than 95%, but adds nearly 10% to the cost of line construction and also wastes energy from induced currents. The leader inception model [8] has also been used to analyze shielding failures.

17.3 Stroke Current Parameters

Once the downward leader contacts a power system component through an upward-connecting leader, the stored charge will be impressed through a high-channel impedance of 600 to 2000 Ω. With this high source impedance, compared to grounded towers or lines, an impulse current source model is suitable.

Berger made the most reliable direct measurements of negative downward cloud-to-ground lightning parameters on an instrumented tower from 1947 to 1977 [9]. Additional observations have been provided by many researchers and then summarized [10,11]. The overall stroke current distribution can be approximated [11] as lognormal with a mean of 31 kA and a log standard deviation of 0.48. The waveshape rises with a concave front, giving the maximum steepness near the crest of the wave, and then decays with a time to half-value of 50 μs or more. The median value of maximum steepness [11] is 24 kA/μs, with a log standard deviation of 0.60. Steepness has a positive correlation to the peak amplitude [11] that allows simplified modeling using a single equivalent front time (peak current divided by peak rate of rise). The mean equivalent front is 1.4 μs for the median 31 kA current, rising to 2.7 μs as peak stroke current increases to the 5% level of 100 kA [11]. An equivalent front time of 2 μs is recommended for simplified analysis [12].

17.4 Calculation of Lightning Overvoltages on Shielded Lines

The voltage rise V_R of the ground resistance R at each tower will be proportional to peak stroke current: $V_R = RI$. A relation between the tower base geometry and its resistance is

$$R = \frac{\rho}{2\pi g} \ln\left(\frac{11.8g^2}{A}\right) + \frac{\rho}{l} \tag{17.4}$$

where ρ is the soil resistivity (Ω m), g is the square root of the sum of the squares of the insulator extent in each direction (m), A is the surface area (sides + base) of the hole needed to excavate the electrode (m^2), and l is the total length (m) of wire in the wire-frame approximation to the electrode (infinite for solid electrodes).

For large surge currents, local ionization will reduce the second ρ/l contact resistance term but not the first geometric resistance term in Eq. (17.4).

The voltage rise V_L associated with conductor and tower series inductance L and the equivalent front time ($dt = 2$ μs) is $V_L = LI/dt$. The V_L term will add to, and sometimes dominate, V_R. Lumped inductance can be approximated from the expression

$$L = Z\tau = 60 \ln\left(\frac{2h}{r}\right) \cdot \frac{l}{c} \tag{17.5}$$

L is the inductance (H), Z is the element antenna impedance (Ω), τ is the travel time (s), h is the wire height above conducting ground (m), r is the wire radius (m), l is the wire length (m), and c is the speed of light (3×10^8 m/s).

In numerical analyses, series and shunt impedance elements can be populated using the same procedure. Tall transmission towers have longer travel times and thus higher inductance, which further exacerbates the increase of stroke incidence with line height.

The high electromagnetic fields surrounding any stricken conductor will induce currents and couple voltages in nearby, unstricken conductors through their mutual surge impedances. In the case where lightning strikes a grounded overhead shield wire, this coupling increases common-mode voltage and reduces differential voltage across insulators. Additional shield wires and corona [11,12] can improve this desirable surge–impedance coupling to mitigate half of the total tower potential rise ($V_R + V_L$).

The strong electromagnetic fields from vertical lightning strokes can induce large overvoltages in nearby overhead lines without striking them directly. This is a particular concern only for MV and LV systems.

17.5 Insulation Strength

Power system insulation is designed to withstand all anticipated power system overvoltages. Unfortunately, even the weakest direct stroke from a shielding failure to a phase conductor will cause a lightning flashover. Once an arc appears across an insulator, the power system fault current keeps this arc alive until voltage is removed by protective relay action. Effective overhead shielding is essential on transmission lines in areas with moderate- to high-GFD.

When the overhead shield wire is struck, the potential difference on insulators is the sum of the resistive and inductive voltage rises on the tower, minus the coupled voltage on the phase conductors. The potential difference can lead to a "backflashover" from the tower to the phase conductor. Backflashover is more frequent when the stroke current is large (5% > 100 kA), when insulation strength is low (<1 m or 600 kV basic impulse level), and/or when footing resistance is high (>30 Ω). Simplified models [11,12] are available to carry out the overvoltage calculations and coordinate the results with insulator strength, giving lightning outage rates, in units of interruptions per 100 km/year.

17.6 Mitigation Methods

Lightning mitigation methods need to be appropriate for the expected long-term GFD and power system reliability requirements. Table 17.1 summarizes typical practices at five different levels of lightning activity to achieve a reliability of one outage per 100 km of line per year on an HV line.

17.7 Conclusion

Direct lightning strokes to any overhead transmission line are likely to cause impulse flashover of supporting insulation, leading to a circuit interruption. The use of overhead shield wires, located above the phase conductors and grounded adequately at each tower, can reduce the risk of flashover by 95–99.5%, depending on system voltage.

TABLE 17.1 Lightning Mitigation Methods for Transmission Lines

Ground Flash Density Range	Typical Design Approaches
0.1–0.3 Ground flashes/km^2 per year	Unshielded, one- or three-pole reclosing
0.3–1 Ground flashes/km^2 per year	Single overhead shield wire
1–3 Ground flashes/km^2 per year	Two overhead shield wires
3–10 Ground flashes/km^2 per year	Two overhead shield wires with good grounding or line surge arresters
10–30 Ground flashes/km^2 per year	Three or more overhead and underbuilt shield wires with good grounding, line surge arresters; underground transmission cables

References

1. Anderson, R.B., Eriksson, A.J., Kroninger, H., and Meal, D.V., Lightning and thunderstorm parameters, IEE conference publication 236, *Lightning and Power Systems*, London, June 1984.
2. MacGorman, D.R., Maier, M.W., and Rust, W.D., *Lightning Strike Density for the Contiguous United States from Thunderstorm Duration Records*. Report to U.S. Nuclear Regulatory Commission, NUREG/CR-3759, 1984.
3. Heydt, G., Instrumentation, in *Handbook of Atmospherics*, Vol. II, edited by Volland, H., CRC Press, Boca Raton, FL, 1982, pp. 203–256.
4. Krider, E.P., Noggle, R.C., and Uman, M.A., A gated, wideband direction finder for lightning return strokes, *Journal of Applied Meteorology*, 15, 301, 1976.
5. Christian, H.J., Blakeslee, R.J., Boccippio, D., Boeck, W., Buechler, D., Driscoll, K., Goodman, Hall, J., Koshak, W., Mach, D., and Stewart, M., Global frequency and distribution of lightning as observed from space by the optical transient detector, *Journal of Geophysical Research*, 108(D1), 4005, 2003 or http://thunder.msfc.nasa.gov.
6. http://www.vaisala.com/businessareas/measurementsystems/thunderstorm/products/networks
7. Rakov, V.A. and Uman M.A., *Lightning: Physics and Effects*, Cambridge University Press, Cambridge, 2003.
8. Rizk, F.A.M., Modeling of transmission line exposure to direct lightning strokes, *IEEE Transactions on PWRD*, 5(4), p. 1983, 1990.
9. Berger, K., The earth flash, in *Lightning*, edited by Golde, R., Academic Press, London, 1977, pp. 119–190.
10. Anderson, R.B. and Eriksson, A.J., Lightning parameters for engineering applications, *Electra* 69, 65–102, 1980.
11. CIGRE Working Group 01 (Lightning) of Study Committee 33, Guide to Procedures for Estimating the Lightning Performance of Transmission Lines, *CIGRE Brochure 63*, Paris, October 1991.
12. *IEEE Guide for Improving the Lightning Performance of Transmission Lines*, IEEE Standard 1243–1997, December 1997.

18

Reactive Power Compensation

Rao S. Thallam
Salt River Project

18.1 The Need for Reactive Power Compensation

Except in a very few special situations, electrical energy is generated, transmitted, distributed, and utilized as alternating current (AC). However, alternating current has several distinct disadvantages. One of these is the necessity of reactive power that needs to be supplied along with active power. Reactive power can be leading or lagging. While it is the active power that contributes to the energy consumed, or transmitted, reactive power does not contribute to the energy. Reactive power is an inherent part of the "total power." Reactive power is either generated or consumed in almost every component of the system, generation, transmission, and distribution and eventually by the loads. The impedance of a branch of a circuit in an AC system consists of two components, resistance and reactance. Reactance can be either inductive or capacitive, which contribute to reactive power in the circuit. Most of the loads are inductive, and must be supplied with lagging reactive power. It is economical to supply this reactive power closer to the load in the distribution system.

In this chapter, reactive power compensation, mainly in transmission systems installed at substations, is discussed. Reactive power compensation in power systems can be either shunt or series. Both will be discussed.

18.1.1 Shunt Reactive Power Compensation

Since most loads are inductive and consume lagging reactive power, the compensation required is usually supplied by leading reactive power. Shunt compensation of reactive power can be employed either at load level, substation level, or at transmission level. It can be capacitive (leading) or inductive (lagging) reactive power, although in most cases as explained before, compensation is

capacitive. The most common form of leading reactive power compensation is by connecting shunt capacitors to the line.

18.1.2 Shunt Capacitors

Shunt capacitors are employed at substation level for the following reasons:

1. Voltage regulation: The main reason that shunt capacitors are installed at substations is to control the voltage within required levels. Load varies over the day, with very low load from midnight to early morning and peak values occurring in the evening between 4 PM and 7 PM. Shape of the load curve also varies from weekday to weekend, with weekend load typically low. As the load varies, voltage at the substation bus and at the load bus varies. Since the load power factor is always lagging, a shunt connected capacitor bank at the substation can raise voltage when the load is high. The shunt capacitor banks can be permanently connected to the bus (fixed capacitor bank) or can be switched as needed. Switching can be based on time, if load variation is predictable, or can be based on voltage, power factor, or line current.
2. Reducing power losses: Compensating the load lagging power factor with the bus connected shunt capacitor bank improves the power factor and reduces current flow through the transmission lines, transformers, generators, etc. This will reduce power losses (I^2R losses) in this equipment.
3. Increased utilization of equipment: Shunt compensation with capacitor banks reduces kVA loading of lines, transformers, and generators, which means with compensation they can be used for delivering more power without overloading the equipment.

Reactive power compensation in a power system is of two types—shunt and series. Shunt compensation can be installed near the load, in a distribution substation, along the distribution feeder, or in a transmission substation. Each application has different purposes. Shunt reactive compensation can be inductive or capacitive. At load level, at the distribution substation, and along the distribution feeder, compensation is usually capacitive. In a transmission substation, both inductive and capacitve reactive compensation are installed.

18.2 Application of Shunt Capacitor Banks in Distribution Systems—A Utility Perspective

The Salt River Project (SRP) is a public power utility serving more than 720,000 (April 2000) customers in central Arizona. Thousands of capacitor banks are installed in the entire distribution system. The primary usage for capacitor banks in the distribution system is to maintain a certain power factor at peak loading conditions. The target power factor is .98 leading at system peak. This figure was set as an attempt to have a unity power factor on the 69-kV side of the substation transformer. The leading power factor compensates for the industrial substations that have no capacitors. The unity power factor maintains a balance with ties to other utilities.

The main purpose of the capacitors is not for voltage support, as the case may be at utilities with long distribution feeders. Most of the feeders in the SRP service area do not have long runs (substations are about two miles apart) and load tap changers on the substation transformers are used for voltage regulation.

The SRP system is a summer peaking system. After each summer peak, a capacitor study is performed to determine the capacitor requirements for the next summer. The input to the computer program for evaluating capacitor additions consists of three major components:

- Megawatts and megavars for each substation transformer at peak.
- A listing of the capacitor banks with size and operating status at time of peak.
- The next summer's projected loads.

By looking at the present peak MW and Mvars and comparing the results to the projected MW loads, Mvar deficiencies can be determined. The output of the program is reviewed and a listing of potential

TABLE 18.1 Number and Size of Capacitor Banks in the SRP System

	Number of Banks	
Kvar	Line	Station
150	1	
300	140	
450	4	
600	758	2
900	519	
1200	835	581
Total	2257	583

TABLE 18.2 SRP Line Capacitors by Type of Control

Type of Control	Number of Banks
Current	4
Fixed	450
Time	1760
Temperature	38 (used as fixed)
Voltage	5

needs is developed. The system operations personnel also review the study results and their input is included in making final decisions about capacitor bank additions.

Once the list of additional reactive power requirements is finalized, determinations are made about the placement of each bank. The capacitor requirement is developed on a per-transformer basis. The ratio of the kvar connected to kVA per feeder, the position on the feeder of existing capacitor banks, and any concentration of present or future load are all considered in determining the position of the new capacitor banks. All new capacitor banks are 1200 kvar. The feeder type at the location of the capacitor bank determines if the capacitor will be pole-mounted (overhead) or pad-mounted (underground).

Capacitor banks are also requested when new feeders are being proposed for master plan communities, large housing developments, or heavy commercial developments.

Table 18.1 shows the number and size of capacitor banks in the SRP system in 1998. Table 18.2 shows the number of line capacitors by type of control.

Substation capacitor banks (three or four per transformer) are usually staged to come on and go off at specific load levels.

18.3 Static VAR Control (SVC)

Static VAR compensators, commonly known as SVCs, are shunt connected devices, vary the reactive power output by controlling or switching the reactive impedance components by means of power electronics. This category includes the following equipment:

Thyristor controlled reactors (TCR) with fixed capacitors (FC)
Thyristor switched capacitors (TSC)
Thyristor controlled reactors in combination with mechanically or Thyristor switched capacitors

SVCs are installed to solve a variety of power system problems:

1. Voltage regulation
2. Reduce voltage flicker caused by varying loads like arc furnace, etc.
3. Increase power transfer capacity of transmission systems
4. Increase transient stability limits of a power system
5. Increase damping of power oscillations
6. Reduce temporary overvoltages
7. Damp subsynchronous oscillations

A view of an SVC installation is shown in Fig. 18.1.

18.3.1 Description of SVC

Figure 18.2 shows three basic versions of SVC. Figure 18.2a shows configuration of TCR with fixed capacitor banks. The main components of a SVC are thyristor valves, reactors, the control system, and the step-down transformer.

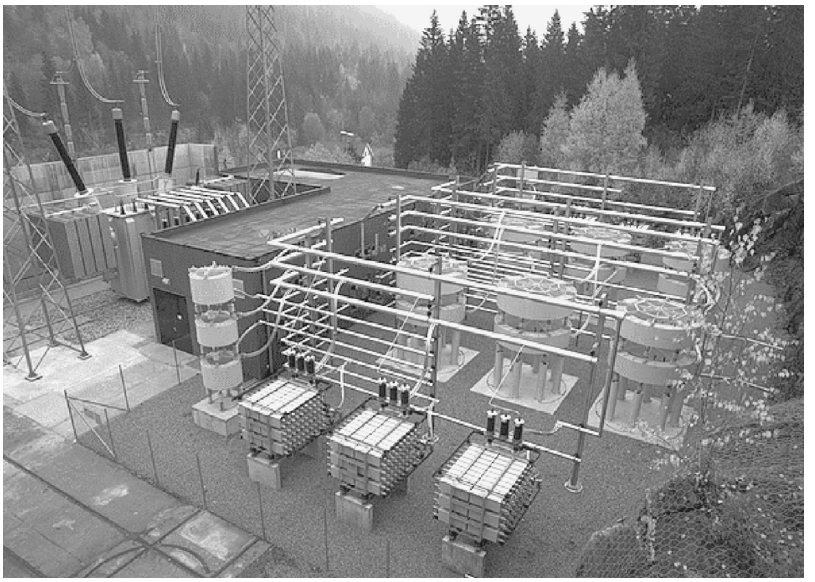

FIGURE 18.1 View of static VAR compensator (SVC) installation. (Photo courtesy of ABB.)

18.3.2 How Does SVC Work?

As the load varies in a distribution system, a variable voltage drop will occur in the system impedance, which is mainly reactive. Assuming the generator voltage remains constant, the voltage at the load bus will vary. The voltage drop is a function of the reactive component of the load current, and system and transformer reactance. When the loads change very rapidly, or fluctuate frequently, it may cause "voltage flicker" at the customers' loads. Voltage flicker can be annoying and irritating to customers because of the "lamp flicker" it causes. Some loads can also be sensitive to these rapid voltage fluctuations.

An SVC can compensate voltage drop for load variations and maintain constant voltage by controlling the duration of current flow in each cycle through the reactor. Current flow in the reactor can be controlled by controlling the gating of thyristors that control the conduction period of the thyristor in each cycle, from zero conduction (gate signal off) to full-cycle conduction. In Fig. 18.2a, for example, assume the MVA of the fixed capacitor bank is equal to the MVA of the reactor when the reactor branch is conducting for full cycle. Hence, when the reactor branch is conducting full cycle, the net reactive power drawn by the SVC (combination of capacitor bank and thyristor controlled reactor) will be zero. When the load reactive power (which is usually inductive) varies, the SVC reactive power will be varied to match the load reactive power by controlling the duration of the conduction of current in the thyristor controlled reactive power branch. Figure 18.3 shows current waveforms for three conduction levels, 60, 120 and 180°. Figure 18.3a shows waveforms for thyristor gating angle (α) of 90°, which gives a conduction angle (σ) of 180° for each thyristor. This is the case for full-cycle conduction, since the two back-to-back thyristors conduct in each half-cycle. This case is equivalent to shorting the thyristors. Figure 18.3b is the case when the gating signal is delayed for 30° after the voltage peak, and results in a conduction angle of 120°. Figure 18.3c is the case for $\alpha = 150°$ and $\sigma = 60°$

With a fixed capacitor bank as shown in Fig. 18.2a, it is possible to vary the net reactive power of the SVC from 0 to the full capacitive VAR only. This is sufficient for most applications of voltage regulation, as in most cases only capacitive VARs are required to compensate the inductive VARs of the load. If the capacitor can be switched on and off, the MVAR can be varied from full inductive to full capacitive, up to the rating of the inductive and capacitive branches. The capacitor bank can be switched by mechanical

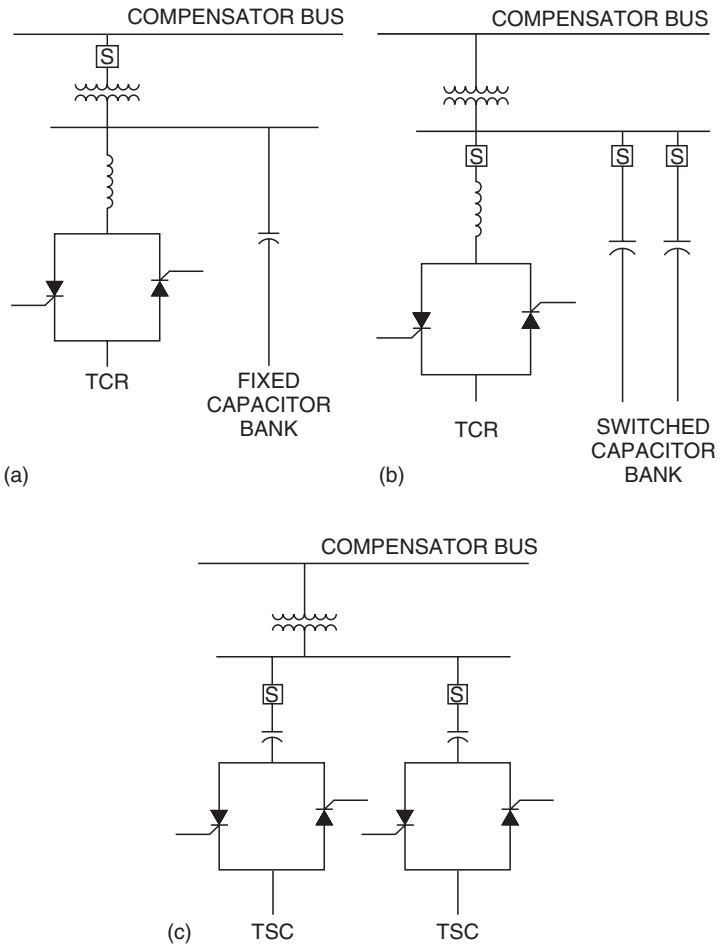

FIGURE 18.2 Three versions of SVC. (a) TCR with fixed capacitor bank; (b) TCR with switched capacitor banks; and (c) thyristor switched capacitor compensator.

breakers (see Fig. 18.2b) if time delay (usually five to ten cycles) is not a consideration, or they can be switched fast (less than one cycle) by thyristor switches (see Fig. 18.2c).

Reactive power variation with switched capacitor banks for an SVC is shown in Fig. 18.4.

18.4 Series Compensation

Series compensation is commonly used in high-voltage AC transmission systems. They were first installed in that late 1940s. Series compensation increases power transmission capability, both steady state and transient, of a transmission line. Since there is increasing opposition from the public to construction of EHV transmission lines, series capacitors are attractive for increasing the capabilities of transmission lines. Series capacitors also introduce some additional problems for the power system. These will be discussed later.

Power transmitted through the transmission system (shown in Fig. 18.5) is given by:

$$P_2 = \frac{V_1 \cdot V_2 \cdot \sin \delta}{X_L} \tag{18.1}$$

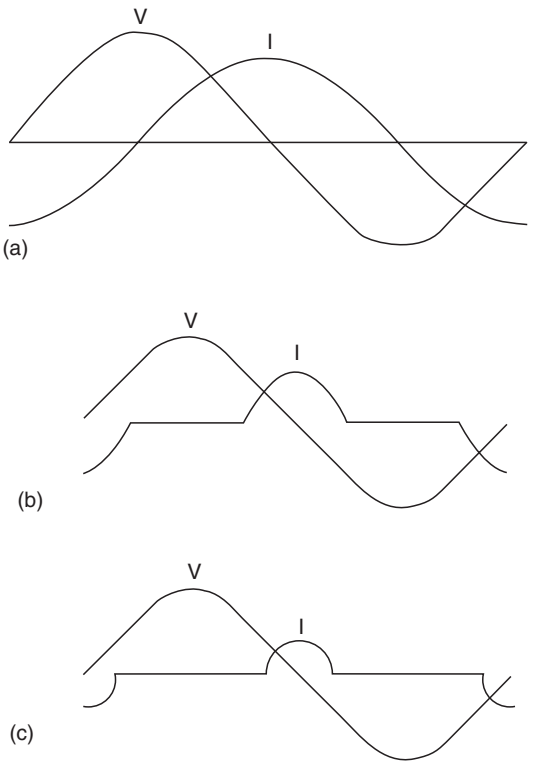

FIGURE 18.3 TCR voltage (V) and current (I) waveforms for three conduction levels. Thyristor gating angle = α; conduction angle = σ. (a) α = 90° and σ = 180°; (b) α = 120° and σ = 120°; and (c) α = 150° and σ = 60°.

where P_2 = Power transmitted through the transmission system
V_1 = Voltage at sending end of the line
V_2 = Voltage at receiving end of transmission line
X_L = Reactance of the transmission line
δ = Phase angle between V_1 and V_2

Equation (18.1) shows that if the total reactance of a transmission system is reduced by installing capacitance in series with the line, the power transmitted through the line can be increased.

With a series capacitor installed in the line, Eq. (18.1) can be written as

$$P_2 = \frac{V_1 \cdot V_2 \cdot \sin\delta}{X_L - X_C} \tag{18.2}$$

$$= \frac{V_1 \cdot V_2 \cdot \sin\delta}{X_L(1 - K)} \tag{18.3}$$

where $K = \dfrac{X_C}{X_L}$ is degree of the compensation, usually expressed in percent. A 70% series compensation means the value of the series capacitor in ohms is 70% of the line reactance.

18.5 Series Capacitor Bank

A series capacitor bank consists of a capacitor bank, overvoltage protection system, and a bypass breaker, all elevated on a platform, which is insulated for the line voltage. See Fig. 18.6. The overvoltage protection is comprised of a zinc oxide varistor and a triggered spark gap, which are connected in parallel to the capacitor bank, and a damping reactor. Prior to the development of the high-energy zinc oxide varistor in the 1970s, a silicon carbide nonlinear resistor was used for overvoltage protection. Silicon carbide resistors require a spark gap in series because the nonlinearity of the resistors is not high enough. The zinc oxide varistor has better nonlinear resistive characteristics, provides better protection, and has become the standard protection system for series capacitor banks.

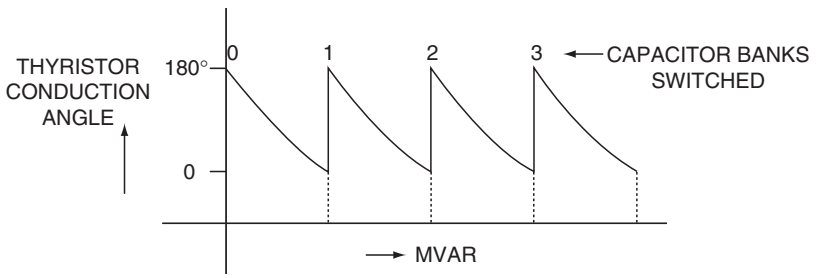

FIGURE 18.4 Reactive power variation of TCR with switched capacitor banks.

The capacitor bank is usually rated to withstand the line current for normal power flow conditions and power swing conditions. It is not economical to design the capacitors to withstand the currents and voltages associated with faults. Under these conditions capacitors are protected by a metal oxide varistor (MOV) bank. The MOV has a highly nonlinear resistive characteristic and conducts negligible current until the voltage across it reaches the protective level. For internal faults, which are defined as faults within the line section in which the series capacitor bank is located, fault currents can be very high. Under these conditions, both the capacitor bank and MOV will be bypassed by the "triggered spark gap." The damping reactor (D) will limit the capacitor discharge current and damps the oscillations caused by spark gap operation or when the bypass breaker is closed. The amplitude, frequency of oscillation, and rate of damping of the capacitor discharge current will be determined by the circuit parameters, C (series capacitor), L (damping inductor), and resistance in the circuit, which in most cases is losses in the damping reactor.

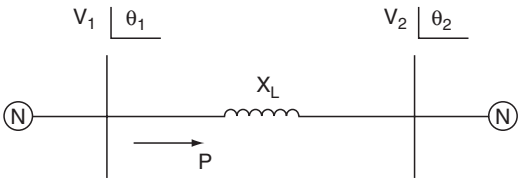

FIGURE 18.5 Power flow through transmission line.

A view of series capacitor bank installation is shown in Fig. 18.7

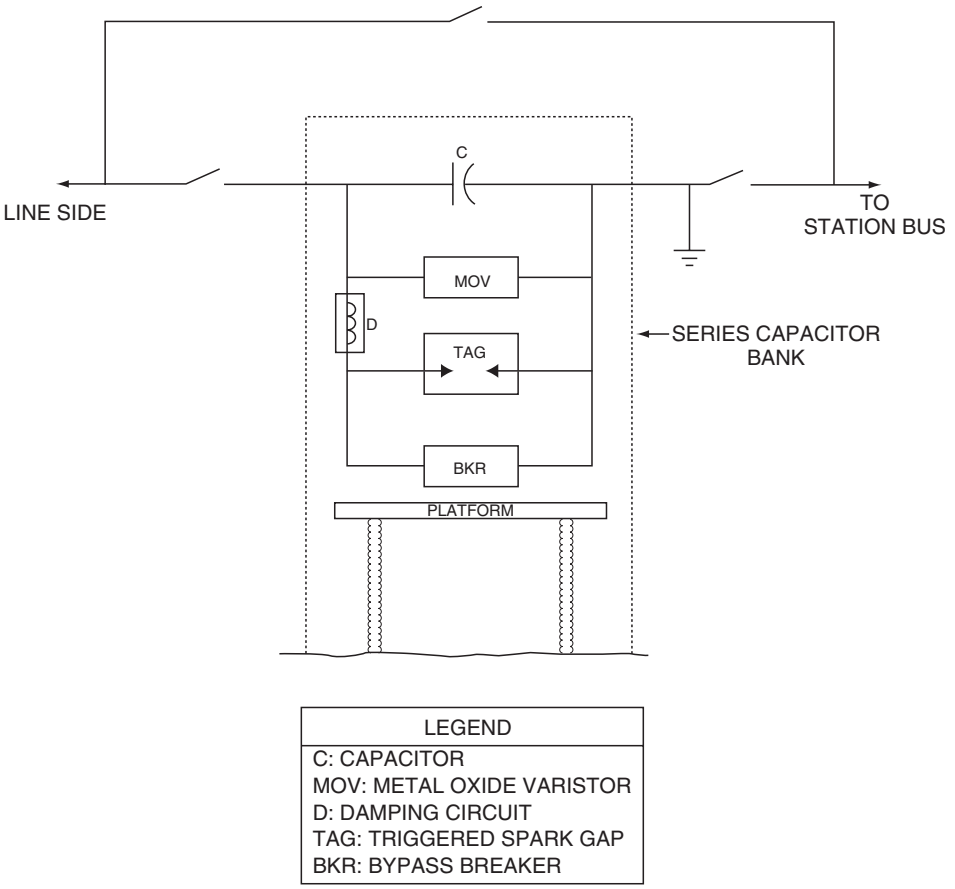

FIGURE 18.6 Schematic one-line diagram of series capacitor bank.

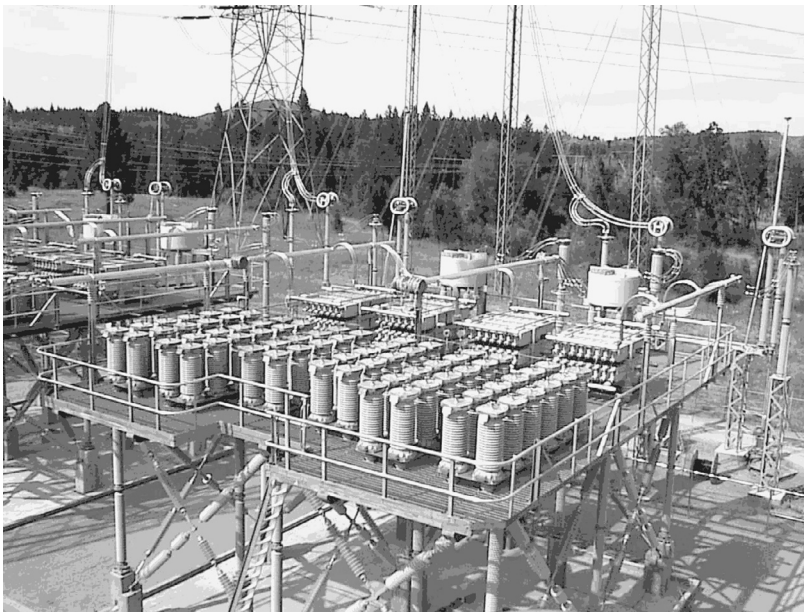

FIGURE 18.7 Aerial view of 500-kV series capacitor installation. (Photo courtesy of ABB.)

18.5.1 Description of Main Components

18.5.1.1 Capacitors

The capacitor bank for each phase consists of several capacitor units in series-parallel arrangement, to make up the required voltage, current, and Mvar rating of the bank. Each individual capacitor unit has one porcelain bushing. The other terminal is connected to the stainless steel casing. The capacitor unit usually has a built-in discharge resistor inside the case. Capacitors are usually all film design with insulating fluid that is non-PCB. Two types of fuses are used for individual capacitor units—internally fused or externally fused. Externally fused units are more commonly used in the U.S. Internally fused capacitors are prevalent in European installations.

18.5.1.2 Metal Oxide Varistor (MOV)

A metal oxide varistor is built from zinc oxide disks in series and parallel arrangement to achieve the required protective level and energy requirement. One to four columns of zinc oxide disks are installed in each sealed porcelain container, similar to a high-voltage surge arrester. A typical MOV protection system contains several porcelain containers, all connected in parallel. The number of parallel zinc oxide disk columns required depends on the amount of energy to be discharged through the MOV during the worst-case design scenario. Typical MOV protection system specifications are as follows.

The MOV protection system for the series capacitor bank is usually rated to withstand energy discharged for all faults in the system external to the line section in which the series capacitor bank is located. Faults include single-phase, phase-to-phase, and three-phase faults. The user should also specify the fault duration. Most of the faults in EHV systems will be cleared by the primary protection system in 3 to 4 cycles. Back-up fault clearing can be from 12 to 16 cycles duration. The user should specify whether the MOV should be designed to withstand energy for back-up fault clearing times. Sometimes it is specified that the MOV be rated for all faults with primary protection clearing time, but for only single-phase faults for back-up fault clearing time. Statistically, most of the faults are single-phase faults.

The energy discharged through the MOV is continuously monitored and if it exceeds the rated value, the MOV will be protected by the firing of a triggered air gap, which will bypass the MOV.

18.5.1.3 Triggered Air Gap

The triggered air gap provides a fast means of bypassing the series capacitor bank and the MOV system when the trigger signal is issued under certain fault conditions (for example, internal faults) or when the energy discharged through the MOV exceeds the rated value. It typically consists of a gap assembly of two large electrodes with an air gap between them. Sometimes two or more air gaps in series can also be employed. The gap between the electrodes is set such that the gap assembly sparkover voltage without trigger signal will be substantially higher than the protective level of the MOV, even under the most unfavorable atmospheric conditions.

18.5.1.4 Damping Reactor

A damping reactor is usually an air-core design with parameters of resistance and inductance to meet the design goal of achieving the specified amplitude, frequency, and rate of damping. The capacitor discharge current when bypassed by a triggered air gap or a bypass breaker will be damped oscillation with amplitude, rate of damping, and frequency determined by circuit parameters.

18.5.1.5 Bypass Breaker

The bypass breaker is usually a standard line circuit breaker with a rated voltage based on voltage across the capacitor bank. In most of the installations, the bypass breaker is located separate from the capacitor bank platform and outside the safety fence. This makes maintenance easy. Both terminals of the breaker standing on insulator columns are insulated for the line voltage. It is usually a SF_6 puffer-type breaker, with controls at ground level.

18.5.1.6 Relay and Protection System

The relay and protection system for the capacitor bank is located at ground level, in the station control room, with information from and to the platform transmitted via fiber-optic cables. The present practice involves all measured quantities on the platform being transmitted to ground level, with all signal processing done at ground level.

18.5.2 Subsynchronous Resonance

Series capacitors, when radially connected to the transmission lines from the generation near by, can create a subsynchronous resonance (SSR) condition in the system under some circumstances. SSR can cause damage to the generator shaft and insulation failure of the windings of the generator. This phenomenon is well-described in several textbooks, given in the reference list at the end of this chapter.

18.5.3 Adjustable Series Compensation (ASC)

The ability to vary the series compensation will give more control of power flow through the line, and can improve the dynamic stability limit of the power system. If the series capacitor bank is installed in steps, bypassing one or more steps with bypass breakers can change the amount of series compensation of the line. For example, as shown in Fig. 18.8, if the bank consists of 33% and 67% of the total

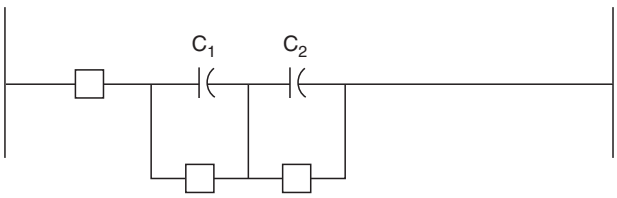

FIGURE 18.8 Breaker controlled variable series compensation.

compensation, four steps, 0%, 33%, 67%, and 100%, can be obtained by bypassing both banks, smaller bank (33%), larger bank (67%), and not bypassing both banks, respectively.

Varying the series compensation by switching with mechanical breakers is slow, which is acceptable for control of steady-state power flow. However, for improving the dynamic stability of the system, series compensation has to be varied quickly. This can be accomplished by thyristor controlled series compensation (TCSC).

18.5.4 Thyristor Controlled Series Compensation (TCSC)

Thyristor controlled series compensation provides fast control and variation of the impedance of the series capacitor bank. To date (1999), three prototype installations, one each by ABB, Siemens, and the General Electric Company (GE), have been installed in the U.S. TCSC is part of the Flexible AC Transmission System (FACTS), which is an application of power electronics for control of the AC system to improve the power flow, operation, and control of the AC system. TCSC improves the system performance for subsynchronous resonance damping, power swing damping, transient stability, and power flow control.

The latest of the three prototype installations is the one at the Slatt 500-kV substation in the Slatt-Buckley 500-kV line near the Oregon-Washington border in the U.S. This is jointly funded by the Electric Power Research Institute (EPRI), the Bonneville Power Administration (BPA), and the General Electric Company (GE). A one-line diagram of the Slatt TCSC is shown in Fig. 18.9. The capacitor bank (8 ohms) is divided into six identical TCSC modules. Each module consists of a capacitor (1.33 ohms), back-to-back thyristor valves controlling power flow in both directions, a reactor (0.2 ohms), and a varistor. The reactors in each module, in series with thyristor valves, limit the rate of change of current through the thyristors. The control of current flow through the reactor also varies the impedance of the combined capacitor-reactor combination, giving the variable impedance. When thyristor gating is blocked, complete line current flows through the capacitance only, and the impedance is 1.33 ohms capacitive (see Fig. 18.10a). When the thyristors are gated for full conduction (Fig. 18.10b), most of the line current flows through the reactor-thyristor branch (a small current flows through the capacitor) and the resulting impedance is 0.12 ohms inductive. If thyristors are gated for partial conduction only (Fig. 18.10c), circulating current will flow between capacitor and inductor, and the impedance can be varied from 1.33 ohms and 4.0 ohms, depending on the angle of conduction of the thyristor valves. The latter is called the vernier operating mode.

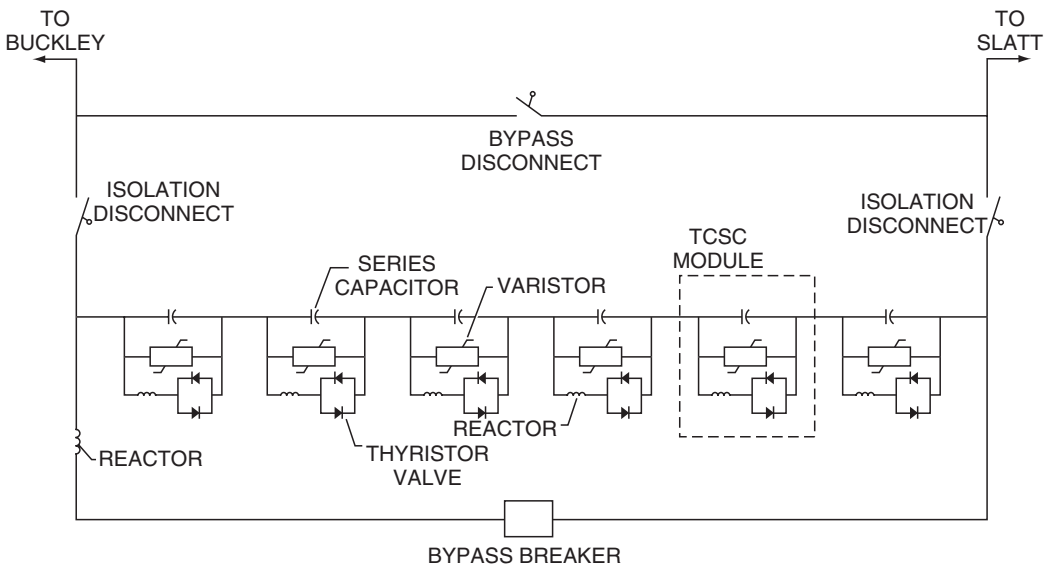

FIGURE 18.9 One-line diagram of TCSC installed at slatt substation.

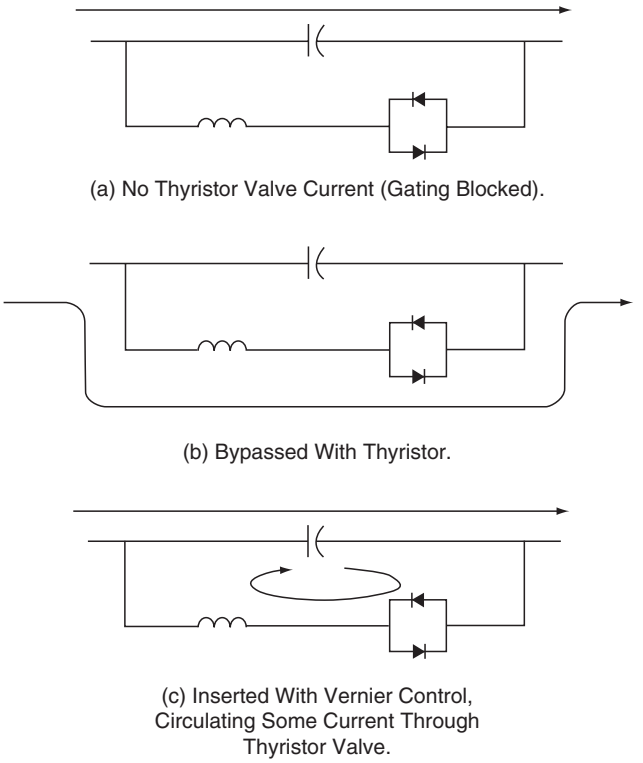

FIGURE 18.10 Current flow during various operating modes of TCSC.

The complete capacitor bank with all six modules can be bypassed by the bypass breaker. This bypass breaker is located outside the main capacitor bank platform, similar to the case for the conventional series capacitor bank. There is also a reactor connected in series with the bypass breaker to limit the magnitude of capacitor discharge current through the breaker. All reactors are of air-core dry-type design and rated for the full line current rating. Metal oxide varistors (MOV) connected in parallel with the capacitors in each module provide overvoltage protection. The MOV for a TCSC requires significantly less energy absorption capability than is the case for a conventional series capacitor of comparable size, because gating of thyristor valves provides quick protection for faulted conditions.

18.5.5 STATic COMpensator (STATCOM)

STATCOM provides variable reactive power from lagging to leading, but with no inductors or capacitors for var generation. Reactive power generation is achieved by regulating the terminal voltage of the converter. The STATCOM consists of a voltage source inverter using gate turn-off thyristors (GTOs) which produces an alternating voltage source in phase with the transmission voltage, and is connected to the line through a series inductance which can be the transformer leakage inductance required to match the inverter voltage with line voltage. If the terminal voltage (V_t) of the voltage source inverter is higher than the bus voltage, STATCOM generates leading reactive power. If V_t is lower than the bus voltage, STATCOM generates lagging reactive power. The performance is similar to the performance of a synchronous condenser (unloaded synchronous motor with varying excitation).

Reactive power generated or absorbed by STATCOM is not a function of the capacitor on the DC bus side of the inverter. The capacitor is rated to limit only the ripple current, and hence the harmonics in the output voltage.

The first demonstration STATCOM of ±100 Mvar rating was installed at the Tennessee Valley Authority's Sullivan substation in 1994.

18.6 Defining Terms

Shunt capacitor bank—A large number of capacitor units connected in series and parallel arrangement to make up the required voltage and current rating, and connected between the high-voltage line and ground, between line and neutral, or between line-to-line.

Voltage flicker—Commonly known as "flicker" and "lamp flicker," this is a rapid and frequent fluctuation of supply voltage that causes lamps to flicker. Lamp flicker can be annoying, and some loads are sensitive to these frequent voltage fluctuations.

Subsynchronous resonance—Per IEEE, subsynchronous resonance is an electric power system condition where the electric network exchanges energy with a turbine generator at one or more of the natural frequencies of the combined system below the synchronous frequency of the system.

References

Anderson, P.M., Agrawal, B.L., and Van Ness, J.E., *Subsynchronous Resonance in Power Systems*, IEEE Press, 1990.

Anderson, P.M. and Farmer, R.G., *Series Compensation in Power Systems*, PBLSH! Inc. 1996.

Gyugyi, L., Otto, R.A., and Putman, T.H., Principles and application of thyristor-controlled shunt compensators, *IEEE Trans. on Power Appar. and Syst.*, 97, 1935–1945, Sept/Oct 1978.

Gyugyi, L. and Taylor, Jr., E.R., Characteristics of static thyristor-controlled shunt compensators for power transmission applications, *IEEE Trans. on Power Appar. and Syst.*, PAS-99, 1795–1804, 1980.

Hammad, A.E., Analysis of power system stability enhancement by static VAR compensators, *IEEE Trans. on Power Syst.*, 1, 222–227, 1986.

Miller, T.J.E., Ed., *Reactive Power Control in Electric Systems*, John Wiley & Sons, New York, 1982.

Miske, Jr., S.A. et al., Recent Series Capacitor Applications in North America, Paper presented at *CEA Electricity '95 Vancouver Conference*, March 1995.

Padiyar, K.R., *Analysis of Subsynchronous Resonance in Power Systems*, Kluwer Academic Publishers, 1999.

Schauder, C. et al., Development of a ±100 MVAR static condenser for voltage control of transmission systems, *IEEE Trans. on Power Delivery*, 10(3), 1486–1496, July 1995.

19

Environmental Impact of Transmission Lines

George G. Karady
Arizona State University

19.1 Introduction

The appearance of the first transmission lines more than one hundred years ago immediately started discussion and public concerns. When the first transmission line was built, more electrocutions occurred because of people climbing up the towers, flying kites, and touching wet conducting ropes. As the public became aware of the danger of electrocution, the aesthetical effect of the transmission lines generated pubic discussion. In fact, there is a story of Frank Lloyd Wright, the famous architect, calling President Roosevelt and demanding the removal of high-voltage lines obstructing his view in Scottsdale, Arizona. Undoubtedly, a transmission line corridor with several lines would disturb the appearance of a quite green valley.

The rapid increase of radio and television transmission has produced the occurrence of electromagnetic interference (EMI) problems. The high voltage on the transmission line produces corona discharge that generates electromagnetic waves. These waves disturb the radio and television reception, which resulted in public protests and opposition to build lines too near towns.

In the 1960s, the electrical field surrounding the high-voltage lines became subject to public concerns. The electrical field can produce minor sparks and small electric shocks under a high-voltage line. An example of this would be, if a woman were to walk under a line holding an umbrella, the woman would feel the electric shocks produced by these small discharges.

In the 1970s, the transmission line current produced magnetic fields and became a public issue. Several newspaper articles discussed the adverse health effects of magnetic fields. This generated intensive research all over the world. The major concern is that exposure to magnetic fields caused cancer, mostly leukemia. The U.S. government report concluded that there was no evidence that moderate 60 Hz magnetic field caused cancer. However, this opinion is not shared by all.

This chapter will discuss the listed environmental effects of transmission lines.

19.2 Aesthetical Effects of Lines

The first transmission towers were small wooden poles that were tempting for children to climb but had no environmental impact. However, the increase of voltage resulted in large steel structures over 100 ft high and 50 ft wide.

In North America, the large wooden structures were common until the Second World War. The typical voltage of transmission lines with wooden poles is less than 132 kV, although 220 kV lines with H-frame wooden towers are also built in the Midwest.

Figure 19.1 shows a transmission line with H-frame wooden towers. This construction fits well in the rural environment and does not produce environmental concerns.

The increasing voltage and need for crossing large valleys and rivers resulted in the appearance of steel towers. These towers are welded or riveted lattice structures. Several different conductor arrangements are used. Figure 19.2a shows a lattice tower with conductors arranged horizontally. The horizontal arrangement increases the widths of the tower, which produces a more visible effect. Figure 19.2b shows a double circuit line with vertically arranged conductors. This results in a taller and more compact appearance.

The presented pictures demonstrate that the transmission lines with large steel towers are not very aesthetically pleasing. They do not blend in with the environment and can interrupt a beautiful landscape.

The increasing demand of electricity and the public objection to build new transmission lines resulted in the development of transmission line corridors. The utilities started to build lines in parallel on right-of-ways land that they already owned. Figure 19.3 shows a typical transmission line corridor. The appearance of the maze of conductors and large steel structures are not an aesthetically pleasing sight.

The public displeasure with the lattice tower triggered research work on the development of aesthetically more pleasing structures. Several attempts were made to develop nonmetallic transmission line

FIGURE 19.1 220 kV line with H-frame wooden towers.

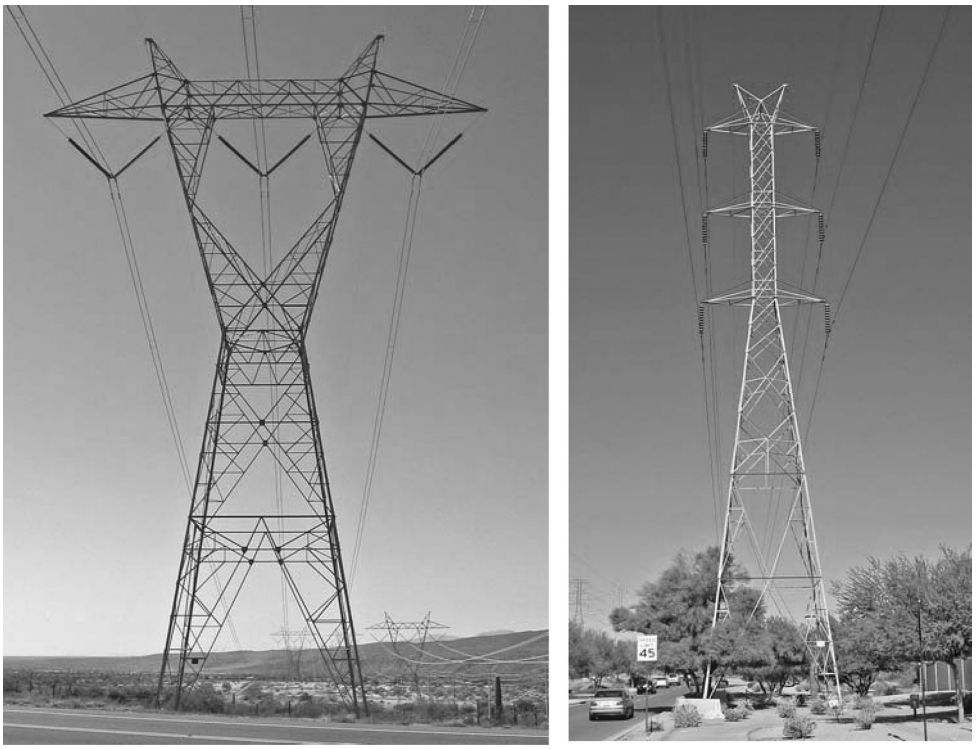

(a) (b)

FIGURE 19.2 High-voltage transmission lines. (a) Single circuit line with horizontally arranged conductors. (b) Double circuit line with vertically arranged conductors.

structure using fiberglass rods, where the insulators are replaced by the tower itself. Although the development of nonmetallic structures was unsuccessful, the development of tubular steal towers led to a more pleasing appearance. Figure 19.4 shows tubular steel tower used in Arizona at the 220 kV high-voltage lines.

FIGURE 19.3 Transmission line corridor.

FIGURE 19.4 A 220 kV suspension tower.

Figure 19.4 demonstrates that the slender tubular structure is less disturbing and aesthetically more pleasing. These towers blend in better with the desert environment and cause less visual interruptions.

The presented examples prove that the aesthetical appearance of the transmission lines is improving although even the best tower structures disturb the environment. The ultimate solution is the replacement of the lines by an underground cable system. Unfortunately, both technical and economic problems are preventing the use of underground energy transmission systems.

19.3 Magnetic Field Generated by HV Lines

Several newspaper articles presented survey results showing that the exposure to magnetic fields increases the cancer occurrence. Studies linked the childhood leukemia to transmission line generated magnetic field exposure. This triggered research in both biological and electrical engineering fields. The biological research studied the magnetic field effect on cells and performed statistical studies to determine the correlation between field exposure and cancer occurrence. The electrical engineering research aimed the determination of magnetic field strength near to transmission lines, electric equipment, motors, and appliances. A related engineering problem is the reduction of magnetic field generated by lines and other devices.

In this chapter we will present a calculation method to determine a transmission line generated magnetic field and summarize the major results of biological research.

19.3.1 Magnetic Field Calculation

The electric current in a cylindrical transmission line conductor generates magnetic field surrounding the conductor. The magnetic field lines are concentric circles. At each point around the conductor, the magnetic field strength or intensity is described by a field vector that is perpendicular to the radius drawn from the center of the conductor.

Figure 19.5 shows the current-carrying conductor, a circular magnetic field line, and the magnetic field vector H in a selected observation point. The magnetic field vector is perpendicular to the radius of the circular magnetic field line. The H field vector is divided into horizontal and vertical components. The location of both the observation point and the conductor is described by the x, y coordinates.

The magnetic field intensity is calculated by using the ampere law. The field intensity is

$$H = \frac{I}{2\pi r} = \frac{I}{2\pi\sqrt{(x_i - X)^2 + (y_i - Y)^2}}$$

where H is the field intensity in A/m, I is the current in the conductor, r is the distance from the conductor, (X, Y) are the coordinates of the observation point, and (x_i, y_i) are the coordinates of the conductor.

The horizontal and vertical components of the field are calculated from the triangle formed by the field vectors. The angle is calculated from the triangle formed with the coordinate's differences as shown in Fig. 19.5.

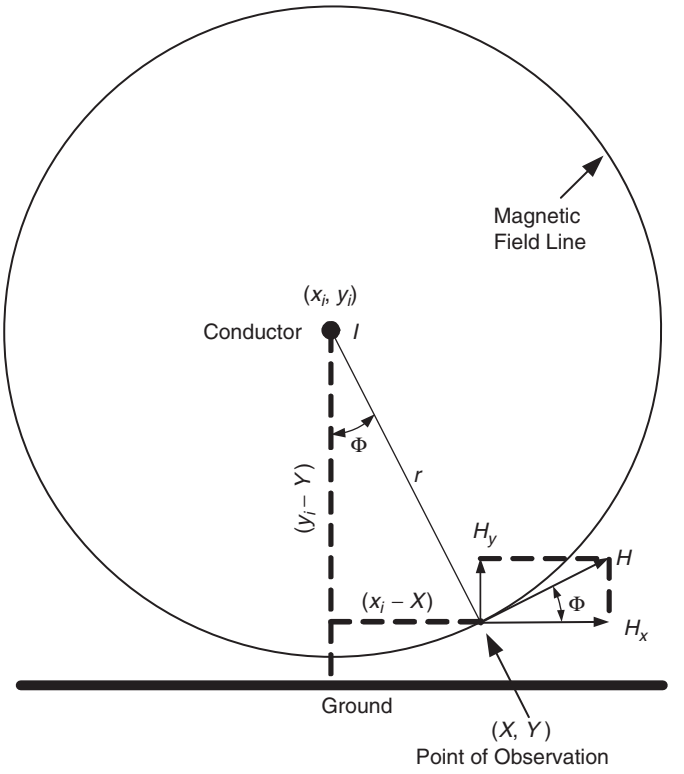

FIGURE 19.5 Magnetic field generation.

$$\cos(\Phi) = \frac{x_i - X}{\sqrt{(x_i - X)^2 + (y_i - Y)^2}} \quad \sin(\Phi) = \frac{y_i - Y}{\sqrt{(x_i - X)^2 + (y_i - Y)^2}}$$

The vertical and horizontal field components are

$$H_x = H\cos(\Phi) = \frac{1}{2\pi}\frac{x_i - X}{(x_i - X)^2 + (y_i - Y)^2}$$
$$H_y = H\sin(\Phi) = \frac{1}{2\pi}\frac{y_i - Y}{(x_i - X)^2 + (y_i - Y)^2}$$

In a three-phase system, each of the three-phase currents generates magnetic fields. The phase currents and corresponding field vectors are shifted by 120°. The three-phase currents are

$$I_1 = I \quad I_2 = Ie^{-120^\circ} \quad I_3 = Ie^{-240^\circ}$$

The three-phase line generated field intensity is calculated by substituting the conductor currents and coordinates in the equations describing the horizontal and vertical field components. This produces three horizontal and three vertical field vectors. The horizontal and vertical components of the three-phase line generated magnetic field are the sum of the three-phase components:

$$H_x = X_{x\_1} + H_{x\_2} + H_{x\_3} \qquad H_y = X_{y\_1} + H_{y\_2} + H_{y\_3}$$

where H_x is the horizontal component of three-phase generated magnetic field, H_y is the vertical component of three-phase generated magnetic field, H_{x_1}, H_{x_2}, H_{x_3} are the horizontal components of phases 1, 2, and 3 generated magnetic field, and H_{y_1}, H_{y_2}, H_{y_3} are the vertical components of phases 1, 2, and 3 generated magnetic field.

The vector sum of the horizontal and vertical components gives the three-phase line generated total magnetic field intensity:

$$H_{3\_\text{phase}} = \sqrt{H_x^2 + H_y^2}$$

The magnetic field flux density is calculated by multiplying the field intensity by the free space permeability:

$$\mu_o = 4\pi \times 10^{-7}\frac{\text{H}}{\text{m}} \quad B_{3\_\text{phase}} = \mu_o H_{3\_\text{phase}}$$

For the demonstration of the expected results, we calculated a 500-kV transmission line generated magnetic flux density under the line in 1 m distance from the ground. The conductors are arranged horizontally. The average conductor height is 24.38 m (80 ft); the distance between the conductors is 10.66 m (35 ft). The line current is 2000 A. Figure 19.6 shows the magnetic flux density distribution under the line in 1 m from the ground. The locations of the line conductors are marked on the figure. It can be seen that the maximum flux density is under the middle conductor and it decreases rapidly with distance.

The right-of-way is around 200 ft in this transmission line. The maximum flux density is around 116 mG (milligauss) or 11.6 μT and around 18 mG (1.8 μT) at the edge of the right-of-way.

Although the acceptable level of magnetic flux density is not specified by national or international standards, the utilities maintain less than 100 mG (10 μT) at the edge of the right-of-way and less than 10 mG (1 μT) at the neighboring residential area.

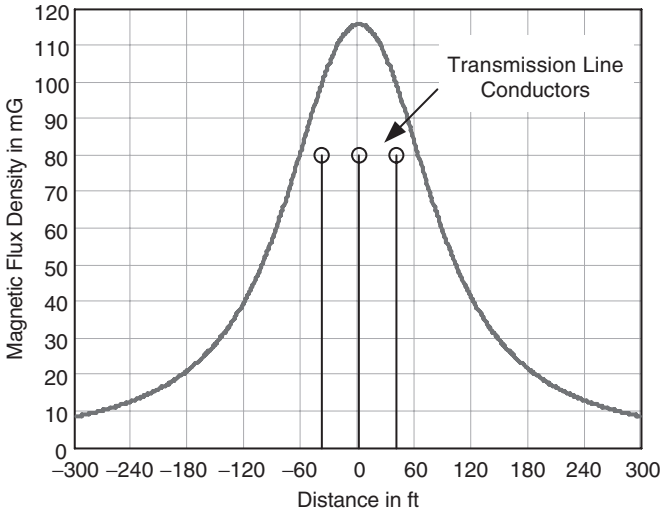

FIGURE 19.6 Magnetic field density under a 500-kV line when the load current is 2000 A.

19.3.2 Health Effect of Magnetic Field

The health effects of magnetic fields are a controversial subject, which generated an emotional discussion. The first study that linked the occurrence of childhood leukemia to electrical current generated magnetic fields was published in 1979 by Wertheimer and Leeper [1]. This was a statistical study where the electric wiring configuration near the house of the victim was related to the occurrence of childhood cancer. The researchers compared the wiring of the configuration including transmission lines close to the childhood leukemia victim's house and close to the house of a controlled population group. The study found a correlation between the occurrence of cancer and the power lines carrying high current. The study was dismissed because of inconsistencies and repeated in 1988 by Savitz et al. [2]. They measured the magnetic field in the victim's house and used the electric wiring configuration. The study found a modest statistical correlation between the cancer and wiring code but not between the cancer and the measured magnetic field. These findings initiated worldwide research on magnetic field health effects. The studies can be divided into three major categories:

- Epidemiological studies
- Laboratory studies
- Exposure assessment studies

Epidemiological studies: These statistical studies connect the exposure to magnetic and electric fields to health effects, particularly to occurrence of cancer. The early studies investigated the childhood cancer occurrence and residential wiring [1–3]. This was followed by studies relating the occupation (electrical worker) to cancer occurrence. In this category, the most famous one is a Swedish study [4], which found elevated risk for lymphoma among electric workers. However, other studies found no elevated cancer risk [5]. The uncertainty in all of these studies is the assessment of actual exposure to electromagnetic fields. As an example, some of the studies estimated the exposure to magnetic field using the job title of the worker or the postal code where the worker lived. The results of these studies are inconclusive, some of the studies showed elevated risk to cancer, most of them not.

Laboratory studies: These studies are divided into two categories: tissue studies and live animal studies. The tissue studies investigated the effect of electric and magnetic field on animal tissues. The studies showed that the electromagnetic field could cause chromosomal changes, single strand breaks, or alteration of ornithine decarboxylase, etc. [6,7]. Some of the studies speculate that the electromagnetic

exposure can be a promoter of cancer together with other carcinogen material. The general conclusion is that the listed effects do not prove that the EMF can be linked to cancer or other health effects.

The study on live animals showed behavioral changes in rats and mice. Human studies observed changes of heart rates and melatonin production as a result of EMF exposure [8,9]. The problem with the laboratory studies are that they use a much higher field than what occurs in residential areas. None of these studies showed that the EMF produces toxicity that is typical for carcinogens. An overall conclusion is that laboratory studies cannot prove that magnetic fields are related to cancer in humans.

Exposure assessment studies: In the U.S., the Electrical Power Research Institute led the research effort to assess the exposure to magnetic fields [10]. One of the interesting conclusions is the effect of ground current flowing through main water pipes. This current can generate a significant portion of magnetic fields in a residential area. Typically in 1 m distance from a TV, the magnetic field can be 0.01–0.2 μT; an electric razor and a fluorescent table lamp can produce a maximum of 0.3 μT. The worst is the microwave oven that can produce magnetic field around 0.3–0.8 μT in 1 m distance. The electric field produced by appliances varies between 30 and 130 V/m in a distance of 30 cm. The worst is the electric blanket that may generate 250 V/m [11].

The measurement of magnetic fields also created problems. EPRI developed a movable magnetic field measuring instrument. IEEE developed a standard ANSI/IEEE Std. 644, that presents a procedure to measure electric and magnetic field emitted by power lines. The conclusion is that both measuring techniques and instruments provide accurate exposure measurement.

Summary: The health effect of magnetic field remains a controversial topic in spite of the U.S. Environmental Protection Agency report [12,13] that concluded that the low frequency, low level electric and magnetic fields are not producing any health risks.

Many people believe that the prudent approach is the "prudent avoidance" to long-term exposure.

19.4 Electrical Field Generated by HV Lines

The energized transmission line produces electric field around the line. The high voltage on a transmission line drives capacitive current through the line. Typically, the capacitive current is maximum at the supply and linearly reduced to zero at the end of a no-loaded line, because of the evenly distributed line capacitance. The capacitive current generates sinusoidal variable charges on the conductors. The rms value of the sinusoidal charge is calculated and expressed as coulomb per meter. The equations describing the relation between the voltage and charge were derived in Chapter 21. For a better understanding, we summarize the derivation of equations for field calculation.

Figure 19.7 shows a long energized cylindrical conductor. This conductor generates an electrical field. The emitted electrical field lines are radial and the field inside the conductor is zero. The electric field intensity is

$$E = \frac{D}{\varepsilon_o} = \frac{Q}{2\pi\varepsilon_o}\frac{1}{x} \quad \varepsilon_o = \frac{10^{-9}}{36\pi}\frac{\text{F}}{\text{m}},$$

where D is the electric field flux density, ε_o is the free place permeability, Q is the charge on the conductor, X is the radial distance, and E is the electric field intensity.

The integral of the electric field between two points gives the voltage differences:

$$V_{D_1\_D_2} = \int_{D_1}^{D_2} \frac{Q}{2\pi\varepsilon_{ox}} dx = \frac{Q}{2\pi\varepsilon_o} \ln\left(\frac{D_2}{D_1}\right)$$

Typically, the three-phase transmission line is built with three conductors placed above the ground. The voltage between the conductors is the line-to-line voltage and between the conductor and ground is the line-to-ground voltage. As we described before, the line energization generates charges on the conductors. The conductor charges produce an electric field around the conductors. The electric field lines are radial close to the conductors. In case of one conductor above the ground the electric field lines are circles. In addition to the electrical field, the conductor is surrounded by equipotential lines.

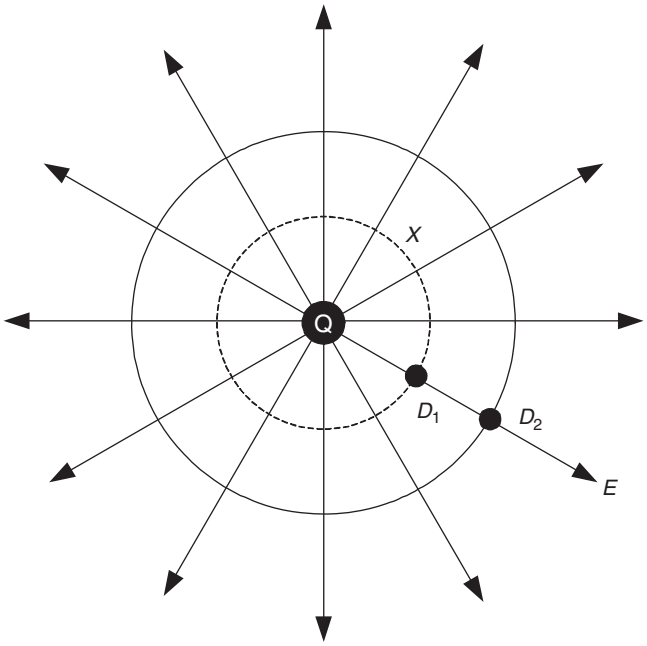

FIGURE 19.7 A charge generated electric field.

The equipotential lines are circles in case of one conductor above the ground. The voltage difference between the conductor and the equipotential line is constant.

From a practical point of view, the voltage difference between a point in the space and the ground is important. This voltage difference is called space potential. Figure 19.8 shows the electric field lines and equipotential lines for a charged conductor above ground.

19.4.1 Electric Charge Calculation

Figure 19.9 shows a three-phase, horizontally arranged transmission line. The ground in this figure is represented by the negatively charged image conductors. This means that each conductor of the line is represented by a positively charged line and a negatively charged image conductor. The voltage difference between the phase conductor and the corresponding image conductor is $2V_{ln}$. The electric charge on an energized conductor is calculated by repetitive use of the voltage difference equation presented before.

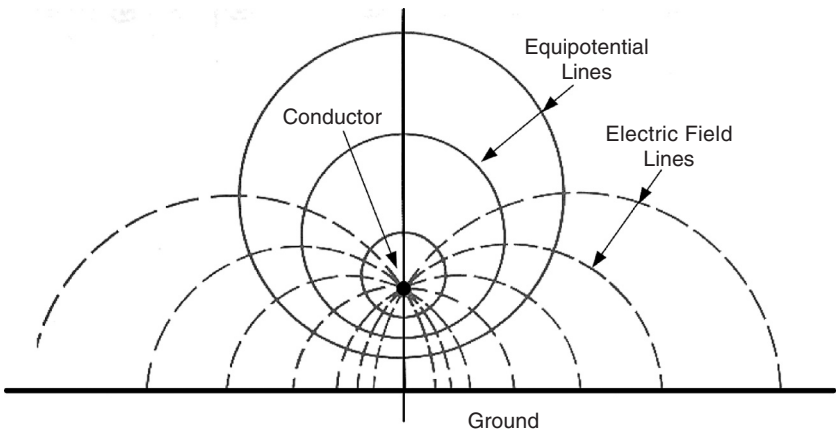

FIGURE 19.8 Electric field around an energized conductor above the ground.

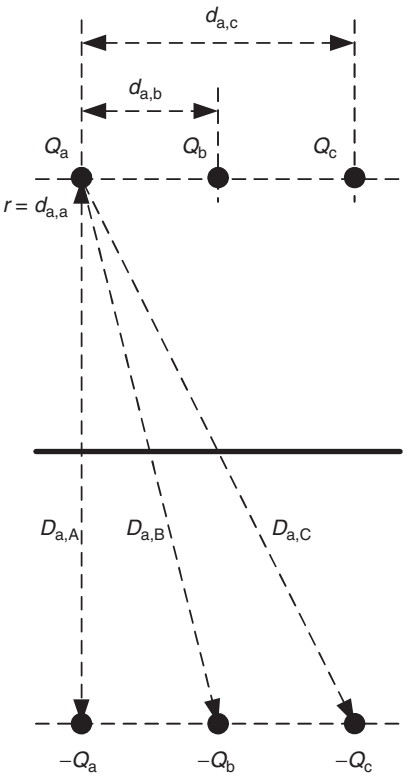

FIGURE 19.9 Representation of three-phase line generated electric field by image conductors.

The voltage difference between phase conductor "A" and its image conductor is generated by all charges (Q_a, Q_b, Q_c, and $-Q_a$, $-Q_b$, $-Q_c$) in the system. Using the voltage difference equations, we obtained the voltage difference between conductor A and its image:

$$V_{a,A} = \frac{Q_A}{2\pi\varepsilon_o}\ln\left(\frac{D_{a,A}}{r_{cond}}\right) + \frac{-Q_A}{2\pi\varepsilon_o}\ln\left(\frac{r_{cond}}{D_{a,A}}\right) + \frac{Q_B}{2\pi\varepsilon_o}\ln\left(\frac{D_{a,B}}{d_{a,b}}\right) + \frac{-Q_B}{2\pi\varepsilon_o}\ln\left(\frac{d_{a,b}}{D_{a,B}}\right) + \frac{Q_C}{2\pi\varepsilon_o}\ln\left(\frac{D_{a,C}}{d_{a,c}}\right) + \frac{-Q_C}{2\pi\varepsilon_o}\ln\left(\frac{d_{a,c}}{D_{a,C}}\right)$$

This equation can be simplified by combining the $+Q$ and $-Q$ terms. The result is

$$V_{a,A} = 2V_{a\_ln} = \frac{2Q_A}{2\pi\varepsilon_o}\ln\left(\frac{D_{a,A}}{r_{cond}}\right) + \frac{2Q_B}{2\pi\varepsilon_o}\ln\left(\frac{D_{a,B}}{d_{a,b}}\right) + \cdots + \frac{2Q_C}{2\pi\varepsilon_o}\ln\left(\frac{D_{a,C}}{d_{a,c}}\right)$$

Further simplification is the division of both sides of the equation by 2, which results in an equation for the line to neutral voltage. Similar equations can be derived for phases B and C. The results are

$$V_{a\_ln} = \frac{Q_A}{2\pi\varepsilon_o}\ln\left(\frac{D_{a,A}}{r_{cond}}\right) + \frac{Q_B}{2\pi\varepsilon_o}\ln\left(\frac{D_{a,B}}{d_{a,b}}\right) + \frac{Q_C}{2\pi\varepsilon_o}\ln\left(\frac{D_{a,C}}{d_{a,c}}\right)$$

$$V_{b\_ln} = \frac{Q_A}{2\pi\varepsilon_o}\ln\left(\frac{D_{b,A}}{d_{a,b}}\right) + \frac{Q_B}{2\pi\varepsilon_o}\ln\left(\frac{D_{b,B}}{r_{cond}}\right) + \frac{Q_C}{2\pi\varepsilon_o}\ln\left(\frac{D_{b,C}}{d_{b,c}}\right)$$

$$V_{c\_ln} = \frac{Q_A}{2\pi\varepsilon_o}\ln\left(\frac{D_{c,A}}{d_{c,b}}\right) + \frac{Q_B}{2\pi\varepsilon_o}\ln\left(\frac{D_{c,B}}{d_{b,c}}\right) + \frac{Q_C}{2\pi\varepsilon_o}\ln\left(\frac{D_{c,C}}{r_{cond}}\right)$$

In these equations, the line to neutral voltages and dimensions are given. The equations can be solved for the charges (Q_a, Q_b, Q_c).

19.4.2 Electric Field Calculation

The horizontal and vertical components of the electric field generated by the six charges (Q_a, Q_b, Q_c, and $-Q_a$, $-Q_b$, $-Q_c$) are calculated. The sum of the horizontal components and vertical components gives the X and Y components of the total electric field. The vector sum of the X and Y components gives the magnitude of the total field.

Figure 19.10 shows a Q charge generated electric field. The field lines are radial to the charge.

The absolute value of electric field generated by a charge Q is described by the Gauss equation. The observation point coordinates are X and Y. The conductor coordinates are x_i and y_i.

The electric field magnitude is

$$E_i = \frac{Q_i}{2\pi r} = \frac{Q_i}{2\pi\sqrt{(x_i - X)^2 + (y_i - Y)^2}}$$

The Φ angle between the E vector and its vertical components is

$$\Phi = \text{atn}\left(\frac{x_i - X}{y_i - Y}\right)$$

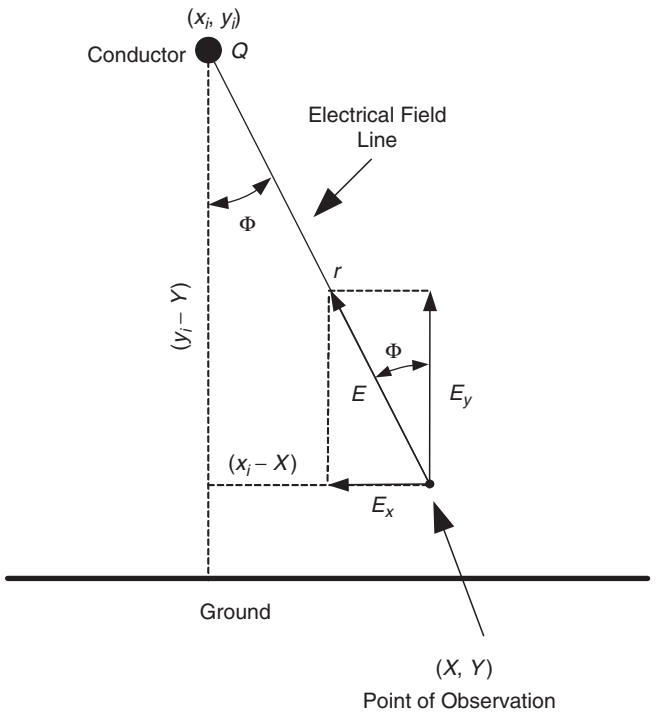

FIGURE 19.10 Electric field generated by a charge in an observation point (X, Y).

The horizontal and vertical components of the electric field are

$$E_{i\_x} = \frac{Q_i}{2\pi\sqrt{(x_i - X)^2 + (y_i - Y)^2}} \sin(\Phi_i) = \frac{Q_i}{2\pi} \frac{x_i - X}{\left[(x_i - X)^2 + (y_i - Y)^2\right]}$$

$$E_{i\_y} = \frac{Q_i}{2\pi\sqrt{(x_i - X)^2 + (y_i - Y)^2}} \cos(\Phi_i) = \frac{Q_i}{2\pi} \frac{y_i - Y}{\left[(x_i - X)^2 + (y_i - Y)^2\right]}$$

The x and y components generated by all six charges are calculated using the equations above.

The magnitude of the total electric field is calculated by the summation of the components. The magnitude of the total field is

$$E = \sqrt{\left(\sum_i E_{i\_x}\right)^2 + \left(\sum_i E_{i\_y}\right)^2}$$

For the demonstration of the expected results, we calculated a 500-kV transmission line generated electric field magnitude under the line in 1 m distance from the ground. The conductors are arranged horizontally. The average conductor height is 24.38 m (80 ft); the distance between the conductors is 10.66 m (35 ft). The line-to-ground voltage is

$$V_{\ln} = \frac{500 \text{ kV}}{\sqrt{3}} = 288.7 \text{ kV}$$

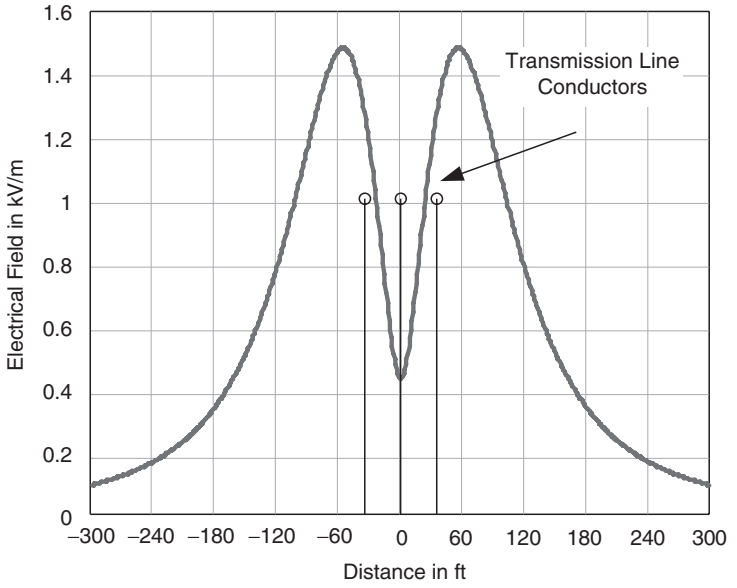

FIGURE 19.11 Magnetic field density under a 500-kV line.

Figure 19.11 shows the electric field distribution under the line in 1 m from the ground. The locations of the line conductors are marked on the figure. It can be seen that the maximum electric field is nearly under the side conductors. The electric field under the middle conductor is less than the side conductors because of the field cancellation caused by the 120° phase shift of the line voltages. The electric field decreases rapidly with the distance.

Typically, the electric field under high-voltage transmission lines varies between 2 and 15 kV/m. The desired electric field at the edge of the right-of-way is less than 1 kV/m. The right-of-way varies with the voltage, at 500 kV the right-of-way is 100–150 ft, at 220 kV it is around 70–90 ft.

19.4.3 Environmental Effect of Electric Field

In general, the electric field generated by a transmission line has no harmful health effects. Large number of studies investigated the biological effect of small 1–20 kV/m, 60 Hz electrical fields. None of the studies has shown any harmful effects. However, the electrical field can produce annoying disturbances.

The electrical field surrounding a transmission line can charge ungrounded objects close to the space potential. If the object is large, like a truck, parking under the line affects the field distribution and space potential.

The simplest visualization of the problem is a truck parking under a transmission line; the rubber tires insulate the truck from the ground. The voltage difference between the truck and the ground is determined by the capacitance between the truck and the line, and the capacitance between the truck and ground. The two capacitances form a capacitive voltage divider. The truck potential to ground can be few kilovolts. A person standing on the ground and touching the truck will discharge the capacitor between the truck and ground. This produces a small spark discharge. The person touching the truck suffers minor electric shock, which is not dangerous but uncomfortable.

After the discharge the person touching the truck grounds it, which results in a constant current through the person. This current is determined by the capacitance between the object, in

this case the truck and the line. EPRI-published *Redbook* (*Transmission Line Reference Book—345 kV and Above*) [14] gives an approximate formula for the expected current:

$$I_{\text{cap}} = 2\pi f \varepsilon_{\text{o}} E_y \text{ surface},$$

where E_y is the vertical component of the electric field, f is the frequency (60 Hz), "surface" is the equivalent charge collecting area of the object, and I_{cap} is the capacitive current flowing through the person grounding the object.

Another potentially dangerous accident scenario is when a worker climbs on a wooden ladder to repair something close to a transmission line. A grounded coworker hands him a tool. This produces a discharge and a minor spark, which is harmless. However, the shock may cause dropping the tool or falling off the ladder.

People walking under the line may experience a tingling sensation on their skin and hair stimulation if the electrical field is larger than 6–7 kV/m. This is an annoying but harmless effect.

The electric field effect is discussed in great details in the *Transmission Line Reference Book—345 kV and Above* [14].

19.5 Audible Noise

The corona discharge on the high-voltage transmission line generates audible noise. The corona discharge produced by a well-designed transmission line is very low in fair weather. Consequently, the transmission line produced audible noise in fair weather conditions is negligible.

Fog and light rain produce droplets on the surface of line conductors. The droplets increase the local electric field and generate corona discharge. The corona discharge produced air movement or pressure wave generates the audible noise. The light rain and fog generated noise intensity varies, fluctuates depending on the level of wetting.

Heavy rain produces more or less constant noise. The corona discharge bursts the water droplets and disperses the water. However, the heavy rain replacing the dispersed water drops immediately.

Snowflakes also can increase corona level and audible noise. The dry, low temperature snow generally does not produce audible noise. The audible noise generated by wet melting snow can be significant and the noise level will be similar to the heavy rain generated noise.

Typically the line generated noise has two components:

- Broadband noise, which is mainly generated by the discharge on water droplets. This is a hissing, crackling noise with significant high-frequency components.
- Low-frequency humming noise with 120, 240 Hz, etc. components. This noise is generated by the oscillatory movement of the corona generated ions around the conductors. The humming noise occurs mostly in good weather condition, if the line corona level is low.

From a practical point of view, the broadband noise is the most important. The utilities accept a noise level of 50–52 dB at the edge of right-of-way. The noise level is measured in dB. The base is 20 μPa. The noise attenuates with the distance due to the divergence of the sound and the absorption of trees and other objects. Practical value is around 3 dB, when the distance is doubled.

A numerical example is presented to estimate the approximate sound level in a residential area if the sound level is 52 dB at the edge of the right-of-way. The distance between the line and the edge of right-of-way is 100 ft. The sound level in a distance of 200 ft is 52 dB – 3 dB = 49 dB and in a distance of 400 ft is 49 dB – 3 dB = 46 dB.

The transmission line generated noise level can be reduced by reduction of corona discharge level. The most effective method is the use of bundle conductors. The rearrangement of the line conductors also can reduce corona discharge and audible noise.

Section 15.2.3 in Chapter 15 presents a method to calculate the approximate sound level produced by a high-voltage line. The EPRI-published *Transmission Line Reference Book—345 kV and Above* [14] gives curves to determine the expected audible noise level produced by a transmission line.

19.6 Electromagnetic Interference (EMI)

The corona discharge produces radio noise and in lesser extent television (TV) disturbances around high-voltage transmission lines. This can be easily observed by all of us when we drive under a high-voltage line. The radio produces hissing, crackling noise close to the line or under the line, but disturbance diapering fast as we drive away from the line crossing the highway. In a similar way, TV picture disturbance can be observed close to a transmission line. The disturbance varies from the snowy picture to the collapse of the picture.

The corona discharge causes short duration (few microseconds) repetitive current pulses. The repetition frequency can be in the MHz range. As was discussed before, the corona discharge is low in fair weather and increases rapidly in foul weather. The most severe EMI disturbance was observed during heavy rain, when the water droplets on the conductor caused corona discharge.

Additional sources of the EMI disturbance are discharge in faulty insulators or discharge generated by spikes, needles, and other sharp objects subjected to electric field. The sharp object produces an increase in the local electric field, which can lead to surface discharge. This discharge can produce EMI and unacceptable disturbances of local TV or radio reception.

The generated EMI disturbance decreases with the distance from the line. Typically, a 100 MHz signal decreases about 20 dB if we move 100 m from the line; simultaneously, a 1 MHz components attenuation is around 35–40 dB in the same distance. The radio and TV noise is measured in dB; the base is 1 $\mu V/m$.

The actual disturbance depends on the signal-to-noise ratio. As an example, the same level of EMI disturbance can produce an unacceptable radio or TV reception if the broadcasted signal is weak, and no disturbance in case of strong signal.

The EPRI-published *Transmission Line Reference Book—345 kV and Above* [14] gives curves to determine the expected radio or TV disturbance level produced by a transmission line.

References

1. Wertheimer, N., Leeper, E., Electric wiring configuration and childhood cancer, *American Journal of Epidemiology*, 109 (3), 273–284, March 1979.
2. Savitz, D.A., Wachtel, H., Barnes, F.A., John, E.M., and Tvrdik, R.G., Case control study of childhood cancer and residential exposure to electric and magnetic fields, *American Journal of Epidemiology*, 128 (1), 21–38, January 1988.
3. London, S.J., et al., Exposure to residential electric and magnetic fields and risk of childhood leukemia, *American Journal of Epidemiology*, 131 (9), 923–937, November 1992.
4. Floderus, B., Persson, T., Stenlund, et al., Occupational exposure to electromagnetic fields in relation to leukemia and brain tumor, Department of Neuromedicine, National Institute of Occupational Health, Solna, Sweden, 1992.
5. Tynes, T., Hanevik, M., Vistnes, A.I., A nested case-control study of leukemia and brain tumors in Norwegian railway workers, Conference Proceedings Fifteenth Annual Meeting of the Bioelectromagnetic Society, Los Angeles, CA, June 1993.
6. Scarfi, M.R., Bersani, F., Brooks, A.L., et al., 50 Hz, sinusoidal electric field do not exert genotaxis effects (micronucleus formation) in human lymphocytes, *Radiation Research*, 135(1), 64–68, 1992.
7. Byus, C.V., Piper, S.A., Adey, W.R., The effect of low energy 60 Hz environmental electromagnetic fields upon the growth related enzyme ornithine decarboxylase, *Carcinogenesis*, 8, 1385–1389, 1987.

8. Korpinen L., Influence of 50 Hz electric and magnetic fields on the human heart, *Bioelectromagnetics*, 14 (4), 329–340, 1993.
9. Graham, C., et al., EMF suppression of nocturnal melatonin in human volunteers, Annual Review of Research in Biological Effects of Electric and Magnetic Fields from the Generation, Delivery and Use of Electricity, Savannah, GA, October 31–November 4, 98–99, 1994.
10. EPRI Report, TR-100194, Survey of Residential Power Magnetic Field Sources, Phase 1, RP2942, Electric Power Research Institute, Palo Alto, CA, 1990.
11. Electric and Magnetic Field Fundamentals, Electric Power Research Institute, Palo Alto, CA, March 1994.
12. U.S. Environmental Protection Agency, Evaluation of the potential carcinogenicity of electromagnetic fields, EAP/600/6-90/005B, October 1990.
13. U.S. Environmental Protection Agency, Office of Research and Development, Electric and Magnetic Fields Annual Environmental Protection Agency, *Prospective on Research Needs and Priorities for Improving Health Risk Assessment*, Washington D.C., U.S. Government Printing, 1992.
14. *Transmission Line Reference Book—345 kV and Above*, 2nd ed., Electric Power Research Institute, Palo Alto, CA, 1987.
15. Kaune, W.T., Zaffranella, L.E., Analysis of magnetic fields produced far from electric power lines, *IEEE Transactions on Power Delivery*, 7 (4), 2082–2091, October 1992.

IV

Distribution Systems

William H. Kersting
New Mexico State University

20

Power System Loads

Raymond R. Shoults
University of Texas at Arlington

Larry D. Swift
University of Texas at Arlington

The physical structure of most power systems consists of generation facilities feeding bulk power into a high-voltage bulk transmission network, that in turn serves any number of distribution substations. A typical distribution substation will serve from one to as many as ten feeder circuits. A typical feeder circuit may serve numerous loads of all types. A light to medium industrial customer may take service from the distribution feeder circuit primary, while a large industrial load complex may take service directly from the bulk transmission system. All other customers, including residential and commercial, are typically served from the secondary of distribution transformers that are in turn connected to a distribution feeder circuit. Figure 20.1 illustrates a representative portion of a typical configuration.

20.1 Load Classification

The most common classification of electrical loads follows the billing categories used by the utility companies. This classification includes residential, commercial, industrial, and other. Residential customers are domestic users, whereas commercial and industrial customers are obviously business and industrial users. Other customer classifications include municipalities, state and federal government agencies, electric cooperatives, educational institutions, etc.

Although these load classes are commonly used, they are often inadequately defined for certain types of power system studies. For example, some utilities meter apartments as individual residential customers, while others meter the entire apartment complex as a commercial customer. Thus, the common classifications overlap in the sense that characteristics of customers in one class are not unique to that class. For this reason some utilities define further subdivisions of the common classes.

A useful approach to classification of loads is by breaking down the broader classes into individual load components. This process may altogether eliminate the distinction of certain of the broader classes, but it is a tried and proven technique for many applications. The components of a particular load, be it residential, commercial, or industrial, are individually defined and modeled. These load components as a whole constitute the composite load and can be defined as a "load window."

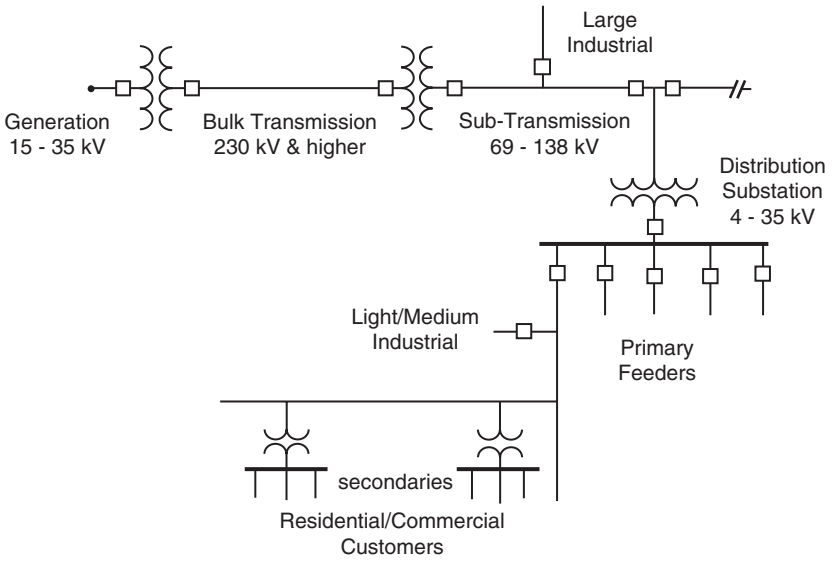

FIGURE 20.1 Representative portion of a typical power system configuration.

20.2 Modeling Applications

It is helpful to understand the applications of load modeling before discussing particular load characteristics. The applications are divided into two broad categories: static ("snap-shot" with respect to time) and dynamic (time varying). Static models are based on the steady-state method of representation in power flow networks. Thus, static load models represent load as a function of voltage magnitude. Dynamic models, on the other hand, involve an alternating solution sequence between a time-domain solution of the differential equations describing electromechanical behavior and a steady-state power flow solution based on the method of phasors. One of the important outcomes from the solution of dynamic models is the time variation of frequency. Therefore, it is altogether appropriate to include a component in the static load model that represents variation of load with frequency. The lists below include applications outside of Distribution Systems but are included because load modeling at the distribution level is the fundamental starting point.

Static applications: Models that incorporate only the voltage-dependent characteristic include the following.

- Power flow (PF)
  - Distribution power flow (DPF)
  - Harmonic power flow (HPF)
  - Transmission power flow (TPF)
- Voltage stability (VS)

Dynamic applications: Models that incorporate both the voltage- and frequency-dependent characteristics include the following.

- Transient stability (TS)
- Dynamic stability (DS)
- Operator training simulators (OTS)

Strictly power-flow based solutions utilize load models that include only voltage dependency characteristics. Both voltage and frequency dependency characteristics can be incorporated in load modeling for those hybrid methods that alternate between a time-domain solution and a power flow solution,

such as found in Transient Stability and Dynamic Stability Analysis Programs, and Operator Training Simulators.

Load modeling in this section is confined to static representation of voltage and frequency dependencies. The effects of rotational inertia (electromechanical dynamics) for large rotating machines are discussed in Chapters 11 and 12. Static models are justified on the basis that the transient time response of most composite loads to voltage and frequency changes is fast enough so that a steady-state response is reached very quickly.

20.3 Load Modeling Concepts and Approaches

There are essentially two approaches to load modeling: component based and measurement based. Load modeling research over the years has included both approaches (EPRI, 1981; 1984; 1985). Of the two, the component-based approach lends itself more readily to model generalization. It is generally easier to control test procedures and apply wide variations in test voltage and frequency on individual components.

The component-based approach is a "bottom-up" approach in that the different load component types comprising load are identified. Each load component type is tested to determine the relationship between real and reactive power requirements versus applied voltage and frequency. A load model, typically in polynomial or exponential form, is then developed from the respective test data. The range of validity of each model is directly related to the range over which the component was tested. For convenience, the load model is expressed on a per-unit basis (i.e., normalized with respect to rated power, rated voltage, rated frequency, rated torque if applicable, and base temperature if applicable). A composite load is approximated by combining appropriate load model types in certain proportions based on load survey information. The resulting composition is referred to as a "load window."

The measurement approach is a "top-down" approach in that measurements are taken at either a substation level, feeder level, some load aggregation point along a feeder, or at some individual load point. Variation of frequency for this type of measurement is not usually performed unless special test arrangements can be made. Voltage is varied using a suitable means and the measured real and reactive power consumption recorded. Statistical methods are then used to determine load models. A load survey may be necessary to classify the models derived in this manner. The range of validity for this approach is directly related to the realistic range over which the tests can be conducted without damage to customers' equipment. Both the component and measurement methods were used in the EPRI research projects EL-2036 (1981) and EL-3591 (1984–85). The component test method was used to characterize a number of individual load components that were in turn used in simulation studies. The measurement method was applied to an aggregate of actual loads along a portion of a feeder to verify and validate the component method.

20.4 Load Characteristics and Models

Static load models for a number of typical load components appear in Tables 20.1 and 20.2 (EPRI 1984–85). The models for each component category were derived by computing a weighted composite from test results of two or more units per category. These component models express per-unit real power and reactive power as a function of per-unit incremental voltage and/or incremental temperature and/or per-unit incremental torque. The incremental form used and the corresponding definition of variables are outlined below:

$\Delta V = V_{act} - 1.0$ (incremental voltage in per unit)
$\Delta T = T_{act} - 95°F$ (incremental temperature for Air Conditioner model)
$= T_{act} - 47°F$ (incremental temperature for Heat Pump model)
$\Delta\tau = \tau_{act} - \tau_{rated}$ (incremental motor torque, per unit)

TABLE 20.1 Static Models of Typical Load Components—AC, Heat Pump, and Appliances

Load Component	Static Component Model
1-ϕ Central Air Conditioner	$P = 1.0 + 0.4311*\Delta V + 0.9507*\Delta T + 2.070*\Delta V^2 + 2.388*\Delta T^2 - 0.900*\Delta V*\Delta T$
	$Q = 0.3152 + 0.6636*\Delta V + 0.543*\Delta V^2 + 5.422*\Delta V^3 + 0.839*\Delta T^2 - 1.455*\Delta V*\Delta T$
3-ϕ Central Air Conditioner	$P = 1.0 + 0.2693*\Delta V + 0.4879*\Delta T + 1.005*\Delta V^2 - 0.188*\Delta T^2 - 0.154*\Delta V*\Delta T$
	$Q = 0.6957 + 2.3717*\Delta V + 0.0585*\Delta T + 5.81*\Delta V^2 + 0.199*\Delta T^2 - 0.597*\Delta V*\Delta T$
Room Air Conditioner (115V Rating)	$P = 1.0 + 0.2876*\Delta V + 0.6876*\Delta T + 1.241*\Delta V^2 + 0.089*\Delta T^2 - 0.558*\Delta V*\Delta T$
	$Q = 0.1485 + 0.3709*\Delta V + 1.5773*\Delta T + 1.286*\Delta V^2 + 0.266*\Delta T^2 - 0.438*\Delta V*\Delta T$
Room Air Conditioner (208/230V Rating)	$P = 1.0 + 0.5953*\Delta V + 0.5601*\Delta T + 2.021*\Delta V^2 + 0.145*\Delta T^2 - 0.491*\Delta V*\Delta T$
	$Q = 0.4968 + 2.4456*\Delta V + 0.0737*\Delta T + 8.604*\Delta V^2 - 0.125*\Delta T^2 - 1.293*\Delta V*\Delta T$
3-ϕ Heat Pump (Heating Mode)	$P = 1.0 + 0.4539*\Delta V + 0.2860*\Delta T + 1.314*\Delta V^2 - 0.024*\Delta V*\Delta T$
	$Q = 0.9399 + 3.013*\Delta V - 0.1501*\Delta T + 7.460*\Delta V^2 - 0.312*\Delta T^2 - 0.216*\Delta V*\Delta T$
3-ϕ Heat Pump (Cooling Mode)	$P = 1.0 + 0.2333*\Delta V + 0.5915*\Delta T + 1.362*\Delta V^2 + 0.075*\Delta T^2 - 0.093*\Delta V*\Delta T$
	$Q = 0.8456 + 2.3404*\Delta V - 0.1806*\Delta T + 6.896*\Delta V^2 + 0.029*\Delta T^2 - 0.836*\Delta V*\Delta T$
1-ϕ Heat Pump (Heating Mode)	$P = 1.0 + 0.3953*\Delta V + 0.3563*\Delta T + 1.679*\Delta V^2 + 0.083*\Delta V*\Delta T$
	$Q = 0.3427 + 1.9522*\Delta V - 0.0958*\Delta T + 6.458*\Delta V^2 - 0.225*\Delta T^2 - 0.246*\Delta V*\Delta T$
1-ϕ Heat Pump (Cooling Mode)	$P = 1.0 + 0.3630*\Delta V + 0.7673*\Delta T + 2.101*\Delta V^2 + 0.122*\Delta T^2 - 0.759*\Delta V*\Delta T$
	$Q = 0.3605 + 1.6873*\Delta V + 0.2175*\Delta T + 10.055*\Delta V^2 - 0.170*\Delta T^2 - 1.642*\Delta V*\Delta T$
Refrigerator	$P = 1.0 + 1.3958*\Delta V + 9.881*\Delta V^2 + 84.72*\Delta V^3 + 293*\Delta V^4$
	$Q = 1.2507 + 4.387*\Delta V + 23.801*\Delta V^2 + 1540*\Delta V^3 + 555*\Delta V^4$
Freezer	$P = 1.0 + 1.3286*\Delta V + 12.616*\Delta V^2 + 133.6*\Delta V^3 + 380*\Delta V^4$
	$Q = 1.3810 + 4.6702*\Delta V + 27.276*\Delta V^2 + 293.0*\Delta V^3 + 995*\Delta V^4$
Washing Machine	$P = 1.0 + 1.2786*\Delta V + 3.099*\Delta V^2 + 5.939*\Delta V^3$
	$Q = 1.6388 + 4.5733*\Delta V + 12.948*\Delta V^2 + 55.677*\Delta V^3$
Clothes Dryer	$P = 1.0 - 0.1968*\Delta V - 3.6372*\Delta V^2 - 28.32*\Delta V^3$
	$Q = 0.209 + 0.5180*\Delta V + 0.363*\Delta V^2 - 4.7574*\Delta V^3$
Television	$P = 1.0 + 1.2471*\Delta V + 0.562*\Delta V^2$
	$Q = 0.243l + 0.9830*\Delta V + 1.647*\Delta V^2$
Fluorescent Lamp	$P = 1.0 + 0.6534*\Delta V - 1.65*\Delta V^2$
	$Q = -0.1535 - 0.0403*\Delta V + 2.734*\Delta V^2$
Mercury Vapor Lamp	$P = 1.0 + 0.1309*\Delta V + 0.504*\Delta V^2$
	$Q = -0.2524 + 2.3329*\Delta V + 7.811*\Delta V^2$
Sodium Vapor Lamp	$P = 1.0 + 0.3409*\Delta V - 2.389*\Delta V^2$
	$Q = 0.060 + 2.2173*\Delta V + 7.620*\Delta V^2$
Incandescent	$P = 1.0 + 1.5209*\Delta V + 0.223*\Delta V^2$
	$Q = 0.0$
Range with Oven	$P = 1.0 + 2.1018*\Delta V + 5.876*\Delta V^2 + 1.236*\Delta V^3$
	$Q = 0.0$
Microwave Oven	$P = 1.0 + 0.0974*\Delta V + 2.071*\Delta V^2$
	$Q = 0.2039 + 1.3130*\Delta V + 8.738*\Delta V^2$
Water Heater	$P = 1.0 + 0.3769*\Delta V + 2.003*\Delta V^2$
	$Q = 0.0$
Resistance Heating	$P = 1.0 + 2*\Delta V + \Delta V^2$
	$Q = 0.0$

If ambient temperature is known, it can be used in the applicable models. If it is not known, the temperature difference, ΔT, can be set to zero. Likewise, if motor load torque is known, it can be used in the applicable models. If it is not known, the torque difference, $\Delta\tau$, can be set to zero.

Based on the test results of load components and the developed real and reactive power models as presented in these tables, the following comments on the reactive power models are important.

- The reactive power models vary significantly from manufacturer to manufacturer for the same component. For instance, four load models of single-phase central air-conditioners show a Q/P ratio that varies between 0 and 0.5 at 1.0 p.u. voltage. When the voltage changes, the $\Delta Q/\Delta V$ of each unit is quite different. This situation is also true for all other components, such as refrigerators, freezers, fluorescent lights, etc.

TABLE 20.2 Static Models of Typical Load Components—Transformers and Induction Motors

Load Component	Static Component Model
Transformer Core Loss Model	$P = \frac{KVA(rating)}{KVA(systembase)}\left[0.00267V^2 + 0.73 \times 10^{-9} \times e^{13.5V^2}\right]$ $Q = \frac{KVA(rating)}{KVA(systembase)}\left[0.00167V^2 + 0.268 \times 10^{-13} \times e^{22.76V^2}\right]$ where V is voltage magnitude in per unit
1-ϕ Motor Constant Torque	$P = 1.0 + 0.5179*\Delta V + 0.9122*\Delta\tau + 3.721*\Delta V^2 + 0.350*\Delta\tau^2 - 1.326*\Delta V*\Delta\tau$ $Q = 0.9853 + 2.7796*\Delta V + 0.0859*\Delta\tau + 7.368*\Delta V^2 + 0.218*\Delta\tau^2 - 1.799*\Delta V*\Delta\tau$
3-ϕ Motor (1–10HP) Const. Torque	$P = 1.0 + 0.2250*\Delta V + 0.9281*\Delta\tau + 0.970*\Delta V^2 + 0.\ 086*\Delta\tau^2 - 0.329*\Delta V*\Delta\tau$ $Q = 0.7810 + 2.3532*\Delta V + 0.1023*\Delta\tau - 5.951*\Delta V^2 + 0.446*\Delta\tau^2 - 1.48*\Delta V*\Delta\tau$
3-ϕ Motor (10HP/Above) Const. Torque	$P = 1.0 + 0.0199*\Delta V + 1.0463*\Delta\tau + 0.341*\Delta V^2 + 0.116*\Delta\tau^2 - 0.457*\Delta V*\Delta\tau$ $Q = 0.6577 + 1.2078*\Delta V + 0.3391*\Delta\tau + 4.097*\Delta V^2 + 0.289\Delta\tau^2 - 1.477*\Delta V*\Delta\tau$
1-ϕ Motor Variable Torque	$P = 1.0 + 0.7101*\Delta V + 0.9073*\Delta\tau + 2.13*\Delta V^2 + 0.245*\Delta\tau^2 - 0.310*\Delta V*\Delta\tau$ $Q = 0.9727 + 2.7621*\Delta V + 0.077*\Delta\tau + 6.432*\Delta V^2 + 0.174*\Delta\tau^2 - 1.412*\Delta V*\Delta\tau$
3-ϕ Motor (1–10HP) Variable Torque	$P = 1.0 + 0.3122*\Delta V + 0.9286*\Delta\tau + 0.489*\Delta V^2 + 0.081*\Delta\tau^2 - 0.079*\Delta V*\Delta\tau$ $Q = 0.7785 + 2.3648*\Delta V + 0.1025*\Delta\tau + 5.706*\Delta V^2 + 0.13*\Delta\tau^2 - 1.00*\Delta V*\Delta\tau$
3-ϕ Motor (10HP & Above) Variable Torque	$P = 1.0 + 0.1628*\Delta V + 1.0514*\Delta\tau \angle 0.099*\Delta V^2 + 0.107*\Delta\tau^2 + 0.061*\Delta V*\Delta\tau$ $Q = 0.6569 + 1.2467*\Delta V + 0.3354*\Delta\tau + 3.685*\Delta V^2 + 0.258*\Delta\tau^2 - 1.235*\Delta V*\Delta\tau$

- It has been observed that the reactive power characteristic of fluorescent lights not only varies from manufacturer to manufacturer, from old to new, from long tube to short tube, but also varies from capacitive to inductive depending upon applied voltage and frequency. This variation makes it difficult to obtain a good representation of the reactive power of a composite system and also makes it difficult to estimate the $\Delta Q/\Delta V$ characteristic of a composite system.
- The relationship between reactive power and voltage is more non-linear than the relationship between real power and voltage, making Q more difficult to estimate than P.
- For some of the equipment or appliances, the amount of Q required at the nominal operating voltage is very small; but when the voltage changes, the change in Q with respect to the base Q can be very large.
- Many distribution systems have switchable capacitor banks either at the substations or along feeders. The composite Q characteristic of a distribution feeder is affected by the switching strategy used in these banks.

20.5 Static Load Characteristics

The component models appearing in Tables 20.1 and 20.2 can be combined and synthesized to create other more convenient models. These convenient models fall into two basic forms: exponential and polynomial.

20.5.1 Exponential Models

The exponential form for both real and reactive power is expressed in Eqs. (20.1) and (20.2) below as a function of voltage and frequency, relative to initial conditions or base values. Note that neither temperature nor torque appear in these forms. Assumptions must be made about temperature and/or torque values when synthesizing from component models to these exponential model forms.

$$P = P_o\left[\frac{V}{V_o}\right]^{\alpha_v}\left[\frac{f}{f_o}\right]^{\alpha_f} \tag{20.1}$$

$$Q = Q_o\left[\frac{V}{V_o}\right]^{\beta_v}\left[\frac{f}{f_o}\right]^{\beta_f} \tag{20.2}$$

The per-unit models of Eqs. (20.1) and (20.2) are as follows.

$$P_u = \frac{P}{P_o} = \left[\frac{V}{V_o}\right]^{\alpha_v}\left[\frac{f}{f_o}\right]^{\alpha_f} \tag{20.3}$$

$$Q_u = \frac{Q}{P_o} = \frac{Q_o}{P_o}\left[\frac{V}{V_o}\right]^{\beta_v}\left[\frac{f}{f_o}\right]^{\beta_f} \tag{20.4}$$

The ratio Q_o/P_o can be expressed as a function of power factor (pf) where $\pm$ indicates a lagging/leading power factor, respectively.

$$R = \frac{Q_o}{P_o} = \pm\sqrt{\frac{1}{pf^2} - 1}$$

After substituting R for Q_o/P_o, Eq. (20.4) becomes the following.

$$Q_u = R\left[\frac{V}{V_o}\right]^{\beta_v}\left[\frac{f}{f_o}\right]^{\beta_f} \tag{20.5}$$

Equations (20.1) and (20.2) [or (20.3) and (20.5)] are valid over the voltage and frequency ranges associated with tests conducted on the individual components from which these exponential models are derived. These ranges are typically $\pm 10\%$ for voltage and $\pm 2.5\%$ for frequency. The accuracy of these models outside the test range is uncertain. However, one important factor to note is that in the extreme case of voltage approaching zero, both P and Q approach zero.

EPRI-sponsored research resulted in model parameters such as found in Table 20.3 (EPRI, 1987; Price et al., 1988). Eleven model parameters appear in this table, of which the exponents α and β and the power factor (pf) relate directly to Eqs. (20.3) and (20.5). The first six parameters relate to general load models, some of which include motors, and the remaining five parameters relate to nonmotor loads—typically resistive type loads. The first is load power factor (pf). Next in order (from left to right) are the exponents for the voltage (α_v, α_f) and frequency (β_v, β_f) dependencies associated with real and reactive power, respectively. N_m is the motor-load portion of the load. For example, both a refrigerator and a freezer are 80% motor load. Next in order are the power factor (pf_{nm}) and voltage (α_{vnm}, α_{fnm}) and frequency (β_{vnm}, β_{fnm}) parameters for the nonmotor portion of the load. Since the refrigerator and freezer are 80% motor loads (i.e., $N_m = 0.8$), the nonmotor portion of the load must be 20%.

20.5.2 Polynomial Models

A polynomial form is often used in a Transient Stability program. The voltage dependency portion of the model is typically second order. If the nonlinear nature with respect to voltage is significant, the order can be increased. The frequency portion is assumed to be first order. This model is expressed as follows.

$$P = P_o\left[a_o + a_1\left(\frac{V}{V_o}\right) + a_2\left(\frac{V}{V_o}\right)^2\right][1 + D_p\ \Delta f] \tag{20.6}$$

$$Q = Q_o\left[b_o + b_1\left(\frac{V}{V_o}\right) + b_2\left(\frac{V}{V_o}\right)^2\right][1 + D_q\ \Delta f] \tag{20.7}$$

TABLE 20.3 Parameters for Voltage and Frequency Dependencies of Static Loads

Component/Parameters	pf	α_v	α_f	β_v	β_f	N_m	pf_{nm}	α_{vnm}	α_{fnm}	β_{vnm}	β_{fnm}
Resistance Space Heater	1.0	2.0	0.0	0.0	0.0	0.0	—	—	—	—	—
Heat Pump Space Heater	0.84	0.2	0.9	2.5	−1.3	0.9	1.0	2.0	0.0	0.0	0.0
Heat Pump/Central A/C	0.81	0.2	0.9	2.5	−2.7	1.0	—	—	—	—	—
Room Air Conditioner	0.75	0.5	0.6	2.5	−2.8	1.0	—	—	—	—	—
Water Heater & Range	1.0	2.0	0.0	0.0	0.0	0.0	—	—	—	—	—
Refrigerator & Freezer	0.84	0.8	0.5	2.5	−1.4	0.8	1.0	2.0	0.0	0.0	0.0
Dish Washer	0.99	1.8	0.0	3.5	−1.4	0.8	1.0	2.0	0.0	0.0	0.0
Clothes Washer	0.65	0.08	2.9	1.6	1.8	1.0	—	—	—	—	—
Incandescent Lighting	1.0	1.54	0.0	0.0	0.0	0.0	—	—	—	—	—
Clothes Dryer	0.99	2.0	0.0	3.3	−2.6	0.2	1.0	2.0	0.0	0.0	0.0
Colored Television	0.77	2.0	0.0	5.2	−4.6	0.0	—	—	—	—	—
Furnace Fan	0.73	0.08	2.9	1.6	1.8	1.0	—	—	—	—	—
Commercial Heat Pump	0.84	0.1	1.0	2.5	−1.3	0.9	1.0	2.0	0.0	0.0	0.0
Heat Pump Comm. A/C	0.81	0.1	1.0	2.5	−1.3	1.0	—	—	—	—	—
Commercial Central A/C	0.75	0.1	1.0	2.5	−1.3	1.0	—	—	—	—	—
Commercial Room A/C	0.75	0.5	0.6	2.5	−2.8	1.0	—	—	—	—	—
Fluorescent Lighting	0.90	0.08	1.0	3.0	−2.8	0.0	—	—	—	—	—
Pump, Fan, (Motors)	0.87	0.08	2.9	1.6	1.8	1.0	—	—	—	—	—
Electrolysis	0.90	1.8	−0.3	2.2	0.6	0.0	—	—	—	—	—
Arc Furnace	0.72	2.3	−1.0	1.61	−1.0	0.0	—	—	—	—	—
Small Industrial Motors	0.83	0.1	2.9	0.6	−1.8	1.0	—	—	—	—	—
Industrial Motors Large	0.89	0.05	1.9	0.5	1.2	1.0	—	—	—	—	—
Agricultural H_2O Pumps	0.85	1.4	5.6	1.4	4.2	1.0	—	—	—	—	—
Power Plant Auxiliaries	0.80	0.08	2.9	1.6	1.8	1.0	—	—	—	—	—

where $a_o + a_1 + a_2 = 1$
$b_o + b_1 + b_2 = 1$
$D_p \equiv$ real power frequency damping coefficient, per unit
$D_q \equiv$ reactive power frequency damping coefficient, per unit
$\Delta f \equiv$ frequency deviation from scheduled value, per unit

The per-unit form of Eqs. (20.6) and (20.7) is the following.

$$P_u = \frac{P}{P_o} = \left[a_o + a_1\left(\frac{V}{V_o}\right) + a_2\left(\frac{V}{V_o}\right)^2\right][1 + D_p\ \Delta f] \tag{20.8}$$

$$Q_u = \frac{Q}{P_o} = \frac{Q_o}{P_o}\left[b_o + b_1\left(\frac{V}{V_o}\right) + b_2\left(\frac{V}{V_o}\right)^2\right][1 + D_q\ \Delta f] \tag{20.9}$$

20.5.3 Combined Exponential and Polynomial Models

The two previous kinds of models may be combined to form a synthesized static model that offers greater flexibility in representing various load characteristics (EPRI, 1987; Price et al., 1988). The mathematical expressions for these per-unit models are the following.

$$P_u = \frac{P_{poly} + P_{exp1} + P_{exp2}}{P_o} \tag{20.10}$$

$$Q_u = \frac{Q_{poly} + Q_{exp1} + Q_{exp2}}{P_o} \tag{20.11}$$

TABLE 20.4 Static Load Frequency Damping Characteristics

	Frequency Parameters	
Component	D_p	D_q
Three-Phase Central AC	1.09818	−0.663828
Single-Phase Central AC	0.994208	−0.307989
Window AC	0.702912	−1.89188
Duct Heater w/blowers	0.528878	−0.140006
Water Heater, Electric Cooking	0.0	0.0
Clothes Dryer	0.0	−0.311885
Refrigerator, Ice Machine	0.664158	−1.10252
Incandescent Lights	0.0	0.0
Florescent Lights	0.887964	−1.16844
Induction Motor Loads	1.6	−0.6

where

$$P_{poly} = a_0 + a_1\left(\frac{V}{V_o}\right) + a_3\left(\frac{V}{V_o}\right)^2 \tag{20.12}$$

$$P_{exp1} = a_4\left(\frac{V}{V_o}\right)^{\alpha_1}[1 + D_{p1}\,\Delta f] \tag{20.13}$$

$$P_{exp2} = a_5\left(\frac{V}{V_o}\right)^{\alpha_2}[1 + D_{p2}\,\Delta f] \tag{20.14}$$

The expressions for the reactive components have similar structures. Devices used for reactive power compensation are modeled separately.

The flexibility of the component models given here is sufficient to cover most modeling needs. Whenever possible, it is prudent to compare the computer model to measured data for the load.

Table 20.4 provides typical values for the frequency damping characteristic, D, that appears in Eqs. (20.6) through (20.9), (20.13), and (20.14) (EPRI, 1979). Note that nearly all of the damping coefficients for reactive power are negative. This means that as frequency declines, more reactive power is required which can cause an exacerbating effect for low-voltage conditions.

20.5.4 Comparison of Exponential and Polynomial Models

Both models provide good representation around rated or nominal voltage. The accuracy of the exponential form deteriorates when voltage significantly exceeds its nominal value, particularly with exponents (α) greater than 1.0. The accuracy of the polynomial form deteriorates when the voltage falls significantly below its nominal value when the coefficient a_o is non zero. A nonzero a_o coefficient represents some portion of the load as constant power. A scheme often used in practice is to use the polynomial form, but switch to the exponential form when the voltage falls below a predetermined value.

20.5.5 Devices Contributing to Modeling Difficulties

Some load components have time-dependent characteristics that must be considered if a sequence of studies using static models is performed that represents load changing over time. Examples of such a study include Voltage Stability and Transient Stability. The devices that affect load modeling by contributing abrupt changes in load over periods of time are listed below.

Protective Relays—Protective relays are notoriously difficult to model. The entire load of a substation can be tripped off line or the load on one of its distribution feeders can be tripped off line as a result of

protective relay operations. At the utilization level, motors on air conditioner units and motors in many other residential, commercial, and industrial applications contain thermal and/or over-current relays whose operational behavior is difficult to predict.

Thermostatically Controlled Loads—Air conditioning units, space heaters, water heaters, refrigerators, and freezers are all controlled by thermostatic devices. The effects of such devices are especially troublesome to model when a distribution load is reenergized after an extended outage (cold-load pickup). The effect of such devices to cold-load pickup characteristics can be significant.

Voltage Regulation Devices—Voltage regulators, voltage controlled capacitor banks, and automatic LTCs on transformers exhibit time-dependent effects. These devices are present at both the bulk power and distribution system levels.

Discharge Lamps (Mercury Vapor, Sodium Vapor, and Fluorescent Lamps)—These devices exhibit time-dependent characteristics upon restart, after being extinguished by a low-voltage condition—usually about 70% to 80% of rated voltage.

20.6 Load Window Modeling

The static load models found in Tables 20.1 and 20.2 can be used to define a composite load referred to as the "load window" mentioned earlier. In this scheme, a distribution substation load or one of its feeder loads is defined in as much detail as desired for the model. Using the load window scheme, any number of load windows can be defined representing various composite loads, each having as many load components as deemed necessary for accurate representation of the load. Figure 20.2 illustrates the load window concept. The width of each subwindow denotes the percentage of each load component to the total composite load.

Construction of a load window requires certain load data be available. For example, load saturation and load diversity data are needed for various classes of customers. These data allow one to (1) identify the appropriate load components to be included in a particular load window, (2) assign their relative percentage of the total load, and (3) specify the diversified total amount of load for that window. If load modeling is being used for Transient Stability or Operator Training Simulator programs, frequency dependency can be added. Let P(V) and Q(V) represent the composite load models for P and Q, respectively, with only voltage dependency (as developed using components taken from Tables 20.1 and 20.2). Frequency dependency is easily included as illustrated below.

$$P = P(V) \times (1 + D_p\ \Delta f)$$
$$Q = Q(V) \times (1 + D_q\ \Delta f)$$

Table 20.5 shows six different composite loads for a summer season in the southwestern portion of the U.S. This "window" serves as an example to illustrate the modeling process. Note that each column must

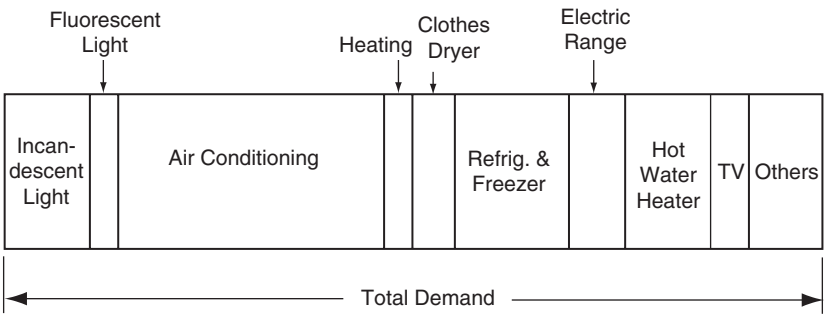

FIGURE 20.2 A typical load window with % composition of load components.

TABLE 20.5 Composition of Six Different Load Window Types

Load Window Type Load Component	LW 1 Res. 1 (%)	LW 2 Res. 2 (%)	LW 3 Res. 3 (%)	LW 4 Com 1 (%)	LW 5 Com 2 (%)	LW 6 Indust (%)
3-Phase Central AC	25	30	10	35	40	20
Window Type AC	5	0	20	0	0	0
Duct Heater with Blower	5	0	0	0	0	0
Water Heater, Range Top	10	10	10	0	0	0
Clothes Dryer	10	10	10	0	0	0
Refrigerator, Ice Machine	15	15	10	30	0	0
Incandescent Lights	10	5	10	0	0	0
Fluorescent Lights	20	30	30	25	30	10
Industrial (Induct. Motor)	0	0	0	10	30	70

add to 100%. The entries across from each component load for a given window type represent the percentage of that load making up the composite load.

References

EPRI User's Manual—Extended Transient/Midterm Stability Program Package, version 3.0, June 1992.

General Electric Company, Load modeling for power flow and transient stability computer studies, *EPRI Final Report EL-5003*, January 1987 (four volumes describing LOADSYN computer program).

Kundur, P., *Power System Stability and Control,* EPRI Power System Engineering Series, McGraw-Hill, Inc., 271–314, 1994.

Price, W.W., Wirgau, K.A., Murdoch, A., Mitsche, J.V., Vaahedi, E., and El-Kady, M.A., Load Modeling for Power Flow and Transient Stability Computer Studies, *IEEE Trans. on Power Syst.,* 3(1), 180–187, February 1988.

Taylor, C.W., *Power System Voltage Stability,* EPRI Power System Engineering Series, McGraw-Hill, Inc., 67–107, 1994.

University of Texas at Arlington, Determining Load Characteristics for Transient Performances, *EPRI Final Report EL-848*, May 1979 (three volumes).

University of Texas at Arlington, Effect of Reduced Voltage on the Operation and Efficiency of Electrical Loads, *EPRI Final Report EL-2036*, September 1981 (two volumes).

University of Texas at Arlington, Effect of Reduced Voltage on the Operation and Efficiency of Electrical Loads, *EPRI Final Report EL-3591*, June 1984 and July 1985 (three volumes).

Warnock, V.J. and Kirkpatrick, T.L., Impact of Voltage Reduction on Energy and Demand: Phase II, *IEEE Trans. on Power Syst.,* 3(2), 92–97, May 1986.

21

Distribution System Modeling and Analysis

William H. Kersting
New Mexico State University

21.1 Modeling

Radial distribution feeders are characterized by having only one path for power to flow from the source (distribution substation) to each customer. A typical distribution system will consist of one or more distribution substations consisting of one or more "feeders." Components of the feeder may consist of the following:

- Three-phase primary "main" feeder
- Three-phase, two-phase ("V" phase), and single-phase laterals
- Step-type voltage regulators or load tap changing transformer (LTC)
- In-line transformers
- Shunt capacitor banks
- Three-phase, two-phase, and single-phase loads
- Distribution transformers (step-down to customer's voltage)

The loading of a distribution feeder is inherently unbalanced because of the large number of unequal single-phase loads that must be served. An additional unbalance is introduced by the nonequilateral conductor spacings of the three-phase overhead and underground line segments.

Because of the nature of the distribution system, conventional power-flow and short-circuit programs used for transmission system studies are not adequate. Such programs display poor convergence characteristics for radial systems. The programs also assume a perfectly balanced system so that a single-phase equivalent system is used.

If a distribution engineer is to be able to perform accurate power-flow and short-circuit studies, it is imperative that the distribution feeder be modeled as accurately as possible. This means that three-phase models of the major components must be utilized. Three-phase models for the major components will be developed in the following sections. The models will be developed in the "phase frame" rather than applying the method of symmetrical components.

Figure 21.1 shows a simple one-line diagram of a three-phase feeder; it illustrates the major components of a distribution system. The connecting points of the components will be referred to as "nodes." Note in the figure that the phasing of the line segments is shown. This is important if the most accurate models are to be developed.

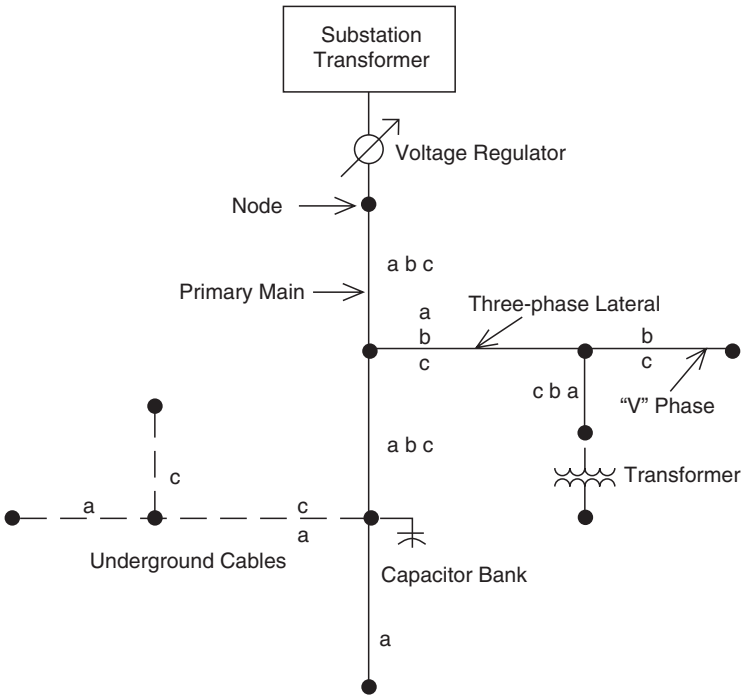

FIGURE 21.1 Distribution feeder.

The following sections will present generalized three-phase models for the "series" components of a feeder (line segments, voltage regulators, transformer banks). Additionally, models are presented for the "shunt" components (loads, capacitor banks). Finally, the "ladder iterative technique" for power-flow studies using the models is presented along with a method for computing short-circuit currents for all types of faults.

21.1.1 Line Impedance

The determination of the impedances for overhead and underground lines is a critical step before analysis of the distribution feeder can begin. Depending upon the degree of accuracy required, impedances can be calculated using Carson's equations where no assumptions are made, or the impedances can be determined from tables where a wide variety of assumptions are made. Between these two limits are other techniques, each with their own set of assumptions.

21.1.1.1 Carson's Equations

Since a distribution feeder is inherently unbalanced, the most accurate analysis should not make any assumptions regarding the spacing between conductors, conductor sizes, or transposition. In a classic paper, John Carson developed a technique in 1926 whereby the self and mutual impedances for ncond overhead conductors can be determined. The equations can also be applied to underground cables. In 1926, this technique was not met with a lot of enthusiasm because of the tedious calculations that had to be done on the slide rule and by hand. With the advent of the digital computer, Carson's equations have now become widely used.

In his paper, Carson assumes the earth is an infinite, uniform solid, with a flat uniform upper surface and a constant resistivity. Any "end effects" introduced at the neutral grounding points are not large at power frequencies, and therefore are neglected. The original Carson equations are given in Eqs. (21.1) and (21.2).

Self-impedance:

$$\hat{z}_{ii} = r_i + 4\varpi P_{ii} G + j\left(X_i + 2\varpi G_{ii} \times \ln\frac{S_{ii}}{R_i} + 4\varpi Q_{ii} G\right)\ \Omega/\text{mile} \tag{21.1}$$

Mutual impedance:

$$\hat{z}_{ij} = 4\varpi P_{ij} G + j\left(2\varpi G\ \ln\frac{S_{ij}}{D_{ij}} + 4\varpi Q_{ij} G\right)\ \Omega/\text{mile} \tag{21.2}$$

where $\hat{z}_{ii}$ = self-impedance of conductor i in Ω/mile
$\hat{z}_{ij}$ = mutual impedance between conductors i and j in Ω/mile
r_i = resistance of conductor i in Ω/mile
v = system angular frequency in radians per second
G = 0.1609347×10^{-7} Ωcm/abohm-mile
R_i = radius of conductor i in feet
GMR_i = geometric mean radius of conductor i in feet
f = system frequency in Hertz
r = resistivity of earth in Ωm
D_{ij} = distance between conductors i and j in feet
S_{ij} = distance between conductor i and image j in feet
q_{ij} = angle between a pair of lines drawn from conductor i to its own image and to the image of conductor j

$$X_i = 2\omega G \ln\frac{R_i}{\text{GMR}_i}\ \Omega/\text{mile} \tag{21.3}$$

$$P_{ij} = \frac{\pi}{8} - \frac{1}{3\sqrt{2}} k_{ij}\cos(\theta_{ij}) + \frac{k_{ij}^2}{16}\cos(2\theta_{ij})\left(0.6728 + \ln\frac{2}{k_{ij}}\right) \tag{21.4}$$

$$Q_{ij} = -0.0386 + \frac{1}{2}\ln\frac{2}{k_{ij}} + \frac{1}{3\sqrt{2}} k_{ij}\cos(\theta_{ij}) \tag{21.5}$$

$$k_{ij} = 8.565 \times 10^{-4} \times S_{ij} \times \sqrt{\frac{f}{\rho}} \tag{21.6}$$

As indicated above, Carson made use of conductor images; that is, every conductor at a given distance above ground has an image conductor the same distance below ground. This is illustrated in Fig. 21.2.

21.1.1.2 Modified Carson's Equations

Only two approximations are made in deriving the "modified Carson equations." These approximations involve the terms associated with P_{ij} and Q_{ij}. The approximations are shown below:

$$P_{ij} = \frac{\pi}{8} \tag{21.7}$$

$$Q_{ij} = -0.03860 + \frac{1}{2}\ln\frac{2}{k_{ij}} \tag{21.8}$$

It is also assumed
f = frequency = 60 Hertz
r = resistivity = 100 Ωm

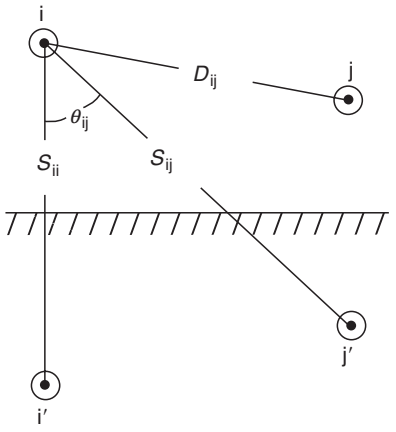

FIGURE 21.2 Conductors and images.

Using these approximations and assumptions, Carson's equations reduce to:

$$\hat{z}_{ii} = r_i + 0.0953 + j0.12134\left(\ln\frac{1}{\text{GMR}_i} + 7.93402\right)\ \Omega/\text{mile} \tag{21.9}$$

$$\hat{z}_{ij} = 0.0953 + j0.12134\left(\ln\frac{1}{D_{ij}} + 7.93402\right)\ \Omega/\text{mile} \tag{21.10}$$

21.1.1.3 Overhead and Underground Lines

Equations (21.9) and (21.10) can be used to compute an ncond × ncond "primitive impedance" matrix. For an overhead four wire, grounded wye distribution line segment, this will result in a 4 × 4 matrix. For an underground grounded wye line segment consisting of three concentric neutral cables, the resulting matrix will be 6 × 6. The primitive impedance matrix for a three-phase line consisting of *m* neutrals will be of the form

$$\left[z_{\text{primitive}}\right] = \left[\begin{array}{ccc|ccc} \hat{z}_{aa} & \hat{z}_{ab} & \hat{z}_{ac} & \hat{z}_{an1} & \cdot & \hat{z}_{anm} \\ \hat{z}_{ba} & \hat{z}_{bb} & \hat{z}_{bc} & \hat{z}_{bn1} & \cdot & \hat{z}_{bnm} \\ \hat{z}_{ca} & \hat{z}_{cb} & \hat{z}_{cc} & \hat{z}_{cn1} & \cdot & \hat{z}_{cnm} \\ \hline \hat{z}_{n1a} & \hat{z}_{n1b} & \hat{z}_{n1c} & \hat{z}_{n1n1} & \cdot & \hat{z}_{n1nm} \\ \cdot & \cdot & \cdot & \cdot & \cdot & \cdot \\ \hat{z}_{nma} & \hat{z}_{nmb} & \hat{z}_{nmc} & \hat{z}_{nmn1} & \cdot & \hat{z}_{nmnm} \end{array}\right] \tag{21.11}$$

In partitioned form Eq. (20.11) becomes

$$\left[z_{\text{primitive}}\right] = \begin{bmatrix} \left[\hat{z}_{ij}\right] & \left[\hat{z}_{in}\right] \\ \left[\hat{z}_{nj}\right] & \left[\hat{z}_{nn}\right] \end{bmatrix} \tag{21.12}$$

21.1.1.4 Phase Impedance Matrix

For most applications, the primitive impedance matrix needs to be reduced to a 3 × 3 phase frame matrix consisting of the self and mutual equivalent impedances for the three phases. One standard method of reduction is the "Kron" reduction (1952) where the assumption is made that the line has a multigrounded neutral. The Kron reduction results in the "phase impedances matrix" determined by using Eq. (21.13) below:

$$\left[z_{abc}\right] = \left[\hat{z}_{ij}\right] - \left[\hat{z}_{in}\right]\left[\hat{z}_{nn}\right]^{-1}\left[\hat{z}_{nj}\right] \tag{21.13}$$

It should be noted that the phase impedance matrix will always be of rotation a–b–c no matter how the phases appear on the pole. That means that always row and column 1 in the matrix will represent phase a, row and column 2 will represent phase b, row and column 3 will represent phase c.

For two-phase (V-phase) and single-phase lines in grounded wye systems, the modified Carson equations can be applied, which will lead to initial 3 × 3 and 2 × 2 primitive impedance matrices. Kron reduction will reduce the matrices to 2 × 2 and a single element. These matrices can be expanded to 3 × 3 phase frame matrices by the addition of rows and columns consisting of zero elements for the missing phases. The phase frame matrix for a three-wire delta line is determined by the application of Carson's equations without the Kron reduction step.

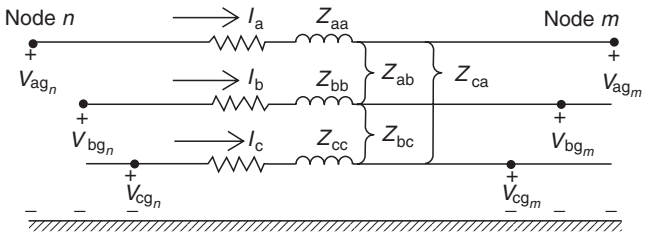

FIGURE 21.3 Three-phase line segment.

The phase frame matrix can be used to accurately determine the voltage drops on the feeder line segments once the currents flowing have been determined. Since no approximations (transposition, for example) have been made regarding the spacing between conductors, the effect of the mutual coupling between phases is accurately taken into account. The application of Carson's equations and the phase frame matrix leads to the most accurate model of a line segment. Figure 21.3 shows the equivalent circuit of a line segment.

The voltage equation in matrix form for the line segment is given by the following equation:

$$\begin{bmatrix} V_{ag} \\ V_{bg} \\ V_{cg} \end{bmatrix}_n = \begin{bmatrix} V_{ag} \\ V_{bg} \\ V_{cg} \end{bmatrix}_m + \begin{bmatrix} Z_{aa} & Z_{ab} & Z_{ac} \\ Z_{ba} & Z_{bb} & Z_{bc} \\ Z_{ca} & Z_{cb} & Z_{cc} \end{bmatrix} \begin{bmatrix} I_a \\ I_b \\ I_c \end{bmatrix} \tag{21.14}$$

where $Z_{ij} = z_{ij} \times \text{length}$

The phase impedance matrix is defined in Eq. (21.15). The phase impedance matrix for single-phase and V-phase lines will have a row and column of zeros for each missing phase

$$[Z_{abc}] = \begin{bmatrix} Z_{aa} & Z_{ab} & Z_{ac} \\ Z_{ba} & Z_{bb} & Z_{bc} \\ Z_{ca} & Z_{cb} & Z_{cc} \end{bmatrix} \tag{21.15}$$

Equation (21.14) can be written in condensed form as

$$[VLG_{abc}]_n = [VLG_{abc}]_m + [Z_{abc}][I_{abc}] \tag{21.16}$$

This condensed notation will be used throughout the document.

21.1.1.5 Sequence Impedances

Many times the analysis of a feeder will use the positive and zero sequence impedances for the line segments. There are basically two methods for obtaining these impedances. The first method incorporates the application of Carson's equations and the Kron reduction to obtain the phase frame impedance matrix. The 3×3 "sequence impedance matrix" can be obtained by

$$[z_{012}] = [A_s]^{-1}[z_{abc}][A_s] \ \Omega/\text{mile} \tag{21.17}$$

where

$$[A_s] = \begin{bmatrix} 1 & 1 & 1 \\ 1 & a_s^2 & a_s \\ 1 & a_s & a_s^2 \end{bmatrix} \tag{21.18}$$

$$a_s = 1.0 \angle 120 \qquad a_s^2 = 1.0 \angle 240$$

The resulting sequence impedance matrix is of the form:

$$[z_{012}] = \begin{bmatrix} z_{00} & z_{01} & z_{02} \\ z_{10} & z_{11} & z_{12} \\ z_{20} & z_{21} & z_{22} \end{bmatrix} \Omega/\text{mile} \tag{21.19}$$

where z_{00} = the zero sequence impedance
z_{11} = the positive sequence impedance
z_{22} = the negative sequence impedance

In the idealized state, the off-diagonal terms of Eq. (21.19) would be zero. When the off-diagonal terms of the phase impedance matrix are all equal, the off-diagonal terms of the sequence impedance matrix will be zero. For high-voltage transmission lines, this will generally be the case because these lines are transposed, which causes the mutual coupling between phases (off-diagonal terms) to be equal. Distribution lines are rarely if ever transposed. This causes unequal mutual coupling between phases, which causes the off-diagonal terms of the phase impedance matrix to be unequal. For the nontransposed line, the diagonal terms of the phase impedance matrix will also be unequal. In most cases, the off-diagonal terms of the sequence impedance matrix are very small compared to the diagonal terms and errors made by ignoring the off-diagonal terms are small.

Sometimes the phase impedance matrix is modified such that the three diagonal terms are equal and all of the off-diagonal terms are equal. The usual procedure is to set the three diagonal terms of the phase impedance matrix equal to the average of the diagonal terms of Eq. (21.15) and the off-diagonal terms equal to the average of the off-diagonal terms of Eq. (21.15). When this is done, the self and mutual impedances are defined as

$$z_s = \frac{1}{3}(z_{aa} + z_{bb} + z_{cc}) \tag{21.20}$$

$$z_m = \frac{1}{3}(z_{ab} + z_{bc} + z_{ca}) \tag{21.21}$$

The phase impedance matrix is now defined as

$$[z_{abc}] = \begin{bmatrix} z_s & z_m & z_m \\ z_m & z_s & z_m \\ z_m & z_m & z_s \end{bmatrix} \tag{21.22}$$

When Eq. (21.17) is used with this phase impedance matrix, the resulting sequence matrix is diagonal (off-diagonal terms are zero). The sequence impedances can be determined directly as

$$\begin{aligned} z_{00} &= z_s + 2z_m \\ z_{11} &= z_{22} = z_s - z_m \end{aligned} \tag{21.23}$$

A second method that is commonly used to determine the sequence impedances directly is to employ the concept of geometric mean distances (GMDs). The GMD between phases is defined as

$$D_{ij} = \text{GMD}_{ij} = \sqrt[3]{D_{ab} D_{bc} D_{ca}} \tag{21.24}$$

The GMD between phases and neutral is defined as

$$D_{in} = \text{GMD}_{in} = \sqrt[3]{D_{an} D_{bn} D_{cn}} \tag{21.25}$$

The GMDs as defined above are used in Eqs. (21.9) and (21.10) to determine the various self and mutual impedances of the line resulting in

$$\hat{z}_{ii} = r_i + 0.0953 + j0.12134\left[\ln\left(\frac{1}{\text{GMR}_i}\right) + 7.93402\right] \tag{21.26}$$

$$\hat{z}_{nn} = r_n + 0.0953 + j0.12134\left[\ln\left(\frac{1}{\text{GMR}_n}\right) + 7.93402\right] \tag{21.27}$$

$$\hat{z}_{ij} = 0.0953 + j0.12134\left[\ln\left(\frac{1}{D_{ij}}\right) + 7.93402\right] \tag{21.28}$$

$$\hat{z}_{in} = 0.0953 + j0.12134\left[\ln\left(\frac{1}{D_{in}}\right) + 7.93402\right] \tag{21.29}$$

Equations (21.26) through (21.29) will define a matrix of order ncond × ncond, where ncond is the number of conductors (phases plus neutrals) in the line segment. Application of the Kron reduction [Eq. (21.13)] and the sequence impedance transformation [Eq. (21.23)] lead to the following expressions for the zero, positive, and negative sequence impedances:

$$z_{00} = \hat{z}_{ii} + 2\hat{z}_{ij} - 3\left(\frac{\hat{z}_{in}^2}{\hat{z}_{nn}}\right)\ \Omega/\text{mile} \tag{21.30}$$

$$z_{11} = z_{22} = \hat{z}_{ii} - \hat{z}_{ij}$$

$$z_{11} = z_{22} = r_i + j0.12134 \times \ln\left(\frac{D_{ij}}{\text{GMR}_i}\right)\ \Omega/\text{mile} \tag{21.31}$$

Equation (21.31) is recognized as the standard equation for the calculation of the line impedances when a balanced three-phase system and transposition are assumed.

Example 21.1

The spacings for an overhead three-phase distribution line are constructed as shown in Fig. 21.4. The phase conductors are 336,400 26/7 ACSR (Linnet) and the neutral conductor is 4/0 6/1 ACSR.

a. Determine the phase impedance matrix.
b. Determine the positive and zero sequence impedances.

Solution

From the table of standard conductor data, it is found that

336,400 26/7 ACSR: GMR = 0.0244 ft
Resistance = 0.306 Ω/mile
4/0 6/1 ACSR: GMR = 0.00814 ft
Resistance = 0.5920 Ω/mile

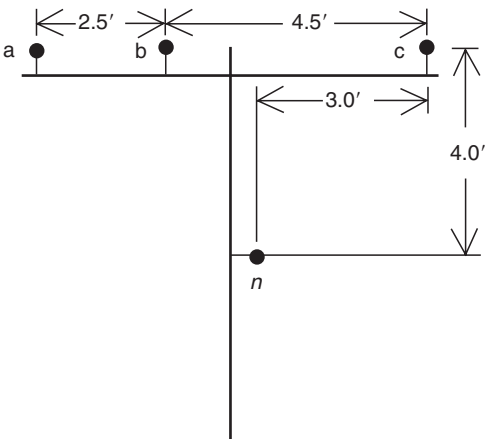

FIGURE 21.4 Three-phase distribution line spacings.

From Fig. 21.4 the following distances between conductors can be determined:

$$D_{ab} = 2.5 \text{ ft} \qquad D_{bc} = 4.5 \text{ ft} \qquad D_{ca} = 7.0 \text{ ft}$$
$$D_{an} = 5.6569 \text{ ft} \quad D_{bn} = 4.272 \text{ ft} \qquad D_{cn} = 5.0 \text{ ft}$$

Applying Carson's modified equations [Eqs. (21.9) and (21.10)] results in the primitive impedance matrix.

$$[\hat{z}] = \begin{bmatrix} 0.4013 + j1.4133 & 0.0953 + j0.8515 & 0.0953 + j0.7266 & 0.0953 + j0.7524 \\ 0.0953 + j0.8515 & 0.4013 + j1.4133 & 0.0953 + j0.7802 & 0.0953 + j0.7865 \\ 0.0953 + j0.7266 & 0.0953 + j0.7802 & 0.4013 + j1.4133 & 0.0953 + j0.7674 \\ 0.0953 + j0.7524 & 0.0953 + j0.7865 & 0.0953 + j.7674 & 0.6873 + j1.5465 \end{bmatrix} \tag{21.32}$$

The Kron reduction of Eq. (21.13) results in the phase impedance matrix

$$[z_{abc}] = \begin{bmatrix} 0.4576 + j1.0780 & 0.1560 + j0.5017 & 0.1535 + j0.3849 \\ 0.1560 + j0.5017 & 0.4666 + j1.0482 & 0.1580 + j0.4236 \\ 0.1535 + j0.3849 & 0.1580 + j0.4236 & 0.4615 + j1.0651 \end{bmatrix} \Omega/\text{mile} \tag{21.33}$$

The phase impedance matrix of Eq. (21.33) can be transformed into the sequence impedance matrix with the application of Eq. (21.17)

$$[z_{012}] = \begin{bmatrix} 0.7735 + j1.9373 & 0.0256 + j0.0115 & -0.0321 + j0.0159 \\ -0.0321 + j0.0159 & 0.3061 + j0.6270 & -0.0723 - j0.0060 \\ 0.0256 + j0.0115 & 0.0723 - j0.0059 & 0.3061 + j0.6270 \end{bmatrix} \Omega/\text{mile} \tag{21.34}$$

In Eq. (21.34), the 1,1 term is the zero sequence impedance, the 2,2 term is the positive sequence impedance, and the 3,3 term is the negative sequence impedance. Note that the off-diagonal terms are not zero, which implies that there is mutual coupling between sequences. This is a result of the nonsymmetrical spacing between phases. With the off-diagonal terms nonzero, the three sequence networks representing the line will not be independent. However, it is noted that the off-diagonal terms are small relative to the diagonal terms.

In high-voltage transmission lines, it is usually assumed that the lines are transposed and that the phase currents represent a balanced three-phase set. The transposition can be simulated in this example by replacing the diagonal terms of Eq. (21.33) with the average value of the diagonal terms $(0.4619 + j1.0638)$ and replacing each off-diagonal term with the average of the off-diagonal terms $(0.1558 + j0.4368)$. This modified phase impedance matrix becomes

$$[z1_{abc}] = \begin{bmatrix} 0.3619 + j1.0638 & 0.1558 + j0.4368 & 0.1558 + j0.4368 \\ 0.1558 + j0.4368 & 0.3619 + j1.0638 & 0.1558 + j0.4368 \\ 0.1558 + j0.4368 & 0.1558 + j0.4368 & 0.3619 + j1.0638 \end{bmatrix} \Omega/\text{mile} \tag{21.35}$$

Using this modified phase impedance matrix in the symmetrical component transformation, Eq. (21.17) results in the modified sequence impedance matrix

$$[z1_{012}] = \begin{bmatrix} 0.7735 + j1.9373 & 0 & 0 \\ 0 & 0.3061 + j0.6270 & 0 \\ 0 & 0 & 0.3061 + j0.6270 \end{bmatrix} \Omega/\text{mile} \tag{21.36}$$

Note now that the off-diagonal terms are all equal to zero, meaning that there is no mutual coupling between sequence networks. It should also be noted that the zero, positive, and negative sequence impedances of Eq. (21.36) are exactly equal to the same sequence impedances of Eq. (21.34).

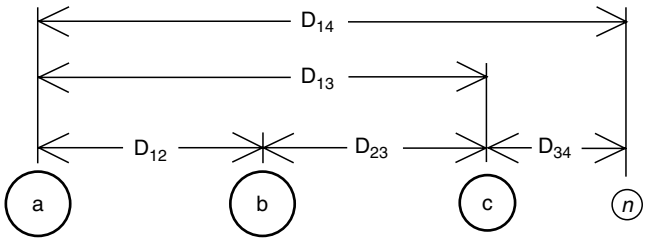

FIGURE 21.5 Three-phase underground with additional neutral.

The results of this example should not be interpreted to mean that a three-phase distribution line can be assumed to have been transposed. The original phase impedance matrix of Eq. (21.33) must be used if the correct effect of the mutual coupling between phases is to be modeled.

21.1.1.6 Underground Lines

Figure 21.5 shows the general configuration of three underground cables (concentric neutral, or tape shielded) with an additional neutral conductor.

Carson's equations can be applied to underground cables in much the same manner as for overhead lines. The circuit of Fig. 21.5 will result in a 7×7 primitive impedance matrix. For underground circuits that do not have the additional neutral conductor, the primitive impedance matrix will be 6×6.

Two popular types of underground cables in use today are the "concentric neutral cable" and the "tape shield cable." To apply Carson's equations, the resistance and GMR of the phase conductor and the equivalent neutral must be known.

21.1.1.7 Concentric Neutral Cable

Figure 21.6 shows a simple detail of a concentric neutral cable. The cable consists of a central phase conductor covered by a thin layer of nonmetallic semiconducting screen to which is bonded the insulating material. The insulation is then covered by a semiconducting insulation screen. The solid strands of concentric neutral are spiralled around the semiconducting screen with a uniform spacing between strands. Some cables will also have an insulating "jacket" encircling the neutral strands.

In order to apply Carson's equations to this cable, the following data needs to be extracted from a table of underground cables:

d_c = phase conductor diameter (in.)
d_{od} = nominal outside diameter of the cable (in.)
d_s = diameter of a concentric neutral strand (in.)
GMR_c = geometric mean radius of the phase conductor (ft)

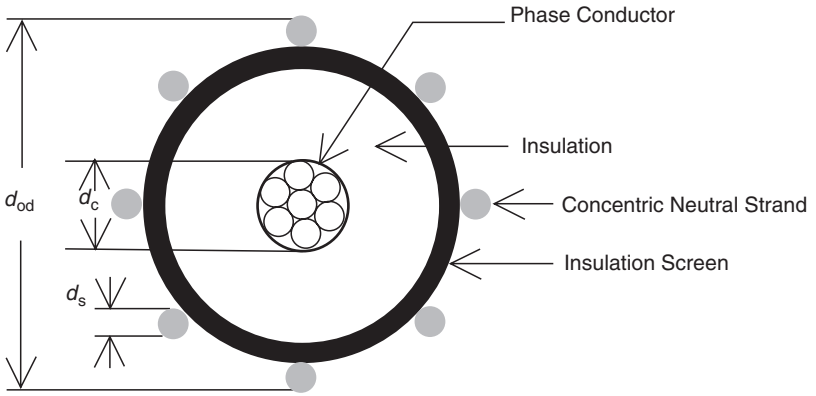

FIGURE 21.6 Concentric neutral cable.

GMR_s = geometric mean radius of a neutral strand (ft)
r_c = resistance of the phase conductor (Ω/mile)
r_s = resistance of a solid neutral strand (Ω/mile)
k = number of concentric neutral strands

The geometric mean radii of the phase conductor and a neutral strand are obtained from a standard table of conductor data. The equivalent geometric mean radius of the concentric neutral is given by

$$GMR_{cn} = \sqrt[k]{GMR_s \times kR^{k-1}} \text{ ft} \tag{21.37}$$

where R = radius of a circle passing through the center of the concentric neutral strands

$$R = \frac{d_{od} - d_s}{24} \text{ ft} \tag{21.38}$$

The equivalent resistance of the concentric neutral is

$$r_{cn} = \frac{r_s}{k} \ \Omega/\text{mile} \tag{21.39}$$

The various spacings between a concentric neutral and the phase conductors and other concentric neutrals are as follows:
Concentric neutral to its own phase conductor

$$D_{ij} = R[\text{Eq. (21.38) above}]$$

Concentric neutral to an adjacent concentric neutral

$$D_{ij} = \text{center-to-center distance of the phase conductors}$$

Concentric neutral to an adjacent phase conductor

Figure 21.7 shows the relationship between the distance between centers of concentric neutral cables and the radius of a circle passing through the centers of the neutral strands.

The GMD between a concentric neutral and an adjacent phase conductor is given by the following equation:

$$D_{ij} = \sqrt[k]{D_{nm}^k - R^k} \text{ ft} \tag{21.40}$$

where D_{nm} = center-to-center distance between phase conductors

For cables buried in a trench, the distance between cables will be much greater than the radius R and therefore very little error is made if D_{ij} in Eq. (21.40) is set equal to D_{nm}. For cables in conduit, that assumption is not valid.

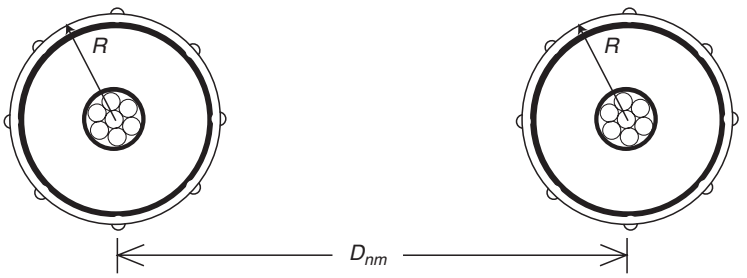

FIGURE 21.7 Distances between concentric neutral cables.

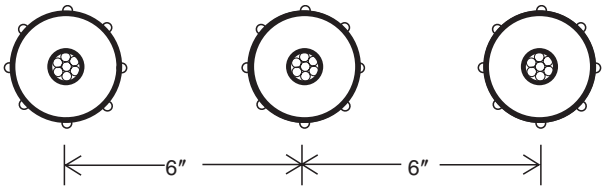

FIGURE 21.8 Three-phase concentric neutral cable spacing.

Example 21.2

Three concentric neutral cables are buried in a trench with spacings as shown in Fig. 21.8. The cables are 15 kV, 250,000 CM stranded all aluminum with 13 strands of #14 annealed coated copper wires (1/3 neutral). The data for the phase conductor and neutral strands from a conductor data table are

250,000 AA phase conductor: $GMR_p = 0.0171$ ft, resistance $= 0.4100\ \Omega$/mile
#14 copper neutral strands: $GMR_s = 0.00208$ ft, resistance $= 14.87\ \Omega$/mile
Diameter $(d_s) = 0.0641$ in.

The equivalent GMR of the concentric neutral [Eq. (21.37)] $= 0.04864$ ft
The radius of the circle passing through strands [Eq. (21.38)] $= 0.0511$ ft
The equivalent resistance of the concentric neutral [Eq. (21.39)] $= 1.1440\ \Omega$/mile
Since R (0.0511 ft) is much less than D_{12} (0.5 ft) and D_{13} (1.0 ft), then the distances between concentric neutrals and adjacent phase conductors are the center-to-center distances of the cables.

Applying Carson's equations results in a 6×6 primitive impedance matrix. This matrix in partitioned form [Eq. (21.12)] is:

$$[z_{ij}] = \begin{bmatrix} 0.5053 + j1.4564 & 0.0953 + j1.0468 & 0.0953 + j0.9627 \\ 0.0953 + j1.0468 & 0.5053 + j1.4564 & 0.0953 + j1.0468 \\ 0.0953 + j0.9627 & 0.0953 + j1.0468 & 0.5053 + j1.4564 \end{bmatrix}$$

$$[z_{in}] = \begin{bmatrix} 0.0953 + j1.3236 & 0.0953 + j1.0468 & 0.0953 + j0.9627 \\ 0.0953 + j1.0468 & 0.0953 + j1.3236 & 0.0953 + j1.0468 \\ 0.0953 + j0.9627 & 0.0953 + j1.0468 & 0.0953 + j1.3236 \end{bmatrix}$$

$$[z_{nj}] = [z_{in}]$$

$$[z_{nn}] = \begin{bmatrix} 1.2393 + j1.3296 & 0.0953 + j1.0468 & 0.0953 + j0.9627 \\ 0.0953 + j1.0468 & 1.2393 + j1.3296 & 0.0953 + j1.0468 \\ 0.0953 + j0.9627 & 0.0953 + j1.0468 & 1.2393 + j1.3296 \end{bmatrix}$$

Using the Kron reduction [Eq. (21.13)] results in the phase impedance matrix

$$[z_{abc}] = \begin{bmatrix} 0.7982 + j0.4463 & 0.3192 + j0.0328 & 0.2849 - j0.0143 \\ 0.3192 + j0.0328 & 0.7891 + j0.4041 & 0.3192 + j0.0328 \\ 0.2849 - j0.0143 & 0.3192 + j0.0328 & 0.7982 + j0.4463 \end{bmatrix} \Omega/\text{mile}$$

The sequence impedance matrix for the concentric neutral three-phase line is determined using Eq. (21.3). The resulting sequence impedance matrix is

$$[z_{012}] = \begin{bmatrix} 1.4106 + j0.4665 & -0.0028 - j0.0081 & -0.0056 + j0.0065 \\ -0.0056 + j0.0065 & 0.4874 + j0.4151 & -0.0264 + j0.0451 \\ -0.0028 - j0.0081 & 0.0523 + j0.0003 & 0.4867 + j0.4151 \end{bmatrix} \Omega/\text{mile}$$

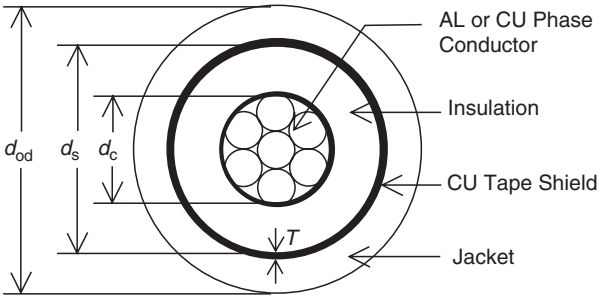

FIGURE 21.9 Taped shielded cable.

21.1.1.8 Tape Shielded Cables

Figure 21.9 shows a simple detail of a tape shielded cable.
Parameters of Fig. 21.9 are

d_c = diameter of phase conductor (in.)
d_s = inside diameter of tape shield (in.)
d_{od} = outside diameter over jacket (in.)
T = thickness of copper tape shield in mils
= 5 mils (standard)

Once again, Carson's equations will be applied to calculate the self-impedances of the phase conductor and the tape shield as well as the mutual impedance between the phase conductor and the tape shield.

The resistance and GMR of the phase conductor are found in a standard table of conductor data.

The resistance of the tape shield is given by

$$r_{\text{shield}} = \frac{18.826}{d_s T}\ \Omega/\text{mile} \tag{21.41}$$

The resistance of the tape shield given in Eq. (21.41) assumes a resistivity of 100 Ωm and a temperature of 50°C. The diameter of the tape shield d_s is given in inches and the thickness of the tape shield T is in mils.

The GMR of the tape shield is given by

$$\text{GMR}_{\text{shield}} = \frac{\frac{d_s}{2} - \frac{T}{2000}}{12}\ \text{ft} \tag{21.42}$$

The various spacings between a tape shield and the conductors and other tape shields are as follows:
Tape shield to its own phase conductor

$$D_{ij} = \text{GMR}_{\text{tape}} = \text{radius to midpoint of the shield} \tag{21.43}$$

Tape shield to an adjacent tape shield

$$D_{ij} = \text{center-to-center distance of the phase conductors} \tag{21.44}$$

Tape shield to an adjacent phase or neutral conductor

$$D_{ij} = D_{nm} \tag{21.45}$$

where D_{nm} = center-to-center distance between phase conductors.

In applying Carson's equations for both concentric neutral and tape shielded cables, the numbering of conductors and neutrals is important. For example, a three-phase underground circuit with an additional neutral conductor must be numbered as

1 = phase conductor #1
2 = phase conductor #2
3 = phase conductor #3
4 = neutral of conductor #1
5 = neutral of conductor #2
6 = neutral of conductor #3
7 = additional neutral conductor (if present)

Example 21.3

A single-phase circuit consists of a 1/0 AA tape shielded cable and a 1/0 CU neutral conductor as shown in Fig. 21.10.
Cable Data: 1/0 AA

Inside diameter of tape shield = $d_s = 1.084$ in.
Resistance = 0.97 Ω/mile
$GMR_p = 0.0111$ ft
Tape shield thickness = $T = 8$ mils

Neutral Data: 1/0 Copper, 7 strand

Resistance = 0.607 Ω/mile
$GMR_n = 0.01113$ ft

Distance between cable and neutral = $D_{nm} = 3$ in.
The resistance of the tape shield is computed according to Eq. (21.41):

$$r_{\text{shield}} = \frac{18.826}{d_s T} = \frac{18.826}{1.084 \times 8} = 2.1705 \ \Omega/\text{mile}$$

The GMR of the tape shield is computed according to Eq. (21.42):

$$\text{GMR}_{\text{shield}} = \frac{\frac{d_s}{2} - \frac{T}{2000}}{12} = \frac{\frac{1.084}{2} - \frac{8}{2000}}{12} = 0.0455 \text{ ft}$$

Using the relations defined in Eqs. (21.43) through (21.45) and Carson's equations results in a 3×3 primitive impedance matrix:

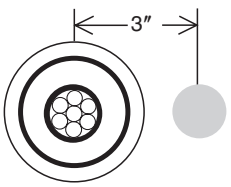

FIGURE 21.10 Single-phase tape shield with neutral.

$$z_{\text{primitive}} = \begin{bmatrix} 1.0653 + j1.5088 & 0.0953 + j1.3377 & 0.0953 + 1.1309 \\ 0.0953 + j1.3377 & 2.2658 + j1.3377 & 0.0953 + j1.1309 \\ 0.0953 + j1.1309 & 0.0953 + j1.1309 & 0.7023 + j1.5085 \end{bmatrix} \Omega/\text{mile}$$

Applying Kron's reduction method will result in a single impedance that represents the equivalent single-phase impedance of the tape shield cable and the neutral conductor.

$$z\text{l}_p = 1.3368 + j0.6028 \ \Omega/\text{mile}$$

21.1.2 Shunt Admittance

When a high-voltage transmission line is less than 50 miles in length, the shunt capacitance of the line is typically ignored. For lightly loaded distribution lines, particularly underground lines, the shunt capacitance should be modeled.

The basic equation for the relationship between the charge on a conductor to the voltage drop between the conductor and ground is given by

$$Q_n = C_{ng} V_{ng} \tag{21.46}$$

where Q_n = charge on the conductor
C_{ng} = capacitance between the conductor and ground
V_{ng} = voltage between the conductor and ground

For a line consisting of ncond (number of phase plus number of neutral) conductors, Eq. (21.46) can be written in condensed matrix form as

$$[Q] = [C][V] \tag{21.47}$$

where $[Q]$ = column vector of order ncond
$[C]$ = ncond × ncond matrix
$[V]$ = column vector of order ncond

Equation (21.47) can be solved for the voltages

$$[V] = [C]^{-1}[Q] = [P][Q] \tag{21.48}$$

$$\text{where} \quad [P] = [C]^{-1} \tag{21.49}$$

21.1.2.1 Overhead Lines

The determination of the shunt admittance of overhead lines starts with the calculation of the "potential coefficient matrix" (Glover and Sarma, 1994). The elements of the matrix are determined by

$$P_{ii} = 11.17689 \times \ln \frac{S_{ii}}{RD_i} \tag{21.50}$$

$$P_{ij} = 11.17689 \times \ln \frac{S_{ij}}{D_{ij}} \tag{21.51}$$

See Fig. 21.2 for the following definitions.

S_{ii} = distance between a conductor and its image below ground in feet
S_{ij} = distance between conductor i and the image of conductor j below ground in feet
D_{ij} = overhead spacing between two conductors in feet
RD_i = radius of conductor i in feet

The potential coefficient matrix will be an ncond × ncond matrix. If one or more of the conductors is a grounded neutral, then the matrix must be reduced using the Kron method to an *n*phase × *n*phase matrix $[P_{abc}]$.

The inverse of the potential coefficient matrix will give the *n*phase × *n*phase capacitance matrix $[C_{abc}]$. The shunt admittance matrix is given by

$$[y_{abc}] = j\omega[C_{abc}] \ \mu\text{S/mile} \tag{21.52}$$

where $\omega = 2\pi f = 376.9911$

Example 21.4

Determine the shunt admittance matrix for the overhead line of Example 21.1. Assume that the neutral conductor is 25 ft above ground.

Solution

For this configuration, the image spacing matrix is computed to be

$$[S] = \begin{bmatrix} 58 & 58.0539 & 58.4209 & 54.1479 \\ 58.0539 & 58 & 58.1743 & 54.0208 \\ 58.4209 & 58.1743 & 58 & 54.0833 \\ 54.1479 & 54.0208 & 54.0835 & 50 \end{bmatrix} \text{ ft}$$

The primitive potential coefficient matrix is computed to be

$$[P_{\text{primitive}}] = \begin{bmatrix} 84.56 & 35.1522 & 23.7147 & 25.2469 \\ 35.4522 & 84.56 & 28.6058 & 28.359 \\ 23.7147 & 28.6058 & 84.56 & 26.6131 \\ 25.2469 & 28.359 & 26.6131 & 85.6659 \end{bmatrix}$$

Kron reduce to a 3×3 matrix

$$[P] = \begin{bmatrix} 77.1194 & 26.7944 & 15.8714 \\ 26.7944 & 75.172 & 19.7957 \\ 15.8714 & 19.7957 & 76.2923 \end{bmatrix}$$

Invert $[P]$ to determine the shunt capacitance matrix

$$[Y_{\text{abc}}] = j376.9911[C_{\text{abc}}] = \begin{bmatrix} j5.6711 & -j1.8362 & -j0.7033 \\ -j1.8362 & j5.9774 & -j1.169 \\ -j0.7033 & -j1.169 & j5.391 \end{bmatrix} \mu\text{S/mile}$$

Multiply $[C_{\text{abc}}]$ by the radian frequency to determine the final three-phase shunt admittance matrix.

21.1.2.2 Underground Lines

Because the electric fields of underground cables are confined to the space between the phase conductor and its concentric neutral to tape shield, the calculation of the shunt admittance matrix requires only the determination of the "self" admittance terms.

21.1.2.3 Concentric Neutral

The self-admittance in μS/mile for a concentric neutral cable is given by

$$Y_{cn} = j\frac{77.582}{\ln\left(\frac{R_b}{R_a}\right) - \frac{1}{k}\ln\left(\frac{kR_n}{R_b}\right)} \tag{21.53}$$

where R_b = radius of a circle to center of concentric neutral strands (ft)
R_a = radius of phase conductor (ft)
R_n = radius of concentric neutral strand (ft)
k = number of concentric neutral strands

Example 21.5

Determine the three-phase shunt admittance matrix for the concentric neutral line of Example 21.2.

Solution

$$R_b = R = 0.0511 \text{ ft}$$

Diameter of the 250,000 AA phase conductor = 0.567 in.

$$R_a = \frac{0.567}{24} = 0.0236 \text{ ft}$$

Diameter of the #14 CU concentric neutral strand = 0.0641 in.

$$R_n = \frac{0.0641}{24} = 0.0027 \text{ ft}$$

Substitute into Eq. (21.53):

$$Y_{cn} = j\frac{77.582}{\ln\left(\frac{R_b}{R_a}\right) - \frac{1}{k}\ln\left(\frac{kR_n}{R_b}\right)} = j\frac{77.582}{\ln\left(\frac{0.0511}{0.0236}\right) - \frac{1}{13}\ln\left(\frac{13 \times 0.0027}{0.0511}\right)} = j96.8847$$

The three-phase shunt admittance matrix is:

$$[Y_{abc}] = \begin{bmatrix} j96.8847 & 0 & 0 \\ 0 & j96.8847 & 0 \\ 0 & 0 & j96.8847 \end{bmatrix} \mu\text{S/mile}$$

21.1.2.4 Tape Shield Cable

The shunt admittance in μS/mile for tape shielded cables is given by

$$Y_{ts} = j\frac{77.586}{\ln\left(\frac{R_b}{R_a}\right)} \ \mu\text{S/mile} \tag{21.54}$$

where R_b = inside radius of the tape shield
R_a = radius of phase conductor

Example 21.6

Determine the shunt admittance of the single-phase tape shielded cable of Example 21.3 in Section 21.1.1.

Solution

$$R_b = \frac{d_s}{24} = \frac{1.084}{24} = 0.0452$$

The diameter of the 1/0 AA phase conductor = 0.368 in.

$$R_a = \frac{d_p}{24} = \frac{0.368}{24} = 0.0153$$

Substitute into Eq. (21.54):

$$Y_{ts} = j\frac{77.586}{\ln\left(\frac{R_b}{R_a}\right)} = j\frac{77.586}{\ln\left(\frac{0.0452}{0.0153}\right)} = j71.8169\ \mu\text{S/mile}$$

21.1.3 Line Segment Models

21.1.3.1 Exact Line Segment Model

The exact model of a three-phase line segment is shown in Fig. 21.11. For the line segment in Fig. 21.11, the equations relating the input (node n) voltages and currents to the output (node m) voltages and currents are

$$[VLG_{\text{abc}}]_n = [\text{a}][VLG_{\text{abc}}]_m + [\text{b}][I_{\text{abc}}]_m \tag{21.55}$$

$$[I_{\text{abc}}]_n = [\text{c}][VLG_{\text{abc}}]_m + [\text{d}][I_{\text{abc}}]_m \tag{21.56}$$

where

$$[\text{a}] = [U] - \frac{1}{2}[Z_{\text{abc}}][Y_{\text{abc}}] \tag{21.57}$$

$$[\text{b}] = [Z_{\text{abc}}] \tag{21.58}$$

$$[\text{c}] = [Y_{\text{abc}}] - \frac{1}{4}[Z_{\text{abc}}][Y_{\text{abc}}]^2 \tag{21.59}$$

$$[\text{d}] = [U] - \frac{1}{2}[Z_{\text{abc}}][Y_{\text{abc}}] \tag{21.60}$$

In Eqs. (21.57) through (21.60), the impedance matrix $[Z_{\text{abc}}]$ and the admittance matrix $[Y_{\text{abc}}]$ are defined earlier in this document.

Sometimes it is necessary to determine the voltages at node m as a function of the voltages at node n and the output currents at node m. The necessary equation is

$$[VLG_{\text{abc}}]_m = [\text{A}][VLG_{\text{abc}}]_n - [\text{B}][I_{\text{abc}}]_m \tag{21.61}$$

where

$$[\text{A}] = \left([U] + \frac{1}{2}[Z_{\text{abc}}][Y_{\text{abc}}]\right)^{-1} \tag{21.62}$$

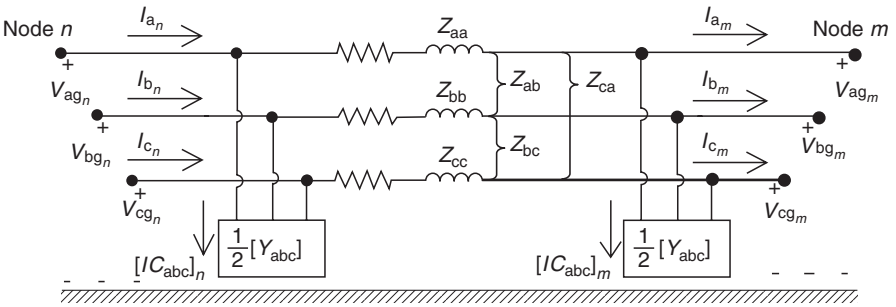

FIGURE 21.11 Three-phase line segment model.

$$[\mathrm{B}] = \left([U] + \frac{1}{2}[Z_{\mathrm{abc}}][Y_{\mathrm{abc}}]\right)^{-1}[Z_{\mathrm{abc}}] \tag{21.63}$$

$$[U] = \begin{bmatrix} 1 & 0 & 0 \\ 0 & 1 & 0 \\ 0 & 0 & 1 \end{bmatrix} \tag{21.64}$$

In many cases the shunt admittance is so small that it can be neglected. However, for all underground cables and for overhead lines longer than 15 miles, it is recommended that the shunt admittance be included. When the shunt admittance is neglected, the [a], [b], [c], [d], [A], and [B] matrices become

$$[\mathrm{a}] = [U] \tag{21.65}$$

$$[\mathrm{b}] = [Z_{\mathrm{abc}}] \tag{21.66}$$

$$[\mathrm{c}] = [0] \tag{21.67}$$

$$[\mathrm{d}] = [U] \tag{21.68}$$

$$[\mathrm{A}] = [U] \tag{21.69}$$

$$[\mathrm{B}] = [Z_{\mathrm{abc}}] \tag{21.70}$$

When the shunt admittance is neglected, Eqs. (21.55), (21.56), and (21.61) become

$$[VLG_{\mathrm{abc}}]_n = [VLG_{\mathrm{abc}}]_m + [Z_{\mathrm{abc}}][I_{\mathrm{abc}}]_m \tag{21.71}$$

$$[I_{\mathrm{abc}}]_n = [I_{\mathrm{abc}}]_m \tag{21.72}$$

$$[VLG_{\mathrm{abc}}]_m = [VLG_{\mathrm{abc}}]_n - [Z_{\mathrm{abc}}][I_{\mathrm{abc}}]_m \tag{21.73}$$

If an accurate determination of the voltage drops down a line segment is to be made, it is essential that the phase impedance matrix $[Z_{\mathrm{abc}}]$ be computed based upon the actual configuration and phasing of the overhead or underground lines. No assumptions should be made, such as transposition. The reason for this is best demonstrated by an example.

Example 21.7

The phase impedance matrix for the line configuration in Example 21.1 was computed to be

$$[z_{\mathrm{abc}}] = \begin{bmatrix} 0.4576 + j1.0780 & 0.1560 + j0.5017 & 0.1535 + j0.3849 \\ 0.1560 + j0.5017 & 0.4666 + j1.0482 & 0.1580 + j0.4236 \\ 0.1535 + j0.3849 & 0.1580 + j0.4236 & 0.4615 + j1.0651 \end{bmatrix} \Omega/\mathrm{mile}$$

Assume that a 12.47 kV substation serves a load 1.5 miles from the substation. The metered output at the substation is balanced 10,000 kVA at 12.47 kV and 0.9 lagging power factor. Compute the three-phase line-to-ground voltages at the load end of the line and the voltage unbalance at the load.

Solution

The line-to-ground voltages and line currents at the substation are

$$[VLG_{\mathrm{abc}}] = \begin{bmatrix} 7200\angle 0 \\ 7200\angle -120 \\ 7200\angle 120 \end{bmatrix} \qquad [I_{\mathrm{abc}}]_n = \begin{bmatrix} 463\angle -25.84 \\ 463\angle -145.84 \\ 463\angle 94.16 \end{bmatrix}$$

Solve Eq. (21.71) for the load voltages:

$$[VLG_{\text{abc}}]_m = [VLG_{\text{abc}}]_n - 1.5[Z_{\text{abc}}][I_{\text{abc}}]_n = \begin{bmatrix} 6761.10\angle 2.32 \\ 6877.7\angle -122.43 \\ 6836.33\angle 117.21 \end{bmatrix}$$

The voltage unbalance at the load using the NEMA definition is

$$V_{\text{unbalance}} = \frac{\max(V_{\text{deviation}})}{V_{\text{avg}}} 100 = 0.937\%$$

The point of Example 21.7 is to demonstrate that even though the system is perfectly balanced at the substation, the unequal mutual coupling between the phases results in a significant voltage unbalance at the load; significant because NEMA requires that induction motors be derated when the voltage unbalance is 1% or greater.

21.1.3.2 Approximate Line Segment Model

Many times the only data available for a line segment will be the positive and zero sequence impedances. An approximate three-phase line segment model can be developed by applying the "reverse impedance transformation" from symmetrical component theory.

Using the known positive and zero sequence impedances, the "sequence impedance matrix" is given by

$$[Z_{\text{seq}}] = \begin{bmatrix} Z_0 & 0 & 0 \\ 0 & Z_+ & 0 \\ 0 & 0 & Z_+ \end{bmatrix} \tag{21.74}$$

The reverse impedance transformation results in the following "approximate phase impedance matrix:"

$$[Z_{\text{approx}}] = [A_s][Z_{\text{seq}}][A_s]^{-1} = \frac{1}{3}\begin{bmatrix} (2Z_+ - Z_0) & (Z_0 - Z_+) & (Z_0 - Z_+) \\ (Z_0 - Z_+) & (2Z_+ - Z_0) & (Z_0 - Z_+) \\ (Z_0 - Z_+) & (Z_0 - Z_+) & (2Z_+ - Z_0) \end{bmatrix} \tag{21.75}$$

Notice that the approximate phase impedance matrix is characterized by the three diagonal terms being equal and all mutual terms being equal. This is the same result that is achieved if the line is assumed to be transposed. Substituting the approximate phase impedance matrix into Eq. (21.71) results in

$$\begin{bmatrix} V_{an} \\ V_{bn} \\ V_{cn} \end{bmatrix}_n = \begin{bmatrix} V_{an} \\ V_{bn} \\ V_{cn} \end{bmatrix}_m + \frac{1}{3}\begin{bmatrix} (2Z_+ - Z_0) & (Z_0 - Z_+) & (Z_0 - Z_+) \\ (Z_0 - Z_+) & (2Z_+ - Z_0) & (Z_0 - Z_+) \\ (Z_0 - Z_+) & (Z_0 - Z_+) & (2Z_+ - Z_0) \end{bmatrix} \begin{bmatrix} I_a \\ I_b \\ I_c \end{bmatrix}_n \tag{21.76}$$

Equation (21.76) can be expanded and an equivalent circuit for the approximate line segment model can be developed. This approximate model is shown in Fig. 21.12.

The errors made by using this approximate line segment model are demonstrated in the following example.

Example 21.8

For the line of Example 21.7, the positive and zero sequence impedances were determined to be

$$Z_+ = 0.3061 + j0.6270\ \Omega/\text{mile}$$
$$Z_0 = 0.7735 + j1.9373\ \Omega/\text{mile}$$

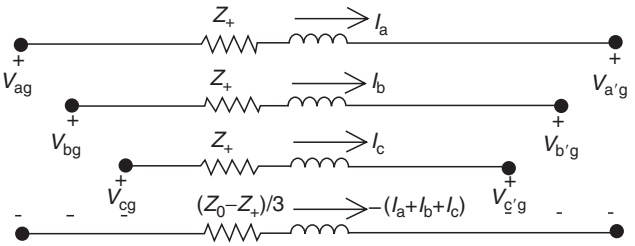

FIGURE 21.12 Approximate line segment model.

Solution

The sequence impedance matrix is

$$\left[z_{\text{seq}}\right] = \begin{bmatrix} 0.7735 + j1.9373 & 0 & 0 \\ 0 & 0.3061 + j0.6270 & 0 \\ 0 & 0 & 0.3061 + j0.6270 \end{bmatrix}$$

Performing the reverse impedance transformation results in the approximate phase impedance matrix.

$$\left[z_{\text{approx}}\right] = [A_s]\left[z_{\text{seq}}\right][A_s]^{-1} = \begin{bmatrix} 0.4619 + j1.0638 & 0.1558 + j0.4368 & 0.1558 + j0.4368 \\ 0.1558 + j0.4368 & 0.4619 + j1.0638 & 0.1558 + j0.4368 \\ 0.1558 + j0.4368 & 0.1558 + j0.4368 & 0.4619 + j1.0638 \end{bmatrix}$$

Note in the approximate phase impedance matrix that the three diagonal terms are equal and all of the mutual terms are equal.

Use the approximate impedance matrix to compute the load voltage and voltage unbalance as specified in Example 21.1.

Note that the voltages are computed to be balanced. In the previous example it was shown that when the line is modeled accurately, there is a voltage unbalance of almost 1%.

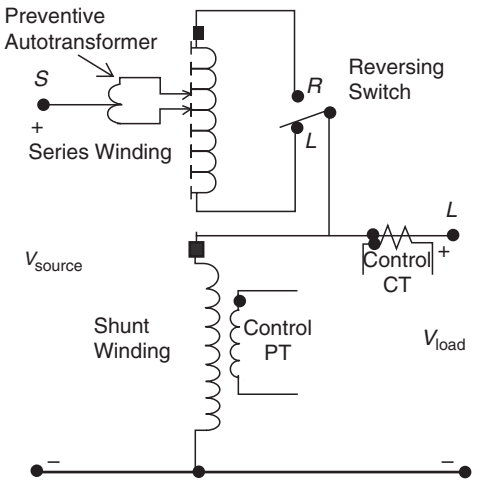

FIGURE 21.13 Type B step-voltage regulator.

21.1.4 Step-Voltage Regulators

A step-voltage regulator consists of an autotransformer and a load tap changing mechanism. The voltage change is obtained by changing the taps of the series winding of the autotransformer. The position of the tap is determined by a control circuit (line drop compensator). Standard step regulators contain a reversing switch enabling a $\pm 10\%$ regulator range, usually in 32 steps. This amounts to a 5/8% change per step or 0.75 V change per step on a 120 V base.

A type B step-voltage regulator is shown in Fig. 21.13. There is also a type A step-voltage regulator where the load and source sides of the regulator are reversed from that shown in Fig. 21.13.

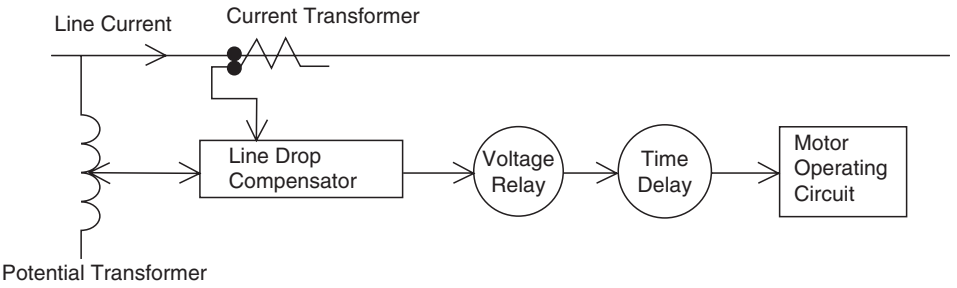

FIGURE 21.14 Regulator control circuit.

Since the type B regulator is more common, the remainder of this section will address the type B step-voltage regulator.

The tap changing is controlled by a control circuit shown in the block diagram of Fig. 21.14. The control circuit requires the following settings:

1. Voltage Level—The desired voltage (on 120 V base) to be held at the "load center." The load center may be the output terminal of the regulator or a remote node on the feeder.
2. Bandwidth—The allowed variance of the load center voltage from the set voltage level. The voltage held at the load center will be $\pm\frac{1}{2}$ of the bandwidth. For example, if the voltage level is set to 122 V and the bandwidth set to 2 V, the regulator will change taps until the load center voltage lies between 121 and 123 V.
3. Time Delay—Length of time that a raise or lower operation is called for before the actual execution of the command. This prevents taps changing during a transient or short time change in current.
4. Line Drop Compensator—Set to compensate for the voltage drop (line drop) between the regulator and the load center. The settings consist of R and X settings in volts corresponding to the equivalent impedance between the regulator and the load center. This setting may be zero if the regulator output terminals are the load center.

The rating of a regulator is based on the kVA transformed, not the kVA rating of the line. In general this will be 10% of the line rating since rated current flows through the series winding that represents the $\pm 10\%$ voltage change.

21.1.4.1 Voltage Regulator in the Raise Position

Figure 21.15 shows a detailed and abbreviated drawing of a type B regulator in the raise position. The defining voltage and current equations for the type B regulator in the raise position are as follows:

Voltage equations	Current equations	
$\frac{V_1}{N_1} = \frac{V_2}{N_2}$	$N_1 I_1 = N_2 I_2$	(21.77)
$V_S = V_1 - V_2$	$I_L = I_s - I_1$	(21.78)
$V_L = V_1$	$I_2 = I_S$	(21.79)
$V_2 = \frac{N_2}{N_1} V_1 = \frac{N_2}{N_1} V_L$	$I_1 = \frac{N_2}{N_1} I_2 = \frac{N_2}{N_1} I_S$	(21.80)

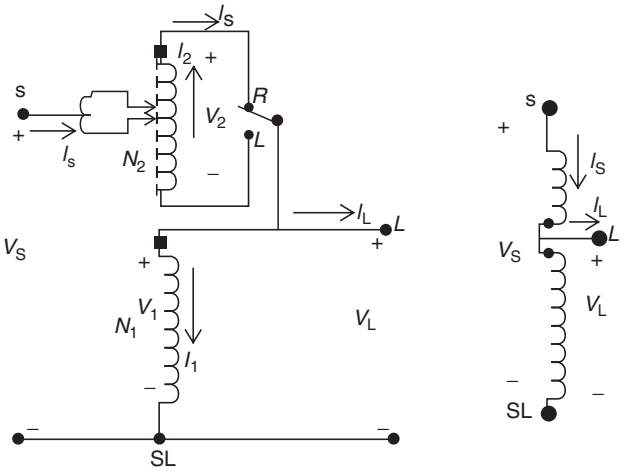

FIGURE 21.15 Type B voltage regulator in the raise position.

$$V_S = \left(1 - \frac{N_2}{N_1}\right) V_l \qquad I_L = \left(1 - \frac{N_2}{N_1}\right) I_S \tag{21.81}$$

$$V_S = a_R V_L \qquad I_L = a_R I_S \tag{21.82}$$

$$a_R = 1 - \frac{N_2}{N_1} \tag{21.83}$$

Equations (21.82) and (21.83) are the necessary defining equations for modeling a regulator in the raise position.

21.1.4.2 Voltage Regulator in the Lower Position

Figure 21.16 shows the detailed and abbreviated drawings of a regulator in the lower position. Note in the figure that the only difference between the lower and the raise models is that the polarity of the series winding and how it is connected to the shunt winding is reversed.

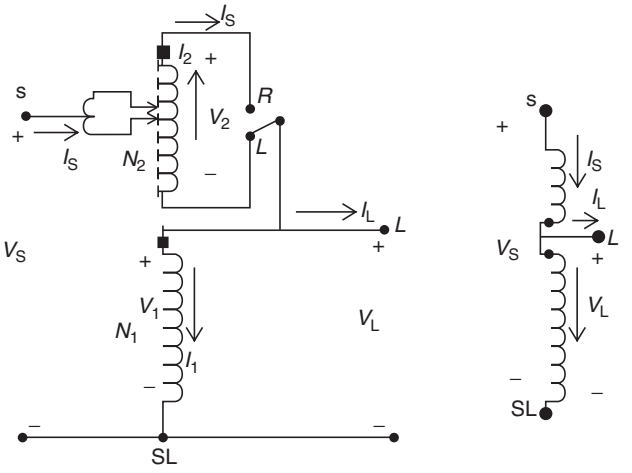

FIGURE 21.16 Type B regulator in the lower position.

The defining voltage and current equations for a regulator in the lower position are as follows:

Voltage equations	Current equations	
$\frac{V_1}{N_1} = \frac{V_2}{N_2}$	$N_1 I_1 = N_2 I_2$	(21.84)
$V_S = V_1 + V_2$	$I_L = I_s - I_1$	(21.85)
$V_L = V_1$	$I_2 = -I_S$	(21.86)
$V_2 = \frac{N_2}{N_1} V_1 = \frac{N_2}{N_1} V_L$	$I_1 = \frac{N_2}{N_1} I_2 = \frac{N_2}{N_1}(-I_S)$	(21.87)
$V_S = \left(1 + \frac{N_2}{N_1}\right) V_l$	$I_L = \left(1 + \frac{N_2}{N_1}\right) I_S$	(21.88)
$V_S = a_R V_L$	$I_L = a_R I_S$	(21.89)
$a_R = 1 + \frac{N_2}{N_1}$		(21.90)

Equations (21.83) and (21.90) give the value of the effective regulator ratio as a function of the ratio of the number of turns on the series winding (N_2) to the number of turns on the shunt winding (N_1). The actual turns ratio of the windings is not known. However, the particular position will be known. Equations (21.83) and (21.90) can be modified to give the effective regulator ratio as a function of the tap position. Each tap changes the voltage by 5/8% or 0.00625 per unit. On a 120 V base, each step change results in a change of voltage of 0.75 V. The effective regulator ratio can be given by

$$a_R = 1 \mp 0.00625 \cdot Tap \tag{21.91}$$

In Eq. (21.91), the minus sign applies to the "raise" position and the positive sign for the "lower" position.

21.1.4.3 Line Drop Compensator

The changing of taps on a regulator is controlled by the "line drop compensator." Figure 21.17 shows a simplified sketch of the compensator circuit and how it is connected to the circuit through a potential transformer and a current transformer.

The purpose of the line drop compensator is to model the voltage drop of the distribution line from the regulator to the load center. Typically, the compensator circuit is modeled on a 120 V base. This requires the potential transformer to transform rated voltage (line-to-neutral or line-to-line) down to 120 V. The current transformer turns ratio (CT_p:CT_s) where the primary rating (CT_p) will typically be the rated current of the feeder. The setting that is most critical is that of R' and X'. These values must represent the equivalent impedance from the regulator to the load center. Knowing the equivalent impedance in Ohms from the regulator to the load center (R_{line_ohms} and X_{line_ohms}), the required value for the compensator settings are calibrated in volts and determined by

$$R'_{volts} + jX'_{volts} = (R_{line\_ohms} + jX_{line\_ohms}) \cdot \frac{Ct_p}{N_{pt}} \text{ V} \tag{21.92}$$

The value of the compensator settings in ohms is determined by

$$R'_{ohms} + jX'_{ohms} = \frac{R'_{volts} + jX'_{volts}}{Ct_s} \ \Omega \tag{21.93}$$

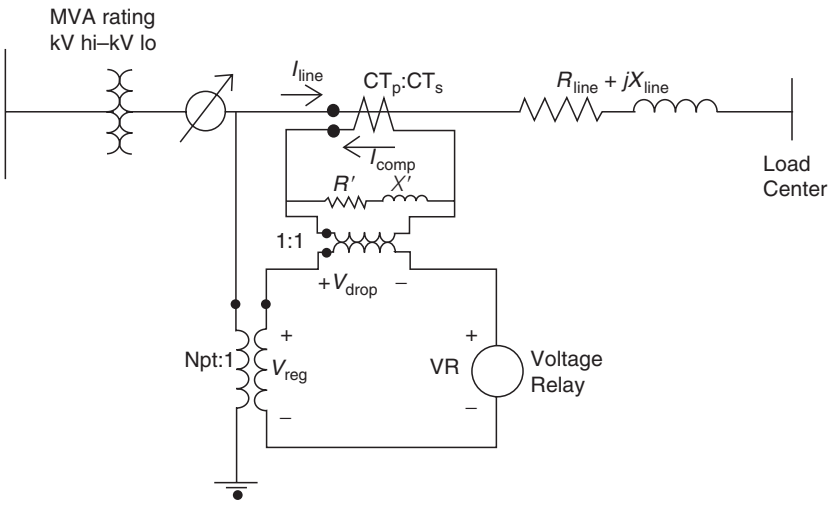

FIGURE 21.17 Line drop compensator circuit.

It is important to understand that the value of $R_{\text{line\_ohms}} + jX_{\text{line\_ohms}}$ is not the impedance of the line between the regulator and the load center. Typically the load center is located down the primary main feeder after several laterals have been tapped. As a result, the current measured by the CT of the regulator is not the current that flows all the way from the regulator to the load center. The proper way to determine the line impedance values is to run a power-flow program of the feeder without the regulator operating. From the output of the program, the voltages at the regulator output and the load center are known. Now the "equivalent" line impedance can be computed as

$$R_{\text{line}} + jX_{\text{line}} = \frac{V_{\text{regulator\_output}} - V_{\text{load\_center}}}{I_{\text{line}}} \ \Omega \tag{21.94}$$

In Eq. (21.94), the voltages must be specified in system volts and the current in system amps.

21.1.4.4 Wye Connected Regulators

Three single-phase regulators connected in wye are shown in Fig. 21.18. In Fig. 21.18 the polarities of the windings are shown in the raise position. When the regulator is in the lower position, a reversing switch will have reconnected the series winding so that the polarity on the series winding is now at the output terminal.

Regardless of whether the regulator is raising or lowering the voltage, the following equations apply:

21.1.4.5 Voltage Equations

$$\begin{bmatrix} V_{An} \\ V_{Bn} \\ V_{Cn} \end{bmatrix} = \begin{bmatrix} a_{R\_a} & 0 & 0 \\ 0 & a_{R\_b} & 0 \\ 0 & 0 & a_{R\_c} \end{bmatrix} \begin{bmatrix} V_{an} \\ V_{bn} \\ V_{cn} \end{bmatrix} \tag{21.95}$$

Equation (21.95) can be written in condensed form as

$$[VLN_{\text{ABC}}] = [aRV_{\text{abc}}][VLN_{\text{abc}}] \tag{21.96}$$

also

$$[VLN_{\text{abc}}] = [aRV_{\text{ABC}}][VLN_{\text{ABC}}] \tag{21.97}$$

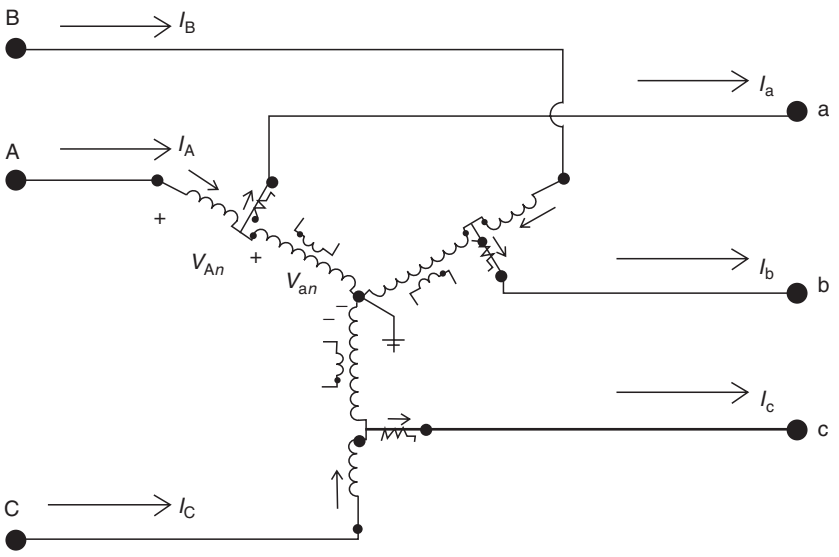

FIGURE 21.18 Wye connected type B regulators.

where

$$[aRV_{ABC}] = [aRV_{abc}]^{-1} \tag{21.98}$$

21.1.4.6 Current Equations

$$\begin{bmatrix} I_A \\ I_B \\ I_C \end{bmatrix} = \begin{bmatrix} \frac{1}{a_{R\_a}} & 0 & 0 \\ 0 & \frac{1}{a_{R\_b}} & 0 \\ 0 & 0 & \frac{1}{a_{R\_c}} \end{bmatrix} \begin{bmatrix} I_a \\ I_b \\ I_c \end{bmatrix} \tag{21.99}$$

or

$$[I_{ABC}] = [aRI_{abc}][I_{abc}] \tag{21.100}$$

also

$$[I_{abc}] = [aRI_{ABC}][I_{ABC}] \tag{21.101}$$

where

$$[aRI_{ABC}] = [aRI_{abc}]^{-1} \tag{21.102}$$

where $0.9 \leq a_{R\_abc} \leq 1.1$ in 32 steps of 0.625% per step (0.75 V/step on 120 V base).

Note: The effective turn ratios (a_{R_a}, a_{R_b}, and a_{R_c}) can take on different values when three single-phase regulators are connected in wye. It is also possible to have a three-phase regulator connected in wye where the voltage and current are sampled on only one phase and then all three phases are changed by the same value of aR (number of taps).

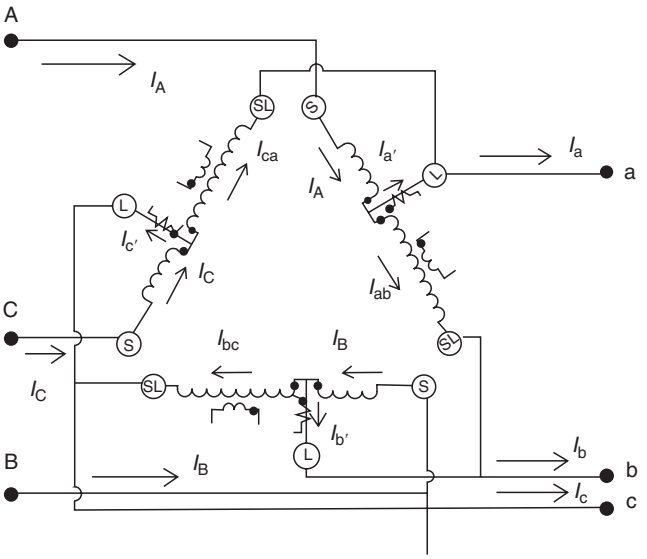

FIGURE 21.19 Delta connected type B regulators.

21.1.4.7 Closed Delta Connected Regulators

Three single-phase regulators can be connected in a closed delta as shown in Fig. 21.19. In the figure, the regulators are shown in the raise position. The closed delta connection is typically used in three-wire delta feeders. Note that the potential transformers for this connection are monitoring the load side line-to-line voltages and the current transformers are monitoring the load side line currents.

Applying the basic voltage and current Eqs. (21.77) through (21.83) of the regulator in the raise position, the following voltage and current relations are derived for the closed delta connection.

$$\begin{bmatrix} V_{AB} \\ V_{BC} \\ V_{CA} \end{bmatrix} = \begin{bmatrix} a_{R\_ab} & 1 - a_{R\_bc} & 0 \\ 0 & a_{R\_bc} & 1 - a_{R\_ca} \\ 1 - a_{R\_ab} & 0 & a_{R\_ca} \end{bmatrix} \begin{bmatrix} V_{ab} \\ V_{bc} \\ V_{ca} \end{bmatrix} \tag{21.103}$$

Equation (21.101) in abbreviated form can be written as

$$[VLL_{ABC}] = [aRVD_{abc}][VLL_{abc}] \tag{21.104}$$

When the load side voltages are known, the source side voltages can be determined by

$$[VLL_{abc}] = [aRVD_{ABC}][VLL_{ABC}] \tag{21.105}$$

where

$$[aRVD_{ABC}] = [aRVD_{abc}]^{-1} \tag{21.106}$$

In a similar manner, the relationships between the load side and source side line currents are given by

$$\begin{bmatrix} I_a \\ I_b \\ I_c \end{bmatrix} = \begin{bmatrix} a_{R\_ab} & 0 & 1 - a_{R\_ca} \\ 1 - a_{R\_ab} & a_{R\_bc} & 0 \\ 0 & 1 - a_{R\_bc} & a_{R\_ca} \end{bmatrix} \begin{bmatrix} I_A \\ I_B \\ I_C \end{bmatrix} \tag{21.107}$$

or

$$[I_{abc}] = [AID_{ABC}][I_{ABC}] \tag{21.108}$$

also

$$[I_{ABC}] = [AID_{abc}][I_{abc}] \tag{21.109}$$

where

$$[IAD_{abc}] = [IAD_{ABC}]^{-1} \tag{21.110}$$

The closed delta connection can be difficult to apply. Note in both the voltage and current equations that a change of the tap position in one regulator will affect voltages and currents in two phases. As a result, increasing the tap in one regulator will affect the tap position of the second regulator. In most cases the bandwidth setting for the closed delta connection will have to be wider than that for wye connected regulators.

21.1.4.8 Open Delta Connection

Two single-phase regulators can be connected in the "open" delta connection. Shown in Fig. 21.20 is an open delta connection where two single-phase regulators have been connected between phases AB and CB.

Two other open connections can also be made where the single-phase regulators are connected between phases BC and AC and also between phases CA and BA.

The open delta connection is typically applied to three-wire delta feeders. Note that the potential transformers monitor the line-to-line voltages and the current transformers monitor the line currents. Once again, the basic voltage and current relations of the individual regulators are used to determine the relationships between the source side and load side voltages and currents.

For all three open connections, the following general equations will apply:

$$[VLL_{ABC}] = [aRV_{abc}][VLL_{abc}] \tag{21.111}$$

$$[VLL_{abc}] = [aRV_{ABC}][VLL_{ABC}] \tag{21.112}$$

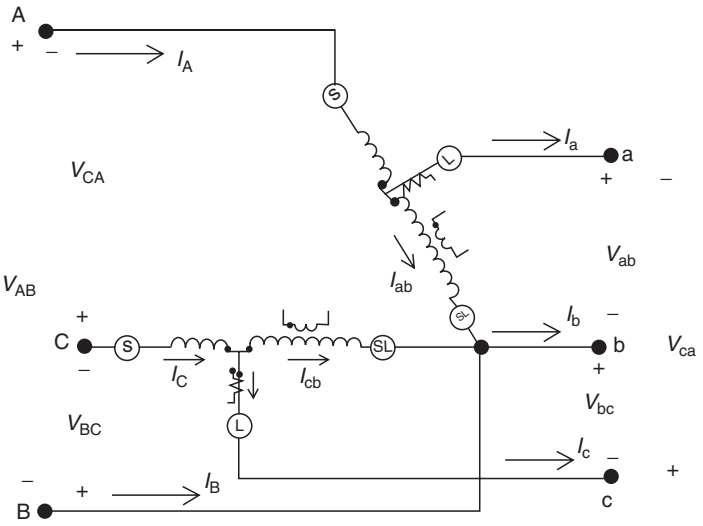

FIGURE 21.20 Open delta type B regulator connection.

$$[I_{ABC}] = [aRI_{abc}][I_{abc}] \tag{21.113}$$

$$[I_{abc}] = [aRI_{ABC}][I_{ABC}] \tag{21.114}$$

The matrices for the three open connections are defined as follows:
Phases AB and CB

$$[aRV_{abc}] = \begin{bmatrix} a_{R\_A} & 0 & 0 \\ 0 & a_{R\_C} & 0 \\ -a_{R\_A} & -a_{R\_C} & 0 \end{bmatrix} \tag{21.115}$$

$$[aRV_{ABC}] = \begin{bmatrix} \dfrac{1}{a_{R\_A}} & 0 & 0 \\ 0 & \dfrac{1}{a_{R\_C}} & 0 \\ -\dfrac{1}{a_{R\_A}} & -\dfrac{1}{a_{R\_C}} & 0 \end{bmatrix} \tag{21.116}$$

$$[aRI_{abc}] = \begin{bmatrix} \dfrac{1}{a_{R\_A}} & 0 & 0 \\ -\dfrac{1}{a_{R\_A}} & 0 & -\dfrac{1}{a_{R\_C}} \\ 0 & 0 & \dfrac{1}{a_{R\_C}} \end{bmatrix} \tag{21.117}$$

$$[aRI_{ABC}] = \begin{bmatrix} a_{R\_A} & 0 & 0 \\ -a_{R\_A} & 0 & a_{R\_C} \\ 0 & 0 & a_{R\_C} \end{bmatrix} \tag{21.118}$$

Phases BC and AC

$$[aRV_{abc}] = \begin{bmatrix} 0 & -a_{R\_B} & -a_{R\_A} \\ 0 & a_{R\_B} & 0 \\ 0 & 0 & a_{R\_A} \end{bmatrix} \tag{21.119}$$

$$[aRV_{ABC}] = \begin{bmatrix} 0 & -\dfrac{1}{a_{R\_B}} & -\dfrac{1}{a_{R\_A}} \\ 0 & \dfrac{1}{a_{R\_B}} & 0 \\ 0 & 0 & \dfrac{1}{a_{R\_A}} \end{bmatrix} \tag{21.120}$$

$$[aRI_{abc}] = \begin{bmatrix} \dfrac{1}{a_{R\_A}} & 0 & 0 \\ 0 & \dfrac{1}{a_{R\_B}} & 0 \\ -\dfrac{1}{a_{R\_A}} & -\dfrac{1}{a_{R\_B}} & 0 \end{bmatrix} \tag{21.121}$$

$$[aRI_{ABC}] = \begin{bmatrix} a_{R\_A} & 0 & 0 \\ 0 & a_{R\_B} & 0 \\ -a_{R\_A} & -a_{R\_B} & 0 \end{bmatrix} \tag{21.122}$$

Phases CA and BA

$$[aRV_{\text{abc}}] = \begin{bmatrix} a_{R\_\text{B}} & 0 & 0 \\ -a_{R\_\text{B}} & 0 & -a_{R\_\text{C}} \\ 0 & 0 & a_{R\_\text{C}} \end{bmatrix} \tag{21.123}$$

$$[aRV_{\text{ABC}}] = \begin{bmatrix} \dfrac{1}{a_{R\_\text{B}}} & 0 & 0 \\ -\dfrac{1}{a_{R\_\text{B}}} & 0 & -\dfrac{1}{a_{R\_\text{C}}} \\ 0 & 0 & \dfrac{1}{a_{R\_\text{C}}} \end{bmatrix} \tag{21.124}$$

$$[aRI_{\text{abc}}] = \begin{bmatrix} 0 & -\dfrac{1}{a_{R\_\text{B}}} & -\dfrac{1}{a_{R\_\text{C}}} \\ 0 & \dfrac{1}{a_{R\_\text{B}}} & 0 \\ 0 & 0 & \dfrac{1}{a_{R\_\text{C}}} \end{bmatrix} \tag{21.125}$$

$$[aRI_{\text{ABC}}] = \begin{bmatrix} 0 & -a_{R\_\text{B}} & -a_{R\_\text{C}} \\ 0 & a_{R\_\text{B}} & 0 \\ 0 & 0 & a_{R\_\text{C}} \end{bmatrix} \tag{21.126}$$

21.1.4.9 Generalized Equations

The voltage regulator models used in power-flow studies are generalized for the various connections in a form similar to the ABCD parameters that are used in transmission line analysis. The general form of the power-flow models in matrix form is

$$[V_{\text{ABC}}] = [\text{a}][V_{\text{abc}}] + [\text{b}][I_{\text{abc}}] \tag{21.127}$$

$$[I_{\text{ABC}}] = [\text{c}][V_{\text{abc}}] + [\text{d}][I_{\text{abc}}] \tag{21.128}$$

$$[V_{\text{abc}}] = [\text{A}][V_{\text{ABC}}] - [\text{B}][I_{\text{abc}}] \tag{21.129}$$

Depending upon the connection, the matrices $[V_{\text{ABC}}]$ and $[V_{\text{abc}}]$ can be either line-to-line or line-to-ground. The current matrices represent the line currents regardless of the regulator connection. For all voltage regulator connections, the generalized constants are defined as

$$[\text{a}] = [aRV_{\text{abc}}] \tag{21.130}$$

$$[\text{b}] = [0] \tag{21.131}$$

$$[\text{c}] = [0] \tag{21.132}$$

$$[\text{d}] = [aRI_{\text{abc}}] \tag{21.133}$$

$$[\text{A}] = [aRV_{\text{ABC}}] \tag{21.134}$$

$$[\text{B}] = [0] \tag{21.135}$$

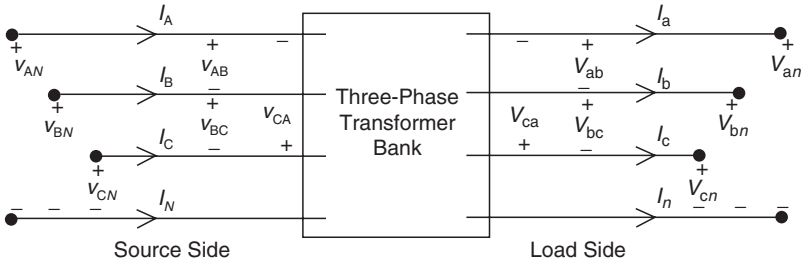

FIGURE 21.21 General transformer bank.

21.1.5 Transformer Bank Connections

Unique models of three-phase transformer banks applicable to radial distribution feeders have been developed (Kersting, 1999). Models for the following three-phase connections are included in this document:

- Delta–grounded wye
- Grounded wye–delta
- Ungrounded wye–delta
- Grounded wye–grounded wye
- Delta–delta

Figure 21.21 defines the various voltages and currents for the transformer bank models. The models can represent a step-down (source side to load side) or a step-up (source side to load side) transformer bank. The notation is such that the capital letters A,B,C,N will always refer to the source side of the bank and the lower case letters a,b,c,n will always refer to the load side of the bank. It is assumed that all variations of the wye–delta connections are connected in the "American Standard Thirty Degree" connection. The standard is such that:
Step-down connection

V_{AB} leads V_{ab} by 30°
I_A leads I_a by 30°

Step-up connection

V_{ab} leads V_{AB} by 30°
I_a leads I_A by 30°

21.1.5.1 Generalized Equations

The models to be used in power-flow studies are generalized for the connections in a form similar to the ABCD parameters that are used in transmission line analysis. The general form of the power-flow models in matrix form are

$$[VLN_{ABC}] = [a_t][VLN_{abc}] + [b_t][I_{abc}] \tag{21.136}$$

$$[I_{ABC}] = [c_t][V_{abc}] + [d_t][I_{abc}] \tag{21.137}$$

$$[VLN_{abc}] = [A_t][VLN_{ABC}] - [B_t][I_{abc}] \tag{21.138}$$

In Eqs. (21.136) through (21.138), the matrices $[VLN_{ABC}]$ and $[VLN_{abc}]$ will be the equivalent line-to-neutral voltages on delta and ungrounded wye connections and the line-to-ground voltages for grounded wye connections.

When the "ladder technique" or "sweep" iterative method is used, the "forward" sweep is assumed to be from the source working toward the remote nodes. The "backward" sweep will be working from the remote nodes toward the source node.

21.1.5.2 Common Variable and Matrices

All transformer models will use the following common variable and matrices:

- Transformer turns ratio

$$n_t = \frac{V_{\text{rated\_source}}}{V_{\text{rated\_load}}} \tag{21.139}$$

where $V_{\text{rated\_source}}$ = transformer winding rating on the source side. Line-to-line voltage for delta connections and line-to-neutral for wye connections.
$V_{\text{rated\_load}}$ = transformer winding rating on the load side. Line-to-line voltage for delta connections and line-to-neutral for wye connections.

Note that the transformer "winding" ratings may be either line-to-line or line-to-neutral, depending upon the connection. The winding ratings can be specified in actual volts or per-unit volts using the appropriate base line-to-neutral voltages.

- Source to load matrix voltage relations:

$$[V_{\text{ABC}}] = [AV][V_{\text{abc}}] \tag{21.140}$$

The voltage matrices may be line-to-line or line-to-neutral voltages depending upon the connection.

- Load to source matrix current relations:

$$[I_{\text{abc}}] = [AI][I_{\text{ABC}}] \tag{21.141}$$

The current matrices may be line currents or delta currents depending upon the connection.

- Transformer impedance matrix:

$$[Zt_{\text{abc}}] = \begin{bmatrix} Zt_{\text{a}} & 0 & 0 \\ 0 & Zt_{\text{b}} & 0 \\ 0 & 0 & Zt_{\text{c}} \end{bmatrix} \tag{21.142}$$

The impedance elements in the matrix will be the per-unit impedance of the transformer windings on the load side of the transformer whether it is connected in wye or delta.

- Symmetrical component transformation matrix:

$$[A_{\text{s}}] = \begin{bmatrix} 1 & 1 & 1 \\ 1 & a_{\text{s}}^2 & a_{\text{s}} \\ 1 & a_{\text{s}} & a_{\text{s}}^2 \end{bmatrix} \tag{21.143}$$

where $a_{\text{s}} = 1\angle 120$

- Phaseshift matrix

$$[T_{\text{s}}] = \begin{bmatrix} 1 & 0 & 0 \\ 0 & t_{\text{s}}^* & 0 \\ 0 & 0 & t_{\text{s}} \end{bmatrix} \tag{21.144}$$

where $t_s = \frac{1}{\sqrt{3}} \angle 30$

- Matrix to convert line-to-line voltages to equivalent line-to-neutral voltages:

$$[W] = [A_s][T_s][A_s]^{-1} = \frac{1}{3}\begin{bmatrix} 2 & 1 & 0 \\ 0 & 2 & 1 \\ 1 & 0 & 2 \end{bmatrix} \tag{21.145}$$

Example: $[VLN] = [W][VLL]$

- Matrix to convert delta currents into line currents:

$$[DI] = \begin{bmatrix} 1 & 0 & -1 \\ -1 & 1 & 0 \\ 0 & -1 & 1 \end{bmatrix} \tag{21.146}$$

Example: $[I_{abc}] = [DI][ID_{abc}]$

- Matrix to convert line-to-ground or line-to-neutral voltages to line-to-line voltages:

$$[D] = \begin{bmatrix} 1 & -1 & 0 \\ 0 & 1 & -1 \\ -1 & 0 & 1 \end{bmatrix} \tag{21.147}$$

Example: $[VLL_{abc}] = [D][VLN_{abc}]$

21.1.5.3 Per-Unit System

All transformer models were developed so that they can be applied using either "actual" or "per-unit" values of voltages, currents, and impedances. When the per-unit system is used, all per-unit voltages (line-to-line and line-to-neutral) use the line-to-neutral base as the base voltage. In other words, for a balanced set of three-phase voltages, the per-unit line-to-neutral voltage magnitude will be 1.0 at rated voltage and the per-unit line-to-line voltage magnitude will be the $\sqrt{3}$. In a similar fashion, all currents (line currents and delta currents) are based on the base line current. Again, $\sqrt{3}$ relationship will exist between the line and delta currents under balanced conditions. The base line impedance will be used for all line impedances and for wye and delta connected transformer impedances. There will be different base values on the two sides of the transformer bank.

Base values are computed following the steps listed below:

- Select a base three-phase kVA_{base} and the rated line-to-line voltage, $kVLL_{source}$, on the source side as the base line-to-line voltage.
- Based upon the voltage ratings of the transformer bank, determine the rated line-to-line voltage, $kVLL_{load}$, on the load side.
- Determine the transformer ratio, a_x, as

$$a_x = \frac{kVLL_{source}}{kVLL_{load}} \tag{21.148}$$

- The source side base values are computed as

$$kVLN_S = \frac{kVLL_S}{\sqrt{3}} \tag{21.149}$$

$$I_S = \frac{kVA_{base}}{\sqrt{3}kVLL_{source}} \tag{21.150}$$

$$Z_S = \frac{kVLL^2_{source}1000}{kVA_B} \tag{21.151}$$

- The load side base values are computed by

$$kVLN_L = \frac{kVLN_S}{a_x} \tag{21.152}$$

$$I_L = a_x I_S \tag{21.153}$$

$$Z_L = \frac{Z_S}{a_x^2} \tag{21.154}$$

The matrices $[a_t]$, $[b_t]$, $[c_t]$, $[d_t]$, $[A_t]$, and $[B_t]$ [see Eqs. (21.136) through (21.138)] for each connection are defined as follows:

21.1.5.4 Matrix Definitions

21.1.5.4.1 Delta–Grounded Wye

Backward sweep:

$$[VLN_{ABC}] = [a_t][VLG_{abc}] + [b_t][I_{abc}]$$
$$[I_{ABC}] = [c_t][VLG_{abc}] + [d_t][I_{abc}]$$

Forward sweep:

$$[VLG_{abc}] = [A_t][VLN_{ABC}] - [B_t][I_{abc}]$$

The matrices used for the step-down connection are

$$[a_t] = \frac{-n_t}{3}\begin{bmatrix} 0 & 2 & 1 \\ 1 & 0 & 2 \\ 2 & 1 & 0 \end{bmatrix}$$

$$[b_t] = \frac{-n_t}{3}\begin{bmatrix} 0 & 2Zt_b & Zt_c \\ Zt_a & 0 & 2Zt_c \\ 2Zt_a & Zt_b & 0 \end{bmatrix}$$

$$[c_t] = \begin{bmatrix} 0 & 0 & 0 \\ 0 & 0 & 0 \\ 0 & 0 & 0 \end{bmatrix}$$

$$[d_t] = \frac{1}{n_t}\begin{bmatrix} 1 & -1 & 0 \\ 0 & 1 & -1 \\ -1 & 0 & 1 \end{bmatrix}$$

$$[A_t] = \frac{1}{n_t}\begin{bmatrix} 1 & 0 & -1 \\ -1 & 1 & 0 \\ 0 & -1 & 1 \end{bmatrix}$$

$$[B_t] = \begin{bmatrix} Zt_a & 0 & 0 \\ 0 & Zt_b & 0 \\ 0 & 0 & Zt_c \end{bmatrix}$$

21.1.5.4.2 Ungrounded Wye–Delta

Power-flow equations:
Backward sweep:

$$[VLN_{ABC}] = [a_t][VLN_{abc}] + [b_t][I_{abc}]$$
$$[I_{ABC}] = [c_t][VLN_{abc}] + [d_t][I_{abc}]$$

Forward sweep:

$$[VLN_{abc}] = [A_t][VLN_{ABC}] - [B_t][I_{abc}]$$

Matrices used for the step-down connection are

$$[a_t] = n_t\begin{bmatrix} 1 & -1 & 0 \\ 0 & 1 & -1 \\ -1 & 0 & 1 \end{bmatrix}$$

$$[b_t] = \frac{n_t}{3}\begin{bmatrix} Zt_{ab} & -Zt_{ab} & 0 \\ Zt_{bc} & 2Zt_{bc} & 0 \\ -2Zt_{ca} & -Zt_{ca} & 0 \end{bmatrix}$$

$$[c_t] = \begin{bmatrix} 0 & 0 & 0 \\ 0 & 0 & 0 \\ 0 & 0 & 0 \end{bmatrix}$$

$$[d_t] = \frac{1}{3n_t}\begin{bmatrix} 1 & -1 & 0 \\ 1 & 2 & 0 \\ -2 & -1 & 0 \end{bmatrix}$$

$$[A_t] = \frac{1}{3n_t}\begin{bmatrix} 2 & 1 & 0 \\ 0 & 2 & 1 \\ 1 & 0 & 2 \end{bmatrix}$$

$$[B_t] = \frac{1}{9}\begin{bmatrix} 2Zt_{ab} + Zt_{bc} & 2Zt_{bc} - 2Zt_{ab} & 0 \\ 2Zt_{bc} - 2Zt_{ca} & 4Zt_{bc} - Zt_{ca} & 0 \\ Zt_{ab} - 4Zt_{ca} & -Zt_{ab} + 2Zt_{ca} & 0 \end{bmatrix}$$

where Zt_{ab}, Zt_{bc}, and Zt_{ca} are the transformer impedances inside the delta secondary connection.

21.1.5.4.3 Grounded Wye–Delta

Power-flow equations:
Backward sweep:

$$[VLG_{ABC}] = [a_t][VLN_{abc}] + [b_t][I_{abc}]$$
$$[I_{ABC}] = [c_t][VLN_{abc}] + [d_t][I_{abc}]$$

Forward sweep:

$$[VLN_{abc}] = [A_t][VLG_{ABC}] - [B_t][I_{abc}]$$

The matrices used for the step-down connection are

$$[a_t] = n_t \begin{bmatrix} 1 & -1 & 0 \\ 0 & 1 & -1 \\ -1 & 0 & 1 \end{bmatrix}$$

$$[b_t] = \frac{n_t}{Zt_{ab} + Zt_{bc} + Zt_{ca}} \begin{bmatrix} Zt_{ab}Zt_{ca} & -Zt_{ab}Zt_{bc} & 0 \\ Zt_{bc}Zt_{ca} & Zt_{bc}(Zt_{ca} + Zt_{ab}) & 0 \\ Zt_{ca}(-Zt_{ab} - Zt_{bc}) & -Zt_{bc}Zt_{ca} & 0 \end{bmatrix}$$

$$[c_t] = \begin{bmatrix} 0 & 0 & 0 \\ 0 & 0 & 0 \\ 0 & 0 & 0 \end{bmatrix}$$

$$[d_t] = \frac{1}{n_t(Zt_{ab} + Zt_{bc} + Zt_{ca})} \begin{bmatrix} Zt_{ca} & -Zt_{bc} & 0 \\ Zt_{ca} & Zt_{ab} + Zt_{ca} & 0 \\ -Zt_{ab} - Zt_{bc} & -Zt_{ca} & 0 \end{bmatrix}$$

$$[A_t] = \frac{1}{3n_t} \begin{bmatrix} 2 & 1 & 0 \\ 0 & 2 & 1 \\ 1 & 0 & 2 \end{bmatrix}$$

$$[B_t] = \frac{1}{3\sum Zt} \begin{bmatrix} 2Zt_{ab}Zt_{ca} + Zt_{bc}Zt_{ca} & -2Zt_{ab}Zt_{bc} + Zt_{bc}(Zt_{ab} + Zt_{ca}) & 0 \\ 2Zt_{bc}Zt_{ca} - Zt_{bc}(Zt_{ab} + Zt_{bc}) & 2Zt_{bc}(Zt_{ab} + Zt_{ca}) - Zt_{bc}Zt_{ca} & 0 \\ Zt_{ab}Zt_{ca} - 2Zt_{ca}(Zt_{ab} + Zt_{bc}) & -Zt_{ab}Zt_{bc} - 2Zt_{bc}Zt_{ca} & 0 \end{bmatrix}$$

where

$$\sum Zt = Zt_{ab} + Zt_{bc} + Zt_{ca}$$

21.1.5.4.4 The Grounded Wye–Grounded Wye Connection

Power-flow equations:
Backward sweep:

$$[VLG_{ABC}] = [a_t][VLG_{abc}] + [b_t][I_{abc}]$$

$$[I_{ABC}] = [c_t][VLG_{abc}] + [d_t][I_{abc}]$$

Forward sweep:

$$[VLG_{abc}] = [A_t][VLG_{ABC}] - [B_t][I_{abc}]$$

The matrices used are

$$[a_t] = n_t \begin{bmatrix} 1 & 0 & 0 \\ 0 & 1 & 0 \\ 0 & 0 & 1 \end{bmatrix}$$

$$[b_t] = n_t \begin{bmatrix} Zt_{\mathrm{a}} & 0 & 0 \\ 0 & Zt_{\mathrm{b}} & 0 \\ 0 & 0 & Zt_{\mathrm{c}} \end{bmatrix}$$

$$[c_t] = \begin{bmatrix} 0 & 0 & 0 \\ 0 & 0 & 0 \\ 0 & 0 & 0 \end{bmatrix}$$

$$[d_t] = \frac{1}{n_t} \begin{bmatrix} 1 & 0 & 0 \\ 0 & 1 & 0 \\ 0 & 0 & 1 \end{bmatrix}$$

$$[A_t] = \frac{1}{n_t} \begin{bmatrix} 1 & 0 & 0 \\ 0 & 1 & 0 \\ 0 & 0 & 1 \end{bmatrix}$$

$$[B_t] = \begin{bmatrix} Zt_{\mathrm{a}} & 0 & 0 \\ 0 & Zt_{\mathrm{b}} & 0 \\ 0 & 0 & Zt_{\mathrm{c}} \end{bmatrix}$$

21.1.5.4.5 Delta–Delta

Power-flow equations:
Backward sweep:

$$[VLN_{\mathrm{ABC}}] = [a_t][VLN_{\mathrm{abc}}] + [b_t][I_{\mathrm{abc}}]$$
$$[I_{\mathrm{ABC}}] = [c_t][VLN_{\mathrm{abc}}] + [d_t][I_{\mathrm{abc}}]$$

Forward sweep:

$$[VLN_{\mathrm{abc}}] = [A_t][VLN_{\mathrm{ABC}}] - [B_t][I_{\mathrm{abc}}]$$

The matrices used are

$$[a_t] = \frac{n_t}{3} \begin{bmatrix} 2 & -1 & -1 \\ -1 & 2 & -1 \\ -1 & -1 & 2 \end{bmatrix}$$

$$[b_t] = \frac{n_t}{3\sum Zt} \begin{bmatrix} 2Zt_{\mathrm{ab}}Zt_{ca} + Zt_{\mathrm{bc}}Zt_{\mathrm{ca}} & -2Zt_{\mathrm{ab}}Zt_{\mathrm{bc}} + Zt_{\mathrm{bc}}(Zt_{\mathrm{ab}} + Zt_{\mathrm{ca}}) & 0 \\ 2Zt_{\mathrm{bc}}Zt_{\mathrm{ca}} - Zt_{\mathrm{bc}}(Zt_{\mathrm{ab}} + Zt_{\mathrm{bc}}) & 2Zt_{\mathrm{bc}}(Zt_{\mathrm{ab}} + Zt_{\mathrm{ca}}) - Zt_{\mathrm{bc}}Zt_{\mathrm{ca}} & 0 \\ Zt_{\mathrm{ab}}Zt_{\mathrm{ca}} - 2Zt_{\mathrm{ca}}(Zt_{\mathrm{ab}} + Zt_{\mathrm{bc}}) & -Zt_{\mathrm{ab}}Zt_{\mathrm{bc}} - 2Zt_{\mathrm{bc}}Zt_{\mathrm{ca}} & 0 \end{bmatrix}$$

where

$$\sum Zt = Zt_{ab} + Zt_{bc} + Zt_{ca}$$

$$[c_t] = \begin{bmatrix} 0 & 0 & 0 \\ 0 & 0 & 0 \\ 0 & 0 & 0 \end{bmatrix}$$

$$[d_t] = \frac{1}{n_t}\begin{bmatrix} 1 & 0 & 0 \\ 0 & 1 & 0 \\ 0 & 0 & 1 \end{bmatrix}$$

$$[A_t] = \frac{1}{3n_t}\begin{bmatrix} 2 & -1 & -1 \\ -1 & 2 & -1 \\ -1 & -1 & 2 \end{bmatrix}$$

$$[B_t] = \frac{1}{3\sum Zt}\begin{bmatrix} 2Zt_{ab}Zt_{ca} + Zt_{bc}Zt_{ca} & -2Zt_{ab}Zt_{bc} + Zt_{bc}(Zt_{ab} + Zt_{ca}) & 0 \\ 2Zt_{bc}Zt_{ca} - Zt_{bc}(Zt_{ab} + Zt_{bc}) & 2Zt_{bc}(Zt_{ab} + Zt_{ca}) - Zt_{bc}Zt_{ca} & 0 \\ Zt_{ab}Zt_{ca} - 2Zt_{ca}(Zt_{ab} + Zt_{bc}) & -Zt_{ab}Zt_{bc} - 2Zt_{bc}Zt_{ca} & 0 \end{bmatrix}$$

where

$$\sum Zt = Zt_{ab} + Zt_{bc} + Zt_{ca}$$

21.1.5.5 Thevenin Equivalent Circuit

The study of short-circuit studies that occur on the load side of a transformer bank requires the three-phase Thevenin equivalent circuit referenced to the load side terminals of the transformer. In order to determine this equivalent circuit, the Thevenin equivalent circuit up to the primary terminals of the "feeder" transformer must be determined. It is assumed that the transformer matrices as defined above are known for the transformer connection in question. A one-line diagram of the total system is shown in Fig. 21.22.

The desired Thevenin equivalent circuit on the secondary side of the transformer is shown in Fig. 21.23.

In Fig. 21.22 the system voltage source $[ELN_{ABC}]$ will typically be a balanced set of per-unit voltages. The Thevenin equivalent voltage on the secondary side of the transformer will be:

$$[Eth_{abc}] = [A_t] \cdot [ELN_{ABC}] \tag{21.155}$$

The Thevenin equivalent impedance in Fig. 21.23 from the source to the primary terminals of the feeder transformer is given by

$$[Zth_{abc}] = [A_t][Zsys_{ABC}][d_t] + [B_t] \tag{21.156}$$

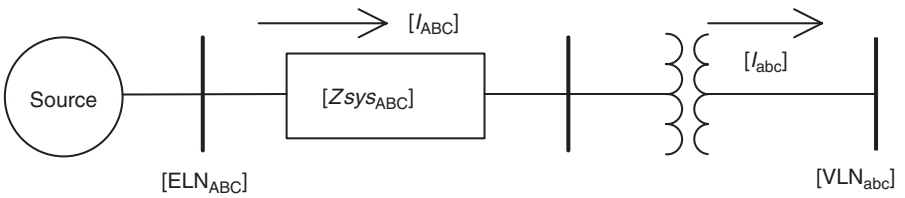

FIGURE 21.22 Total system.

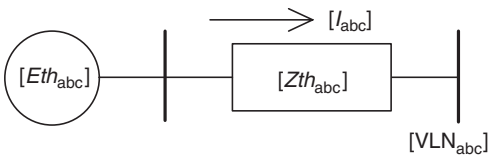

FIGURE 21.23 Three-phase Thevenin equivalent circuit.

The values of the source side Thevenin equivalent circuit will be the same regardless of the type of connection of the feeder transformer. For each three-phase transformer connection, unique values of the matrices [Eth_{abc}] and [Zth_{abc}] are defined as functions of the source side Thevenin equivalent circuit. These definitions are shown for each transformer connection below.

21.1.5.6 Center Tapped Transformers

The typical single-phase service to a customer is 120/240 V. This is provided from a center tapped single-phase transformer through the three-wire secondary and service drop to the customer's meter. The center tapped single-phase transformer with the three-wire secondary and 120/240 V loads can be modeled as shown in Fig. 21.24.

Notice in Fig. 21.24 that three impedance values are required for the center tapped transformer. These three impedances typically will not be known. In fact, usually only the magnitude of the transformer impedance will be known as found on the nameplate. In order to perform a reasonable analysis, some assumptions have to be made regarding the impedances. It is necessary to know both the per-unit R_A and the X_A components of the transformer impedance. References Gonen (1986) and Hopkinson (1977) are two sources for typical values. From Hopkinson (1977) the center tapped transformer impedances as a function of the transformer impedance are given. For interlaced transformers the three impedances are given by

$$\begin{aligned} Z_0 &= 0.5R_A + j0.8X_A \\ Z_1 &= R_A + j0.4X_A \\ Z_2 &= R_A + j0.4X_A \end{aligned} \tag{21.157}$$

The equations for the noninterlaced design are

$$\begin{aligned} Z_0 &= 0.25R_A - j0.6X_A \\ Z_1 &= 1.5R_A + j3.3X_A \\ Z_2 &= 1.5R_A + j3.1X_A \end{aligned} \tag{21.158}$$

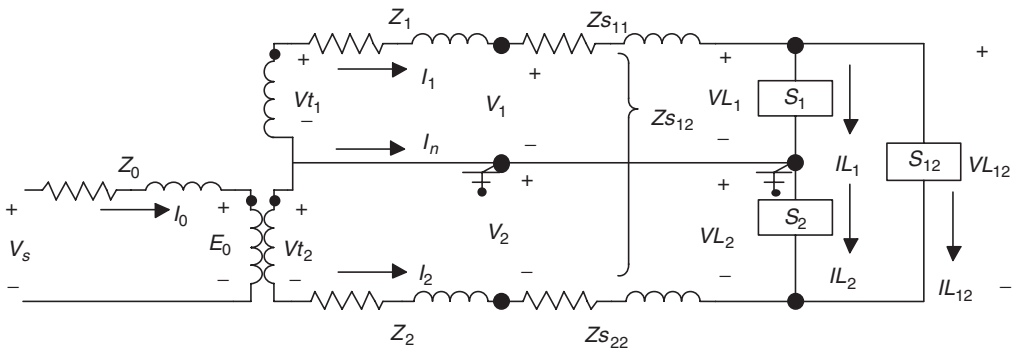

FIGURE 21.24 Center tapped single-phase transformer with secondary.

The transformer turns ratio is defined as

$$n_t = \frac{\text{high side rated voltage}}{\text{low side half winding rated voltage}} \tag{21.159}$$

$$\text{Example: } n_t = \frac{7200}{120} = 60$$

With reference to Fig. 21.24, note that the secondary current I_1 flows out of the dot of the secondary half winding whereas the current I_2 flows out of the undotted terminal. This is done in order to simplify the voltage drop calculations down the secondary. The basic transformer equations that must apply at all times are

$$\begin{aligned} E_0 &= n_t Vt_1 = n_t Vt_2 \\ I_0 &= \frac{1}{n_t}(I_1 - I_2) \end{aligned} \tag{21.160}$$

General matrix equations similar to those of the three-phase transformer connections are used in the analysis. For the backward sweep (working from the load toward the source), the equations are

$$\begin{aligned} [V_{ss}] &= [a_{ct}][V12] + [b_{ct}][I_{12}] \\ [I_{00}] &= [d_{ct}][I_{12}] \end{aligned} \tag{21.161}$$

where

$$\begin{aligned} [V_{ss}] &= \begin{bmatrix} V_s \\ V_s \end{bmatrix} \\ [I_{00}] &= \begin{bmatrix} I_0 \\ I_0 \end{bmatrix} \\ [I_{12}] &= \begin{bmatrix} I_1 \\ I_2 \end{bmatrix} \\ [a_{ct}] &= \begin{bmatrix} n_t & 0 \\ 0 & n_t \end{bmatrix} \\ [b_{ct}] &= \begin{bmatrix} n_t\left(Z_1 + \dfrac{Z_0}{n_t^2}\right) & -\dfrac{Z_0}{n_t} \\ \dfrac{Z_0}{n_t} & -n_t\left(Z_2 + \dfrac{Z_0}{n_t^2}\right) \end{bmatrix} \\ [d_{ct}] &= \frac{1}{n_t}\begin{bmatrix} 1 & -1 \\ 1 & -1 \end{bmatrix} \end{aligned} \tag{21.162}$$

For the forward sweep (working from the source toward the loads) the equations are

$$[V_{12}] = [A_{ct}][V_{ss}] - [B_{ct}][I_{12}] \tag{21.163}$$

where

$$\begin{aligned} [A_{ct}] &= \frac{1}{n_t}\begin{bmatrix} 1 & 0 \\ 0 & 1 \end{bmatrix} \\ [B_{ct}] &= \begin{bmatrix} Z_1 + \dfrac{Z_0}{n_t^2} & -\dfrac{Z_0}{n_t^2} \\ \dfrac{Z_0}{n_t^2} & -\left(Z_2 + \dfrac{Z_0}{n_t^2}\right) \end{bmatrix} \end{aligned} \tag{21.164}$$

The three-wire secondary is modeled by first applying the Carson's equations and Kron reduction method to determine the 2×2 phase impedance matrix:

$$[Z_s] = \begin{bmatrix} Z_{s_{11}} & Z_{s_{12}} \\ Z_{s_{21}} & Z_{s_{22}} \end{bmatrix} \tag{21.165}$$

The backward sweep equation becomes

$$[V_{12}] = [a_s][VL_{12}] + [b_s][I_{12}]$$

where

$$\begin{aligned} [a_s] &= \begin{bmatrix} 1 & 0 \\ 0 & 1 \end{bmatrix} \\ [b_s] &= [Z_s] \end{aligned} \tag{21.166}$$

The forward sweep equation is:

$$[VL_{12}] = [A_s][V_{12}] - [B_s][I_{12}] \tag{21.167}$$

where

$$\begin{aligned} [A_s] &= [a_s]^{-1} \\ [B_s] &= [Z_s] \end{aligned} \tag{21.168}$$

21.1.6 Load Models

Loads can be represented as being connected phase-to-phase or phase-to-neutral in a four-wire wye systems or phase-to-phase in a three-wire delta system. The loads can be three-phase, two-phase, or single-phase with any degree of unbalance and can be modeled as

- Constant real and reactive power (constant PQ)
- Constant current
- Constant impedance
- Any combination of the above

The load models developed in this document are used in the iterative process of a power-flow program. All models are initially defined by a complex power per phase and either a line-to-neutral (wye load) or a line-to-line voltage (delta load). The units of the complex power can be in volt-amperes and volts or per-unit volt-amperes and per-unit volts.

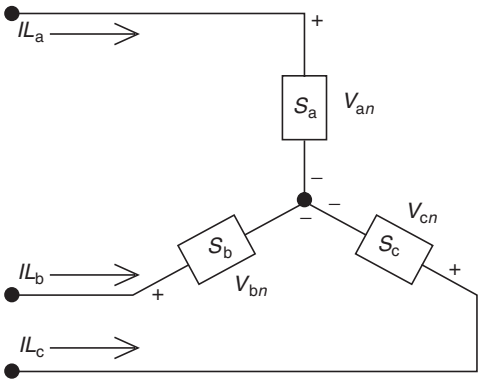

FIGURE 21.25 Wye connected load.

For both the wye and delta connected loads, the basic requirement is to determine the load component of the line currents coming into the loads. It is assumed that all loads are initially specified by their complex power ($S = P + jQ$) per phase and a line-to-neutral or line-to-line voltage.

21.1.6.1 Wye Connected Loads

Figure 21.25 shows the model of a wye connected load.

The notation for the specified complex powers and voltages is as follows:

$$\text{Phase a: } |S_a|\angle\theta_a = P_a + jQ_a \quad \text{and } |V_{an}|\angle\delta_a \tag{21.169}$$

$$\text{Phase b: } |S_b|\angle\theta_b = P_b + jQ_b \quad \text{and } |V_{bn}|\angle\delta_b \tag{21.170}$$

$$\text{Phase c: } |S_c|\angle\theta_c = P_c + jQ_c \quad \text{and } |V_{cn}|\angle\delta_c \tag{21.171}$$

1. Constant real and reactive power loads

$$\begin{aligned} IL_a &= \left(\frac{S_a}{V_{an}}\right)^* = \frac{|S_a|}{|V_{an}|}\angle\delta_a - \theta_a = |IL_a|\angle\alpha_a \\ IL_b &= \left(\frac{S_b}{V_{bn}}\right)^* = \frac{|S_b|}{|V_{bn}|}\angle\delta_b - \theta_b = |IL_b|\angle\alpha_b \\ IL_c &= \left(\frac{S_c}{V_{cn}}\right)^* = \frac{|S_c|}{|V_{cn}|}\angle\delta_c - \theta_c = |IL_c|\angle\alpha_c \end{aligned} \tag{21.172}$$

In this model the line-to-neutral voltages will change during each iteration until convergence is achieved.

2. Constant impedance loads

The "constant load impedance" is first determined from the specified complex power and line-to-neutral voltages according to the following equation:

$$\begin{aligned} Z_a &= \frac{|V_{an}|^2}{S_a^*} = \frac{|V_{an}|^2}{|S_a|}\angle\theta_a = |Z_a|\angle\theta_a \\ Z_b &= \frac{|V_{bn}|^2}{S_b^*} = \frac{|V_{bn}|^2}{|S_b|}\angle\theta_b = |Z_b|\angle\theta_b \\ Z_c &= \frac{|V_{cn}|^2}{S_c^*} = \frac{|V_{cn}|^2}{|S_c|}\angle\theta_c = |Z_c|\angle\theta_c \end{aligned} \tag{21.173}$$

The load currents as a function of the constant load impedances are given by the following equation:

$$\begin{aligned} IL_a &= \frac{V_{an}}{Z_a} = \frac{|V_{an}|}{|Z_a|}\angle\delta_a - \theta_a = |IL_a|\angle\alpha_a \\ IL_b &= \frac{V_{bn}}{Z_b} = \frac{|V_{bn}|}{|Z_b|}\angle\delta_b - \theta_b = |IL_b|\angle\alpha_b \\ IL_c &= \frac{V_{cn}}{Z_c} = \frac{|V_{cn}|}{|Z_c|}\angle\delta_c - \theta_c = |IL_c|\angle\alpha_c \end{aligned} \tag{21.174}$$

In this model the line-to-neutral voltages will change during each iteration until convergence is achieved.

3. Constant current loads

In this model the magnitudes of the currents are computed according to Eq. (21.172) and then held constant while the angle of the voltage (δ) changes during each iteration. In order to keep the power factor constant, the angles of the load currents are given by

$$\begin{aligned} IL_a &= |IL_a|\angle\delta_a - \theta_a \\ IL_b &= |IL_b|\angle\delta_b - \theta_b \\ IL_c &= |IL_c|\angle\delta_c - \theta_c \end{aligned} \tag{21.175}$$

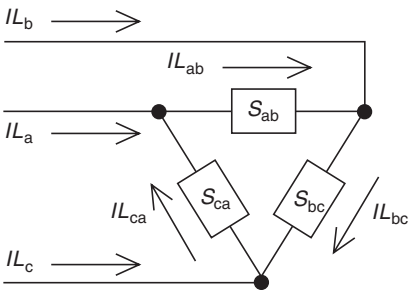

FIGURE 21.26 Delta connected load.

4. Combination loads

Combination loads can be modeled by assigning a percentage of the total load to each of the above three load models. The total line current entering the load is the sum of the three components.

21.1.6.2 Delta Connected Loads

Figure 21.26 shows the model of a delta connected load.

The notation for the specified complex powers and voltages is as follows:

$$\text{Phase ab: } |S_{ab}|\angle\theta_{ab} = P_{ab} + jQ_{ab} \quad \text{and } |V_{ab}|\angle\delta_{ab} \tag{21.176}$$

$$\text{Phase bc: } |S_{bc}|\angle\theta_{bc} = P_{bc} + jQ_{bc} \quad \text{and } |V_{bc}|\angle\delta_{bc} \tag{21.177}$$

$$\text{Phase ca: } |S_{ca}|\angle\theta_{ca} = P_{ca} + jQ_{ca} \quad \text{and } |V_{ca}|\angle\delta_{ca} \tag{21.178}$$

1. Constant real and reactive power loads

$$\begin{aligned} IL_{ab} &= \left(\frac{S_{ab}}{V_{ab}}\right)^* = \frac{|S_{ab}|}{|V_{ab}|}\angle\delta_{ab} - \theta_{ab} = |IL_{ab}|\angle\alpha_{ab} \\ IL_{bc} &= \left(\frac{S_{bc}}{V_{bc}}\right)^* = \frac{|S_{bc}|}{|V_{bc}|}\angle\delta_{bc} - \theta_{bc} = |IL_{bc}|\angle\alpha_{bc} \\ IL_{ca} &= \left(\frac{S_{ca}}{V_{ca}}\right)^* = \frac{|S_{ca}|}{|V_{ca}|}\angle\delta_{ca} - \theta_{ca} = |IL_{ca}|\angle\alpha_{ac} \end{aligned} \tag{21.179}$$

In this model the line-to-line voltages will change during each iteration until convergence is achieved.

2. Constant impedance loads

The constant load impedance is first determined from the specified complex power and line-to-neutral voltages according to the following equation:

$$\begin{aligned} Z_{ab} &= \frac{|V_{ab}|^2}{S_{ab}^*} = \frac{|V_{ab}|^2}{|S_{ab}|}\angle\theta_{ab} = |Z_{ab}|\angle\theta_{ab} \\ Z_{bc} &= \frac{|VL_{bc}|^2}{S_{bc}^*} = \frac{|V_{bc}|^2}{|S_{bc}|}\angle\theta_{bc} = |Z_{bc}|\angle\theta_{bc} \\ Z_{ca} &= \frac{|V_{ca}|^2}{S_{ca}^*} = \frac{|V_{ca}|^2}{|S_{ca}|}\angle\theta_{ca} = |Z_{ca}|\angle\theta_{ca} \end{aligned} \tag{21.180}$$

The load currents as a function of the constant load impedances are given by the following equation:

$$\begin{aligned} IL_{ab} &= \frac{V_{ab}}{Z_{ab}} = \frac{|V_{arb}|}{|Z_{ab}|}\angle\delta_{ab} - \theta_{ab} = |IL_{ab}|\angle\alpha_{ab} \\ IL_{bc} &= \frac{V_{bc}}{Z_{bc}} = \frac{|V_{bc}|}{|Z_{bc}|}\angle\delta_{bc} - \theta_{bc} = |IL_{bc}|\angle\alpha_{bc} \\ IL_{ca} &= \frac{V_{ca}}{Z_{ca}} = \frac{|V_{ca}|}{|Z_{ca}|}\angle\delta_{ca} - \theta_{ca} = |IL_{ca}|\angle\alpha_{ca} \end{aligned} \tag{21.181}$$

In this model the line-to-line voltages in Eq. (21.181) will change during each iteration until convergence is achieved.

3. Constant current loads

In this model the magnitudes of the currents are computed according to Eq. (21.179) and then held constant while the angle of the voltage (δ) changes during each iteration. This keeps the power factor of the load constant.

$$\begin{aligned} IL_{ab} &= |IL_{ab}|\angle\delta_{ab} - \theta_{ab} \\ IL_{bc} &= |IL_{bc}|\angle\delta_{bc} - \theta_{bc} \\ IL_{ca} &= |IL_{ca}|\angle\delta_{ca} - \theta_{ca} \end{aligned} \tag{21.182}$$

4. Combination loads

Combination loads can be modeled by assigning a percentage of the total load to each of the above three load models. The total delta current for each load is the sum of the three components.

The line currents entering the delta connected load for all models are determined by

$$\begin{bmatrix} IL_a \\ IL_b \\ IL_c \end{bmatrix} = \begin{bmatrix} 1 & 0 & -1 \\ -1 & 1 & 0 \\ 0 & -1 & 1 \end{bmatrix} \begin{bmatrix} IL_{ab} \\ IL_{bc} \\ IL_{ca} \end{bmatrix} \tag{21.183}$$

In both the wye and delta connected loads, single-phase and two-phase loads are modeled by setting the complex powers of the missing phases to zero. In other words, all loads are modeled as three-phase loads and by setting the complex power of the missing phases to zero, the only load currents computed using the above equations will be for the nonzero loads.

21.1.7 Shunt Capacitor Models

Shunt capacitor banks are commonly used in a distribution system to help in voltage regulation and to provide reactive power support. The capacitor banks are modeled as constant susceptances connected in either wye or delta. Similar to the load model, all capacitor banks are modeled as three-phase banks with the kVAr of missing phases set to zero for single-phase and two-phase banks.

21.1.7.1 Wye Connected Capacitor Bank

A wye connected capacitor bank is shown in Fig. 21.27. The individual phase capacitor units are specified in kVAr and kV. The constant susceptance for each unit can be computed in either Siemans or per unit. When per unit is desired, the specified kVAr of the capacitor must be divided by the base single-phase kVAr and the kV must be divided by the base line-to-neutral kV.

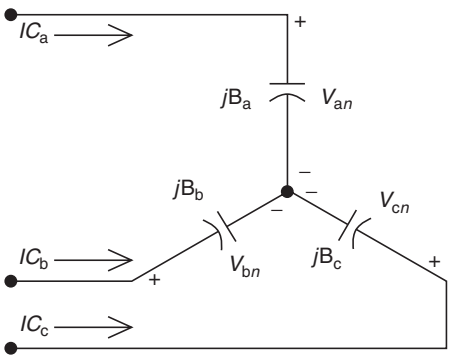

FIGURE 21.27 Wye connected capacitor bank.

The susceptance of a capacitor unit is computed by

$$B_{actual} = \frac{kVAr}{kV^2 1000} \quad \text{Siemans} \tag{21.184}$$

$$B_{pu} = \frac{kVAr_{pu}}{V_{pu}^2} \quad \text{per unit} \tag{21.185}$$

$$\text{where } kVAr_{pu} = \frac{kVAr_{actual}}{kVA_{single\_phase\_base}} \tag{21.186}$$

$$V_{pu} = \frac{kV_{actual}}{kV_{line\_to\_neutral\_base}} \tag{21.187}$$

The per-unit value of the susceptance can also be determined by first computing the actual value [Eq. (21.184)] and then dividing by the base admittance of the system.

With the susceptance computed, the line currents serving the capacitor bank are given by

$$\begin{aligned} IC_{\mathrm{a}} &= jB_{\mathrm{a}}V_{an} \\ IC_{\mathrm{b}} &= jB_{\mathrm{b}}V_{bn} \\ IC_{\mathrm{c}} &= jB_{\mathrm{c}}V_{cn} \end{aligned} \tag{21.188}$$

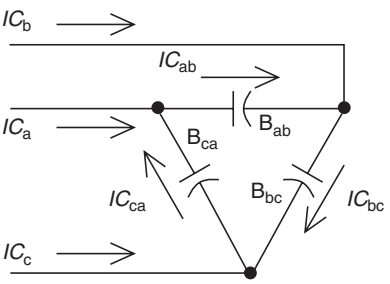

FIGURE 21.28 Delta connected capacitor bank.

21.1.7.2 Delta Connected Capacitor Bank

A delta connected capacitor bank is shown in Fig. 21.28.

Equations (21.184) through (21.187) can be used to determine the value of the susceptance in actual Siemans or per unit. It should be pointed out that in this case, the kV will be a line-to-line value of the voltage. Also, it should be noted that in Eq. (21.187), the base line-to-neutral voltage is used to compute the per-unit line-to-line voltage. This is a variation from the usual application of the per-unit system where the actual line-to-line voltage would be divided by a base line-to-line voltage in order to get the per-unit line-to-line voltage. That is not done here so that under normal conditions, the per-unit line-to-line voltage will have a magnitude of $\sqrt{3}$ rather than 1.0. This is done so that Kirchhoff's current law (KCL) at each node of the delta connection will apply for either the actual or per-unit delta currents. The currents flowing in the delta connected capacitors are given by

$$\begin{aligned} IC_{\mathrm{ab}} &= jB_{\mathrm{ab}}V_{\mathrm{ab}} \\ IC_{\mathrm{bc}} &= jB_{\mathrm{bc}}V_{\mathrm{bc}} \\ IC_{\mathrm{ca}} &= jB_{\mathrm{ca}}V_{\mathrm{ca}} \end{aligned} \tag{21.189}$$

The line currents feeding the delta connected capacitor bank are given by

$$\begin{bmatrix} IC_{\mathrm{a}} \\ IC_{\mathrm{b}} \\ IC_{\mathrm{c}} \end{bmatrix} = \begin{bmatrix} 1 & 0 & -1 \\ -1 & 1 & 0 \\ 0 & -1 & 1 \end{bmatrix} \begin{bmatrix} IC_{\mathrm{ab}} \\ IC_{\mathrm{bc}} \\ IC_{\mathrm{ca}} \end{bmatrix} \tag{21.190}$$

21.2 Analysis

21.2.1 Power-Flow Analysis

The power-flow analysis of a distribution feeder is similar to that of an interconnected transmission system. Typically what will be known prior to the analysis will be the three-phase voltages at the substation and the complex power of all the loads and the load model (constant complex power, constant impedance, constant current, or a combination). Sometimes, the input complex power supplied to the feeder from the substation is also known.

In Sections 21.1.3, 21.1.4, and 21.1.5, phase frame models were presented for the series components of a distribution feeder. In Sections 21.1.6 and 21.1.7, models were presented for the shunt components (loads and capacitor banks). These models are used in the "power-flow" analysis of a distribution feeder.

A power-flow analysis of a feeder can determine the following by phase and total three-phase:

- Voltage magnitudes and angles at all nodes of the feeder
- Line flow in each line section specified in kW and kVAr, amps and degrees, or amps and power factor

- Power loss in each line section
- Total feeder input kW and kVAr
- Total feeder power losses
- Load kW and kVAr based upon the specified model for the load

Because the feeder is radial, iterative techniques commonly used in transmission network power-flow studies are not used because of poor convergence characteristics (Trevino, 1970). Instead, an iterative technique specifically designed for a radial system is used. The ladder iterative technique (Kersting and Mendive, 1976) will be presented here.

21.2.1.1 The Ladder Iterative Technique

21.2.1.1.1 Linear Network

A modification of the ladder network theory of linear systems provides a robust iterative technique for power-flow analysis. A distribution feeder is nonlinear because most loads are assumed to be constant kW and kVAr. However, the approach taken for the linear system can be modified to take into account the nonlinear characteristics of the distribution feeder.

For the ladder network in Fig. 21.29, it is assumed that all of the line impedances and load impedances are known along with the voltage at the source (V_s).

The solution for this network is to assume a voltage at the most remote load (V_5). The load current I_5 is then determined as

$$I_5 = \frac{V_5}{ZL_5} \tag{21.191}$$

For this "end-node" case, the line current I_{45} is equal to the load current I_5. The voltage at node 4 (V_4) can be determined using Kirchhoff's voltage law (KVL):

$$V_4 = V_5 + Z_{45} I_{45} \tag{21.192}$$

The load current I_4 can be determined and then KCL applied to determine the line current I_{34}.

$$I_{34} = I_{45} + I_4 \tag{21.193}$$

KVL is applied to determine the node voltage V_3. This procedure is continued until a voltage (V_1) has been computed at the source. The computed voltage V_1 is compared to the specified voltage V_s. There will be a difference between these two voltages. The ratio of the specified voltage to the compute voltage can be determined as

$$\text{Ratio} = \frac{V_s}{V_1} \tag{21.194}$$

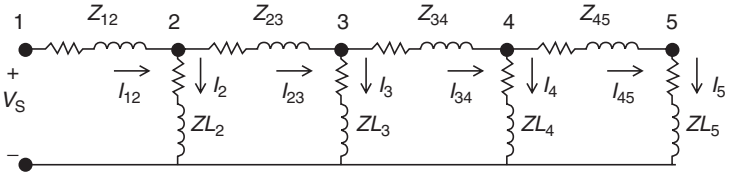

FIGURE 21.29 Linear ladder network.

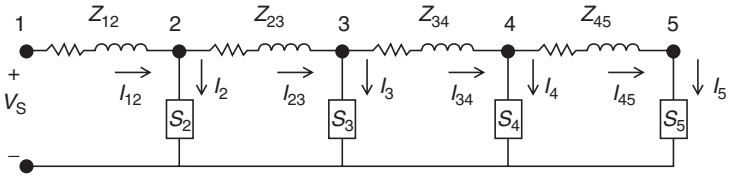

FIGURE 21.30 Nonlinear ladder network.

Since the network is linear, all of the line and load currents and node voltages in the network can be multiplied by the Ratio for the final solution to the network.

21.2.1.1.2 Nonlinear Network

The linear network of Fig. 21.29 is modified to a nonlinear network by replacing all of the constant load impedances by constant complex power loads as shown in Fig. 21.30.

The procedure outlined for the linear network is applied initially to the nonlinear network. The only difference being that the load current (assuming constant P and Q) at each node is computed by

$$I_n = \left(\frac{S_n}{V_n}\right)^* \tag{21.195}$$

The backward sweep will determine a computed source voltage V_1. As in the linear case, this first iteration will produce a voltage that is not equal to the specified source voltage V_s. Because the network is nonlinear, multiplying currents and voltages by the ratio of the specified voltage to the computed voltage will not give the solution. The most direct modification to the ladder network theory is to perform a forward sweep. The forward *d* sweep commences by using the specified source voltage and the line currents from the backward sweep. KVL is used to compute the voltage at node 2 by

$$V_2 = V_s - Z_{12}I_{12} \tag{21.196}$$

This procedure is repeated for each line segment until a "new" voltage is determined at node 5. Using the new voltage at node 5, a second backward sweep is started that will lead to a new computed voltage at the source. The backward and forward sweep process is continued until the difference between the computed and specified voltage at the source is within a given tolerance.

21.2.1.1.3 General Feeder

A typical distribution feeder will consist of the "primary main" with laterals tapped off the primary main, and sublaterals tapped off the laterals, etc. Figure 21.30 shows an example of a typical feeder.

The ladder iterative technique for the feeder of Fig. 21.31 would proceed as follows:

1. Assume voltages (1.0 per unit) at the "end" nodes (6, 8, 9, 11, and 13).
2. Starting at node 13, compute the node current (load current plus capacitor current if present).
3. With this current, apply KVL to calculate the node voltages at 12 and 10.
4. Node 10 is referred to as a "junction" node since laterals branch in two directions from the node. This feeder goes to node 11 and computes the node current. Use that current to compute the voltage at node 10. This will be referred to as "the most recent voltage at node 10."
5. Using the most recent value of the voltage at node 10, the node current at node 10 (if any) is computed.
6. Apply KCL to determine the current flowing from node 4 toward node 10.
7. Compute the voltage at node 4.

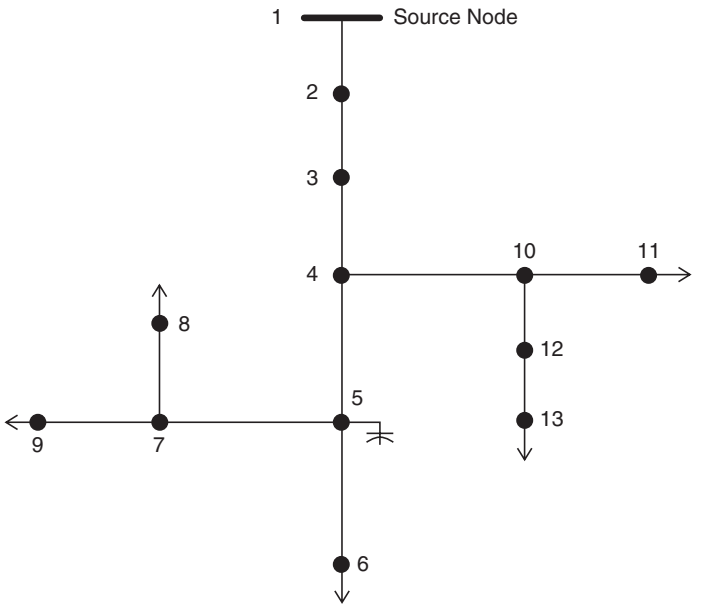

FIGURE 21.31 Typical distribution feeder.

8. Node 4 is a junction node. An end-node downstream from node 4 is selected to start the forward sweep toward node 4.
9. Select node 6, compute the node current, and then compute the voltage at junction-node 5.
10. Go to downstream end-node 8. Compute the node current and then the voltage at junction-node 7.
11. Go to downstream end-node 9. Compute the node current and then the voltage at junction-node 7.
12. Compute the node current at node 7 using the most recent value of node 7 voltage.
13. Apply KCL at node 7 to compute the current flowing on the line segment from node 5 to node 7.
14. Compute the voltage at node 5.
15. Compute the node current at node 5.
16. Apply KCL at node 5 to determine the current flowing from node 4 toward node 5.
17. Compute the voltage at node 4.
18. Compute the node current at node 4.
19. Apply KCL at node 4 to compute the current flowing from node 3 to node 4.
20. Calculate the voltage at node 3.
21. Compute the node current at node 3.
22. Apply KCL at node 3 to compute the current flowing from node 2 to node 3.
23. Calculate the voltage at node 2.
24. Compute the node current at node 2.
25. Apply KCL at node 2.
26. Calculate the voltage at node 1.
27. Compare the calculated voltage at node 1 to the specified source voltage.
28. If not within tolerance, use the specified source voltage and the backward sweep current flowing from node 1 to node 2 and compute the new voltage at node 2.
29. The forward sweep continues using the new upstream voltage and line segment current from the forward sweep to compute the new downstream voltage.
30. The forward sweep is completed when new voltages at all end nodes have been completed.
31. This completes the first iteration.
32. Now repeat the backward sweep using the new end voltages rather than the assumed voltages as was done in the first iteration.

33. Continue the backward and forward sweeps until the calculated voltage at the source is within a specified tolerance of the source voltage.
34. At this point, the voltages are known at all nodes and the currents flowing in all line segments are known. An output report can be produced giving all desired results.

21.2.1.2 The Unbalanced Three-Phase Distribution Feeder

The previous section outlined the general procedure for performing the ladder iterative technique. This section will address how that procedure can be used for an unbalanced three-phase feeder.

Figure 21.32 is the one-line diagram of an unbalanced three-phase feeder. The topology of the feeder in Fig. 21.32 is the same as the feeder in Fig. 21.31. Figure 21.32 shows more detail of the feeder however. The feeder in Fig. 21.32 can be broken into the series components and the shunt components.

21.2.1.2.1 Series Components

The series components of a distribution feeder are

- Line segments
- Transformers
- Voltage regulators

Models for each of the series components have been developed in prior areas of this section. In all cases, models (three-phase, two-phase, and single-phase) were developed in such a manner that they can be generalized. Figure 21.33 shows the "general model" for each of the series components.

The general equations defining the "input" (node n) and "output" (node m) voltages and currents are given by

$$[V_{abc}]_n = [a][V_{abc}]_m + [b][I_{abc}]_m \tag{21.197}$$

$$[I_{abc}]_n = [c][V_{abc}]_m + [d][I_{abc}]_m \tag{21.198}$$

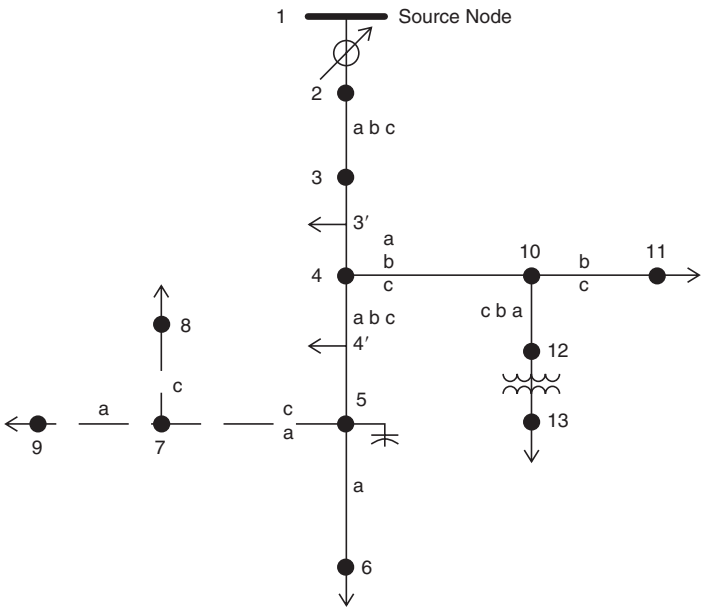

FIGURE 21.32 Unbalanced three-phase distribution feeder.

FIGURE 21.33 Series feeder component.

The general equation relating the output (node m) and input (node n) voltages is given by

$$[V_{abc}]_m = [A][V_{abc}]_n - [B][I_{abc}]_m \tag{21.199}$$

In Eqs. (21.197) through (21.199), the voltages are line-to-neutral for a four-wire wye feeder and equivalent line-to-neutral for a three-wire delta system. For transformers and voltage regulators, the voltages are line-to-neutral for terminals that are connected to a four-wire wye and line-to-line when connected to a three-wire delta.

21.2.1.2.2 Shunt Components

The shunt components of a distribution feeder are

- Spot loads
- Distributed loads
- Capacitor banks

Spot loads are located at a node and can be three-phase, two-phase, or single-phase and connected in either a wye or a delta connection. The loads can be modeled as constant complex power, constant current, constant impedance, or a combination of the three.

Distributed loads are located at the midsection of a line segment. A distributed load is modeled when the loads on a line segment are uniformly distributed along the length of the segment. As in the spot load, the distributed load can be three-phase, two-phase, or single-phase and connected in either a wye or a delta connection. The loads can be modeled as constant complex power, constant current, constant impedance, or a combination of the three. To model the distributed load, a "dummy" node is created in the center of a line segment with the distributed load of the line section modeled at this dummy node.

Capacitor banks are located at a node and can be three-phase, two-phase, or single-phase and can be connected in a wye or delta. Capacitor banks are modeled as constant admittances.

In Fig. 21.32 the solid line segments represent overhead lines while the dashed lines represent underground lines. Note that the phasing is shown for all of the line segments. In the area of the section entitled "Line Impedances," the application of Carson's equations for computing the line impedances for overhead and underground lines was presented. There it was pointed out that two-phase and single-phase lines are represented by a 3×3 matrix with zeros set in the rows and columns of the missing phases.

In the area of the section entitled "Line Admittances," the method for the computation of the shunt capacitive susceptance for overhead and underground lines was presented. Most of the time the shunt capacitance of the line segment can be ignored; however, for long underground segments, the shunt capacitance should be included.

The "node" currents may be three-phase, two-phase, or single-phase and consist of the sum of the load current at the node plus the capacitor current (if any) at the node.

21.2.1.3 Applying the Ladder Iterative Technique

The previous section outlined the steps required for the application of the ladder iterative technique. For the general feeder of Fig. 21.32 the same outline applies. The only difference is that Eq. (21.197) and (21.198) are used for computing the node voltages on the backward sweep and Eq. (21.199) is used for

computing the downstream voltages on the forward sweep. The [a], [b], [c], [d], [A], and [B] matrices for the various series components are defined in the following areas of this section:

- Line segments: Line segment models
- Voltage regulators: Step-voltage regulators
- Transformer banks: Transformer bank connections

The node currents are defined in the following area:

- Loads: Load models
- Capacitors: Shunt capacitor models

21.2.1.4 Final Notes

21.2.1.4.1 Line Segment Impedances

It is extremely important that the impedances and admittances of the line segments be computed using the exact spacings and phasing. Because of the unbalanced loading and resulting unbalanced line currents, the voltage drops due to the mutual coupling of the lines become very important. It is not unusual to observe a voltage rise on a lightly loaded phase of a line segment that has an extreme current unbalance.

21.2.1.4.2 Power Loss

The real power losses of a line segment must be computed as the difference (by phase) of the input power to a line segment minus the output power of the line segment. It is possible to observe a negative power loss on a phase that is lightly loaded compared to the other two phases. Computing power loss as the phase current squared times the phase resistance does not give the actual real power loss in the phases.

21.2.1.4.3 Load Allocation

Many times the input complex power (kW and kVAr) to a feeder is known because of the metering at the substation. This information can be either total three-phase or for each individual phase. In some cases the metered data may be the current and power factor in each phase.

It is desirable to have the computed input to the feeder match the metered input. This can be accomplished (following a converged iterative solution) by computing the ratio of the metered input to the computed input. The phase loads can now be modified by multiplying the loads by this ratio. Because the losses of the feeder will change when the loads are changed, it is necessary to go through the ladder iterative process to determine a new computed input to the feeder. This new computed input will be closer to the metered input, but most likely not within a specified tolerance. Again, a ratio can be determined and the loads modified. This process is repeated until the computed input is within a specified tolerance of the metered input.

21.2.1.5 Short-Circuit Analysis

The computation of short-circuit currents for unbalanced faults in a normally balanced three-phase system has traditionally been accomplished by the application of symmetrical components. However, this method is not well-suited to a distribution feeder that is inherently unbalanced. The unequal mutual coupling between phases leads to mutual coupling between sequence networks. When this happens, there is no advantage to using symmetrical components. Another reason for not using symmetrical components is that the phases between which faults occur is limited. For example, using symmetrical components, line-to-ground faults are limited to phase a to ground. What happens if a single-phase lateral is connected to phase b or c? This section will present a method for short-circuit analysis of an unbalanced three-phase distribution feeder using the phase frame (Kersting, 1980).

21.2.1.5.1 General Theory

Figure 21.34 shows the unbalanced feeder as modeled for short-circuit calculations. In Fig. 21.34, the voltage sources E_a, E_b, and E_c represent the Thevenin equivalent line-to-ground voltages at the faulted

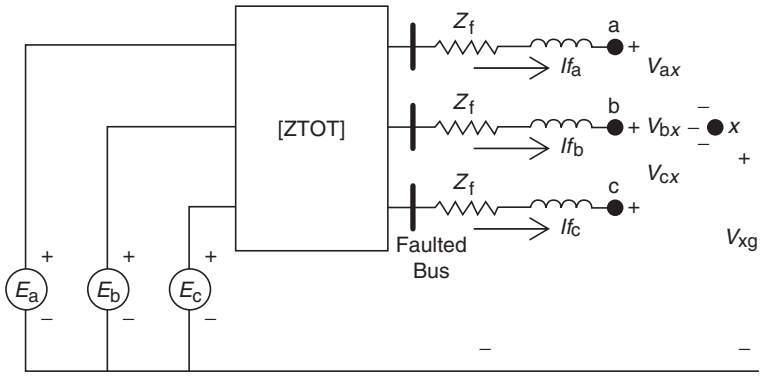

FIGURE 21.34 Unbalanced feeder short-circuit analysis model.

bus. The matrix [ZTOT] represents the Thevenin equivalent impedance matrix at the faulted bus. The fault impedance is represented by Z_f in Fig. 21.34.
Kirchhoff's voltage law in matrix form can be applied to the circuit of Fig. 21.33.

$$\begin{bmatrix} E_a \\ E_b \\ E_c \end{bmatrix} = \begin{bmatrix} Z_{aa} & Z_{ab} & Z_{ac} \\ Z_{ba} & Z_{bb} & Z_{bc} \\ Z_{ca} & Z_{cb} & Z_{cc} \end{bmatrix} \begin{bmatrix} If_a \\ If_b \\ If_c \end{bmatrix} + \begin{bmatrix} Z_f & 0 & 0 \\ 0 & Z_f & 0 \\ 0 & 0 & Z_f \end{bmatrix} \begin{bmatrix} If_a \\ If_b \\ If_c \end{bmatrix} + \begin{bmatrix} V_{ax} \\ V_{bx} \\ V_{cx} \end{bmatrix} + \begin{bmatrix} V_{xg} \\ V_{xg} \\ V_{xg} \end{bmatrix} \tag{21.200}$$

Equation (21.188) can be written in compressed form as

$$[E_{abc}] = [ZTOT][If_{abc}] + [ZF][If_{abc}] + [V_{abcx}] + [V_{xg}] \tag{21.201}$$

Combine terms in Eq. (21.201).

$$[E_{abc}] = [ZEQ][If_{abc}] + [V_{abcx}] + [V_{xg}] \tag{21.202}$$

$$\text{where } [ZEQ] = [ZTOT] + [ZF] \tag{21.203}$$

Solve Eq. (21.202) for the fault currents:

$$[If_{abc}] = [YEQ][E_{abc}] - [YEQ][V_{abcx}] - [YEQ][V_{xg}] \tag{21.204}$$

$$\text{where } [YEQ] = [ZEQ]^{-1} \tag{21.205}$$

Since the matrices [YEQ] and [E_{abc}] are known, define

$$[IP_{abc}] = [YEQ][E_{abc}] \tag{21.206}$$

Substituting Eq. (21.206) into Eq. (21.204) results in the following expanded equation:

$$\begin{bmatrix} If_a \\ If_b \\ If_c \end{bmatrix} = \begin{bmatrix} IP_a \\ IP_b \\ IP_c \end{bmatrix} - \begin{bmatrix} Y_{aa} & Y_{ab} & Y_{ac} \\ Y_{ba} & Y_{bb} & Y_{bc} \\ Y_{ca} & Y_{cb} & Y_{cc} \end{bmatrix} \begin{bmatrix} V_{ax} \\ V_{bx} \\ V_{cx} \end{bmatrix} - \begin{bmatrix} Y_{aa} & Y_{ab} & Y_{ac} \\ Y_{ba} & Y_{bb} & Y_{bc} \\ Y_{ca} & Y_{cb} & Y_{cc} \end{bmatrix} \begin{bmatrix} V_{xg} \\ V_{xg} \\ V_{xg} \end{bmatrix} \tag{21.207}$$

Performing the matrix operations in Eq. (21.195):

$$\begin{aligned} If_a &= IP_a - (Y_{aa}V_{ax} + Y_{ab}V_{bx} + Y_{ac}V_{cx}) - Y_a V_{xg} \\ If_b &= IP_b - (Y_{ba}V_{ax} + Y_{bb}V_{bx} + Y_{bc}V_{cx}) - Y_b V_{xg} \\ If &= IP_c - (Y_{ca}V_{ax} + Y_{cb}V_{bx} + Y_{cc}V_{cx}) - Y_c V_{xg} \end{aligned} \tag{21.208}$$

where

$$\begin{aligned} Y_a &= Y_{aa} + Y_{ab} + Y_{ac} \\ Y_b &= Y_{ba} + Y_{bb} + Y_{bc} \\ Y_c &= Y_{ca} + Y_{cb} + Y_{cc} \end{aligned} \tag{21.209}$$

Equations (21.208) become the general equations that are used to simulate all types of short circuits. Basically there are three equations and seven unknowns (If_a, If_b, If_c, V_{ax}, V_{bx}, V_{cx}, and V_{xg}). The other three variables in the equations (IP_a, IP_b, and IP_c) are functions of the total impedance and the Thevenin voltages and are therefore known. In order to solve Eq. (21.208), it will be necessary to specify four of the seven unknowns. These specifications are functions of the type of fault being simulated. The additional required four knowns for various types of faults are given below:
Three-phase faults

$$\begin{aligned} V_{ax} &= V_{bx} = V_{cx} = 0 \\ I_a + I_b + I_c &= 0 \end{aligned} \tag{21.210}$$

Three-phase-to-ground faults

$$V_{ax} = V_{bx} = V_{cx} = V_{xg} = 0 \tag{21.211}$$

Line-to-line faults (assume i–j fault with phase k unfaulted)

$$\begin{aligned} V_{ix} &= V_{jx} = 0 \\ If_k &= 0 \\ If_i + If_j &= 0 \end{aligned} \tag{21.212}$$

Line-to-line-to-ground faults (assume i–j to ground fault with k unfaulted)

$$\begin{aligned} V_{ix} &= V_{jx} = V_{xg} = 0 \\ V_{kx} &= \frac{IP_k}{Y_{kk}} \end{aligned} \tag{21.213}$$

Line-to-ground faults (assume phase k fault with phases i and j unfaulted)

$$\begin{aligned} V_{kx} &= V_{xg} = 0 \\ If_i &= If_j = 0 \end{aligned} \tag{21.214}$$

Notice that Eqs. (21.212) through (21.214) will allow the simulation of line-to-line, line-to-line-to-ground, and line-to-ground faults for all phases. There is no limitation to b–c faults for line-to-line and a–g for line-to-ground as is the case when the method of symmetrical components is employed.

References

Carson, J.R., Wave propagation in overhead wires with ground return, *Bell Syst. Tech. J.*, 5, 1926.

Glover, J.D. and Sarma, M., *Power System Analysis and Design*, 2nd ed., PWS Publishing Company, Boston, Chap. 5, 1994.

Gonen, T., *Electric Power Distribution System Engineering*, McGraw-Hill Book Company, 1986.

Hopkinson, R.H., Approximate Distribution Transformer Impedances, from an internal GE Memo dated August 30, 1977.

Kersting, W.H., Distribution system short circuit analysis, 25th Intersociety Energy Conversion Conference, Reno, Nevada, August 1980.

Kersting, W.H., *Milsoft Transformer Models—Theory, Research Report*, Milsoft Integrated Solutions, Inc., Abilene, TX, 1999.

Kersting, W.H. and Mendive, D.L., An application of ladder network theory to the solution of three-phase radial load-flow problems, IEEE Conference Paper presented at the IEEE Winter Power Meeting, New York, January 1976.

Kron, G., Tensorial analysis of integrated transmission systems, Part I: The six basic reference frames, *AIEE Trans.*, 71, 1952.

Trevino, C., Cases of difficult convergence in load-flow problems, IEEE Paper no. 71-62-PWR, presented at the IEEE Summer Power Meeting, Los Angeles, CA, 1970.

22

Power System Operation and Control

George L. Clark
Alabama Power Company

Simon W. Bowen
Alabama Power Company

22.1 Implementation of Distribution Automation

The implementation of "distribution automation" within the continental U.S. is as diverse and numerous as the utilities themselves. Particular strategies of implementation utilized by various utilities have depended heavily on environmental variables such as size of the utility, urbanization, and available communication paths. The current level of interest in distribution automation is the result of:

- The August 14, 2003 northeast blackout, which focused attention on infrastructure deficiencies and increased industry attention on sensor technology and digital control systems.
- Recent initiatives such as the DOE's GridWise program and EPRI's IntelliGrid program that have funded distribution research and development projects.
- The availability of low-cost, high-performance general purpose microprocessors, embedded processors, and digital signal processors, which have extended technology choices by blurring the lines between traditional RTU, PLC, meter, and relay technologies, specifically capabilities that include meter accuracy measurements and calculations with power quality information including harmonic content.

- Increased performance in host servers for the same or lower cost, lower cost of memory, and in particular the movement to Windows and Linux architectures.
- The threat of deregulation and competition as a catalyst to automate.
- Strategic benefits to be derived (e.g., potential of reduced labor costs, better planning from better information, optimizing of capital expenditures, reduced outage time, increased customer satisfaction).

While not meant to be all-inclusive, this section on distribution automation attempts to provide some dimension to the various alternatives available to the utility engineer. The focus will be on providing insight on the elements of automation that should be included in a scalable and extensible system. The approach will be to describe the elements of a "typical" distribution automation system in a simple manner, offering practical observations as required.

The supervisory control and data acquisition (SCADA) vendors are now delivering systems on the Windows platform running on PC workstations. The PC-based systems provide opportunities to distribute the SCADA technology throughout the electric distribution network.

22.2 Distribution SCADA History

SCADA is the foundation for the distribution automation system. The ability to remotely monitor and control electric power system facilities found its first application within the power generation and transmission sectors of the electric utility industry. The ability to significantly influence the utility bottom line through the effective dispatch of generation and the marketing of excess generating capacity provided economic incentive. The interconnection of large power grids in the Midwestern and the Southern U.S. (1962) created the largest synchronized system in the world. The blackout of 1965 prompted the U.S. Federal Power Commission to recommend closer coordination between regional coordination groups (Electric Power Reliability Act of 1967), and gave impetus to the subsequent formation of the National Electric Reliability Council (1970). From that time (1970) forward, the priority of the electric utility has been to engineer and build a highly reliable and secure transmission infrastructure. The importance and urgency of closer coordination was re-emphasized with the northeast blackout of 2003. Transmission SCADA became the base for the large energy management systems that were required to manage the transmission grid.

Distribution SCADA was not given equal consideration during this period. For electric utilities, justification for automating the distribution system, while being highly desirable, was not readily attainable based on a high cost/benefit ratio due to the size of the distribution infrastructure and cost of communication circuits. Still there were tactical applications deployed on parts of distribution systems that were enough to keep the dream alive.

The first real deployments of distribution SCADA systems began in the late 1980s and early 1990s when SCADA vendors delivered reasonably priced "small" SCADA systems on low-cost hardware architectures to the small co-ops and municipality utilities. As the market expanded, SCADA vendors who had been providing transmission SCADA began to take notice of the distribution market. These vendors initially provided host architectures based on VAX/VMS and later on Alpha/OpenVMS platforms and on UNIX platforms. These systems were required for the large distribution utility (100,000–250,000 point ranges). These systems often resided on company-owned LANs with communication front-end (CFE) processors and user interface (UI) attached either locally on the same LAN or across a WAN.

In the mid-1980s, EPRI published definitions for distribution automation and associated elements. The industry generally associates distribution automation with the installation of automated distribution line devices such as switches, reclosers, sectionalizers, etc. The author's definition of distribution automation encompasses the automation of the distribution substations and the distribution line

devices. The automated distribution substations and the automated distribution line devices are then operated as a system to facilitate the operation of the electric distribution system.

22.2.1 SCADA System Elements

At a high level, the elements of a distribution automation system can be divided into three main areas:

- SCADA application and servers
- DMS applications and servers
- Trouble management applications and servers

22.2.2 Distribution SCADA

As was stated in the introduction, the SCADA system is the heart of distribution management system (DMS) architecture. A SCADA system should have all of the infrastructure elements to support the multifaceted nature of distribution automation and the higher level applications of a DMS. A distribution SCADA system's primary function is in support of distribution operations telemetry, alarming, event recording, and remote control of field equipment. Historically, SCADA systems have been notorious for their lack of support for the import, and more importantly, the export of power system data values. A modern SCADA system should support the engineering budgeting and planning functions by providing access to power system data without requiring possession of an operational workstation. The main elements of a SCADA system are:

- Host equipment
- Communication infrastructure (network and serial communications)
- Field devices (in sufficient quantity to support operations and telemetry requirements of a DMS platform)

22.2.3 Host Equipment

The authors feel that the essential elements of a distribution SCADA host are:

- Host servers (redundant servers with backup/failover capability)
- Communication front-end nodes (network based)
- Full graphics user interfaces
- Relational database server (for archival of historical power system values) and data server/Web server (for access to near real-time values and events)

The elements and components of the typical distribution automation system are illustrated in Fig. 22.1.

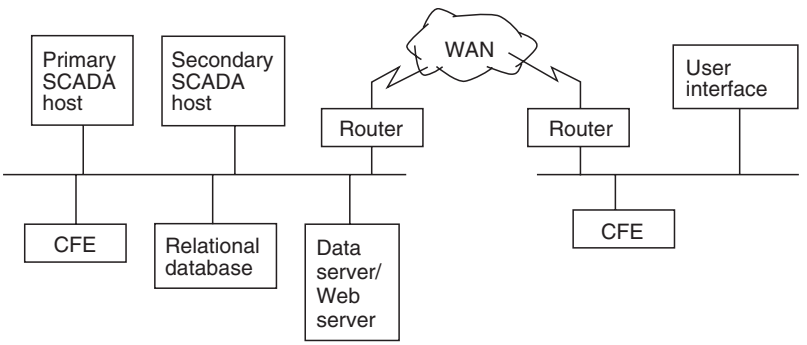

FIGURE 22.1 DA system architecture.

22.2.4 Host Computer System

22.2.4.1 SCADA Servers

As SCADA has proven its value in operation during inclement weather conditions, service restoration, and daily operations, the dependency on SCADA has created a requirement for highly available and high-performance systems. High-performance servers with abundant physical memory, RAID hard disk systems, and LAN connection are typical of today's SCADA high-performance servers. Redundant server hardware operating in a "live" backup/failover mode is required to meet the high availability criteria. In meeting the high availability criteria, electric utilities may also include a remote SCADA host configuration for disaster recovery.

22.2.5 Communication Front-End Processors

Most utilities will utilize more than one communication medium with the particular choice based on system requirements and other variables (e.g., radio coverage). However the preponderance of host to field device communications still depends heavily on serial communications. That is to say no matter what the communication medium used, the electrical interface to the SCADA system (CFE) is still most often a serial interface, not a network interface. The host/RTU interface requirement is filled by the CFE. The CFE can come in several forms based on bus architecture (older CFE technologies were most often based on VME or PCI bus systems with custom serial controllers). Currently CFE architectures are moving to Intel/Windows architectures with the serial controller function performed by the main processor instead of having the serial controllers located on the serial card. Location of the CFE in relation to the SCADA server can vary based on requirement. In some configurations the CFE is located on the LAN with the SCADA server. In other cases, existing communications hubs may dictate that the CFE resides at the communication hub. The incorporation of the WAN into the architecture requires a more robust CFE application to compensate for intermittent interruptions of network connectivity (relatively speaking—comparing WAN to LAN communication reliability).

The advent of new architectures for CFEs will offer new capabilities and opportunities for sharing data within the utility. The ability to serve data through a nonproprietary protocol such as ICCP offers the possibility for rethinking SCADA architectures within large utilities that may have more than one SCADA system or more than one audience for SCADA information.

In general the CFE will include three functional devices: a network/CPU board, serial cards, and possibly a time code receiver. Functionality should include the ability to download configuration and scan tables. The CFE should also support the ability to dead band values (i.e., report only those analog values that have changed by a user-defined amount). Even when exception scanning/reporting is used, the CFE, network and SCADA servers should be capable of supporting worst-case conditions (i.e., all points changing outside of the dead band limits), which typically occur during severe system disturbances. Deterministic communications with known data solicitation rates facilitate the sizing of the SCADA database and the performance of the SCADA system during wide-area storm events. Deterministic serial communications with the RTU are required for secure predictable data acquisition and supervisory control.

22.2.6 Full Graphics User Interface

The current distribution SCADA UI is a full graphics (FG) user interface. While character graphics consoles are still in use by some utilities today, SCADA vendors have aggressively moved their platforms to an FGUI. Initially the SCADA vendors implemented their FGUI on low-cost NT and XP workstations using third-party applications to emulate the X11 window system. Today the UI is being more natively integrated into the Windows architecture or as "browser"-like application. Full graphic displays provide the ability to display power system data along with the electric distribution facilities in a geographical (or semigeographical) perspective. The advantage of using a full graphics interface becomes evident (particularly for distribution utilities) as SCADA is deployed beyond the substation fence where feeder diagrams become critical to distribution operations.

22.2.7 Relational Databases, Data Servers, and Web Servers

The traditional SCADA systems were poor providers of data to anyone not connected to the SCADA system by an operational console. This occurred due to the proprietary nature of the performance (in memory) database and its design optimization for putting scanned data in and pushing display values out. Power system quantities such as bank and feeder loading (MW, MWH, MQH, and ampere loading) and bus volts provide valuable information to the distribution planning engineer. The maintenance engineer frequently uses the externalized SCADA data to identify trends and causality information to provide more effective and efficient equipment maintenance. The availability of event (log) data is important in postmortem analysis. The use of relational databases, data servers, and Web servers by the corporate and engineering functions provides access to power system information and data while isolating the SCADA server from nonoperations personnel.

22.2.8 Host to Field Communications

There are many communication mediums available to distribution SCADA for host/remote communications today. Some SCADA implementations utilize a network protocol over fiber to connect the SCADA hosts to substation automation systems; typically this is more often found in a small co-op or PUD who may have a relatively small substation count. Communication technologies such as frame-relay, multiple address system (MAS) radio, 900 MHz unlicensed, and even satellite find common usage today. Additionally there are new technologies emerging that may enter the mix of host/RTU communications (e.g., WiFi, WiMAX, and even broadband over power line [BPL] are possibilities at least for data acquisition). The authors do not recommend supervisory control over BPL.

Radio technologies offer good communications value. One such technology is the MAS radio. The MAS operates in the 900 MHz range and is omni-directional, providing radio coverage in an area with radius up to 20–25 miles depending on terrain. A single MAS master radio can communicate with many remote sites. The 900 MHz remote radio depends on a line-of-sight path to the MAS master radio. Protocol and bandwidth limit the number of remote terminal units that can be communicated with by a master radio. The protocol limit is simply the address range supported by the protocol. Bandwidth limitations can be offset by the use of efficient protocols, or slowing down the scan rate to include more remote units. Spread-spectrum and point-to-point radio (in combination with MAS) offer an opportunity to address specific communication problems, e.g., terrain changes or buildings within the MAS radio line-of-sight. At the present time MAS radio is preferred (authors' opinion) to packet radio (another new radio technology); MAS radio communications tend to be more deterministic providing for smaller timeout values on communication no-responses and controls.

22.3 Field Devices

Distribution automation (DA) field devices are multifeatured installations meeting a broad range of control, operations, planning, and system performance issues for the utility personnel. Each device provides specific functionality, supports system operations, includes fault detection, captures planning data, and records power quality information. These devices are found in the distribution substation and at selected locations along the distribution line. The multifeatured capability of the DA device increases its ability to be integrated into the electric distribution system. The functionality and operations capabilities complement each other with regard to the control and operation of the electric distribution system. The fault detection feature is the "eyes and ears" for the operating personnel. The fault detection capability becomes increasingly more useful with the penetration of DA devices on the distribution line.

The real-time data collected by the SCADA system are provided to the planning engineers for inclusion in the radial distribution line studies. As the distribution system continues to grow, the utility makes annual investments to improve the electric distribution system to maintain adequate facilities to meet the

increasing load requirements. The use of the real-time data permits the planning engineers to optimize the annual capital expenditures required to meet the growing needs of the electric distribution system.

The power quality information includes capturing harmonic content to the 15th harmonic and recording percent total harmonic distortion (%THD). This information is used to monitor the performance of the distribution electric system.

22.3.1 Modern RTU

Today's modern RTU is modular in construction with advanced capabilities to support functions that heretofore were not included in the RTU design. The modular design supports installation configurations ranging from the small point count required for the distribution line pole-mounted units to the very large point count required for large bulk-power substations and power plant switchyard installations. The modern RTU modules include analog units with 9 points, control units with 4 control pair points, status units with 16 points, and communication units with power supply. The RTU installation requirements are met by accumulating the necessary number of modern RTU modules to support the analog, control, status, and communication requirements for the site to be automated. Packaging of the minimum point count RTUs is available for the distribution line requirement. The substation automation requirement has the option of installing the traditional RTU in one cabinet with connections to the substation devices or distributing the RTU modules at the devices within the substation with fiber optic communications between the modules. The distributed RTU modules are connected to a data concentrating unit which in turn communicates with the host SCADA computer system.

The modern RTU accepts direct AC inputs from a variety of measurement devices including line-post sensors, current transformers, potential transformers, station service transformers, and transducers. Direct AC inputs with the processing capability in the modern RTU support fault current detection and harmonic content measurements. The modern RTU has the capability to report the magnitude, direction, and duration of fault current with time tagging of the fault event to 1-ms resolution. Monitoring and reporting of harmonic content in the distribution electric circuit are capabilities that are included in the modern RTU. The digital signal processing capability of the modern RTU supports the necessary calculations to report %THD for each voltage and current measurement at the automated distribution line or substation site.

The modern RTU includes logic capability to support the creation of algorithms to meet specific operating needs. Automatic transfer schemes have been built using automated switches and modern RTUs with the logic capability. This capability provides another option to the distribution line engineer when developing the method of service and addressing critical load concerns. The logic capability in the modern RTU has been used to create the algorithm to control distribution line switched capacitors for operation on a per-phase basis. The capacitors are switched on at zero voltage crossing and switched off at zero current crossing. The algorithm can be designed to switch the capacitors for various system parameters such as voltage, reactive load, time, etc. The remote control capability of the modern RTU then allows the system operator to take control of the capacitors to meet system reactive load needs.

The modern RTU has become a dynamic device with increased capabilities. The new logic and input capabilities are being exploited to expand the uses and applications of the modern RTU.

22.3.2 PLCs and IEDs

Programmable logic controllers (PLCs) and intelligent electronic devices (IEDs) are components of the distribution automation system, which meet specific operating and data gathering requirements. While there is some overlap in capability with the modern RTU, the authors are familiar with the use of PLCs for automatic isolation of the faulted power transformer in a two-bank substation and automatic transfer of load to the unfaulted power transformer to maintain an increased degree of reliability. The PLC communicates with the modern RTU in the substation to facilitate the remote operation of the substation facility. The typical PLC can support serial communications to a SCADA server. The modern RTU has the capability to communicate via an RS-232 interface with the PLC.

IEDs include electronic meters, electronic relays, and controls on specific substation equipment such as breakers, regulators, LTC on power transformers, etc. The IEDs also have the capability to support serial communications to a SCADA server. The authors' experience indicates that substation IEDs are either connected to a substation automation master via a substation LAN or reporting to the modern RTU (and thus to the SCADA host) via a serial interface using ASCII or vendor-specific protocol. Recent improvement in measurement accuracy and inclusion of power quality (harmonic content) especially in the realm of electronic relays are making the IED an important part of the substation protection and automation strategy.

22.3.3 Substation

The installation of the SCADA technology in the DA substation provides for the full automation of the distribution substation functions and features. The modular RTU supports the various substation sizes and configuration. The load on the power transformer is monitored and reported on a per-phase basis. The substation low-side bus voltage is monitored on a per-phase basis. The distribution feeder breaker is fully automated. Control of all breaker control points is provided including the ability to remotely set up the distribution feeder breaker to support energized distribution line work. The switched capacitor banks and substation regulation are controlled from the typical modular RTU installation. The load on the distribution feeder breaker is monitored and reported on a per-phase basis as well as on a three-phase basis. This capability is used to support the normal operations of the electric distribution system and to respond to system disturbances. The installation of the SCADA technology in the DA substation eliminates the need to dispatch personnel to the substation except for periodic maintenance and equipment failure.

22.3.4 Line

The DA distribution line applications include line monitoring, pole-mounted reclosers, gang-operated switches equipped with motor operators, switched capacitor banks, pole-mounted regulators, and pad-mounted automatic transfer switchgear. The modular RTU facilitates the automation of the distribution line applications. The use of the line post sensor facilitates the monitoring capability on a per-phase basis. The direct AC input from the sensors to the RTU supports monitoring of the normal load, voltage, and power factor measurements, and also the detection of fault current. The multifeatured distribution line DA device can be used effectively to identify the faulted sections of the distribution circuit during system disturbances, isolate the faulted sections, and restore service to the unfaulted sections of the distribution circuit. The direct AC inputs to the RTU also support the detection and reporting of harmonics and the %THD per phase for voltage and current. Fault detection (forward and reverse) per phase as well as fault detection on the residual current is supported in the RTU.

22.3.5 Tactical and Strategic Implementation Issues

As the threat of deregulation and competition emerges, retention of industrial and large commercial customers will become the priority for the electric utility. Every advantage will be sought by the electric utility to differentiate itself from other utilities. Reliable service, customer satisfaction, fast storm restorations, and power quality will be the goals of the utility. Differing strategies will be employed based on the customer in question and the particular mix of goals that the utility perceives will bring customer loyalty.

For large industrial and commercial customers, where the reliability of the electric service is important and outages of more than a few seconds can mean lost production runs or lost revenue, tactical automation solutions may be required. Tactical solutions are typically transfer schemes or switching schemes that can respond independently of operator action, reporting the actions that were initiated in response to loss of preferred service and/or line faults. The requirement to transfer source power, or

reconfigure a section of the electric distribution system to isolate and reconnect in a matter of seconds is the primary criteria. Tactical automation based on local processing provides the solution.

In cases where there are particularly sensitive customer requirements, tactical solutions are appropriate. When the same requirements are applied to a large area and/or customer base, a strategic solution based on a distribution management platform is preferred. This solution requires a DMS with a system operational model that reflects the current configuration of the electric distribution system. Automatic fault isolation and restoration applications, which can reconfigure the electric distribution system, require a "whole and dynamic system" model in order to operate correctly and efficiently.

22.3.6 Distribution Management Platform

So, while tactical automation requirements exist and have significant impact and high profile, goals that target system issues require a strategic solution. A DMS is the capstone for automation of the distribution system and includes advance distribution applications, integrated SCADA, integrated trouble call and outage management, and distribution operations training simulator (DOTS) at a minimum.

22.3.7 Advanced Distribution Applications

Transmission EMS systems have had advanced applications for many years. The distribution management platform will include advanced applications for distribution operations. A true DMS should include advanced applications such as volt/VAR control, automatic fault isolation and service restoration, operational power flows, contingency analysis, loss minimization, switching management, etc.

22.4 Integrated SCADA System

A functional DMS platform should be fully integrated with the distribution SCADA system. The SCADA–DMS interface should be fully implemented with the capability of passing data [discrete indication (status) and values (analog)] bi-directionally. The SCADA interface should also support device control. Figure 22.2 details the components of a DMS.

22.4.1 Trouble Call and Outage Management System

In addition to the base SCADA functionality and high-level DMS applications, the complete distribution automation system will include a trouble call and outage management system (TCOMS). TCOMS

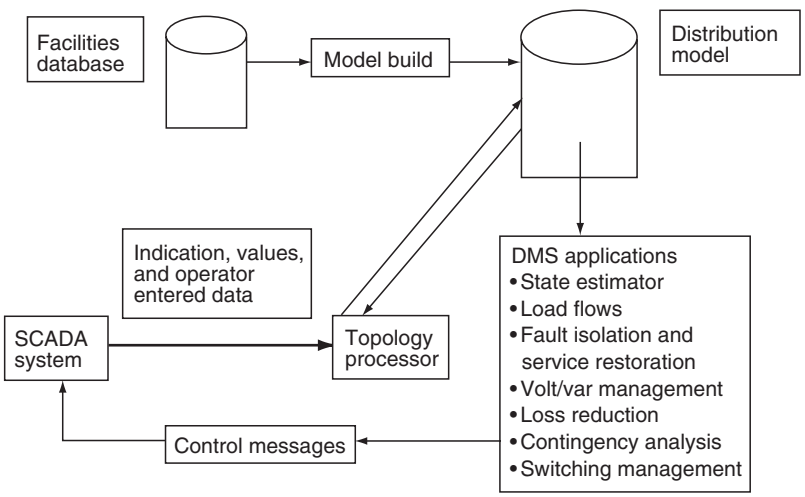

FIGURE 22.2 A DMS platform with SCADA interface.

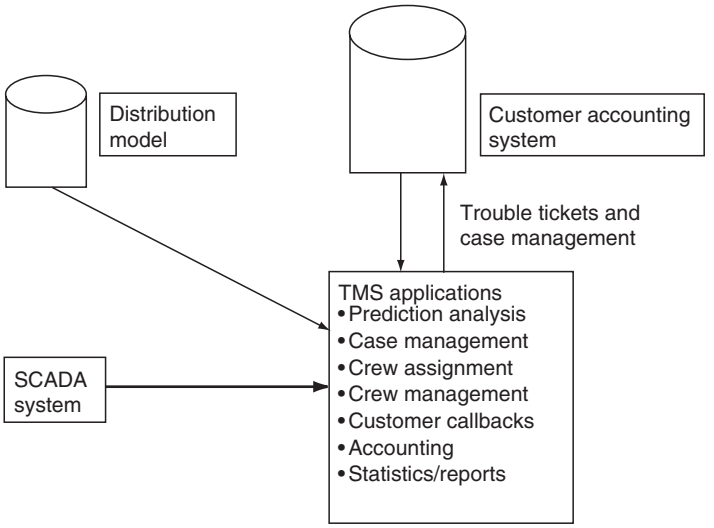

FIGURE 22.3 A TCOMS platform with SCADA interface.

collect trouble calls received by human operators and interactive voice recorders (IVR). The trouble calls are fed to an analysis/prediction engine that has a model of the distribution system with customer to electrical address relationships. Outage prediction is presented on a full graphics display that overlays the distribution system on CAD base information. A TMS also provides for the dispatch and management of crews, customer callbacks, accounting, and reports. A SCADA interface to a TCOMS provides the means to provide confirmed (SCADA telemetry) outage information to the prediction engine. Figure 22.3 shows a typical TCOMS.

22.4.2 Distribution Operations Training Simulator

With the graying of the American workforce and subsequent loss of expertise there is a requirement to provide better training for the distribution operator. A DOTS will provide the ability to train and test the distribution operator with real world scenarios captured (and replayed) through the DOTS. The DOTS instructor will be able to "tweak" the scenarios, varying complexity and speed of the simulation providing the distribution operator with the opportunity to learn best practices and to test his skills in an operational simulation without consequences of making operational mistakes on the "real distribution system."

22.5 Security

In today's environment, security of control systems has become an important topic. The dependence by electric utilities on digital control systems for operations coupled with the threat of terrorist activity whether by governments or individuals is beyond the scope of this article. However, it should be noted that most distribution SCADA systems (unlike transmission SCADA and EMS systems which are often on their own separate network) often reside on the utilities corporate networks elevating the risk of exposure to viruses, worms, and Trojan horses.

Every electric utility, no matter what size, should have the appropriate policy and procedures in place to secure their distribution "control system" from malicious or accidental harm. Securing administrator accounts, password aging policies, passwords with requirements on length and requirements on the mixture of character types, two factor authentication, virus protection, firewalls, intrusion detection, and securing the physical and electronic perimeter have all become a part of the vocabulary for SCADA system support staffs.

22.6 Practical Considerations

22.6.1 Choosing the Vendor

22.6.1.1 Choosing a Platform Vendor

In choosing a platform (SCADA, DMS, TCOMS) vendor there are several characteristics that should be kept in mind (these should be considered as a rule of thumb based on experience of what works and what does not). Choosing the right vendor is as important as choosing the right software package.

Vendor characteristics that the authors consider important are:

- A strong "product" philosophy. Having a strong product philosophy is typically a chicken and egg proposition. Which came first, the product or the philosophy? Having a baseline SCADA application can be a sign of maturity and stability. Did the platform vendor get there by design or did they back into it? Evidence of a product philosophy includes a baseline system that is in production and enhancements that are integrated in a planned manner with thorough testing on the enhancement and regression testing on the product along with complete and comprehensive documentation.
- A documented development and release path projected three to five years into the future.
- By inference from the first two bullets, a vendor who funds planned product enhancements from internal funds.
- A strong and active user group that is representative of the industry and industry drivers.
- A platform vendor that actively encourages its user group by incentive (e.g., dedicating part of its enhancement funding to user group initiatives).
- A vendor that is generally conservative in moving its platform to a new technology; one that does not overextend its own resources.
- Other considerations.
- As much as possible, purchase the platform as an off-the-shelf product (i.e., resist the urge to ask for customs that drive your system away from the vendor's baseline).
- If possible, maintain/develop your own support staff.

All "customization" should be built around the inherent capabilities and flexibility of the system (i.e., do not generate excessive amounts of new code). Remember, you will have to reapply any code that you may have developed to every new release; or worse, you will have to pay the vendor to do it for you.

22.7 Standards

22.7.1 Internal Standards

The authors highly recommend the use of standards (internal to your organization) as a basis for ensuring a successful distribution automation or SCADA program. Well-documented construction standards that specify installation of RTUs, switches, and line sensors with mechanical and electrical specifications will ensure consistent equipment installations from site to site. Standards that cover nontrivial, but often overlooked issues can often spell the difference between acceptance and rejection by operational users and provide the additional benefit of having a system that is "maintainable" over the 10–20 years (or more) life of a system. Standards that fall in this category include standards that cover point-naming conventions, symbol standards, display standards, and the all-important operations manual.

22.7.2 Industry Standards

In general, standards fall into two categories: standards that are developed by organizations and commissions (e.g., EPRI, IEEE, ANSI, CCITT, ISO, etc.) and de facto standards that become standards

by virtue of widespread acceptance. As an example of what can occur, the reader is invited to consider what has happened in network protocols over the recent past with regard to the OSI model and TCP/IP.

Past history of SCADA and automation has been dominated by the proprietary nature of the various system vendor offerings. Database schemas and RTU communication protocols are exemplary of proprietary design philosophies utilized by SCADA platform and RTU vendors. Electric utilities that operate as part of the interconnected power grid have been frustrated by the lack of ability to share power system data between dissimilar energy management systems. The same frustration exists at the device level; RTU vendors, PLC vendors, electronic relay vendors, and meter vendors each having their own product protocols have created a "tower of babel" problem for utilities. Recently several communications standards organizations and vendor consortiums have proposed standards to address these deficiencies in intersystem data exchange, intrasystem data exchange (corporate data exchange), and device level interconnectivity. Some of the more notable examples of network protocol communication standards are ICCP (intercontrol center protocol), UCA (utility communication architecture), CCAPI (control center applications interface), and UIB (utility integration bus). For database schemas, EPRI's CIM (common information model) is gaining supporters. In RTU, PLC, and IED communications, DNP 3.0 has also received much attention from the industry's press.

In light of the number of standards that have appeared (and then disappeared) and the number of possibly competing "standards" that are available today, the authors, while acknowledging the value of standards, prefer to take (and recommend) a cautious approach to standards. A wait-and-see posture may be an effective strategy. Standards by definition must have proven themselves over time. Difficulties in immediately embracing new standards are due in part to vendors having been allowed to implement only portions of a standard, thereby nullifying the hopefully "plug-and-play" aspect for adding new devices. Also, the trend in communication protocols has been to add functionality in an attempt to be all-inclusive, which has resulted in an increased requirement on bandwidth. Practically speaking, utilities that have already existing infrastructure may find it economical to resist the deployment of new protocols. In the final analysis, as in any business decision, a "standard" should be accepted only if it adds value and benefit that exceeds the cost of implementation and deployment.

22.8 Deployment Considerations

The definition of the automation technology to be deployed should be clearly delineated. This definition includes the specification of the host systems, the communication infrastructure, the automated end-use devices, and the support infrastructure. This effort begins with the development of a detailed installation plan that takes into consideration the available resources. The pilot installation will never be any more than a pilot project until funding and manpower resources are identified and dedicated to the enterprise of implementing the technologies required to automate the electric distribution system. The implementation effort is best managed on an annual basis with stated incremental goals and objectives for the installation of automated devices. With the annual goals and objectives identified, then the budget process begins to ensure that adequate funding is available to support the implementation plan. To ensure adequate time to complete the initial project tasks, the planning should begin 18 to 24 months prior to the budget year. During this period, the identification of specific automation projects is completed. The initial design work is commenced with the specification of field automation equipment (e.g., substation RTU based on specific point count requirements and distribution line RTU). The verification of the communication to the selected automation site is an urgent early consideration in order to minimize the cost of achieving effective remote communications. As the installation year approaches, the associated automation equipment (e.g., switches, motor operators, sensors, etc.) must be verified to ensure that adequate supplies are stocked to support the implementation plan.

The creation of a SCADA database and display is on the critical path for new automated sites. The database and display are critical to the efficient completion of the installation and checkout tasks. Data must be provided to the database and display team with sufficient lead time to create the database and display for the automated site. The database and display are subsequently used to check out the

completed automated field device. The point assignment (PA) sheet is a project activity that merits serious attention. The PA sheet is the basis for the creation of the site-specific database in the SCADA system. The PA sheet should be created in a consistent and standard fashion. The importance of an accurate database and display cannot be overemphasized. The database and display form the basis for the remote operational decisions for the electric distribution system using the SCADA capability. Careful coordination of these project tasks is essential to the successful completion of the annual automation plans.

Training is another important consideration during the deployment of the automation technology. The training topics are as varied as the multidisciplined nature of the distribution automation project. Initial training requirements include the system support personnel in the use and deployment of the automation platform, the end user (operator) training, and installation teams. Many utilities now install new distribution facilities using energized line construction techniques. The automated field device adds a degree of complexity to the construction techniques to ensure adherence to safe practices and construction standards. These training issues should be addressed at the outset of the planning effort to ensure a successful distribution automation project.

22.8.1 Support Organization

The support organization must be as multidisciplined as the distribution automation system is multifeatured. The support to maintain a deployed distribution automation system should not be underestimated. Functional teams should be formed to address each discipline represented within the distribution automation system. The authors recommend forming a core team that is made up of representation from each area of discipline or area of responsibility within the distribution automation project. These areas of discipline include the following:

- Host SCADA system
- User interface
- Communication infrastructure
- Facilities design personnel for automated distribution substation and distribution line devices
- System software and interface developments
- Installation teams for automated distribution substation and distribution line devices
- End users (i.e., the operating personnel)

The remaining requirement for the core team is project leadership with responsibility for the project budget, scheduling, management reports, and overall direction of the distribution automation project. The interaction of the various disciplines within the distribution automation team will ensure that all project decisions are supporting the overall project goals. The close coordination of the various project teams through the core team is essential to minimizing decision conflict and maximizing the synergy of project decisions. The involvement of the end user at the very outset of the distribution automation project planning cannot be overemphasized. The operating personnel are the primary users of the distribution automation technology. The participation of the end user in all project decisions is essential to ensure that the distribution automation product meets business needs and improves the operating environment in the operating centers. One measure of good project decisions is found in the response of the end user. When the end user says, "I like it," then the project decision is clearly targeting the end user's business requirements. With this goal achieved, the distribution automation system is then in a position to begin meeting other corporate business needs for real-time data from the electric distribution system.

23

Hard to Find Information (on Distribution System Characteristics and Protection)

Jim Burke
InfraSource Technology

23.1 Overcurrent Protection

23.1.1 Introduction

The distribution system shown in Fig. 23.1 illustrates many of the features of a distribution system making it unique. The voltage level of a distribution system can be anywhere from about 5 kV to as high as 35 kV with the most common voltages in the 15 kV class. Areas served by a given voltage are proportional to the voltage itself, indicating that, for the same load density, a 35 kV system can serve considerably longer lines. Lines can be as short as a mile or two and as long as 20 or 30 miles. Typically,

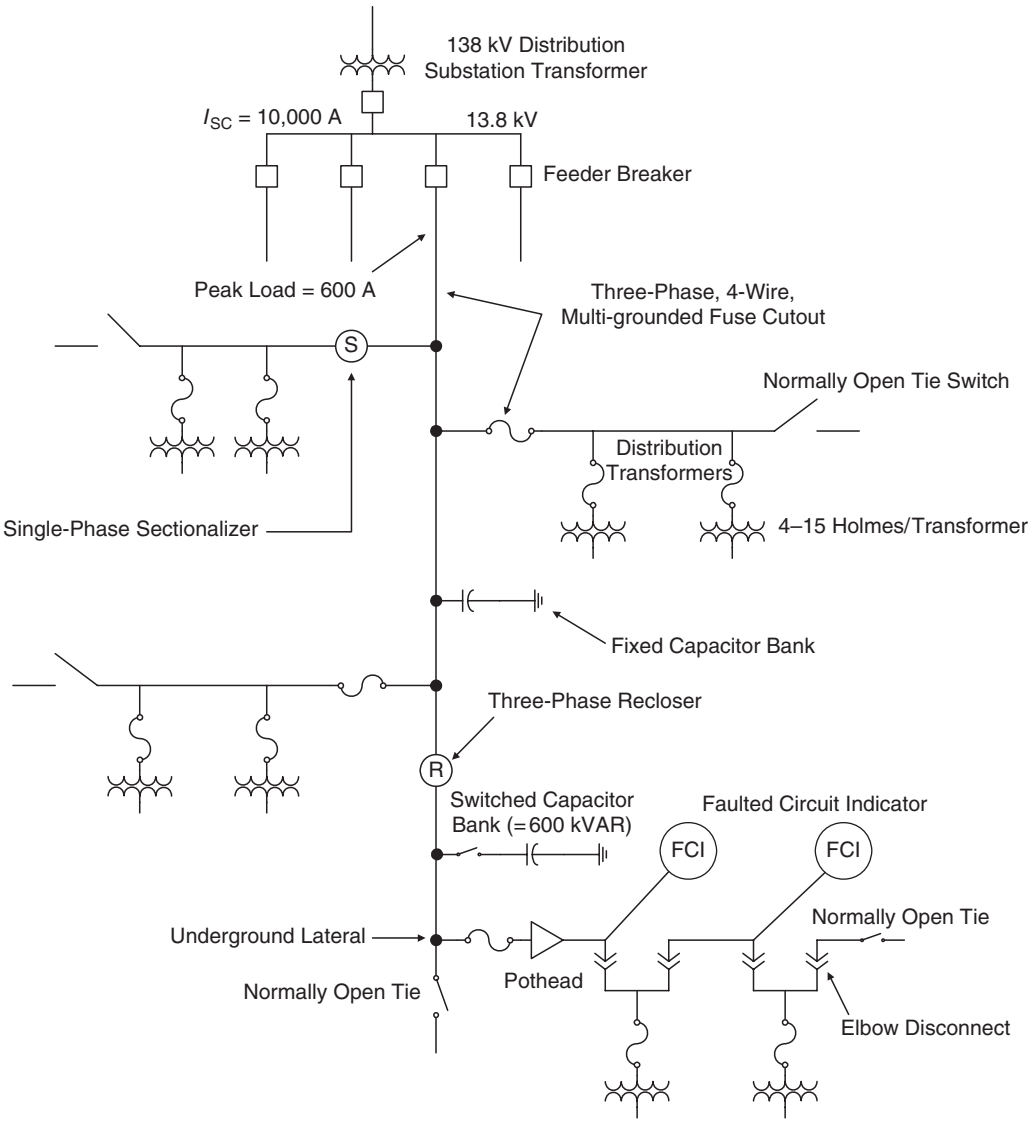

FIGURE 23.1 Typical distribution system.

however, lines are generally 10 miles or less. Short-circuit levels at the substation are dependent on voltage level and substation size. The average short-circuit level at a distribution substation has been shown, by survey, to be about 10,000 A. Feeder load current levels can be as high as 600 A but rarely exceed about 400 A with many never exceeding a couple of hundred amperes.

23.1.2 Fault Levels

There are two types of faults, low impedance and high impedance. A high impedance fault is considered to be a fault that has a high Z due to the contact of the conductor to the earth, i.e., Z_f is high. By this definition, a bolted fault at the end of a feeder is still classified as a low impedance fault. A summary of findings on faults and their effects is as follows.

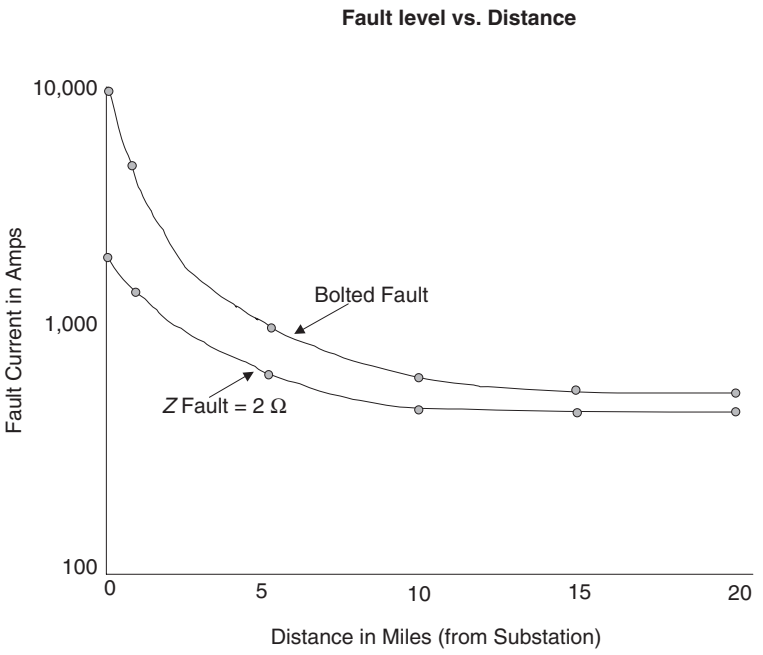

FIGURE 23.2 Low impedance faults.

23.1.2.1 Low Impedance Faults

Low impedance faults or bolted faults can be either very high in current magnitude (10,000 A or above) or fairly low, e.g., 300 A at the end of a long feeder. Faults that can be detected by normal protective devices are all low impedance faults. These faults are such that the calculated value of fault current assuming a "bolted fault" and the actual are very similar. Most detectable faults, per study data, do indeed show that fault impedance is close to 0 Ω. This implies that the phase conductor either contacts the neutral wire or that the arc to the neutral conductor has a very low impedance. An EPRI study performed by the author over 10 years ago indicated that the maximum fault impedance for a detectable fault was 2 Ω or less. Figure 23.2 indicates that 2 Ω of fault impedance influences the level of fault current depending on location of the fault. As can be seen, 2 Ω of fault impedance considerably decreases the level of fault current for close-in faults but has little effect for faults some distance away. What can be concluded is that *fault impedance does not significantly affect faulted circuit indicator performance* since low level faults are not greatly altered.

23.1.2.2 High Impedance Faults

High impedance faults are faults that are low in value, i.e., generally less than 100 A due to the impedance between the phase conductor and the surface on which the conductor falls. Figure 23.3 illustrates that most surface areas, whether wet or dry, do not conduct well. If one considers the fact that an 8-ft ground rod sunk into the earth more often than not results in an impedance of 100 Ω or greater, then it is not hard to visualize the fact that a conductor simply lying on a surface cannot be expected to have a low impedance. These faults, called high impedance faults, do not contact the neutral and do not arc to the neutral. They are not detectable by any conventional means and are not to be considered at all in the evaluation of fault current indicators (FCIs) and most other protective devices.

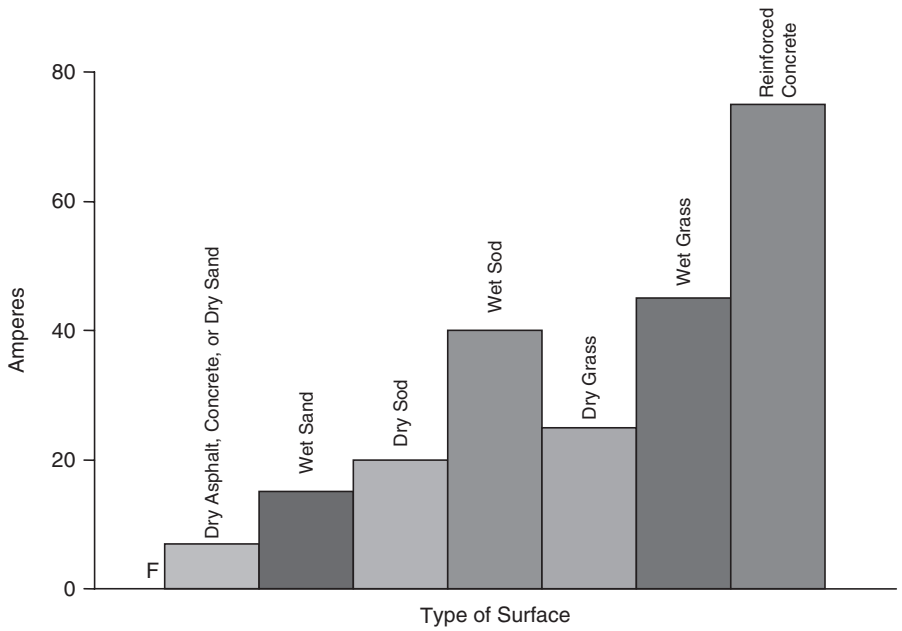

FIGURE 23.3 High impedance fault current levels.

23.1.3 Surface Current Levels

See Figure 23.3.

23.1.4 Reclosing and Inrush

On most systems where most faults are temporary, the concept of reclosing and the resulting inrush currents are a fact of life. Typical reclosing cycles for breakers and reclosers are different and are shown in Fig. 23.4.

These reclosing sequences produce inrush primarily resulting from the connected transformer kVA. This inrush current is high and can approach the actual fault current level in many instances. Figure 23.5 shows the relative magnitude of these currents. What keeps most protective devices from operating is that the duration of the inrush is generally short and as a consequence will not melt a fuse or operate a time delay relay.

23.1.5 Cold Load Pickup

Cold load pickup, occurring as the result of a permanent fault and long outage, is often maligned as the cause of many protective device misoperations. Figure 23.6 illustrates several cold load pickup curves developed by various sources. These curves are normally considered to be composed of the following three components:

1. Inrush—lasting a few cycles
2. Motor starting—lasting a few seconds
3. Loss of diversity—lasting many minutes

When a lateral fuse misoperates, it is probably not the result of this loss of diversity, i.e., the fuse is overloaded. This condition is rare on most laterals. Relay operation during cold load pickup is generally the result of a trip of the instantaneous unit and probably results from high inrush. Likewise, an FCI

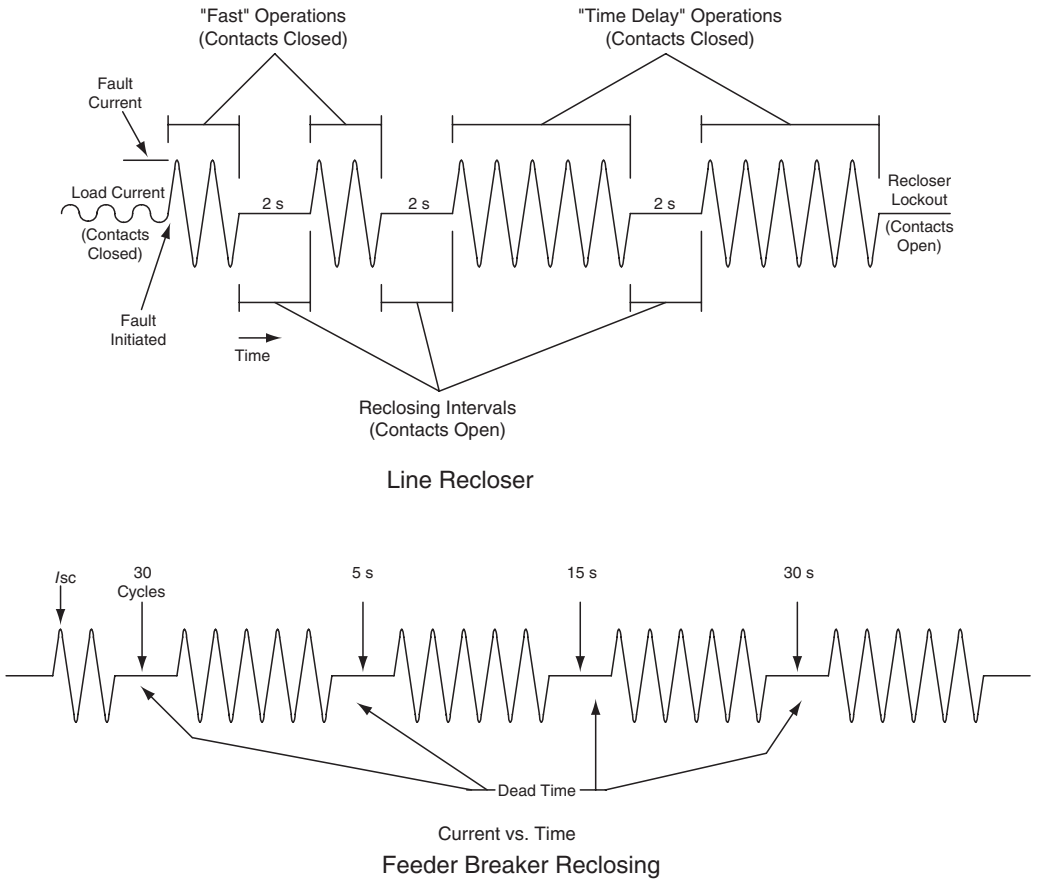

FIGURE 23.4 Reclosing sequences.

operation would not appear to be the result of loss of diversity but rather the high inrush currents. Since inrush occurs during all energization and not just as a result of cold load pickup, it can be concluded that cold load pickup is not a major factor in the application of FCIs.

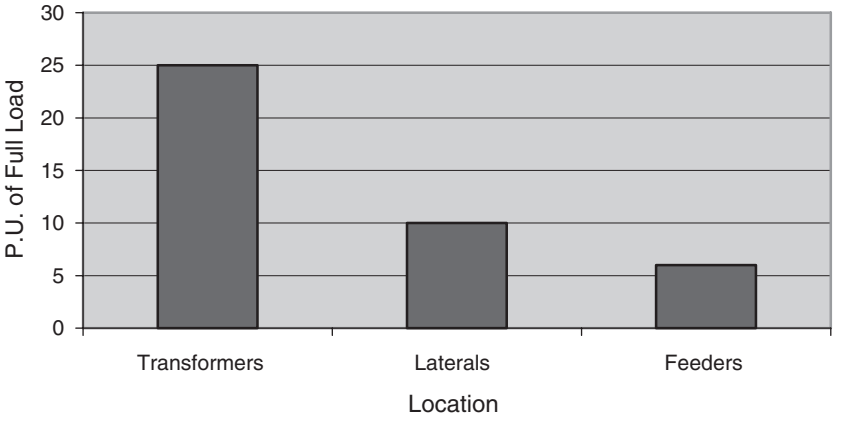

FIGURE 23.5 Magnitudes of inrush current.

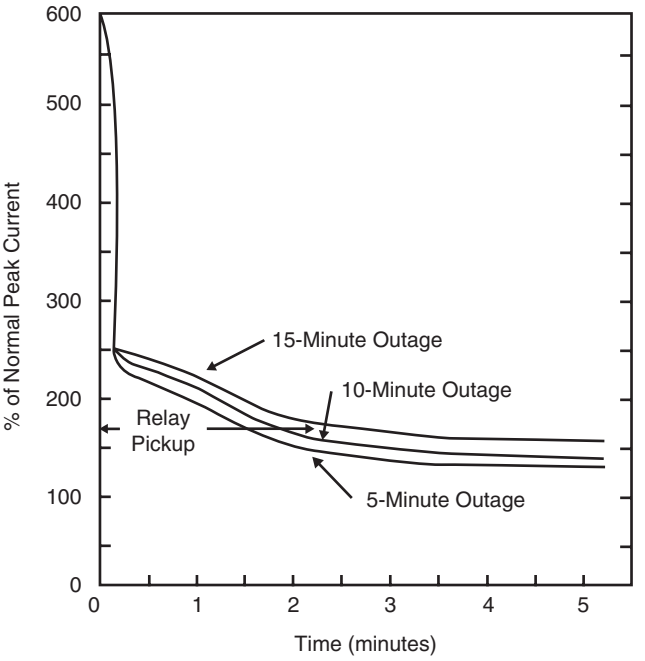

FIGURE 23.6 Cold load inrush current characteristics for distribution circuits.

23.1.6 Calculation of Fault Current

Line Faults

$$\text{Line-to-neutral fault} = \frac{E}{\sqrt{3}2Z_\ell}$$

where Z_ℓ is the line impedance and $2Z_\ell$ is the loop impedance assuming the impedance of the phase conductor and the neutral conductor are equal (some people use a 1.5 factor).

$$\text{Line-to-line fault} = E/2Z_\ell$$

Transformer Faults

$$\text{Line-to-neutral or three-phase} = \frac{\text{E}}{\sqrt{3}Z_T}$$

$$\text{Line-to-line} = \frac{E}{2(Z_\text{T} + Z_\ell)} \quad \text{where} \quad Z_\ell = \sqrt{R_L^2 + X_L^2}$$

$$Z_\text{T} = \frac{Z_{\text{T}\%}10E^2}{\text{kVA}}$$

23.1.7 Current Limiting Fuses

Current limiting fuses (CLFs) use a fusible element (usually silver) surrounded by sand (Fig. 23.7). When the element melts, it causes the sand to turn into fulgerite (glass). Since glass is a good insulator,

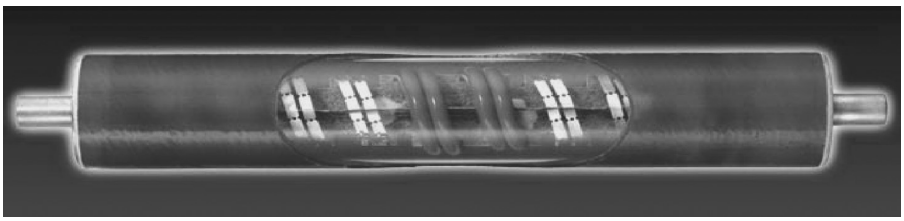

FIGURE 23.7 Full range current limiting fuse. (Courtesy T&B. With permission.)

FIGURE 23.8 Back-up CLF.

this results in a high resistance in series with the faults. This not only limits the magnitude of the fault but also the energy. All this can happen in less than a half cycle.

CLFs are very good at interrupting high currents (e.g., 50,000 A). They historically have had trouble (General Purpose, and Back-up) with low level fault currents and overloads, where the fuse tube melts before the element (i.e., these two fuses are not considered to be "full range," since they do not necessarily interrupt low currents that melt the element). There are now "full range" CLFs in the market (see Fig. 23.7).

The three types of CLFs are defined as follows:

- General purpose—A fuse capable of interrupting all currents from the rated maximum interrupting current down to the current that causes melting of the fusible element in 1 h.
- Back-up—A fuse capable of interrupting all currents from the rated maximum interrupting current down to the rated minimum interrupting current (Fig. 23.8).
- Full range—A fuse capable of interrupting all currents from the rated maximum current down to any current that melts the element.

23.1.8 Rules for Application of Fuses

1. Cold load pickup.

After 15-min outage	200% for 0.5 s
	140% for 5 s
After 4 h, all electric	300% for 5 min

2. "Damage" curve—75% of minimum melt.
3. Two expulsion fuses cannot be coordinated if the available fault current is great enough to indicate an interruption of less than 0.8 cycles.
4. "T"-SLOW and "K"-FAST.
5. CLFs can be coordinated in the subcycle region.
6. Capacitor protection:
   - The fuse should be rated for 165% of the normal capacitor current. The fuse should also clear within 300 s for the minimum short-circuit current.

- If current exceeds the maximum case rupture point, a CLF must be used.
- CLFs should be used if a single parallel group exceeds 300 kVAR.

7. Transformer
   - Inrush—12 times for 0.1 s.
   - 25 times for 0.01 s.
   - Self protected—primary fuse rating is 10–14 times continuous when secondary breaker is used.
   - Self protected—weak link is selected to be about 2.5 times the continuous when no secondary breaker is used (which means that minimum melt is in the area of 4–6 times rating).
   - Conventional—primary fuse rated 2–3 times.
   - General-purpose current limiting—2–3 times continuous.
   - Back-up current limiting—the expulsion and CLF are usually coordinated such that the minimum melt I^2t of the expulsion fuse is equal to or less than that of the back-up CLF.
8. Conductor burn down—not as great a problem today because loads are higher and hence conductors are larger.
9. General purpose—one which will successfully clear any current from its rated maximum interrupting current down to the current that will cause melting of the fusible element in 1 h.
10. Back-up—one which will successfully clear any current from its rated maximum interrupting down to the rated minimum interrupting current, which may be at the 10-s time period on the minimum melting time–current curve.
11. CLF—approximately 1/4 cycle operation; can limit energy by as much as 60 to 1.
12. Weak link—in oil is limited to between 1500 and 3500 A.
13. Weak link—in cutout is limited to 6,000–15,000 asymmetrical.
14. Lightning minimum fuse (12T-SLOW), (25K-FAST).
15. Energy stored in inductance $= \frac{1}{2}Li^2$.
16. The maximum voltage produced by a CLF typically will not exceed 3.1 times the fuse rated maximum voltage.
17. The minimum sparkover allowed for a gapped arrester is $1.5 \times 1.414 = 2.1$ times arrester rating.
18. General practice is to keep the minimum sparkover of a gapped arrester at about $2.65 \times$ arrester rating.
19. Metal oxide varistors (MOVs) do not have a problem with CLF "kick voltages".

23.1.9 More Overcurrent Rules

1. *Hydraulically controlled reclosers* are limited to about 10,000 A for the 560 A coil and 6,000 A for the 100 A coil.
2. Many companies set ground minimum trip at maximum load level and phase trip at two times load level.
3. A *K factor* of 1 (now used in the standards) means the interrupting current is constant for any operating voltage. A recloser is rated on the maximum current it can interrupt. This current generally remains constant throughout the operating voltage range.
4. A *recloser* is capable of its full interrupting rating for a complete four-operation sequence. The sequence is determined by the standard. A breaker is subject to derating.
5. A recloser can handle any degree of asymmetrical current. A breaker is subject to an S factor derating.
6. A *sectionalizer* is a self-contained circuit-opening device that automatically isolates a faulted portion of a distribution line from the source only after the line has been de-energized by an upline primary protective device.
7. A *power fuse* is applied close to the substation (2.8–169 kV and X/R between 15 and 25).
8. A *distribution fuse* is applied farther out on the system (5.2–38 kV and X/R between 8 and 15).
9. The *fuse tube* (in cutout) determines the interrupting capability of the fuse. There is an auxiliary tube that usually comes with the fuse that aids in low current interruption.

10. Some *expulsion fuses* can handle 100% continuous and some 150%.
11. Type "K" is a fast fuse link with a speed ratio of melting time–current characteristics from 6 to 8.1. (Speed is the ratio of the 0.1-s minimum melt current to the 300-s minimum melt current. Some of the larger fuses use the 600-s point.)
12. Type "T" is a slow fuse link with a speed ratio of melt time–current characteristics from 10 to 13.
13. After about ten fuse link operations, the *fuse holder* should be replaced.
14. *Slant ratings* can be used on grounded wye, wye, or delta systems as long as the line-to-neutral voltage of the system is lower than the smaller number and the line-to-line voltage is lower than the higher number. A slant rated cutout can withstand the full line-to-line voltage whereas a cutout with a single voltage rating could not withstand the higher line-to-line voltage.
15. *Transformer fusing*—25 at 0.01; 12 at 0.1; 3 at 10 s.
16. *Unsymmetrical transformer connections (delta/wye)*

Fault Type	Multiplying Factor
Three-phase	N
Phase-to-phase	87 (N)
Phase-to-ground	1.73 (N)

    where N is the ratio of $V_{\text{primary}}/V_{\text{secondary}}$.

17. Multiply the high side device *current points* by the appropriate factor.
18. *K factor for load side fuses*
    a. Two fast operations and dead time 1–2 s = 1.35.
19. *K factor for source side fuses*
    a. Two fast—Two delayed and dead time of 2 s = 1.7.
    b. Two fast—Two delayed and dead time of 10 s = 1.35.
    c. Sometimes these factors go as high as 3.5 so check.
20. *Sequence coordination*—Achievement of true "trip coordination" between an upline electronic recloser and a downline recloser is made possible through a feature known as "sequence" coordination. Operation of sequence coordination requires that the upline electronic recloser be programmed with "fast curves" whose control response time is slower than the clearing time of the downline recloser fast operation, through the range of fault currents within the reach of the upline recloser. Assume a fault beyond the downline recloser that exceeds the minimum trip setting of both reclosers. The downline recloser trips and clears before the upline recloser has a chance to trip. However, the upline control does see the fault and the subsequent cutoff of fault current. The sequence coordination feature then advances its control through its fast operation, such that both controls are at their second operation, even though only one of them has actually tripped. Should the fault persist, and a second fast trip occur, sequence coordination repeats the procedure. Sequence coordination is active only on the programmed fast operations of the upline recloser. In effect, sequence coordination maintains the downline recloser as the faster device.
21. *Recloser time–current characteristics*
    a. Some curves are average. Maximum is 10% higher.
    b. Response curves are the responses of the sensing device and do not include arc extinction.
    c. Clearing time is measured from fault initiation to power arc extinction.
    d. The response time of the recloser is sometimes the only curve given. To obtain the interrupting time, you must add approximately 0.045 s to the curve (check . . . they are different).
    e. Some curves show maximum clearing time. On the new electronic reclosers, you usually get a control response curve and a clearing curve.
    f. $Z_\ell - g = (2Z_1 + Z_0)/3$
22. The "75% Rule" considers TCC tolerances, ambient temperature, pre-loading, and pre-damage. Pre-damage only uses 90%.

23. *A back-up CLF* with a designation like "12 K" means that the fuse will coordinate with a K link rated 12 A or less.
24. *Capacitor Fusing*:
    a. The 1.35 factor may result in nuisance fuse operations. Some utilities use 1.65.
    b. Case rupture is not as big a problem as years ago due to all film designs.
    c. Tank rupture curves may be probable or definite in nature. Probable means there is a probability chance of not achieving coordination. Definite indicates there is effectively no chance of capacitor tank rupture with the proper 0% probability curve.
    d. T links are generally used up to about 25 A and K link above that to reduce nuisance fuse operations from lightning.
25. *Line Impedance*—Typical values for line impedance (350 kcm) on a per mile basis are as follows:

	Z_{positive}	Z_0
Cable UG	$0.31 + j0.265$	$1.18 + j0.35$
Spacer	$0.3 + j0.41$	$1.25 + j2.87$
Tree wire	$0.3 + j0.41$	$1.25 + j2.87$
Armless	$0.3 + j0.61$	$0.98 + j2.5$
Open	$0.29 + j0.66$	$0.98 + j2.37$

26. 1A–3B is necessary when sectionalizers are used downstream from the recloser.
27. Vacuum reclosers have interrupting ratings as high as 10–20 kA.
28. Highest recloser continuous ratings are 800 and 1200 A.
29. Sectionalizer actuating current should be <80% of back-up device trip current.
30. Interrupting ratings of cutouts are approximately 7–10 kA symmetrical.
31. *K factor* can mean a "voltage range" factor or a "shift factor" caused by the recloser heating up the fuse.
32. *Sectionalizer counts* should normally be one count less than the operations to lockout of the breaker or recloser.
33. *Sectionalizer memory* time must be greater than cumulative trip and recloser time.
34. Fuses melt at about 200% of rating.
35. Sectionalizers have momentary ratings for 1 and 10 s.
36. *Twenty five percent rule* for fuses includes pre-load, ambient temperature, and pre-damage.
37. **Characteristics of Chance Sectionalizers include:**
    - 100 A continuous
    - 160 A actuating
    - 2 counts
    - 12,000 A momentary
    - 4,000 A at 1 s
    - 2,500 A at 10 s
    - 0.3 A detector threshold
    - Minimum time delay = 80 ms
    - Reset time approximately 25 s
    - Minimum duration of current impulse approximately 1–3 cycles
    - *Short time curves* are 20% of the normal curve (in time)
    - *Long time curves* are ten times the normal

23.1.10 Capacitor Fusing

1. Purpose of fusing:
    a. To isolate faulted bank from system
    b. To protect against bursting

c. To give indication
d. To allow manual switching (fuse control)
e. To isolate faulted capacitor from bank

2. Recommended rating:
   a. The continuous-current capability of the fuse should be at least 165% of the normal capacitor bank (for delta and floating wye banks the factor may be reduced to 150% if necessary).
   b. The total clearing characteristics of the fuse link must be coordinated with the capacitor "case bursting" curves.
3. Tests have shown that expulsion fuse links will not satisfactorily protect against violent rupture where the fault current through the capacitor is greater than 5000 A.
4. The capacitor bank may be connected in a floating wye to limit short-circuit current to less than 5000 A.
5. *Inrush*—for a single bank, the inrush current is always less than the short-circuit value at the bank location.
6. *Inrush*—for parallel banks, the inrush current is always much greater than for a single bank.
7. *Expulsion fuses* offer the following advantages:
   a. They are inexpensive and easily replaced
   b. They offer a positive indication of operation
8. *CLFs* are used where:
   a. a high available short circuit exceeds the expulsion or non-vented fuse rating.
   b. a CLF is needed to limit the high energy discharge from adjacent parallel capacitors effectively.
   c. a non-venting fuse is needed in an enclosure.
9. The fuse link rating should be such that the link will melt in 300 s at 240–350% of normal load current.
10. The fuse link rating should be such that it melts in 1 s at not over 220 A and in 0.015 s at not over 1700 A.
11. The fuse rating must be chosen through the use of melting time–current characteristic curves, because fuse links of the same rating, but of different types and makes have a wide variation in the melting time at 300 s and at high currents.
12. *Safe zone*—usually greater damage than a slight swelling.
    a. *Zone* 1—suitable for locations where case rupture or fluid leakage would present no hazard.
    b. *Zone* 2—suitable for locations that have been chosen after careful consideration of possible consequences associated with violent case ruptures.
    c. *Hazardous zone*—unsafe for most applications. The case will often rupture with sufficient violence to damage adjacent units.
13. Manufacturers normally recommend that the group fuse size be limited by the 50% probability curve or the upper boundary of Zone 1.
14. Short-circuit current in an open wye bank is limited to approximately three times the normal current.
15. CLFs can be used for delta or grounded wye banks, provided there is sufficient short-circuit current to melt the fuse within $\frac{1}{2}$ cycle.

23.1.11 Conductor Burndown

Conductor burndown is a function of (i) conductor size, (ii) whether the wire is bare or covered, (iii) the magnitude of the fault current, (iv) climatic conditions such as wind, and (v) the duration of the fault current.

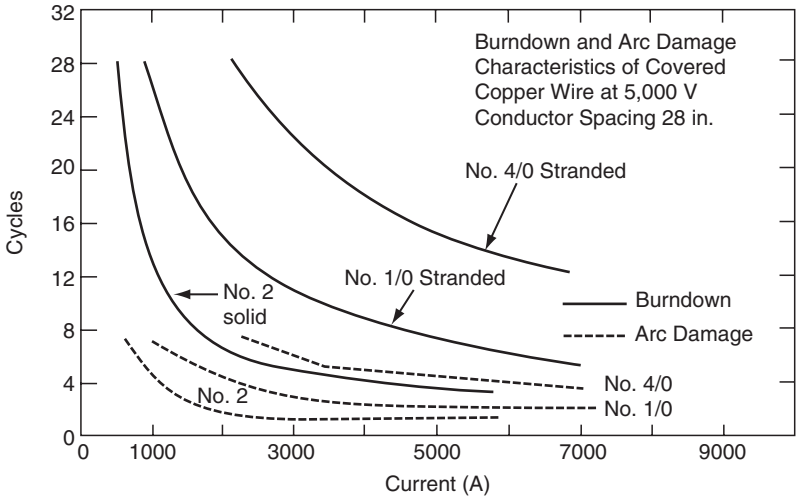

FIGURE 23.9 Burndown characteristics of several weatherproof conductors.

If burndown is less of a problem today than in years past, it must be attributed to the trend of using heavier conductors and a lesser use of covered conductors. However, extensive outages and hazards to life and property still occur as the result of primary lines being burned down by flashover, tree branches falling on lines, etc. Insulated conductors, which are used less and less, anchor the arc at one point and thus are the most susceptible to being burned down. With bare conductors, except on multi-grounded neutral circuits, the motoring action of the current flux of an arc always tends to propel the arc along the line away from the power source until the arc elongates sufficiently to automatically extinguish itself. However, if the arc encounters some insulated object, the arc will stop traveling and may cause line burndown.

With tree branches falling on bare conductors, the arc may travel away and clear itself; however, the arc will generally reestablish itself at the original point and continue this procedure until the line burns down or the branch falls off the line. Limbs of soft spongy wood are more likely to burn clear than hard wood. However ½-in. diameter branches of any wood, which cause a flashover, are apt to burn the lines down unless the fault is cleared quickly enough.

Figure 23.9 shows the burndown characteristics of several weatherproof conductors. Arc damage curves are given as arc is extended by traveling along the phase wire; it is extinguished but may be reestablished across the original path. Generally, the neutral wire is burned down.

23.1.12 Protective Device Numbers

The devices in the switching equipment are referred to by numbers, with appropriate suffix letters (when necessary), according to the functions they perform. These numbers are based on a system that has been adopted as standard for automatic switchgear by the American Standards Association (Table 23.1).

23.1.13 Protection Abbreviations

CS—Control switch
X—Auxiliary relay
Y—Auxiliary relay
YY—Auxiliary relay
Z—Auxiliary relay

TABLE 23.1 Protective Device Numbers

Device No.	Function and Definition
11	*Control power transformer* is a transformer that serves as the source of AC control power for operating AC devices.
24	*Bus-tie circuit breaker* serves to connect buses or bus sections together.
27	*AC undervoltage relay* is one which functions on a given value of single-phase AC under voltage.
43	*Transfer device* is a manually operated device that transfers the control circuit to modify the plan of operation of the switching equipment or of some of the devices.
50	*Short-circuit selective relay* is one which functions instantaneously on an excessive value of current.
51	*AC overcurrent relay* (inverse time) is one which functions when the current in an AC circuit exceeds a given value.
52	*AC circuit breaker* is one whose principal function is usually to interrupt short-circuit or fault currents.
64	*Ground protective relay* is one which functions on failure of the insulation of a machine, transformer, or other apparatus to ground. This function is, however, not applied to devices 51N and 67N connected in the residual or secondary neutral circuit of current transformers.
67	*AC power directional or AC power directional overcurrent relay* is one which functions on a desired value of power flow in a given direction or on a desired value of overcurrent with AC power flow in a given direction.
78	*Phase–angle measuring relay* is one which functions at a predetermined phase angle between voltage and current.
87	*Differential current relay* is a fault-detecting relay that functions on a differential current of a given percentage or amount.

1. To denote the location of the main device in the circuit or the type of circuit in which the device is used or with which it is associated, or otherwise identify its application in the circuit or equipment, the following are used:
   N—Neutral
   SI—Seal-in
2. To denote parts of the main device, the following are used:
   H—High set unit of relay
   L—Low set unit of relay
   OC—Operating coil
   RC—Restraining coil
   TC—Trip coil
3. To denote parts of the main device such as auxiliary contacts that move as part of the main device and are not actuated by external means. These auxiliary switches are designated as follows:
   "a"—closed when main device is in energized or operated position
   "b"—closed when main device is in de-energized or non-operated position
4. To indicate special features, characteristics, the conditions when the contacts operate, or are made operative or placed in the circuit, the following are used:
   A—Automatic
   ER—Electrically reset
   HR—Hand rest
   M—Manual
   TDC—Time-delay closing
   TDDO—Time-delay dropping out
   TDO—Time-delay opening

To prevent any possible conflict, one letter or combination of letters has only one meaning on individual equipment. Any other words beginning with the same letter are written out in full each time, or some other distinctive abbreviation is used.

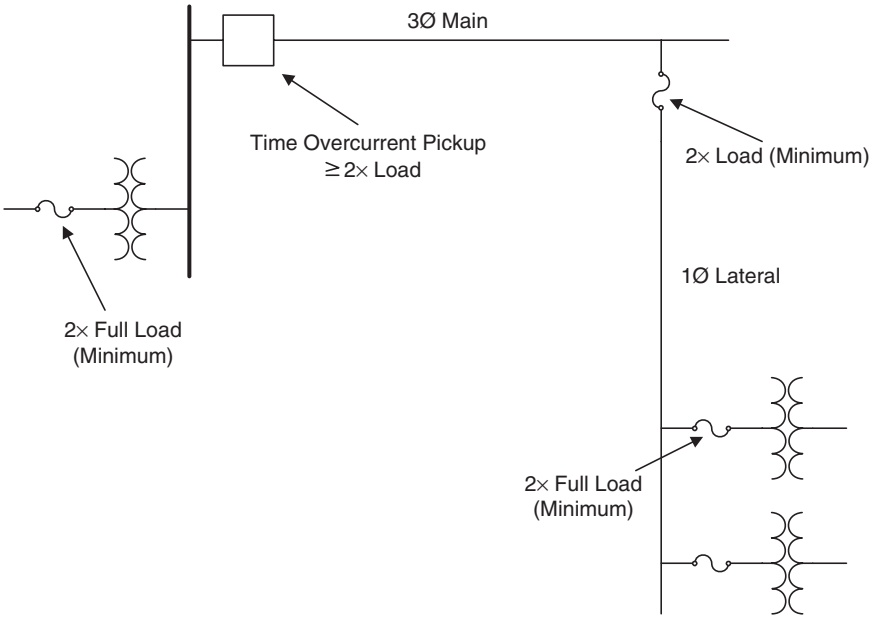

FIGURE 23.10 Burke 2× rule.

23.1.14 Simple Coordination Rules

There are few things more confusing in distribution engineering than trying to find out rules of overcurrent coordination, i.e., what size fuse to pick or where to set a relay, etc. The patented (*just kidding*) Burke 2× rule states that when in doubt, pick a device of twice the rating of what it is you are trying to protect as shown in Fig. 23.10. This rule picks the minimum value you should normally consider and is generally as good as any of the much more complicated approaches you might see. For various reasons, you might want to go higher than this, which is usually okay. To go lower, you will generally get into trouble. One exception to this rule is the fusing of capacitors where minimum size fusing is important to prevent case rupture.

23.1.15 Lightning Characteristics

1. Stroke currents
   a. Maximum—220,000 A
   b. Minimum—200 A
   c. Average—10,000–15,000 A
2. Rise times—1–100 μs
3. Lightning polarity—approximately 95% are negative
4. Annual variability (Empire State Building)
   a. Maximum number of hits—50
   b. Average—21
   c. Minimum—3
5. Direct strokes to T line—one per mile per year with keraunic levels between 30 and 65
6. Lightning discharge currents in distribution arresters on primary distribution lines (composite of urban and rural)
   Maximum measured to date—approximately 40,000 A
   1% of records at least 22,000 A

TABLE 23.2 Lightning Discharge Current vs. Location

Col. 1 Urban Circuits (%)	Col. 2 Semi-urban Circuits (%)	Col. 3 Rural Circuits (%)	Col. 4 Discharge Currents (A)
20	35	45	1,000
1.6	7	12	5,000
0.55	3.5	6	10,000
0.12	0.9	2.4	20,000
		0.4	40,000

5% of records at least 10,500 A
10% of records at least 6,000 A
50% of records at least 1,500 A

7. Percent of distribution arresters receiving lightning currents at least as high as in Col. 4 in Table 23.2.
8. Number of distribution arrester operations per year (excluding repeated operations on multiple strokes):
   a. Average on different systems—0.5 to 1.1 per year
   b. Maximum recorded—6 per year
   c. Maximum number of successive operations of one arrester during one multiple lightning stroke—12 operations

23.1.16 Arc Impedance

Although arcs are quite variable, a commonly accepted value for currents between 70 and 20,000 A has been an arc drop of 440 V/ft, essentially independent of current magnitude:

$Z_{arc} = 440l/I$ l = length of arc (in feet) I = current

Assume:

$I_F = 5000$ A $= I$

Arc length = 2 ft.

$Z_{arc} = 440 \times (2/5000) = 0.176\ \Omega$ $\therefore$ Arc impedance is pretty small.

Let us say you have a 120 V secondary fault and the distance between the phase and neutral is 1 ft. If the current level was 500 A then the arc resistance would be $(440 \times 1)/500 = 0.88\ \Omega$, which is significant in its effect on fault levels.

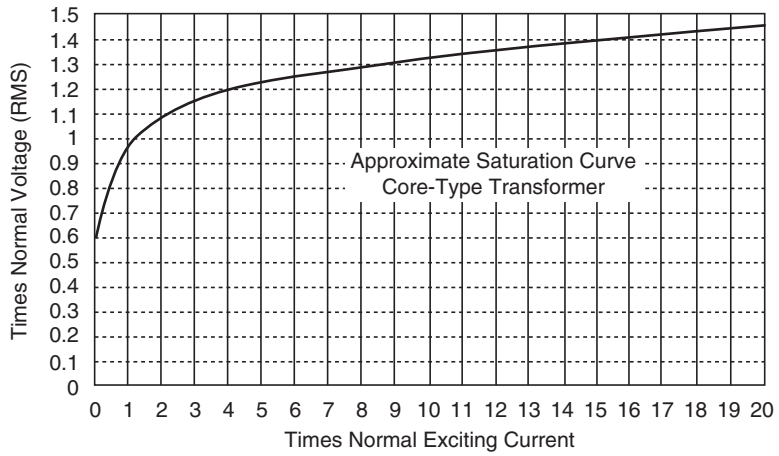

FIGURE 23.11 Transformer saturation curve.

TABLE 23.3 Insulation Levels for Transformer Windings and Bushings

Insulation Class and Nominal Bushing Rating kV	Low-frequency Dielectric Tests kV	Windings: Impulse Tests (1.2 × 50 Wave): Chopped Wave: Minimum Time to Flashover: kV	Windings: Impulse Tests (1.2 × 50 Wave): Chopped Wave: Minimum Time to Flashover: μs	Windings: Impulse Tests (1.2 × 50 Wave): Full Wave kV	Bushings: Bushing Withstand Voltages: 60-cycle 1-min Dry kV (Rms)	Bushings: Bushing Withstand Voltages: 60-cycle 10-s Wet kV (Rms)	Bushings: Bushing Withstand Voltages: Impulse 1.2 × 50 Wave kV (Crest)
1.2	10	36	1.0	10	10	6	30
5.0	19	69	1.5	60	21	20	60
8.66	26	88	1.6	75	27	24	75
15.0	34	110	1.8	95	35	30	95
25.0	40	145	1.9	125	70	60	150
34.5	70	175	3.0	150	95	95	200
46.0	95	290	3.0	250	120	120	250
69.0	140	400	3.0	350	175	175	350

23.2 Transformers

23.2.1 Saturation Curve

See Figure 23.11.

23.2.2 Insulation Levels

Table 23.3 gives the American standard test levels for insulation of distribution transformers.

23.2.3 Δ-Y Transformer Banks

Figure 23.12 is a review of fault current magnitudes for various secondary faults on a Δ-Y transformer bank connection.

23.2.3.1 Transformer Loading

When the transformer is overloaded, the high temperature decreases the mechanical strength and increases the brittleness of the fibrous insulation. Even though the insulation strength of the unit may not be seriously decreased, transformer failure rate increases due to this mechanical brittleness.

- Insulation life of the transformer is where it loses 50% of its tensile strength. A transformer may continue beyond its predicted life if it is not disturbed by short-circuit forces, etc.
- The temperature of top oil should never exceed 100°C for power transformers with a 55° average winding rise insulation system. Oil overflow or excessive pressure could result.
- The temperature of top oil should not exceed 110°C for those with a 65°C average winding rise.
- Hotspot should not exceed 150°C for 55°C systems and 180°C for 65°C systems. Exceeding these temperature could result in free bubbles that could weaken dielectric strength.
- Peak short duration loading should never exceed 200%.
- Standards recommend that the transformer should be operated for normal life expectancy. In the event of an emergency, a 2.5% loss of life per day for a transformer may be acceptable.
- Percent Daily Load for Normal Life Expectancy with 30°C Cooling Air (see Table 23.4).

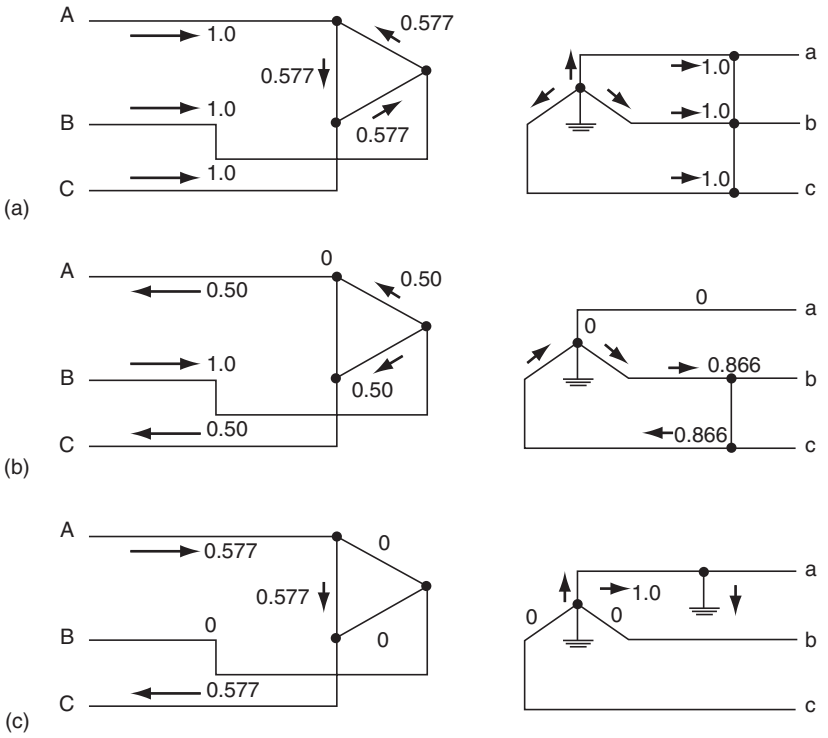

FIGURE 23.12 Δ-Y transformer banks.

TABLE 23.4 Distribution Transformer Overload with Normal Loss of Life

Duration of Peak Load (Hours)	Self-cooled with % Load before Peak of:		
	50	70	90
0.5	189	178	164
1	158	149	139
2	137	132	124
4	119	117	113
8	108	107	106

23.3 Instrument Transformers

23.3.1 Two Types

1. Potential (usually 120 V secondary)
2. Current (5 A secondary at rated primary current)

23.3.2 Accuracy

Three factors will influence accuracy:

1. Design and construction of transducer
2. Circuit conditions (*V*, *I*, and *f*)
3. Burden (in general, the higher the burden, the greater the error)

23.3.3 Potential Transformers

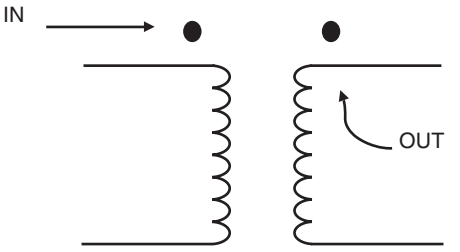

$$\text{Ratio correction factor (RCF)} = \frac{\text{true ratio}}{\text{marked ratio}} \quad (\text{RCF generally} > 1)$$

$$\text{Burden is measured in VA} \quad \therefore \text{VA} = \frac{E^2}{Z_b}$$

Assume

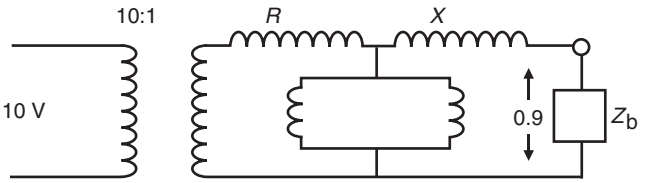

$$\text{True ratio} = \frac{10}{0.9} = 11.1$$

$$\Rightarrow \text{RCF} = \frac{11.1}{10} = 1.11$$

$$\text{Marked ratio} = \frac{10}{1} = 10$$

Voltage at secondary is low and must be compensated by 11% to get the actual primary voltage using the marked ratio.

23.3.4 Current Transformer

$$\text{True ratio} = \text{marked ratio} \times \text{RCF}$$

$$\therefore \text{RCF} = \frac{\text{true ratio}}{\text{marked ratio}}$$

23.3.5 H-Class

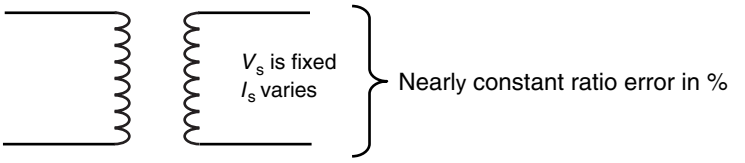

Burdens are in series
e.g., 10H200 $\Rightarrow$ 10% error at 200 V

$\therefore$ 20 (5 As) = 100 A $\Rightarrow Z_b = 200/100 = 2\ \Omega$

$\Rightarrow$ 5 A to 100 A has $\leq$ 10% error if $Z_b = 4\ \Omega$
or

If $Z_b = 4\ \Omega$

200 V/4 Ω = 50 A (ten times normal)

H-class—constant magnitude error (variable %)
L-class—constant % error (variable magnitude)

Example

True ratio = marked ratio $\times$ RCF
Assume marked is 600/5 or 120:1 at rated amps and 2 Ω

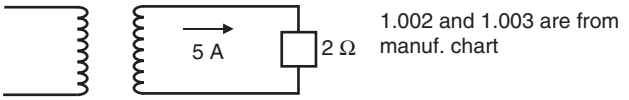

At 100% A true = 120 $\times$ 1.002 $\times$ 5 secondary
primary = 600 $\times$ 1.002 = 601.2
At 20% A true = 600 $\times$ 0.2 $\times$ 1.003 = 120.36 (marked was 120)

23.3.6 Current Transformer Facts

1. Bushing current transformers (BCTs) tend to be accurate more on high currents (due to large core and less saturation) than other types.
2. At low currents, BCTs are less accurate due to their larger exciting currents.
3. Rarely, if ever, it is necessary to determine the phase–angle error.
4. Accuracy calculations need to be made only for three-phase and single-phase to ground faults.
5. CT burden decreases as secondary current increases, because of saturation in the magnetic circuits of relays and other devices. At high saturation, the impedance approaches the DC resistance.
6. It is usually sufficiently accurate to add series burden impedance arithmetically.
7. The reactance of a tapped coil varies as the square of the coil turns, and the resistance varies approximately as the turns.
8. Impedance varies as the square of the pickup current.
9. Burden impedances are always connected in wye.
10. "Ratio correction factor" is defined as that factor by which the marked ratio of a current transformer must be multiplied to obtain the true ratio. These curves are considered standard application data.
11. The secondary-excitation-curve method of accuracy determination does not lend itself to general use except for bushing-type, or other, CTs with completely distributed secondary leakage, for which the secondary leakage reactance is so small that it may be assumed to be zero.
12. The curve of rms terminal voltage vs. rms secondary current is approximately the secondary-excitation curve for the test frequency.
13. ASA accuracy classification:
    a. This method assumes CT is supplying 20 times its rated secondary current to its burden.
    b. The CT is classified on the basis of the maximum rms value of voltage that it can maintain at its secondary terminals without its ratio error exceeding a specified amount.

c. "H" stands for high internal secondary impedance.
d. "L" stands for low internal secondary impedance (bushing type).
e. 10H800 means the ratio error is 10% at 20 times rated voltage with a maximum secondary voltage of 800 and high internal secondary impedance.
f. Burden (max)—maximum specified voltage/20 × rated second.
g. The higher the number after the letter, the better the CT.
h. A given 1200/5 bushing CT with 240 secondary turns is classified as 10L400: if a 120-turn completely distributed tap is used, then the applicable classification is 10L200.
i. For the same voltage and error classifications, the H transformer is better than the L for currents up to 20 times rated.

23.3.7 Glossary of Transducer Terms

Voltage transformers—They are used whenever the line voltage exceeds 480 V or whatever lower voltage may be established by the user as a safe voltage limit. They are usually rated on a basis of 120 V secondary voltage and used to reduce primary voltage to usable levels for transformer-rated meters.

Current transformers—Current transformers are usually rated on a basis of 5 A secondary current and used to reduce primary current to usable levels for transformer-rated meters and to insulate and isolate meters from high-voltage circuits.

Current transformer ratio—Current transformer ratio is the ratio of primary to secondary current. For current transformer rated 200:5, the ratio is 200:5 or 40:1.

Voltage transformer ratio—Voltage transformer ratio is the ratio of primary to secondary voltage. For voltage transformer rated 480:120, the ratio is 4:1, 7200:120, or 60:1.

Transformer ratio (TR)—Transformer ratio is the total ratio of current and voltage transformers. For 200:5 CT and 480:120 PT, TR = 40 × 4 = 160.

Weatherability—Transformers are rated as indoor or outdoor, depending on construction (including hardware).

Accuracy classification—Accuracy classification is the accuracy of an instrument transformer at specified burdens. The number used to indicate accuracy is the maximum allowable error of the transformer for specified burdens. For example, 0.3 accuracy class means the maximum error will not exceed 0.3% at stated burdens.

Rated burden—Rated burden is the load that may be imposed on the transformer secondaries by associated meter coils, leads, and other connected devices without causing an error greater than the stated accuracy classification.

Current transformer burdens—Current transformer burdens are normally expressed in ohms impedance such as B-0.1, B-0.2, B-0.5, B-0.9, or B-1.8.Corresponding volt–ampere values are 2.5, 5.0, 12.5, 22.5, and 45.

Voltage transformer burdens—Voltage transformer burdens are normally expressed as volt–amperes at a designated power factor. May be W, X, M, Y, or Z where W is 12.5 VA at 0.10 pf, X is 25 VA at 0.70 pf, M is 35 VA at 0.20 pf, Y is 75 VA at 0.85 pf, and Z is 200 VA at 0.85 pf. The complete expression for a current transformer accuracy classification might be 0.3 at B-0.1, B-0.2, and B-0.5, while the potential transformer might be 0.3 at W, X, M, and Y.

Continuous thermal rating factor (TRF)—Continuous TRF is normally designated for current transformers and is the factor by which the rated primary current is multiplied to obtain the maximum allowable primary current without exceeding temperature rise standards and accuracy requirements. For example, if a 400:5 CT has a TRF of 4.0, the CT will continuously accept 400 × 4 or 1600 primary amperes with 5 × 4 or 20 A from the secondary. The thermal burden rating of a voltage transformer shall be specified in terms of the maximum burden in volt–amperes that the transformer can carry at rated secondary voltage without exceeding a given temperature rise.

Rated insulation class—Rated insulation class denotes the nominal (line-to-line) voltage of the circuit on which it should be used. Associated Engineering Company has transformers rated for 600 V through 138 kV.

Polarity—The relative polarity of the primary and secondary windings of a current transformer is indicated by polarity marks (usually white circles), associated with one end of each winding. When current enters at the polarity end of the primary winding, a current in phase with it leaves the polarity end of the secondary winding. Representation of primary marks on wiring diagrams is shown as black squares.

Hazardous open circulating—The operation of CTs with the secondary winding open can result in a high voltage across the secondary terminals, which may be dangerous to personnel or equipment. Therefore, the secondary terminals should always be short circuited before a meter is removed from service. This may be done automatically with a bypass in the socket or by a test switch for A-base meters.

23.4 Loading

Probably no area of distribution engineering causes more confusion than does loading. Reading the standards does not seem to help much since everyone appears to have their own interpretation. Manufacturers of equipment are very conservative since they really never know how the user will actually put the product to use so they must expect the worst. On the other hand, many users seem to take the approach that since it did not fail last year with traditional overloading values, it will not fail this year either. In fact, it will not fail until after retirement. Heck! "Save a buck and get a promotion." The author of this document is not a psychology major and frankly has no idea of what the thinking was when much of the following was produced. The material that follows, however, was taken from sources with excellent reputation. Use it with caution.

23.4.1 Transformer Loading Basics

- All modern transformers have insulation systems designed for operation at 65°C average winding temperature and 80°C hottest-spot winding rise over ambient in an average ambient of 30°C. This means:
  - 65°C average winding rise + 30°C ambient = 95°C average winding temperature
  - 80°C hottest-spot rise + 30°C ambient = 110°C hottest spot

(Old system: 55°C winding rise + 30°C ambient = 85°C average winding temperature)
  - 65°C hotttest spot + 30°C ambient = 95°C hottest spot
- Notice that 95°C is the average winding temperature for the new insulation system and the hottest spot for the old—A source of immense confusion for many of us.
- The temperature of the top oil should not exceed 100°C. Obviously, top-oil temperature is always less than hottest spot.
- The maximum hotspot temperature should not exceed 150°C for a 55°C rise transformer or 180°C for a 65°C rise transformer.
- Peak 0.5 h loading should not exceed 200%.
- The conditions of 30°C ambient temperature and 100% load factor establish the basis of transformer ratings.
- The ability of the transformer to carry more than nameplate rating under certain conditions without exceeding 95°C is basically due to the fact that top-oil temperature does not instantaneously follow changes in transformer load due to thermal storage.

- An average loss of life of 1% per year (or 5% in any emergency) incurred during emergency operations is considered reasonable.
- Most companies do not allow normal daily peaks to exceed the permissible load for normal life expectancy.
- The firm capacity is usually the load that the substation can carry with one supply line or one transformer out of service.
- "Emergency 24-h firm capacity" usually means a loss of life of 1% but is sometimes as much as 5% or 6%.
- The following measures can be used for emergency conditions lasting more than 24 h:
  - Portable fans
  - Water spray
  - Interconnect cooling equipment of FOA units
  - Use transformer thermal relays to drop certain loads

23.4.2 Examples of Substation Transformer Loading Limits

The following is an example of maximum temperature limits via the IEEE for a 65°C rise transformer:

	IEEE Normal Life Expectancy
Top-oil temperature	105°C
Hotspot temperature	120°C

This next example shows the loading practice of various utilities for substation transformers:

	Utility A	Utility B	Utility C	Utility D	Utility E	Utility F	Utility G
Normal Conditions							
Top-oil	95	110	95	95	95	110	110
Hotspot	125	130	120	110	120	140	120
Emergency Conditions							
Top-oil	110	110	110	110	110	110	110
Hotspot	140	140	140	130	140	140	140

What happens when the hotspot is raised from 125°C to 130°C? This is shown as follows:

Maximum Hotspot (°C)	% Loss of Life, Annual
125	0.3366
130	0.5372

An example of the effect of load cycle (3-h peak with 70% pre-load for 13 h and 45% load for 8 h) and ambient on transformer capability via the ANSI guide is shown below:

	Peak Load for Normal Life Expectancy		Emergency Peak Load with 24-h Loss of Life	
Transformer Type	10°C Ambient	30°C Ambient	0.25%	1.0%
20,000—OA	30,000	24,200	28,400	32,000
15,000/2,000—OA/FA	28,700	23,800	27,500	30,700
12,000/16,000/ 20,000—OA/FA/FOA	27,500	23,200	26,800	29,700
20,000—FOA	27,500	23,200	26,800	29,700

The following is the effect on transformer ratings for various limits of top-oil temperature:

	MVA	Top-Oil Temperature (°C)
Normal rating	50	95
New rating	55	105
Emergency rating	59	110

23.4.3 Distribution Transformers

The loading of distribution transformers varies more widely than substation units. Some utilities try to never exceed the loading of the transformer nameplate. Others, particularly those using TLM, greatly overload smaller distribution transformers with no apparent increase in failure rates. An example of one utilities practice is as follows:

	Padmounted		Submersible	
kVA	Install Range	Removal Point	Install Range	Removal Point
25	0–40	55	0–34	42
50	41–69	88	35–64	79
75	70–105	122	65–112	112
100	106–139	139	113–141	141

23.4.4 Ampacity of Overhead Conductors

The table below shows the rating of conductors via a typical utility:

	ACSR		All Aluminum	
Conductor Size	Normal	Emergency	Normal	Emergency
1/0	319	331	318	334
2/0	365	379	369	388
3/0	420	435	528	450
4/0	479	496	497	523
267	612	641	576	606
336	711	745	671	705
397	791	830	747	786

23.4.5 Emergency Ratings of Equipment

The following are some typical 2-h overload ratings of various substation equipment. Use at your own risk:

Station transformer	140%
Current transformer	125%
Breakers	110%
Reactors	140%
Disconnects	110%
Regulators	150%

23.5 Miscellaneous Loading Information

The following are some miscellaneous loading information and thoughts from a number of actual utilities:

a. Commercial and industrial transformer loading

Load Factor (%)	Transformer Load Limit (%)
0–64	130
65–74	125
75–100	120

b. Demand factor
Lights—50%
Air conditioning—70%
Major appliances—40%

c. Transformer loading

- Distribution transformer life is in excess of five times the present guide levels.
- Distribution guide shows that life expectancy is about 500,000 h for 100°C hottest-spot operation, compared to 200,000 h for a power transformer. Same insulation system.
- Using present loading guides, only 2.5% of power transformer thermal life is used up after 15 years.
- Results of one analysis showed that the transition from acceptable to unacceptable risk (approximately an order of magnitude) was accompanied (by this utility) by only an 8.5% investment savings and a 12% increase in transformer loading.
- Application of transformers in *excess of normal loading* can cause the following:
  - Evolution of *free gas* from insulation of winding and lead conductors.
  - Evolution of free gas from insulation adjacent to metallic structural parts linked by magnetic flux produced by winding or lead currents may also reduce dielectric strength.
  - Operation at high temperatures will cause *reduced mechanical strength* of both conductor and structural insulation.
  - Thermal expansion of conductors, insulation materials, or structural parts at high temperature may result in permanent *deformations* that could contribute to mechanical or dielectric failures.
  - *Pressure buildup in bushings* for currents above rating could result in leaking gaskets, loss of oil, and ultimate dielectric failure.
  - *Increased resistance in the contacts* of tap changers can result from a buildup of oil decomposition products in a very localized high temperature region.
  - Reactors and current transformers are also at risk.
  - *Oil expansion* could become greater than the holding capacity of the tank.
- *Aging or deterioration of insulation* is a time function of temperature, moisture content, and oxygen content. With modern oil preservation systems, the moisture and oxygen contributions to insulation deterioration can be minimized, leaving insulation temperature as the controlling parameter.
- Distribution and power transformer model tests indicate that the *normal life expectancy* at a continuous hottest-spot temperature of 110°C is 20.55 years.
- Input into *a transformer loading program* should be as follows:
  - Transformer characteristics (loss ratio, top-oil rise, hottest-spot rise, total loss, gallons of oil, and weight of tank and fittings)
  - Ambient temperatures
  - Initial continuous load

- Peak load durations and the specified daily percent loss of life
- Repetitive 24-h load cycle if desired

- *Maximum permitted loading* is 200% for a power transformer and 300% for a distribution transformer.
- Suggested limits of *loading for distribution transformers* are as follows:
  - Top oil—120°C
  - Hottest spot—200°C
  - Short time (0.5 h)—300%
- Suggested *limits for power transformers* are as follows:
  - Top oil—100°C
  - Hottest spot—180°C
  - Maximum loading—200%
- Overload limits for *coordination of bushings* with transformers are as follows:
  - Ambient air—40°C maximum
  - Transformer top oil—110°C maximum
  - Maximum current—two times bushing rating
  - Bushing insulation hottest spot—150°C maximum
- Current ratings for the *load tap changer* (*LTC*) are:
  - Temperature rise limit of 20°C for any current carrying contact in oil when carrying 1.2 times the maximum rated current of the LTC
  - Capable of 40 breaking operations at twice the rate current and kVA
- Planned *loading beyond nameplate* rating defines a condition wherein a transformer is so loaded that its hottest-spot temperature is in the temperature range of 120–130°C.
- Long term *emergency loading* defines a condition wherein a power transformer is so loaded that its hottest-spot temperature is in the temperature range of 120–140°C.
- The *principal gases* found dissolved in the mineral oil of a transformer are as follows:
  - *Nitrogen*: from external atmosphere or from gas blanket over the free surface of the oil.
  - *Oxygen*: from external atmosphere.
  - *Water*: from moisture absorbed in cellulose insulation or from decomposition of the cellulose.
  - *Carbon dioxide*: from thermal decomposition of cellulose insulation.
  - *Carbon monoxide*: from thermal decomposition of cellulose insulation.
  - *Other gases*: may be present in very small amounts (e.g., acetylene) as a result of oil or insulation decomposition by overheated metal, partial discharge, arcing, etc. These are very important in any analysis of transformers, which may be in the process of failing.
- *Moisture* affects insulation strength, power factor, aging, losses, and the mechanical strength of the insulation. Bubbles can form at 140°C, which enhance the chances of partial discharge and the eventual breakdown of the insulation as they rise to the top of the insulation. If a transformer is to be overloaded, it is important to know the moisture content of the insulation, especially if it is an older transformer. Bubbles evolve fast, so temperature is important to bubble formation but not the time at that temperature. Transformer insulation with 3.5% moisture content should not be operated above nameplate for a hottest spot of 120°C. Tests have shown that the use of circulated oil for the drying process takes some time. For a processing time of 70 h the moisture content of the test transformers was reduced from 2% to 1.9% at a temperature of 50–75°C. Apparently only surface moisture was affected. A more effective method is to remove the oil and heat the insulation under vacuum.

24

Real-Time Control of Distributed Generation

Murat Dilek
Electrical Distribution Design, Inc.

Robert P. Broadwater
Virginia Polytechnic Institute and State University

Distributed generation (DG) can be operated to control voltages and power flows within the distribution system. Improvements in distribution system reliability and overall power system efficiency can be realized. For load growth with short-lived peaks that occur during extreme weather, DGs may provide lower-cost solutions than other approaches to system capacity upgrades.

DG provides a means for increasing the capacity of existing distribution facilities. When considering increasing distribution system capacity, DGs can be an alternative to new substation addition and replacing existing equipment with larger ones. A DG installed at the distribution level releases capacity throughout the system, from transmission through distribution. Transmission system losses are eliminated, and distribution system losses are reduced.

Some customer facilities have DGs that are installed for back-up power. These DGs are employed during grid-power outages or periods of high-cost grid power. They are operated for only a small fraction of time over the year. Moreover, back-up DGs are usually oversized, which means that they can provide more power than their facility loads need. These DGs can be equipped with a set of devices that will enable them to seamlessly interconnect to the grid and be dispatched if needed. The available capacity from such DGs can then be used for utility purposes.

DGs across many circuits in distribution areas can be controlled from a single control point. That is, such DGs can be aggregated into a block of generation and made available for transmission system use.

Although specifically intended for DGs, the aggregate control may also include other means of capacity release. When equipped with the necessary control and interconnection instrumentation, capacitors can be involved in aggregate control also. Some loads may also participate in the aggregation process in the form of curtailable or interruptible load. The aggregate control handles the collection of all of these participating entities.

The total power made available to the transmission system by the aggregate control is exhibited as a capacity release. That is, it is not the power injected into the transmission system from the distribution side, rather it is less power drawn by the distribution side. In the discussion to follow, the phrases DG power by aggregate control and capacity release by aggregate control are used interchangeably.

The aggregate control of DGs may serve a number of purposes. For instance, aggregated DGs can be activated if the transmission system or the distribution utility is having supply emergencies. Thus, DG aggregation provides a means to increase operating reserve. DGs can also help utilities manage energy purchases during times when the transmission grid electricity price is excessively high.

In the next section, local control for common DGs is discussed first. Next, controlling a group of DGs as an aggregate is addressed. Then, the DG as part of a hierarchical control system for controlling voltages and system power flows is investigated. Finally, load estimation for real-time DG control and also for forecasting aggregate control of DGs is presented.

24.1 Local Site DG Control

A DG operates basically in two modes in regard to being connected to the utility grid. In parallel mode, the DG remains connected to the grid. Hence, both the DG and the grid provide power for the local load in the customer facility (or DG site). In stand-alone (isolated or island) mode the DG is the sole power source to the local loads. In this section, consideration will be given only to DGs operating in parallel with the grid.

There are several forms of control for parallel DG. In one form of control, a local controller maintains a constant kW and kVar generation. In most cases, the local load is greater than the DG. Therefore, the power mismatch is supplied by the grid.

In another form of local control, the DG is controlled in order to maintain a constant power flow at the point of common coupling (PCC)—the point where the DG site interfaces with the grid, which is basically the metering point. The power flow maintained might be from the grid into the DG site (import) or from the site into the grid (export). As the local load varies, the local controller acts to change the kW and kVar generation at the DG in an attempt to keep the power flow constant at the PCC.

The most common DGs in service utilize synchronous machines. They prevail in grid-scale power exchanges between the utility and DG sites. Internal combustion (IC) engines and combustion turbines are the main prime movers for the synchronous generators. IC engines are much more common. Diesel fuel and natural gas are chosen for powering these engines.

The control of a synchronous machine is achieved by adjusting the fuel flow into the engine and the excitation of the generator. The fuel flow control by the governor determines the horsepower (kW) developed on the shaft of the engine. In a parallel DG, the shaft speed must be maintained very close to system frequency. The governor uses the kW set-point signal from the local controller and the speed signal from the DG output. The governor adjusts the fuel control to cause the kW output of the DG to match the kW set point that is set by the local controller.

The excitation control achieved by the voltage regulator determines terminal voltage and kVar output of the generator. Parallel DGs are required not to actively participate in regulating voltage at the PCC where the grid is supposed to set the voltage. Therefore, the excitation control is used to adjust kVar generation only. Rather than a kVar set point, a power factor (pf) set point is used for the excitation control. The local controller feeds the pf set point to the regulator. The regulator then adjusts the excitation to match the pf measured at the DG to the provided pf setting.

Basic functionality of the control system for parallel-connected DGs can be seen in Fig. 24.1. For simplicity, it is assumed that the customer facility has only one DG. The local control receives the desired kW and kVar generation set points from an upper-level controller. The strategy can be a constant kW and kVar generation level for the DG or a constant kW and kVar flow at the PCC. Based on the control strategy, the local controller sends the required set points to the controller of the DG. An operator can supervise the control process and intervene as needed.

24.2 Hierarchical Control: Real-Time Control

The hierarchical DG control consists of three levels and is illustrated in Fig. 24.2. The control functionality is used for two purposes: (1) for real-time DG control and (2) for forecasting future generation.

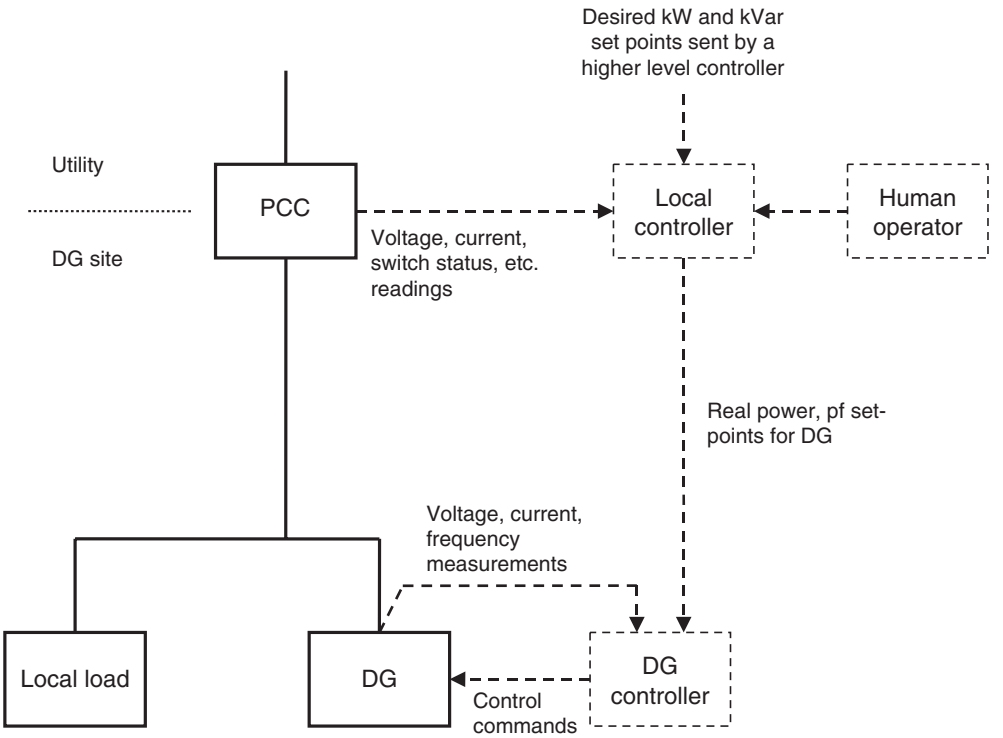

FIGURE 24.1 Block diagram for local control of a parallel DG at a customer site.

The aggregate control at level 3 shown in Fig. 24.2 groups DGs together from many distribution circuits within a distribution service area. The aggregate control talks to both a transmission system entity (let us refer to this entity as the independent system operator, ISO) at a higher level and the circuit controls below at level 2. Each circuit might have a number of DG sites from which the circuit can import power. Each such DG site has a local controller (level 1) that can handle the import/export processes as explained in the previous section.

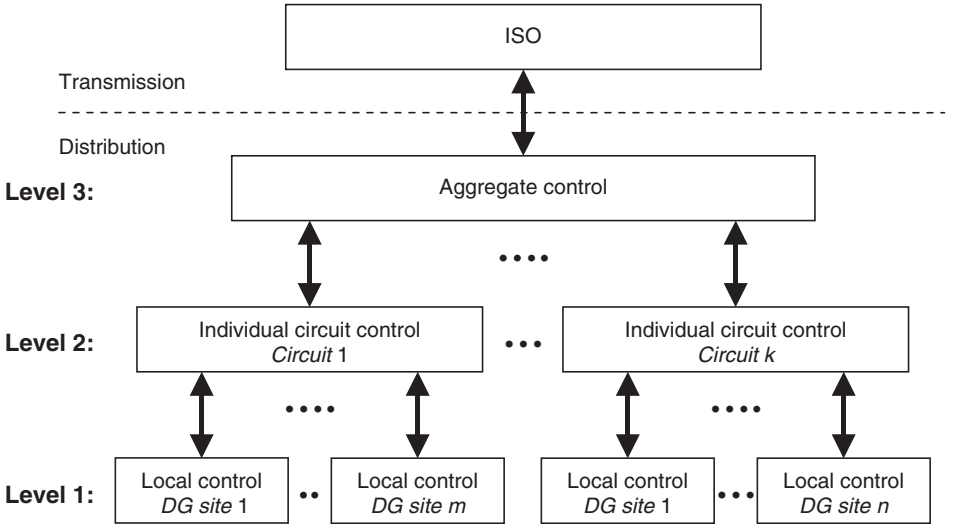

FIGURE 24.2 Hierarchical view of the control of aggregated DGs.

The challenge of DG control is to implement the control without having to install measurement or monitoring equipment throughout the many miles of the distribution circuits. Each circuit control at level 2 has a model of the corresponding circuit, which includes such data as any existing circuit measurements and historical load measurements. Given weather and circuit conditions, the circuit control can make use of the available circuit model to estimate the power flows rather than measure the flows via instrumentation that would have to be installed throughout the circuit. This will be discussed further.

In essence, the aggregate control evaluates the DG power present at its lower levels and informs the ISO about the DG power that can be made available for transmission system use. After some negotiations, the ISO informs the aggregate control of the power it needs. The aggregate control then talks to the circuit controls in an attempt to provide the requested power in the best way possible. Data traffic among the layers of the control hierarchy in Fig. 24.2 can be seen in Fig. 24.3. Note that in order to simplify the discussion only a partial view of the data flow is presented. The view shown considers one circuit and one DG site in that circuit. One can extend this view to understand the data flow for the general case where multiple circuits with multiple DGs would be involved.

The data flow will be examined from two perspectives: flow from lower to higher layers and flow from higher to lower layers. The nomenclature used in Fig. 24.3 is as follows:

Pdg-mr: must-run real power (kW) generation from DG site
Qdg-mr: must-run reactive power (kVar) generation from DG site
Pdg-sp: desired kW generation from DG site
Qdg-sp: desired kVar generation from DG site
Pckt-mr: must-run kW generation needed by circuit
Qckt-mr: must-run kVar generation needed by circuit
Pckt-max: maximum kW generation available from circuit
Qckt-max: maximum kVar generation available from circuit
Pckt-des: desired kW generation from circuit
Qckt-des: desired kVar generation from circuit
Ptot-mr: total must-run kW generation needed by all circuits
Qtot-mr: total must-run kVar generation needed by all circuits

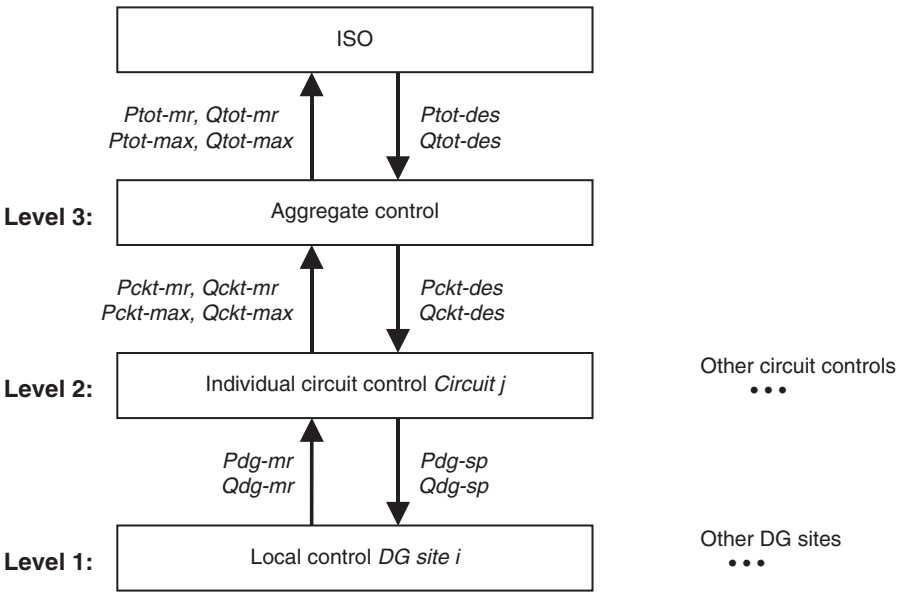

FIGURE 24.3 Data flow among ISO, aggregate controller, controller of a particular *Circuit j*, and controller of a particular *DG site i* in *Circuit j*.

Ptot-max: total kW generation available from all circuits
Qtot-max: total kVar generation available from all circuits
Ptot-des: total desired kW generation needed by ISO from aggregate DG control
Qtot-des: total desired kVar generation needed by ISO from aggregate DG control

24.2.1 Data Flow to Upper Layers

As mentioned earlier, level-2 circuit controllers have their corresponding circuit models, which are used to estimate power flows throughout the circuits. Given weather and circuit conditions such as voltage and current measurements taken at the start of circuit, the circuit controllers evaluate flows and voltages for the circuits. Consider for example *Circuit j* shown in level 2 in Fig. 24.3. The circuit controller of *Circuit j* examines voltages and loadings in the circuit. If there exist any circuit problems such as under-voltage or overloaded locations in the circuit, then the circuit controller attempts to use the controllable DGs in the circuit to eliminate the problems. If employing the DGs helps to solve the circuit problems, then the DG kW and kVar generation levels at which the problems disappear are recorded. Such generation quantities are labeled as "must run," which means that the circuit itself needs that DG for solving its own problems.

Consider *DG site i* at level 1 in Fig. 24.3. *Pdg-mr* and *Qdg-mr* represent the kW and kVar amounts that *DG site i* needs to produce in order to remove the problems that *Circuit j* will experience. *Pdg-mr* and *Qdg-mr* will be zero if no circuit problems occur when the *DG site i* produces no power.

Each circuit controller at level 2 sums up must-run generation. Each circuit controller also calculates the total available generation within the circuit. Must-run and maximum generation amounts are passed to the aggregate control at level 3. In Fig. 24.3, *Pckt-mr*, *Qckt-mr*, *Pckt-max,* and *Qckt-max* indicate must-run and maximum generations from *Circuit j*. Note that *Pckt-max* and *Qckt-max* may also include curtailable load and reactive power available from capacitors installed in *Circuit j*. The *Circuit j* controller at level 2 may also know the type and operating characteristics of the DGs. Therefore, *Pckt-max* and *Qckt-max* may actually be further subdivided into available base-load generation and available load-following generation.

The aggregate control at level 3 sums both the totals of must-run generation and the maximum available generation across the individual circuit controllers at level 2. These sums are communicated to the ISO, as indicated by *Ptot-mr*, *Qtot-mr*, *Ptot-max,* and *Qtot-max* in Fig. 24.3. Generation costs may also be communicated to the ISO, which is not considered here.

24.2.2 Data Flow to Lower Layers

The aggregate control negotiates with the ISO. When the negotiation is complete, the ISO informs the aggregate control of the total desired real and reactive generation. *Ptot-des* and *Qtot-des* in Fig. 24.3 indicate the kW and kVar amounts requested by the ISO, respectively.

The aggregate control takes the total amount of desired generation and divides it among the DGs in the circuits under its control. *Pckt-des* and *Qckt-des*, for instance, represent kW and kVar generation that the aggregate control allocates for *Circuit j* to provide. A circuit controller at level 2 addresses control for all DG sites located in the corresponding circuit. Each circuit controller determines the generation sharing among the individual generators, based upon economic and reliability considerations. Thus, kW and kVar generation levels for all DGs under a circuit are calculated and communicated to the corresponding local controllers at DG sites. These kW and kVar values become the set points for the generator controllers. For instance, *Pdg-sp* and *Qdg-sp* in Fig. 24.3 are the kW and kVar set points for the DG at *DG site i* in *Circuit j*.

24.3 Control of DGs at Circuit Level

Basic functions used in circuit-level control are depicted in Fig. 24.4. The direction of arrows in the figure is interpreted such that what is at the tail-side of an arrow is available for use by what is at the head

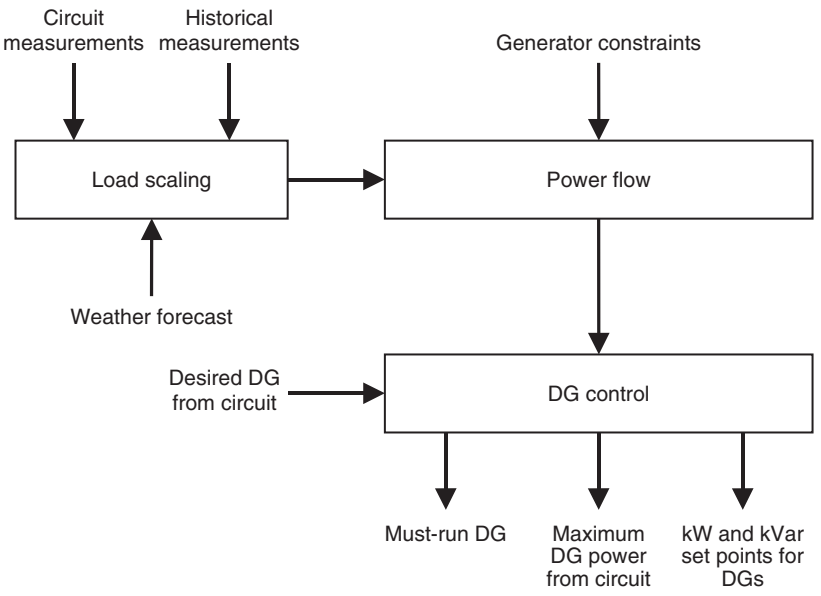

FIGURE 24.4 Level-2 DG control functions.

of the arrow. For instance, the arrow between *Power Flow* and *DG Control* indicates that *Power Flow* is used by the *DG Control* task. That is, *DG Control* can run *Power Flow* and obtain power flow results. Similarly, it can be seen that circuit measurements are made available for use in the load scaling.

All the functions shown in Fig. 24.4 share the same circuit model and circuit data. Exchange of results among these functions takes place through the common circuit model. The circuit model and data include the following:

- Topology information of the circuit
- Type, status, rating, configuration, impedance, and/or admittance of the components present in the circuit
- Location and class of loads connected throughout the circuit
- Historical load measurements
- Load research data for the various classes of loads

Typically, measurements are taken at a very limited number of locations such as at the start of the circuit and DG sites. Therefore, the main task is to use the circuit model and the available measurements to estimate the flows in the circuit. That is, the majority of flows are determined by calculations instead of measurements obtained via data acquisition systems.

The most common scenario concerning control is as follows. Real-time current and voltage measurements taken at the start of the circuit are fed into the circuit model. Real-time kW and kVar measurements taken at the DGs are also fed into the model. *Power Flow* then calculates voltages and currents throughout the circuit. Since the load data (location, class, historical measurements, and load research data such as load curves, coincidence, and diversity factors) are already available, *Power Flow* uses *Load Scaling* for matching the calculated flows to the measurements. *Load Scaling* adjusts the circuit loads until the calculated flows match the measured flows. This is thus an estimation process for the loads that result in the measured flows.

In case real-time circuit measurements are not available, historical measurements and weather data are used to estimate loading. From this information, the flows at the start of circuit can be estimated. Then the estimated flows are used as if they were measurements at the start of the circuit, and *Load Scaling* again adjusts load sizes so that the estimated and measured flows match.

Once the circuit flows are estimated, *DG Control* can check to see if there are any circuit problems such as overloaded equipment and/or locations with voltages below specified limits. If problems exist, *DG Control* runs power flow calculations and uses the controllable DGs to attempt to eliminate the problems. If the problems are removed, the generation levels required are referred to as must-run generation.

In another scenario, suppose that initially there are no problems in the circuit. However, the real-time kW and kVar DG measurements show that some DGs are running. In this case, *DG Control* tries reducing the generation to check if the no-problem condition can be obtained with less DG. If so, the reduced generation levels will be reported as must run.

Besides the must-run generation, *DG Control* also calculates the total power that can be dispatched by the circuit control. Circuit loading and generator constraints are used in this process. When DGs are dispatched, circuit losses and voltage profiles in the circuit are affected. Therefore, when looked at from the transmission side, the maximum power flow change that the DGs can achieve is greater than their rated capacities. The additional capacity achieved is due to reduced losses in the circuit and DG effects on circuit voltage profiles.

The explanation given in the preceding paragraphs is from the point of view of what happens in level 2 when data flows upward in the control hierarchy. The result of this flow is must-run generation levels and additional capacity release that can be provided for the transmission side. On the other hand, when the data flows downward from level 3, the aggregate control informs the circuit control of how much DG power is desired from the circuit. This desired power quantity is given as an input parameter to *DG Control* as shown in Fig. 24.4. *DG Control* then evaluates how the desired power can be realized from the participating DGs in the circuit. This is basically an assignment problem: How much power should each generator produce so that the desired total power can be obtained in the most effective way possible? Generator constraints, fuel costs, generator operating characteristics, circuit-loss effects, reliability effects, and other parameters can be considered in this assignment process. At the end, the settings for kW and kVar generation that need to be supplied from individual DG sites are determined and sent to local controllers.

24.3.1 Estimating Loading throughout Circuit

The control of the DGs at the circuit level constitutes a major computational element in the control hierarchy. As stated earlier, the control primarily uses estimates of circuit conditions rather than measurements. Estimating the loading of customers throughout the circuit model plays a central role in the success of the control. Because system load is usually monitored at only a few points in the circuit, determining circuit loads accurately is a challenging process. In general, load is monitored at substations, major system equipment locations, and major customer (load) sites. Besides such load data, the only load information commonly available is billing-cycle customer kilowatt-hour (kWh) consumptions. The estimation of load has features described next.

Historical load measurements: Historical load measurements consist of monthly kWh measurements or periodic (such as every 15-minute or hourly) kW/kVar measurements obtained at customer sites. These measurements are used in the estimation of loading at each customer site in the circuit model.

Load research statistics: With the help of electronic recorders, utilities can automatically gather hourly sample load data from diverse classes of customers. This raw data (load research data) is then analyzed to obtain load research statistics. The purpose of load research statistics is to convert kWh measurements to kW and kVar load estimates. Load research statistics consist of the following elements:

- *Kilowatt-hour parsing factors* are defined as a function of customer class. They represent the fractional annual energy use as a function of the day of the year. Thus, they vary from 0 to 1. They are used to split a kWh measurement made across monthly boundaries into estimates of how much of the measurement was used in each month.
- *kWh-to-peak-kW conversion coefficients* (referred to as C-factors) are used to convert kWh measurements for a customer to peak-kW estimates. The C-factor is calculated as a function of

class of customer, type of month, type of day, and weather condition. C-factor curves are typically parameterized by the customer class, type of day, and weather condition, and plotted against the month of year.

- *Diversity factors* are used to find the aggregated demand of a group of customers. It is defined as the ratio of the sum of individual noncoincident customer peaks in the group to the coincident peak demand of the group itself. The diversity factors are greater than unity. They are defined as function of class of customer, type of month, type of day, weather conditions, and number of customers. Diversity factor curves are typically parameterized by the customer class, type of day, type of month, and weather condition, and plotted against number of customers.
- *Diversified load curves* are parameterized by class of customer, type of month, type of day, and weather conditions. They show the expected energy use for each hour of the day. Diversified load curves may be used to estimate loading as a function of the hour of day. Diversified load curves may be normalized by dividing each point on the diversified load curve by the peak of the diversified curve itself.
- *Temperature/humidity load sensitivity coefficients* are defined as a function of class of customer. They are used to scale loads to take into account temperature/humidity load sensitivities. They are calculated by correlating load research data with the weather conditions that existed at the time the load research measurements were made.

Start-of-circuit measurements: Start-of-circuit measurements generally consist of voltage magnitude, current magnitude, and/or power flows. They are used to affect scaling of estimated loads throughout the distribution circuit model such that the power flow solution matches the start-of-circuit measurements.

Examples of load research statistics for a residential class of customer are shown in Figs. 24.5 through 24.9. Figure 24.5 illustrates a parsing-factor curve as a function of the day of the year. The parsing factor may be used together with monthly kWh measurements to estimate the energy usage between any two days of the year.

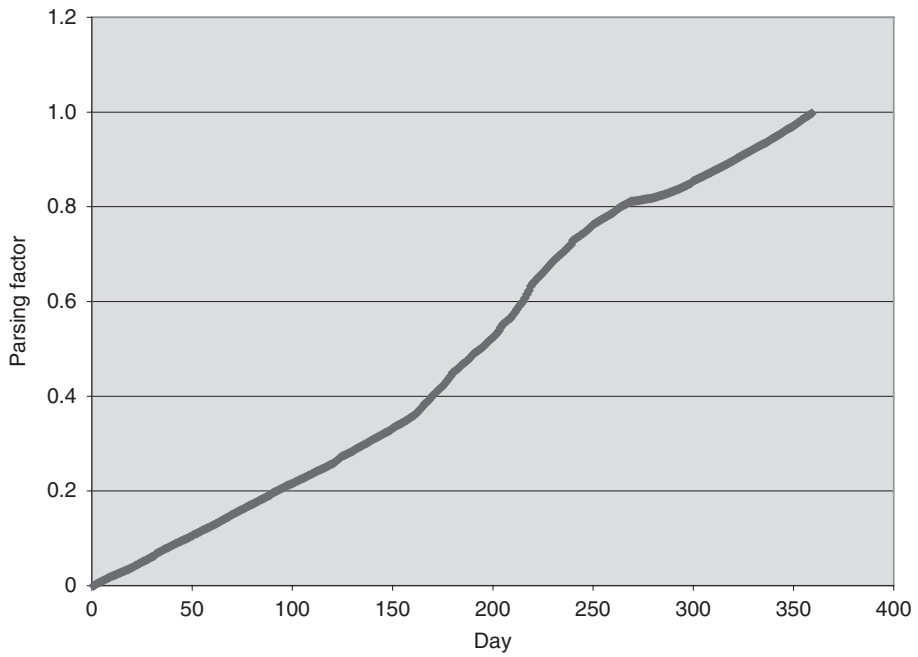

FIGURE 24.5 A representative parsing-factor curve for residential customer.

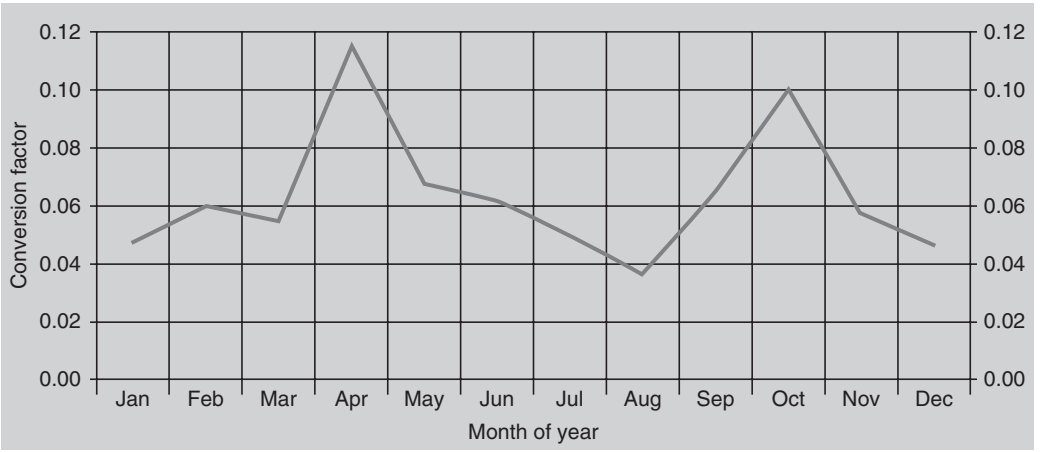

FIGURE 24.6 kWh-to-peak-kW conversion coefficients for residential class for weekdays at normal weather conditions.

Figure 24.6 illustrates a representative C-factor curve for residential customers for weekdays at typical weather conditions, where the C-factor is plotted as a function of month. Values read from this curve may be used to convert kWh measurements into kW-peak estimates for weekdays.

Figure 24.7 illustrates a diversified load curve for weekdays during February at normal temperatures as a function of hour of day.

Figure 24.8 illustrates a diversity factor curve for weekdays during February at normal temperatures as a function of the number of customers.

Figure 24.9 represents variation of load scaling factors for residential customers as a function of weather condition. Note that weather condition incorporates not only the temperature, but also other factors such as humidity and wind speed. Variations in these quantities are compounded into a single index.

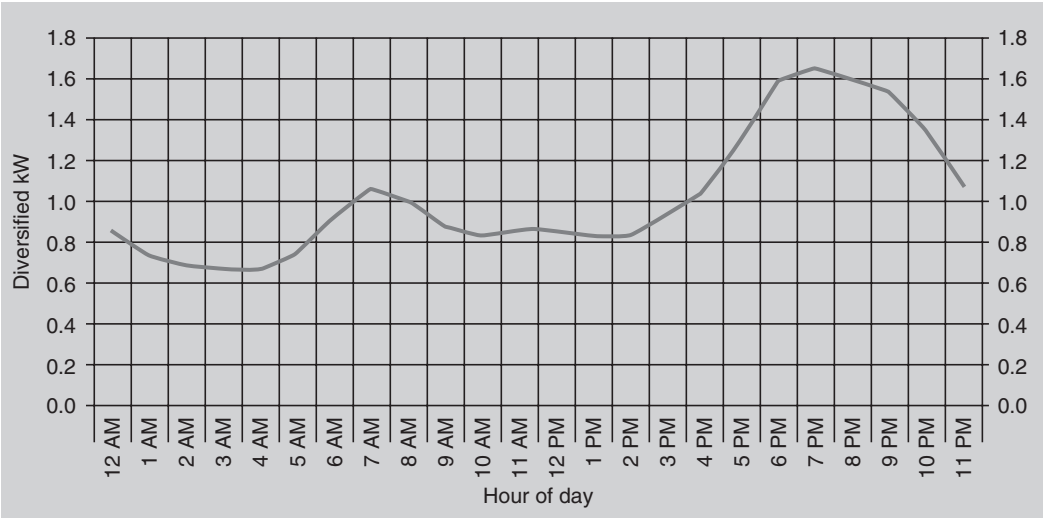

FIGURE 24.7 Diversified load curve for residential class for weekdays during February at normal weather conditions.

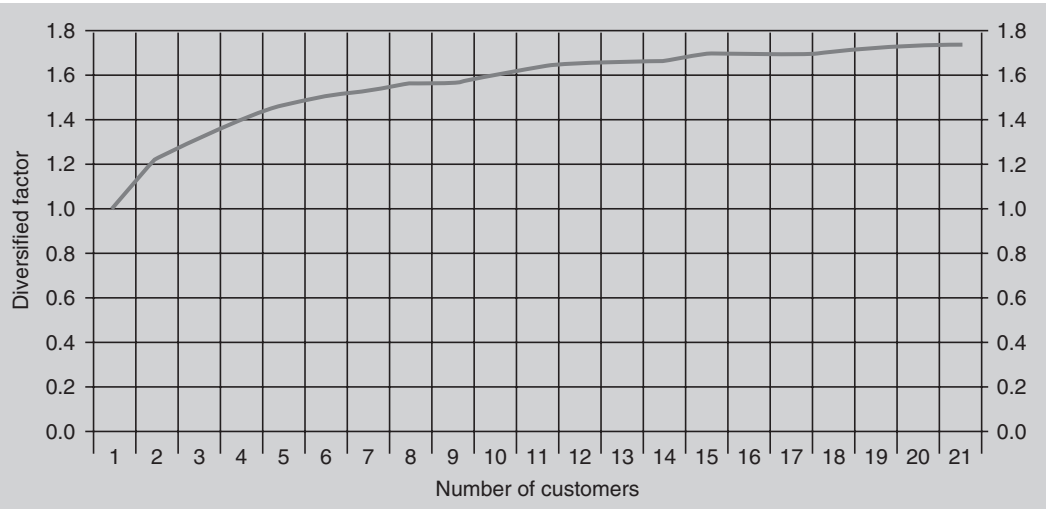

FIGURE 24.8 Diversity factor curve for residential class for weekdays during February at normal weather conditions.

As an example of calculating a load estimate at a point in a circuit, assume the following (where for simplicity, weather considerations have been neglected):

- Below the point selected, the circuit is radial.
- It is desired to estimate the peak-kW of the group of customers for a weekday in February. It is also desired to calculate the combined kW load of the two customers at 2 pm on a weekday in February.

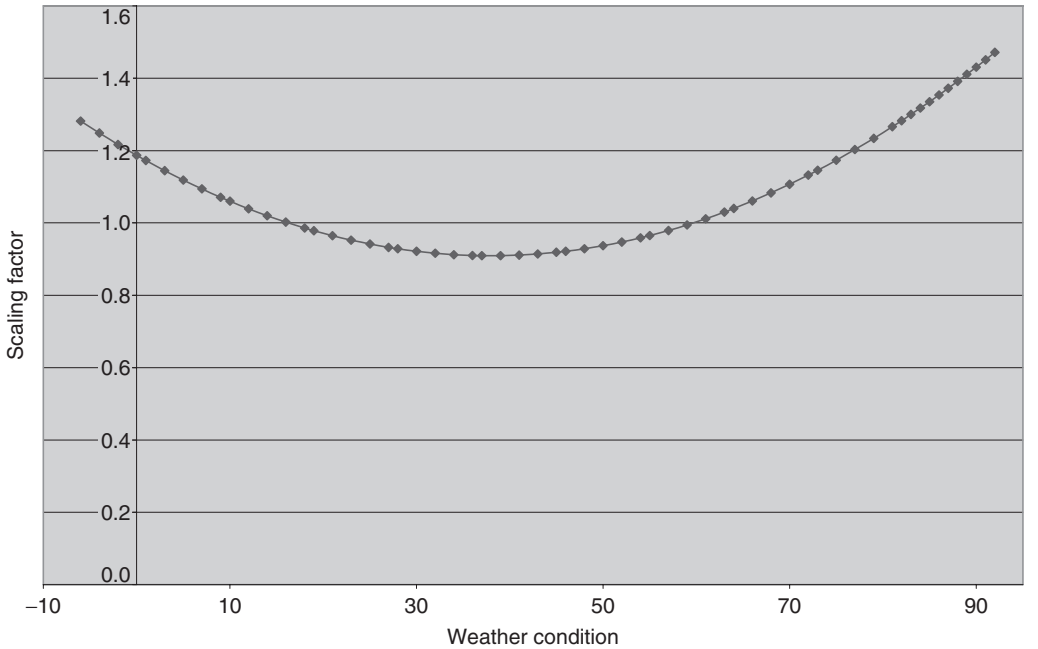

FIGURE 24.9 Representative variation of load scaling factors for residential customers as a function of weather condition.

- There are only two customers of the same load research class, say Class R, fed from the selected point.

Assume that each customer only has monthly kWh measurements as given by:

$KWH_{m1}(Jan18, Feb16)$ = Measured kWh usage of first customer between the dates January 18 and February 16.
$KWH_{m1}(Feb17, Mar17)$ = Measured kWh usage of first customer between the dates February 17 and March 17.
$KWH_{m2}(Jan20, Feb17)$ = Measured kWh usage of second customer between the dates January 20 and February 17.
$KWH_{m2}(Feb18, Mar19)$ = Measured kWh usage of second customer between the dates February 18 and March 19.

The first step is to estimate the energy usages of each customer during the month of February. Note that the recorded measurements do not directly reflect the February usages. Parsing factors provide the ability to estimate the February energy usage from the two measurements available.

Let $p(MonX)$ represent the parsing-factor value for customers of Class R for day X in month Mon. Then using the kWh measurements given above, the estimated kWh energy use of Customer 1 during February is calculated as follows:

$$KWH_{e1}(Feb1, Feb16) = KWH_{m1}(Jan18, Feb16)x\frac{p(Feb16) - p(Feb1)}{p(Feb16) - p(Jan18)}$$

$$KWH_{e1}(Feb17, Feb28) = KWH_{m1}(Feb17, Mar17)x\frac{p(Feb28) - p(Feb17)}{p(Mar17) - p(Feb17)}$$

$$KWH_{e1}(Feb) = KWH_{e1}(Feb1, Feb16) + KWH_{e1}(Feb17, Feb28)$$

where $KWH_{e1}(Feb)$ = Estimated kWh usage of Customer 1 during February.
$KWH_{e1}(Feb1, Feb16)$ = Estimated kWh usage of Customer 1 between February 1 and February 16.
$KWH_{e1}(Feb17, Feb28)$ = Estimated kWh usage of Customer 1 between February 17 and February 28.

A similar calculation can be performed to estimate the kWh usage of Customer 2 during February:

$$KWH_{e2}(Feb1, Feb17) = KWH_{m2}(Jan20, Feb17)x\frac{p(Feb17) - p(Feb1)}{p(Feb17) - p(Jan20)}$$

$$KWH_{e2}(Feb18, Feb28) = KWH_{m2}(Feb18, Mar19)x\frac{p(Feb28) - p(Feb18)}{p(Mar19) - p(Feb18)}$$

$$KWH_{e2}(Feb) = KWH_{e2}(Feb1, Feb17) + KWH_{e2}(Feb18, Feb28)$$

The next step is to estimate the peak kW demand by the two customers together. For this, we use the C-factors and diversity factors (d) from the load research statistics. Consider the following:

$C(weekday, Feb, R)$ = The kWh-to-peak-kW factor value for customers of Class R for weekdays during February.
$d(weekday, Feb, R, 2)$ = The diversity-factor value for two customers of Class R for weekdays during February.
$KW_{peak}(Sum)$ = Sum of the individual kW peaks (noncoincident peaks) for the two customers.
$KW_{peak}(Group)$ = The group peak (coincident peak) for the two customers.

Then,

$$KW_{\text{peak}}(Sum) = C(weekday, Feb, R) \times (KWH_{e1}(Feb) + KWH_{e2}(Feb))$$
$$KW_{\text{peak}}(Group) = KW_{\text{peak}}(Sum)/d(weekday, Feb, R, 2)$$

This is the first answer that was sought, which is the estimated peak of the group of customers on a weekday in February. The diversified load curve corresponding to the given conditions can be referred to for finding the time point (hour) of day at which the peak would occur. One can examine kW demands at any other time points, say at 2 pm, as well. The normalized diversified load curve is used for this purpose. The normalized curve has the maximum value of unity at its peak-kW time point. To estimate the load of the two customers at 2 pm on a weekday in February, let $k(2\ pm, weekday, Feb)$ be the normalized diversified load curve value for customers of Class R at 2 pm for weekdays during February. Then, the estimated load at 2 pm, $KW_e(Group, 2\ pm, weekday, Feb)$ is given by

$$KW_e(Group, 2pm, weekday, Feb) = k(2pm, weekday, Feb) \times KW_{\text{peak}}(Group)$$

24.3.2 Siting DGs for Improving Efficiency and Reliability

Along with voltage and power flow control, DGs can be placed within the distribution system for simultaneously improving efficiency and reliability. That is, there are many locations within a circuit from which a DG can implement some desired voltage or flow control, and of these many locations, the location that results in the optimum improvement in efficiency and/or reliability can be selected.

Within a system of circuits, the circuits can be reconfigured via switching operations and DG can be shifted from one circuit to another in order to implement some desired control. With such switching operations, the DG does not necessarily need to be operated as an island. That is, a DG that is connected to an unenergized circuit may be switched to an energized circuit, and then brought on line. Thus, a DG can be placed to serve a number of circuits, and can be looked at as increasing both efficiency and reliability for the system of circuits.

For a single circuit or a system of circuits, the DG site placement for best reliability is generally not the same as the placement for best efficiency. Percent changes in system reliability and efficiency can be used to determine desirable locations from a limited set of geographical locations where the DG may be placed.

To obtain good locations for efficiency and/or reliability improvements, exhaustive searches and/or optimization methods may be applied. The exhaustive search approach often works well because there are generally only a very limited number of physical sites for placing DGs. This is due to constraints placed on the siting from community impact and available land considerations.

The method that is used to site the DG should take into account the time-varying loading of the circuits involved. Placing a DG based upon just peak loading conditions will generally not result in the best reliability or efficiency when the entire time-varying load pattern is considered.

24.4 Hierarchical Control: Forecasting Generation

The load estimation discussed above is combined with a weather forecast and used to forecast system loading on an hourly basis. This load forecast is used to provide a generation schedule to the ISO, and is typically performed for the 24 hours of the next day. Forecasting the next day's generation uses functionality found in levels 2 and 3 of the hierarchical control shown in Fig. 24.2.

The load forecast is used to predict a schedule of must-run generation located in the distribution system. The forecast is also used to provide the ISO with the amount of base load and load following generation available at the distribution level. The amount of available generation is a function of the circuit loading. DGs provide the possibility of causing the power to flow from the distribution system to the transmission system. Since typical distribution systems are not designed to handle reverse power flows, including reverse fault currents, IEEE 1574 recommends that DGs be operated at a generation

level that is 25% or less of existing circuit loading. This is taken into account when calculating the maximum amount of generation available from the distribution system.

In the forecast, DG that is just for standby must be treated specially. The load that the standby generation serves is what must be reported to the ISO as a capacity release, and not the capability of the standby generation itself. Load research statistics coupled with the weather forecast are used to estimate the hourly variation of the load that is served by the standby generation. It is this release of load estimate that is then reported to the ISO.

References

Broadwater, R.P., Sargent, A., Yarali, A., Shaalan, H.E., and Nazarko, J., Estimating substation peaks from load research data, *IEEE Transactions on Power Delivery,* 12(1), 451–456, 1997.

Daley, J.M. and Siciliano, R.L., Application of emergency and standby generation for distributed generation. I. Concepts and hypotheses, *IEEE Transactions on Industry Applications*, 39(4), 1214–1225, 2003.

IEEE Std. 1547-2003, *Standard for Interconnecting Distributed Resources with Electric Power Systems.*

NREL SR-560-34779, *Aggregation of Distributed Generation Assets in New York State*, National Renewable Energy Laboratory (NREL), Colorado, 2004.

Sargent, A., Broadwater, R.P., Thompson, J.C., and Nazarko, J., Estimation of diversity and kWHR-to-peak-kW factors from load research data, *IEEE Transactions on Power Systems,* 9(3), 1450–1456, 1994.

Westinghouse Electric Cooperation, *Electric Utility Engineering Reference Book—Distribution Systems,* vol. 3, Westinghouse Electric Cooperation, East Pittsburg, PA, 1965.

V

Electric Power Utilization

Andrew Hanson
PowerComm Engineering

25

Metering of Electric Power and Energy

John V. Grubbs
Alabama Power Company

Electrical metering deals with two basic quantities: *energy* and *power*. Energy is equivalent to work. Power is the rate of doing work. Power applied (or consumed) for any length of time is energy. In mathematical terms, power integrated over time is energy. The basic electrical unit of energy is the watthour. The basic unit of power is the watt. The watthour meter measures energy (in watthours), while the wattmeter measures the rate of energy, power (in watthours per hour or simply watts). For a constant power level, power multiplied by time is energy. For example, a watthour meter connected for two hours in a circuit using 500 watts (500 watthours per hour) will register 1000 watthours.

25.1 The Electromechanical Meter

The electromechanical watthour meter is basically a very specialized electric motor, consisting of

- A *stator* and a *rotor* that together produce torque
- A *brake* that creates a counter torque
- A *register* to count and display the revolutions of the rotor

25.1.1 Single Stator Electromechanical Meter

A two-wire single stator meter is the simplest electromechanical meter. The single stator consists of two electromagnets. One electromagnet is the potential coil connected between the two circuit conductors. The other electromagnet is the current coil connected in series with the load current. Figure 25.1 shows the major components of a single stator meter.

The electromagnetic fields of the current coil and the potential coil interact to generate torque on the rotor of the meter. This torque is proportional to the product of the source voltage, the line current, and the cosine of the phase angle between the two. Thus, the torque is also proportional to the power in the metered circuit.

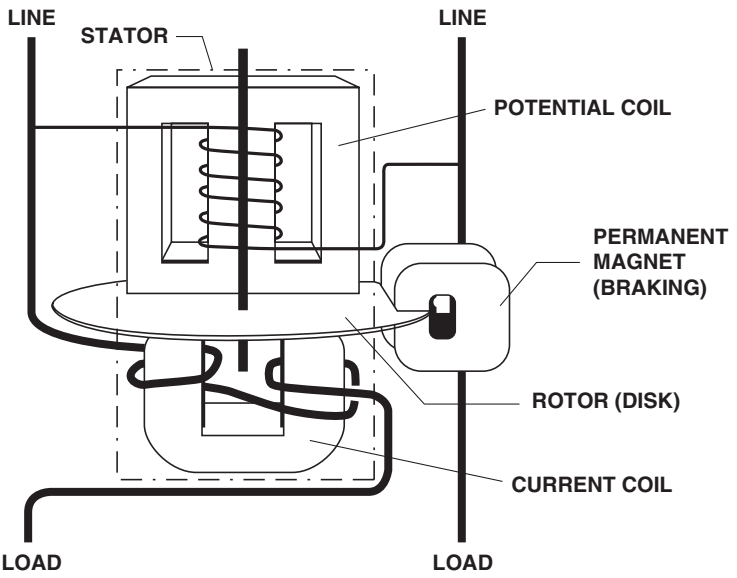

FIGURE 25.1 Main components of electromechanical meter.

The device described so far is incomplete. In measuring a steady power in a circuit, this meter would generate constant *torque* causing steady acceleration of the rotor. The rotor would spin faster and faster until the torque could no longer overcome friction and other forces acting on the rotor. This ultimate speed would not represent the level of power present in the metered circuit.

To address these problems, designers add a permanent magnet whose magnetic field acts on the rotor. This field interacts with the rotor to cause a *counter torque* proportional to the speed of the rotor. Careful design and adjustment of the magnet strength yields a meter that rotates at a *speed* proportional to power. This speed can be kept relatively slow. The product of the rotor speed and time is revolutions of the rotor. The revolutions are proportional to energy consumed in the metered circuit. One revolution of the rotor represents a fixed number of watthours. The revolutions are easily converted via mechanical gearing or other methods into a display of watthours or, more commonly, kilowatthours.

25.2 Blondel's Theorem

Blondel's theorem of polyphase metering describes the measurement of power in a polyphase system made up of an arbitrary number of conductors. The theorem provides the basis for correctly metering power in polyphase circuits. In simple terms, Blondel's theorem states that the total power in a system of (N) conductors can be properly measured by using (N) wattmeters or watt-measuring elements. The elements are placed such that one current coil is in each of the conductors and one potential coil is connected between each of the conductors and some common point. If this common point is chosen to be one of the (N) conductors, there will be zero voltage across one of the measuring element potential coils. This element will register zero power. *Therefore, the total power is correctly measured by the remaining (N − 1) elements.*

In application, this means that to accurately measure the power in a four-wire three-phase circuit (N = 4), the meter must contain (N − 1) or three measuring elements. Likewise, for a three-wire three-phase circuit (N = 3), the meter must contain two measuring elements. There are meter designs available that, for commercial reasons, employ less than the minimum number of elements (N − 1) for a given circuit configuration. These designs depend on *balanced* phase voltages for proper operation. Their accuracy suffers as voltages become unbalanced.

25.3 The Electronic Meter

Since the 1980s, meters available for common use have evolved from (1) electromechanical mechanisms driving mechanical, geared registers to (2) the same electromechanical devices driving electronic registers to (3) totally electronic (or solid state) designs. All three types remain in wide use, but the type that is growing in use is the solid state meter.

The addition of the electronic register to an electromechanical meter provides a digital display of energy and demand. It supports enhanced capabilities and eliminates some of the mechanical complexity inherent in the geared mechanical registers.

Electronic meters contain no moving mechanical parts—rotors, shafts, gears, bearings. They are built instead around large-scale integrated circuits, other solid state components, and digital logic. Such meters are much more closely related to computers than to electromechanical meters.

The operation of an electronic meter is very different than that described in earlier sections for an electromechanical meter. Electronic circuitry samples the voltage and current waveforms during each electrical cycle and converts these samples to digital quantities. Other circuitry then manipulates these values to determine numerous electrical parameters, such as kW, kWh, kvar, kvarh, kQ, kQh, power factor, kVA, rms current, rms voltage.

Various electronic meter designs also offer some or all of the following capabilities:

- **Time of use (TOU)**. The meter keeps up with energy and demand in multiple daily periods. (See section on Time of Use Metering.)
- **Bi-directional**. The meter measures (as separate quantities) energy delivered to and received from a customer. This feature is used for a customer that is capable of generating electricity and feeding it back into the utility system.
- **Loss compensation**. The meter can be programmed to automatically calculate watt and var losses in transformers and electrical conductors based on defined or tested loss characteristics of the transformers and conductors. It can internally add or subtract these calculated values from its measured energy and demand. This feature permits metering to be installed at the most economical location. For instance, we can install metering on the secondary (e.g., 4 kV) side of a customer substation, even when the contractual service point is on the primary (e.g., 110 kV) side. The 4 kV metering installation is much less expensive than a corresponding one at 110 kV. Under this situation, the meter compensates its secondary-side energy and demand readings to simulate primary-side readings.
- **Interval data recording**. The meter contains solid state memory in which it can record up to several months of interval-by-interval data. (See section on Interval Data Metering.)
- **Remote communications**. Built-in communications capabilities permit the meter to be interrogated remotely via telephone, radio, or other communications media.
- **Diagnostics**. The meter checks for the proper voltages, currents, and phase angles on the meter conductors. (See section on Site Diagnostic Meter.)
- **Power quality**. The meter can measure and report on momentary voltage or current variations and on harmonic conditions.

Note that many of these features are available only in the more advanced (and expensive) models of electronic meters.

As an example of the benefits offered by electronic meters, consider the following two methods of metering a large customer who is capable of generating and feeding electricity back to the utility. In this example, the metering package must perform these functions:

Measure kWh delivered to the customer
Measure kWh received from the customer
Measure kvarh delivered
Measure kvarh received

Measure kW delivered
Measure kW received
Compensate received quantities for transformer losses
Record the measured quantities for each demand interval

Method A. (2) kW/kWh electromechanical meters with pulse generators (one for delivered, one for received)
(2) kWh electromechanical meters with pulse generators (to measure kvarh)
(2) Phase shifting transformers (used along with the kWh meters to measure kvarh)
(2) Transformer loss compensators
(1) Pulse data recorder

Method B. (1) Electronic meter

Obviously, the electronic installation is much simpler. In addition, it is less expensive to purchase and install and is easier to maintain.

Benefits common to most solid state designs are high accuracy and stability. Another less obvious advantage is in the area of error detection. When an electromechanical meter develops a serious problem, it may produce readings in error by any arbitrary amount. An error of 10%, 20%, or even 30% can go undetected for years, resulting in very large over- or under-billings. However, when an electronic meter develops a problem, it is more likely to produce an obviously bad reading (e.g., all zeroes; all 9s; a demand 100 times larger than normal; or a blank display). This greatly increases the likelihood that the error will be noticed and reported soon after it occurs. The sooner such a problem is recognized and corrected, the less inconvenience and disruption it causes to the utility and to the customer.

25.3.1 Multifunction Meter

Multifunction or *extended function* refers to a meter that can measure reactive or apparent power (e.g., kvar or kVA) in addition to real power (kW). By virtue of their designs, many electronic meters inherently measure the quantities and relationships that define reactive and apparent power. It is a relatively simple step for designers to add meter intelligence to calculate and display these values.

25.3.2 Voltage Ranging and Multiform Meter

Electronic meter designs have introduced many new features to the watthour metering world. Two features, typically found together, offer additional flexibility, simplified application, and opportunities for reduced meter inventories for utilities.

- *Voltage ranging* – Many electronic meters incorporate circuitry that can sense the voltage level of the meter input signals and adjust automatically to meter correctly over a wide range of voltages. For example, a meter with this capability can be installed on either a 120 volt or 277 volt service.
- *Multiform* – Meter form refers to the specific combination of voltage and current signals, how they are applied to the terminals of the meter, and how the meter uses these signals to measure power and energy. For example, a Form 15 meter would be used for self-contained application on a 120/240 volt 4-wire delta service, while a Form 16 meter would be used on a self-contained 120/208 volt 4-wire wye service. A *multiform* 15/16 meter can work interchangeably on either of these services.

25.3.3 Site Diagnostic Meter

Newer meter designs incorporate the ability to measure, display, and evaluate the voltage and current magnitudes and phase relationships of the circuits to which they are attached. This capability offers important advantages:

- At the time of installation or reinstallation, the meter analyzes the voltage and current signals and determines if they represent a recognizable service type.
- Also at installation or reinstallation, the meter performs an initial check for wiring errors such as crossed connections or reversed polarities. If it finds an error, it displays an error message so that corrections can be made.
- Throughout its life, the meter continuously evaluates voltage and current conditions. It can detect a problem that develops weeks, months, or years after installation, such as tampering or deteriorated CT or VT wiring.
- Field personnel can switch the meter display into diagnostic mode. It will display voltage and current magnitudes and phase angles for each phase. This provides a quick and very accurate way to obtain information on service characteristics.

If a diagnostic meter detects any error that might affect the accuracy of its measurements, it will lock its display in error mode. The meter continues to make energy and demand measurements in the background. However, these readings cannot be retrieved from the meter until the error is cleared. This ensures the error will be reported the next time someone tries to read the meter.

25.4 Special Metering

25.4.1 Demand Metering

25.4.1.1 What is Demand?

Electrical energy is commonly measured in units of kilowatthours. Electrical power is expressed as kilowatthours per hour or, more commonly, kilowatts.

Demand is defined as power averaged over some specified period. Figure 25.2 shows a sample power curve representing instantaneous power. In the time interval shown, the integrated area under the power curve represents the energy consumed during the interval. This energy, divided by the length of the interval (in hours) yields "demand." In other words, the demand for the interval is that value of power that, if held constant over the interval, would result in an energy consumption equal to that energy the customer actually used.

Demand is most frequently expressed in terms of real power (kilowatts). However, demand may also apply to reactive power (kilovars), apparent power (kilovolt-amperes), or other suitable units. Billing for demand is commonly based on a customer's maximum demand reached during the billing period.

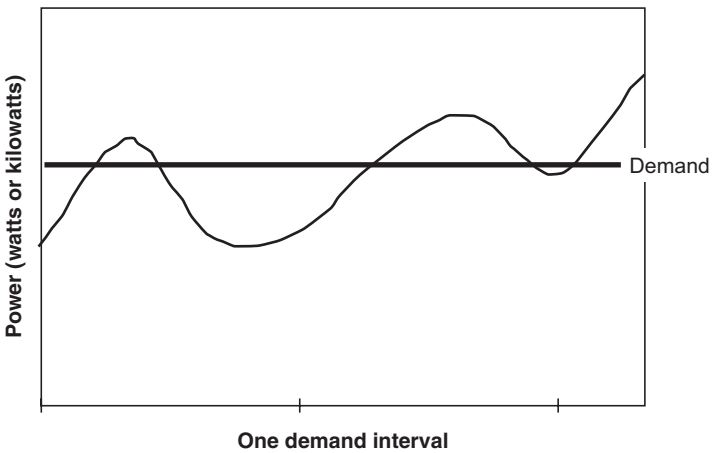

FIGURE 25.2 Instantaneous power vs. demand.

25.4.1.2 Why is Demand Metered?

Electrical conductors and transformers needed to serve a customer are selected based on the expected maximum demand for the customer. The equipment must be capable of handling the maximum levels of voltages and currents needed by the customer. A customer with a higher maximum demand requires a greater investment by the utility in equipment. Billing based on energy usage alone does not necessarily relate directly to the cost of equipment needed to serve a customer. Thus, energy billing alone may not equitably distribute to each customer an appropriate share of the utility's costs of doing business.

For example, consider two commercial customers with very simple electricity needs. Customer A has a demand of 25 kW and operates at this level 24 hours per day. Customer B has a maximum demand of 100 kW but operates at this level only 4 hours per day. For the remaining 20 hours of the day, "B" operates at a 10 kW power level.

$$\text{"A" uses } 25 \text{ kW} \times 24 \text{ hr} = 600 \text{ kWh per day}$$
$$\text{"B" uses } (100 \text{ kW} \times 4 \text{ hr}) + (10 \text{ kW} \times 20 \text{ hr}) = 600 \text{ kWh per day}$$

Assuming identical billing rates, each customer would incur the same energy costs. However, the utility's equipment investment will be larger for Customer B than for Customer A. By implementing a charge for demand as well as energy, the utility would bill Customer A for a maximum demand of 25 kW and Customer B for 100 kW. "B" would incur a larger total monthly bill, and each customer's bill would more closely represent the utility's cost to serve.

25.4.1.3 Integrating Demand Meters

By far the most common type of demand meter is the integrating demand meter. It performs two basic functions. First, it measures the *average* power during each *demand interval.* (Common demand interval lengths are 15, 30, or 60 min.) See Table 25.1. The meter makes these measurements interval-by-interval throughout each day. Second, it retains the maximum of these interval measurements.

The demand calculation function of an electronic meter is very simple. The meter measures the energy consumed during a demand interval, then multiplies by the number of demand intervals per hour. In effect, it calculates the energy that would be used if the rate of usage continued for one hour. The following table illustrates the correspondence between energy and demand for common demand interval lengths.

After each measurement, the meter compares the new demand value to the stored *maximum demand.* If the new value is greater than that stored, the meter replaces the stored value with the new one. Otherwise, it keeps the previously stored value and discards the new value. The meter repeats this process for each interval. At the end of the billing period, the utility records the maximum demand, then resets the stored *maximum demand* to zero. The meter then starts over for the new billing period.

25.4.2 Time of Use Metering

A time of use (TOU) meter measures and stores energy (and perhaps demand) for multiple periods in a day. For example, a service rate might define one price for energy used between the hours of 12 noon and 6 P.M. and another rate for that used outside this period. The TOU meter will identify the hours from 12 noon until 6 P.M. as "Rate 1." All other hours would be "Rate 2." The meter will maintain separate

TABLE 25.1 Energy/Demand Comparisons

Demand Interval	Intervals per Hour	Energy During Demand Interval	Resulting Demand
60 min	1	100 kWh	100 kW
30 min	2	50 kWh	100 kW
15 min	4	25 kWh	100 kW

measurements of Rate 1 energy (and demand) and Rate 2 energy (and demand) for the entire billing period. Actual TOU service rates can be much more complex than this example, including features such as

- more than two periods per day,
- different periods for weekends and holidays, and
- different periods for different seasons of the year.

A TOU meter depends on an internal clock/calendar for proper operation. It includes battery backup to maintain its clock time during power outages.

25.4.3 Interval Data Metering

The standard method of gathering billing data from a meter is quite simple. The utility reads the meter at the beginning of the billing period and again at the end of the billing period. From these readings, it determines the energy and maximum demand for that period. This information is adequate to determine the bills for the great majority of customers. However, with the development of more complex service rates and the need to study customer usage patterns, the utility sometimes wants more detail about how a customer uses electricity. One option would be to read the meter daily. That would allow the utility to develop a day-by-day pattern of the customer's usage. However, having someone visit the meter site every day would quickly become very expensive. What if the meter could record usage data every day? The utility would have more detailed usage data, but would only have to visit the meter when it needed the data, for instance, once per month. And if the meter is smart enough to do that, why not have it record data even more often, for instance every hour?

In very simple terms, this is what *interval data metering* does. The interval meter includes sufficient circuitry and intelligence to record usage multiple times per hour. The length of the recording interval is programmable, often over a range from 1 to 60 minutes. The meter includes sufficient solid state memory to accumulate these interval readings for a minimum of 30 days at 15-minute intervals. Obviously, more frequent recording times reduce the days of storage available.

A simple kWh/kW recording meter typically records one set of data representing kWh. This provides the detailed usage patterns that allow the utility to analyze and evaluate customer "load profiles" based on daily, weekly, monthly, or annual bases. An extended function meter is commonly programmed to record two channels of data, e.g., kWh and kvarh. This provides the additional capability of analyzing customers' power factor patterns over the same periods. Though the meter records information in energy units (kWh or kvarh), it is a simple matter to convert this data to equivalent demand (kW or kvar). Since demand represents energy per unit time, simply divide the energy value for one recorder interval by the length of the interval (in hours). If the meter records 16.4 kWh in a 30-minute period, the equivalent demand for that period is 16.4 kWh/(0.5 hours) = 32.8 kW.

A sample 15-minute interval load shape for a 24-hour period is shown in the graph in Fig. 25.3. The minimum demand for that period was 10.5 kW, occurring during the interval ending at 04:30. The maximum demand was 28.7 kW, occurring during the interval ending at 15:15, or 3:15 P.M.

25.4.4 Pulse Metering

Metering pulses are signals generated in a meter for use outside the meter. Each pulse represents a discrete quantity of the metered value, such as kWh, kVAh, or kvarh. The device receiving the pulses determines the energy or demand at the meter by counting the number of pulses occurring in some time interval. A pulse is indicated by the transition (e.g., open to closed) of the circuit at the meter end. Pulses are commonly transmitted on small conductor wire circuits. Common uses of pulses include providing signals to

- customer's demand indicator
- customer's energy management system

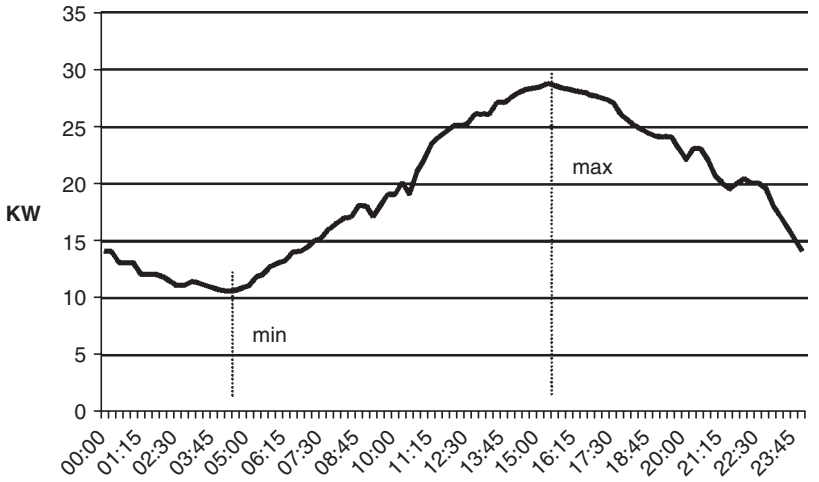

FIGURE 25.3 Graph of interval data.

- a *totalizer* (see section on Totalized Metering)
- a metering data recorder
- a telemetering device that converts the pulses to other signal forms (e.g., telephone line tones or optical signals) for transmission over long distances

Pulse metering is installed when customer service requirements, equipment configurations, or other special requirements exceed the capability of conventional metering. Pulse metering is also used to transmit metered data to a remote location.

25.4.4.1 Recording Pulses

A meter pulse represents a quantity of energy, not power. For example, a pulse is properly expressed in terms of watthours (or kWh) rather than watts (or kW). A pulse recorder will associate time with pulses as it records them. If set up for a 15-minute recording interval, the recorder counts pulses for 15 min, then records that number of pulses. It then counts pulses for the next 15 min, records that number, and so on, interval after interval, day after day. It is a simple matter to determine the number of pulses recorded in a chosen length of time. Since the number of pulses recorded represents a certain amount of energy, simply divide this energy by the corresponding length of time (in hours) to determine average power for that period.

Example: For a metering installation, we are given that each pulse represents 2400 watthours or 2.4 kWh. In a 15-minute period, we record 210 pulses. What is the corresponding energy (kWh) and demand (kW) during this 15-minute interval?

$$\begin{aligned} \text{Total energy in interval} &= 2.4 \text{ kWh per pulse} \times 210 \text{ pulses} \\ &= 504 \text{ kWh} \\ \text{Demand} = \text{Energy/Time} &= 504 \text{ kWh}/0.25 \text{ hour} \\ &= 2016 \text{ kW} \end{aligned}$$

Often, a customer asks for the demand value of a pulse, rather than the energy value. The demand value is dependent on demand interval length. The demand pulse value is equal to the energy pulse value divided by the interval length in hours.

For the previous example, the kW pulse value would be:

$$2.4 \text{ kWh per pulse}/0.25 \text{ hours} = 9.6 \text{ kW per pulse}$$

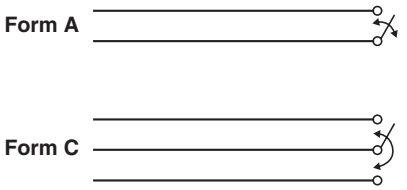

FIGURE 25.4 Pulse circuits.

and the resulting demand calculation is:

$$\text{Demand} = 9.6 \text{ kW per pulse} \times 210 \text{ pulses}$$
$$= 2016\text{kW}$$

Remember, however, that a pulse demand value is meaningful only for a specific demand interval. In the example above, counting pulses for any period other than 15 minutes and then applying the kW pulse value will yield incorrect results for demand.

25.4.4.2 Pulse Circuits

Pulse circuits commonly take two forms (Fig. 25.4):

- *Form A*, a two-wire circuit where a switch toggles between closed and open. Each transition of the circuit (to open or to closed) represents one pulse.
- *Form C*, a three-wire circuit where the switch flip-flops. Each transition (from closed on one side to closed on the other) represents one pulse.

Use care in interpreting pulse values for these circuits. The value will normally be expressed per *transition*. With Form C circuits, a transition is a change from closed on the first side to closed on the second side. Most receiving equipment interprets this properly. However, with Form A circuits, the transition is defined as a change from open to closed or from closed to open. An initially open Form A circuit that closes, then opens has undergone two (2) transitions. If the receiving equipment counts only circuit closures, it will record only half of the actual transitions. This is not a problem if the applicable pulse value of the Form A circuit is *doubled* from the rated pulse weight per transition. For example, if the value of a Form A meter pulse is 3.2 kWh per transition, the value needed for a piece of equipment that only counted circuit closures would be $3.2 \times 2 = 6.4$ kWh per pulse.

25.4.5 Totalized Metering

Totalized metering refers to the practice of combining data to make multiple service points look as if they were measured by a single meter. This is done by combining two or more sets of data from separate meters to generate data equivalent to what would be produced by a single "virtual meter" that measured the total load. This combination can be accomplished by:

- Adding recorded interval data from multiple meters, usually on a computer
- Adding (usually on-site) meter pulses from multiple meters by a special piece of metering equipment known as a totalizer
- Paralleling the secondaries of current transformers located in multiple circuits and feeding the combined current into a conventional meter (this works only when the service voltages and ratios of the current transformers are identical)
- Using a multi-circuit meter, which accepts the voltage and current inputs from multiple services

Totalized demand is the sum of the *coincident* demands and is usually less than the sum of the individual peak demands registered by the individual meters. Totalized energy equals the sum of the energies measured by the individual meters.

Table 25.2 illustrates the effects of totalizing a customer served by three delivery (and metering) points. It presents the customer's demands over a period of four demand intervals and illustrates the difference in the maximum totalized demand compared to the sum of the individual meter maximum demands.

The peak kW demand for each meter point is shown in bold. The sum of these demands is 2240 kW. However, when summed interval-by-interval, the peak of the sums is 2180 kW. This is the *totalized demand*. The difference in the two demands, 60 kW, represents a cost savings to the customer. It should be clear why many customers with multiple service points desire to have their demands totalized.

TABLE 25.2 Example of Totalized Meter Data

Interval	Meter A	Meter B	Meter C	Totalized (A+B+C)
1	**800**	600	700	*2100*
2	780	650	**740**	*2170*
3	750	**700**	500	*1950*
4	780	680	720	***2180***

25.5 Instrument Transformers

Instrument transformers is the general name for members of the family of current transformers (CTs) and voltage transformers (VTs) used in metering. They are high-accuracy transformers that convert load currents or voltages to other (usually smaller) values by some fixed ratio. Voltage transformers are also often called potential transformers (PTs). The terms are used interchangeably in this section. CTs and VTs are most commonly used in services where the current and/or voltage levels are too large to be applied directly to the meter.

A current transformer is rated in terms of its nameplate primary current as a ratio to five amps secondary current (e.g., 400:5). The CT is not necessarily limited to this nameplate current. Its maximum capacity is found by multiplying its nameplate rating by its *rating factor*. This yields the total current the CT can carry while maintaining its rated accuracy and avoiding thermal overload. For example, a 200:5 CT with a rating factor of 3.0 can be used and will maintain its rated accuracy up to 600 amps. Rating factors for most CTs are based on open-air outdoor conditions. When a CT is installed indoors or inside a cabinet, its rating factor is reduced.

A voltage transformer is rated in terms of its nameplate primary voltage as a ratio to either 115 or 120 volts secondary voltage (e.g., 7200:120 or 115000:115). These ratios are sometimes listed as an equivalent ratio to 1 (e.g., 60:1 or 1000:1).

Symbols for a CT and a PT connected in a two-wire circuit are shown in Fig. 25.5.

25.5.1 Measuring kVA

In many cases, a combination watthour demand meter will provide the billing determinants for small- to medium-sized customers served under rates that require only real power (kW) and energy (kWh). Rates for larger customers often require an *extended function* meter to provide the additional reactive or apparent power capability needed to measure or determine kVA demand. There are two common methods for determining kVA demand for billing.

1. **Actual kVA**. This method directly measures actual kVA, a simple matter for electronic meters.
2. **Average Power Factor kVA**. This method approaches the measurement of kVA in a more roundabout fashion. It was developed when most metering was done with mechanical meters that could

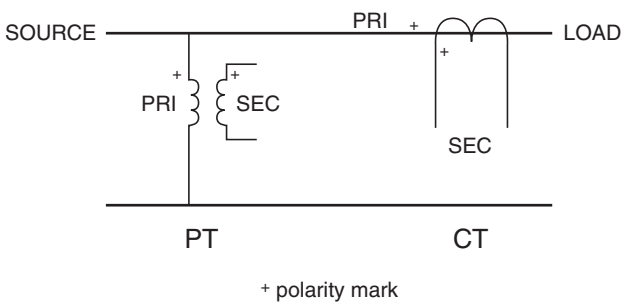

FIGURE 25.5 Instrument transformer symbols.

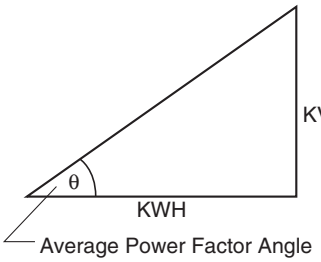

$$\tan(\theta) = \frac{KVARH}{KWH} = \frac{528000}{981600} = 0.5378$$

$$\theta = 28.275^\circ$$

$$APF = \cos(\theta) = 0.881$$

$$KVA\ \text{demand} = \frac{KW\ \text{demand}}{APF} = \frac{1412}{0.881}$$

$$= 1603\ \text{KVA}$$

FIGURE 25.6 Calculation of kVA demand using the Average Power Factor method.

directly measure only real energy and power (kWh and kW). With a little help, they could measure kvarh. Those few meters that could measure actual kVA were very complex and demanded frequent maintenance. The Average Power Factor (APF) method of calculating kVA addressed these limitations. It requires three (3) pieces of meter information:

- Total real energy (kWh)
- Maximum real demand (kW)
- Total reactive energy (kvarh)

These can be measured with two standard mechanical meters. The first meter measures kWh and kW. With the help of a special transformer to shift the voltage signals 90° in phase, the second mechanical meter can be made to measure kvarh.

APF kVA is determined by calculating the customer's "average power factor" over the billing period using the total kWh and kvarh for the period. This APF is then applied to the maximum kW reading to yield APF kVA. An example of this calculation process follows.

Customer: XYZ Corporation

Billing determinants obtained from the meter:

kWh	981,600
kvarh	528,000
kW	1412

The calculations are shown in Fig. 25.6.

25.6 Defining Terms

Class—The class designation of a watthour meter represents the maximum current at which the meter can be operated continuously with acceptable accuracy and without excessive temperature rise. Examples of common watthour meter classes are:

Self-contained—Class 200, 320, or 400

Transformer rated—Class 10 or 20

Test amperes (TA)—The test amperes rating of a watthour meter is the current that is used as a base for adjusting and determining percent registration (accuracy). Typical test current ratings and their relations to meter class are:

Class 10 and 20—TA 2.5

Class 200—TA 30

Self-contained meter—A self-contained meter is one designed and installed so that power flows from the utility system *through* the meter to the customer's load. The meter sees the total load current and full service voltage.

Transformer rated meter—A transformer rated meter is one designed to accept *reduced* levels of current and/or voltage that are directly proportional to the service current and voltage. The primary windings of current transformers and/or voltage transformers are placed in the customer's service and see the total load current and full service voltage. The transformer rated meter connects into the secondary windings of these transformers.

Meter element—A meter element is the basic energy and power measurement circuit for one set of meter input signals. It consists of a current measurement device and a voltage measurement device for one phase of the meter inputs. Usually, a meter will have one less element than the number of wires in the circuit being metered. That is, a 4-wire wye or delta circuit will be metered by a 3-element meter; a 3-wire delta circuit will be metered by a 2-element meter, although there are numerous exceptions.

CT PT ratio—A number or factor obtained by multiplying the current transformer ratio by the potential transformer ratio. Example: If a meter is connected to 7200:120 volt PTs (60:1) and 600:5 CTs (120:1), the CT PT ratio is $60 \times 120 = 7200$. A metering installation may have current transformers but no potential transformer in which case the CT PT ratio is just the CT ratio.

Meter multiplier—Also called the dial constant or kilowatthour constant, this is the multiplier used to convert meter kWh readings to actual kWh. The meter multiplier is the CT PT ratio. For a self-contained meter, this constant is 1.

Further Information

Further information and more detail on many of the topics related to metering can be found in the *Handbook for Electricity Metering*, published by Edison Electric Institute. This authoritative book provides extensive explanations of many aspects of metering, from fundamentals of how meters and instrument transformers operate, to meter testing, wiring, and installation.

26

Basic Electric Power Utilization—Loads, Load Characterization and Load Modeling

Andrew Hanson
PowerComm Engineering

Utilization is the "end result" of the generation, transmission, and distribution of electric power. The energy carried by the transmission and distribution system is turned into useful work, light, heat, or a combination of these items at the utilization point. Understanding and characterizing the utilization of electric power is critical for proper planning and operation of power systems. Improper characterization of utilization can result of over or under building of power system facilities and stressing of system equipment beyond design capabilities. This chapter describes some of the basic concepts used to characterize and model loads in electric power systems.

The term *load* refers to a device or collection of devices that draw energy from the power system. Individual loads (devices) range from small light bulbs to large induction motors to arc furnaces. The term *load* is often somewhat arbitrarily applied, at times being used to describe a specific device, and other times referring to an entire facility and even being used to describe the lumped power requirements of power system components and connected utilization devices downstream of a specific point in large-scale system studies.

26.1 Basic Load Characterization

A number of terms are used to characterize the magnitude and intensity of loads. Several such terms are defined and uses outlined below.

Energy—Energy use (over a specified period of time) is a key identifying parameter for power system loads. Energy use is often recorded for various portions of the power system (e.g., homes, businesses, feeders, substations, districts). Utilities report aggregate system energy use over a variety of time frames (daily, weekly, monthly, and annually). System energy use is tied directly to sales and thus is often used as a measure of the utility or system performance from one period to another.

Demand—Loads require specific amounts of energy over short periods of time. Demand is a measure of this energy and is expressed in terms of power (kilowatts or Megawatts). Instantaneous demand is the peak instantaneous power use of a device, facility, or system. Demand, as commonly referred to in utility discussions, is an integrated demand value, most often integrated over 10, 15, or 30 min. Integrated demand values are determined by dividing the energy used by the time interval of measurement or the demand interval.

$$\text{Demand} = \frac{\text{Energy Use Over Demand Interval}}{\text{Demand Interval}} \tag{26.1}$$

Integrated demand values can be much lower than peak instantaneous demand values for a load or facility.

Demand Factor—Demand factor is a ratio of the maximum demand to the total connected load of a system or the part of the system under consideration. Demand factor is often used to express the expected diversity of individual loads within a facility prior to construction. Use of demand factors allows facility power system equipment to be sized appropriately for the expected loads.

$$\text{Demand Factor} = \frac{\text{Maximum Demand}}{\text{Total Connected Load}} \tag{26.2}$$

Load Factor—Load factor is similar to demand factor and is calculated from the energy use, the demand, and the period of time associated with the measurement.

$$\text{Load Factor} = \frac{\text{Energy Use}}{\text{Demand} \times \text{Time}} \tag{26.3}$$

A high load factor is typically desirable, indicating that a load or group of loads operates near its peak most of the time, allowing the greatest benefit to be derived from any facilities installed to serve the load.

26.2 Composite Loads and Composite Load Characterization

It is impractical to model each individual load connected to a power system to the level of detail at which power is delivered to each individual utilization device. Loads are normally lumped together to represent all of the "downstream" power system components and individual connected loads. This grouping occurs as a result of metering all downstream power use from a certain point in the power system, or as a result of model simplification in which effects of the downstream power system and connected loads are represented by a single load in system analysis.

26.2.1 Coincidence and Diversity

Although individual loads vary unpredictably from hour to hour and minute to minute, an averaging effect occurs as many loads are examined in aggregate. This effect begins at individual facilities (home, commercial establishment, or industrial establishment) where all devices are seldom if ever in operation at the same instant. Progressing from an individual facility to the distribution and transmission systems, the effect is compounded, resulting in somewhat predictable load characteristics.

Diversity is a measure of the dispersion of the individual loads of a system under observation over time. Diversity is generally low in individual commercial and industrial installations. However, at a feeder level, diversity is a significant factor, allowing more economical choices for equipment since the feeder needs to supply power to the aggregate peak load of the connected customers, not the sum of the customer individual (noncoincident) peak loads.

Groups of customers of the same class (i.e., residential, commercial, industrial) tend to have an aggregate peak load per customer that decreases as the number of customers increases. This tendency is termed *coincidence* and has significant impact on the planning and construction of power systems (Willis, 1997). For example, load diversity would allow a feeder or substation to serve a number of customers whose individual (noncoincident) peak demands may exceed the feeder or substation rating by a factor of two or more.

$$\text{Coincidence Factor} = \frac{\text{Aggregate Demand for a Group of Customers}}{\text{Sum of Individual Customer Demands}} \tag{26.4}$$

Note that there is a minor but significant difference between coincidence (and its representation as a coincidence factor) and the demand factor discussed above. The coincidence factor is based on the *observed* peak demand for individuals and groups, whereas the demand factor is based on the *connected* load.

26.2.2 Load Curves and Load Duration

Load curves and load duration curves graphically convey very detailed information about the characteristics of loads over time. Load curves typically display the load of a customer class, feeder, or other portion of a power system over a 24-hour period. Load duration curves display the cumulative amount of time that load levels are experienced over a period of time.

Load curves represent the demand of a load or groups of load over a period of time, typically 24 hours. The curves provide "typical" load levels for a customer class on an hour-by-hour or minute-by-minute basis. The curves themselves represent the demand of a certain class of customers or portion of the system. The area under the curve represents the corresponding energy use over the time period under consideration. Load curves provide easily interpreted information regarding the peak load duration as well as the variation between minimum and maximum load levels. Load curves provide key information for daily load forecasts allowing planners and operators to ensure system capacity is available to meet customer needs. Three sample load curves (for residential, commercial, and industrial customer classes) are shown in Figs. 26.1 through 26.3.

Load curves can also be developed on a feeder or substation basis, as a composite representation of the load profile of a portion of the system.

Load duration curves quickly convey the duration of the peak period for a portion of a power system over a given period of time. Load duration curves plot the cumulative amount of time that load levels are

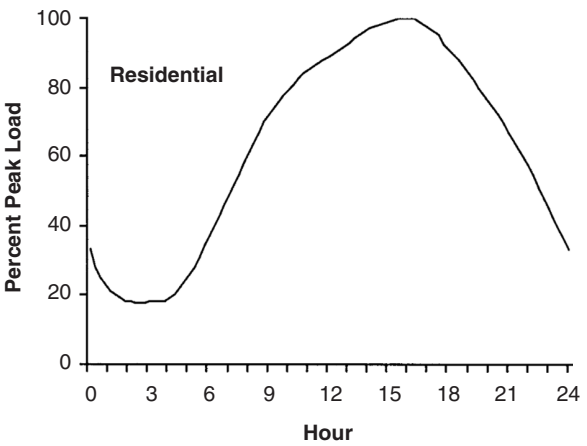

FIGURE 26.1 Residential load curve.

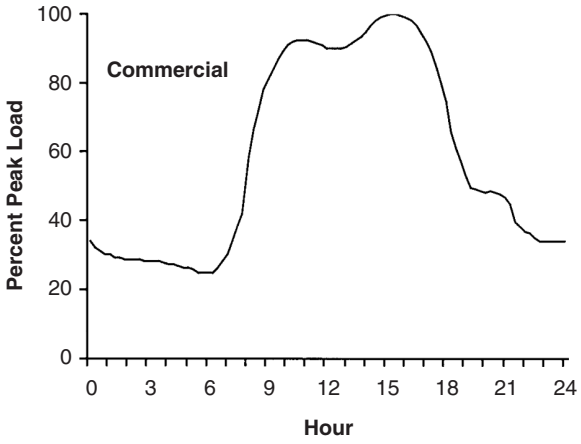

FIGURE 26.2 Commercial load curve.

seen over a specified time period. The information conveyed graphically in a load duration curve, although more detailed, is analogous to the information provided by the load factor discussed above. A sample load duration curve is shown in Fig. 26.4.

Load duration curves are often characterized by very sharp ascents to the peak load value. The shape of the remainder of the curves vary based on utilization patterns, size, and content of the system for which the load duration curve is plotted.

26.3 Composite Load Modeling

Load models can generally be divided into a variety of categories for modeling purposes. The appropriate load model depends largely on the application. For example, for switching transient analyses, simple load models as combinations of time-invariant circuit elements (resistors, inductors, capacitors) and/or voltage sources are usually sufficient. Power flow analyses are performed for a specific operating point at a specific frequency, allowing loads to be modeled primarily as constant impedance or constant power. However, midterm and extended term transient stability analyses require that load voltage and

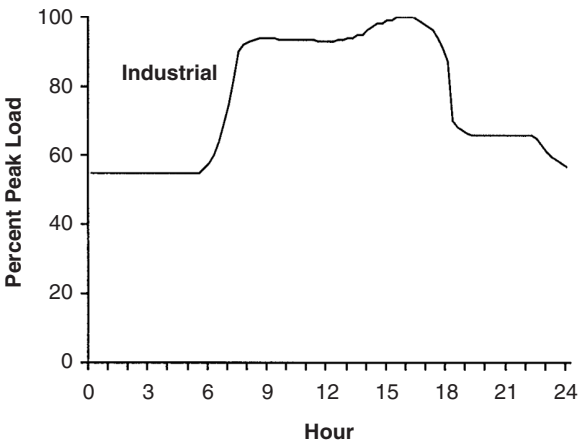

FIGURE 26.3 Industrial load curve.

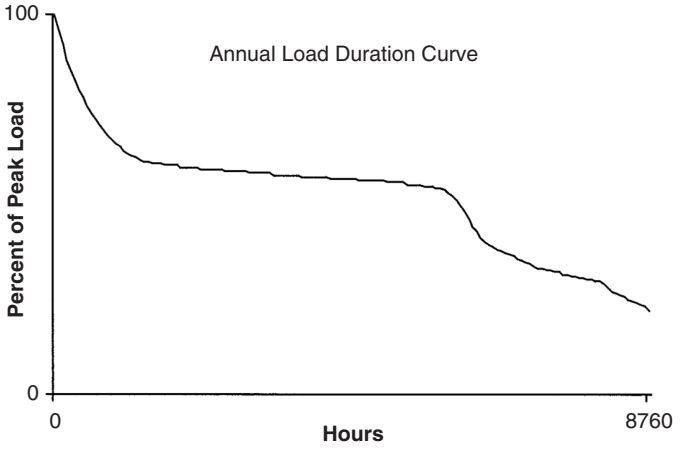

FIGURE 26.4 Annual load duration curve.

frequency dependencies be modeled, requiring more complex aggregate load models. Two load models are discussed below.

Composite loads exhibit dependencies on frequency and voltage. Both linear (Elgerd, 1982; Gross, 1986) and exponential models (Arrillaga and Arnold, 1990) are used for addressing these dependencies.

Linear Voltage and Frequency Dependence Model—The linear model provides excellent representation of load variations as frequency and voltages vary by small amounts about a nominal point.

$$P = P_{nominal} + \frac{\partial P}{\partial |\bar{V}|}\Delta|\bar{V}| + \frac{\partial P}{\partial f}\Delta f \tag{26.5}$$

$$Q = Q_{nominal} + \frac{\partial Q}{\partial |\bar{V}|}\Delta|\bar{V}| + \frac{\partial Q}{\partial f}\Delta f \tag{26.6}$$

where $P_{nominal}$, $Q_{nominal}$ are the real and reactive power under nominal conditions,

$\frac{\partial P}{\partial |\bar{V}|}, \frac{\partial P}{\partial f}, \frac{\partial Q}{\partial |\bar{V}|}, \frac{\partial Q}{\partial f}$ are the rates of change of real and reactive power with respect to voltage magnitude and frequency, and

$\Delta|V|$, Δf are the deviations in voltage magnitude and frequency from nominal values.

The values for the partial derivatives with respect to voltage and frequency can be determined through analysis of metered load data recorded during system disturbances or in the case of very simple loads, through calculations based on the equivalent circuit models of individual components.

Exponential Voltage and Frequency Dependence Model—The exponential model provides load characteristics useful in midterm and extended term stability simulations in which the changes in system frequency and voltage are explicitly modeled in each time step.

$$P = P_{nominal}|\bar{V}|^{pv} f^{pf} \tag{26.7}$$

$$Q = Q_{nominal}|\bar{V}|^{qv} f^{qf} \tag{26.8}$$

where $P_{nominal}$, $Q_{nominal}$ are the real and reactive power of the load under nominal conditions

$|V|$ is the voltage magnitude in per unit

f is the frequency in per unit

pv, *pf*, *qv*, and *qf* are the exponential modeling parameters for the voltage and frequency dependence of the real and reactive power portions of the load, respectively.

26.4 Other Load-Related Issues

26.4.1 Cold Load Pickup

Following periods of extended service interruption, the advantages provided by load diversity are often lost. The term *cold load pickup* refers to the energization of the loads associated with a circuit or substation following an extended interruption during which much of the diversity normally encountered in power systems is lost.

For example, if a feeder suffers an outage, interrupting all customers on the feeder during a particularly cold day, the homes and businesses will cool to levels below the individual thermostat settings. This situation eliminates the diversity normally experienced, where only a fraction of the heating will be required to operate at any given time. Once power is restored, the heating at all customer locations served by the feeder will attempt to operate to bring the building temperatures back to levels near the thermostat settings. The load experienced by the feeder following reenergization can be far in excess of the design loading due to lack of load diversity.

Cold load pickup can result in a number of adverse power system reactions. Individual service transformers can become overloaded under cold load pickup conditions, resulting in loss of life and possible failure due to overheating. Feeder load levels can exceed protective device ratings/settings, resulting in customer interruptions following initial service restoration. Additionally, the heavily loaded system conditions can result in conductors sagging below their designed minimum clearance levels, creating safety concerns.

26.4.2 Harmonics and Other Nonsinusoidal Loads

Electronic loads that draw current from the power system in a nonsinusoidal manner represent a significant portion of the load connected to modern power systems. These loads cause distortions of the generally sinusoidal characteristics traditionally observed. Harmonic loads include power electronic based devices (rectifiers, motor drives, switched mode power supplies, etc.) and arc furnaces. More details on power electronics and their effects on power system operation can be found in the power electronics section of this handbook.

References

Arrillaga, J. and Arnold, C.P., *Computer Analysis of Power Systems*, John Wiley & Sons, West Sussex, 1990.

Elgerd, O.I., *Electric Energy Systems Theory: An Introduction*, 2nd ed., McGraw Hill Publishing Company, New York, 1982.

Gross, C.A., *Power System Analysis*, 2nd ed., John Wiley & Sons, New York, 1986.

1996 National Electric Code, NFPA 70, Article 100, Batterymarch Park, Quincy, MA.

Willis, H.L., *Power Distribution Planning Reference Book*, Marcel-Dekker, Inc., New York, 1997.

Further Information

The references provide a brief treatment of loads and their characteristics. More detailed load characteristics for specific industries can be found in specific industry trade publications. For example, specific characteristics of loads encountered in the steel industry can be found in Fruehan, R.J., Ed., *The Making, Shaping and Treating of Steel*, 11th ed., AISE Steel Foundation, Pittsburgh, Pennsylvania, 1998.

The quarterly journals *IEEE Transactions on Power Systems* and *IEEE Transactions on Power Delivery* contain numerous papers on load modeling, as well as short and long term load forecasting. Papers in these journals also track recent developments in these areas.

Information on load modeling for long term load forecasting for power system planning can be found the following references respectively:

Willis, H.L., *Spatial Electric Load Forecasting*, Marcel-Dekker, Inc., New York, 1996.

Stoll, H.G., *Least Cost Electric Utility Planning*, John Wiley & Sons, New York, 1989.

27

Electric Power Utilization: Motors

Charles A. Gross
Auburn University

A major application of electric energy is in its conversion to mechanical energy. Electromagnetic, or "EM" devices designed for this purpose are commonly called "motors." Actually the machine is the central component of an integrated system consisting of the source, controller, motor, and load. For specialized applications, the system may be, and frequently is, designed as a integrated whole. Many household appliances (e.g., a vacuum cleaner) have in one unit, the controller, the motor, and the load. However, there remain a large number of important stand-alone applications that require the selection of a proper motor and associated control, for a particular load. It is this general issue that is the subject of this chapter.

The reader is cautioned that there is no "magic bullet" to deal with all motor-load applications. Like many engineering problems, there is an artistic, as well as a scientific dimension to its solution. Likewise, each individual application has its own peculiar characteristics, and requires significant experience to manage. Nevertheless, a systematic formulation of the issues can be useful to a beginner in this area of design, and even for experienced engineers faced with a new or unusual application.

27.1 Some General Perspectives

Consider the general situation in Fig. 27.1a. The flow of energy through the system is from left to right, or from electrical source to mechanical load. Also, note the positive definitions of currents, voltages, speed, and torques. These definitions are collectively called the "motor convention," and are logically used when motor applications are under study. Likewise, when generator applications are considered, the sign conventions of Fig. 27.1b (called generation convention) will be adopted. This means that variables will be positive under "normal" conditions (motors operating in the motor mode, generators in the generator mode), and negative under some abnormal conditions (motors running "backwards," for example). Using motor convention:

$$T_{dev} - (T_m + T_{RL}) = T_{dev} - T'_m = J(d\omega_{rm}/dt) \tag{27.1}$$

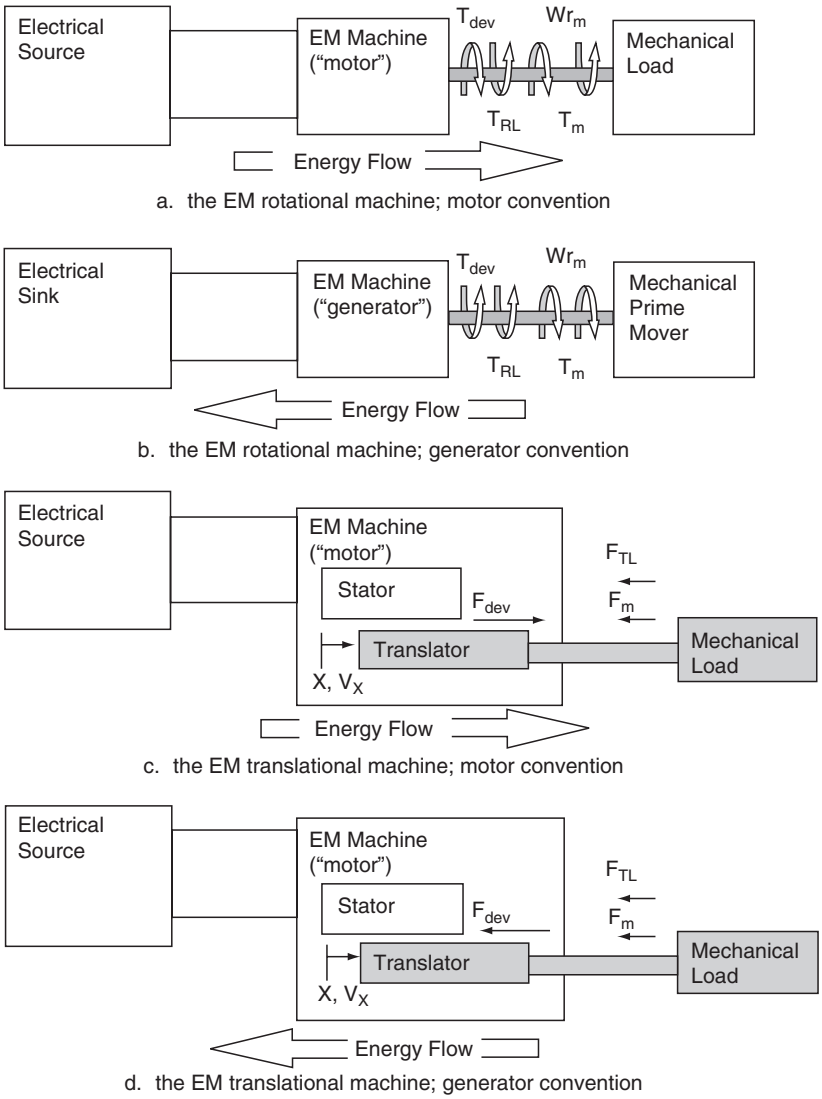

FIGURE 27.1 Motor and generator sign conventions for EM machines.

where T_{dev} = EM torque, produced by the motor, Nm
T_m = torque absorbed by the mechanical load, including the load losses and that used for useful mechanical work, Nm
T_{RL} = rotational loss torque, internal to the motor, Nm
$T'_m = T_m + T_{RL}$ = equivalent load torque, Nm
J = mass polar moment of inertia of all rotating parts, kg-m^2
ω_{rm} = angular velocity of rotating parts, rad/s

Observe that whenever $T_{dev} > T'_m$, the system accelerates; if $T_{dev} < T'_m$, the system decelerates. The system will inherently seek out the equilibrium condition of $T_{dev} = T'_m$, which will determine the running speed. In general, the steady state running speed for any motor-load system occurs at the intersection of the motor and load torque-speed characteristics, i.e., where $T_{dev} = T'_m$. If $T_{dev} > T'_m$, the system is accelerating; for $T_{dev} < T'_m$, the system decelerates. Thus, torque-speed characteristics for motors and loads are necessary for the design of a speed (or position) control system.

The corresponding system powers are:

$P_{dev} = T_{dev}\ \omega_{rm}$ = EM power, converted by the motor into mechanical form, W

$P_m = T_m\ \omega_{rm}$ = power absorbed by the mechanical load, including the load losses and that used for useful mechanical work, W

$P_{RL} = T_{RL}\ \omega_{rm}$ = rotational power loss, internal to the motor, W

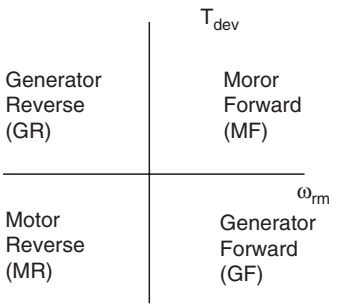

FIGURE 27.2 Operating modes.

27.2 Operating Modes

Equation (27.1) implies that torque and speed are positive. Consider positive speed as "forward," meaning rotation in the "normal" direction, which should be obvious in a specific application. "Reverse" is defined to mean rotation in the direction opposite to "forward," and corresponds to $\omega_{rm} < 0$. Positive EM torque is in the positive speed direction. Using motor convention, first quadrant operation means that (1) speed is positive ("forward") and (2) T_{dev} is positive (also forward), and transferring energy from motor to load ("motoring"). There are four possible operating modes specific to the four quadrants of Fig. 27.2. In any application, a primary consideration is to determine which of these operating modes will be required.

27.3 Motor, Enclosure, and Controller Types

The general types of enclosures, motors, and controllers are summarized in Tables 27.1, 27.2, and 27.3.

27.4 System Design

The design of a proper motor-enclosure-controller system for a particular application is a significant engineering problem requiring engineering expertise and experience. The following issues must be faced and resolved.

TABLE 27.1 General Enclosure Types[a]

Types
Open
Drip-proof
Splash-proof
Semi-guarded
Weather protected
Type I
Type II
Totally enclosed
Nonventillated
Fan-cooled
Explosion-proof
Dust-ignition-proof
Water-proof
Pipe-ventilated
Water-cooled
Water-air-cooled
Air-to-air-cooled
Air-over-cooled

[a]See NEMA Standard MG 1.1.25-1.1.27 for definitions.

TABLE 27.2 General Motor Types[a]

Type
DC motors (commutator devices)
Permanent magnet field
Wound field
Series
Shunt
Compound
AC motors
Single-phase
Cage rotor
Split phase
Resistance-start
Capacitor start
Single capacitor (start-run)
Capacitor start/capacitor run
Shaded pole
Wound rotor
Repulsion
Repulsion start/induction run
Universal
Synchronous
Hysteresis
Three-phase
Synchronous
Permanent magnet field
Wound field
Induction
Cage rotor
NEMA Design A,B,C,D,F
Wound rotor

[a]See NEMA Standard MG 1.1.1-1.1.21 for definitions.

27.4.1 Load Requirements

1. The steady-state duty cycle with torque-speed (position) requirements at each load step.
2. What operating modes are required.
3. Dynamic performance requirements, including starting and stopping, and maximum and minimum accelerations.
4. The relevant torque-speed (position) characteristics.
5. All load inertias (J).
6. Coupling options (direct drive, belt-drive, gearing).
7. Reliability of service. How critical is a system failure?
8. Future modifications.

27.4.2 Environmental Requirements

1. Ambient atmospheric conditions (pressure, temperature, humidity, content)
2. Indoor, outdoor application
3. Wet, dry location
4. Ventilation
5. Acceptable acoustical noise levels
6. Electrical/mechanical hazards to personnel
7. Accessibility for inspection and maintenance

TABLE 27.3 General Motor Controllers

Type
DC motor controllers
Electromechanical
Armature starting resistance; rheostat field control
Power electronic drive
Phase converters: 1, 2, 4 quadrant drives
Chopper control: 1, 2, 4 quadrant drives
AC motor controllers
Single-phase
Electromechanical
Across-the-line: protection only
Step-reduced voltage
Power electronic drive
Armature control: 1, 2, 4 quadrant drives
Three-phase induction
Cage rotor
Electromechanical
Across-the-line: protection only
Step-reduced voltage
Power electronic drive (ASDs)
Variable voltage source inverter
Variable current source inverter
Chopper voltage source inverter
PWM voltage source inverter
Vector control
Wound rotor
Variable rotor resistance
Power electronic rotor power recovery
Three-phase synchronous
Same as cage rotor induction
Brushless DC control

27.4.3 Electrical Source Options

1. DC-AC
2. If AC, single- and/or three-phase
3. Voltage level
4. Frequency
5. Capacity (kVA)
6. Protection options
7. Power quality specifications

27.4.4 Preliminary System Design

Based on the information compiled in the steps above, select an appropriate enclosure, motor type, and controller. In general, the enclosure entries, reading from top to bottom in Table 27.1, are from simplest (and cheapest) to most complex (and expensive). Select the simplest enclosure that meets all the environmental constraints. Next, select a motor and controller combination from Tables 27.2 and 27.3. This requires personal experience and/or consulting with engineers with experience relevant to the application.

In general, DC motors are expensive and require more maintenance, but have excellent speed and position control options. Single-phase AC motors are limited to about 5 kW, but may be desirable in locations where three-phase service is not available and control specifications are not critical.

Three-phase AC synchronous motors are not amenable to frequent starting and stopping, but are ideal for medium and high power applications which run at essentially fixed speeds. Three-phase AC

cage rotor induction motors are versatile and economical, and will be the preferred choice for most applications, particularly in the medium power range. Three-phase AC wound rotor induction motors are expensive, and only appropriate for some unusual applications.

The controller must be compatible with the motor selected; the best choice is the most economical that meets all load specifications. If the engineer's experience with the application under study is lacking, two or more systems should be selected.

27.4.5 System Ratings

Based on the steps above, select appropriate power, voltage, and frequency ratings. For cyclic loads, the power rating may tenatively be selected based on the "rms horsepower" method (calculating the rms power requirements over the load cycle).

27.4.6 System Data Acquisition

Request data from at least two vendors on all systems selected in the steps above, including:

- circuit diagrams
- performance test data
- equivalent circuit values, including inertia constants
- cost data
- warranties and guarantees

27.4.7 Engineering Studies

Perform the following studies using data from the system data acquisition step above.

1. Steady state performance. Verify that each candidate system meets all steady state load requirements.
2. Dynamic performance. Verify that each system meets all dynamic load requirements.
3. Load cycle efficiency. Determine the energy efficiency over the load cycle.
4. Provide a cost estimate for each system, including capital investment, maintenance, and annual operating costs.
5. Perform a power quality assessment.

Based on these studies, select a final system design.

27.4.8 Final System Design

Request a competitive bid on the final design from appropriate vendors. Select a vendor based on cost, expectation of continuing technical support, reputation, warranties, and past customer experience.

27.4.9 Field Testing

Whenever practical, customer and vendor engineers should design and perform field tests on the installed system, demonstrating that it meets or exceeds all specifications. If multiple units are involved, one proto-unit should be installed, tested, and commissioned before delivery is made on the balance of the order.

Further Information

The design of a properly engineered motor-controller system for a particular application requires access to several technical resources, including standards, the technical literature, manufacturers' publications, textbooks, and handbooks. The following section provides a list of references and resource material that

the author recommends for work in this area. In many cases, more recent versions of publications listed are available and should be used.

Organizations

American National Standards Institute (ANSI), 1430 Broadway, New York, NY 10018.
Institute of Electrical and Electronics Engineers (IEEE), 445 Hoes Lane, Piscataway, NJ 08855.
International Organization for Standardization (ISO) 1, rue de Varembe, 1211 Geneva 20, Switzerland.
American Society for Testing and Materials (ASTM), 1916 Race Street, Philadelphia, PA 19103.
National Electrical Manufacturers Association (NEMA), 2101 L Street, NW, Washington, D.C. 20037.
National Fire Protection Association (NFPA), Batterymarch Park Quincy, MA 02269.
The Rubber Manufacturers Association, Inc., 1400 K Street, NW, Suite 300, Washington, D.C. 20005.
Mechanical Power Transmission Association, 1717 Howard Street, Evanston, IL 60201.

Standards

NEMA MG 1-1987, *Motors and Generators.*
NEMA MG 2-1983, *Safety Standard for Construction and Guide for Selection, Installation and Use of Electric Motors and Generators.*
NEMA MG 3-1984, *Sound Level Prediction for Installed Rotating Electrical Machines.*
NEMA MG 13-1984, *Frame Assignments for Alternating-Current Integral-horsepower Induction Motors.*
ANSI/NFPA 70-1998, *National Electrical Code.*
IEEE Std 1-1969, *General Principles for Temperature Limits in the Rating of Electric Equipment.*
IEEE Std 85-1980, *Test Procedure for Airborne Sound Measurements on Rotating Electric Machinery.*
ANSI/IEEE Std 100-1984, *IEEE Standard Dictionary of Electrical and Electronics Terms.*
IEEE Std 112-1984, *Standard Test Procedure for Potyphase Induction Motors and Generators.*
IEEE Std 113-1985, *Guide on Test Procedures for DC Machines.*
ANSI/IEEE Std 114-1984, *Test Procedure for Single-Phase Induction Motors.*
ANSI/IEEE Std 115-1983, *Test Procedures for Synchronous Machines.*
ANSI/IEEE Std 117-1985, *Standard Test Procedure for Evaluation of Systems of Insulating Materials for Random-Wound AC Electric Machinery.*
ANSI/IEEE Std 304-1982, *Test Procedure for Evaluation and Classification of Insulation Systems for DC Machines.*
ISO R-1000, *SI Units and Recommendations for the Use of their Multiples and of Certain Other Units.*

Books (an abridged sample)

Acarnley, P.P., *Stepping Motors*, 2nd ed., Peter Peregrinus, Ltd., London, 1984.
Anderson, L.R., *Electric Machines and Transformers*, Reston Publishing, Reston, VA, 1981.
Bergseth, F.R. and Venkata, S.S., *Introduction to Electric Energy Devices*, Prentice-Hall, Englewood Cliffs, NJ, 1987.
Bose, B.K., Power *Electronics and AC Drives*, Prentice-Hall, Englewood Cliffs, NJ, 1985.
Brown, D. and Hamilton 111, E.P., *Electromechanical Energy Conversion*, Macmillan, New York, 1984.
Chapman, S.J., *Electric Machinery Fundamentals*, McGraw-Hill, New York, 1985.
DC Motors-Speed Controls-Servo Systems—An Engineering Handbook, 5th ed., Electro-Craft Corporation, Hopkins, MN, 1980.
Del Toro, V, *Electric Machinery and Power Systems*, Prentice-Hall, Englewood Cliffs, NJ, 1986.
Electro-Craft Corporation, *DC Motors, Speed Controls, Servo Systems*, 3rd ed., Pergamon Press, Ltd., Oxford, 1977.
Fitzgerald, A.E., Kingsley, Jr., C., and Umans, S.D., *Electric Machinery*, 5th ed., McGraw-Hill, New York, 1990.
Gonen, T., *Engineering Economy for Engineering Managers*, Wiley, New York, 1990.

Kenjo, T. and S. Nagamori, *Permanent-Magnet and Brush-less DC Motors*, Oxford, Claredon, 1985.
Krause, P.C. and Wasynezk, O., *Electromechanical Machines and Devices*, McGraw-Hill, New York, 1989.
Krein, P., *Elements of Power Electronics*; Oxford Press, 1998.
Moha, N., Undeland, and Robbins, *Power Electronics; Converters, Application, and Design, 2nd ed.*, John Wiley & Sons, New York, 1995.
Nasar, S.A. and Boldea, I., *Linear Motion Electric Machines*, John Wiley & Sons, New York, 1976.
Nasar, S.A., Ed., *Handbook of Electric Machines*, McGraw-Hill, New York, 1987.
Patrick, D.R. and Fardo, S.W., *Rotating Electrical Machines and Power Systems*, Prentice-Hall, Englewood Cliffs, NJ, 1985.
Ramshaw, R. and Van Heeswijk, R.G., *Energy Conversion: Electric Motors and Generators*, Saunders College Publishing, Orlando, FL, 1990.
Rashid, M.H., *Power Electronics: Circuits, Devices, and Applications, 2nd ed.*, Prentice-Hall, Englewood Cliffs, NJ, 1993.
Sarma, M.S., *Electric Machines: Steady-State Theory and Dynamic Performance*, Brown Publishers, Dubuque, IA, 1985.
Smeatson, R.W., Ed., *Motor Application and Maintenance Handbook*, McGraw-Hill, New York, 1969.
Stein, R., and Hunt, W.T., *Electric Power System Components: Transformers and Rotating Machines*, Van Nostrand, New York, 1979.
Veinott, C.G. and Martin, J.E., *Fractional- and Subfractional-Horsepower Electric Motors*, 4th ed., McGraw-Hill, New York, 1986.
Wenick, E.H., ed., *Electric Motor Handbook*, McGraw-Hill, London, 1978.

VI

Power Quality

S.M. Halpin
Auburn University

28

Introduction

S.M. Halpin
Auburn University

Electric power quality has emerged as a major area of electric power engineering. The predominant reason for this emergence is the increase in sensitivity of end-use equipment. This chapter is devoted to various aspects of power quality as it impacts utility companies and their customers and includes material on (1) grounding, (2) voltage sags, (3) harmonics, (4) voltage flicker, and (5) long-term monitoring. While these five topics do not cover all aspects of power quality, they provide the reader with a broad-based overview that should serve to increase overall understanding of problems related to power quality.

Proper grounding of equipment is essential for safe and proper operation of sensitive electronic equipment. In times past, it was thought by some that equipment grounding as specified in the U.S. by the National Electric Code was in contrast with methods needed to insure power quality. Since those early times, significant evidence has emerged to support the position that, in the vast majority of instances, grounding according to the National Electric Code is essential to insure proper and trouble-free equipment operation, and also to insure the safety of associated personnel.

Other than poor grounding practices, voltage sags due primarily to system faults are probably the most significant of all power quality problems. Voltage sags due to short circuits are often seen at distances very remote from the fault point, thereby affecting a potentially large number of utility customers. Coupled with the wide-area impact of a fault event is the fact that there is no effective preventive for all power system faults. End-use equipment will, therefore, be exposed to short periods of reduced voltage which may or may not lead to malfunctions.

Like voltage sags, the concerns associated with flicker are also related to voltage variations. Voltage flicker, however, is tied to the likelihood of a human observer to become annoyed by the variations in the output of a lamp when the supply voltage amplitude is varying. In most cases, voltage flicker considers (at least approximately) periodic voltage fluctuations with frequencies less than about 30–35 Hz that are small in size. Human perception, rather than equipment malfunction, is the relevant factor when considering voltage flicker.

For many periodic waveform (either voltage or current) variations, the power of classical Fourier series theory can be applied. The terms in the Fourier series are called harmonics; relevant harmonic terms may have frequencies above or below the fundamental power system frequency. In most cases, nonfundamental frequency equipment currents produce voltages in the power delivery system at those same frequencies. This voltage distortion is present in the supply to other end-use equipment and can lead to improper operation of the equipment.

Harmonics, like most other power quality problems, require significant amounts of measured data in order for the problem to be diagnosed accurately. Monitoring may be short- or long-term and may be

relatively cheap or very costly and often represents the majority of the work required to develop power quality solutions.

In summary, the power quality problems associated with grounding, voltage sags, harmonics, and voltage flicker are those most often encountered in practice. It should be recognized that the voltage and current transients associated with common events like lightning strokes and capacitor switching can also negatively impact end-use equipment. Because transients are covered in a separate chapter of this book, they are not considered further in this chapter.

29

Wiring and Grounding for Power Quality

Christopher J. Melhorn
EPRI

Perhaps one of the most common problems related to power quality is wiring and grounding. It has been reported that approximately 70 to 80% of all power quality related problems can be attributed to faulty connections and/or wiring. This chapter describes wiring and grounding issues as they relate to power quality. It is not intended to replace or supercede the National Electric Code (NEC) or any local codes concerning grounding.

29.1 Definitions and Standards

Defining grounding terminology is outside the scope of this chapter. There are several publications on the topic of grounding that define grounding terminology in various levels of detail. The reader is referred to these publications for the definitions of grounding terminology.

The following is a list of standards and recommended practice pertaining to wiring and grounding issues. See the section on References for complete information.

National Electric Code Handbook, 1996 edition.
IEEE Std. 1100–1999. *IEEE Recommended Practice for Powering and Grounding Electronic Equipment.*
IEEE Std. 142–1991. *IEEE Recommended Practice for Grounding Industrial and Commercial Power Systems.*
FIPS-94 Publication
Electrical Power Systems Quality

29.1.1 The National Electric Code

NFPAs *National Electrical Code Handbook* pulls together all the extra facts, figures, and explanations readers need to interpret the 1999 NEC. It includes the entire text of the Code, plus expert commentary, real-world examples, diagrams, and illustrations that clarify requirements. Code text appears in blue

type and commentary stands out in black. It also includes a user-friendly index that references article numbers to be consistent with the Code.

Several definitions of grounding terms pertinent to discussions in this article have been included for reader convenience. The following definitions were taken from various publications as cited.

29.1.2 From the *IEEE Dictionary—Std. 100*

Grounding: A conducting connection, whether intentional or accidental, by which an electric circuit or equipment is connected to the earth, or to some conducting body of relatively large extent that serves in place of the earth. It is used for establishing and maintaining the potential of the earth (or of the conducting body) or approximately that potential, on conductors connected to it; and for conducting ground current to and from the earth (or the conducting body).

29.1.3 Green Book (IEEE Std. 142) Definitions

Ungrounded System: A system, circuit, or apparatus without an intentional connection to ground, except through potential indicating or measuring devices or other very high impedance devices.

Grounded System: A system of conductors in which at least one conductor or point (usually the middle wire or neutral point of transformer or generator windings) is intentionally grounded, either solidly or through an impedance.

29.1.4 NEC Definitions

Refer to Fig. 29.1.

Bonding Jumper, Main: The connector between the grounded circuit conductor (neutral) and the equipment-grounding conductor at the service entrance.

Conduit/Enclosure Bond: (bonding definition) The permanent joining of metallic parts to form an electrically conductive path which will assure electrical continuity and the capacity to conduct safely any current likely to be imposed.

Grounded: Connected to earth or to some conducting body that serves in place of the earth.

Grounded Conductor: A system or circuit conductor that is intentionally grounded (the grounded conductor is normally referred to as the neutral conductor).

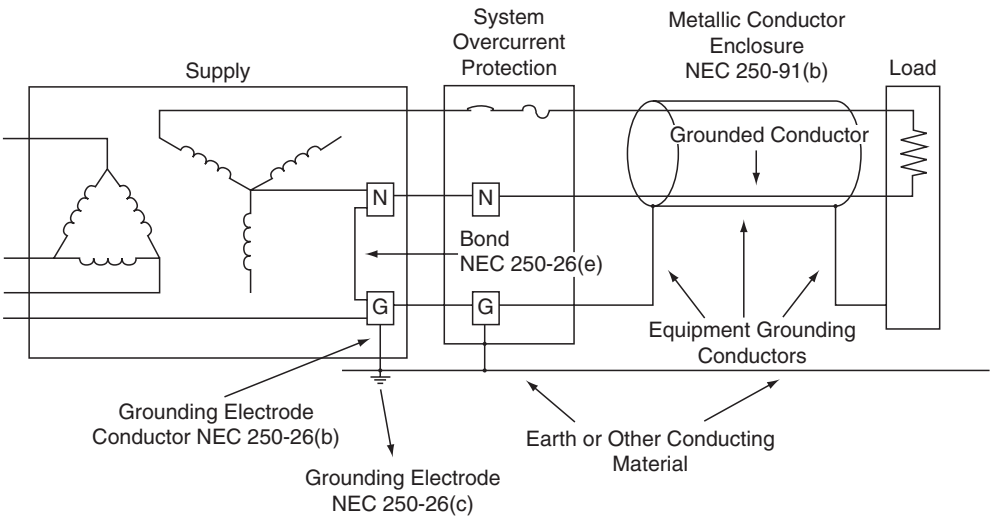

FIGURE 29.1 Terminology used in NEC definitions.

Grounding Conductor: A conductor used to connect equipment or the grounded circuit of a wiring system to a grounding electrode or electrodes.

Grounding Conductor, Equipment: The conductor used to connect the noncurrent-carrying metal parts of equipment, raceways, and other enclosures to the system grounded conductor and/or the grounding electrode conductor at the service equipment or at the source of a separately derived system.

Grounding Electrode Conductor: The conductor used to connect the grounding electrode to the equipment-grounding conductor and/or to the grounded conductor of the circuit at the service equipment or at the source of a separately derived system.

Grounding Electrode: The grounding electrode shall be as near as practicable to and preferably in the same area as the grounding conductor connection to the system. The grounding electrode shall be: (1) the nearest available effectively grounded structural metal member of the structure; or (2) the nearest available effectively grounded metal water pipe; or (3) other electrodes (Section 250-81 & 250-83) where electrodes specified in (1) and (2) are not available.

Grounding Electrode System: Defined in NEC Section 250-81 as including: (a) metal underground water pipe; (b) metal frame of the building; (c) concrete-encased electrode; and (d) ground ring. When these elements are available, they are required to be bonded together to form the grounding electrode system. Where a metal underground water pipe is the only grounding electrode available, it must be supplemented by one of the grounding electrodes specified in Section 250–81 or 250–83.

Separately Derived Systems: A premises wiring system whose power is derived from generator, transformer, or converter windings and has no direct electrical connection, including a solidly connected grounded circuit conductor, to supply conductors originating in another system.

29.2 Reasons for Grounding

There are three basic reasons for grounding a power system: personal safety, protective device operation, and noise control. All three of these reasons will be addressed.

29.2.1 Personal Safety

The most important reason for grounding a device on a power system is personal safety. The safety ground, as it is sometimes called, is provided to reduce or eliminate the chance of a high touch potential if a fault occurs in a piece of electrical equipment. Touch potential is defined as the voltage potential between any two conducting materials that can be touched simultaneously by an individual or animal.

Figure 29.2 illustrates a dangerous touch potential situation. The "hot" conductor in the piece of equipment has come in contact with the case of the equipment. Under normal conditions, with the safety ground intact, the protective device would operate when this condition occurred. However, in Fig. 29.2, the safety ground is missing. This allows the case of the equipment to float above ground since the case of the equipment is not grounded through its base. In other words, the voltage potential between the equipment case and ground is the same as the voltage potential between the hot leg and ground. If the operator would come in contact with the case and ground (the floor), serious injury could result.

In recent years, manufacturers of handheld equipment, drills, saws, hair dryers, etc. have developed double insulated equipment. This equipment generally does not have a safety ground. However, there is never any conducting material for the operator to contact and therefore there is no touch potential hazard. If the equipment becomes faulted, the case or housing of the equipment is not energized.

29.2.2 Protective Device Operation

As mentioned in the previous section, there must be a path for fault current to return to the source if protective devices are to operate during fault conditions. The National Electric Code (NEC) requires that an effective grounding path must be mechanically and electrically continuous (NEC 250–51), have

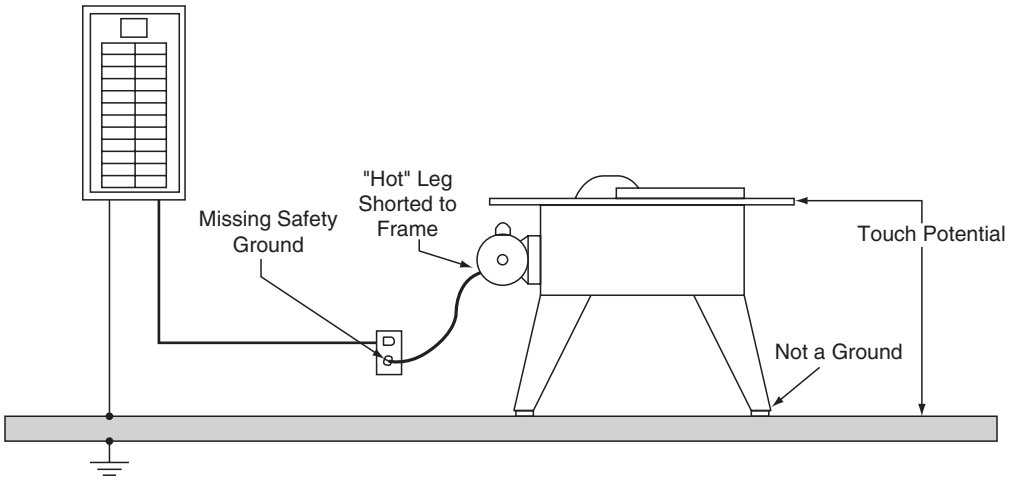

FIGURE 29.2 Illustration of a dangerous touch potential situation.

the capacity to carry any fault currents imposed on it without damage (NEC 250–75). The NEC also states that the ground path must have sufficiently low impedance to limit the voltage and facilitate protective device operation. Finally, the earth cannot serve as the equipment-grounding path (NEC-250–91(c)).

The formula to determine the maximum circuit impedance for the grounding path is:

$$\text{Ground Path Impedance} = \frac{\text{Maximum Voltage to Ground}}{\text{Overcurrent Protection Rating} \times 5}$$

Table 29.1 gives examples of maximum ground path circuit impedances required for proper protective device operation.

29.2.3 Noise Control

Noise control is the third main reason for grounding. Noise is defined as unwanted voltages and currents on a grounding system. This includes signals from all sources whether it is radiated or conducted. As stated, the primary reason for grounding is safety and is regulated by the NEC and local codes. Any changes to the grounding system to improve performance or eliminate noise control must be in addition to the minimum NEC requirements.

When potential differences occur between different grounding systems, insulation can be stressed and circulating currents can be created in low voltage cables (e.g., communications cables). In today's electrical environment, buildings that are separated by large physical distances are typically tied together via a communication circuit. An example of this would be a college campus that may cover several

TABLE 29.1 Example Ground Impedance Values

Protective Device Rating	Voltage to Ground 120 Volts	Voltage to Ground 277 Volts
20 Amps	1.20 Ω	2.77 Ω
40 Amps	0.60 Ω	1.39 Ω
50 Amps	0.48 Ω	1.11 Ω
60 Amps	0.40 Ω	0.92 Ω
100 Amps	0.24 Ω	0.55 Ω

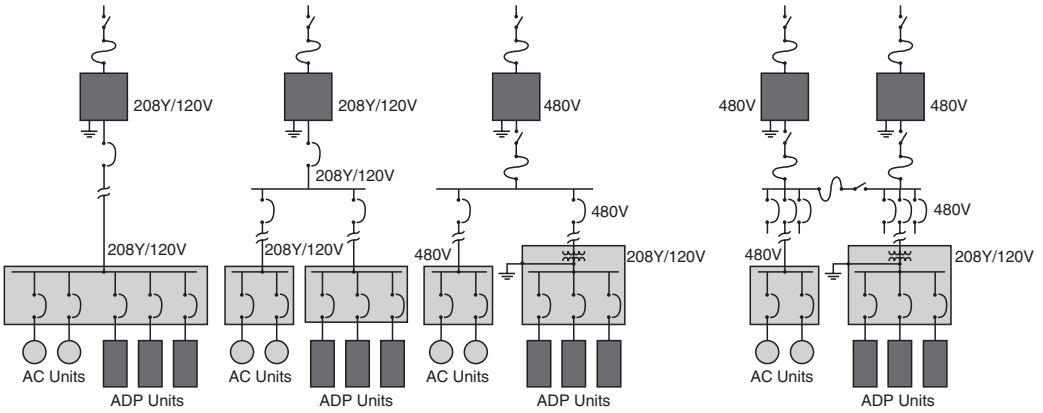

FIGURE 29.3 Separation of loads for noise control.

square miles. Each building has its own grounding system. If these grounding systems are not tied together, a potential difference on the grounding circuit for the communication cable can occur. The idea behind grounding for noise control is to create an equipotential grounding system, which in turn limits or even eliminates the potential differences between the grounding systems. If the there is an equipotential grounding system and currents are injected into the ground system, the potential of the whole grounding system will rise and fall and potential differences will not occur.

Supplemental conductors, ground reference grids, and ground plates can all be used to improve the performance of the system as it relates to power quality. Optically isolated communications can also improve the performance of the system. By using the opto-isolators, connecting the communications to different ground planes is avoided. All improvements to the grounding system must be done in addition to the requirements for safety.

Separation of loads is another method used to control noise. Figure 29.3 illustrates this point. Figure 29.3 shows four different connection schemes. Each system from left to right improves noise control.

As seen in Fig. 29.3, the best case would be the complete separation (system on the far right) of the ADP units from the motor loads and other equipment. Conversely, the worst condition is on the left of Fig. 29.3 where the ADP units are served from the same circuit as the motor loads.

29.3 Typical Wiring and Grounding Problems

In this section, typical wiring and grounding problems, as related to power quality, are presented. Possible solutions are given for these problems as well as the possible causes for the problems being observed on the grounding system. (See Table 29.2.)

The following list is just a sample of problems that can occur on the grounding system.

- Isolated grounds
- Ground loops
- Missing safety ground
- Multiple neutral-to-ground bonds
- Additional ground rods
- Insufficient neutral conductors

29.3.1 Insulated Grounds

Insulated grounds in themselves are not a grounding problem. However, improperly used insulated grounds can be a problem. Insulated grounds are used to control noise on the grounding system. This is

TABLE 29.2 Typical Wiring and Grounding Problems and Causes

Wiring Condition or Problem Observed	Possible Cause
Impulse, voltage drop out	Loose connections
Impulse, voltage drop out	Faulty breaker
Ground currents	Extra neutral-to-ground bond
Ground currents	Neutral-to-ground reversal
Extreme voltage fluctuations	High impedance in neutral circuit
Voltage fluctuations	High impedance neutral-to-ground bonds
High neutral to ground voltage	High impedance ground
Burnt smell at the panel, junction box, or load	Faulted conductor, bad connection, arcing, or overloaded wiring
Panel or junction box is warm to the touch	Faulty circuit breaker or bad connection
Buzzing sound	Arcing
Scorched insulation	Overloaded wiring, faulted conductor, or bad connection
Scorched panel or junction box	Bad connection, faulted conductor
No voltage at load equipment	Tripped breaker, bad connection, or faulted conductor
Intermittent voltage at the load equipment	Bad connection or arcing

accomplished by using insulated ground receptacles, which are indicated by a "Δ" on the face of the outlet. Insulated ground receptacles are often orange in color. Figure 29.4 illustrates a properly wired insulated ground circuit.

The 1996 NEC has this to say about insulated grounds.

NEC 250-74. Connecting Receptacle Grounding Terminal to Box. An equipment bonding jumper shall be used to connect the grounding terminal of a grounding-type receptacle to a grounded box.

Exception No. 4. Where required for the reduction of electrical noise (electromagnetic interference) on the grounding circuit, a receptacle in which the grounding terminal is purposely insulated from the receptacle mounting means shall be permitted. The receptacle grounding terminal shall be grounded by an insulated equipment grounding conductor run with the circuit conductors. This grounding conductor shall be permitted to pass through one or more panelboards without connection to the panelboard grounding terminal as permitted in Section 384-20, Exception so as to terminate within the same building or structure directly at an equipment grounding conductor terminal of the applicable derived system or source.

(FPN): Use of an isolated equipment grounding conductor does not relieve the requirement for grounding the raceway system and outlet box.

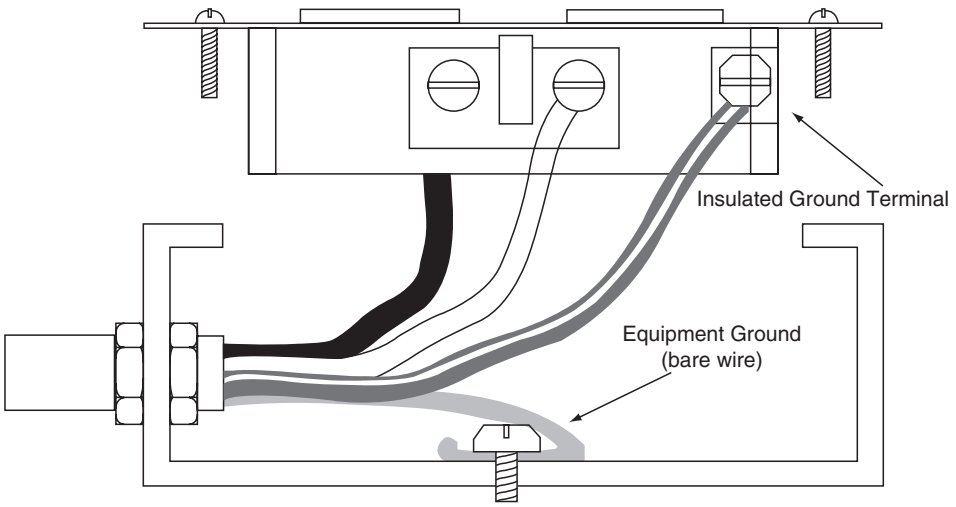

FIGURE 29.4 Properly wired isolated ground circuit.

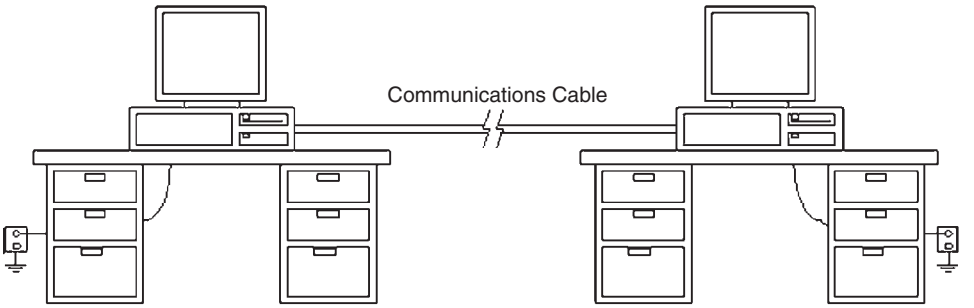

FIGURE 29.5 Circuit with a ground loop.

NEC 517-16. Receptacles with Insulated Grounding Terminals. Receptacles with insulated grounding terminals, as permitted in Section 250-74, Exception No. 4, shall be identified; such identification shall be visible after installation.

(FPN): Caution is important in specifying such a system with receptacles having insulated grounding terminals, since the grounding impedance is controlled only by the grounding conductors and does not benefit functionally from any parallel grounding paths.

The following is a list of pitfalls that should be avoided when installing insulated ground circuits.

- Running an insulated ground circuit to a regular receptacle.
- Sharing the conduit of an insulated ground circuit with another circuit.
- Installing an insulated ground receptacle in a two-gang box with another circuit.
- Not running the insulated ground circuit in a metal cable armor or conduit.
- Do not assume that an insulated ground receptacle has a truly insulated ground.

29.3.2 Ground Loops

Ground loops can occur for several reasons. One is when two or more pieces of equipment share a common circuit like a communication circuit, but have separate grounding systems (Fig. 29.5).

To avoid this problem, only one ground should be used for grounding systems in a building. More than one grounding electrode can be used, but they must be tied together (NEC 250-81, 250-83, and 250-84) as illustrated in Fig. 29.6.

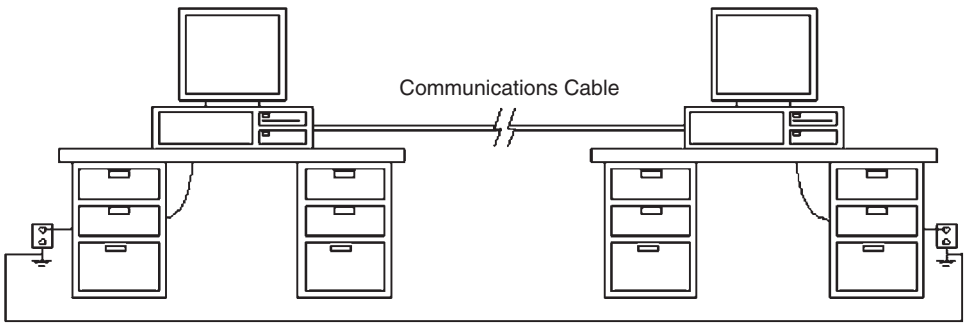

FIGURE 29.6 Grounding electrodes must be bonded together.

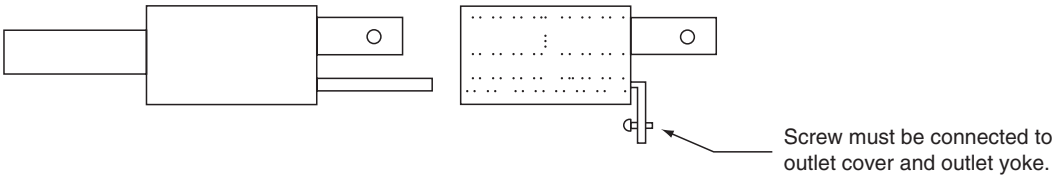

FIGURE 29.7 Proper use of a grounding plug adapter or "cheater plug."

29.3.3 Missing Safety Ground

As discussed previously, a missing safety ground poses a serious problem. Missing safety grounds usually occur because the safety ground has been bypassed. This is typical in buildings where the 120-volt outlets only have two conductors. Modern equipment is typically equipped with a plug that has three prongs, one of which is a ground prong. When using this equipment on a two-prong outlet, a grounding plug adapter or "cheater plug" can be employed provided there is an equipment ground present in the outlet box. This device allows the use of a three-prong device in a two-prong outlet. When properly connected, the safety ground remains intact. Figure 29.7 illustrates the proper use of the cheater plug.

If an equipment ground is not present in the outlet box, then the grounding plug adapter should not be used. If the equipment grounding conductor is present, the preferred method for solving the missing safety ground problem is to install a new three-prong outlet in the outlet box. This method insures that the grounding conductor will not be bypassed. The NEC discusses equipment grounding conductors in detail in Section 250—Grounding.

29.3.4 Multiple Neutral to Ground Bonds

Another misconception when grounding equipment is that the neutral must be tied to the grounding conductor. Only one neutral-to-ground bond is permitted in a system or sub-system. This typically occurs at the service entrance to a facility unless there is a separately derived system. A separately derived system is defined as a system that receives its power from the windings of a transformer, generator, or some type of converter. Separately derived systems must be grounded in accordance with NEC 250-26.

The neutral should be kept separate from the grounding conductor in all panels and junction boxes that are downline from the service entrance. Extra neutral-to-ground bonds in a power system will cause neutral currents to flow on the ground system. This flow of current on the ground system occurs because of the parallel paths. Figures 29.8 and 29.9 illustrate this effect.

As seen in Fig. 29.9, neutral current can find its way onto the ground system due to the extra neutral-to-ground bond in the secondary panel board. Notice that not only will current flow in the ground wire for the power system, but currents can flow in the shield wire for the communication cable between the two PCs.

If the neutral-to-ground bond needs to be reestablished (high neutral-to-ground voltages), this can be accomplished by creating a separately derived system as defined above. Figure 29.10 illustrates a separately derived system.

29.3.5 Additional Ground Rods

Additional ground rods are another common problem in grounding systems. Ground rods for a facility or building should be part of the grounding system. The ground rods should be connected where all the building grounding electrodes are bonded together. Isolated grounds can be used as described in the NEC's Isolated Ground section, but should not be confused with isolated ground rods, which are not permitted.

The main problem with additional ground rods is that they create secondary paths for transient currents, such as lightning strikes, to flow. When a facility incorporates the use of one ground rod, any currents caused by lightning will enter the building ground system at one point. The ground potential of

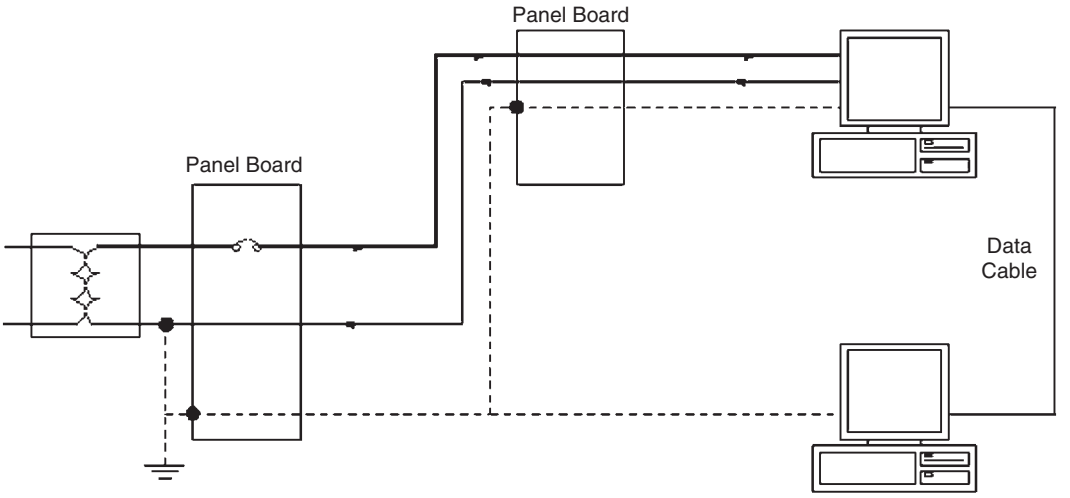

FIGURE 29.8 Neutral current flow with one neutral-to-ground bond.

the entire facility will rise and fall together. However, if there is more than one ground rod for the facility, the transient current enters the facility's grounding system at more than one location and a portion of the transient current will flow on the grounding system causing the ground potential of equipment to rise at different levels. This, in turn, can cause severe transient voltage problems and possible conductor overload conditions.

29.3.6 Insufficient Neutral Conductor

With the increased use of electronic equipment in commercial buildings, there is a growing concern for the increased current imposed on the grounded conductor (neutral conductor). With a typical three-phase load that is balanced, there is theoretically no current flowing in the neutral conductor, as illustrated in Fig 29.11.

However, PCs, laser printers, and other pieces of electronic office equipment all use the same basic technology for receiving the power that they need to operate. Figure 29.12 illustrates the typical power

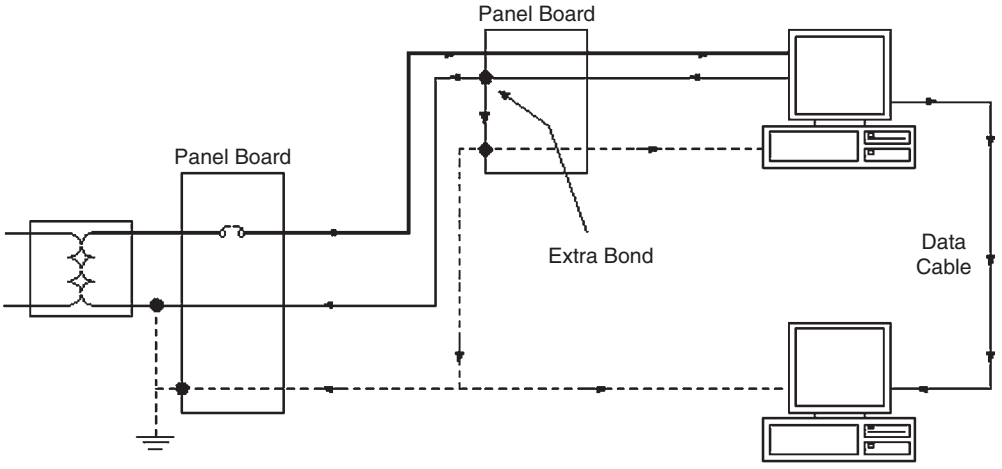

FIGURE 29.9 Neutral current flow with and extra neutral-to-ground bond.

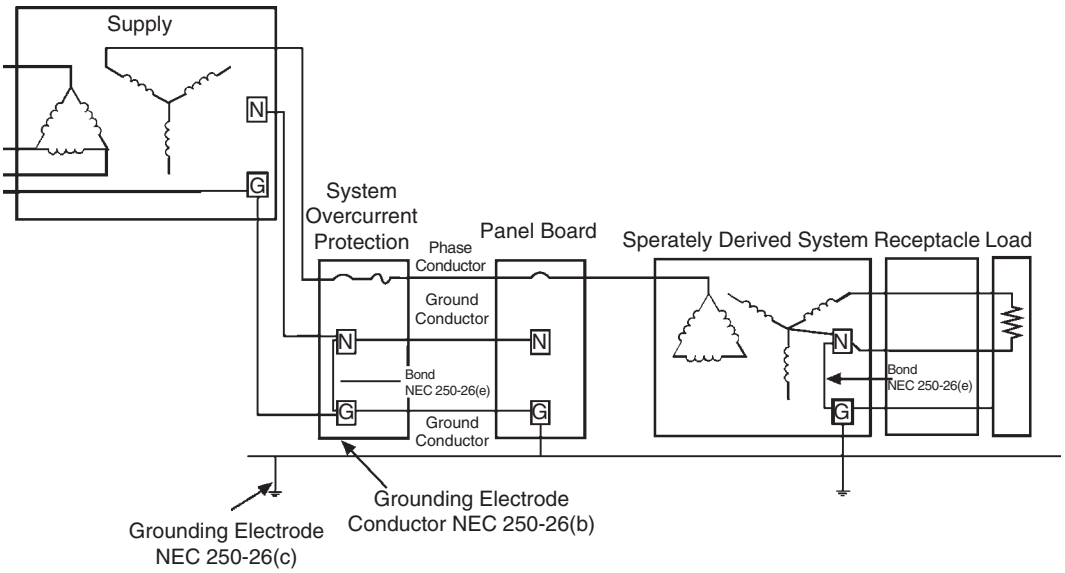

FIGURE 29.10 Example of the use of a separately derived system.

supply of a PC. The input power is generally 120 volts AC, single phase. The internal electronic parts require various levels of DC voltage (e.g., ± 5, 12 volts DC) to operate. This DC voltage is obtained by converting the AC voltage through some type of rectifier circuit as shown. The capacitor is used for filtering and smoothing the rectified AC signal. These types of power supplies are referred to as switch mode power supplies (SMPS).

The concern with devices that incorporate the use of SMPS is that they introduce triplen harmonics into the power system. Triplen harmonics are those that are odd multiples of the fundamental frequency component ($h = 3, 9, 15, 21, \ldots$). For a system that has balanced single-phase loads as illustrated in Fig. 29.13, fundamental and third harmonic components are present. Applying Kirchoff's current law at node N shows that the fundamental current component in the neutral must be zero. But when loads are balanced, the third harmonic components in each phase coincide. Therefore, the magnitude of third harmonic current in the neutral must be three times the third harmonic phase current.

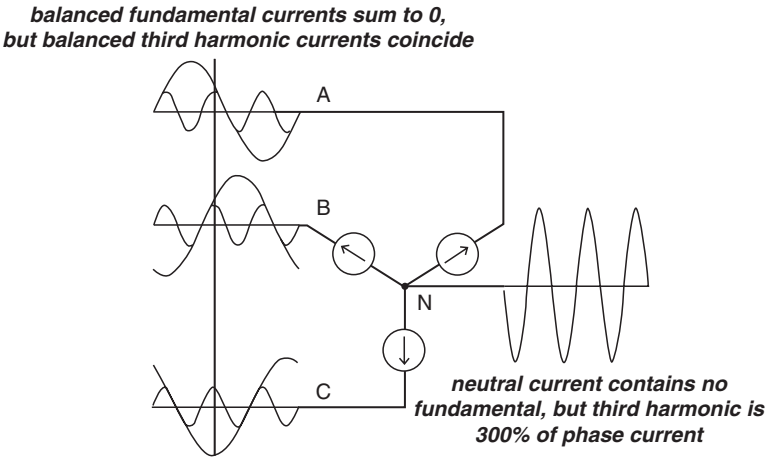

FIGURE 29.11 A balanced three-phase system.

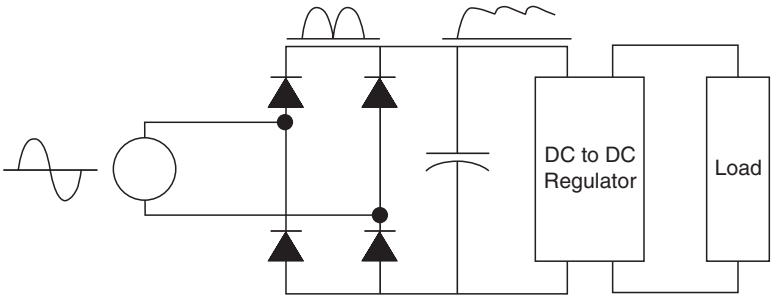

FIGURE 29.12 The basic one-line for a SMPS.

This becomes a problem in office buildings when multiple single-phase loads are supplied from a three-phase system. Separate neutral wires are run with each circuit, therefore the neutral current will be equivalent to the line current. However, when the multiple neutral currents are returned to the panel or transformer serving the loads, the triplen currents will add in the common neutral for the panel and this can cause over heating and eventually even cause failure of the neutral conductor. If office partitions are used, the same, often undersized neutral conductor is run in the partition with three-phase conductors. Each receptacle is fed from a separate phase in order to balance the load current. However, a single neutral is usually shared by all three phases. This can lead to disastrous results if the partition electrical receptacles are used to supply nonlinear loads rich in triplen harmonics.

Under the worst conditions, the neutral current will never exceed 173% of the phase current. Figure 29.13 illustrates a case where a three-phase panel is used to serve multiple single-phase SMPS PCs.

29.3.7 Summary

As discussed previously, the three main reasons for grounding in electrical systems are:

1. Personal safety
2. Proper protective device operation
3. Noise control

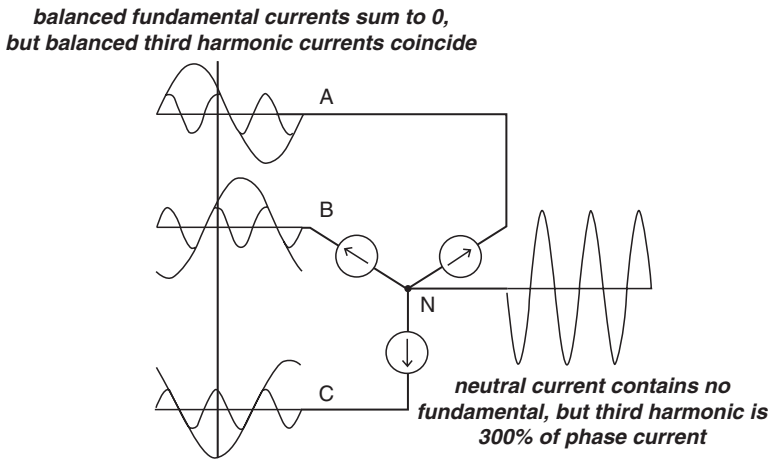

FIGURE 29.13 Balanced single-phase loads.

TABLE 29.3 Summary of Wiring and Grounding Issues

Summary Issues
Good power quality and noise control practices do not conflict with safety requirements.
Wiring and grounding problems cause a majority of equipment interference problems.
Make an effort to put sensitive equipment on dedicated circuits.
The grounded conductor, neutral conductor, should be bonded to the ground at the transformer or main panel, but not at other panel down line except as allowed by separately derived systems.

By following the guidelines found below, the objectives for grounding can be accomplished.

- All equipment should have a safety ground. A safety ground conductor
- Avoid load currents on the grounding system.
- Place all equipment in a system on the same equipotential reference.

Table 29.3 summarizes typical wiring and grounding issues.

29.4 Case Study

This section presents a case study involving wiring and grounding issues. The purpose of this case study is to inform the reader on the procedures used to evaluate wiring and grounding problems and present solutions.

29.4.1 Case Study—Flickering Lights

This case study concerns a residential electrical system. The homeowners were experiencing light flicker when loads were energized and deenergized in their homes.

29.4.1.1 Background

Residential systems are served from single-phase transformers employing a spilt secondary winding, often referred to as a single-phase three-wire system. This type of transformer is used to deliver both 120-volt and 240-volt single-phase power to the residential loads. The primary of the transformer is often served from a 12 to 15 kV distribution system by the local utility. Figure 29.14 illustrates the concept of a split-phase system.

When this type of service is operating properly, 120 volts can be measured from either leg to the neutral conductor. Due to the polarity of the secondary windings in the transformer, the polarity of each 120-volt leg is opposite the other, thus allowing a total of 240 volts between the legs as illustrated. The proper operation of this type of system is dependent on the physical connection of the neutral conductor or center tap of the secondary winding. If the neutral connection is removed, 240 volts will remain across the two legs, but the line-to-neutral voltage for either phase can be shifted, causing either a low or high voltage from line to neutral.

Most loads in a residential dwelling, i.e., lighting, televisions, microwaves, home electronics, etc., are operated from 120 volts. However, there are a few major loads that incorporate the use of the 240 volts available. These loads include electric water heaters, electric stoves and ovens, heat pumps, etc.

29.4.1.2 The Problem

In this case, there were problems in the residence that caused the homeowner to question the integrity of the power system serving his home. On occasion, the lights would flicker erratically when the washing machine and dryer were operating at the same time. When large single-phase loads were operated, low power incandescent light bulb intensity would flicker.

Measurements were performed at several 120-volt outlets throughout the house. When the microwave was operated, the voltage at several of the 120-volt outlets would increase from 120 volts nominal to

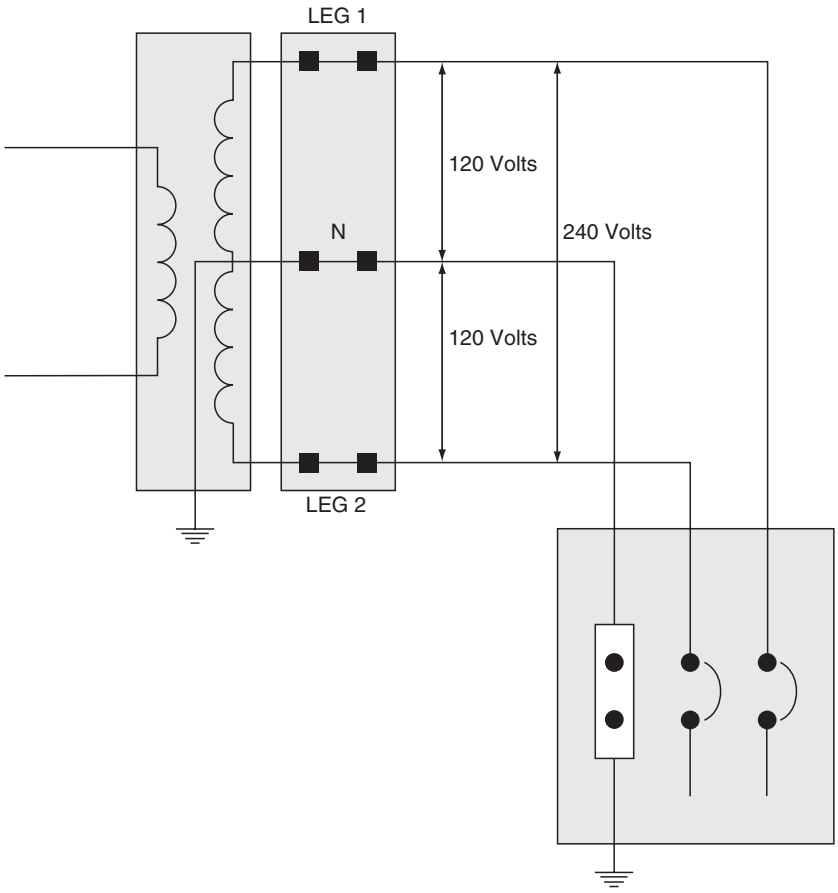

FIGURE 29.14 Split-phase system serving a residential customer.

128 volts. The voltage would return to normal after the microwave was turned off. The voltage would also increase when a 1500-Watt space heater was operated. It was determined that the voltage would decrease to approximately 112 volts on the leg from which the large load was served. After the measurements confirmed suspicions of high and low voltages during heavy load operation, finding the source of the problem was the next task at hand.

The hunt began at the service entrance to the house. A visual inspection was made of the meter base and socket after the meter was removed by the local utility. It was discovered that one of the neutral connectors was loose. While attempting to tighten this connector, the connector fell off of the meter socket into the bottom of the meter base (see Fig. 29.15). Could this loose connector have been the cause of the flickering voltage? Let's examine the effects of the loose neutral connection.

Figures 29.16 and 29.17 will be referred to several times during this discussion. Under normal conditions with a solid neutral connection (Fig. 29.16), load current flows through each leg and is returned to the source through the neutral conductor. There is very little impedance in either the hot or the neutral conductor; therefore, no appreciable voltage drop exists.

When the neutral is loose or missing, a significant voltage can develop across the neutral connection in the meter base, as illustrated in Fig. 29.17. When a large load is connected across Leg 1 to N and the other leg is lightly loaded (i.e., Leg 1 to N is approximately 10 times the load on Leg 2 to N), the current flowing through the neutral will develop a voltage across the loose connection. This voltage is in phase with the voltage from Leg 1 to N′ (see Fig. 29.17) and the total voltage from Leg 1 to N will be 120 volts.

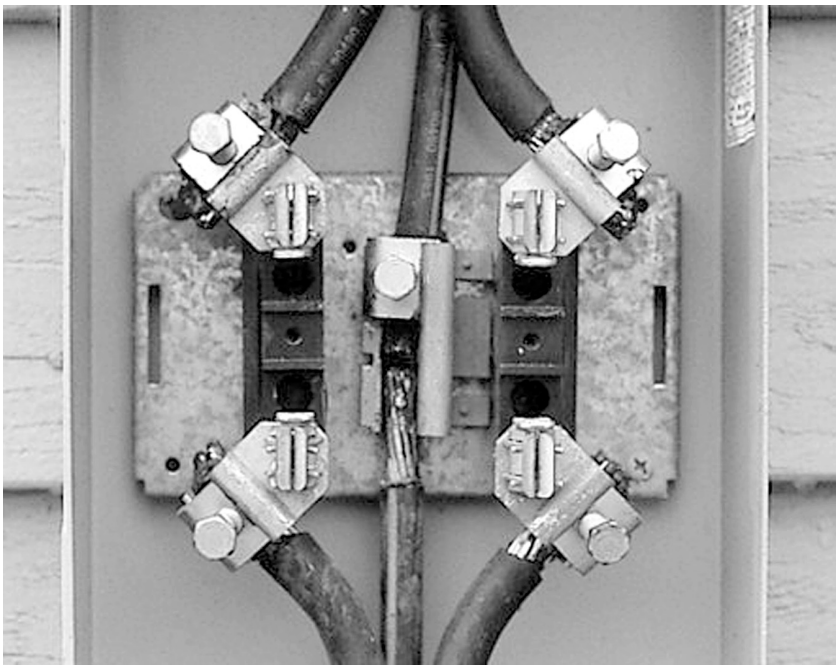

FIGURE 29.15 Actual residential meter base. Notice the missing neutral clamp on load side of meter.

However, the voltage supplied to any loads connected from Leg 2 to N′ will rise to 128 volts, as illustrated in Fig. 29.17. The total voltage across the Leg 1 and Leg 2 must remain constant at 240 volts. It should be noted that the voltage from Leg 2 to N will be 120 volts since the voltage across the loose connection is 180° out of phase with the Leg 2 to N′ voltage.

Therefore, with the missing neutral connection, the voltage from Leg 2 to N′ would rise, causing the light flicker. This explains the rise in voltage when a large load was energized on the system.

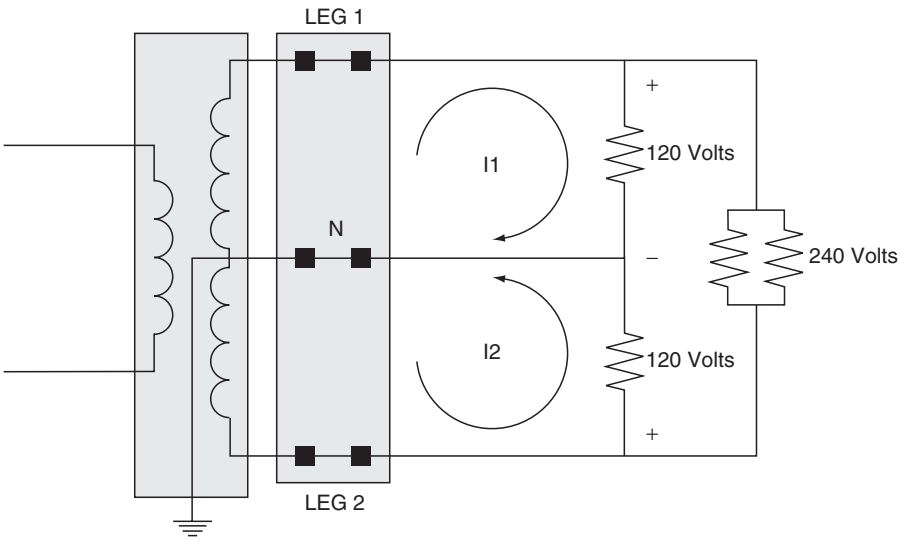

FIGURE 29.16 The effects of a solid neutral connection in the meter base.

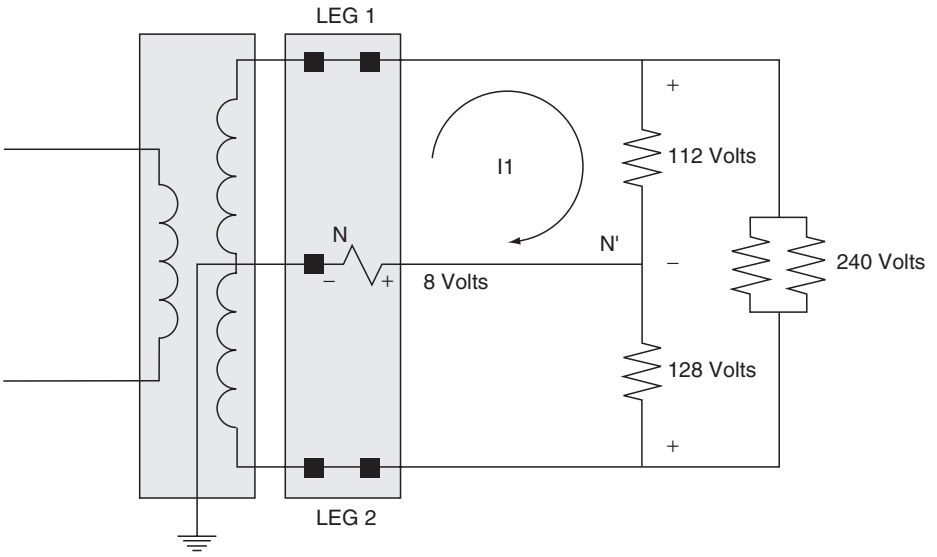

FIGURE 29.17 The effects of a loose neutral connection in the meter base.

29.4.1.3 The Solution

The solution in this case was simple—replace the failed connector.

29.4.1.4 Conclusions

Over time, the neutral connector had become loose. This loose connection caused heating, which in turn caused the threads on the connector to become worn, and the connector failed. After replacing the connector in the meter base, the flickering light phenomena disappeared.

On systems of this type, if a voltage rise occurs when loads are energized, it is a good indication that the neutral connection may be loose or missing.

References

Dugan, R.C. et al., *Electrical Power Systems Quality*, McGraw-Hill, New York, 1995.

FIPS-94 Publication.

IEEE Std. 142–1991. *IEEE Recommended Practice for Grounding Industrial and Commercial Power Systems*, The Institute of Electrical and Electronics Engineers, New York, New York, 1991.

IEEE Std. 1100–1999. *IEEE Recommended Practice for Powering and Grounding Electronic Equipment*, The Institute of Electrical and Electronics Engineers, New York, New York, 1999.

Melhorn, Christopher J., Coping with non-linear computer loads in commercial buildings—Part I, *emf-emi control* 2, 5, September/October, 1995.

Melhorn, Christopher J., Coping with non-linear computer loads in commercial building—Part II, *emf-emi control* 2, 6, January/February, 1996.

Melhorn, Chris, Flickering Lights—A Case of Faulty Wiring, *PQToday*, 3, 4, August 1997.

National Electrical Code Handbook, National Fire Protection Agency, Quincy, MA, 1996 edition.

Understanding the National Electric Code, 1993 Edition, Michael Holt, Delmar Publishers, Inc., 1993.